In vivo analysis of the antihyperalgesic activity of innovative compounds

Louis Hilfiger

UNIVERSITÉ DE STRASBOURG

ÉCOLE DOCTORALE DES SCIENCES DE LA VIE ET DE LA SANTÉ

UPR 3212 - Institut des Neurosciences Cellulaires et Intégratives

-

BENEPHYT

THÈSE

Présentée par :

Louis HILFIGER

Soutenue le : **11 Mars 2022**

Pour obtenir le grade de : **Docteur de l'Université de Strasbourg**

Discipline / Spécialité : **Neurosciences**

Analyse *in vivo* de l'activité anti-hyperalgésique de molécules innovantes.

Thèse dirigée par :

M. CHARLET Alexandre CRCN, Université de Strasbourg, INCI, CNRS UPR 3212.

Rapporteurs :

M. LINGUEGLIA Éric DR, Université de Nice - Sophia Antipolis, IPMC, INSERM UMR 7275.

M. LANDRY Marc PU, Université de Bordeaux, IMN, CNRS UMR 5293.

Examinateur interne :

M. SIMONIN Frédéric DR, Université de Strasbourg, BSC, CNRS UMR 7242.

Co-encadrant CIFRE (Invité) :

M. PETITJEAN Hugues PDG, BENEPHYT, Strasbourg.

REMERCIEMENTS

La thèse est l'aboutissement d'un cheminement personnel s'inscrivant dans un travail et une réflexion collaborative. Je tiens donc à remercier tous ceux qui m'ont accompagné au cours de ces dernières années.

Dans un premier temps je remercie chaleureusement, les membres du jury, le Pr. Marc Landry, ainsi que les Dr Éric Lingugelia et Frédéric Simonin d'avoir accepté d'évaluer mon travail de thèse.

Je tiens particulièrement à te remercier Alex. La liberté scientifique et expérimentale que tu m'as accordé tout en maintenant un encadrement scientifique rigoureux fut un vrai plaisir pendant ces années. Avec toi j'ai aussi eu la chance de prendre part à de nombreux de projets et collaborations différentes qui m'ont permis d'acquérir des compétences scientifiques et professionnelles diversifiées. Je ne pourrais pas ici te remercier pour tout ce que tu m'as apporté. Pour finir je te souhaite le meilleur pour la suite, mais je ne me fais pas trop de soucis, tu es bien accompagné.

Pascal, je vais un peu me répéter du rapport du M2, mais un énorme merci pour le temps passé à relire tous mes documents, rapports, articles et thèse. Tu as toujours pris le temps de répondre avec le sourire à toutes mes questions et interrogations, ta bienveillance et ta bonne humeur sont d'inestimables apports à l'équipe.

Merci à toute l'équipe Damien, Angel, Etienne et Julie, pour le temps passé en salle de patch, les blagues, les débats, les binouzes au chariot, les soirées jeux, les repas du midi, bref merci pour tout et bonne chance pour la suite.

Hugues un très grand merci de m'avoir proposé cette opportunité au sein de BENEPHYT. La confiance que vous m'avez accordé pour la gestion du projet NeuroTerpain et votre rigueur m'ont permis de mûrir scientifiquement, professionnellement et personnellement. Encore merci et bonne chance pour la suite avec BENEPHYT.

Un grand merci Eléa, pour ton aide, pour les relectures de la thèse et des articles mais surtout pour ton soutien. Nos réunions du vendredi matin ont été un super moment durant cette thèse, je te souhaite tout le meilleur pour la suite.

Je tiens aussi à remercier toute l'équipe du Chronobiotronc et tout particulièrement Dominique et Sophie. Votre aide et vos conseils pour la réalisation de mes expériences ont été essentiels tout au long de ma thèse.

Je remercie aussi tous mes collaborateurs, collègues et les membres de Doctoneuro avec qui j'ai pu travailler et échanger pendant ces presque 4 années.

Théo, Thomas, Florian, Guillaume, Zélie et tous les autres, quel chemin parcouru depuis notre rentrée en M1 ; des premières réunions IDSN en passant par les fêtes, les soirées jeux et l'entré en thèse. Merci d'avoir partagé avec moi ce sacré bout de chemin et j'espère vous voir très bientôt.

Merci aussi à tous mes amis Simon, Ben, Daminou, Gusti, Tonio, Meance, Lucas, Jéjé, Martin et tous ceux que je n'ai pas pu nommer ici. Les moments, les verres et les bières partagés ont été un soutien essentiel durant toutes ces années.

Je tiens aussi à remercier toute ma famille pour leurs soutiens avec une mention spéciale pour Nono, Mamama, Sabine, Nathalie et Jean-Pierre.

J'ai aussi une pensée particulière pour Papy et Papapa qui m'ont transmis depuis mon enfance le goût du travail et de la connaissance, cela été décisif dans mon parcours.

Un énorme merci à mes parents, sans votre soutien inconditionnel depuis toujours je ne serais pas là aujourd'hui. Vous avez tout fait pour que je puisse atteindre mes objectifs et toujours soutenu dans mes choix. Vous m'avez appris à avoir confiance en moi (un peu trop même) et à développer mon esprit critique. Encore une fois merci.

Enfin, Elsa par où commencer pour te remercier. Je pourrais remplir un nouveau manuscrit pour expliquer pourquoi tu fais de moi une meilleure personne. Tu lisses mes défauts, tu me pousses à me dépasser à sortir de ma zone de confort, tu sais aussi me tempérer et me ralentir quand il faut prendre le temps de profiter de l'instant. Ton amour inconditionnel est pour moi un moteur dans tous les moments de la vie. Je t'aime et j'ai hâte de voir la prochaine étape de notre vie.

TABLE DES MATIERES

RESUME ETENDU EN FRANÇAIS

RESUME ETENDU EN FRANÇAIS

1. Contexte et cadre de la thèse

Le traitement des douleurs (chroniques ou aigües) est l'un des enjeux importants du 21ème siècle. En effet, avec le vieillissement global de la population et le prolongement de l'espérance de vie, le nombre de personnes souffrant de douleurs chroniques dans le monde dépasse les 100 millions (Institut Pasteur de Lille). Chez l'Homme, une douleur est qualifiée de chronique lorsqu'elle dure plus de 3 mois (Treede et al., 2019). Bien que ces douleurs induisent une diminution de la qualité de vie des personnes atteintes, soulignant le besoin de les soulager, leurs traitements est à ce jour peu satisfaisant.

Le traitement de ces douleurs est complexe et la médecine est aujourd'hui extrêmement dépendante des analgésiques dérivés des opiacés (notamment en Amérique du Nord), qui ont pourtant des effets secondaires particulièrement délétères. De cette situation découle la crise dite « des Opiacés », telle qu'elle a été observée aux Etats-Unis : en 2019, près de 50 000 Américains sont morts d'une overdose d'opioïdes et environ 1,7 millions de personnes ont souffert de troubles liés à l'utilisation d'opioïdes prescrits sur ordonnance (National Institute on Drug Abuse, 2021a, 2021b). En Europe la crise n'est pas aussi marquée : en 2016, 4830 personnes sont décédées. Cependant l'augmentation de la consommation inquiète, comme le souligne l'augmentation de la consommation d'opioïdes forts chez des patients souffrant d'arthrose de 8 % à 20 % (OECD, 2019). Ainsi, pour endiguer cette crise tout en permettant de continuer à traiter les douleurs chroniques et aigües, il est essentiel de développer des traitements alternatifs. Dans ce contexte, mon travail de thèse a consisté à explorer le potentiel analgésique de nouvelles molécules innovantes ciblant les systèmes analgésiques endogènes.

Le travail de thèse a commencé en mars 2019, avec le CNRS et l'entreprise BENEPHYT sur un financement de l'association nationale de la recherche et de la technologie (ANRT). J'ai ainsi pu acquérir une expertise forte dans l'évaluation comportementale du potentiel analgésique d'une molécule sur un modèle animal.

Cette expertise m'a permis de caractériser le potentiel analgésique de deux molécules innovantes, l'une issue de l'ingénierie du récepteur de l'ocytocine, pour lequel mon équipe d'accueil possède une expertise forte ; et la pulégone, un monoterpène analogue du menthol et pourtant largement sous étudié, qui présente un intérêt particulier pour BENEPHYT.

2. Evaluation du potentiel analgésique du système ocytocinergique

Il a été mis en évidence que la stimulation (optogénétique) d'une petite population de neurones ocytocinergiques (≈ 30 neurones) des noyaux paraventriculaires de l'hypothalamus (PVN), est suffisante pour induire une analgésie mécanique et thermique dans un modèle animal de douleur inflammatoire (Eliava et al., 2016). Pourtant, l'utilisation clinique de l'ocytocine (OT) dans le cadre de son potentiel analgésique est largement compromise par sa très faible demi-vie (≃ 10 minutes).

Ainsi, je me suis intéressé au potentiel analgésique d'une molécule, le LIT-001, synthétisée par notre collaborateur le Dr. Marcel Hibert. Cette molécule est un agoniste non peptidergique du récepteur à l'ocytocine (OTR) (Frantz et al., 2018). Le LIT-001 présente l'avantage d'être une molécule particulièrement stable, peu ou pas métabolisée par l'organisme, contrairement à l'OT. Pour évaluer les propriétés analgésiques du LIT-001 j'ai donc effectué différentes expériences de mesures comportementales (sensibilité thermique au chaud et mécanique) dans un modèle de sensibilisation douloureuse inflammatoire (**Figure R1**). J'ai pu observer dans ce modèle, qu'une injection intra-péritonéale (i.p.) de LIT-001 (10 mg/kg) permet d'induire une analgésie d'une durée d'environ 5h pour les sensibilités thermiques (chaud) et mécaniques. J'ai également contrôlé l'implication du récepteur à l'OT dans cette analgésie induite, en réalisant une co-injection i.p. du LIT-001 avec un antagoniste de OTR, L-368,899. L'absence d'analgésie lors de cette co-injection suggère que le LIT-001 exerce bien ses effets analgésiques au travers de l'activation de OTR (**Figure R1**). L'intérêt du LIT-001 en tant que molécule thérapeutique a aussi été approfondi grâce à des dosages par spectrométrie de masse, qui m'ont permis de mettre en évidence le passage du LIT-001 dans le liquide cérébrospinal et dans le cerveau.

Ces travaux ont été réalisés en collaboration avec le Dr. Marcel Hibert et les résultats de ces expériences ont été publiés en février 2020 dans la revue Scientific Reports (Hilfiger et al., 2020). Ces résultats offrent des possibilités nouvelles sur l'utilisation d'un agoniste non peptidergique de l'OT dans une multitude de pathologies et notamment dans le traitement des douleurs inflammatoires.

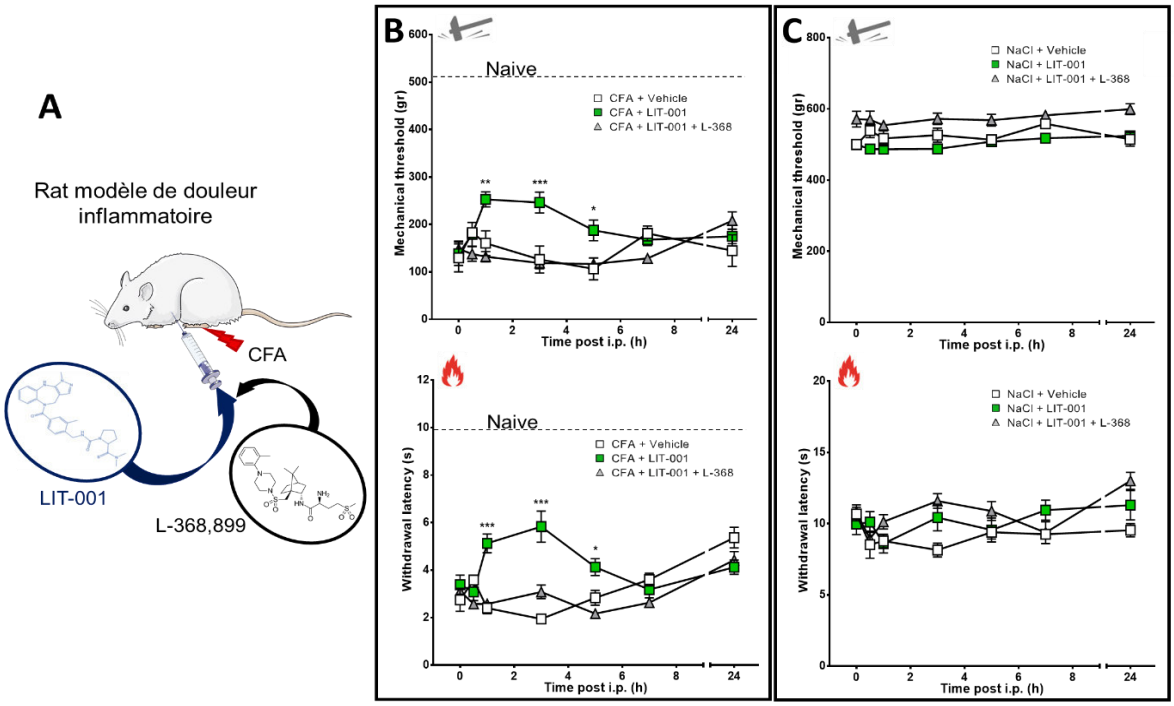

Figure R1 : Décours temporel des propriétés analgésique du LIT-001 sur un modèle de sensibilisation douloureuse inflammatoire.

(**A**) Représentation schématique du modèle de sensibilisation douloureuse inflammatoire induite via une injection d'adjuvant complet de Freund (CFA) dans la patte et injection i.p. de LIT-001 (10 mg/kg) et/ou de L-368,899 (1 mg/kg). (**B**) Effets du Véhicule, de LIT-001 et de la combinaison LIT-001 + L-368 sur les modalités de sensibilité mécanique et thermique chaude dans le modèle de sensibilisation douloureuse inflammatoire. (**C**) Effets du Véhicule, de LIT-001 et de la combinaison LIT-001 + L-368 sur les modalités de sensibilité mécanique et thermique chaude chez les animaux contrôle (injection de NaCl a la place du CFA). CFA + LIT-001 (n = 8), CFA + Vehicule (n = 7), CFA + LIT-001 + L-368 (n = 7), NaCl + LIT-001 (n = 7), NaCl + Vehicule (n = 8), NaCl + LIT-001 + L-368 (n = 6).

En parallèle, j'ai cherché à mieux comprendre comment l'ocytocine endogène exerce son activité analgésique. J'ai ainsi approfondi la compréhension des mécanismes analgésiques de l'OT avec l'étude du rôle d'une population de neurones présentant l'OTR dans la substance périaqueducale grise (PAG), ces derniers étant eux-mêmes contactés par des neurones OT provenant du PVN (une population distincte de ceux évoqués dans (Eliava et al., 2016)).

Dans un premier temps, j'ai cherché à valider fonctionnellement le modèle animal utilisé, le rat OTR-Cre (exprimant la Cre recombinase dans les neurones OTR) nouvellement développé par l'équipe de Dusan Bartsch, à Mannheim. Pour cela, j'ai transfecté les neurones de la PAG avec un virus permettant l'expression de la GFP dans les neurones exprimant la Cre recombinase. J'ai pu ainsi patcher les neurones fluorescents et réaliser des applications de tri-gly-oxytocin (TGOT, agoniste de OTR). L'application de TGOT a mis en évidence une activation directe des neurones par cette dernière (**Figure R2**), démontrant ainsi que OTR est toujours fonctionnel dans les neurones exprimant la green fluorescent protein (GFP) et donc que notre modèle de rat OTR-Cre est valide.

J'ai ensuite cherché à évaluer le potentiel analgésique de la stimulation des neurones exprimant l'OTR dans le ventro-lateral PAG (vlPAG), sur un modèle de sensibilisation douloureuse inflammatoire (CFA) en mesurant la sensibilité mécanique et thermique chaude (**Figure R3**). Pour ce faire, j'ai injecté un virus permettant l'expression d'une hM3D-Gq de manière Cre dépendante dans la vlPAG de rats OTR-Cre. Trois semaines plus tard, le jour du test, j'ai injecté en i.p. la deschloroclozapine (DCZ; un agoniste exogène de hM3D-Gq, théoriquement dépourvu d'effet secondaire) (Nagai et al., 2020). Les résultats ont mis en évidence une analgésie induite par la stimulation de ces neurones dans les deux modalités, mécanique et thermique (**Figure R3**).

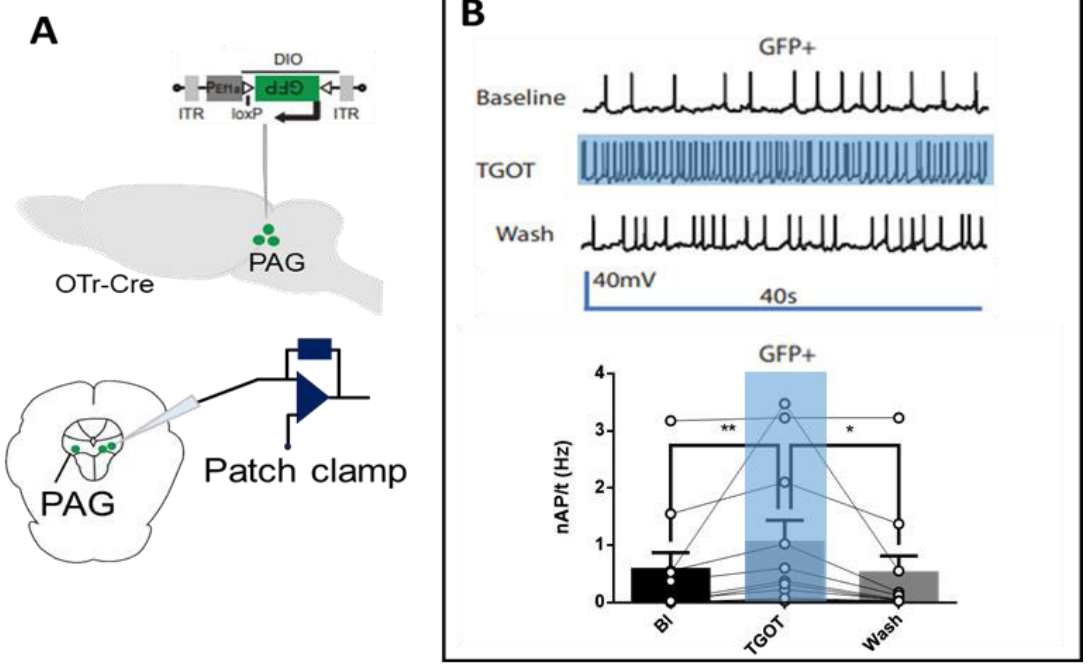

Figure R2 : Validation fonctionnelle *ex-vivo* de la stimulation des neurones OTR de la PAG via l'application d'un agoniste de l'OTR, le TGOT.

(**A**) Représentation schématique de l'injection de virus dans la PAG permettant par la suite d'enregistrer l'activité électrophysiologique (patch clamp en cellule entière) les neurones OTR exprimant la GFP. (**B**) Haut : trace exemple des potentiels d'action (AP) des neurones GFP+/OTR+ suite à une application en bain de TGOT (0.4 µM 20s). Bas : graphique des variations de fréquence des AP des neurones GFP+/TGOT+, suite à l'application de TGOT par rapport au niveau de base et au lavage. Neurones GFP+/OTR+ n = 11.

L'OT est connu pour avoir un rôle très important dans la modulation des émotions (Jurek and Neumann, 2018). Afin de pouvoir discerner les effets antinociceptifs des aspects émotionnels du contrôle de la douleur par le système OT, j'ai réalisé une expérience complémentaire, le test du conditionnement de préférence de place (CPP). Cela m'a permis d'étudier le rôle de cette population de neurones OTR de la PAG dans le contrôle de la douleur, en comparant leurs impacts sur la nociception et sur les aspects émotionnels de la douleur. Je n'ai observé aucun effet hédonique lors de la stimulation de ces neurones, ce qui s'est traduit par l'impossibilité de modifier la préférence des animaux entre deux environnements distincts. Cette expérience permet de discriminer le rôle des neurones OTR de la PAG dans

l'analgésie induite par le système OT, comme étant responsable d'une partie de la modulation purement nociceptive sans moduler a priori l'aspect émotionnel.

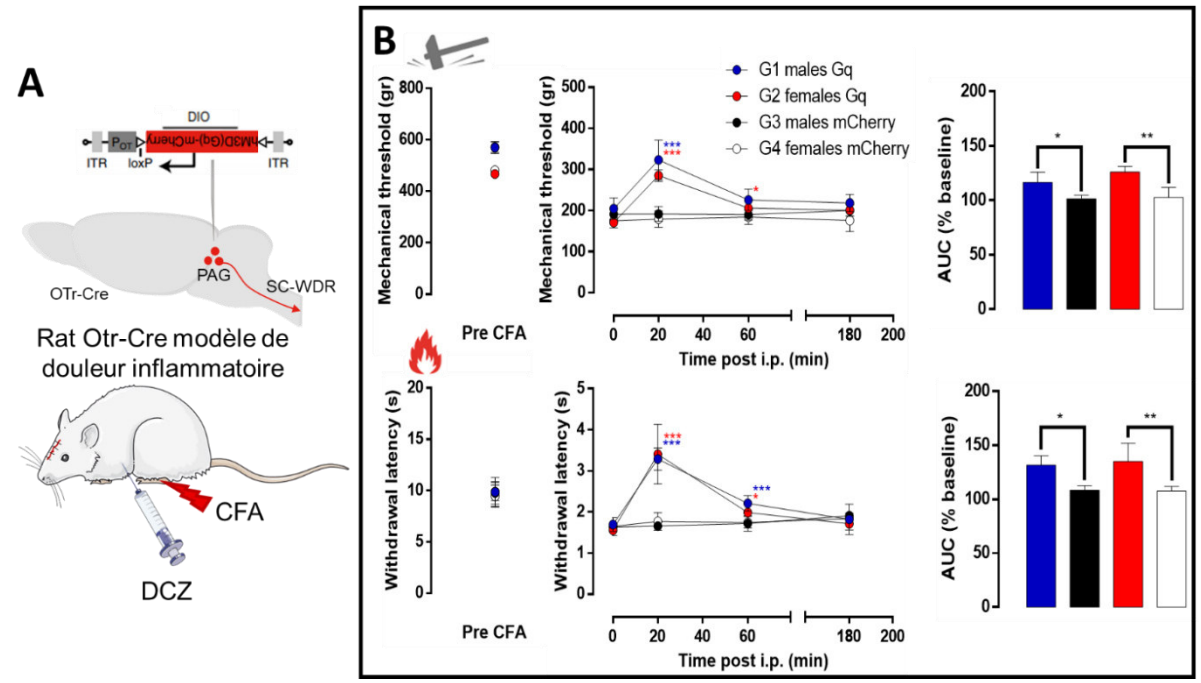

Figure R3 : Décours temporel des propriétés analgésiques de la stimulation chemogénétique des neurones OTR de la PAG via l'activation de hM3DGq par la DCZ dans un modèle de sensibilisation douloureuse inflammatoire.

(**A**) Représentation schématique du modèle de sensibilisation douloureuse inflammatoire induite via une injection de CFA dans la patte et injection i.p. de DCZ (100 µg/kg). (**B**) Décours temporels des effets de la stimulation des neurones OTR de la PAG sur les modalités de sensibilité mécanique et thermique chaude dans les modèles de sensibilisation douloureuse inflammatoire. Les groupes Gq ont été transfectés avec hM3DGq et les groupes contrôles ont été transfectés uniquement avec mCherry. G1 males Gq (n = 6), G2 femelles Gq (n = 5), G3 males mCherry (n = 6), G4 femelles mCherry (n = 6).

Ces expériences s'inscrivent dans la thématique ocytocine de l'équipe et ont été réalisées en collaboration avec Prof. Valery Grinevich. Les résultats sont actuellement en cours de compilation et de mise en forme dans un article pour le moment intitulé : « Oxytocin release in periaqueductal gray induces analgesia through long term suppression of spinal cord neuron activity ». Ces résultats permettent d'approfondir les possibilités de l'utilisation du système OT dans la modulation des douleurs, avec par exemple un ciblage des neurones OTR de la PAG via des injections

de composés tels que le LIT-001 afin moduler sur une longue durée les neurones OTR. Cela afin d'induire une analgésie sans moduler l'aspect émotionnel et ainsi limiter de potentiels effets secondaires, comme des modifications comportementales ou de l'addiction.

3. Evaluation du potentiel analgésique des monoterpènes

On trouve des traces écrites d'utilisation de plantes dans le traitement des douleurs en Europe depuis l'Antiquité. Les données ethnopharmacologiques découlant d'une étude d'herbiers européens du 16ème siècle ont mis en évidence l'utilisation de *C. nepeta* dans le traitement des douleurs arthritiques. Les données ethnopharmacologiques ont mis en évidence l'utilisation de *Clinopodium nepeta* (L.) Kuntze dans le traitement des douleurs arthritiques, les premières traces écrites relatant ces usages sont les herbiers de *Leonhart Fuchs* et *Pietro Andrea Matthiolus* (1543 et 1590 respectivement) (Adams et al., 2009).

Le projet global de BENEPHYT vise à caractériser le potentiel analgésique de certains terpènes, ou mélanges de terpènes, issues de plantes de la pharmacopée locale alsacienne, avec pour objectif de développer des traitements analgésiques à partir de ces molécules. BENEPHYT s'est donc intéressée aux molécules extraites de *Calamintha nepeta* (L.) Savi (synonyme accepté de *Clinopodium nepeta* (L.) Kuntze), plus particulièrement à la classe des monoterpènes (sous-famille des terpènes). Les monoterpènes sont des molécules très utilisées en parfumerie, agroalimentaire et dans les traitements de médecine dite « non conventionnelle » (en tant que composants importants des huiles essentielles) et sont très utilisés dans le traitement des douleurs, mais peu utilisés dans le cadre de la médecine dite « moderne ». Cette famille de molécules présente pourtant une très grande variété d'effets, en plus de leurs effets antinociceptifs (antibactérien, antiviral, anticancéreux, antidiabétique, etc … (Cox-Georgian et al., 2019)) qui sont à l'heure actuelle principalement étudiés dans un contexte préclinique. De plus, les monoterpènes présentent l'avantage de passer facilement la barrière hématoencéphalique et sont présents en grandes quantités dans de nombreuses espèces végétales.

BENEPHYT s'est tourné vers l'équipe du Dr. Eric Marchioni (Chimie Analytique des molécules bioactives et Pharmacognosie) pour extraire et caractériser le principal monoterpène issus de *Clinopodium nepeta* (L.) Kuntze, la pulégone (Triaux et al., 2020, 2021). L'objectif final étant le développement de nouveaux traitements analgésiques innovants à partir de combinaisons originales de monoterpènes.

A l'aide des données obtenues lors d'un important travail bibliographique et de l'expérience acquise lors de l'évaluation des propriétés du LIT-001 (cf : **Evaluation du potentiel analgésique du système ocytocinergique**), j'ai pu caractériser les effets potentiellement analgésiques du pulégone. J'ai pour cela testé différentes mesures comportementales (sensibilité mécanique, thermique au chaud et au froid) dans un modèle de sensibilisation douloureuse inflammatoire (**Figure R4**). J'ai décidé d'étudier ces effets en comparaison avec ceux du menthol, pour lequel il existe quelques rares travaux qui m'ont servi d'appui (Pan et al., 2012). Ces expériences m'ont permis de mettre en évidence que la pulégone (i.p. ; 100 mg/kg) possède des effets analgésiques plus puissants que le menthol (i.p. ; 100 mg/kg). Il faut noter que les doses maximales utilisées lors des tests d'hypersensibilité ne présentent pas d'effets secondaires de type locomoteur ou sédatif. Cela a été testé au travers de deux tests de locomotion (Rotarod et beam walk test) et ni le menthol, ni la pulégone n'ont significativement altéré les performances locomotrices des rats par rapport à un groupe contrôle.

Ces résultats ont été publiés en novembre 2021 dans la revue Frontiers in Pharmacology (Hilfiger et al., 2021). Ils ouvrent ainsi dans un premier temps la voie à l'utilisation de nouvelles molécules terpéniques, dans le cadre de traitements de douleurs inflammatoires, avec ici un exemple de l'intérêt que pourrait avoir le remplacement du menthol par la pulégone. Ils ouvrent également des possibilités de recherche pour améliorer la compréhension fine des effets analgésiques de la pulégone, notamment sur le plan de son mécanisme d'action à l'échelle moléculaire et/ou cellulaire (Pergolizzi et al., 2018).

Dans un second temps, nous avons cherché à réduire les doses de monoterpènes à injecter, en cherchant un potentiel effet synergique entre le menthol et la pulégone. Un effet synergique pourrait présenter l'intérêt de nous permettre de pourvoir diminuer les doses de terpènes et ainsi diminuer les potentiels effets secondaires sans affecter les effets bénéfiques. J'ai donc évalué les propriétés

analgésiques d'un mélange de menthol (i.p. ; 50 mg/kg) et de pulégone (i.p. ; 50 mg/kg) dans un modèle de sensibilisation douloureuse inflammatoire pour les modalités de sensibilité mécanique, thermique au chaud et au froid, afin de comparer les résultats obtenus avec le menthol et la pulégone individuellement (**Figure R4**). Les résultats obtenus montrent des effets analgésiques similaires à ceux de la pulégone a 100 mg/kg.

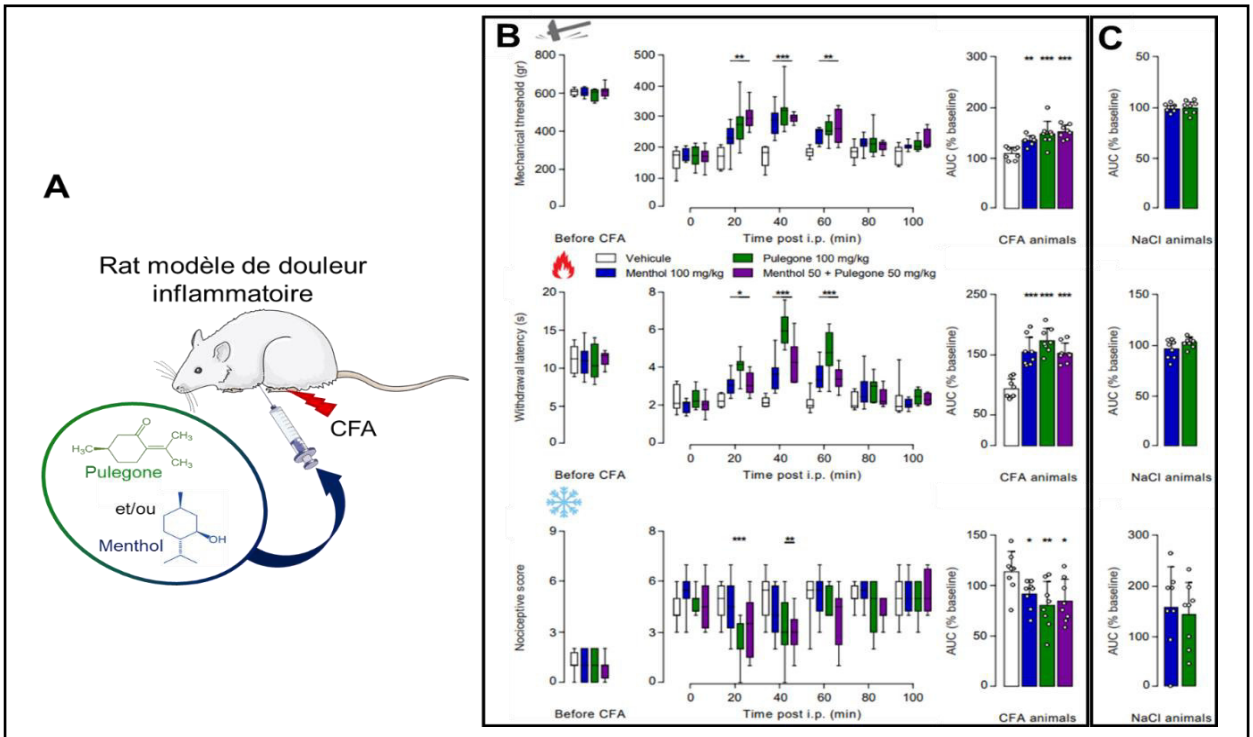

Figure R4 : Décours temporel des propriétés analgésiques du menthol et de la pulégone sur un modèle sensibilisation douloureuse inflammatoire.

(**A**) Représentation schématique du modèle de sensibilisation douloureuse inflammatoire induite via une injection de CFA dans la patte droite et injection i.p. de menthol (100 mg/kg), de pulégone (100 mg/kg) ou d'une combinaison menthol (50 mg/kg) + pulégone (50 mg/kg). (**B**) Effets du menthol, de la pulégone et de la combinaison menthol + pulégone pour les modalités de sensibilité mécanique et thermique (chaud et froid). (**C**) Effets du menthol et de la pulégone sur les modalités de sensibilité mécanique et thermique (chaud et froid) chez les animaux contrôle (injection de NaCl à la place du CFA). CFA + Menthol (n = 8), CFA + Pulegone (n = 8), CFA + Combinaison (n = 8), CFA + Vehicule (n = 8), NaCl + Menthol (n = 8), NaCl + Pulegone (n = 8).

Ces résultats offrent une perspective très intéressante quant à l'utilisation de mélanges de monoterpènes afin d'obtenir des effets synergiques pour le traitement de douleurs inflammatoires. En s'appuyant ainsi sur ces expériences préliminaires et une bibliographie complète, comprenant l'ensemble des cibles connues des monoterpènes, BENEPHYT pourrait à terme développer de potentiels traitements innovants impliquant des mélanges de différents monoterpènes. Ces monoterpènes seront choisis pour leurs cibles moléculaires ou cellulaires, afin de réaliser un cocktail de monterpènes synergique à fort potentiel analgésique.

4. Conclusion

Lors de ma thèse, j'ai eu l'opportunité d'explorer le potentiel analgésique de molécules innovantes variées, ciblant des systèmes moléculaires et cellulaires différents. J'ai effectué cette recherche dans une perspective préclinique, afin de proposer des approches/systèmes alternatifs aux cibles classiques. Cette recherche s'est principalement basée sur une approche comportementale *in vivo* basée sur un modèle de douleur induite et l'étude de différentes modalités de sensibilités. J'ai ainsi pu acquérir une expertise technique et théorique sur ce modèle et ces techniques.

Au vu des résultats obtenus, on peut être intéressé par l'exploration d'approches multi-cibles se basant sur des combinaisons de différents types de molécules. Cela serait une approche novatrice qui permettrait par exemple d'adjoindre le recrutement du système ocytocinergique avec des applications topiques ou orales de mélanges de monoterpènes. Avec une telle approche, on modulerait ainsi le système nociceptif central et périphérique via l'action des agonistes nonpeptidergiques de l'OT, combinés avec la modulation des cellules sensorielles via les récepteurs de types TRP et autres canaux ioniques par des monoterpènes. Cette approche permettrait ainsi de diversifier les cibles à différentes échelles afin d'avoir des effets synergiques et de diminuer les doses pour limiter les effets secondaires.

5. Liste des publications scientifiques

5.1. Articles scientifiques en qualité de premier auteur

Titre: **A Nonpetide Oxytocin Receptor Agonist for a Durable Relief of Inflammatory Pain**

Auteurs : Louis Hilfiger, Qian Zhao, Damien Kerspern, Perrine Inquimbert, Virginie Andry, Yannick Goumon, Pascal Darbon, Marcel Hibert & Alexandre Charlet

Journal: Scientific Reports (2020)

DOI: 10.1038/s41598-020-59929-w

Titre: **Social touch promotes interfemale communication via activation of parvocellular oxytocin neurons**

Auteurs: Yan Tang*, Diego Benusiglio*, Arthur Lefevre*, Louis Hilfiger*, Ferdinand Althammer, Anna Bludau, Daisuke Hagiwara, Angel Baudon, Pascal Darbon, Jonas Schimmer, Matthew K. Kirchner, Ranjan K. Roy, Shiyi Wang, Marina Eliava, Shlomo Wagner, Martina Oberhuber, Karl K. Conzelmann, Martin Schwarz, Javier E. Stern, Gareth Leng, Inga D. Neumann, Alexandre Charlet & Valery Grinevich

(*) représente les premiers auteurs

Journal: Nature Neuroscience (2020)

DOI: 10.1038/s41593-020-0674-y

Titre: **Anti-hyperalgesic Properties of Menthol and Pulegone**

Auteurs: Louis Hilfiger*, Zélie Triaux*, Christophe Marcic, Eléa Héberlé, Fathi Emhemmed, Pascal Darbon, Eric Marchioni, Hugues Petitjean & Alexandre Charlet

(*) représente les premiers auteurs

Journal: Frontiers in Pharmacology (2021)

DOI: 10.3389/fphar.2021.753873

Titre: **TRP channels and monoterpenes: current leads on analgesic properties**

Auteurs: Hugues Petitjean*, Louis Hilfiger*, Eléa Héberlé, & Alexandre Charlet

(*) représente les premiers auteurs

En préparation

5.2. Articles scientifique co-signés

Titre: **Projections from a novel population of parvocellular oxytocin neurons promote analgesia in the periaqueductal gray**

Auteurs: Mai Iwasaki*, Arthur Lefevre*, Ferdinand Althammer, Olga Lapies, Louis Hilfiger, Meggane Melchior, Damien Kerspern, Stéphanie Küppers, Quirin Krablicher, Ryan Patwell, Sabine Herpertz, Beate Ditzen, Kai Schoenig, Dusan Bartsch, Javier Stern, Pascal Darbon, Valery Grinevich & Alexandre Charlet

En préparation

5.3. Articles de vulgarisation scientifique co-signé

Titre: **Le toucher favorise les interactions sociales *via* l'ocytocine**

Auteurs: Arthur Lefevre, Louis Hilfiger & Alexandre Charlet

Journal: Médecine Sciences (2021)

DOI: 10.1051/medsci/2021073

6. Communication Orales

Présentation oral: A Nonpeptide Oxytocin Receptor Agonist for a Durable Relief of Inflammatory Pain – XVI^{ème} Symposium National du Réseau Français de Recherche sur la Douleur (**Bordeaux, Fr - 2020**)

Auteurs: Louis Hilfiger, Qian Zhao, Damien Kerspern, Perrine Inquimbert, Virginie Andry, Yannick Goumon, Pascal Darbon, Marcel Hibert & Alexandre Charlet

Poster: A Nonpeptide Oxytocin Receptor Agonist for a Durable Relief of Inflammatory Pain – 12th FENS 2020 Forum for Neuroscience, the Virtual Forum (**Glasgow, UK / Visioconférence - 2020**)

Auteurs: Louis Hilfiger, Qian Zhao, Damien Kerspern, Perrine Inquimbert, Virginie Andry, Yannick Goumon, Pascal Darbon, Marcel Hibert & Alexandre Charlet

Poster: Anti-Inflammatory and Analgesic Properties of Pulegone, a Major Component in Calamintha nepeta – NeuroFrance 2021, International virtual meeting (**Strasbourg, Fr / Visioconférence - 2021**)

Auteurs: Louis Hilfiger, Zélie Triaux, Christophe Marcic, Fathi Emhemmed, Pascal Darbon, Eric Marchioni, Hugues Petitjean & Alexandre Charlet

LISTE DES FIGURES

LISTE DES TABLEAUX

LISTE DES ABREVIATIONS

- 5-HT : Serotonin/5-hydroxytryptamine
- 5-HT_3 R : 5-HT_3 receptor
- AMPA : Alpha-amino3-hydroxy-5-methy-4-iso-xazoleproprionic acid
- AN : Accessory nuclei
- ANRT : Association Nationale de la Recherche et de la Technologie
- AP : Action potential
- AVP : Vasopressin
- BBB : Blood brain barrier
- Ca^{2+} channel : Calcium channel
- CFA : Complet Freund adjuvant
- CNS : Central nervous system
- COFER : Collège Français des enseignants en rhumatologie
- COVID-19 : Coronavirus disease
- COX : Cyclooxygenase
- CPP : Conditioned place preference
- CSF : Cerebrospinal fluid
- DCZ : Deschloroclozapine
- DMAPP : Dimethylallyl diphosphate
- DRG : Dorsal root ganglion
- GABA : γ-aminobutyric acid
- $GABA_a$ R : $GABA_a$ receptor
- GCT : Gate control theory
- GFP : Green fluorescent protein
- Gly R : Glycine receptor
- GPCR : G protein-coupled receptor
- GPP : Geranyl diphosphate
- HkC : HEK cell line
- i.c.v. : Intracerebroventricular
- i.p. : Intraperitoneal
- i.t. : Intrathecal
- i.v. : Intravenously
- IASP : International Association of the Study of Pain

- IFN : Interferon
- IL : Interleukin
- iNOS : Inducible NO synthase
- IPP : Isopentenyl diphosphate
- K^+ channel : Potassium channel
- MagnOT : Magnocellular OT neuron
- MAPK : Mitogen-activated protein kinase
- MEP : Methylerythritol phosphate
- MVA : Mevalonic acid
- MW : Molecular weight
- NA : Noradrenaline
- Na^+ channel : Sodium channel
- nACh : Nicotinic acetylcholine
- nACh R : nACh receptor
- NGF : Nerve growth factor
- NMDA : N-methyl-D-aspartate
- nNOS : NO synthase
- NO : Nitric oxide
- NSAID : Nonsteroidal anti-inflammatory drugs
- OT : Oxytocin
- OTR : Oxytocin receptor
- p.o. : *Per os*
- PAG : Periaqueductal gray
- ParvOT : Parvocellular OT neuron
- PGE : Prostaglandin
- PI3K : Phosphoinositide 3-kinase
- PLC : Phospholipase C
- PNS : Peripheral nervous system
- PVN : Paraventricular nucleus of hypothalamus
- RVM : Rostral ventromedial medulla
- s.c. : Subcutaneous
- SCI : Spinal cord injury
- SNI : Spared nerve injury
- SON : Supraoptic nucleus

- TGOT : Tri-gly-oxytocin
- TLR : Toll-like receptor
- TNF : Tumor necrosis factor
- TRP : Transient receptor potential
- TRPA : TRP Ankyrin
- TRPM : TRP Melastatin
- TRPV : TRP Vanilloid
- TTX : Tetrodotoxin
- vlPAG : Ventro-lateral periaqueductal gray
- WDR : Wide dynamic range
- WT : Wild type

PREAMBULE

Being in a CIFRE thesis agreement and employed by the BENEPHYT company, most of the research I performed during my PhD was mainly focused on an entrepreneurial approach of research, to open new avenues for innovative pain medication development. It is in this context that we decided to focus on inflammatory pain (acute or chronic) because it is the more common type of pain.

Thus, I studied the analgesic effects of two types of molecules, LIT- 001, a synthetic molecule, and both menthol and pulegone, natural compounds extracted from traditional medicinal plants.

LIT-001 is an oxytocin receptor agonist chemically engineered by a collaborator. We decided to study it because it showed promising results on other oxytocin-related behaviours and my hosting lab has a strong expertise on oxytocin.

The reason why we chose to study pulegone is that most of the studies (around 80 %) focus on 6 - 7 monoterpenes and pulegone is one of the least studied. In addition, since menthol is the most studied terpene and is close to pulegone in the synthesis pathways, we decided that it would make an interesting control for our study. In addition, there is also a commercial interest for BENEPHYT to study and develop monoterpene therapeutic treatments explaining why the anti-hyperalgesic effects of pulegone and menthol have been studied in this thesis.

Moreover, these small molecules also have the interesting property of crossing the blood brain barrier (BBB), which is particularly interesting for a medical application.

For all these reasons, we decided at the beginning of my PhD that I would be focused on these two types of analgesic compound that could be used in the treatment of inflammatory pain.

INTRODUCTION

INTRODUCTION

In this introduction, I will cover several essential points for the understanding of the thesis results. First, I will discuss the subject of nociception and pain, as understanding the nociceptive system and pain is essential to identify molecular and cellular targets for the development of new analgesic compounds. Then I will investigate the analgesic potential of oxytocin-like molecules and finally exogenous molecules from traditional pharmacopoeia, the terpenes.

1. Nociception and pain

On the one hand, nociception is a sensory system that allows the organism to recognize a signal as dangerous or harmful for the organism. On the other hand, pain is the emotional interpretation of this signal, and it is essential to understand these two aspects to treat the pain experienced by patients. For that, it is essential to base this introduction on clearly established definitions (**Table 1**).

1.1. Assessment of pain

1.1.1. In humans

As define by IASP pain is “an unpleasant sensory and emotional experience associated with, or resembling that associated with, actual or potential tissue damage” (**Table 1**). For humans, the easiest way to assess pain (in a clinical study) is through visual analog scales of the pain feeling, because pain is an emotion. Since, the perception of pain is influenced by life experiences as well as biological, psychological and social factors, it can be difficult to score the level of pain (IASP). To overcome this issue, already in 1923 psychologists started to use visual analogue scale (Freyd, 1923). It can be represented by a graphic rating scale form 0, which is qualified as no pain, to 10, which is “pain as bad as it could be” and was studied by Scott and Huskisson (Scott and Huskisson, 1976). In addition, there are other methods of assessing pain. In their review, Haefeli and Elfering also propose direct oral rating scale, pain drawing (the patient is asked to mark the areas of pain on an outline of a human figure and with more or less indication) and even different questionnaires (Pain-O-Meter, McGill Pain Questionnaire) (Haefeli and Elfering, 2006).

Table 1: Definitions and glossary.

From International Association of the Study of Pain (IASP), and Collège français des enseignants en rhumatologie (COFER).

Terms	Definitions
Allodynia:	Pain due to a stimulus that does not normally provoke pain.
Analgesia:	Absence of pain in response to stimulation, which would normally be painful.
Chronic pain:	Pain that persists or recurs for longer than three months.
Hyperalgesia:	Increased pain from a stimulus that normally provokes pain.
Inflammatory pain:	Inflammatory nociceptive pain is associated with tissue damage and the resulting inflammatory process.
Multimodal treatment:	The concurrent use of separate therapeutic interventions with different mechanisms of action within one discipline aimed at different pain mechanisms.
Neuropathic pain:	Pain caused by a lesion or disease of the somatosensory nervous system.
Nociception:	The neural process of encoding noxious stimuli.
Nociceptive neuron:	A central or peripheral neuron of the somatosensory nervous system that can encode noxious stimuli.
Nociceptive pain:	Pain that arises from actual or threatened damage to non-neural tissue and is due to the activation of nociceptors.
Nociceptive stimulus:	An actually or potentially tissue-damaging event transduced and encoded by nociceptors.
Nociceptor:	A high-threshold sensory receptor of the peripheral somatosensory nervous system that is capable of transducing and encoding noxious stimuli.
Noxious stimulus:	A stimulus that is damaging or threatens damage to normal tissues.
Pain:	An unpleasant sensory and emotional experience associated with, or resembling that associated with, actual or potential tissue damage.
Pain threshold:	The minimum intensity of a stimulus that is perceived as painful.
Pain tolerance level:	The maximum intensity of a pain-producing stimulus that a subject is willing to accept in a given situation.
Sensitization:	Increased responsiveness of nociceptive neurons to their normal input, and/or recruitment of a response to normally subthreshold inputs.
Unimodal treatment:	Single therapeutic intervention directed at a specific pain mechanism or pain diagnosis.

However, in some cases, it is difficult to verbalize (vocally, in a written form or even with a scale) pain assessment, particularly in newborns, infant, people with cognitive impairment and some elderly persons (Booker and Herr, 2016). Hopefully there are now methods to evaluate pain for example in newborns and infants. For example, the EVENDOL pain scale is based on behaviours such as facial expression, postures and even interaction with the environment (for review; (Beltramini et al., 2017)).

Given that verbalization is not possible in non-human primates and rodents, pre-clinical evaluation of pain rely on different measurements.

1.1.2. In rodents

As mentioned by IASP the inability to communicate does not negate the possibility that non-human animals experience pain. There are similar scale to those used in pre-clinical studies, such as the Grimace Scale or the Nest Building Behavior Study, which are robust indicators of pain levels in rodents (Turner et al., 2019). However, the stimulus dependent tests are more commonly used to assess the analgesic potential of drug than the stimulus-independent tests.

Many reviews have listed the different types of stimulus-dependent nociceptive tests used to assess the different component of pain (Sandkühler, 2009; Turner et al., 2019; Abboud et al., 2021). Von Frey or calibrated forceps tests are used to evaluate mechanical hypersensitivities as they increase pressure on a specific point. To assess the heat modality of pain, the most used tests are the Plantar and the hot plate which will induce nociception by heating an area (hindpaw generally) of the animal. Conversely, to evaluate cold sensitivity, the most notable test is the cold plate and the acetone evaporation test, which induce cooling of the animal paw by quick evaporation of a drop of acetone. However, this test is not considered as a nociceptive test in naive animals (Deuis et al., 2017). There are also chemical tests, that if injected (i.p.) induce visceral pain, such as the formalin-induce pain test or the acetic acid abdominal constriction test (for review; (Sandkühler, 2009; Turner et al., 2019; Abboud et al., 2021)). Finally, it is important in most of the cases to have a cut-off limit for each test, as the goal is to assess nociception without inducing a damaging injury the animal.

However, to evaluate the analgesic potential of compounds these tests are usually performed on animal models with induced hyperalgesia/allodynia. The first group are the inflammatory pain models induced by complete Freund's adjuvant (CFA)

or carrageenan as example. The second group are the neuropathic pain models induced by spared nerve injury (SNI) or cuffing of sciatic nerve for example (for review; (Sandkühler, 2009; Turner et al., 2019; Abboud et al., 2021)).

Thus, the combination of models and tests are essential to assess pain and nociceptive behaviour in order to investigate the analgesic properties of new compounds that could be transposed to clinical studies.

1.2. Nociception

In the following section, I will approach the nociceptive system based on the pathway of the noxious stimulus from the peripheral nervous system (PNS) to the central nervous system (CNS). The nociceptive stimulus (mechanical, thermal, chemical) is initially transduced by a sensor and can even be induced by an inflammation. These specific sensors are expressed in different types of nociceptors, which transduce the stimulus in a nociceptive signal that will be transmitted via nociceptive fibres. The endings of these primary afferent fibres will then connect to the neurons of the dorsal horn of the spinal cord where the signal will be integrated (and sometime modulated) to the supraspinal structures in order to be integrated and perceived as pain.

1.2.1. Transduction of the nociceptive stimulus

An noxious stimulus can be thermal, mechanical or chemical and thus the conversion of the stimulus into an electrical signal in the primary nociceptor involved specific ion channels (Dubin and Patapoutian, 2010). These channels generate an electrical current through either opening, enhancing the influx of Na^+ or Ca^{2+}, or closing if the channels are responsible for a hyperpolarising current, like K^+ channels (Bell, 2018). In addition, many chemical compounds, particularly substances mediating inflammation, acting through G protein-coupled receptors (GPCR), indirectly modify ion channel activity (for review; (Lumpkin and Caterina, 2007; Dubin and Patapoutian, 2010; Julius, 2013; Bell, 2018)).

TRPs represent the most important family of sensors in the conversion of the noxious stimulus into an electrical signal.

1.2.1.1. The TRP Family

Transient receptor potential (TRP) ion channels is a family of ligand-gated ion channels who the main role is to be sensor of various stimuli (**Figure 1**). This family is highly conserved through evolution and can be divided in three subtypes; TRP Vanilloid (TRPV), Melastatin (TRPM) and Ankyrin (TRPA) (Bell, 2018).

TRPV1 is a non-selective cation channel that exhibits calcium permeability and is known to be the target of capsaicin since it was discovered in the late 90's, by the team of the 2021 Nobel Prize in Physiology or Medicine, David Julius (Caterina et al., 1997; Nobel Prize, 2021). TRPV1 is a polymodal receptor because it is also activated by noxious heat (≥ 43°C), acidic pH, and many other exogenous or endogenous agents among then: capsaicin, camphor, allicin, spider toxins and polyamines (for review; (Lumpkin and Caterina, 2007; Julius, 2013; Dai, 2016)). TRPV1 is a thermal nociceptor mainly expressed in periphery of the body, especially in nociceptors from the dorsal root ganglion (DRG) (nociceptive fibres C & Aδ), (Kobayashi et al., 2005; Dai, 2016).

TRPV3 is also a cation channel that also exhibits calcium permeability and which is activated by non-nociceptive warm temperatures (≥ 34°C) and some phytochemical agent like monoterpenes (Peier et al., 2002b; Vogt-Eisele et al., 2007). It is expressed in DRG and in the spinal cord and even in some brain areas (for review; (Dai, 2016)).

TRPV2 and TRPV4 are also members of the Vanilloid family but are less studied. However, they are known to be heat sensitive to (≥ 52°C) and (≥ 27°C) respectively (Caterina et al., 1997; Güler et al., 2002). Moreover, TRPV4 is also a mechanosensitive channel and they are both expressed in ending of nociceptive fibres and in DRG (for review; (Dai, 2016)).

TRPA1 is with TRPV1 the most critically involved TRP in nociception. TRPA1 is a non-selective cation channel that exhibits a major sodium permeability. It can be activated by multiple stimuli such as; noxious cold (≤ 18°C), osmotic change and some chemical agents (Story et al., 2003; Zhang et al., 2008). The chemical sensor function of TRPA1 is responsible for the pungent ingredients; mustard, garlic or even ginger which induce acute painful burning an pricking sensation (Macpherson et al., 2005). Additionally, as the other TRPs, TRPA1 is expressed in periphery of the body, especially at ending of nociceptor and in DRG (for review; (Dai, 2016)).

TRPM8 is the well known sensor of cool temperature (≤ 25°C) that was studied by both David Julius and Ardem Patapoutian (McKemy et al., 2002; Peier et al., 2002a; Nobel Prize, 2021). TRPM8 is a non-selective cation channel that exhibits sodium permeability. It can be activated by multiple stimuli such as; cool temperature (≤ 25°C) but also by some monoterpenes and especially menthol (McKemy et al., 2002; Peier et al., 2002a). TRPM8 is also expressed in DRG sensory neurons but it is never coexpressed in these neurons with TRPV1, suggesting that in physiological condition TRPM8 is not involved in the detection of noxious stimuli (for review; (Dai, 2016)). However it was demonstrated that TRPM8 are required for cold aversion (Dhaka et al., 2007; Pogorzala et al., 2013).

To summarize, TRP channels in DRG sensory neurons play a key role in the perception of our environment, as they are sensors of various stimuli. In addition, some stimuli can affect some TRPs and will evoke nociceptive pain (**Figure 1**). Therefore, TRP channels are strategic targets for analgesic compounds, to inhibit the generation of nociceptive signals directly at the nociceptor level. However, TRPs are not the only sensors of such noxious stimulus.

1.2.1.2. Others channels and receptors involved

Other important groups of channels and receptors are implied in the transduction of the nociceptive signal in the peripheral part of the nervous system.

One of them is the potassium channels (K^+ channel) including voltage-gated potassium channels (e.g. K_v 1, K_v 3.4) and two-pore background KCNK potassium channels (e.g. TREK-1, TRAAK). These channels play an important role as nociceptor sensor, especially for mechanical and thermal stimuli, as mice depleted of these channels display abnormal sensitivity to pressure, cold and heat (Basbaum et al., 2009; Madrid et al., 2009; Noël et al., 2009).

Another group are the degenerin/epithelia sodium channel families in which we found the ASIC (1, 2 and 3) channels. ASIC channels are sensor of mechanical stimuli and acidic compounds as they are receptors for extracellular protons (for review; (Basbaum et al., 2009)). ASIC channels are present in epithelial cells (keratinocytes, Merkel cells), in nociceptors and in the nerve ending surrounding the cardiovascular walls, where they serve as baroreceptors (Lumpkin and Caterina, 2007; Yang et al., 2021).

The Piezo (1 and 2) discovered by Patapoutian (Nobel Prize, 2021) show some similarities to ASIC channels (Murthy et al., 2017). However, they are only specialized in mechanoreception (Coste et al., 2010; Woo et al., 2015).

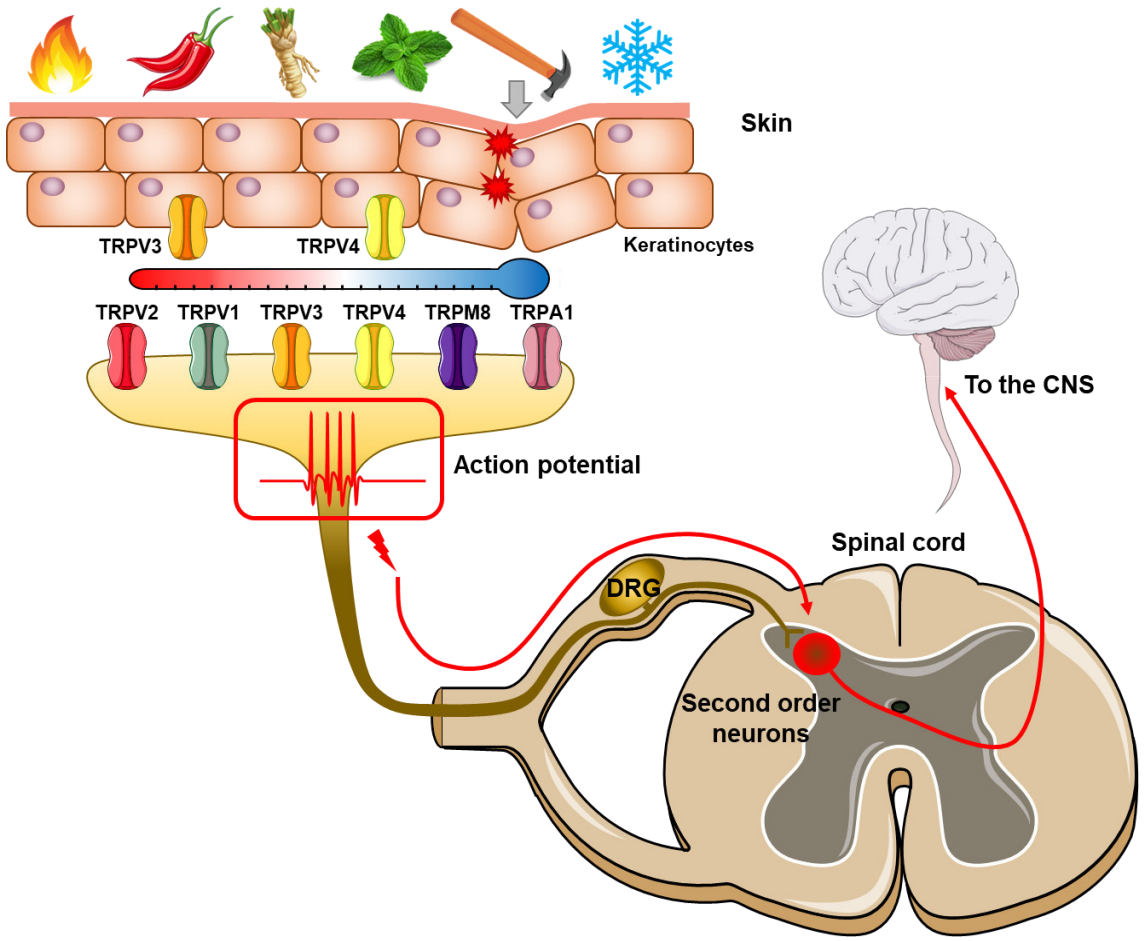

Figure 1: TRPs in nociceptive pain.

TRP channels in DRG sensory neurons are sensors of various nociceptive stimuli. *Inspired from: Dai (2015).*

However, another important aspect of the nociceptive perception is the triggering of sensor during the mediation of inflammation, as it is the most common context in which we experience pain is the inflammatory context. Additionally, some analgesic compounds such as paracetamol inhibit pro-inflammatory factors (VIDAL, 2021a).

1.2.2. Mediation of the inflammation

Tissue damage is often followed by the release of inflammatory mediators/factors by a multitude of immune cells (e.g. macrophage, mast cells), non-

immune cells (e.g. fibroblasts, keratinocytes) and nociceptors at the injured area (Basbaum et al., 2009; Chiu et al., 2012; Bell, 2018). These factors are collectively called the “inflammatory soup” and include a wide array of molecules e.g.: neurotransmitters, peptides (substance P, bradykinin), eicosinoids and related lipids (prostaglandins [PGE], leukotrienes, endocannabinoids), neurotrophins (nerve growth factor [NGF]) (Yaksh et al., 2015), cytokines (tumor necrosis factor [TNF], interleukins [IL], interferons [IFN]) and chemokines (extracellular proteases and protons) (**Figure 2**) (for review (Basbaum et al., 2009; Bell, 2018)).

Moreover, these factors can sensitise nociceptors, which will lower their response threshold and *de facto* increase their response to a stimulus. This whole process is called peripheral sensitisation and results in hyperalgesia in animals (**Figure 2**). Sensitisation occur through 3 mechanisms; (**1**) direct opening of cation channels (ASICs, TRPV1, TRPA1) leading to the nociceptor activation, (**2**) activation of intracellular pathways through G-proteins to indirectly modify membrane proteins, or (**3**) alterations in the transcriptional mechanisms of the cell (**Figure 2**) (Dawes et al., 2013; Bell, 2018). For example NGF activates downstream signalling pathways (**2**), such as phospholipase C (PLC), mitogen-activated protein kinase (MAPK), and phosphoinositide 3-kinase (PI3K) (Basbaum et al., 2009). This results in a potentiation of sensor at the peripheral ending of nociceptor, most notably TRPV1, leading to a change in thermal, mechanical and chemical sensitivity (Chuang et al., 2001). Additionally, NGF is also retrogradely transported to the nucleus of the nociceptor (**3**), where it promotes increased expression of pro-nociceptive proteins (sensor, substance P) (Ji et al., 2002; Chao, 2003). Some evidences support a direct action of cytokines and chemokines on nociceptors (Pethő and Reeh, 2012), however they mostly contribute to pain hypersensitivity by potentiating the inflammatory response (for review (Basbaum et al., 2009; Bell, 2018)).

To summarize, after an injury a nociceptive signal will be transduced through different sensors (TRPs, TREK, TRAAK, ASICs) in sensory cells. However, if an inflammation is initiated at the injury site, the “inflammatory soup” will sensitize the area. Additionally, most of the stimuli will trigger a nociceptive signal due to the lowering of the nociceptor threshold (hyperalgesia). The nociceptive stimulus, after being transduced by the sensors in the nociceptors, will be sent to the spinal cord via the PNS.

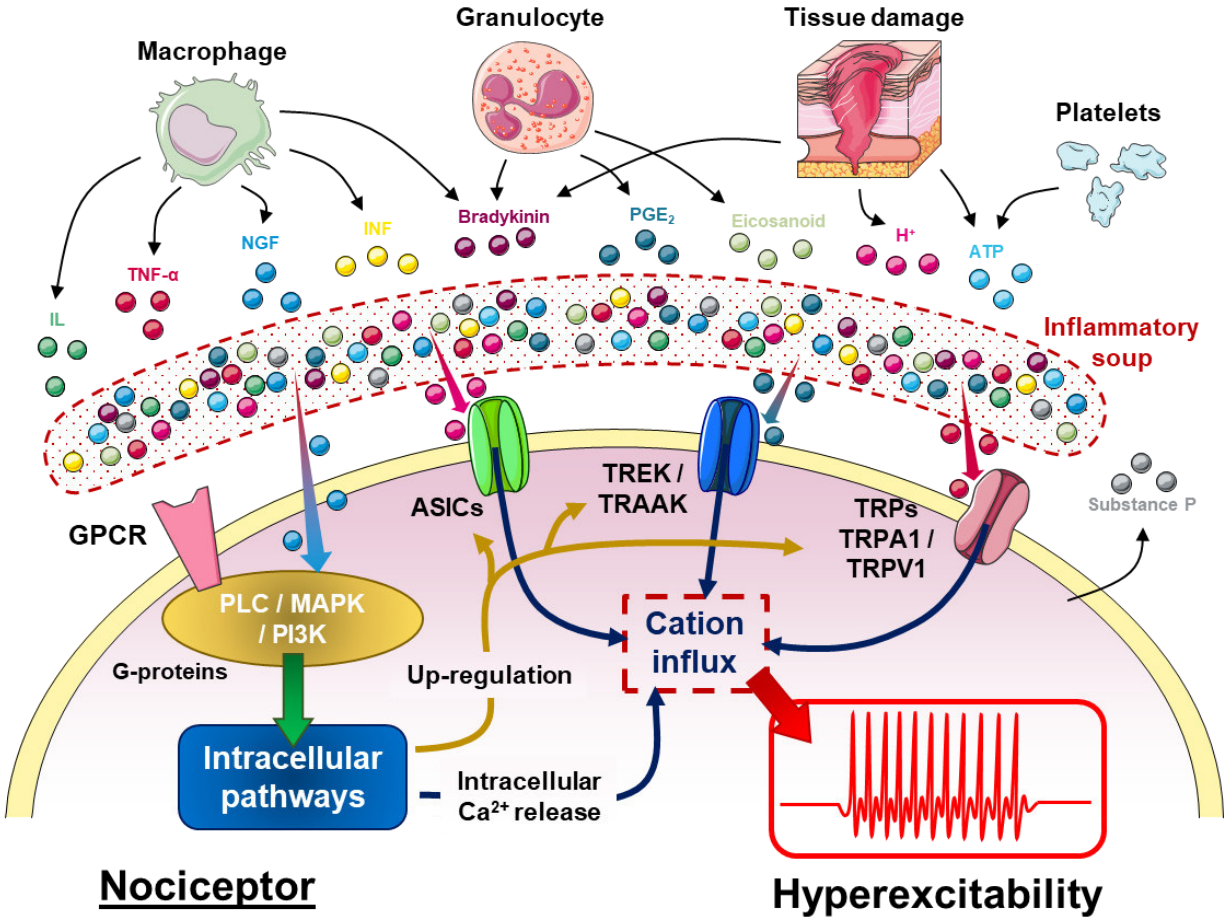

Figure 2: Peripheral sensitisation during inflammation.

Inflammatory soup factors, released by elements (macrophage, platelets, etc…) of the immune system, sensitize nociceptors close to the inflammation site. *Inspired from: Basbaum (2009).*

1.2.3. Nociceptive system

1.2.3.1. Peripheral

As seen previously, stimuli are transduced by various sensor. These sensors are largely express in the periphery of the body, especially into the skin and guts to be the closest to the potential injury site (**Figure 3**).

Information of the nociceptive stimulus arise from sensory channels expressed at the peripheral ending of nociceptors (see. *1.2.1. Transduction of the nociceptive stimulus*) (Basbaum et al., 2009). Nociceptors are somatosensory afferent neurons, which belong to one of the three major types: Aβ, Aδ and C-fibres, that project from tissues (skin, muscle, joints or viscera) to the spinal cord (or to the trigeminal for facial

pain). Nociceptors cell bodies are located in the DRG adjacent to the spinal cord or in the trigeminal ganglia. Axons arise from these pseudo-unipolar neurons and carry both a peripheral and a central tract, which respectively innervates the tissues and the spinal cord. It is at the peripheral ending that stimuli are transduced and are transmitted to the spinal cord through the axon (**Figure 3**) (for review; (Lumpkin and Caterina, 2007; Basbaum et al., 2009; Bell, 2018)).

Primary afferent neurons involved in nociception are classically characterised by their diameter and myelination level, which both determine their conduction velocity (**Figure 3**).

First, the Aβ-fibres are the largest myelinated fibres. They respond to touch or hair movement (Piezo channels) (Abraira and Ginty, 2013) and can be involved in mechanical nociception under specific conditions (dry skin and aging) (Feng and Hu, 2019). Second, the Aδ-fibres have a medium diameter, are myelinated, and constitute one of the two major classes of nociceptors. They are responsible for the transmission of well-localised “first” pain (for review; (Bell, 2018)). Third, the C-fibres have a small diameter, are unmyelinated and are the other major classes of nociceptors, as they are responsible for the poorly localised pain (for review; (Bell, 2018)). These fibres can be subdivided into two molecular-based groups, peptidergic C-fibres marked by the expression of calcitonin gene-related peptide and non-peptidergic C-fibres are identified by their isolectin B4 binding (for review; (Bell, 2018)).

Most of the knowledge about nociceptors is coming from studies about cutaneous nociceptors. Although visceral nociceptors are less studied, they dispose of similar ability to convey nociceptive information that can lead to the sensation of visceral pain.

Visceral sensory neurons are similar to cutaneous nociceptors; cell bodies are localised in the DRG (or nodose ganglia for vagal visceral afferents), and their axons are usually thinly myelinated or unmyelinated (Aδ- or C-fibres) (for review; (Bell, 2018)). Importantly, the viscera are sparsely innervated compared to other tissues, and visceral nociception does not come from organ cutting or burning, rather it arises from distension, traction, ischaemia and through release of chemical mediators of inflammation (Robinson and Gebhart, 2008).

Following transduction of thermal, mechanical and chemical signals by the TRP and other ion channel sensors, a large number of voltage-gated ion channels are

involved in the conduction of the nociceptive signal across nociceptors (Basbaum et al., 2009; Bell, 2018). These channels generate an electrical current either opening, allowing the influx of Na^+ or Ca^{2+}, or closing if the channel is responsible for a hyperpolarising current, such as the potassium voltage-gated channels K_v that are expressed in C-fibre nociceptors (Bell, 2018). Within these voltage-gated channels, there are also the tetrodotoxin (TTX)-sensitive (e.g. Na_v 1.1, 1.6) and TTX-insensitive (e.g. Na_v 1.8, 1.9) sodium channels (Na^+ channel) that are involved in ion influx. Interestingly, patients presenting loss-of-function mutations in Na_v genes are unable to detect noxious stimuli and, conversely, gain-of-function mutation lead to nociceptor hyperexcitability associated with pain disorder (Cox et al., 2006; Estacion et al., 2008). Additionally, there is a diversity of calcium channel (Ca^{2+} channel) especially the voltage-gated channels Ca_v (e.g. 2.2, 3.2) that are expressed from nociceptors (C-fibres) to laminae II-IV of the dorsal horn (Basbaum et al., 2009; Bell, 2018).

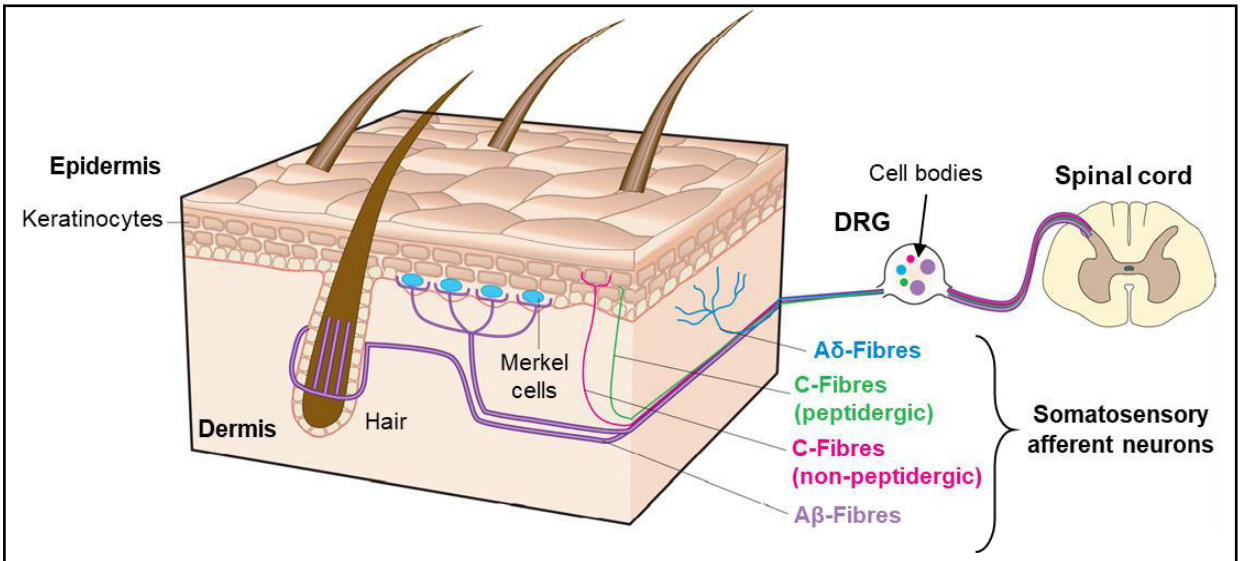

Figure 3: Somatosensory neurons of the skin.

The skin is innervated by somatosensory fibres, which are pseudo-unipolar neurons whose cell bodies are located within the DRG, and which project to the spinal cord. *Adapted from: Lumkin & Caterina (2007).*

The nociceptive signal is conducted from the peripheral ending of the nociceptors to the dorsal horn of the spinal cord. The conduction of this signal involves several ion channels. These channels are potential targets to modulate the nociceptive signal.

1.2.3.2. Spinal cord

The spinal cord (and the brainstem for trigeminal system) and more precisely the dorsal horn, is an innervation area of primary afferent neuron. Inputs from nociceptors arrive there and are integrated and modulated by different interneurons (and descending controls) and then projected (or not) to the brain.

Grey matter of the spinal cord is divided into laminæ according to cytoarchitecture criteria (Rexed, 1952). Primary afferents end-up in different laminæ of the dorsal horn determined by fibre type. Aδ-fibres terminate primarily in lamina I. Next peptidergic-C fibres afferents arborize mainly in laminae I and II. Most of non-peptidergic-C fibres occupy the central part of lamina II. Then Aβ-fibres end mainly in the deeper laminæ III–V (Abraira et al., 2017) (for review; (West et al., 2015; Bell, 2018). In the laminæ I-V of the dorsal horn, in addition of the terminals of primary afferent neurons, there are 3 other major neural components: excitatory and inhibitory interneurons, projection neurons and descending modulatory axons (Todd, 2010, 2017).

Primary afferents all use glutamate as their main/primary neurotransmitter and, therefore, all synapses with “second order neurons” are excitatory (Basbaum et al., 2009). Glutamate acts on three types of ionotropic receptors (kainate, alpha-amino3-hydroxy-5-methy-4-iso-xazoleproprionic acid [AMPA] and N-methyl-D-aspartate [NMDA]) and on the metabotropic receptors (mGlu) (Bell, 2018). The “second order neurons” could be projection neurons or interneurons, which may form complex circuits within the dorsal horn (Ribeiro-Da-Silva and Coimbra, 1982). Inhibitory interneurons use γ-aminobutyric acid (GABA) or glycine as neurotransmitters although many co-express both (Todd, 2010) while excitatory interneurons use glutamate as a neurotransmitter (Todd, 2017).

Thus, after passing from the primary afferents through glutamate release to second-order neurons, the nociceptive signal is sent to the brain via projection axons and modulated within the dorsal horn by interneurons (for review; (Bell, 2018)). The concept of the dorsal horn as a modulation site for noxious signals dates back to Wall and Melzack’s gate control theory (GCT) of pain (Melzack and Wall, 1965). GCT proposed that at the centre of gate control circuit, lies an inhibitory interneuron that can be activated by the large afferent non nociceptive fibres (Aβ), and inhibited by small afferent nociceptive fibres (Aδ, C) resulting in a feed-forward control of the inhibitory

interneuron (**Figure 4**) (Melzack and Wall, 1965). Thus, nociceptive primary afferents will not only activate projection neurons (or excitatory interneurons) but will also reduce the activity of the "gating" inhibitory interneurons (**Figure 4**) (for review; (Bell, 2018)).

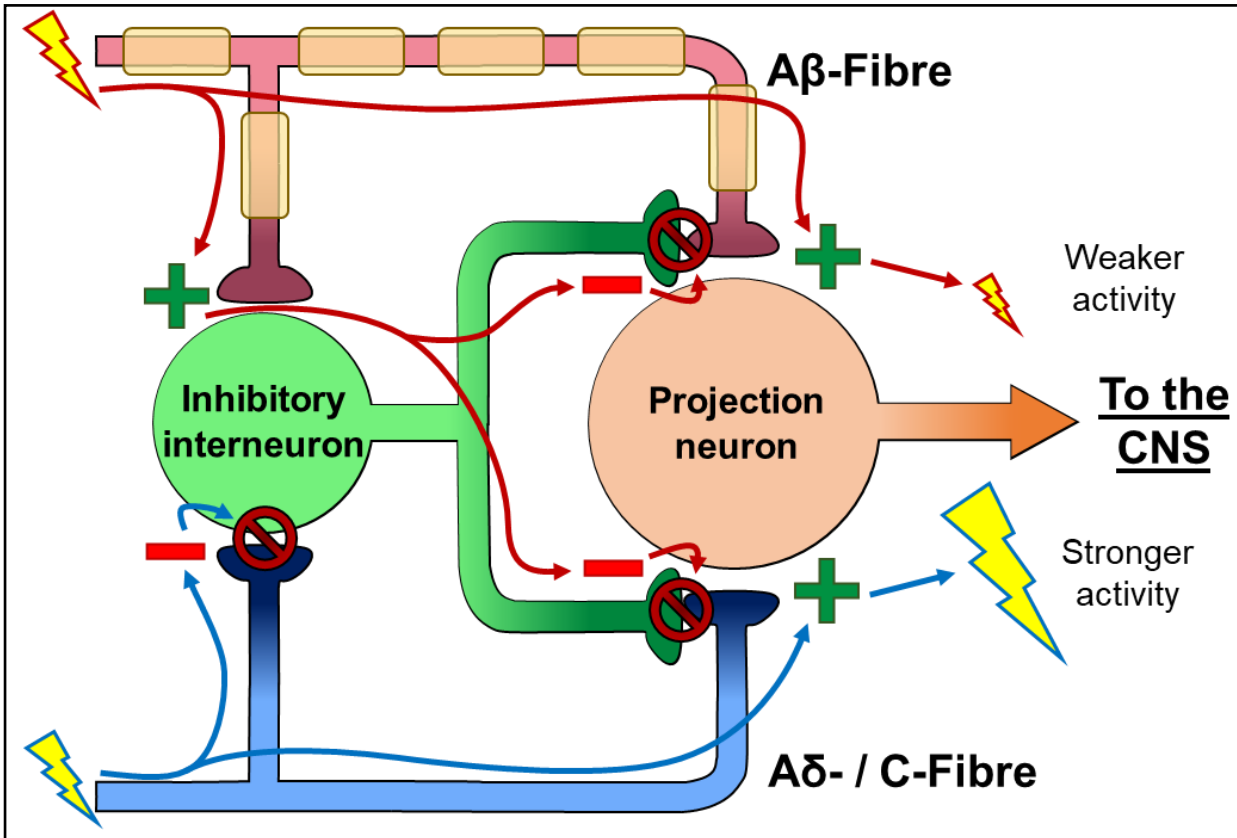

Figure 4: Gate control theory of pain.

GCT proposed that an inhibitory interneuron of the dorsal horn could be activated by large non-nociceptive fibres and inhibited by small nociceptive fibres. This results in a feed-forward control of the inhibitory interneuron, which is connected to the projection neurons.

Finally, there is also GPCR (e.g.; opioid, cannabinoid, muscarinic acetylcholine, $GABA_b$, and α2-adrenergic receptors) and ligand-gated ion channel ($GABA_a$, nicotinic acetylcholine [nACh R] and serotonin type-3 [$5\text{-}HT_3$ R] receptors) that are involved in the modulation of the nociceptive signal particularly at the spinal level (for review ; (Basbaum et al., 2009; Bell, 2018)). GPCR generally appear to act via modulation of Ca^{2+} channels to reducing the influx in projection neurons or in inhibitory interneurons.

Numerous clinical studies have demonstrated that the administration of exogenous agonist of the GPCR (especially opioid and cannabinoid) can produce significant analgesic and anti-inflammatory effects (van Loon et al., 2010; Iwaszkiewicz

et al., 2013). On their side, these ion channel receptors modulate the nociceptive signal by inhibiting or activating directly the neurons or the interneurons (Lummis, 2012; Dineley et al., 2015; Wilke et al., 2020).

After being modulated (or not) in the dorsal horn, the nociceptive stimulus converge on nociceptive specific projection neurons that are concentrated in lamina I and spread out in laminæ III–VI (Bell, 2018). Projection neurons of the lamina V are not specific to noxious stimuli and are known as wide dynamic range (WDR) neurons because they respond to a wide range of inputs (Sikandar et al., 2013). The axons of these projection neurons cross the midline, travel in ascending spinal white matter tracts and innervate various supraspinal targets (Bell, 2018). The nociceptive signal will then be projected to the supraspinal level in order to be integrated or not as pain by the cortex.

1.2.3.3. Supraspinal

Dorsal horn projections, travel along ascending spinal white matter tracts and innervate various nuclei in the brainstem and thalamus (Bell, 2018). These targets include the medulla (especially the rostral ventromedial medulla [RVM]), the parabrachial area, the periaqueductal grey (PAG), the nucleus of the solitary tract and the thalamus (**Figure 5**). Each of these areas is presumed to encode for specific dimensions of the pain perception (West et al., 2015). The parabrachial area is an important structure for the affective component of pain as its output provides a fast connection to the amygdala (Kato et al., 2018). Amygdala is a region that contributes to processing information related to the aversive properties of the pain experience (Basbaum et al., 2009). On the other hand, the thalamus has been linked to the sensory-discriminatory aspects of pain due to its connections with the somatosensory cortex (Vierck et al., 2013). At this point, the nociceptive signal is integrated in brain structures and can be called pain if it is perceived as such (IASP).

However, the nociceptive signal may still be modulate by the PAG and RVM, that control powerful descending inputs to the dorsal horn of the spinal cord, these descending inputs are called descending controls (**Figure 5**) (for review; (West et al., 2015; Bell, 2018)). They represent a mechanism whereby the transmitted nociceptive signal can be facilitated (enhanced pain) or inhibited (reduced pain). They provide a

top-down mechanism by which cognitive, emotional or autonomic factors can regulate nociceptive signal at the dorsal horn (Bannister and Dickenson, 2017). These descending control pathways start with PAG and RVM neurons that project bilaterally to the dorsal horn where they release noradrenaline (NA) and serotonin/5-hydroxytryptamine (5-HT) (for review; (Bannister and Dickenson, 2017; Bell, 2018)). On the one hand, NA acts via α_2-adrenergic receptors to induce antinociceptive effects (Bannister and Dickenson, 2017). On the other hand, 5-HT release can mediate both anti- or pro-nociceptive effects through either the 5-HT_7 R or 5-HT_3 R respectively (Dogrul et al., 2009).

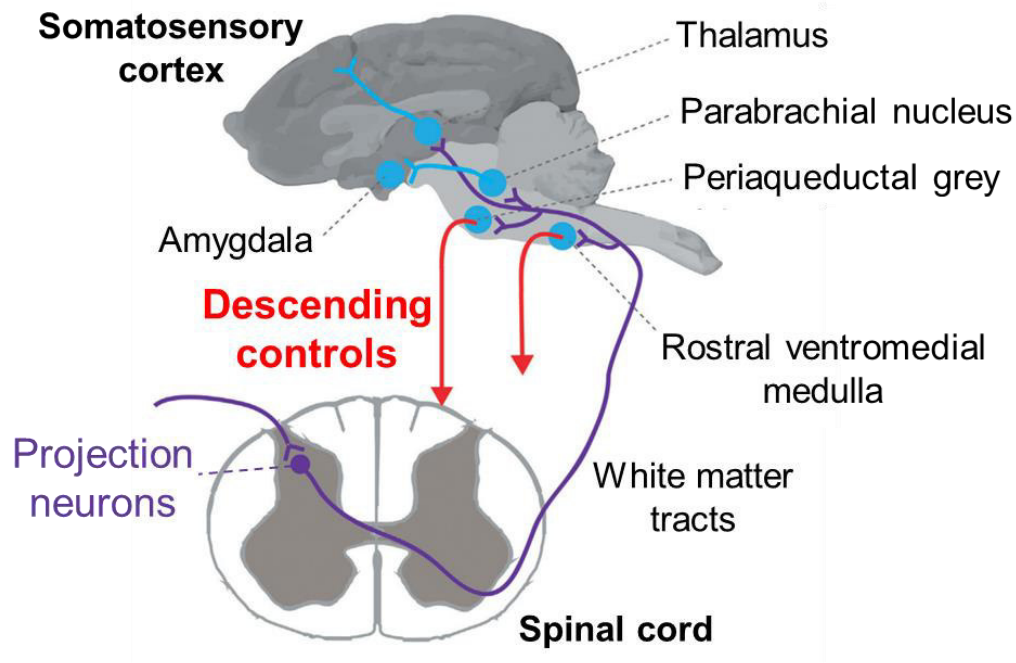

Figure 5: Projections and major supraspinal sites of the nociceptive system.

Projection neurons arise from the dorsal horn of the spinal cord. These innervate various higher centres responsible for aspects of the pain experience. *Adapted from: Bell (2018).*

After being modulated (or not) in the dorsal horn the nociceptive stimulus converged on nociceptive specific projection neurons that are concentrated in lamina I and spread out in laminæ III–VI (Bell, 2018). Projection neurons of the lamina V are not specific to noxious stimuli and are known as wide dynamic range (WDR) neurons because they respond to a wide range of input (Sikandar et al., 2013). The axons of these projection neurons cross the midline, travel in ascending spinal white matter tracts and innervate various supraspinal targets (Bell, 2018). The nociceptive signal

will then be projected to the supraspinal level in order to be integrated or not as pain by the cortex.

Starting from the molecular sensors of the nociceptors up to the integration in brain structures, the nociceptive stimulus can be modulated in many steps. Each of these steps involves different molecular (ion channels, GPCRs) and cellular (nociceptors, interneurons, WDR neurons) actors that can potentially be targeted to modulate nociception and thus reducing pain perception.

1.3. Pain

Pain is the emotional interpretation of the nociception and a valence will be associated to the nociceptive experience. As such, the appreciation (the emotional valence) of pain is not simply the result of abnormal sensory stimulation causing an unpleasant sensation, but rather a combination of the recognition of somatic discomfort in association with an emotional response to that discomfort. Thus, the perception of pain and the extent of associated emotions (distress, disability) may vary depending on previous experience, cultural back-ground, situational factors, and comorbid psychiatric disease (Wang and Mullally, 2020).

1.3.1. Pain and emotions

Melzack and Casey proposed in 1968 that the human pain experience is composed of three dimensions (Melzack and Casey, 1968). The first one is the sensory-discriminative aspect that identifies the location, timing, and physical characteristics (e.g., mechanical, chemical, heat) of the noxious stimulus. Then, the cognitive-evaluative dimension influences the evaluation of the meanings and consequences of the pain (or injury). Finally, the affective/motivational dimension (closely related to emotion) underlies the unpleasantness associated with exposure to a noxious stimulus and activates the appropriate behaviour (for review; (Lumley et al., 2011)).

There are many evidence, that negative valence emotions such as fear and anxiety influence pain perception. Fear is triggered by a present or imminent threat and motivates defensive responses such as flight. Anxiety, on the other hand, arises from anticipation of threat and is characterized by hypervigilance and passive defensive responses (for review; (Lumley et al., 2011)). Studies show that fear of an external

stimulus can inhibit pain through activation of the endogenous opioids system (Pugh et al., 1996; Godoi et al., 2020), whereas anxiety increases pain (Rhudy and Meagher, 2000).

In opposition, positive valence emotion generally reduce pain perception, this phenomenon is known as “affective analgesia” (Franklin, 1998). The major system presumed to be responsible for this phenomenon is the dopaminergic system. It has been found that its activation reduces emotional responses to pain (Kender et al., 2008).

To summarize, the emotional aspect of pain is complex and supported by various cortical and subcortical systems. At the same time, pain influences the emotional state, and emotions in return affect the pain perception. So anxiolytic treatment by reducing anxiety can improve the perception of pain. Thus, a molecule with both analgesic and anxiolytic effects is interesting for the treatment of pain, particularly chronic pain.

1.3.2. Acute and chronic pain

Pain can be categorised according to its different origins, for example: inflammatory (acute injury, rheumatoid arthritis), osteoarthritis (joint degeneration), or neuropathic (damaged nerves) (**Table 1**). However, in the following section, I will not discuss the origins of pain but the dichotomy between acute or chronic pain.

Acute pain is an indicator of potential tissue damage and can therefore be considered as an adaptive alarm. It alerts the person to the cause of pain and motivates the person to act to avoid tissue damage, protect the affected area and prevent similar situations in the future (Bell, 2018).

Understanding chronic pain, which is defined as lasting at least 3 months (Treede et al., 2019), is more complicated than acute pain. Especially due to the adaptive changes that occur at the neurobiological, psychological, and social levels that can maintain the pain. As a result, chronic pain patients are much more likely needing a psychological follow-up than those with acute pain. In fact, in addition to treating the pain itself, it helps to deal with maladaptive outcomes of the pain (mood problems, substance abuse or relationship difficulties) (for review; (Lumley et al., 2011)).

As there are different types of pain, their treatment must also be adapted in order to treat the different facets of the pain according to the type(s) of pain.

1.3.3. Nociception modulation and pain treatment

Acute and chronic pain can be a comorbidity associated with many diseases, affections, surgical procedures, and this constitutes a burden for the patients and society. Indeed, pain strongly affects our society, affecting the patient in his daily activities such as work, hobbies, social relationships and, emotional state notably the anxiodepressive state (Mick et al., 2013; Malfliet et al., 2017).

However, medical management of pain aims to reduce its intensity, preventing the risk of chronicization to improve life quality. The choice of treatment given by the physician depends on the intensity of the pain, its type, location, context, and the patient. To achieve this, the physician can rely on different types of treatment, for which I will describe the main categories.

1.3.3.1. Current treatment

Majority of the analgesic treatments available are known as antalgics. They are divided in three groups according to their analgesic potency.

The first group is composed of non-opioid analgesic and anti-inflammatory drugs such as paracetamol, aspirin or nonsteroidal anti-inflammatory drugs (NSAID) (VIDAL, 2021c). They are all inhibitor of cyclooxygenase (COX) which are responsible for the production of pro-inflammatory factors (prostaglandins) (Rajan and Behrends, 2019). They are usually the first line of treatment as they are weak and well tolerated analgesics (Blondell et al., 2013; Hylands-White et al., 2017; Rajan and Behrends, 2019). The second group consists in weak opioids such as codeine and tramadol (VIDAL, 2021c). They attenuate transmission of nociceptive signals by activating opioid receptors in the central nervous system (Hylands-White et al., 2017). They are used for mild to moderate pain that persists or increases after the use of first group drugs (Hylands-White et al., 2017). The third and last group of analgesic drugs are the strong opioids (morphine, fentanyl) (VIDAL, 2021c). They are more potent that the second group opioids, however, they also have more severe side effects such as respiratory depression which can be fatal (even at therapeutic doses) (Hylands-White et al., 2017).

In the previous section, only unimodal treatments were listed, which are treatments that target a single mechanism of pain. However, today the approach of pain management and treatment is mainly based on a multimodal treatment, that is, a combination of different treatments to target different mechanisms of pain in order to have stronger analgesic effects, fewer side effects or even both (**Figure 6**) (Dale and Stacey, 2016). For example there are many drugs that are combining different types of molecules, such as cocktail of codeine and paracetamol, to achieve a more powerful effect than codeine alone, without having to use strong opioids because the two molecules have different target (Blondell et al., 2013; VIDAL, 2021a).

However, despite the interesting possibilities offered by multimodal treatments and the global awareness of the risks of abuse of opioid related compounds in the therapeutic context, we still observe here that opioids are the gold standard treating severe pain. In addition, the diversity of therapeutic targets offered by analgesics is particularly limited, either NSAIDs or opioid related. The development of non-NSAID and/or non-opioid related analgesic compounds would therefore be a significant advance in the treatment of pain, notably in the context of the opioid crisis.

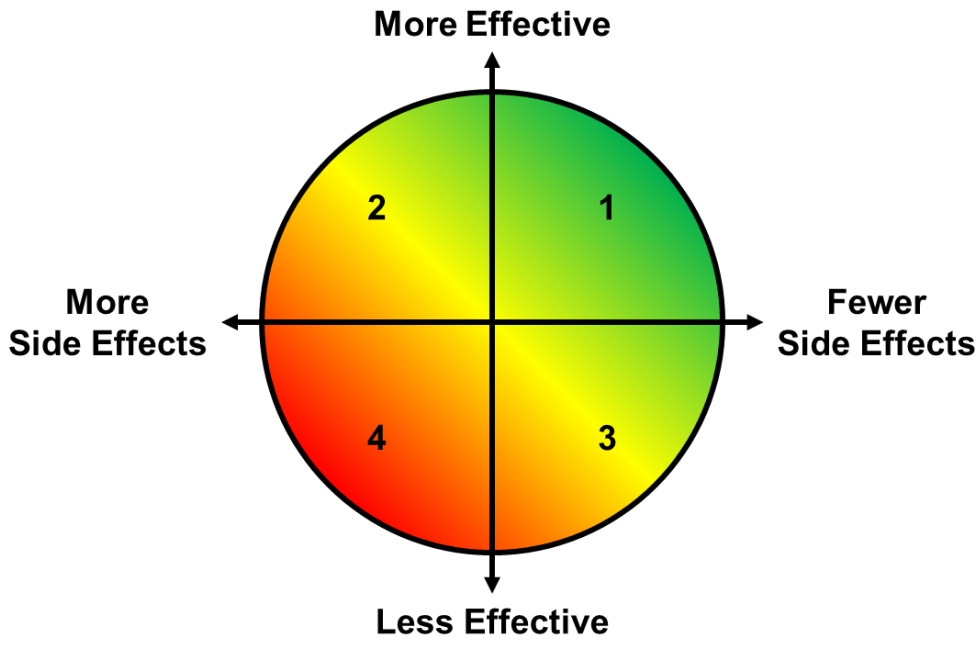

Figure 6: Potential outcomes of combination pharmacotherapy.

(**1**) Better pain control and improved side effect profile. (**2**) Better pain control, but worsened side effects. (**3**) No change in pain control with improved side effect. (**4**) Worsening pain control and worsened side effect. *Adapted from: Dale & Stacey (2015).*

1.3.3.2. Opioid crisis

The use and abuse of opioid related analgesic compounds, especially in North America, has led to the opioid crisis as observed in the United States.

This crisis started in the late 1990s, where pharmaceutical companies tried to convince the medical community that their patients would not become addicted to analgesic therapeutic opioid compounds (National Institute on Drug Abuse, 2021a). As a result, physicians and healthcare providers started prescribing these compounds in greater amounts, which led to their widespread detour and misuse, as they are indeed now recognized as highly addictive compounds (Kolodny et al., 2015). In 2019, nearly 50 000 Americans died from opioid overdoses (**Figure 7A**) and approximately 1.7 million people suffered from disorders (e.g. sedation, dizziness, nausea, vomiting, constipation, dependence, respiratory depression, mood disorders) associated to prescribed opioids (Benyamin et al., 2008; National Institute on Drug Abuse, 2021a, 2021b). It is therefore a major health crisis in North America, in terms of death rate, effects on society and number of people affected (**Figure 7A**).

However, in Europe the crisis is not as strong, in 2016, 4830 people died (**Figure 7B**). Nevertheless, the increase in consumption is a cause for concern, as highlighted by the rise in the use of strong opioids in patients with osteoarthritis from 8% to 20% (OECD, 2019).

Thus, to stem this crisis while continuing to treat chronic and acute pain, it is essential to develop alternative analgesic treatments.

1.3.3.3. Actual need of new treatment

The opioid crisis and its dramatic consequences reflect our medical dependence to opioid compounds and, as seen in the previous section, this has tremendous drawbacks that affect patients' health. In addition, patients treated with opioids develop tolerance, which leads to a loss of efficacy of the treatment and increase the risk of abuse (Allegri et al., 2012). However, there are also alternative treatments that are efficient but are usually highly specific to certain diseases or conditions (e.g. gabapentin, a GABA established analgesic drug specifically for neuropathic pain (Hylands-White et al., 2017)).

As discussed previously, the cost of all these mistreated pains, coupled with the cost of the opioids crisis, places a significant burden on society and health care system, both in the U.S. and in Europe (**Figure 7**). This demonstrates that there is a need to identify and develop new analgesic compounds that do not rely on the opioid system.

One possibility it to use exogenous molecules from the traditional pharmacopoeia, the terpenes, which are extracts from medicinal plants and used to relieve pain. These molecules are known to target several essential sensors and ion channels involved in the nociceptive system such as TRPs, Ca^{2+}, Na^{+}, K^{+} channels or even $GABA_a$ R. It is therefore necessary to investigate the analgesic potential of terpenes.

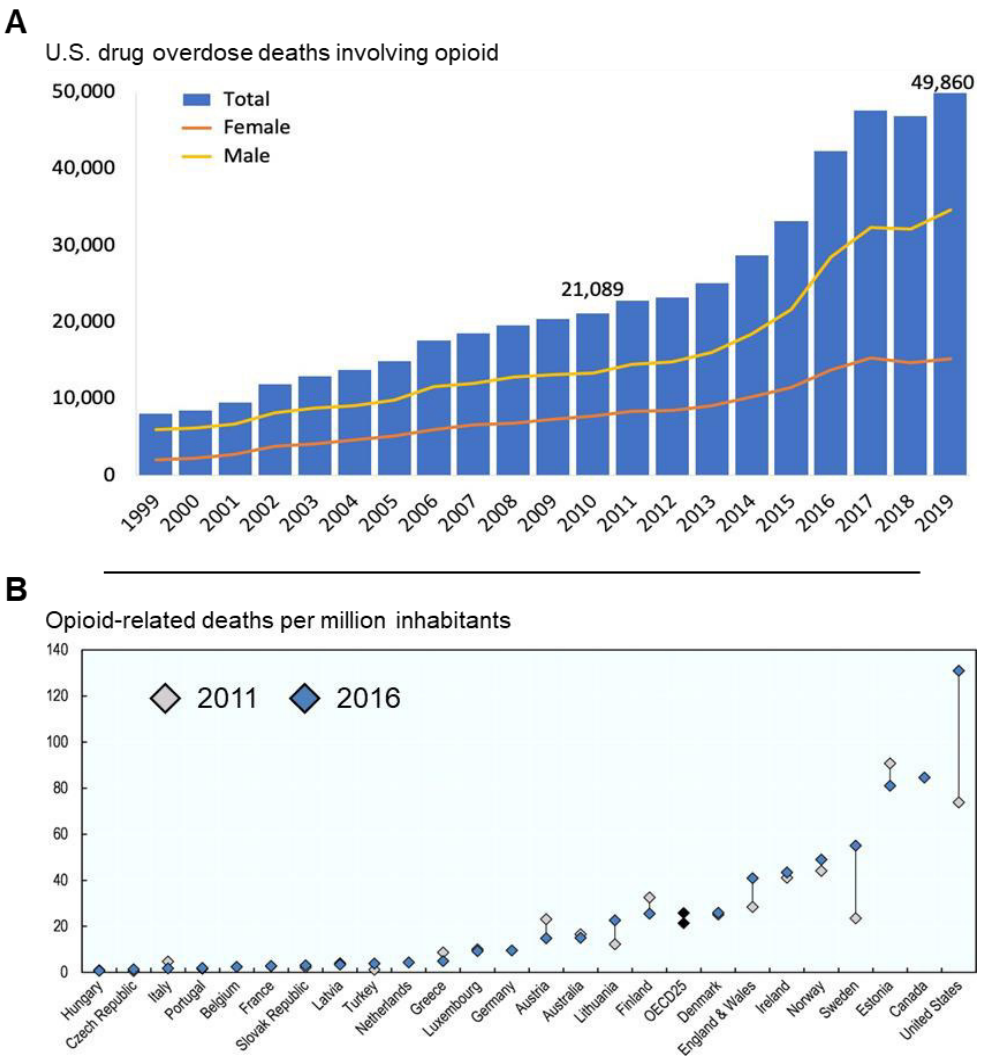

Figure 7: Opioid-related deaths per year.

(**A**) Evolution from 1999 to 2019 in the United State. (**B**) Evolution between 2011 and 2016 in OECD countries. *From: (A) https://www.drugabuse.gov/drug-topics/trends-statistics/overdose-death-rates (2019) / (B) https://www.oecd.org/fr/sante/addressing-problematic-opioid-use-in-oecd-countries-a18286f0-en.htm (2019).*

2. Terpenes

2.1. Structures, synthesis and effects

2.1.1. Terpenes: general informations

Terpenes are a family of molecules classified according to their natural origins, their structures and their biosynthesis origins. They are a large class of organic compounds (hydrocarbon) and are produced by a wide variety of plants, mainly gymnosperms (conifers) and angiosperms (flowering plants). Exceptionally, they are also produced by some insects, which might represent a convergent evolution (Beran et al., 2019).

As terpenes are elements of the primary and secondary metabolites of plant cells, they play a major role in their lives and ecosystems. For example, terpenes are known to be the main molecules responsible for the scent of plants. Their terpene compositions can change from a plant to another even if it is the same species. Terpenes production depends on many conditions: environmental factors (temperature, humidity, wind and soil composition), the stage of development of the plants and their organs (fruits, flower, leaf, roots) (Zgheib et al., 2016). To summarize, these natural compounds are produced in different parts of the plant in order to respond to their biological and physiological needs. Indeed, terpenes have a response function to biotic and abiotic factors for the plants; they are attractors for pollinators, deterrents for herbivores, repellents, antibacterial compounds, thermotolerance and photoprotection molecules (Bergman et al., 2019) (**Figure 8**).

Due to this diversity of effects, terpenes are used in industry to produce biofuels, rubbers, cosmetics, and food products (menthol, which is commonly found in chewing gum, is a major terpene of mint (*Mentha sp.*)). In addition, in alternative medicine, they have been use for decades in essential oils but this will be further explored in a dedicated section (for review; (Tetali, 2018)). However, the analgesic properties of terpenes remain understudied.

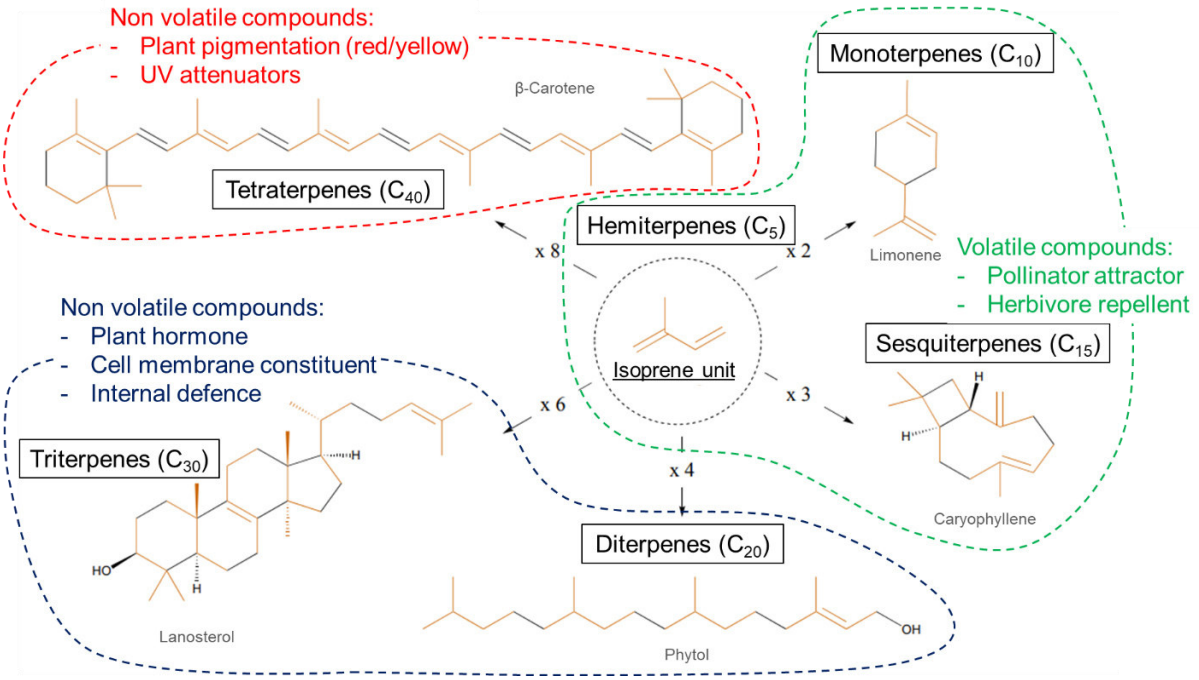

Figure 8: Terpenes families and major functions in plants.

Terpenes families are classified according to their isoprene structures. *Adapted from: Zélie Triaux thesis (2019).*

2.1.2. Structures and biosynthesis of terpenes

With about 70 000 structures known today, the terpene family (including both terpenes and terpenoids, which are oxidized terpenes) is the largest family of natural compounds (Vavitsas et al., 2018). Their structures follow the biogenetic isoprene rule; a variable number of five-carbon elements, called the isoprene unit, composes all terpenes. Hemiterpenes (C_5) are composed by one isoprene unit, monoterpenes (C_{10}) are composed by two isoprene units, sesquiterpenes (C_{15}) three isoprene units, diterpenes (C_{20}) four units, etc… until tetraterpenes (C_{40}) which are made of eight or more units (**Figure 8**). This diversity of molecules is also increased by the variety of enzymes and secondary modifications mediated by terpene synthases (Tetali, 2018; Bergman et al., 2019).

Moreover, this diversity is even more impressive since they all derived from the same constituent elements. The isoprene unit present in all terpenes is originating from two isomeric 5-carbon molecules, the isopentenyl diphosphate (IPP) and dimethylallyl diphosphate (DMAPP). It is also interesting to note that these two molecules can be converted into each other by the IPP isomerase. We now know that there are two

independent pathways for the biosynthesis of IPP and DMAPP, which evolved in taxonomically different organisms (Pulido et al., 2012). The mevalonic acid (MVA) pathway, which occurs mainly in the cytosol, begins with acetyl-coenzyme A and is mainly responsible for the biosynthesis of sesquiterpenes, triterpenes and diterpenes. On the other hand, the methylerythritol phosphate (MEP) pathway is mainly present in the chloroplast and starts with the condensation of pyruvate with the glyceraldehyde-3-phosphate, leading to smaller terpenes such as hemiterpenes, monoterpenes and diterpenes (Tholl, 2015). The IPP and the DMAPP synthesized by the MEP pathway can then assemble in a head-to-tail manner to form geranyl diphosphate (GPP). GPP is thus the precursor of all monoterpenes, which will then be generated through the action of terpene synthase (**Figure 9**) (for review; (Tetali, 2018; Vavitsas et al., 2018; Bergman et al., 2019)).

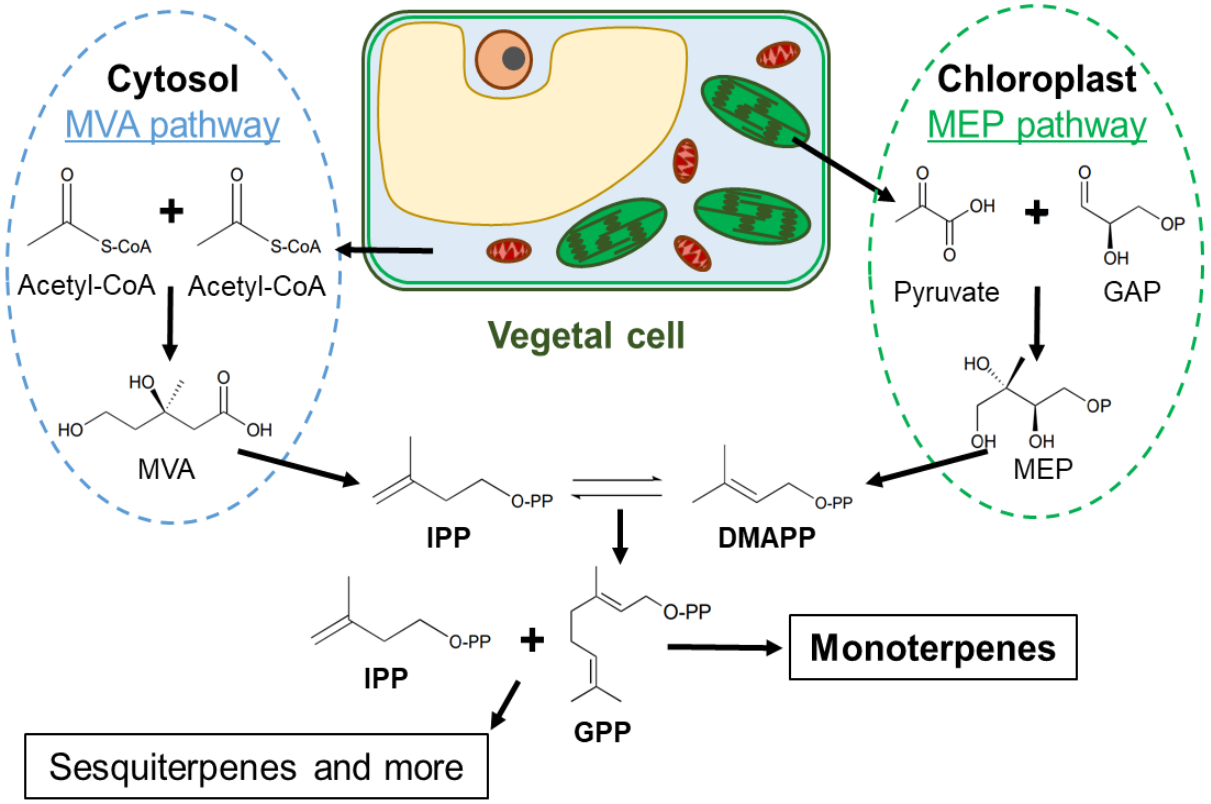

Figure 9: Simplified biosynthetic pathways of the precursors, IPP and DMAPP.

The two biosynthetic pathways of the terpenes in plants are the MVA and MEP pathways, respectively occurring in the cytosol and in chloroplast. *Adapted from: Zélie Triaux thesis (2019).*

Monoterpenes all derive from the GPP precursor, and it is important to highlight that the tremendous diversity of these compounds is due to the action of different terpene synthases. Acyclic monoterpenes are made from modifications (gain of H_20 or loss of H^+) of the geranyl cation, whereas cyclic and bicyclic monoterpenes are synthesized by a similar modification of the a-terpinyl cation (Bergman et al., 2019). (**Figure 10**).

In this project, we decided to solely focus on the potential effects of monoterpenes (therefore, I will not go further with the description of the other families of terpenes). Monoterpenes form a chemical group that is well defined; however, their individual effects are widely uncharacterized, and only a few monoterpenes are really well studied and described in the literature. This consideration is further developed in the next section.

2.2. Monoterpenes

Monoterpenes are small volatile molecules with a tremendous diversity of structures (**Figure 10**), which play an important role in the fragrances of flowers and leaves (**Figure 8**). As such, they are frequent amongst the main constituents of plant essential oils.

Aromatic plants and essential oils preparation, used in folk medicine for pain relief for centuries, happen to contain high levels of monoterpenes (Bakkali et al., 2008; Adams et al., 2009; Tsuchiya, 2017). For example, “bing pian” a medicinal substance extracted from the fruits of *Bassia scoparia* (L.) used in traditional Chinese medicine as a topical analgesic balm, is chemically almost exclusively composed of a single monoterpene, borneol (Wang et al., 2017). Furthermore, only about 25 monoterpenes are known to exert analgesic properties ((Guimarães et al., 2013; de Cássia da Silveira e Sá et al., 2017; Tsuchiya, 2017; Quintans et al., 2019; Perri et al., 2020)).

In addition, monoterpenes are highly lipophilic/hydrophobic compounds and end welled with an important anti-microbial action that has been attributed to their membrane disrupting properties (Bakkali et al., 2008). On top of that, the combination of their small size and lipophilic nature makes them perfectly able to cross the BBB. This ability is a major asset for their therapeutic applications (Wojtunik-Kulesza et al., 2017).

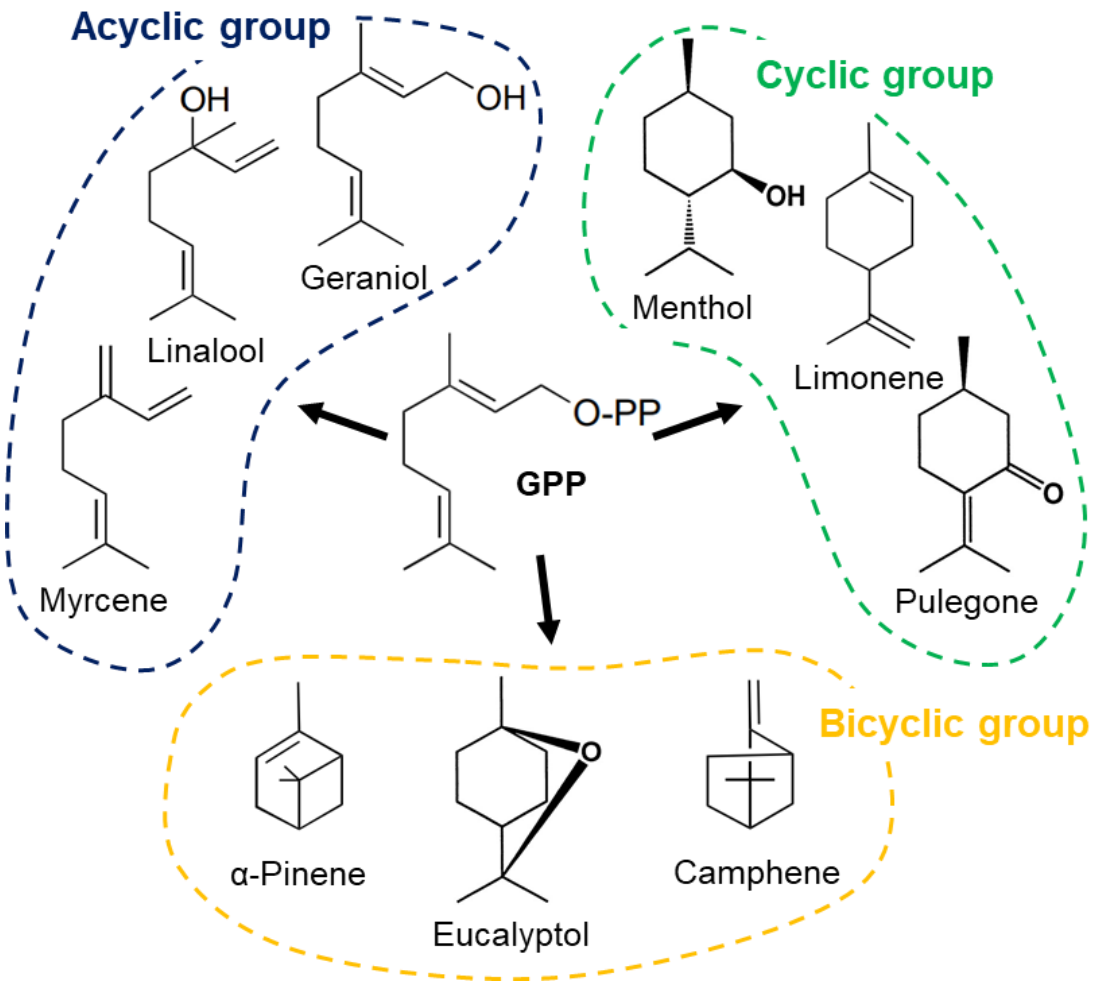

Figure 10: Example of monoterpenes from the three different structural groups.

All monoterpenes from the three different groups (acyclic, cyclic and bicyclic) derive from the GGP precursor.

2.2.1. Analgesic properties

Pure monoterpenes are studied for their analgesic properties since the early 90's and the number of studies increased at the beginning of the 21st century. This development is due to the democratization of the synthesis process of these pure compounds by large chemical companies. Before that, extraction and isolation of monoterpenes directly from essential oil was done by maceration, which was a time-consuming and complicated process (Triaux et al., 2020).

With the accessibility of affordable molecules, it is possible to study their properties and understand which monoterpenes are the major contributors to analgesia within essential oils. For example, Katsuyama et *al.* studied the analgesic effect induced by bergamot essential oil (10 µg) and compared it with the one induced

by linalool (5 µg) in a model of formalin-induced nociceptive behaviours. Results have shown that even with a lower dose, pure linalool induces stronger analgesia than the bergamot essential oil. Linalool might thus be the principal contributor to this analgesia (Katsuyama et al., 2015). However, a study of Djenane published the same year described the chemical profile of the essential oil of Algerian bergamot. Monoterpenes are 85% of the essential oil total components, and among these, limonene represents 77 %, and linalool only 1 % of the mixture (Djenane, 2015). Comparatively, another study has shown that the essential oil of Italian bergamot is composed by more than 95% of monoterpenes, 34 % of which being limonene and 18 % being linalool (Marchese et al., 2020).

These three studies taken together show us the importance of using pure monoterpenes to study and discriminate their properties. Indeed, the composition of an essential oil, even from a same subspecies, can drastically change because of biotic and abiotic factors, making the results difficult to compare (Zgheib et al., 2016; Tetali, 2018).

To study the analgesic properties of monoterpenes, it is required to use *in vivo* pain models and different tests. Most of them are induced pain models. As an example, the main models to study visceral pain are hyperalgesia induced by acetic acid or formalin (Almeida et al., 2013; Quintans-Júnior et al., 2013). Otherwise, the main models in order to study inflammatory pain are hyperalgesia induced by capsaicin, CFA or carrageenan (Liu et al., 2013; de Santana et al., 2015) (for review; (Sandkühler, 2009; Abboud et al., 2021)) (**Table 2**).

Based on these models, it has been shown that monoterpenes are able to induce different types of analgesia (for review; (De Sousa, 2011; Guimarães et al., 2013; de Cássia da Silveira e Sá et al., 2017)). For example, menthol, the most studied monoterpene, is capable of inducing thermal hot, thermal cold, mechanical and visceral analgesia (Klein et al., 2010; Pan et al., 2012; Liu et al., 2013) (**Table 2**). Almost all other monoterpenes share these thermal hot, mechanical and visceral analgesic abilities. There are multiple documented examples, such as citral (Nishijima et al., 2014; Gonçalves et al., 2020) or linalool (Berliocchi et al., 2009; Souto-Maior et al., 2017) (**Table 2**). However, cold analgesia is less studied, and this activity was investigated for only six different monoterpenes (Batista et al., 2010; Patel et al., 2014; Wang et al., 2017; Soleimani et al., 2019; Koohsari et al., 2020; Hilfiger et al., 2021)

(**Table 2**). Cold analgesia induction might be a less shared feature among monoterpenes; it is however impossible to conclude, due to the lack of knowledge on this subject.

To summarize, all the information stated in the last section will be classified in the following table (**Table 2**). This table is a non-exhaustive compilation of studies on analgesic monoterpenes. The aim of this table is to inventorize the important diversity of monoterpenes displaying analgesic activities. Although it does not reflect, all of the existing studies performed in the field of monoterpenes analgesia *in vivo,* it still gives a good picture of their analgesic properties.

In the following section, I will discuss the two main analgesic mechanisms of monoterpenes. The two major target systems of the monoterpene-induced analgesia are the modulation of the inflammation and the modulation of the nociceptive system. These two pathways are therefore of significant interest for the development of monoterpenes based analgesic treatments that would modulate both inflammation and nociceptive signal.

Table 2: Monoterpenes and analgesia.

Inventory of the different types of analgesia (thermal hot, thermal cold, mechanical, visceral) induced by monoterpenes. References are listed in the **Annex 1**.

Abbreviation Models : **AA** = Acetic acid; **Fm** = Formalin; **Glu** = gluamate; **Cap** = Capsaicin; **CCI** = Chronic constriction injury; **CFA** = Complete Freund adjuvant; **Car** = Carrageenan; **LPS** = Lipopolysaccharide; **PGE2** = Prostaglandin E2; **TNF-α** = Tumor necrosis factor alpha; **Zy** = zymosan; **SNI** = Spared nerve injury ; **SNL** = Spinal nerve ligation ; **M** = Mice; **R** = Rats

Abbreviation Methods : **AAACT** = Acetic acid abdominal constriction test; **AT** = Acetone test; **CF** = Calibrated forceps; **CP** = Cold plate; **EvF** = Electronic von Frey; **HP** = Hot plate; **IndP** = Induce pain; **PIT** = Paw immersion test; **Pl** = Plantar; **RST** = Randall-Selitto test; **TFT** = Tail flick test; **vF** = von Frey; **2-t°PT** = 2-temperature preference test

Terpenes	Types of analgesia				Models	Methods	Doses	Reference
	Thermal hot	Thermal cold	Mechanical	Visceral				
Borneol					Visceral (**AA** or **Fm**) hyperalgesia (**M**)	**AAACT**, **HP** and **IndP**	Borneol (5 - 50 mg/kg; i.p.)	Almeida J.R. et al., 2013
					Inflammatory (**CFA**) / Neuropathic (**SNL**) hyperalgesia (**M**)	**vF**	(+)-Borneol (125 - 500 mg/kg; p.o. / 15 - 60 µg; i.t.)	Jiang J. et al., 2015
					Inflammatory (**Cap** or **CFA**) / Visceral (**Fm**) hyperalgesia (**M**)	**CP**, **HP**, **IndP** and **vF**	(+)-Borneol (15 %; topical)	Wang S. et al., 2017
Camphene					Visceral (**AA** or **Fm**) hyperalgesia (**M**)	**AAACT** and **IndP**	(+)-Camphene (200 mg/kg; i.p.)	Quintans-Junior L. et al., 2013
Carvacrol					Inflammatory (**Cap**) / Visceral (**AA**, **Fm** or **Glu**) hyperalgesia (**M**)	**AAACT**, **HP** and **IndP**	Carvacrol (100 mg/kg i.p.)	Guimaraes A.G. et al., 2010
					Visceral (**AA** or **Fm**) hyperalgesia (**M**)	**AAACT**, **HP** and **IndP**	Carvacrol (100 - 200 mg/kg; p.o.)	Cavalcante Melo F.H. et al., 2012
Carvone					Visceral (**AA**) hyperalgesia (**M**)	**AAACT**	(±)-Carvone (250 mg/kg; i.p.)	de Sousa D.P. et al., 2007
Citral					Inflammatory (**Cap**) / Neuropathic (**SNL**) / Visceral (**AA**, **Fm** or **Glu**) hyperalgesia (**M**)	**IndP** and **vF**	Citral (100 mg/kg; i.g.)	Nishijima C.M. et al., 2014
					Inflammatory (**Car**, **LPS** or **Zy**) hyperalgesia (**M**)	**IndP** and **PIT**	Citral (50 - 300 mg/kg; p.o.)	Gonçalves E.C.D. et al., 2020
Citronellal					Inflammatory (**Cap**) / Visceral (**Fm**) orofacial hyperalgesia (**M**)	**IndP**	Citronellal (50 - 200 mg/kg; s.c.)	Quintans-Junior L. et al., 2011
					Inflammatory (**Car**, **PGE2** or **TNF-α**) hyperalgesia (**M**)	**vF**	Citronellal (25 - 100 mg/kg; i.p.)	de Santana M.T. et al., 2013

Citronellol					Inflammatory (**Cap**) / Visceral (**Fm** or **Glu**) hyperalgesia (**M**)	**IndP**	(-)-Citronellol (25 - 100 mg/kg; i.p.)	Brito R.G. et al., 2013
					Inflammatory (**Car**, **PGE2** or **TNF-α**) hyperalgesia (**M**)	**EvF**	(-)-Citronellol (25 - 100 mg/kg; i.p.)	Brito R.G. et al., 2015
Cuminaldehyde					Neuropathic (**CCl**) / Visceral (**AA** or **Fm**) hyperalgesia (**M** or **R**)	**AT**, **IndP**, **HP**, **PI** and **vF**	Cuminaldehyde (12.5 - 200 mg/kg i.p.)	Koohsari S. et al., 2020
p-Cymene					Visceral (**AA** or **Fm**) hyperalgesia (**M**)	**AAACT** and **IndP**	p-Cymene (50 mg/kg; i.p.)	Quintans-Junior L. et al., 2013
					Inflammatory (**Car**, **PGE2** or **TNF-α**) hyperalgesia (**M**)	**EvF** and **TFT**	p-Cymene (25 - 100 mg/kg; i.p.)	de Santana M.F. et al., 2015
Eucalyptol/ 1.8-Cineole					(**M** or **R**)	**HP** and **TFT**	Eucalyptol (0.3 mg/kg; i.p.)	Liapi C. et al., 2007
					Inflammatory (**Cap** or **CFA**) / Visceral (**AA**) hyperalgesia (**M**)	**AAACT**, **HP**, **TFT** and **vF**	Eucalyptol (200 mg/kg; p.o.)	Liu B. et al., 2013
Geraniol					Visceral (**Fm** or **Glu**) hyperalgesia (**M**)	**IndP**	Geraniol (12.5 - 50 mg/kg; i.p. / 50 - 200 mg/kg; p.o.)	La Rocca V. et al., 2017
Geranyl acetate					Visceral (**AA** or **Fm**) hyperalgesia (**M**)	**AAACT** and **IndP**	Geranyl acetate (100 mg/kg; i.p.)	Quintans-Junior L. et al., 2013
Limonene					Visceral (**AA**) hyperalgesia (**M**)	**AAACT**	Limonene (250 mg/kg; i.p.)	de Sousa D.P. et al., 2007
					Inflammatory / Visceral (H_2O_2) hyperalgesia (**M**)	**IndP**	(±)-Limonene (5 µM; i.itp.)	Kaimoto T. et al., 2016
					Visceral (**AA** or **Fm**) hyperalgesia (**M**)	**HP** and **IndP**	Limonene (75 mg/kg; i.p.)	de Almeida A.A. et al., 2017
					Visceral (**AA** or oxazolone-induced colitis) hyperalgesia (**M**)	**IndP** and **vF**	Limonene (30 - 300 mg/kg; p.o.)	Adriana Estrella G.R. et al., 2021

Linalool					Visceral (**Fm**) hyperalgesia (**M**)	**HP** and **IndP**	(-)-Linalool (100 - 150 mg/kg; s.c.)	Peana A.T. et al., 2003
					Neuropathic (**SNL**) hyperalgesia (**M**)	**PI** and **vF**	(-)-Linalool (100 mg/kg; s.c.)	Berliocchi L. et al., 2009
					Inflammatory (**CFA**) / Neuropathic (**SNL**) hyperalgesia (**M**)	**AT**, **IndP** and **vF**	(-)-Linalool (50 - 200 mg/kg; i.p.)	Batista P.A. et al., 2010
					Visceral (**Fm**) hyperalgesia (**M**)	**IndP**	(±)-Linalool (5 µg; i.p.)	Katsuyama S. et al., 2015
					Visceral (**Fm** or **AA**) hyperalgesia (**M**)	**AAACT** and **IndP**	Linalool (100 - 150 mg/kg; i.p.)	Souto-Maior F.N. et al., 2017
Menthol					Visceral (**AA**) hyperalgesia (**M**)	**AAACT** and **HP**	(-) Menthol (10 mg/kg; p.o. / 10 µg i.c.v.)	Galeotti N. et al., 2002
					(**R**)	**CP**, **PI**, **vF** and **2-t°PT**	Menthol (0.64 mM - 6.4 M; topical)	Klein A.H. et al., 2010
					Inflammatory (**CFA**) / Visceral (**Fm**) hyperalgesia (**M**)	**IndP**, **PI** and **vF**	Menthol (50 - 100 mg/kg; i.p.)	Pan R. et al., 2012
					Inflammatory (**Cap** or **CFA**) / Visceral (**AA**) hyperalgesia (**M**)	**AAACT**, **HP**, **TFT** and **vF**	(L)-Menthol (10 mg/kg; p.o.)	Liu B. et al., 2013
					Neuropathic (**SNL**) hyperalgesia (**R**)	**AT** and **vF**	Menthol (10 - 40 %; topical)	Patel R. et al., 2014
					Inflammatory (**CFA**) hyperalgesia (**R**)	**CF** and **PI**	Menthol (10 - 150 mg/kg; i.p.)	Hilfiger L. et al., 2021
Myrcene					Visceral (**AA**) hyperalgesia (**M**)	**AAACT** and **HP**	Myrcene (10 - 20 mg/kg; i.p. / 20 - 40 mg/kg s.c.)	Rao V.S.N. et al., 1990
					Inflammatory (**PGE2**) / Visceral (**AA**) hyperalgesia (**M** or **R**)	**AAACT** and **RST**	Myrcene (45 - 135 mg/kg; p.o.)	Lorenzetti B.B. et al., 1991

Myrtenol					Inflammatory (**Cap**) / Visceral (**AA**, **Fm** or **Glu**) hyperalgesia (**M**)	**AAACT**, **HP** and **IndP**	(-)-Myrtenol (75 mg/kg; i.p.)	Silva R.O. et al., 2014
Nerol					Visceral (oxazolone-induced colitis) hyperalgesia (**M**)	**vF**	Nerol (30 - 300 mg/kg; p.o.)	González-Ramírez A.E. et al., 2016
α-Pinene					Inflammatory (**Cap**) hyperalgesia (**R**)	**IndP**	α-Pinene (0.4 µg; i.lv.)	Rahbar I. et al., 2018
α-Phellandrene					Inflammatory (**Cap**) / Visceral (**AA**, **Fm** or **Glu**) hyperalgesia (**M**)	**AAACT**, **IndP** and **vF**	α-Phellandrene (25 -50 mg/kg; p.o.)	Lima D.F. et al., 2011
Pulegone					Visceral (**AA**) hyperalgesia (**M**)	**AAACT**	(+)-Pulegone (250 mg/kg; i.p.)	de Sousa D.P. et al., 2007
					Visceral (**Fm**) hyperalgesia (**M**)	**HP** and **IndP**	(+)-Pulegone (62.5 - 125 mg/kg; i.p.)	de Sousa D.P. et al., 2011
					Inflammatory (**CFA**) hyperalgesia (**R**)	**AT**, **CF** and **PI**	Pulegone (10 - 150 mg/kg; i.p.)	Hilfiger L. et al., 2021
Rotundifolone					Visceral (**AA**) hyperalgesia (**M**)	**AAACT**	Rotundifolone (250 mg/kg; i.p.)	de Sousa D.P. et al., 2007
γ-Terpinene					Inflammatory (**Cap**) / Visceral (**Fm** or **Glu**) hyperalgesia (**M**)	**IndP**	γ-Terpinene (12.5 - 50 mg/kg; p.o.)	Passos F.F. et al., 2015
α-Terpineol					Neuropathic (**CCI**) hyperalgesia (**R**)	**AT**, **PI** and **vF**	α-Terpineol (25 - 100 mg/kg; i.p.)	Soleimani M. et al., 2019
Thymol					Visceral (**AA**) hyperalgesia (**M**)	**AAACT** and **HP**	Thymol (100 mg/kg; p.o.)	Angeles-López G. et al., 2010

2.2.1.1. Anti-inflammatory effects

The study of the anti-inflammatory effects of monoterpenes generally starts with the investigation of the anti-inflammatory properties of an essential oil. Subsequently, researchers tried to isolate the major monoterpene, in order to study its properties alone. However, the mechanisms that support these properties are still little known. In comparison, the anti-inflammatory properties of monoterpenes have been well studied for the past two decades. Three major reviews cover almost all the work that has been done in this field. De Cássia da Silveira e Sá et *al.* and Guimarães et *al.* have both classified monoterpenes that present anti-inflammatory activity *in vitro* or/and *in vivo* (de Cássia da Silveira e Sá et al., 2013; Guimarães et al., 2013). In a more up-to-date review, Quintans et *al.* highlight the modulation of cytokines by monoterpenes (Quintans et al., 2019). In the following paragraph, we will summarize the most remarkable effects, mechanisms and properties that can be found in these reviews.

Different teams have proven that linalool *per os* (p.o.) (10 – 40 mg/kg) is able to reduce the level of pro-inflammatory cytokines, such as TNF-α, IL-1β or IL-6, in a context of induced inflammation. Furthermore, they show evidence that linalool modulates the regulatory pathways such as the NK-κB and the MAPK signalling pathways. Based on these results, the authors suggest that linalool modulates inflammation by playing a regulatory function in the pro- and anti-inflammatory cytokine pathways (Deepa and Venkatraman Anuradha, 2013; Li et al., 2014; Sabogal-Guáqueta et al., 2016). Similar results were observed with many other monoterpenes, such as carvacrol (Guimarães et al., 2012), citral (Shen et al., 2015), eucalyptol (1,8-cineole synonyme) (Greiner et al., 2013), geraniol (Medicherla et al., 2015) or limonene (d'Alessio et al., 2014; Rehman et al., 2014). Quintans et *al.* propose that carvacrol might block the activation of Toll-like receptors (TLR) signalling pathways. This would result in the decrease of the MAPK phosphorylation levels, and the inhibition of NK-κB, leading to a decrease of pro-inflammatory cytokines and chemokines, reducing inflammation *de facto*. This could be a shared property among different monoterpenes.

Inhibition of pro-inflammatory cytokines are the most extensively studied mechanisms for the anti-inflammatory effects of monoterpenes. However, there are also studies focusing on the up-regulation of anti-inflammatory cytokines. Lima et *al.* investigated the ability of carvacrol to stimulate the anti-inflammatory cytokine IL-10 and its implication in the anti-inflammatory effect of carvacrol using an IL-10 knockout

mice model (Lima et al., 2013a). Similar results were observed with other monoterpenes, such as borneol (Juhás et al., 2008), eucalyptol (Lima et al., 2013b) or menthol (Rozza et al., 2014). To summarize, not only can monoterpenes down-regulate the synthesis of pro-inflammatory cytokines, but they can also up-regulate the release of anti-inflammatory cytokines (**Figure 11**).

Other studies show the modulation of pro-inflammatory factors by monoterpenes through different pathways than the direct regulation of cytokines. Both Hotta et *al.* and Guimarães et *al.* demonstrated that carvacrol is a suppressor of the COX-2 enzyme expression (Hotta et al., 2010) and that it inhibits inducible nitric oxide synthase (iNOS), resulting in the blockage of NO release (Guimarães et al., 2012). Similar results were observed with other monoterpenes, such as citral (Lee et al., 2008; Katsukawa et al., 2010) or myrcene (Souza et al., 2003) (**Figure 11**) (for review; (de Cássia da Silveira e Sá et al., 2013; Guimarães et al., 2013; Quintans et al., 2019; Perri et al., 2020)).

In conclusion, almost all monoterpenes, regardless of their structure (acyclic, monocyclic or bicyclic), have anti-inflammatory properties through different mechanisms: by decreasing the synthesis of pro-inflammatory cytokines; by modulating pro-inflammatory factors; or by increasing the production of anti-inflammatory cytokines (**Figure 11**). This combination of actions seems to be shared by many monoterpenes, which may explain why essential oils have anti-inflammatory properties.

Moreover, interest in anti-inflammatory molecules against TNF-α or IL-6 have been on the rise over the last two decades, as promising treatments for numerous autoimmune diseases, including rheumatoid arthritis (Atzeni et al., 2005), and monoterpenes may be a major compound in these treatments.

Despite this recent trend, many monoterpenes, targets and mechanisms have yet to be studied. Anti-inflammatory properties are just the one side of the coin that is the effects of monoterpenes on inflammatory pain; the other side is the modulation of nociception.

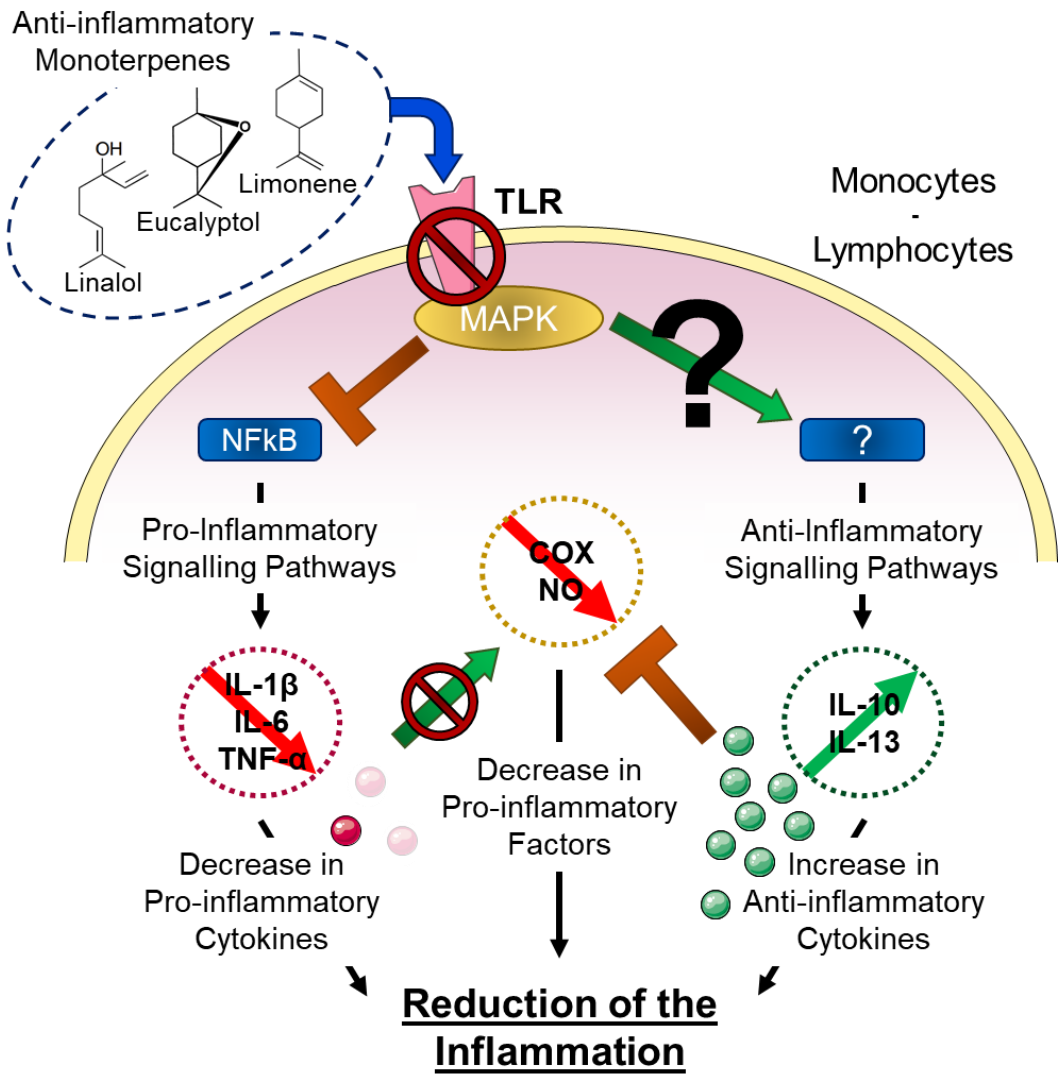

Figure 11: The effects of monoterpenes on inflammation.

Monoterpenes modulate inflammation through various mechanisms involving pro- and anti-inflammatory cytokines. "?" means that the mechanism is currently unknown, but we hypothesized that this could be a possible mechanism.

2.2.1.2. Anti-nociceptive effects

Modulation of nociception is the other side of the analgesic properties of monoterpenes on inflammatory pain (**Table 2**). These effects are mainly directed towards ion channel receptors, the effect of menthol on the TRPM8 being the most studied. The following section will thus be a "case study" of menthol, the most studied monoterpene. The purpose of this section is to describe a monoterpene with all its interactions with ion channel receptors. In order to extrapolate putative mechanisms to the other selected monoterpenes from the following tables (**Tables 3 & 4**).

Everyone experienced this at least once in its life: upon chewing a menthol-flavored gum, we start feeling a cool/cold sensation in the mouth. This is due to the non-noxious agonistic activation of the cold sensor, TRPM8, by menthol. TRPM8 is a protein receptor expressed at the sensory ending of the nerve cells of the tongue (taste papillae) (Abe et al., 2005). The activation of TRPM8 through menthol has been established in different models; for example *in vivo* using TRPM8 antagonists (Liu et al., 2013) (**Table 3**) or *in vitro* using specific the expression of TRPM8+ in HEK cell lines (HkC) (Behrendt et al., 2004; Takaishi et al., 2016) (**Table 4**). Xu et *al.* have recently studied the mechanism of TRPM8 binding and its activation by menthol (Xu et al., 2020). This activation of TRPM8 is an interesting mechanism in order to explain the analgesic properties of menthol, as TRPM8 activation has been shown to induce cold analgesia (Dhaka et al., 2007). One hypothesis from Proudfoot et *al.* suggests that the activation of TRPM8 sensory neurons exerts an inhibitory gate control by releasing glutamate, which then acts through the inhibitory metabotropic glutamate receptors (group II/III) in dorsal horn neurons, thus resulting in the inhibition of the nociceptive signal (Proudfoot et al., 2006).

Furthermore, menthol also has a biphasic effect on TRPA1, the latter receptor being capable of responding to noxious cold temperatures and functioning as a mechanical and chemical stress sensor (García-Añoveros and Nagata, 2007). This biphasic effect depends on menthol concentration. At lower concentrations, it activates the channel, whereas at higher concentrations, it blocks it (Macpherson et al., 2006; Liu et al., 2013; Luo et al., 2019) (**Table 4**). Perri et *al.* suggested in their review that after an initial activation, the channel might shift into an inactive state that can be reversed to the active state only after the wash-out of the agonist compounds (Perri et al., 2020). This could explain the burning, irritation and painful sensation sometimes induced by menthol, as reported in some studies (Eccles, 1994; Wasner, 2004). These effects could also be due to the TRPV3 activation by menthol (Macpherson et al., 2006; Sherkheli et al., 2009; Nguyen et al., 2021) (**Table 4**). As TRPV3 is the sensor of warm temperatures, this could also be an explanation. In addition, this receptor is known to be subject to sensitization and desensitization after prolonged signal exposure (Yang and Zhu, 2014), and could explain the initial warmth impression that quickly disappears after an application of mint balm. This has been shown with another monoterpene, camphor (Macpherson et al., 2006), which is known to be a strong TRPV3 agonist (**Table 4**). However, it is also more than probable that all these effects are the result of

co-activation phenomenon between TRPM8, TRPA1 and TRPV3. Although menthol is the most studied monoterpene, little is known about its action on TRPV1, the noxious warm temperature and acidic pH sensor (**Table 4**). Furthermore, the first study by Takaishi et *al.* showed that menthol inhibits TRPV1 and the second from Nguyen et al. observed that menthol activates TRPV1(Takaishi et al., 2016; Nguyen et al., 2021). In the current state of knowledge, it is impossible to conclude, but it is possible to propose, according to the bibliography, that menthol might have biphasic effect depending on the concentration, similarly to TRPA1 (**Table 4**).

Besides, it is important to take into account the agonistic action of menthol on $GABA_a$ R and, less investigated, on glycine receptor (Gly R) (**Table 4**). In the first study on the subject, Hall et *al.* found, with $GABA_a$ R and Gly R expressed in *Xenopus* oocytes, that menthol enhances GABA and glycine currents (Hall et al., 2004). Later Pan et *al.* show, on cultured DRG neurons, that at higher concentrations, menthol can also activate $GABA_a$ R itself (Pan et al., 2012). Activation (or facilitation) of the $GABA_a$ or Gly chloride channel in the DRG results in an inhibitory depolarization due to the high intracellular chloride concentration maintained through the active chloride transporters (Wilke et al., 2020). This depolarization leads to a decrease of transmitters release from afferent terminals by shunting inhibition (described by (Fatt and Katz, 1953)) or to the inactivation of voltage-gated Ca^{2+} and Na^{+} channels (Rudomin and Schmidt, 1999; Lidierth, 2006; Witschi et al., 2011). This leads to neural suppression of the nociceptive signal, and providing another possible mechanism for menthol-induced analgesia (Wilke et al., 2020).

Another group of receptors modulated by menthol is the nACh R and the 5-HT_3 R. They participate in a variety of physiological functions, such as the nociception and regulation of neuronal excitability (Lummis, 2012; Dineley et al., 2015). Menthol is mainly described as an inhibitor of these receptors (Ashoor et al., 2013; Walstab et al., 2014; Ton et al., 2015). However, a recent study highlights menthol as a positive allosteric modulator in *Xenopus* oocytes that express nematode nACh R (Choudhary et al., 2019) (**Table 4**).

The last known direct targets of menthol are ion channels: Ca^{2+} channel, Na^{+} channel and K^{+} channel families (**Table 4**). Menthol appears to block Ca^{2+} and Na^{+} voltage gated channels (Pan et al., 2012), on the other hand, Arazi et *al.* show that menthol activates a K^{+} channel (Arazi et al., 2020). Despite the fact that these channels play an essential role in each neuron and the knowledge that some local anaesthetic

drugs block Na^+ channels, it is still unclear how modulation of these channels by monoterpenes can play a role in analgesia, other than by a local modulation of neurons.

Finally, the last target is the opioid system. Although it is not a direct target, it plays an important role in the *in vivo* analgesic effect. Galeotti et *al.* investigated the involvement of the opioid system in the menthol-induced analgesia, by reversing the analgesic effect with naloxone (unselective opioid antagonist) (Galeotti et al., 2002) (**Table 3**).

To sum-up the last section, menthol has the ability to modulate many different ion channels, allowing it to induce analgesia using different types of targets and pathways (**Figure 12**) (for review; (Guimarães et al., 2013; Oz et al., 2015, 2017; Perri et al., 2020)). Finally, it is the most studied molecule, out of the 31 monoterpenes (number of different monoterpenes in the **Tables 2, 3 & 4**). It is thus important to study the pharmacology of other monoterpenes as they have many targets and their therapeutic applications (especially analgesia) are really interesting compared to their production cost.

All the information presented in the last section are classified within the two following tables (**Table 3 & 4**). These tables are an exhaustive compilation of studies on the molecular and neuronal targets of monoterpenes. The aim of these tables is to report all monoterpene targets (ion channel, receptor and system) and how they are modulated by the corresponding molecules. **Table 3** focuses on *in vivo* studies to show the *in vivo* effect of monoterpenes on their targets, while **Table 4** focuses on *ex vivo* and *in vitro* studies.

Table 3: Monoterpenes *in vivo* targets.

Inventory of the *in vivo* effects induced by monoterpenes and their targets. The green tick indicates that the target has been pharmacologically modulated by an agonist or/and an antagonist in the study. References are listed in the **Annex 2**.

Abbreviation Models : **AA** = Acetic acid; **Fm** = Formaline; **Glu** = gluamate; **Cap** = Capsaicin; **CCI** = Chronic constriction injury; **CFA** = Complete Freund adjuvant; **Car** = Carrageenan; **LPS** = Lipopolysaccharide; **PGE2** = Prostaglandin E2; **TNF-α** = Tumor necrosis factor alpha; **Zy** = zymosan; **SNL** = Spinal nerve ligation ; **M** = Mice; **R** = Rats

Abbreviation Methods : **AAACT** = Acetic acid abdominal constriction test; **AT** = Acetone test; **CP** = Cold plate; **CPP** = Conditioned place preference; **ECG** = Electrocardiogram; **EEG** = Electroencephalogram; **EMG** = Electromyogram; **EvF** = Electronic von Frey; **EPM** = Elevated plus maze; **HP** = Hot plate; **IndP** = Induce pain; **OF** = Open field; **PI** = Plantar; **PIT** = Paw immersion test; **TFT** = Tail flick test; **TST** = Tail suspension test; **vF** = von Frey

Terpenes	Targets	Effects	Doses	Pharmacological validation	Models	Methods	Reference
Borneol	**TRPM8**	**Analgesia**	(+)-Borneol (15 %; topical)	✓	Inflammatory (**Cap** or **CFA**) / Visceral (**Fm**) hyperalgesia (TRPM8-/-(**M**))	**CP**, **HP**, **IndP** and **vF**	Wang S. et al., 2017
	$GABA_a$ R	**Analgesia**	(+)-Borneol (125 - 500 mg/kg; p.o. / 15 - 60 µg; i.t.)	✓	Inflammatory (**CFA**) / Neuropathic (**SNL**) hyperalgesia (**M**)	**vF**	Jiang J. et al., 2015
Citral	**TRPV1**	**Analgesia**	Citral (100 mg/kg; i.g.)		Neuropathic (**SNL**) / Visceral (**AA**, **Fm** or **Glu**) hyperalgesia (**M**)	**IndP** and **vF**	Nishijima C.M. et al., 2014
		Hyperalgesia	Citral (100 mg/kg; i.g.)		Inflammatory (**Cap**) hyperalgesia (**M**)	**IndP** and **vF**	Nishijima C.M. et al., 2014
	Monoamine system	**Analgesia**	Citral (100 mg/kg; i.g.)	✓	Neuropathic (**SNL**) / Visceral (**AA**, **Fm** or **Glu**) hyperalgesia (**M**)	**IndP** and **vF**	Nishijima C.M. et al., 2014
		Hyperalgesia	Citral (100 mg/kg; i.g.)	✓	Inflammatory (**Cap**) hyperalgesia (**M**)	**IndP** and **vF**	Nishijima C.M. et al., 2014
	CB_2 R	**Analgesia**	Citral (50 - 300 mg/kg; i.p.)	✓	Inflammatory (**Car**, **LPS** or **Zy**) hyperalgesia (**M**)	**IndP** and **PIT**	Gonçalves E.C.D. et al., 2020
	K^+ channel	**Analgesia**	Citral (50 - 300 mg/kg; i.p.)	✓	Inflammatory (**Car**, **LPS** or **Zy**) hyperalgesia (**M**)	**IndP** and **PIT**	Gonçalves E.C.D. et al., 2020
Citronellal	**K^+ channel**	**Analgesia**	Citronellal (25 - 100 mg/kg; i.p.)	✓	Inflammatory (**Car**, **PGE2** or **TNF-α**) hyperalgesia (**M**)	**vF**	de Santana M.T. et al., 2013
	NO pathways	**Analgesia**	Citronellal (25 - 100 mg/kg; i.p.)	✓	Inflammatory (**Car**, **PGE2** or **TNF-α**) hyperalgesia (**M**)	**vF**	de Santana M.T. et al., 2013
Cuminaldehyde	**Opioid system**	**Analgesia**	Cuminaldehyde (12.5 - 200 mg/kg i.p.)	✓	Neuropathic (**CCI**) / Visceral (**AA** or **Fm**) hyperalgesia (**M** or **R**)	**AT**, **IndP**, **HP**, **PI** and **vF**	Koohsari S. et al., 2020
	NO pathways	**Analgesia**	Cuminaldehyde (12.5 - 200 mg/kg i.p.)	✓	Neuropathic (**CCI**) / Visceral (**AA** or **Fm**) hyperalgesia (**M** or **R**)	**AT**, **IndP**, **HP**, **PI** and **vF**	Koohsari S. et al., 2020

p-Cymene	**Opioid system**	**Analgesia**	p-Cymene (25 - 100 mg/kg; i.p.)	✓	Inflammatory (**Car**, **PGE2** or **TNF-α**) hyperalgesia (**M**)	**EvF** and **TFT**	de Santana M.F. et al., 2015
Eucalyptol/ 1.8-Cineole	**TRPM8**	**Analgesia**	Eucalyptol (200 mg/kg; p.o.)	✓	Inflammatory (**Cap** or **CFA**) / Visceral (**AA**) hyperalgesia (TRPM8-/-(**M**))	**AAACT**, **HP**, **TFT** and **vF**	Liu B. et al., 2013
	Opioid system	**Analgesia**	Eucalyptol (0.3 mg/kg; i.p.)	✓	(**M** or **R**)	**HP** and **TFT**	Liapi C. et al., 2007
Hydroxy-citronellal	**GABAa R**	**Anxiolytic**	Hydroxycitronellal (12.5 - 50 mg/kg; i.p.)	✓	(**M**)	**EPM** and **OF**	Andrade J.C. et al., 2021
Limonene	**TRPA1**	**Analgesia / Hyperalgesia**	Limonene (5 µM; i.itp.)		Inflammatory / Visceral (H_2O_2) hyperalgesia (TRPA1-/-(**M**))	**IndP**	Kaimoto T. et al., 2016
	Opioid system	**Analgesia**	Limonene (75 mg/kg; i.p.)	✓	Visceral (**AA** and **Fm**) hyperalgesia (**M**)	**HP** and **IndP**	de Almeida A.A. et al., 2017
Linalool	**Monoamine system**	**Analgesia**	(-)-Linalool (100 - 150 mg/kg; s.c.)	✓	Visceral (**Fm**) hyperalgesia (**M**)	**HP** and **IndP**	Peana A.T. et al., 2003
	Opioid system	**Analgesia**	(-)-Linalool (100 - 150 mg/kg; s.c.)	✓	Visceral (**Fm**) hyperalgesia (**M**)	**HP** and **IndP**	Peana A.T. et al., 2003
		Analgesia	(±)-Linalool (5 µg; i.p.)	✓	Visceral (**Fm**) hyperalgesia (**M**)	**IndP**	Katsuyama S. et al., 2015
Menthol	**TRPM8**	**Analgesia**	(L)-Menthol (10 mg/kg; p.o.)	✓	Inflammatory (**Cap** or **CFA**) / Visceral (**AA**) hyperalgesia (TRPM8-/-(**M**))	**AAACT**, **HP**, **TFT** and **vF**	Liu B. et al., 2013
		Analgesia	Menthol (10 - 40 %; topical)		Neuropathic (**SNL**) hyperalgesia (**R**)	**AT** and **vF**	Patel R. et al., 2014
	Opioid system	**Analgesia**	(-) Menthol (10 mg/kg; p.o. / 10 µg i.c.v.)	✓	Visceral (**AA**) hyperalgesia (**M**)	**AAACT** and **HP**	Galeotti N. et al., 2002
Myrcene	**Opioid system**	**Analgesia**	Myrcene (10 - 20 mg/kg; i.p. / 20 - 40 mg/kg s.c.)	✓	Visceral (**AA**) hyperalgesia (**M**)	**AAACT** and **HP**	Rao V.S.N. et al., 1990
α-Pinene	**$GABA_a$ R**	**↗ sleep duration / Alter sleep waves**	(-)-α-Pinene (100 mg/kg; i.p.)		Induce sleep (**M**)	**EEG** and **EMG**	Yang H. et al., 2016
		Analgesia	α-Pinene (0.4 µg; i.lv.)	✓	Inflammatory (**Cap**) hyperalgesia (**R**)	**IndP**	Rahbar I. et al., 2018

	Opioid system	**Analgesia**	α-Pinene (0.4 µg; i.lv.)	✓	Inflammatory (**Cap**) hyperalgesia (**R**)	**IndP**	Rahbar I. et al., 2018
α-Phellandrene	**Cholinergic system**	**Analgesia**	α-Phellandrene (25 - 50 mg/kg; p.o.)	✓	Inflammatory (**Cap**) / Visceral (**AA**, **Fm** or **Glu**) hyperalgesia (**M**)	**AAACT**, **IndP** and **vF**	Lima D.F. et al., 2011
	Monoamine system	**Analgesia**	α-Phellandrene (25 - 50 mg/kg; p.o.)	✓	Inflammatory (**Cap**) / Visceral (**AA**, **Fm** or **Glu**) hyperalgesia (**M**)	**AAACT**, **IndP** and **vF**	Lima D.F. et al., 2011
	K^+ channel	**Analgesia**	α-Phellandrene (25 - 50 mg/kg; p.o.)	✓	Inflammatory (**Cap**) / Visceral (**AA**, **Fm** or **Glu**) hyperalgesia (**M**)	**AAACT**, **IndP** and **vF**	Lima D.F. et al., 2011
	Opioid system	**Analgesia**	α-Phellandrene (25 - 50 mg/kg; p.o.)	✓	Inflammatory (**Cap**) / Visceral (**AA**, **Fm** or **Glu**) hyperalgesia (**M**)	**AAACT**, **IndP** and **vF**	Lima D.F. et al., 2011
	NO pathways	**Analgesia**	α-Phellandrene (25 - 50 mg/kg; p.o.)	✓	Inflammatory (**Cap**) / Visceral (**AA**, **Fm** or **Glu**) hyperalgesia (**M**)	**AAACT**, **IndP** and **vF**	Lima D.F. et al., 2011
Pulegone	**Ca^{2+} channel**	**↗ ambulatory activity**	(+)-Pulegone (400 mg/kg; i.p.)	✓	(**M**)	**CPP**, **EPM**, grasping test, **OF** and rotarod	da Silveira N.S.S. et al., 2014
	K^+ channel	**↘ heart beat**	Pulegone (100 mg/kg; i.j.)		(**R**)	**ECG**	Santos-Miranda A. et al., 2014
γ-Terpinene	**Cholinergic system**	**Analgesia**	γ-Terpinene (25 - 50 mg/kg; p.o.)	✓	Inflammatory (**Cap**) / Visceral (**Fm** or **Glu**) hyperalgesia (**M**)	**IndP**	Passos F.F. et al., 2015
	K^+ channel	**Analgesia**	γ-Terpinene (25 - 50 mg/kg; p.o.)	✓	Inflammatory (**Cap**) / Visceral (**Fm** or **Glu**) hyperalgesia (**M**)	**IndP**	Passos F.F. et al., 2015
	Opioid system	**Analgesia**	γ-Terpinene (25 - 50 mg/kg; p.o.)	✓	Inflammatory (**Cap**) / Visceral (**Fm** or **Glu**) hyperalgesia (**M**)	**IndP**	Passos F.F. et al., 2015
Terpineol	**Monoamine system**	**↘ depressive like behaviors**	Terpineol (200 mg/kg p.o. / 100 mg/kg i.p.)	✓	Induce depressive behavirour (**M**)	Splash test and **TST**	Vieira G. et al., 2020
	Opioid system	**↘ depressive like behaviors**	Terpineol (200 mg/kg p.o. / 100 mg/kg i.p.)	✓	Induce depressive behavirour (**M**)	Splash test and **TST**	Vieira G. et al., 2020
Thymol	**$GABA_a$ R**	**Sedation / Anesthesia**	Thymol (25 - 100 mg/L in water tank)	✓	(Silver catfish)	Sedation scoring	Bianchini A.E. et al., 2017

The next section summarizes the action of monoterpenes on their targets (**Figure 12**) (see **Tables 3 & 4** for references).

a. TRP family; The TRP family (related to TRPM8, TRPA1, TRPVx) is the most studied group of targets in **Table 4** and, by extension, includes almost all the monoterpenes from **Tables 3 & 4**. Moreover, they generally have an agonist/activator effect on them. **Table 3:** Borneol, Citral, Eucalyptol, Limonene, Menthol. **Table 4:** Borneol, Camphor, Carvacrol, Carveol, Dihydro-Carveol, Carvone, 1,4-Cineole, Citral, Citronellol, Cuminaldehyde, Eucalyptol, Geraniol, Limonene, Linalool, Menthol, Myrcene, Nerol, Pulegone, Thymol.

b. $GABA_a$ R, Gly R; Receptors of the major inhibitory neurotransmitters are mostly activated by monoterpenes, but not by all of them (**Table 4**). This could be a lead to evaluate the most potent monoterpenes to induce analgesia. **Table 3:** Borneol, Hydroxy-citronellal, α-Pinene, Thymol. **Table 4:** Borneol, Carvacrol, Menthol, α-Pinene, α-Thujone, Thymol.

c. nACh R, Cholinergic system; All monoterpenes that have been shown to interact with nACh R have inhibitor effects towards it (**Table 4**). Furthermore, the cholinergic system *in vivo* is involved in monoterpene-induced analgesia (**Table 3**). **Table 3:** α-Phellandrene, γ-Terpinene. **Table 4:** Borneol, Camphor, Carvacrol, Carvone, Citronellol, Limonene, Linalool, Menthol, Pulegone.

d. $5\text{-}HT_3$ R, Monoamine system; A majority of monoterpene are found to have inhibitory effects on $5\text{-}HT_3$ R, with the notable exception of carvacrol and thymol which have activator effects (**Table 4**). **Table 3:** Citral, Linalool, α-Phellandrene, Terpineol. **Table 4:** Carvacrol, Citral, Eucalyptol, Linalool, Menthol, α-Thujone, Thymol.

e. Ca^{2+}, Na^+ and K^+ channels; There is a significant variability in the results of this group, for the same channel and the same monoterpenes will be described with different outcomes from one study to another change (**Table 4**). However, monoterpenes still modulate these channels. **Table 4:** Carvacrol, Carveol, Carvone, Citral, Citronellol, p-Cymene, Geraniol, Linalool, Menthol, Nerol, Pulegone, Thymol.

f. Opioid system; As shown previously, the opioid system appears to be only an intermediary in the *in vivo* effects of monoterpenes, especially for induced analgesia (**Table 3**). However, some studies show that for some monoterpenes (e.g., geraniol), naloxone or any other opioid antagonist did not antagonize induced analgesia (La Rocca et al., 2017). Thus, it is possible that not all monoterpenes recruit this system. **Table 3:** Cuminaldehyde, p-Cymene, Eucalyptol, Limonene, Linalool, Menthol, Myrcene, α-Pinene, α-Phellandrene, γ-Terpinene, Terpineol.

g. NO pathways; As mentioned in section *3.2.1.1. Anti-inflammatory effects* many monoterpenes are known to modulate iNOs and by extension NO pathways, leading to *in vivo* analgesia (**Table 3**). **Table 3:** Citronellal, Cuminaldehyde, α-Phellandrene.

Some studies have also attempted to examine the effect of monoterpenes on the cannabinoid system, and a single study shows direct or indirect *in vivo* implication of CB_2 receptor in the citral induce analgesia (Gonçalves et al., 2020) (**Table 3**). Moreover, Santiago et *al.* determined in an *in vitro* study that 6 different monoterpenes were not agonists of CB_1 and CB_2 receptors (Santiago et al., 2019).

Important notes related to the tables: It is important to emphasize that monoterpenes are used and are effective at higher concentrations/doses than for more conventional compounds (such as morphine). For example, the concentration range of monoterpenes used in *ex vivo* and *in vitro* studies for the TRP receptors is usually between 0.3 and 3 mM (**Table 4**). Moreover, in *in vivo* studies, monoterpenes are generally injected i.p. between 50 and 200 mg/kg and at this concentration range they induce nociception in all the different sensory modalities (mechanical, visceral, thermal hot and cold) (**Tables 2 & 3**). Taken together these observations define a recommended dose-framework in order to investigate the effect of new monoterpenes on pain behaviours.

Table 4: Monoterpenes *ex vivo* and *in vitro* targets.

Inventory of molecular targets of monoterpenes and how they modulate them in *ex vivo* and *in vitro* studies. The first green tick indicates that the study used a model with a genetic modification that allows the target to be expressed and/or not expressed. The second green tick indicates that the target has been pharmacologically modulated by an agonist or/and an antagonist in the study. References are listed in the **Annex 3**.

Abbreviation Models : **C** = Cells; ch = Chiken; **CHO** = Chinese hamster ovary cells; DRG = Dorsal root ganglion; **HkC** = Hek cells; h = Human; m = Mice; **N** = Neurons; **Ooc** = Oocytes (Xenopus); PAG = Periaqueductal gray; r = Rat; **S** = Slices

Abbreviation Methods : **CaI** = Ca^{2+} imaging; **ClI** = Cl^- influx test; **ECG** = Electrocardiogram; **MeR** = Microelectrode recordings; **PC** = Patch-clamp

Terpenes	Targets	Activity	Concentrations	Models	Genetic validation	Methods	Pharmacological validation	Reference
Borneol	**TRPM8**	+	(+)-Borneol (0.1 - 1 mM)	**HkC** ((h)TRPM8+)	✓	**CaI** and **PC** *in vitro*	✓	Wang S. et al., 2017
	TRPA1	−	(±)-Borneol (1 mM)	**HkC** (TRPA1+)	✓	**CaI** and **PC** *in vitro*	✓	Takaishi M. et al., 2014
	TRPV3	+	(±)-Borneol (2 mM)	**HkC** or **Ooc** (TRPV3+)	✓	**PC** *in vitro*	✓	Vogt-Eisele A.K. et al., 2007
	$GABA_a$ R	+	(-)-Borneol (100 - 300 µM)	**Ooc** (GABAa R+)	✓	**PC** *in vitro*	✓	Hall A.C. et al., 2004
		+	(-)-Borneol (0.1 - 1 mM)	**Ooc** ((h)GABAa R+)	✓	**PC** *in vitro*	✓	Granger R.E. et al., 2005
		+	Borneol (0.2 - 0.3 mM)	Substantia gelatinosa **N** from trigeminal subnucleus caudalis **S** (m)		**PC** *ex-vivo*	✓	Nguyen P.T.T. et al., 2020
	Gly R	+	Borneol (0.3 mM)	Substantia gelatinosa **N** from trigeminal subnucleus caudalis **S** (m)		**PC** *ex-vivo*	✓	Nguyen P.T.T. et al., 2020
	nACh R	−	(-)-Borneol (100 µM)	Chromaffin **C**		**CaI** *in vitro*	✓	Park T.J. et al., 2003
Camphor	**TRPM8**	+	(+)-Camphor (2 mM)	**HkC** or **Ooc** (TRPM8+)	✓	**PC** *in vitro*	✓	Vogt-Eisele A.K. et al., 2007
		+	Camphor (1 - 10 mM)	**HkC** ((h or r)TRPA1+)	✓	**CaI** and **PC** *in vitro*	✓	Selescu T. et al., 2013
	TRPA1	−	(±)-Camphor (10 mM)	**HkC** ((m)TRPA1+)	✓	**CaI** and **PC** *in vitro*	✓	Xu H. et al., 2005
		−	Camphor (68 µM)	**CHO** ((m)TRPA1+)	✓	**CaI** and **PC** *in vitro*		Macpherson L.J. et al., 2006
		−	Camphor (1 mM)	**HkC** ((h)TRPA1+)	✓	**CaI** and **PC** *in vitro*	✓	Takaishi M. et al., 2014
	TRPV1	+	(±)-Camphor (3 mM)	**HkC** ((m)TRPV1+) / DRG **N** (r)	✓	**CaI** and **PC** *in vitro*		Xu H. et al., 2005
		+	Camphor (4.5 mM)	**CHO** ((m)TRPA1+)	✓	**CaI** and **PC** *in vitro*		Macpherson L.J. et al., 2006
		+	Camphor (10 mM)	**HkC** ((r)TRPV1+)	✓	**PC** *in vitro*		Nguyen T.H.D. et al., 2021
	TRPV3	+	(±)-Camphor (10 mM)	**HkC** ((m)TRPV3+)	✓	**CaI** and **PC** *in vitro*		Xu H. et al., 2005

		+	Camphor (5 mM)	Primary keratinocyte / DRG **N** (WT or TRPV3-/- (m))	✓	**PC** *in vitro*		Moqrich A. et al., 2005
		+	Camphor (40 mM)	**CHO** (TRPV3+)	✓	**Cal** and **PC** *in vitro*		Macpherson L.J. et al., 2006
		+	Camphor (2 mM)	**HkC** or **Ooc** (TRPV3+)	✓	**PC** *in vitro*		Vogt-Eisele A.K. et al., 2007
		+	Camphor (10 mM)	**Ooc** (TRPV3+)	✓	**PC** *in vitro*		Sherkheli M.A. et al., 2009
		+	Camphor (10 mM)	**HkC** ((m)TRPV3+)	✓	**PC** *in vitro*		Nguyen T.H.D. et al., 2021
	$GABA_a$ R	+	(±)-Camphor (300 µM)	**Ooc** (GABAa R+)	✓	**PC** *in vitro*	✓	Hall A.C. et al., 2004
		+	Camphor (0.3 - 1 mM)	**Ooc** ((h)GABAa R+)	✓	**PC** *in vitro*	✓	Granger R.E. et al., 2005
	nACh R	−	Camphor (100 µM)	Chromaffin **C**		**Cal** *in vitro*	✓	Park T.J. et al., 2001
Carvacrol	**TRPA1**	+	Carvacrol (250 µM)	**HkC** ((h or m)TRPA1+)	✓	**Cal** and **PC** *in vitro*		Xu H. et al., 2006
		+	Carvacrol (500 µM)	**HkC** (TRPA1+)	✓	**Cal** *in vitro*		Lee S.P. et al., 2008
		+	Carvacrol (0.1 - 1.5 mM)	Lamina I and III **N** from spinal cord **S** (r)		**PC** *ex-vivo*	✓	Luo Q.T. et al., 2014
		+	Carvacrol (50 - 150 µM)	**HkC** ((h or r)TRPA1+)	✓	**Cal** *in vitro*	✓	Ghosh M. et al., 2020
	TRPV3	+	Carvacrol (500 µM)	**HkC** ((h or m)TRPV3+)	✓	**Cal** and **PC** *in vitro*		Xu H. et al., 2006
		+	Carvacrol (2 mM)	**HkC** or **Ooc** (TRPV3+)	✓	**PC** *in vitro*	✓	Vogt-Eisele A.K. et al., 2007
	TRPM7	−	Carvacrol (0.1 - 1 mM)	**HkC** (TRPM7+)	✓	**PC** *in vitro*	✓	Parnas M. et al., 2009
	$GABA_a$ R	+	Carvacrol (500 µM)	Primary cortical **N** (m)		**CII** *in vitro*	✓	Reiner G.N. et al., 2013
	nACh R	−	Carvacrol (0.1 - 1 mM)	**Ooc** ((nematode) nACh R+)	✓	**PC** *in vitro*		Choudhary S. et al., 2019
	$5\text{-}HT_3$ R	+	Carvacrol (100 µM)	**Ooc** ((h)$5\text{-}HT_3$ R+)	✓	**PC** *in vitro*	✓	Lansdell S.J. et al., 2014
	Ca^{2+} channel	−	Carvacrol (0.1 - 1 mM)	Ventricular cardiomyocytes		**PC** *in vitro*		Magyar J. et al., 2004
		+/−	Carvacrol (100 - 300 µM)	Heart (rabbit) / ventricle (h)		**ECG** and **MeR** *ex vivo*		Almanaitytė M. et al 2020

	Na^+ channel	−	Carvacrol (10 mM)	De-sheathed sciatic nerves (r)		**MeR** *ex vivo*		Gonçalves J.C. et al., 2010
		+/−	Carvacrol (0.6 - 1 mM)	DRG **N** (r)		**PC** *in vitro*		Joca H.C. et al., 2012
		+/−	Carvacrol (100 - 300 µM)	Heart (rabbit) / ventricle (h)		**ECG** and **MeR** *ex vivo*		Almanaitytė M. et al 2020
	K^+ channel	+	Carvacrol (300 µM)	**Ooc** (K2p leak channel+)	✓	**PC** *in vitro*	✓	Arazi E. et al., 2020
Carveol	**TRPV3**	+	(-)-Carveol (2 mM)	**HkC** or **Ooc** (TRPV3+)	✓	**PC** *in vitro*	✓	Vogt-Eisele A.K. et al., 2007
	Na^+ channel	−	Carveol (10 mM)	De-sheathed sciatic nerves (r)		**MeR** *ex vivo*		Gonçalves J.C. et al., 2010
Dihydro-Carveol	**TRPM8**	+	Dihydro-Carveol (2 mM)	**HkC** or **Ooc** (TRPM8+)	✓	**PC** *in vitro*		Vogt-Eisele A.K. et al., 2007
	TRPV3	+	Dihydro-Carveol (2 mM)	**HkC** or **Ooc** (TRPV3+)	✓	**PC** *in vitro*	✓	Vogt-Eisele A.K. et al., 2007
Carvone	**TRPV1**	+	(-)-Carvone (1 - 10 mM)	**HkC** ((m)TRPV1+) / DRG **N** (r)	✓	**Cal** *in vitro*	✓	Gonçalves J.C. et al., 2013
	nACh R	−	(-)-Carvone (100 µM)	**Ooc** ((nematode) nACh R+)	✓	**PC** *in vitro*		Choudhary S. et al., 2019
	Na^+ channel	−	Carvone (10 mM)	De-sheathed sciatic nerves (r)		**MeR** *ex vivo*		Gonçalves J.C. et al., 2010
	K^+ channel	+	β-Citronellol (300 µM)	**Ooc** (K2p leak channel+)	✓	**PC** *in vitro*	✓	Arazi E. et al., 2020
1,4-Cineole	**TRPM8**	+	1,4-Cineole (5 mM)	**HkC** ((h)TRPM8+)	✓	**Cal** and **PC** *in vitro*		Takaishi M. et al., 2012
	TRPA1	+	1,4-Cineole (5 mM)	**HkC** ((h)TRPV1+)	✓	**Cal** and **PC** *in vitro*		Takaishi M. et al., 2012
Citral	**TRPM8**	+/−	Citral (300 µM)	**HkC** ((r)TRPM8+)	✓	**Cal** and **PC** *in vitro*	✓	Stotz S.C. et al., 2008
	TRPA1	+/−	Citral (300 µM)	**HkC** ((r)TRPA1+)	✓	**Cal** and **PC** *in vitro*	✓	Stotz S.C. et al., 2008
	TRPV1	+/−	Citral (1 mM)	**HkC** ((r)TRPV1+)	✓	**Cal** and **PC** *in vitro*	✓	Stotz S.C. et al., 2008
	TRPV2	−	Citral (1 mM)	**HkC** ((r)TRPV2+)	✓	**Cal** and **PC** *in vitro*	✓	Stotz S.C. et al., 2008
	TRPV3	+/−	Citral (1 mM)	**HkC** ((m)TRPV3+)	✓	**Cal** and **PC** *in vitro*	✓	Stotz S.C. et al., 2008
	TRPV4	−	Citral (1 mM)	**HkC** ((m)TRPV4+)	✓	**Cal** and **PC** *in vitro*		Stotz S.C. et al., 2008

	5-HT$_3$ R	−	Citral (200 - 500 µM)	**Ooc** (5-HT$_3$ R+)	✓	**PC** *in vitro*	✓	Jarvis G.E. et al., 2016
	K$^+$ channel	−	Citral (1 mM)	**HkC** ((m)Kv channel+)	✓	**PC** *in vitro*		Ye C-J. et al., 2019
Citronellol/ β-Citronellol	**TRPA1**	+	Citronellol (200 µM)	**HkC** ((r)TRPA1+)	✓	**Cal** *in vitro*		Ortar G. et al., 2014
	nACh R	−	(-)-β-Citronellol (100 µM)	**Ooc** ((nematode) nACh R+)	✓	**PC** *in vitro*		Choudhary S. et al., 2019
	K$^+$ channel	−	β-Citronellol (1 mM)	**HkC** ((m)Kv channel+)	✓	**PC** *in vitro*		Ye C-J. et al., 2019
		+	β-Citronellol (300 µM)	**Ooc** (K2p leak channel+)	✓	**PC** *in vitro*	✓	Arazi E. et al., 2020
Cuminaldehyde	**TRPA1**	+	Cuminaldehyde (0.3 - 5 mM)	**CHO** (TRPA1+)	✓	**Cal** and **PC** *in vitro*	✓	Legrand C. et al., 2020
p-Cymene	**K$^+$ channel**	+	p-Cymene (300 µM)	**Ooc** (K2p leak channel+)	✓	**PC** *in vitro*	✓	Arazi E. et al., 2020
Eucalyptol/ 1,8-Cineole	**TRPM8**	+	Eucalyptol (5 mM)	**HkC** (TRPM8+)	✓	**Cal** *in vitro*		Behrendt H.J. et al., 2004
		+	1,8-Cineole (5 mM)	**HkC** ((h)TRPM8+)	✓	**Cal** and **PC** *in vitro*		Takaishi M. et al., 2012
	TRPA1	−	1,8-Cineole (2 - 15 mM)	**HkC** ((h)TRPA1+)	✓	**Cal** and **PC** *in vitro*	✓	Takaishi M. et al., 2012
		−	1,8-Cineole (1 mM)	**HkC** ((h)TRPA1+)	✓	**Cal** and **PC** *in vitro*	✓	Takaishi M. et al., 2014
	TRPV3	+	1,8-Cineole (10 mM)	**Ooc** (TRPV3+)	✓	**PC** *in vitro*		Sherkheli M.A. et al., 2009
	5-HT$_3$ R	−	(±)-Eucalyptol (100 µM)	**Ooc** ((h)5-HT$_3$ R+)	✓	**PC** *in vitro*	✓	Ashoor A. et al., 2013
		−	Eucalyptol (0.5 - 2 mM)	**Ooc** (5-HT$_3$ R+)	✓	**PC** *in vitro*	✓	Jarvis G.E. et al., 2016
Geraniol	**TRPM8**	+	Geraniol (5 mM)	**HkC** (TRPM8+)	✓	**Cal** *in vitro*		Behrendt H.J. et al., 2004
	TRPA1	+/−	Geraniol (300 µM)	**HkC** ((r)TRPM8+)	✓	**Cal** and **PC** *in vitro*	✓	Stotz S.C. et al., 2008
	TRPV1	−	Geraniol (1 mM)	**HkC** ((r)TRPV1+)	✓	**Cal** and **PC** *in vitro*	✓	Stotz S.C. et al., 2008
	Ca^{2+} channel	−	Geraniol (300 µM)	Dissociated cardiomyocytes **C** (m)		**PC** *ex-vivo*		de Menezes-Filho J.E. et al., 2014
	K$^+$ channel	−	Geraniol (300 µM)	Dissociated cardiomyocytes **C** (m)		**PC** *ex-vivo*		de Menezes-Filho J.E. et al., 2014

		−	Geraniol (1 mM)	**HkC** ((m)Kv channel+)	✓	**PC** *in vitro*		Ye C-J. et al., 2019
		+	Geraniol (300 µM)	**Ooc** (K2p leak channel+)	✓	**PC** *in vitro*	✓	Arazi E. et al., 2020
Limonene	**TRPA1**	+	(±)-Limonene (1 mM)	**HkC** ((m)TRPV1+) / primary DRG **N** (TRPA1-/-(m))	✓	**Cal** *in vitro*	✓	Kaimoto T. et al., 2016
	nACh R	−	(+)-Limonene (100 µM)	**Ooc** ((nematode) nACh R+)	✓	**PC** *in vitro*		Choudhary S. et al., 2019
Linalool	**TRPM8**	+	Linalool (5 mM)	**HkC** (TRPM8+)	✓	**Cal** *in vitro*		Behrendt H.J. et al., 2004
	$GABA_a$ R	−	Linalool (0.025 - 1 mM)	WSS-1 **C** (GABAa R+(r))	✓	**PC** *in vitro*	✓	Li A.S. et al., 2020
	nACh R	−	Linalool (20 - 80 µg/mL)	Neuromuscular junction of hemidiaphragm (m)		Loose **PC** *ex-vivo*	✓	Re L. et al., 2000
		−	Linalool (0.025 - 1 mM)	WSS-1 **C** (nACh R+(r))	✓	**PC** *in vitro*	✓	Li A.S. et al., 2020
	$5\text{-}HT_3$ R	−	Linalool (200 - 500 µM)	**Ooc** ($5\text{-}HT_3$ R+)	✓	**PC** *in vitro*	✓	Jarvis G.E. et al., 2016
	Ca^{2+} channel	+	Linalool (0.4 mM)	Isolated subesophageal ganglia **N** (land snail)		**PC** *ex-vivo*	✓	Vatanparast J. et al., 2017
	Na^+ channel	−	Linalool (0.3 - 2 mM)	Dissociated DRG **N** (r)		**PC** *ex-vivo*	✓	Leal-Cardoso J.H. et al., 2010
		+/−	Linalool (0.1 mM)	Isolated subesophageal ganglia **N** (land snail)		**PC** *ex-vivo*		Vatanparast J. et al., 2017
	K^+ channel	−	Linalool (1 mM)	**HkC** ((m)Kv channel+)	✓	**PC** *in vitro*		Ye C-J. et al., 2019
Menthol	**TRPM8**	+	(±)-Menthol (10 - 100 µM)	**CHO** (TRPM8+)	✓	**PC** *in vitro*		Peier A.M. et al., 2002
		+	(±)-Menthol (300 µM)	**HkC** (TRPM8+)	✓	**Cal** *in vitro*		Behrendt H.J. et al., 2004
		+	Menthol (30 µM)	**CHO** ((m)TRPM8+)	✓	**Cal** and **PC** *in vitro*		Macpherson L.J. et al., 2006
		+	Menthol (0.5 mM)	**HkC** ((h)TRPM8+)	✓	**Cal** and **PC** *in vitro*		Takaishi M. et al., 2016
		+	(-)-Menthol (100 µM)	Spinal lamina II **S** (TRPM8 -/-(m))	✓	**PC** *ex-vivo*	✓	Luo Y. et al., 2019
		+	Menthol (500 µM)	**HkC** ((m)TRPM8+)	✓	**PC** *in vitro*		Nguyen T.H.D. et al., 2021
	TRPA1	−	Menthol (250 µM)	**CHO** ((m)TRPA1+)	✓	**Cal** and **PC** *in vitro*		Macpherson L.J. et al., 2006

		+/–	Menthol (250 - 1000 µM)	DRG **N** (m)		**Cal** *in vitro*		Liu B. et al., 2013
		+	(-)-Menthol (100 µM)	Spinal lamina II **S** (TRPM8 -/-(m))	✓	**PC** *ex-vivo*	✓	Luo Y. et al., 2019
	TRPV1	–	Menthol (10 mM)	**HkC** ((h)TRPV1+)	✓	**Cal** and **PC** *in vitro*	✓	Takaishi M. et al., 2016
		+	Menthol (3 mM)	**HkC** ((r)TRPV1+)	✓	**PC** *in vitro*		Nguyen T.H.D. et al., 2021
	TRPV3	+	Menthol (20 mM)	**CHO** ((m)TRPV3+)	✓	**Cal** and **PC** *in vitro*		Macpherson L.J. et al., 2006
		+	Menthol (10 mM)	**Ooc** (TRPV3+)	✓	**PC** *in vitro*		Sherkheli M.A. et al., 2009
		+	Menthol (3 mM)	**HkC** ((m)TRPV3+)	✓	**PC** *in vitro*		Nguyen T.H.D. et al., 2021
	$GABA_a$ R	+	(±)-Menthol (30 - 300 µM)	**Ooc** (GABAa R+)	✓	**PC** *in vitro*	✓	Hall A.C. et al., 2004
		+	(±)-Menthol (100 - 1000 µM)	Hippocampus primary **N** / CA1 **S**		**PC** *in vitro / ex-vivo*	✓	Zhang X.B. et al., 2008
		+	Menthol (1.08 mM)	DRG **N**		**PC** *in vitro*	✓	Pan R. et al., 2012
		+	(-)-Menthol (150 - 750 µM)	PAG **S** (r)		**PC** *ex-vivo*		Lau B.K. et al., 2014
	Gly R	+	(±)-Menthol (30 - 300 µM)	**Ooc** (Gly R+)	✓	**PC** *in vitro*	✓	Hall A.C. et al., 2004
	nACh R	–	(-)-Menthol (50 - 500 µM)	**HkC** ((h)α4β2-nACh R+)	✓	**PC** *in vitro*	✓	Hans M. et al., 2012
		–	(±)-Menthol (30 - 100 µM)	**Ooc** ((h)α7-nACh R+) / α7-nAChR **N** (r)	✓	**Cal** and **PC** *in vitro*	✓	Ashoor A. et al., 2013
		–	(-)-Menthol (10 - 300 µM)	**HkC** ((h)α7-nACh R+) / nodose ganglia **N**	✓	**Cal** and **PC** *in vitro*	✓	Ton H.T. et al., 2015
		–	(±)-Menthol (10 - 1000 µM)	**Ooc** (α7-nACh R+) / midbrain **N** (m)	✓	**PC** *in vitro*	✓	Henderson B.J. et al., 2018
		+	Menthol (0.1 - 10 µM)	**Ooc** ((nematode) nACh R+)	✓	**PC** *in vitro*		Choudhary S. et al., 2019
	$5\text{-}HT_3$ R	–	(±)-Menthol (0.1 - 1 mM)	**Ooc** ((h)$5\text{-}HT_3$ R+)	✓	**PC** *in vitro*	✓	Ashoor A. et al., 2013
		–	(±)-Menthol (30 µM)	**Ooc** ((h)$5\text{-}HT_3$ R+)	✓	**Cal** and Membrane binding assay *in vitro*	✓	Walstab J. et al., 2014
	Ca^{2+} channel	–	(-)-Menthol (0.25 mM)	Neuroblastoma **C** (h)		**Cal** of the free cytosolic *in vitro*	✓	Sidell N. et al., 1990

		−	Menthol (300 µM)	Primary DRG **N**		**PC** *in vitro*		Pan R. et al., 2012
		−	Menthol (1 mM)	Cultured smooth muscle **C** or arteries (r)		**Cal** of the free cytosolic *in vitro*		Cheang W.S. et al., 2013
	Na^+ channel	−	Menthol (300 µM)	Primary DRG **N**		**PC** *in vitro*		Pan R. et al., 2012
		−	(+)-Menthol (0.125 - 1 mM)	Primary DRG **N** (r) / F11 **C**		**PC** *in vitro*	✓	Gaudioso C. et al., 2012
	K^+ channel	+	Menthol (300 µM)	**Ooc** (K2p leak channel+)	✓	**PC** *in vitro*	✓	Arazi E. et al., 2020
Myrcene	**TRPA1**	+	β-Myrcene (50 - 150 µM)	**HkC** ((h or r)TRPA1+)	✓	**Cal** *in vitro*	✓	Ghosh M. et al., 2020
	TRPV1	+	Myrcene (10 µM)	**HkC** ((h or r)TRPV1+)	✓	**Cal** and **PC** *in vitro*	✓	Jansen C. et al., 2019
Nerol	**TRPA1**	+/−	Nerol (0.3 - 1 mM)	**HkC** ((r)TRPA1+)	✓	**Cal** and **PC** *in vitro*	✓	Stotz S.C. et al., 2008
		+	Nerol (10 µM)	**HkC** ((r)TRPA1+)	✓	**Cal** *in vitro*		Ortar G. et al., 2014
	TRPV1	+/−	Nerol (0.3 - 1 mM)	**HkC** ((r)TRPA1+)	✓	**Cal** and **PC** *in vitro*	✓	Stotz S.C. et al., 2008
	K^+ channel	−	Nerol (1 mM)	**HkC** ((m)Kv channel+)	✓	**PC** *in vitro*		Ye C-J. et al., 2019
α-Pinene	**$GABA_a$ R**	+	(-)-α-Pinene (10 µM)	Hippocampus CA1 **S** (m)		**PC** *ex-vivo*	✓	Yang H. et al., 2016
Pulegone	**TRPM8**	+/−	(+)-Pulegone (0.3 mM)	**HkC** ((ch)TRPM8+) / DRG **N** (ch)	✓	**Cal** and **PC** *in vitro*	✓	Majikina A. et al., 2018
	TRPV1	+	(+)-Pulegone (1 mM)	**HkC** ((ch)TRPV1+) / DRG **N** (ch)	✓	**Cal** and **PC** *in vitro*	✓	Majikina A. et al., 2018
	nACh R	−	(+)-Pulegone (100 µM)	**Ooc** ((nematode) nACh R+)	✓	**PC** *in vitro*		Choudhary S. et al., 2019
	K^+ channel	−	(+)-Pulegone (1.1 mM)	Cultured cardiomyocyte (r)		**PC** *in vitro*		Santos-Miranda A. et al., 2014
α-Thujone	**$GABA_a$ R**	−	(-)-α-Thujone (30 - 300 µM)	**Ooc** (GABAa R+)	✓	**PC** *in vitro*	✓	Hall A.C. et al., 2004
		−	α-Thujone (100 - 300 µM)	**HkC** (GABAa R+) / isolated **N** (r)	✓	**PC** *in vitro*	✓	Czyzewska M.M. and Mozrzymas J.W., 2013
	5-HT_3 R	−	α-Thujone (0.1 - 3 mM)	**HkC** ((h)5-HT_3 R+)	✓	**PC** *in vitro*	✓	Deiml T. et al., 2003
Thymol	**TRPM8**	+	Thymol (2 mM)	**HkC** or **Ooc** (TRPM8+)	✓	**PC** *in vitro*		Vogt-Eisele A.K. et al., 2007

		+	Thymol (50 µM)	**HkC** ((r)TRPM8+)	✓	**Cal** *in vitro*		Ortar G. et al., 2012
		+	Thymol (50 - 200 µM)	Dissociated DRG **N** (TRPM8 -/-(m))	✓	**Cal** *in vitro*	✓	Wang W. et al., 2020
	TRPA1	+	Thymol (30 -300 µM)	**HkC** ((r)TRPA1+)	✓	**Cal** and **PC** *in vitro*	✓	Lee S.P. et al., 2008
		+	Thymol (300 µM)	**HkC** ((r)TRPA1+)	✓	**Cal** *in vitro*		Ortar G. et al., 2012
		+	Thymol (1 mM)	Glutamatergic **N** of the lamina II spinal cord **S** (r)		**PC** *ex-vivo*	✓	Xu Z.H. et al., 2015
		+	Thymol (50 - 150 µM)	**HkC** ((h or r)TRPA1+)	✓	**Cal** *in vitro*	✓	Ghosh M. et al., 2020
	TRPV3	+	Thymol (0.5 - 1 mM)	**HkC** ((h or m)TRPV3+)	✓	**Cal** and **PC** *in vitro*		Xu H. et al., 2006
		+	Thymol (2 mM)	**HkC** or **Ooc** (TRPV3+)	✓	**PC** *in vitro*		Vogt-Eisele A.K. et al., 2007
		+	Thymol (80 µM)	**HkC** ((r)TRPV3+)	✓	**Cal** *in vitro*		Ortar G. et al., 2012
	$GABA_a$ R	+	Thymol (0.3 - 1 mM)	**HkC** ((r)GABA R+)	✓	**PC** *in vitro*		Mohammadi B. et al., 2001
		+	Thymol (50 - 100 µM)	**HkC** ((h)GABA R+)	✓	**PC** *in vitro*	✓	Priestley C.M. et al., 2003
		+	Thymol (150 µM)	Primary cortical **N** (m)		**CII** *in vitro*	✓	Garcia D.A. et al., 2006
	5-HT_3 R	+	Thymol (100 µM)	**Ooc** ((h)5-HT_3 R+)	✓	**PC** *in vitro*		Lansdell S.J. et al., 2015
	Ca^{2+} channel	−	Thymol (100 - 500 µM)	Ventricular cardiomyocytes (h or dog)		**PC** *in vitro*	✓	Magyar J. et al., 2002
		−	Thymol (100 µM)	Pituitary GH3 **C**		**Cal** and **PC** *in vitro*	✓	Shen A.Y. et al., 2009
	Na^+ channel	−	Thymol (100 - 150 µM)	**HkC** ((h or r)Na^+ channels+)	✓	**PC** *in vitro*		Haeseler G. et al., 2002
	K^+ channel	−	Thymol (100 - 500 µM)	Ventricular cardiomyocytes (h or dog)		**PC** *in vitro*		Magyar J. et al., 2002
		+	Thymol (0.5 - 1mM)	Isolated subesophageal ganglia **N** (land snail)		**PC** *ex-vivo*	✓	Zolfaghari Z. and Vatanparast J., 2020
		+	Thymol (300 µM)	**Ooc** (K2p leak channel+)	✓	**PC** *in vitro*	✓	Arazi E. et al., 2020

To conclude, we could say that monoterpenes have a lot of different targets (**Figure 12**) and that it is important to study the pharmacology of monoterpenes, as many potent targets to modulate nociception are not known well enough now. A simple comparison between **Table 3** and **Table 4** allows us to clearly observe that there is a huge gap between the knowledge of how monoterpenes modulate their molecular targets and their *in vivo response*. Furthermore, despite the lack of knowledge about how molecular targets are modulated by monoterpenes *in vivo*, it appears that the systemic effect of monoterpenes ingestion or injection induces a reduction of noxious pain responses (**Tables 2 & 3**). Therefore, it can be hypothesized that other plants used in traditional medicine contain major monoterpenes, similarly to menthol for *Mentha piperita* L. These monoterpenes could be good candidates to test as analgesic compounds in *in vivo* assays. According to the review of the literature (**Tables 2 & 3**), a range of 50 to 200 mg/kg would be necessary to investigate it and reveal its potential effects. Moreover, the study of the impact of monoterpenes on their targets provides potential mechanisms for the action of monoterpene-based medical herbs (**Tables 3 & 4**).

2.3. Terpenes application in medicine

2.3.1. Historical use in folk medicine

Evidence of the use of medicinal plants to heal or relieve pain are found in ancient civilisations such as Ancient Mesopotamia and Ancient Egypt, through transcribed written documents such as clay tablets (4000 BCE), cuneiform tablets (2000 BCE) (R. Campbell Thompson, 1949) and hieroglyphic texts (2000-1000 BCE) (Von Deines and Grapow, 1959; Daumas, 1961) bearing information about medicinal plants and their uses (Dafni and Böck, 2019). In the early days, people used plants to try to cure illnesses; their knowledge was based on experience and perception of treatment based on either seeds, leaves, roots, fruits, or even the whole plant (Petrovska, 2012). However, in the end, it appeared that a lot of the medicinal plants, which empirically remained in the pharmacopoeia, are indeed indwelled with interesting pharmacological properties. For example, in Homer's literary work, the Iliad and the Odyssey, often considered as one of the first European written trace of medicinal plants (800 BCE), he refers to *Artemisia species* as healing plants.

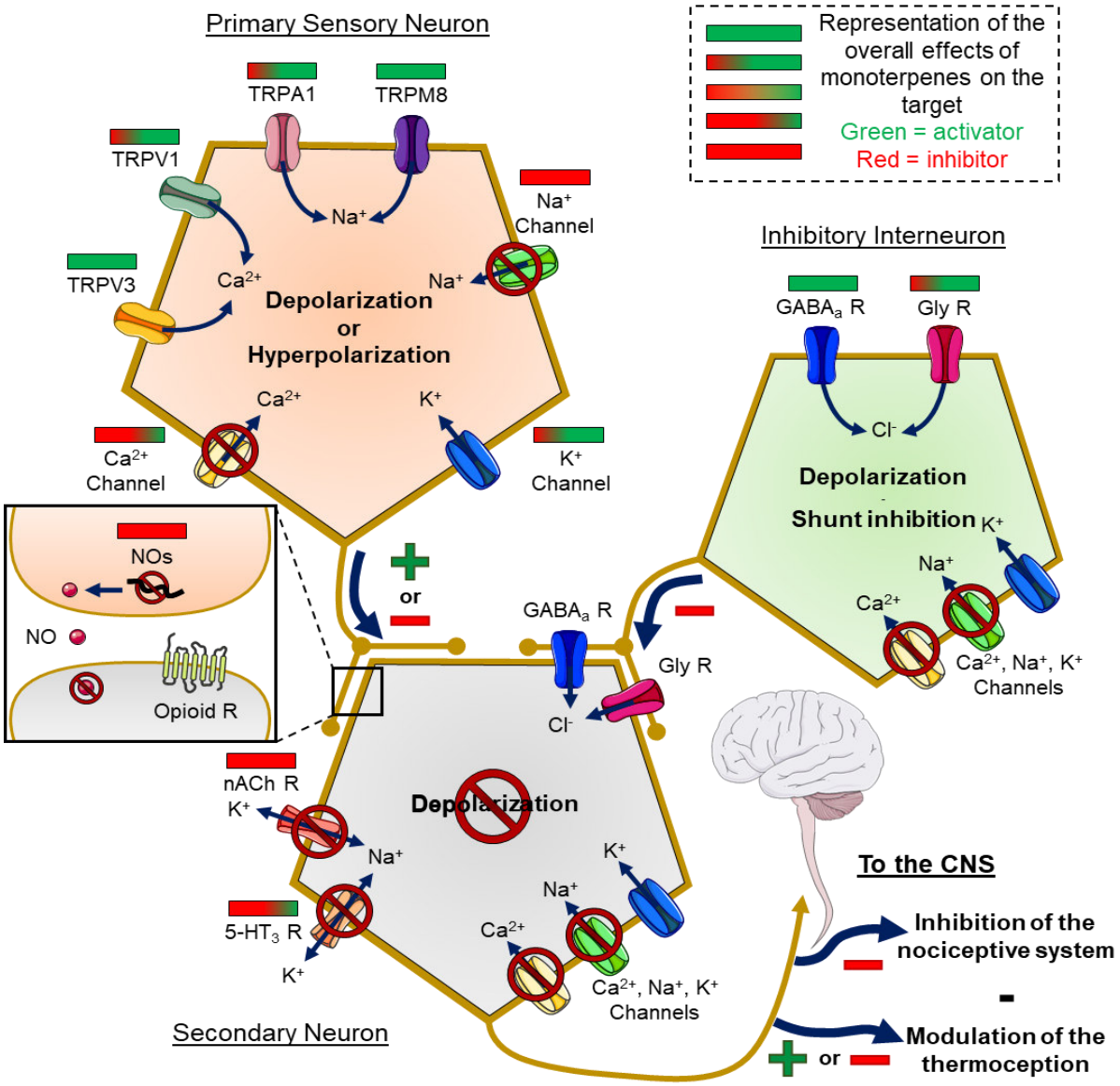

Figure 12: Targets modulated by monoterpenes in nociception.

This illustration summarizes the targets and the effects of monoterpenes from **Tables 3 & 4**. Monoterpenes modulate the nociceptive system through various ion channels by modulating them either positively or negatively. These effects might involve different types of neurons within the same network.

Nowadays, *Artemisia* species are used in many different treatments such as malaria, hepatitis, cancer, inflammation, bacterial, viral and fungal injection (Tan et al., 1998). In addition, the essential oil of *Artemisia caerulescens* L. contain a large number of known analgesic monoterpenes such as borneol, nerol or α- terpineol (Morán et al., 1989) (**Table 2**).

During the 16th and 17th centuries, with the democratisation of the printing press techniques impulsed by Johannes Gutenberg, books on medicinal herbs and herbals became some of the best-sellers of their time, because it was finally possible to access scientific medical advice and knowledge to take care of one's own health. In their review, Adams et *al.* show that plants species of the *Artemisia genus* or of the *Lamiaceae family* (mint, basil, rosemary, oregano, thyme or lavender to name only the most common species) were well known and described for their analgesic properties to alleviate rheumatic-related pains (for review; (Adams et al., 2009)). Besides, thymol is the main constituent of thyme (*Thymys vulgaris* L.) essential oil and its therapeutic applications are promising (Salehi et al., 2018; Kowalczyk et al., 2020).

Today there is an important quantity of studies showing the biological effect of essential oils of these plants, especially their analgesic properties (Bakkali et al., 2008; Katsuyama et al., 2015; Donatello et al., 2020). However, the use of these essential oils is particularly controversial.

2.3.2. Misuses and controversies

The actual use of essential oils and by extension the terpenes they contain, is controversial. Not because they have no pharmacological properties, but because they have many properties that can be harmful in some circumstances (Vigan, 2010; Zárybnický et al., 2018; Stojanović et al., 2019). To quote Vigan: "Essential oils are natural substances, but natural is not synonymous with harmless". In fact, essential oils are often composed of more than 10 different terpenes and understanding all the interactions and side effects remains complicated to this day (Djenane, 2015; Aziz et al., 2018).

Nowadays, essential oil and traditional herbal medicines are not subject to the same rules of sale than conventional medicines. Thus, anyone can sell essential oils (with a few notable exceptions) without any qualification or expertise. It is easy to experience this yourself with a simple search on an internet browser: when you type the keywords "essential oil", the first page is filled with blogs and commercial websites that sell and promote essential oils often under the appellation of "aromatherapy" (classified as non-conventional medicine (Lee et al., 2012)) to relieve various aches and pains. One of them even strongly suggests that Atlas cedar essential oil (that you can buy directly on the website) burns lipids to facilitate dieting and slimming (Nail-

Billaud, 2020). However, the French government agency ANSM (Agence nationale de sécurité du médicament et des produits de santé) strongly recommends that the public and professionals alike should consider essential oils as special substances that are not devoid of side effects. Moreover, they are particularly not recommended for children, pregnant women, elderly people and people suffering from chronic pathologies (Bercy Infos, 2020; ANSM). There is thus an important question about the ethics of selling a health product by unqualified personnel with commercial interests, which in addition may have more negative effects than the intended effect.

The major side effects of the essential oil are their cytotoxicity and their sedative effects. Bakkali et *al.* in their review indicates that the lipophilic nature of monoterpene allows them to pass through the cell membrane, disrupting their structure. So when a high concentration of monoterpenes passes through, the disruption of the membrane is so important that it leads to cytotoxicity (for review; (Bakkali et al., 2008)). Moreover Zárybnický et *al.* also highlighted the hepatotoxicity of monoterpenes, particularly due to the formation of reactive metabolites that could affect the liver, especially after an oral absorption (Zárybnický et al., 2018).

Sedative effects are mainly described in monoterpenes studies that test high doses of monoterpenes *in vivo* (≥ 150 mg/kg). de Sousa et *al.* tested 10 different monoterpenes on mice during a pentobarbital-induced hypnosis test; the results show 7 out of 10 monoterpenes (150 mg/kg i.p.) increased the sleeping time mice (Sousa et al., 2007). In another study, da Silveira et *al.* found that pulegone 400 - 800 mg/kg i.p. in mice induces strong temporary sedative effects resulting in a decrease in ambulatory ability (Silveira et al., 2014). Fortunately, these effects are only observed with high doses of monoterpenes and/or essential oils.

However, despite these side effects and misuses, the pharmacology of essential oil compounds is particularly interesting for medical research, particularly to identify their active compounds (more specifically the monoterpenes in the case of essential oils) with curative properties.

2.3.3. Interest of the monoterpenes pharmacopeia in medicine

Monoterpenes are indeed particularly interesting for medical research because firstly, some of them already beneficiate of a validation of application on the market of

the commercially controlled essential oils, or as agro-alimentary products (e.g. food additives, e-cigarette). Secondly, they have a low cost of production (e.g. menthol 1 g = 0.08 €) and high economic interest. In 2002 the worldwide sales of terpene-related drugs were already approximately 12 $ billions (Wang et al., 2005a). Thirdly, they are already described as potential therapeutic compounds, effective in most cases and with many described targets that monoterpenes are able to modulate (**Tables 3 & 4**) (**Figure 11, 12**) (for review; (Wang et al., 2005b; Cox-Georgian et al., 2019; Perri et al., 2020)). Finally, despite their potential, there is yet little or no monoterpene-based analgesic treatments. This situation is now changing with the democratization of therapeutic cannabis for pain relief (03/2021 - first clinical study of therapeutic cannabis in France; (ANSM)). There is an interest to understand the potential of monoterpenes that are produced by *Cannabis sativa* and how they may interact in synergy with phytocannabinoids ("entourage effect" described by (Russo, 2019)) (for review; (Liktor-Busa et al., 2021).

Recently, different studies even suggested that they might be neuroprotective agents as they are able to cross the BBB (Wojtunik-Kulesza et al., 2017). Lv et *al.* investigated the therapeutic effect of geraniol on functional recovery in a model of spinal cord injury (SCI) inducing neuropathic pain in rats. They show that the treatment of SCI rats with geraniol improves locomotor function, promotes recovery of neuronal function and attenuates neuropathic pain. This is due to the action of geraniol on pro- and anti-inflammatory cytokines (Lv et al., 2017). Another study reveals that carvacrol-induce neuroprotection in gerbils that have undergone ischemic stroke (Guan et al., 2019). These recent results show that there is an important path forward for monoterpenes-based neuroprotectant drugs.

Moreover, this interest for the neuroprotective and analgesic effect of monoterpenes led to clinical trials as well. Sasannejad et *al.* point out that a 15 minute inhalation of lavender essential oil induces, between 1 and 2 hours, a significant reduction of headache symptoms compared to a control placebo in a clinical trial (Sasannejad et al., 2012). Arslan et *al.* observed similar results, in their randomized clinical trial, with children exposed to lavender oil before dental surgery (tooth extraction) (Arslan et al., 2020). These types of results are particularly interesting, although the contribution of the placebo effect in these cases still needs to be studied.

The effect of essential oils and monoterpenes inhalation is described in two studies (Tashiro et *al.* in 2016 and Higa et *al.* in 2021), where they have conducted

functional neuroanatomy on animals. They show that when mice are exposed to linalool vapours, it induces analgesia. In animals with olfactory bulb or epithelium lesion, these effects are completely abolished, suggesting the implication of the nervous system in the effect production. Furthermore, c-Fos, an early transcription factor used to map cellular activity (Dragunow and Faull, 1989) was revealed in hypothalamic orexin neurons after animal exposition to the monoterpene linalool, in an immunochemical analysis. These neurons project to the spinal cord through descending orexinergic pathways to modulate the nociceptive information processing (Higa et al., 2021). To confirm, they made i.t. injection with an orexin receptor antagonist, and observed a complete abolition of the analgesic effects of vaporous linalool (Tashiro et al., 2016; Higa et al., 2021). As such, they demonstrate that it is possible to modulate nociception through the smell of monoterpene, via orexin neurons. This could be the major mechanism in essential oils inhalation-induced analgesia. Moreover, these findings combined with previous knowledge about neuroprotective effects of monoterpenes and their ability to cross the BBB, enhanced the interest of monoterpenes as therapeutic treatments.

As seen in the previous paragraph, the route of intake of monoterpenes/essential oils can be multiple, inhalation, orally and even by cutaneous application. The use of balm in folk medicine is known and there are studies that use topical application of monoterpenes in *in vivo* studies with borneol and menthol (**Tables 2 & 3**). In addition, Wang et *al.* tested the analgesic effect of the topical application of borneol for post-operative pain, in a randomized, double blind, placebo-controlled clinical study. Their results show significant postoperative pain relief, increasing the interest of borneol as a topical analgesic (Wang et al., 2017). These results, taken altogether, show that monoterpenes have a diversity of intake routes, which is really interesting for medical research.

Monoterpenes also raise interest in the context of the current pandemic, Meeran et *al.* in their review speculate on the potential effects of limonene against the Coronavirus disease (COVID-19). They suggest that as SARS-CoV-2 is a viral infection that induces inflammation, it could be possible that the antiviral and anti-inflammatory effects of limonene may be an interesting treatment to reduce the symptoms of COVID-19 (Nagoor Meeran et al., 2021). Although this is only a prospective study, it still shows that monoterpenes are of real interest in medical research, in a slightly broader context than analgesia and inflammation.

Finally the last underlying point that was developed throughout the whole section *3.2.1. Analgesic properties*, is that there are still many monoterpenes that need to be studied and which targets need to be characterized (**Figure 11, 12**) (for review; (Guimarães et al., 2013; Oz et al., 2015; Perri et al., 2020)). As seen in the **Tables 2, 3 & 4**, a few monoterpenes get almost all the attention; menthol, carvacrol, thymol and camphor are the only 4 monoterpenes among the 22 in **Table 4** to be studied in more than 10 articles for their *ex vivo* and *in vitro* molecular targets. This is even more impressive when looking at the molecular targets (**Table 4**) of analgesic monoterpenes (**Table 2**) (**Figure 13**). To summarize, there are large number of monoterpenes (n = 25) (**Figure 13**) that have an effect on pain behaviour modulation but are clearly not fully characterized.

For all the reasons previously discussed, monoterpenes and by extension essential oils, need to be further investigated in order to have a better understanding of their analgesic properties and their mechanisms, with the aim of developing a potent monoterpene-based analgesic treatment. Especially monoterpenes like pulegone, which shows interesting effects but is not enough studied to conclude about its analgesic potential. Its targets and its optimal application and route of intake remain to be defined in order to maximize its effect. However, it is still useful to use more characterized monoterpenes such as menthol to compare the analgesic effects and/or the molecular targets with a “reference” monoterpene.

This is with the aim of developing new innovative analgesic treatments based on monoterpenes extracted from plants. Those will target ion channels (TRPs, Ca^{2+}, Na^{+}, K^{+} channels, or $GABA_a$ R) involved in the emergence and transmission of the nociceptive signals and inflammatory factors.

Monoterpenes are analgesic compounds but their mechanisms are not yet fully understood. Therefore, another possibility is to develop an innovative analgesic compound that will specifically activate an endogenous system. Oxytocin is in this case an ideal endogenous system because it has its own receptors and is known to have analgesic effects.

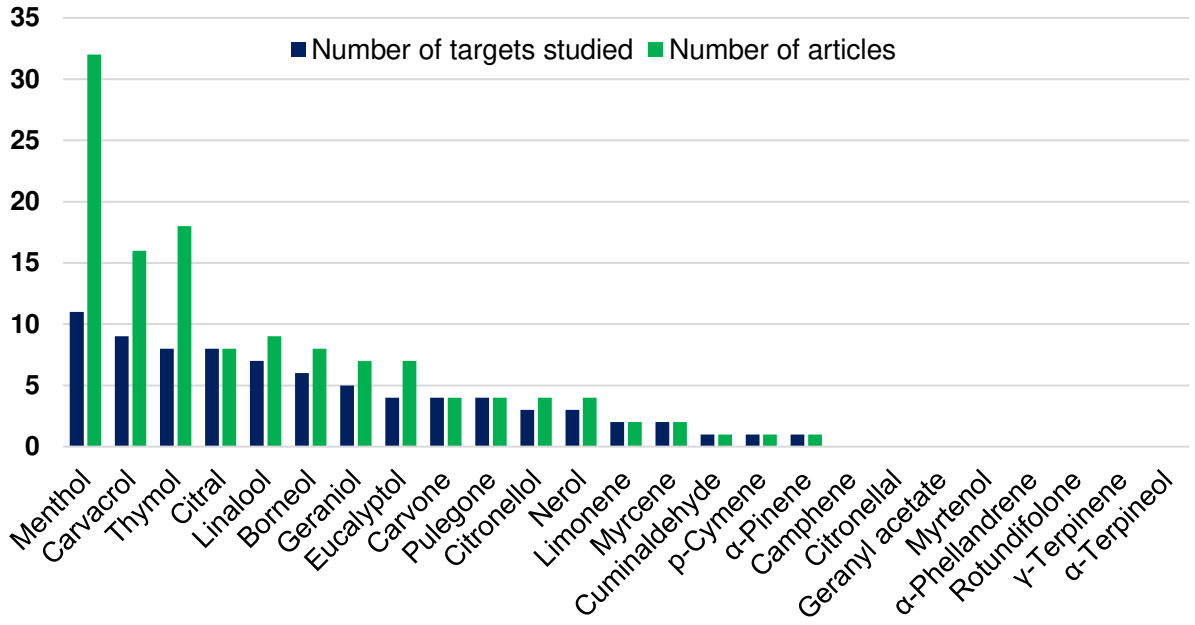

Figure 13: Cross plot of analgesic monoterpenes sorted by targets studied.

Cross plot based on analgesic monoterpenes from **Table 2** and their molecular targets from **Table 4** classified according to the number of targets studied and the number of studies.

3. Oxytocin

Oxytocin (OT) is a neuropeptide and a hormone discovered in 1906 by Sir Henry H. Dale who during experiments on pregnant cats, observed uterine contractions after injecting extracts of posterior pituitary glands (Dale, 1906). The compound responsible for these contractions will be named oxytocin, which means "quick delivery" in Greek and isolated about twenty years later by Kamm et *al.* (Kamm, 1928). In addition, OT was the first hormonal polypeptide to be sequenced and synthesized by Vincent Du Vigneaud, leading to the award of the Nobel Prize of Chemistry in 1955 (for review; (Lee et al., 2009)).

3.1. Endogenous oxytocin

3.1.1. Synthesis and structure

The OT gene is highly conserved in the life tree; it is made up of 850 base pairs and is located on chromosome 20 in humans and chromosome 3 in rats.

The OT gene in mammals is co-located on the same chromosomal locus as the gene coding for the vasopressin (AVP) as these gene are highly related (Donaldson and Young, 2008). Indeed, AVP and OT probably originate from a common hormone and share many similar characteristics, such as their structures, which differ by only two amino acids. Because of their similar structures they also have partial agonistic effects on their respective receptors (for review; (Jurek and Neumann, 2018)). Both genes (OT and AVP) share a common composition, which contains three exons and two introns, but they are transcribed in opposite directions. The first exon encodes the translocation signal, which is the hormone itself, the tripeptide-processing signal and the main part of the associated neurophysin. The second exon encodes for the minor part of the neurophysin, and the third exon encode the carboxy-terminal ending of neurophysin (Gimpl and Fahrenholz, 2001). The expression of the OT gene is highly regulated, particularly at the transcriptional level, at a specific site located at approximately 160 base pairs upstream of the transcription initiation site, on a highly conserved sequence of the OT gene (Stedronsky et al., 2002).

Biosynthesis of OT is identical to other neuropeptides. The initial transcript is translated into a pre-pro-peptide, which is subsequently cleaved into a pro-peptide and then a peptide. The mature product of OT gene biosynthesis consists of a dimer, OT-neurophysin and it is then transported within the cell. Then the dissociation of the OT-neurophysin dimer occurs in the neurosecretory granules, which contain pro-hormone convertase enzymes and carboxypeptidases. Once OT is dissociated, it will be released into the plasma, cerebrospinal fluid (CSF) or intersynaptic space from where the OT can then bind to its receptor (Blumenstein et al., 1979; Breslow and Burman, 1990; Gimpl and Fahrenholz, 2001).

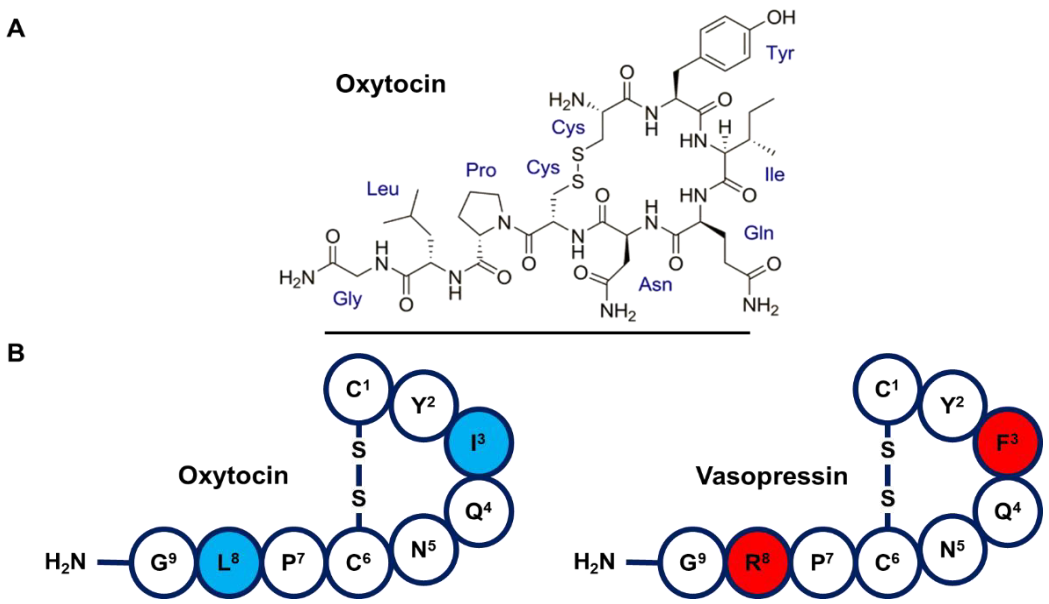

Figure 14: Oxytocin and vasopressin structure.

(**A**) Molecular structure of OT. (**B**) The coloured amino acids represent the differences between OT and AVP.

Regarding the structure OT is a peptide made of nine amino acids: **Cys**-**Tyr**-**Ile**-**Gln**-**Asn**-**Cys**-**Pro**-**Leu**-**Gly**-NH_2 (**Figure 14A**). The two cysteine (**Cys**) compounds constitute a disulfide bridge, which results in the absence of a carboxyterminal end to this molecule. As mentioned before, OT presents a strong structural similarity with AVP; indeed, these two neuropeptides differ only in two neutral amino acids: isoleucine (**Ile**) and leucine (**Leu**) of OT are replaced respectively by phenylalanine (**Phe**) and by arginine (**Arg**) (**Figure 14B**) (Gimpl and Fahrenholz, 2001).

It is therefore, this difference in polarity that made the interaction of OT and AVP possible with their receptors (Barberis et al., 1998). Furthermore, the understanding of the oxytocin receptor (OTR) is essential for the development of a therapeutic compound targeting the OT system.

3.1.2. Receptors

The OTR is a member of the GPCR family made of seven transmembrane domains. The encoding gene for OTR is carried on chromosome 3 in humans (Kimura et al., 1994) and 4 in rats (Rozen et al., 1995). The sequence is 17 kb long and consists of four exons and three introns. The first two exons contain the 5' non-coding region, while exons three and four contain the sequence for the 389 amino acids of OTR.

There are also several regulatory sequences in the 5' region of the OTR gene (for review; (Gimpl and Fahrenholz, 2001; Jurek and Neumann, 2018)).

The study of the ligand-receptor interaction for OTR has identified the N-terminal part (E1) as well as the first two extracellular loops (E2 and E3) as the specific binding site for OT (**Figure 15A**) (Fanelli et al., 1999). As previously mentioned, OT is very similar to AVP, which allows them to bind to their respective receptors. Indeed, both OT and AVP have a high affinity for OTR (OT Ki = 0.79 nM for OTR; AVP Ki = 1.7nM for OTR). Thus, AVP can act as a partial agonist of OT (Chini et al., 1996; Akerlund et al., 1999). Conversely, OT can also bind with lower affinity to AVP receptors (Chini et al., 1996).

Then, after the OT - OTR interaction with the binding sites induces conformational changes and switches the receptor in active state. Thus, this conformational change will affect intracellular loops of the transmembrane domain and the C-terminal of the GPCR, which are linked to the heterotrimeric G protein complex made of three subunits α, β and γ (for review; (Gimpl and Fahrenholz, 2001; Lee et al., 2009)). This conformational change will lead to the phosphorylation of the Gα protein, which will be released from the Gβγ complex. Gα and Gβγ will each activate different types of subunits-specific effectors. Then secondary messengers of GPCR signalling pathways will be activated and may lead to different cellular functions (**Figure 15B**) (for review; (Gimpl and Fahrenholz, 2001; Lee et al., 2009; Viero et al., 2010)).

As OTR is a receptor that is known to be coupled with different type of Gα, such as Gq/11 and Gi/o (Gimpl and Fahrenholz, 2001; Reversi et al., 2005; Busnelli et al., 2016) that can co-exist in a same cell (Gravati et al., 2010). Some type of agonists and antagonists can only affect certain Gα subtypes; they are termed biased agonists and are able to affect only OTR-Gq or OTR-Gi (Luttrell et al., 2015). The intracellular signalling pathways that are activated by OTR are diverse and numerous, thus the (**Figure 15B**) proposed by Viero et *al.* summarizes the intracellular pathways of OTR (for review; (Viero et al., 2010)).

It should be noted that the availability of OTR in the neuronal membrane is determined by the expression of the OTR gene, but also by the desensitization and internalization of the receptor upon ligand binding. Thus, prolonged or repeated activation of the receptor induces desensitization of the receptor and a reduction of OTR expression in the membrane (for review; (Jurek and Neumann, 2018)).

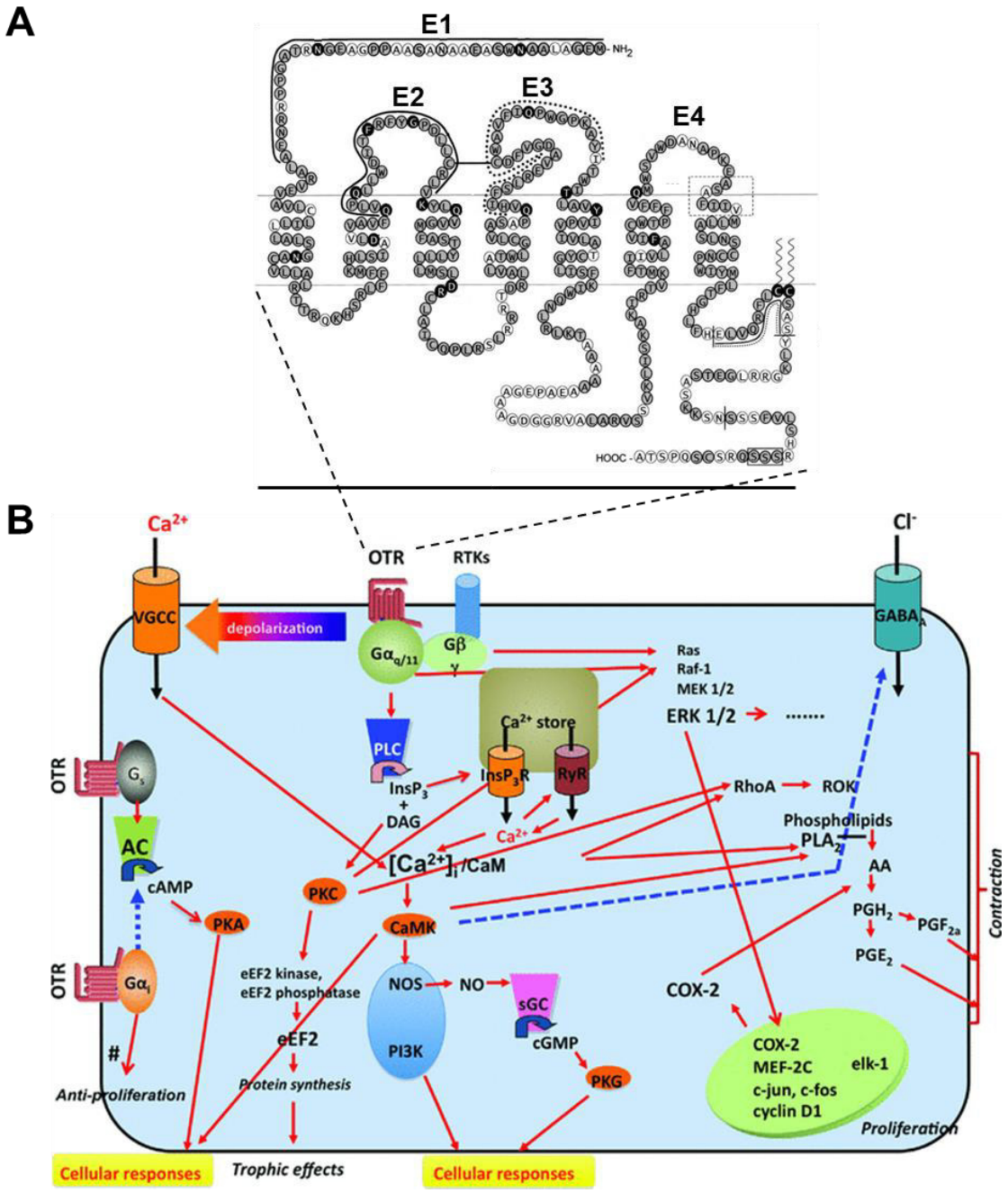

Figure 15: Oxytocin receptor and linked signalling pathways.

(**A**) OTR structure and OT binding domains (E1 – 3). (**B**) OTR linked signalling pathways. References and abbreviations can be found in the original review, Viero et *al.* (2010). *Adapted from: (A) Gimpl & Fahrenholz (2001) / (B) Viero et al. (2010).*

OTR activation induces a cascade of intracellular mechanisms that allow the activation of the OT system, including analgesic effects. In order to develop a therapeutic treatment, based on an OT agonist, it is essential to understand how the OT system is organised, which will be discussed in the next section.

3.1.3. Oxytocinergic system

OT is usually described as synthesized, in the CNS, only in three hypothalamic nuclei: the paraventricular nucleus (PVN), the supraoptic nucleus (SON) and the accessory nuclei (AN) (Sofroniew, 1983; Swanson and Sawchenko, 1983; Burbach et al., 2001; Jurek and Neumann, 2018).

Among these structures, OT neurons are divided into two subtypes, magnocellular (magnOT) and parvocellular (parvOT), each with distinct characteristics in terms of size, shape, location, amount of OT produced and projection sites (**Figure 16**) (for review; (Lee et al., 2009; Jurek and Neumann, 2018)). MagnOT neurons are large neurons projecting into the CNS and particularly to the posterior pituitary gland in order to allow the release of OT into the bloodstream, as OT hardly crosses the blood-brain barrier (about 1 molecule per 1000) (Jurek and Neumann, 2018). Conversely, parvOT neurons are small neurons with long axon whose projections remain exclusively in the CNS (**Figure 16**) (Swanson and Sawchenko, 1983; Jurek and Neumann, 2018).

The PVN is the only one of the three OT-synthesizing nuclei to contain parvOT neurons, which therefore project into many CNS structures (**Figure 16**) (Jurek and Neumann, 2018). The SON is almost exclusively composed of magnOT neurons that project mainly to the posterior pituitary gland. As for the AN, they are made up of 6 different nuclei (anterior commissural, circular, dorsolateral, extra-hypothalamic, fornical and ventrolateral) (Grinevich and Polenov, 1998; Knobloch and Grinevich, 2014) located between the PVN and the SON and contain approximately one third of the magnOT (Rhodes et al., 1981; Knobloch et al., 2012).

In addition to its neurotransmitter function, OT also has a hormonal action, its secretion via the pituitary gland from magnOT neurons mediates these neuroendocrine functions. Once released into the bloodstream OT has a half-life of about 3 to 8 minutes (Morin et al., 2008), although its half-life in the CSF is around 20 minutes (Mens et al., 1983). This difference is due to the accelerated chemical degradation of OT in the blood, which occurs mainly in the liver and kidneys through peptidases that will hydrolyse and cleave OT, such as placental leucine aminopeptidase termed oxytocinase (Claybaugh and Uyehara, 1993).

Moreover, magnOT neurons connect other cortical structures, including amygdala, hippocampus and bed nucleus of the stria terminalis (**Figure 16**) (Knobloch

et al., 2012; Duque-Wilckens et al., 2017). These connections in the CNS are completed by projections from parvOT neurons to diverse cortical area, brainstem and spinal cord (**Figure 16**) (Jurek and Neumann, 2018). Furthermore, it has been shown that parvOT neurons are able to modulate the activity of magnOT neurons through the PVN → SON connection (Eliava et al., 2016; Tang et al., 2020).

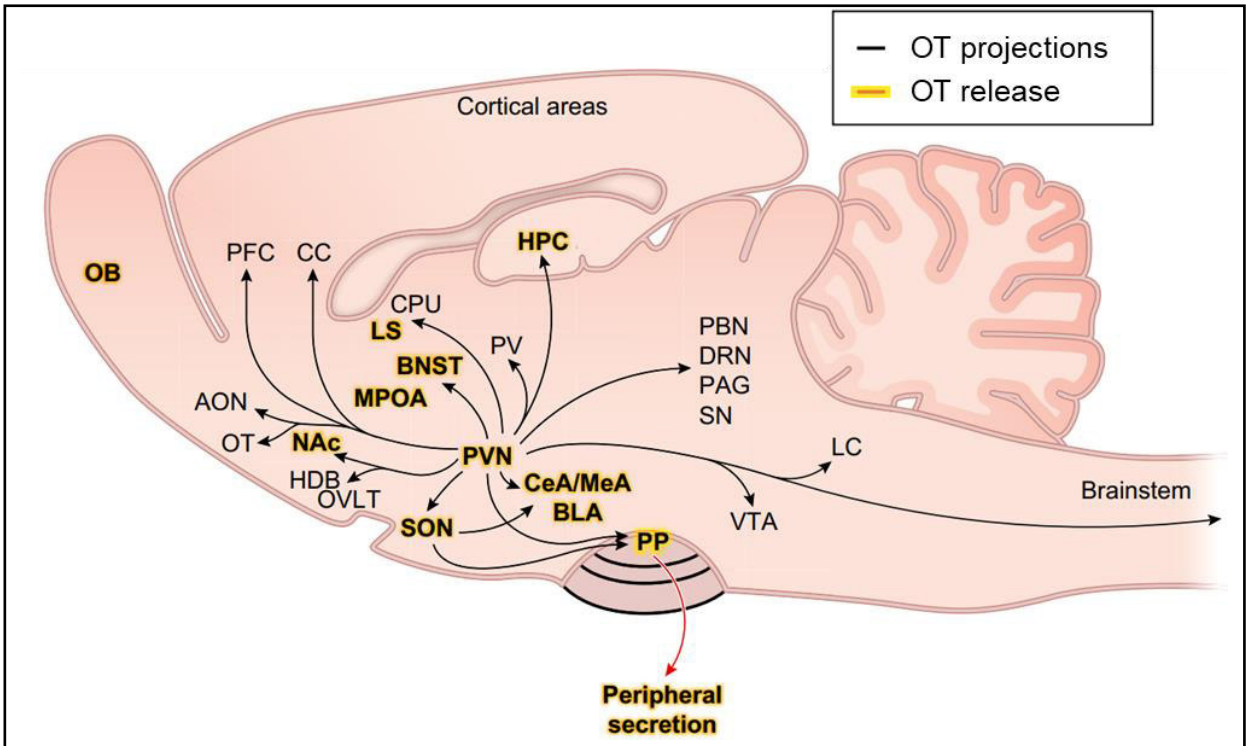

Figure 16: Oxytocin projections in the CNS.

OT projections in the CNS originating from the PVN are shown as black lines, connecting to the brain region where OTR expression has been detected. References and abbreviations can be found in the original review, Jurek and Neumann (2018).

Adapted from: Jurek & Neumann (2018).

In the CNS, once OT is released, it binds to its receptor OTR, which is expressed in numerous cortical areas. Generally, the OTR expression among cortical areas is mainly linked to the OT projection, as in the amygdala, PAG or spinal cord (Juif and Poisbeau, 2013; Eliava et al., 2016) in order to modulate many different physiologic functions (Kita et al., 2006; Baskerville and Douglas, 2008; Atasoy et al., 2012; Eliava et al., 2016) and emotions (Shamay-Tsoory et al., 2009; Hasan et al., 2019; Tang et al., 2020).

Besides the synthesis in the CNS, OT is also synthesized by peripheral tissues and cells such as; female genitalia, male genital tract, cardiovascular tissue, thymus,

pancreas, bone, skin, macrophage and monocytes (for review; (Jurek and Neumann, 2018)). Nevertheless, the concentration of OT reported in these peripheral tissues is 100 to 1000 lower than in the hypothalamic synthesis sites, suggesting a paracrine or autocrine role, conversely to the endocrine mediate by pituitary OT (Banerjee et al., 2017).

To summarize, many of the cortical areas expressing OTR are linked to the regions that synthesize OT, and all of this can be related to the known physiological and psychological functions of OT. Thus, by targeting specific OT-related areas with a therapeutic OT agonist, it should be possible to reproduce some of the effects induced by OT, including analgesia. However, not all effects of OT are beneficial in the therapeutic context of pain management and related comorbidities (anxiety, loss of social connexion). This is why I will develop in the next section, the general functions of OT before deepening the pain-related effects.

3.1.4. General functions

OT is a peptide strongly involved in the regulation of many physiological functions and behaviours associated with social interactions, social recognition, mate choice, sexual behaviours, reproduction, parturition, lactation and parenting behaviours (**Figure 17**) (for review; (Lee et al., 2009; Jurek and Neumann, 2018)). All these physiological functions and behaviours play a key role in the survival and propagation of species, especially mammals, which is why OT has been referred as “the great facilitator of life” (Lee et al., 2009).

In addition to these reproductive and social functions, OT also plays a role in the regulation of other physiological functions (e.g. cardiac, renal, food intake) (**Figure 17**). For example, two studies demonstrated that i.p. injection of OT is able to reduce heartbeat, mean arterial pressure and strength of atrial contraction in rats (Petersson et al., 1996; Favaretto et al., 1997).

Moreover, OT can affect psychological functions such as emotions (**Figure 17**). The relationship between OT and anxiety has been clearly established and it is a potent anxiolytic. For example, the release of OT during mating has been shown to reduce anxiety-related behaviours in male mice, and this effect is inhibited when OTR antagonist are administered (Waldherr and Neumann, 2007; Blume et al., 2008).

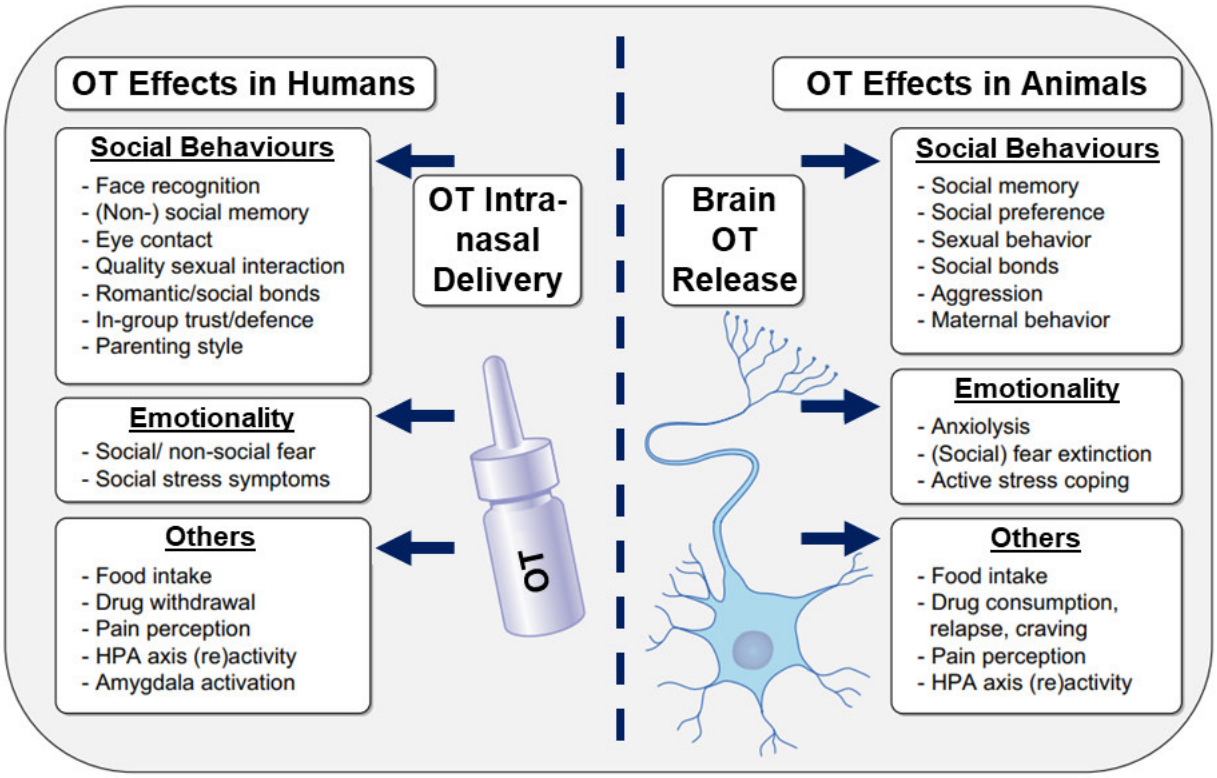

Figure 17: Oxytocin implication on vital and behavioral functions.

Reported effects of synthetic or endogenous OT in human (left) or in animal (right) on social behaviours, emotionality, and other functions. *Adapted from: Jurek & Neumann (2018).*

To summarize, OT is involved in many vital functions and behaviours. Among them, we believe that the most interesting functions of OT to target for the development of a therapeutic compound are the anti-inflammatory, analgesic and anxiolytic effects.

3.2. Oxytocin and pain

3.2.1. Regulation of the immune system

OT is synthetises in the thymus where it plays an important role for the immune system (**Figure 18**) (Geenen et al., 1986). The high concentration of OT and its localization in the cytokeratin network of thymic epithelial cells led to the hypothesis that OT is used as the self-antigen of the neurohypophysial peptides family modulating immune cells (Geenen et al., 2000). Furthermore, it has also been show that the anti-inflammatory actions of OT are related to the decreased superoxide production and

pro-inflammatory cytokines release from OTR monocytes and macrophages (Szeto et al., 2008) (**Figure 18**) (for review; (Wang et al., 2015)).

However, CNS OT is also assumed as essential for the inflammatory system (**Figure 18**). In case of sepsis in rats, SON magnOT neurons related to neurosecretory pathways were activated (Sendemir et al., 2013). Similarly, hypothalamic and pituitary cells, including OT neurons, produce many cytokines, such as IL-1, IL-2, IL-6, IFN-γ, and transforming growth factor-β in response to physiological alteration (**Figure 18**) (Savino et al., 1999).

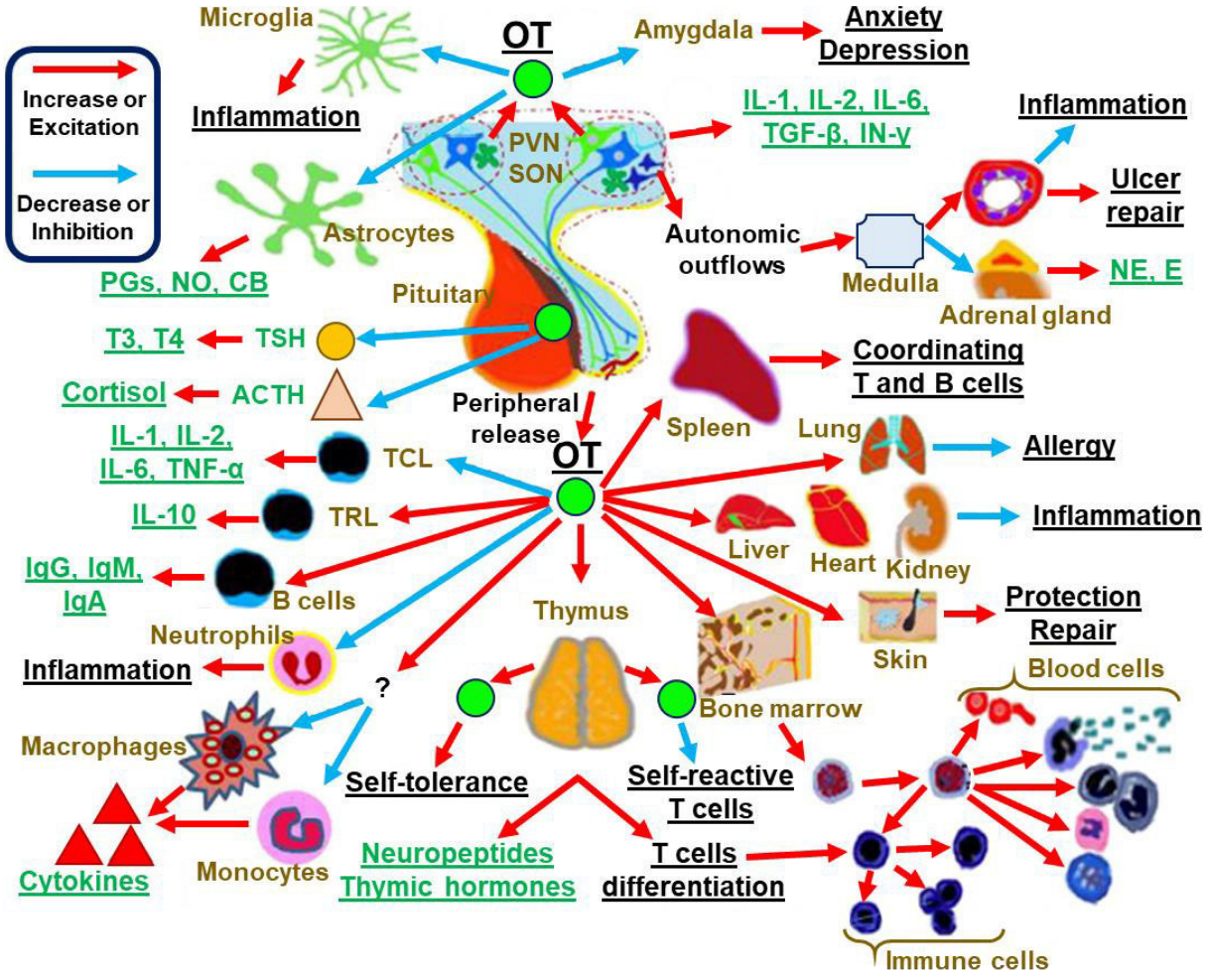

Figure 18: Oxytocin in the neuroendocrine regulation of the immune system.

The OT secreting system play a key role in the neuroendocrine regulation of the immune system. References and abbreviations can be found in the original review, Wang et *al.* (2015). *Adapted from: Wang et al. (2015).*

In addition to these indirect implications, there is also evidence supporting a central role for the OT-secreting system in the neuroendocrine regulation of immunological functions, based on its ability to coordinate activities of other organ systems displaying immune reactions (**Figure 18**) (Yang et al., 2013). For example, OT has been proven to weaken the inflammation cause by labour by reducing the mRNA expressions of chemokines in myometrial cells (Hua et al., 2013).

More generally, the OT and OT secretion system can be considered as an integrating organ of the immune defence (Li et al., 2017a). However, even if the anti-inflammatory effects of OT are limited in the analgesic properties of OT, they still need to be taken into account in the development of an analgesic compound. Indeed, the main effect against pain is based on OT anti-nociceptive properties within the nervous system.

3.2.2. Oxytocin in the modulation of nociception and pain

OT is a recognized mediator of endogenous analgesia (for review; (Tracy et al., 2015; Boll et al., 2018)). It acts on every level of nociception and pain processing, from PNS through the spinal cord and finally to supraspinal levels. Additionally, it is well documented that painful states raise plasma OT concentration (Gimpl and Fahrenholz, 2001; Martínez-Lorenzana et al., 2008; Juif et al., 2013).

3.2.2.1. Peripheral anti-nociceptive effect

OT injected i.p. or i.v. (intravenously) in rats and mice, mediate OTR anti-nociceptive effects (Lundeberg et al., 1994; Kang and Park, 2000; Tracy et al., 2015). Some studies indicate that it might acts on the nociceptors cell bodies. Indeed, OTR is expressed in the cell body of non-peptidergic C-fibre neurons, located in DRG (Moreno-López et al., 2013). A study using cultured DRG neurons (rats) shows that OT decreases membrane excitability, increases outward current and evoked membrane hyperpolarization (Gong et al., 2015). They additionally demonstrate that OT produces an intracellular increase in calcium in these capsaicin-sensitive neurons. An additional study shows that OTR is also present in nociceptive neurons of the trigeminal ganglion. OTR expression was upregulated in these neurons when rats underwent electrocutaneous stimulation or adjuvant-induced inflammation. However,

OT application reduces the capsaicin-induced hyperalgesia is these rats (Tzabazis et al., 2016). De Araujo et *al.* have provided evidence for an anti-hyperalgesic role of peripheral OT during visceral pain (de Araujo et al., 2014).

Nevertheless, there is an ongoing discussion regarding the effects mentioned above that could be partially mediated by $V_{1A}R$ (AVP receptor). In fact as mentioned previously, OT has a physiologically relevant affinity for this receptor. Juif and Poisbeau showed that a low "physiological" i.v. dose of TGOT (OT agonist) had an anti-nociceptive effect. The same anti-nociceptive effect was achieved with AVP, but with a 100-fold higher dose. With even higher doses, pro-nociceptive effects were obtained for both OT and AVP (Juif and Poisbeau, 2013). When OTR or $V_{1A}R$ antagonists were co-injected with TGOT or AVP at anti-nociceptive dose, the anti-nociceptive effects were abolished for both TGOT and AVP only with the OTR antagonist. Conversely, at pro-nociceptive dose, only the $V_{1A}R$ antagonist blocked the proalgesic effects of TGOT and AVP (Juif and Poisbeau, 2013). A potential explanation may arise from the work of Tan et *al.*, who showed that low concentrations of OT increased GABA-evoked currents in DRG neurons, leading to suppression of primary sensory transmission, whereas higher doses reduced GABA-mediated pre-synaptic inhibition (Tan et al., 2000).

The following studies used specific EO agonists and antagonists to avoid potential interaction with the AVP system to investigate the mechanisms and peripheral effects of EO in analgesia.

Eliava et *al.* demonstrated that a minor population of parvOT neurons exerts a dual action, via systemic and central mechanisms (detailed in the following section: *2.2.1.2. Anti-nociceptive effect at the spinal level*), which activates magnOT neurons that will release OT into the bloodstream, and this peripheral OT will then inhibit DRG OTR neurons (**Figure 19**). Additionally, evoked OT release from these parvOT neurons suppresses nociception and promotes anti-hyperalgesia in animal model of inflammatory pain (Eliava et al., 2016). This mechanism of peripheral OT mediated anti-hyperalgesia is extended by a study of González-Hernández et *al.*, who showed that subcutaneous (s.c.) injection of OT attenuates acute pain, exerting long-lasting inhibition of WDR neurons in the spinal cord. In line with these results, the authors detected OTR immunoreactivity in the nociceptive-specific terminals of the superficial skin layers (**Figure 19**) (González-Hernández et al., 2017). These findings are even

more interesting when considering that keratinocyte, are able to deliver OT locally (**Figure 19**) (Peier et al., 2002b; Denda et al., 2012; Dai, 2016).

There is also a discussion about potential OT/TRPV1 interactions initiated by two studies (Nersesyan et al., 2017; Sun et al., 2018). They suggest that OT may interact with TRPV1 expressed by nociceptors. They are based on experiments showing that DRG neurons in TRPV1 knockout mice exhibit reduced sensitivity to OT (Nersesyan et al., 2017) and that i.t. OT reduces capsaicin-induced hyperalgesia (Sun et al., 2018). However, the results and conclusions made by the authors are controversial (for review; (Gonzalez-Hernandez and Charlet, 2018)).

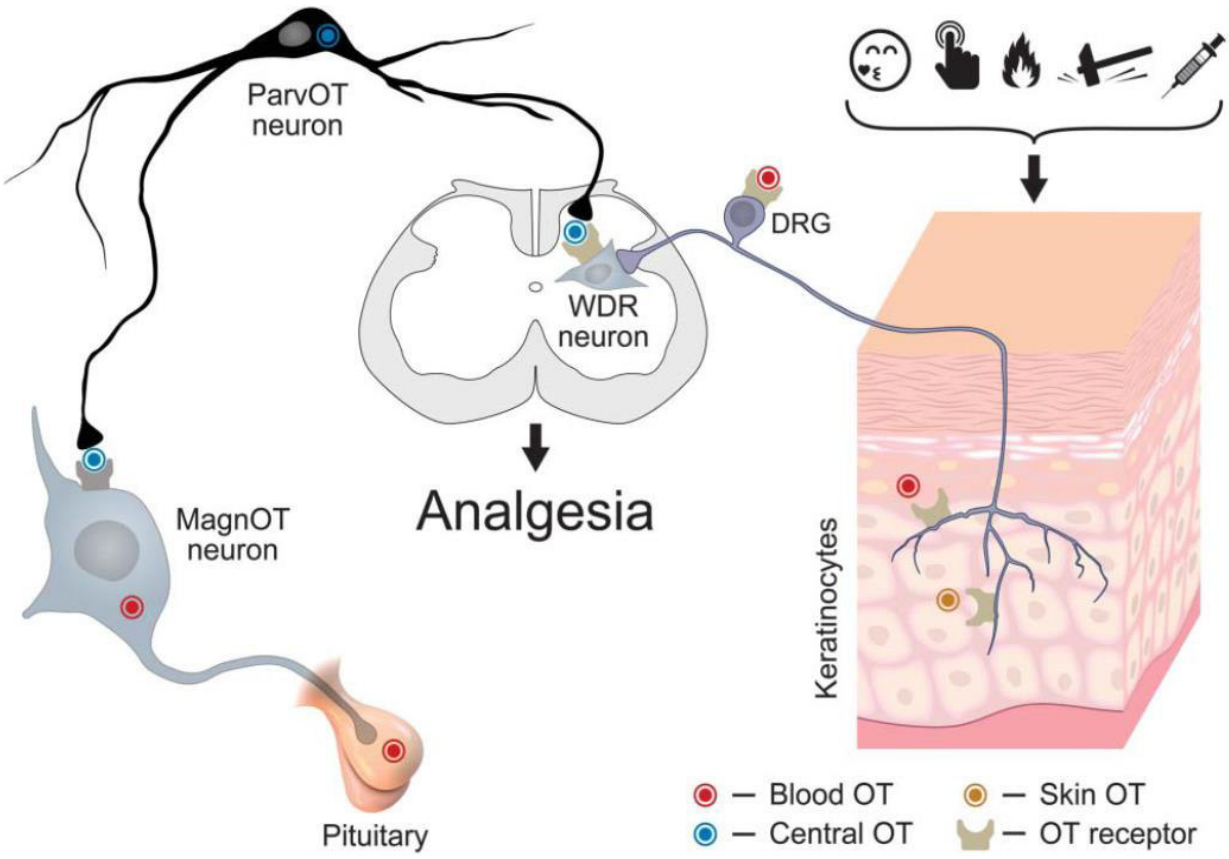

Figure 19: Oxytocin mediated peripheral and central analgesia.

OT acts through a three-way path: central release at the spinal cord level, to directly inhibit the activity of WDR neurons; blood release, via the pituitary, to inhibit either the cell body and peripheral nociceptive fibres of DRG neurons; and skin release after skin stimulation, to inhibit the excitation of nociceptive fibres. *Adapted from: Grinevich & Charlet (2017).*

All together, these elements raise many questions about the cutaneous OT system and its peripheral role in analgesia that will require further studies to better understand it (Grinevich and Charlet, 2017).

However, the analgesic properties of OT are not limited to the PNS, as seen previously. The peripheral effects of OT are mainly induced by its release from the pituitary into the bloodstream. In addition, OT in the WDRs of the spinal cord also modulate the nociceptive signal. Thus, it is necessary to study the anti-nociceptive effects of OT at the spinal and supra-spinal level to best define the cellular and neuronal targets of an analgesic compound targeting OTR.

3.2.2.2. Anti-nociceptive effect at the spinal level

PVN is the only hypothalamic nucleus that contains parvOT neurons and these neurons play a key role in the OT anti-nociceptive effect at the spinal level (**Figure 19**).

ParvOT neurons send axons to different laminae of the spinal and their axons make synaptic contacts with these laminae neurons of the dorsal horn (lamina I and II) and in the central grey (lamina X) (Rousselot et al., 1990; Jójárt et al., 2009; Moreno-López et al., 2013). Additionally OT innervation is particularly pronounced around some section of the spinal cord (e.g. thoracic L3, lumbar L2 and L6) (Swanson and McKellar, 1979; Schoenen et al., 1985). OTR is densely expressed in the superficial laminae of the dorsal horn especially in the most superficial layers (I and II), consistent with the presence of OT fibres (Reiter et al., 1994). Together, these data provide an anatomical support for a direct modulation of spinal cord neurons by OT, likely affecting the nociceptive processing (for review; (Boll et al., 2018)). Unlike the peripheral effect of OT on nociception, it appears that the AVP system is not involved in these effects of OT at the spinal level (Rojas-Piloni et al., 2010).

The anti-nociceptive effects of OT can also be observed by stimulating the descending OT projections from PVN; while recording the nociceptive Aδ- and C-evoked discharge, Condés-Lara et *al.* were able to reduce the duration of such discharge by electrical stimulation of the PVN (Condés-Lara et al., 2006). The effect of PVN stimulation is replicated by exogenous application of OT on the spinal recording site, and both effects were reversed by application of an OTR antagonist. They further proved that, in an *in vivo* model of hyperalgesia and allodynia, intrathecal (i.t.) OT have clear anti-hyperalgesic properties (Condés-Lara et al., 2006). *In vivo* studies by DeLaTorre et *al.* further showed that exogenous OT or endogenous OT released

through PVN stimulation could reduce or prevent the long-term potentiation of WDR neurons (DeLaTorre et al., 2009). More recently, the study of Eliava et *al.* deciphered a new small population of parvOT neurons residing in the PVN, which mediate analgesia via peripheral (see *2.2.1.1. Peripheral anti-nociceptive effect*) and central mechanisms (**Figure 19**). Furthermore, they show that activation of this specific population of parvOT neurons can control the release of OT into the bloodstream from magnOT neurons and directly target deep layers WDR neurons to ensure a coordinated and complementary effect of peripheral and central release OT on nociception (**Figure 19**) (Eliava et al., 2016).

Electrophysiological experiments revealed that OT-sensitive neurons could be glutamatergic. A presynaptic excitation of glutamatergic transmission was found after OT infusion in primary cultures of rat layer I-III spinal cord neurons (Jo et al., 1998). *In vivo* unit recordings of the spinal cord in rats revealed that application of OT could elicit either activation or inhibition of the recorded neurons (Condés-Lara et al., 2003). Later, Breton et *al.* revealed by c-Fos expression that OT-activated spinal cord neurons were always non-GABAergic neurons. They also shown that in lamina II, OT actually activates a subpopulation of glutamatergic interneurons, which allow the recruitment of GABAergic interneurons in the same lamina (Breton et al., 2008). This increased inhibition potentially inhibits incoming nociceptive signal coming through Aδ and C nociceptors (Breton et al., 2008).

It is also important to note that a participation of μ-opioid receptor was also involved in the anti-nociceptive effect of OT but mainly on supraspinal areas (Rash et al., 2014). Indeed, their blockade partially blocked the inhibitory effects of OT application or PVN stimulation (Miranda-Cardenas et al., 2006; Condés-Lara et al., 2009).

OT descending projection to the spinal level that modulate the nociceptive signal are so far established as arising from the hypothalamus. However, whether they are direct or indirect projections, they also involve other supraspinal structures that could trigger analgesic as well as anxiolytic effects.

3.2.2.3. Anti-nociceptive properties in supraspinal structure

Pain stimuli raise the concentration of OT in many supraspinal areas such as thalamic reticular nucleus, PAG, RVM, raphe nucleus, locus coeruleus. Moreover, i.c.v infusion of OT alleviates pain, whereas an anti-OT serum increases it (Yang et al., 2007).

The PAG and RVM are closely interconnected areas and are known to be involved in the descending pathway of pain modulation (West et al., 2015; Bell, 2018). PAG contains OT fibres from the hypothalamus and is also an area where OTR are expressed (**Figure 20**) (Figueira et al., 2008; Campbell et al., 2009). Studies by Yang et *al.* demonstrated that painful stimuli are able to elevate the OT concentration in the PAG and that a PAG infusion of OT can decrease pain threshold (Yang et al., 2011a, 2011b). Furthermore, it was found that the RVM is highly innervated by PVN OT neurons and OT fibres can directly activate RVM nociceptive cells (Mack et al., 2002; Lee et al., 2013).

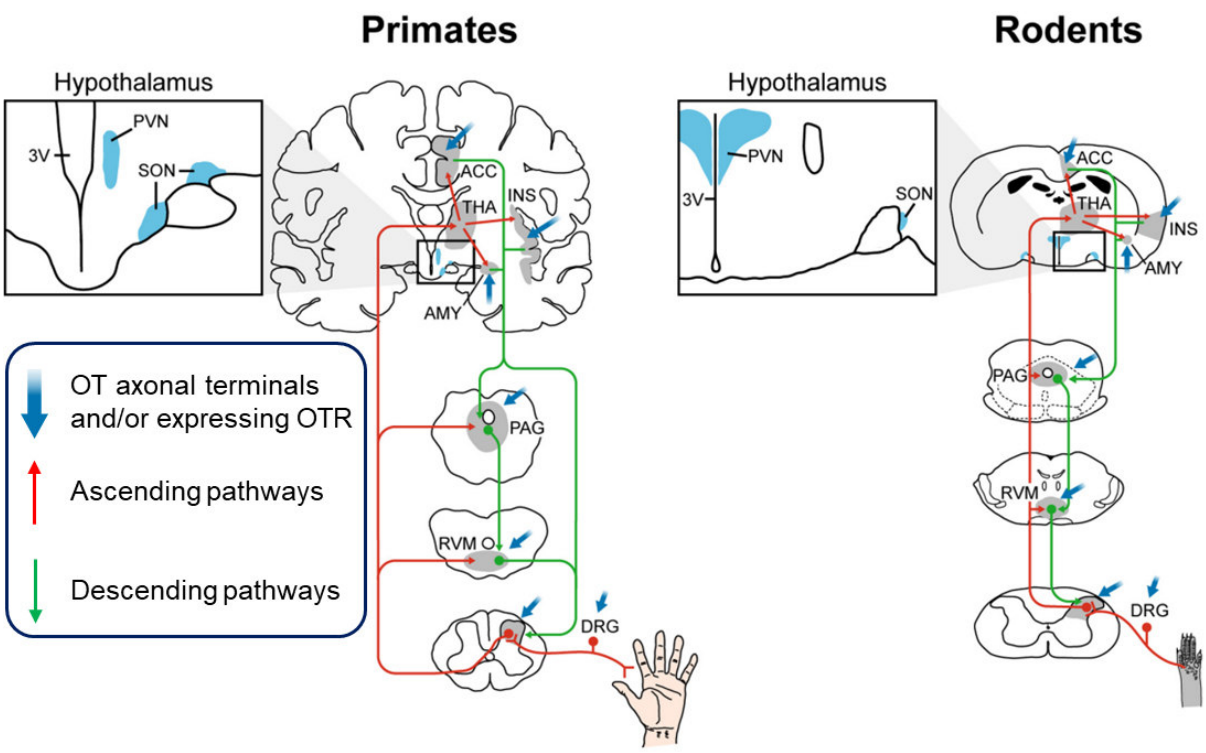

Figure 20: Spinal and supraspinal pain and oxytocin pathways.

Circuitry involved in pain and OT pathways in primates (left) and rodents (right). Abbreviations: AMY, Amygdala; ACC, Anterior cingulate cortex; INS, Insular cortex; THA, Thalamus. *Adapted from: Boll et al. (2018).*

Regarding anxiety, amygdala is known to be involved in the circuitry that assigns emotional significance to sensory information (Sah et al., 2003) and represents a key structure in the emotional regulation of pain (**Figure 20**) (Neugebauer et al., 2009). A study from Han et *al.* showed that injection of OT into the amygdala induces a dose-dependent reduction of the nociceptive threshold level (Han and Yu, 2009). In addition, the release of OT in the amygdala attenuates fear responses (Knobloch et al., 2012).

Finally, hypothalamic OT neurons project axons to various cortical areas, such as the orbitofrontal, cingulate, insular and medial prefrontal cortex, which express moderate levels of OTR (**Figure 20**) (for review; (Boll et al., 2018)). However, no studies nowadays have been conducted to assess the direct effects of OT on cortical processing of pain (Boll et al., 2018).

In conclusion, OT and its system can modulate the nociceptive signal at different levels (peripheral, spinal, supraspinal). They can also affect pain perception by triggering top-down controls (PAG) and modulating pain-related behaviours (anxiety) in cortical structures.

Considering these points, targeting the OT system via an OTR agonist seems to be promising therapeutic approach.

3.2.3. OT as a therapeutic drug?

Based on the observation of these anti-nociceptive effects, one question arises: could OT be used as a therapeutic central or peripheral treatment against pain?

A first element of answer is that the observations of analgesic effects obtained in rodents can be transposed to the treatment of pain in humans, as i.t. OT injections successfully reduced low-back pain (Yang, 1994) and visceral pain (Engle et al., 2012). Moreover, human data corroborates animal ones regarding the analgesic role of OT on peripheral nociceptors (Alfvén et al., 1994; Alfvén, 2004).

However, despite its interesting analgesic properties OT is not used in the treatment of pain, it is only used to initiate labour (Heesen et al., 2019) and stimulate milk ejection (Newton and Egli, 1958). This is due to its low efficiency to cross the BBB (Ermisch et al., 1985; Kang and Park, 2000) and its short half-life in the blood

circulation (Mens et al., 1983). Mens et *al.* estimated that 0.002% of OT in intra-cutaneous injection penetrate to the brain (Mens et al., 1983).

In order to bypass these issues, another route of administration of OT is usually suggested to reach the brain: intranasal application by sprays. Publications about the intranasal application of OT can be found as early as 1958, as a mean to facilitate lactation in women (Newton and Egli, 1958). However, the use of nasal OT spray to affect the CNS is still very controversial (for review; (Leng and Ludwig, 2016)).

In addition to this short half-life in the blood circulation (5 minutes) and in the CSF (20 minutes) (Mens et al., 1983), OT suffers from several additional drawbacks: a lack of specificity. OT has very similar affinities for its receptor OTR and for V1aR, which could led to various side effects (e.g. vasoconstriction, increased heartbeat) (Chini et al., 1996; Kubo et al., 2017). Finally, OT has also an extremely poor oral absorption and distribution since its high molecular weight prevents or strongly limits its absorption from the gastro intestinal tract to the blood or from the blood to the brain (for review; (Gimpl and Fahrenholz, 2001; Lee et al., 2009; Jurek and Neumann, 2018)).

One alternative to use the OT system in the treatment of pain, without suffering from these drawbacks, is to use a specific non-peptidergic agonist (chemically engineered) that would be able to recruit specifically the OT system even with a peripheral administration. Recently, a first non-peptidergic full agonist of OT (LIT-001) has been reported to improve social interactions in a mouse model of autism spectrum disorders after peripheral administration (**Figure 21**) (Frantz et al., 2018). LIT-001 is a pyrazolobenzodiazepine derivative with a non-peptide chemical structure and a low molecular weight (MW) compared to OT (MW = 531 vs. 1007). Frantz et *al.* have found that LIT-001 is a specific OTR agonist with high affinity (EC_{50} = 25 nM vs. 18 nM) and efficacy (E_{max} = 96% and 95%) for human and mouse receptors. Furthermore, the compound poorly antagonized AVP induced calcium release on V1aR and was devoid of agonist or antagonist effect on V1bR (Frantz et al., 2018).

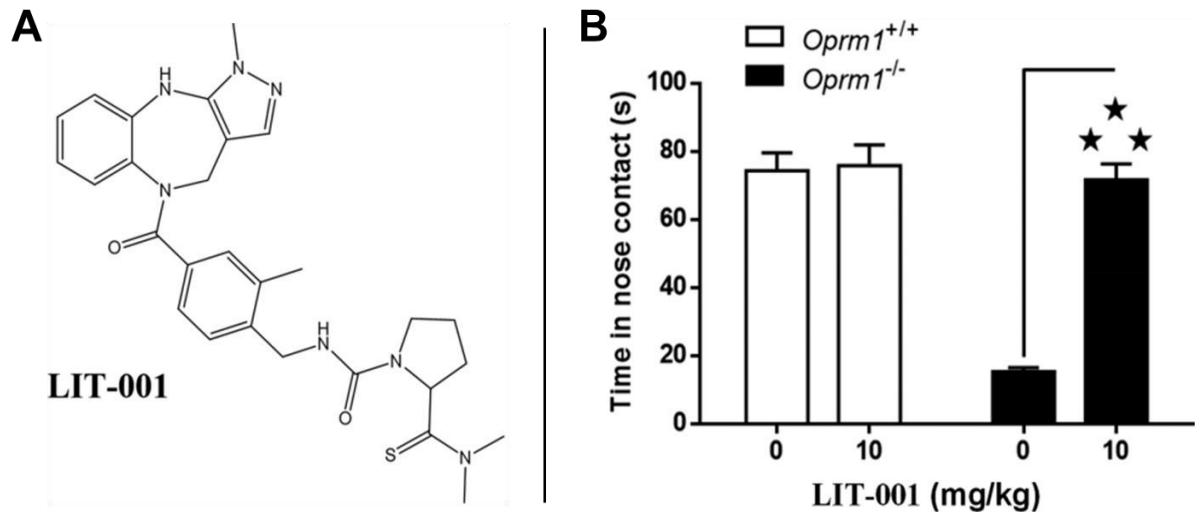

Figure 21: LIT-001, an oxytocin receptor agonist that improves social interaction.

(**A**) Structure of LIT-001. (**B**) LIT-001 restores social interaction in a mouse model of autism spectrum disorders (Oprm $1^{-/-}$). *Adapted from: Frantz et al. (2017).*

For all the above reasons, the OT system needs to be studied in greater depth to better understand its analgesic potential and mechanisms. It would enable develop a potent analgesic treatment based on an OTR agonist that could modulate the nociceptive signal at multiple levels. LIT-001 could be a very promising analgesic therapeutic compound.

PHD OBJECTIVES

The aim of my PhD research consisted in exploring the analgesic potential of new innovative molecules, which targets endogenous analgesic systems.

During these three years, I acquired a strong expertise in the behavioural evaluation of the analgesic potency of a molecule in an animal model. This expertise allowed me to characterize the analgesic potential of two innovative molecules, pulegone, a monoterpene analogue of menthol and yet largely under-studied, which is of particular interest for BENEPHYT; and LIT-001 resulting from the engineering of the oxytocin receptor, for which my host team has a strong expertise.

1. Evaluation of monoterpenes analgesic potential

The general project of BENEPHYT aimed to characterize the analgesic potential of terpenes, or mixtures of terpenes, originating from pharmacopeia plants, with the purpose of developing analgesic treatments based on these molecules. Based on the data obtained from an extensive bibliographic work (**Introduction: 2. Terprenes** [**Tables 2, 3 & 4**]) which will be adapted for publication in a review, I was able to identify some monoterpene profiles of potential interest for BENEPHYT, such as pulegone.

BENEPHYT approached Dr. Eric Marchioni's team to extract and characterize the main monoterpene from *Clinopodium nepeta* (L.) Kuntze, pulegone. Then I characterized the effects of pulegone on mechanical and thermal sensitivity in a model of induced inflammatory pain. These results have been compared with those obtained with menthol. I also undertook locomotion tests to check if monoterpenes presented any locomotive or sedative side effects. This work is presented in the **Article 1**.

Then, we tried to reduce the doses of monoterpenes to be injected, looking for a potential synergistic effect between menthol and pulegone. I therefore evaluated the analgesic properties of a mixture of menthol and pulegone, again in a model of induced inflammatory pain in order to compare the results obtained with menthol and pulegone individually. The results are reported in **Annex 4 Terpene combination**.

2. Evaluation of the analgesic potential of the oxytocinergic system

We saw that OT has a certain analgesic potency. However, the clinical use of OT for its analgesic potential is severely compromised by its short half-life.

Thus, I investigated the analgesic potential of a molecule, synthesized by our collaborator Dr. Marcel Hibert, the LIT-001. This molecule is a non-peptidergic agonist of OTR and is a stable molecule, with little or no metabolisation by the organism, unlike OT. In order to assess the analgesic properties of LIT-001, I performed different behavioural experiments (thermal and mechanical sensitivity) in a model of induced inflammatory pain. I also monitored the involvement of the OTR, by performing a co-injection of LIT-001 with an antagonist of OTR. This work is presented in the **Article 2**.

In collaboration with Prof. Valery Grinevich we also aimed to improve our understanding of how endogenous OT exerts its analgesic activity. We furthered the understanding of the analgesic mechanisms of OT by studying the role of a population of OTR-presenting neurons in the PAG, contacted by OT neurons from the PVN.

We evaluated the analgesic potential of stimulating OTR-expressing neurons in PAG in a model of induced inflammatory pain by measuring mechanical and thermal sensitivity. To be able to discern the antinociceptive effects from the emotional aspects of pain control by the OT system, I performed an additional experiment, the CPP test. The results of this work are reported in the **Article 3**.

RESULTS

RESULTS

1. Article 1: Anti-hyperalgesic Properties of Menthol and Pulegone

1.1. Overview

1.1.1. Introduction

Medicinal plants among the Lamiaceae family, including *Mentha piperita* (L.) and *Calamintha nepeta* (L.), have been used as medicinal plants since the ancient Greece (Carović-Stanko et al., 2016). Additionally, Adams et *al*. found specific mentions of usage of *C. nepeta*, as a treatment of pain and rheumatism in herbals of the 17th century (Adams et al., 2009). The main bioactive compounds of this plant family (Lamiaceae) are secondary metabolites including terpenoids, alkaloids and phenolic compounds. Terpenoids are considered as the largest family of natural compounds, among which we find the monoterpenes group (Vavitsas et al., 2018). However, less than 50 monoterpenes have been described as potential analgesic and/or anti-inflammatory molecules (Guimarães et al., 2013).

Among these monoterpenes, one of the most studied is menthol, which is known to inhibit nociceptor neuronal activity through TRPM8 (Pan et al., 2012). Menthol is also the major monoterpene present in *M. piperita*, and is known to modulate the nociceptive threshold by reducing sensory hypersensitivity in visceral pain (Galeotti et al., 2002) and inflammatory pain (Pan et al., 2012).

Pulegone, on the other hand is a less studied monoterpene but it is the main monoterpene found in the essential oil of *C. nepeta* (Li et al., 2017b). Additionally it is a precursor in the biosynthesis of menthol (Li et al., 2017b). We currently know that pulegone acts as an avian repellents through the modulation of TRPM8 and TRPA1 (Majikina et al., 2018). However, despite the similarities between menthol and pulegone, the analgesic potential of pulegone has been little studied, and there is a lack of information on either the putative effect of pulegone treatment or the nociceptive modalities on which it might act (de Sousa et al., 2011).

Here, we analysed the monoterpenes composition of *C. nepeta* and *M. piperita*. We then investigated the analgesic potential of the main monoterpenes found, menthol

and pulegone, for the thermal and mechanical sensitivity in a rat model of induced inflammatory pain (CFA).

1.1.2. Results

We first analysed by gas chromatography-mass spectrometry the *M. piperita* and *C. nepeta* extracts obtained by pressurized liquid extraction. Respectively, 11 and 10 volatile compounds were identified in *M. piperita* and *C. nepeta* extracts. As expected, the main constituent of the *C. nepeta* extract was pulegone (49.41 %), while the one of the *M. piperita* extract was menthol (42.85 %).

We then assessed the *in vitro* anti-inflammatory activity of menthol and pulegone by measuring the secretion of the TNF-α from THP-1 cells after 4 h incubation with each monoterpene. Interestingly, we observed a similar reduction of TNF-α secretion after incubation with menthol (3 mM) or pulegone (3 mM). Furthermore, before testing the compounds *in vivo* we also evaluated their cytotoxicity *in vitro*. The cytotoxicity curves were significantly different, a 100 % cells death rate for menthol at a concentration of 12.8 mM, while a similar pulegone concentration induced a 45.1 % cells death rate.

Therefore, we tested the putative analgesic properties of menthol and pulegone in a CFA-induced inflammatory pain model. For this purpose, we performed a dose-response of the analgesic action of i.p. injected menthol and pulegone on mechanical, thermal heat, and thermal cold sensitivities. First, we observed that menthol and pulegone induced dose-dependent reduction of the mechanical hypersensitivity, which reaches a plateau value at 50 mg/kg for menthol and 100 mg/kg for pulegone. Secondly, both menthol and pulegone induced a dose-dependent reduction of thermal heat hypersensitivity, which reaches a plateau value at 100 mg/kg. Thirdly, only pulegone (at 100 mg/kg) induced a significant decrease in thermal cold sensitivities. Interestingly, the anti-hyperalgesic effect induced by pulegone was slightly higher than the one induced by menthol for all tested modalities.

These results allowed us to perform a time-course of the anti-hyperagesic effect of menthol and pulegone i.p. at the optimal dose of 100 mg/kg regarding their anti-hyperalgesic effects. Although pulegone induced an anti-hyperalgesic effect on all measured modalities as early as 20 minutes after injection, significant effects of

menthol were only observed 40 minutes after injection. Nevertheless, the effects of the two terpenes fade away 80 min after the i.p. injection.

Interestingly, none of those observations were reproduced on contralateral hindpaw (i.e., paw without inflammatory sensitization), suggesting an absence of anti-nociceptive effects.

Given that monoterpenes might have strong unwilling side effects when injected at high doses (> 200 mg/kg), we performed several controls to assess that the previous experiments are free of motor reflex bias. To do so, we tested the motor activity of the rats after the i.p. injection of either pulegone or menthol (150 mg/kg), using two different experimental paradigms: the beam walk assay and the rotarod assay. In both tests, both menthol and pulegone showed no impairment of the locomotor abilities of the animals.

In conclusion, we showed that pulegone has a significantly higher effect than menthol on nociceptive sensory thresholds in a CFA-induced inflammatory pain model, without negative locomotor side effects. This suggests that traditional treatments based on *C. nepeta* preparations have indeed the potential to reduce pain conditions. This work thus supports the interest and potential of ethnopharmacological research for the discovery of new innovative treatments in the treatment of pain.

Author contribution:

This study was a collective work, I detail below my personal contribution to the following experiments (and consequent analysis):

- Behavioural experiments.

frontiers in Pharmacology

ORIGINAL RESEARCH
published: 30 November 2021
doi: 10.3389/fphar.2021.753873

Anti-Hyperalgesic Properties of Menthol and Pulegone

Louis Hilfiger[1,2†], Zélie Triaux[1,3†], Christophe Marcic[3], Eléa Héberlé[1], Fathi Emhemmed[3], Pascal Darbon[2], Eric Marchioni[3], Hugues Petitjean[1‡] and Alexandre Charlet[2*‡]*

[1]Benephyt, Strasbourg, France, [2]Centre National de la Recherche Scientifique, University of Strasbourg, Institute of Cellular and Integrative Neurosciences, INCI UPR3212, Strasbourg, France, [3]Centre National de la Recherche Scientifique, University of Strasbourg, Institut Pluridisciplinaire Hubert Curien, IPHC UMR, Strasbourg, France

OPEN ACCESS

Edited by:
Marie Jeanne Mukazayire, University of Rwanda, Rwanda

Reviewed by:
Germain Sotoing Taiwe, University of Buea, Cameroon
Armando Caceres, Universidad de San Carlos de Guatemala, Guatemala
Adnan Amin, Gomal University, Pakistan

***Correspondence:**
Alexandre Charlet
acharlet@unistra.fr
Hugues Petitjean
hugues.petitjean@benephyt.fr

‡These authors jointly supervised this work

†These authors have contributed equally to this work and share first authorship

Specialty section:
This article was submitted to Ethnopharmacology, a section of the journal Frontiers in Pharmacology

Received: 05 August 2021
Accepted: 29 October 2021
Published: 30 November 2021

Citation:
Hilfiger L, Triaux Z, Marcic C, Héberlé E, Emhemmed F, Darbon P, Marchioni E, Petitjean H and Charlet A (2021) Anti-Hyperalgesic Properties of Menthol and Pulegone. Front. Pharmacol. 12:753873. doi: 10.3389/fphar.2021.753873

Context: Menthol, the main monoterpene found in *Mentha piperita* L. (*M. piperita*) is known to modulate nociceptive threshold and is present in different curative preparations that reduce sensory hypersensitivities in pain conditions. While for pulegone, a menthol-like monoterpene, only a limited number of studies focus on its putative analgesic effects, pulegone is the most abundant monoterpene present in *Calamintha nepeta* (L.) Savi (*C. nepeta*), a plant of the Lamiaceae family used in traditional medicine to alleviate rheumatic disorders, which counts amongst chronic inflammatory diseases.

Objectives: Here, we analyzed the monoterpenes composition of *C. nepeta* and *M. piperita*. We then compared the putative anti-hyperalgesic effects of the main monoterpenes found, menthol and pulegone, in acute inflammatory pain conditions.

Methods: *C. nepeta* and *M. piperita* extracts were obtained through pressurized liquid extraction and analyzed by gas chromatography-mass spectrometry. The *in vitro* anti-inflammatory activity of menthol or pulegone was evaluated by measuring the secretion of the tumour necrosis factor alpha (TNF α) from LPS-stimulated THP-1 cells. The *in vivo* anti-hyperalgesic effects of menthol and pulegone were tested on a rat inflammatory pain model.

Results: Pulegone and menthol are the most abundant monoterpene found in *C. nepeta* (49.41%) and *M. piperita* (42.85%) extracts, respectively. *In vitro*, both pulegone and menthol act as strong anti-inflammatory molecules, with EC50 values of 1.2 ± 0.2 and 1.5 ± 0.1 mM, respectively, and exert cytotoxicity with EC50 values of 6.6 ± 0.3 and 3.5 ± 0.2 mM, respectively. *In vivo*, 100 mg/kg pulegone exerts a transient anti-hyperalgesic effect on both mechanical (pulegone: 274.25 ± 68.89 g, $n = 8$; vehicle: 160.88 ± 35.17 g, $n = 8$, $p < 0.0001$), thermal heat (pulegone: 4.09 ± 0.62 s, $n = 8$; vehicle: 2.25 ± 0.34 s, $n = 8$, $p < 0.0001$), and cold (pulegone: 2.25 ± 1.28 score, $n = 8$; vehicle: 4.75 ± 1.04 score, $n = 8$, $p = 0.0003$). In a similar way, 100 mg/kg menthol exerts a transient anti-hyperalgesic effect on both mechanical (mechanical: menthol: 281.63 ± 45.52 g, $n = 8$; vehicle: 166.25 ± 35.4 g, $n = 8$, $p < 0.0001$) and thermal heat (menthol: 3.65 ± 0.88 s, $n = 8$; vehicle: 2.19 ± 0.26 s, $n = 8$, <0.0001).

Conclusion: Here, we show that both pulegone and menthol are anti-inflammatory and anti-hyperalgesic monoterpenes. These results might open the path towards new compound mixes to alleviate the pain sensation.

Keywords: pulegone, pain, rodent, menthol, inflammatory pain, monoterpene

INTRODUCTION

Medicinal plants amongst the Lamiaceae family, including *Mentha piperita* L. (*M. piperita*) and *Calamintha nepeta* (L.) Savi (*C. nepeta*), have been used in traditional medicine since the ancient Greeks (Carović-Stanko et al., 2016) and during the Renaissance to alleviate rheumatoid disorders and chronic pain in the upper valley of the Rhine in Europe (Adams et al., 2009). *C. nepeta* was first described by Carl Linneus as "Melissa nepeta." Since 1753, it has been replaced in the *Calamintha*, *Thymus*, *Satureja*, *or Clinopodium* genera. This plant grows as a perennial herb native to Europe and the Mediterranean region. It bears ovate, opposite gray-green leaves, white to pink tubular, two-lipped flowers and is very fragrant when crushed according to the World Checklist of Selected Plant Families (Govaerts, 2020). Adams and collaborators found mentions of usage of *C. nepeta*, a synonym for *Clinopodium nepeta* (L.) Kuntze, as a treatment of pain and rheumatism in two major herbals of the 17th century (Adams et al., 2009). Mattioli's herbal advised the drinking of boiled calamint against gout and tough slime (Mattioli, 1554). Moreover, Fuchs' herbal advises the use of an external application of leaves against hip pain (Fuchs, 1543). Since then, it has not been used much by modern herbalists, making it an interesting plant to re-investigate.

The main bioactive compounds in Lamiaceae plants are secondary metabolites including terpenoids, alkaloids, and phenolic compounds (Tissier et al., 2015). With about 70,000 structures described (Harborne, 1995), terpenoids are considered the largest family of natural compounds (Vavitsas et al., 2018). Those natural compounds are classified by the number of isoprene units containe in their chemical structure. Monoterpenes, composed of two isoprene units, are the main components of essential oils and are responsible for their diverse well-known biological activities (Salakhutdinov et al., 2017). In general, monoterpenes are derived from geranyl diphosphate (GPP) which is a product of the head-to-tail coupling of the primary metabolites isopentenyl diphosphate (IPP) and dimethylallyl diphosphate (DMAPP) (Rehman et al., 2016). Less than 50 monoterpenes have been described as potential analgesic (Guimarães et al., 2013) and/or anti-inflammatory molecules (De Cássia Da Silveira E Sá et al., 2013). However, menthol, the major monoterpene found in *M. piperita* (Ristorcelli et al., 1996), is known to modulate nociceptive threshold and is present in different curative preparations that reduce sensory hypersensitivities in pain type such as visceral pain (Galeotti et al., 2002), inflammatory pain (Pan et al., 2012) as well as neuropathic pain (Patel et al., 2014). One of the known mechanisms enabling menthol to act as a pain-killer is the inhibition of neural activity via the desensibilization of the TRPM8 channels expressed by the nociceptive sensory fiber endings (Pan et al., 2012; Liu et al., 2013).

Pulegone, a major monoterpene found in the essential oil of *C. nepeta* (Božović et al., 2017; Li et al., 2017), is obtained from GPP through limonene and piperitone, isopulegone being its direct precursor (Turner and Croteau, 2004). Pulegone is a precursor in the biosynthesis of menthol through menthone (Li et al., 2017). This monoterpene acts as an avian repellents through the modulation of the TRPM8 and TRPA1 channels expressed by bird sensory neurons (Majikina et al., 2018). In spite of the similarities between menthol and pulegone, the analgesic potential of pulegone was only studied in one visceral pain model (de Sousa et al., 2007) and one spontaneous pain model (de Sousa et al., 2011). Despite these observations, there is not much information on neither the putative effect of a curative pulegone treatment nor on nociceptive modalities on which it may act.

Interestingly, a recent review (Quintans et al., 2019) lists several terpenes that modulate the activity of cytokines, including the tumour necrosis factor (TNF-α), a cytokine involved in the primary onset of inflammatory responses maintenance and in its chronicity (Basbaum et al., 2009). Menthol and pulegone are cited within this list. Despite this potent anti-inflammatory action, only recent works explore the potential analgesic actions of terpenes (Guimarães et al., 2013; Yang et al., 2019a, 2019b; Perri et al., 2020; Bai et al., 2021; Wojtunik-Kulesza et al., 2021). Therefore, in the present study, we hypothesized that pulegone might have potent analgesic action on peripheral painful inflammatory sensitization, and tested its *in vitro* anti-inflammatory effect and cytotoxicity and its *in vivo* anti-hyperalgesic effects in the Freund's Complete Adjuvant (CFA)-induced inflammatory pain model.

RESULTS

Mentha piperita L. and *Calamintha nepeta* L. Extracts Analysis

M. piperita and *C. nepeta* extracts were obtained by pressurized liquid extraction (PLE) and analyzed by gas chromatography-mass spectrometry (GC-MS) (**Figure 1A**; **Supplementary Figure S1**). Overall, 11 volatile compounds were identified in the *M. piperita* extract (**Figure 1B**) and 10 in the *C. nepeta* PLE extract. As expected, the main constituent of the *C. nepeta* extract was pulegone (49.41%), while the one of the *M. piperita* extract was menthol (42.85%). The presence of isopulegone in the *C. nepeta* extract (**Figure 1B**), indicates that the isomerase conversion was not complete. In the same extract, menthol, isomenthone, and menthone can be found at lower concentrations than pulegone. Given the absence of pulegone detection in *M. piperita* extracts, its analgesic effects in traditional medicine cannot be attributed to pulegone. On the other hand, it raises the question of pulegone putative analgesic action, as it is the principal monoterpene found in *C. nepeta* (Adams et al., 2009).

Considering these results, we then restricted our investigation to the potential anti-inflammatory and analgesic properties of these two major compounds, pulegone and menthol.

Menthol and Pulegone Display *In Vitro* Anti-inflammatory Effects

The *in vitro* anti-inflammatory activity of menthol or pulegone was evaluated by measuring the secretion of the TNF-α from THP-1 cells after 4 h incubation with either menthol or pulegone (**Figures 2A–C**; **Supplementary Figure S2**). We used LPS to induce production of

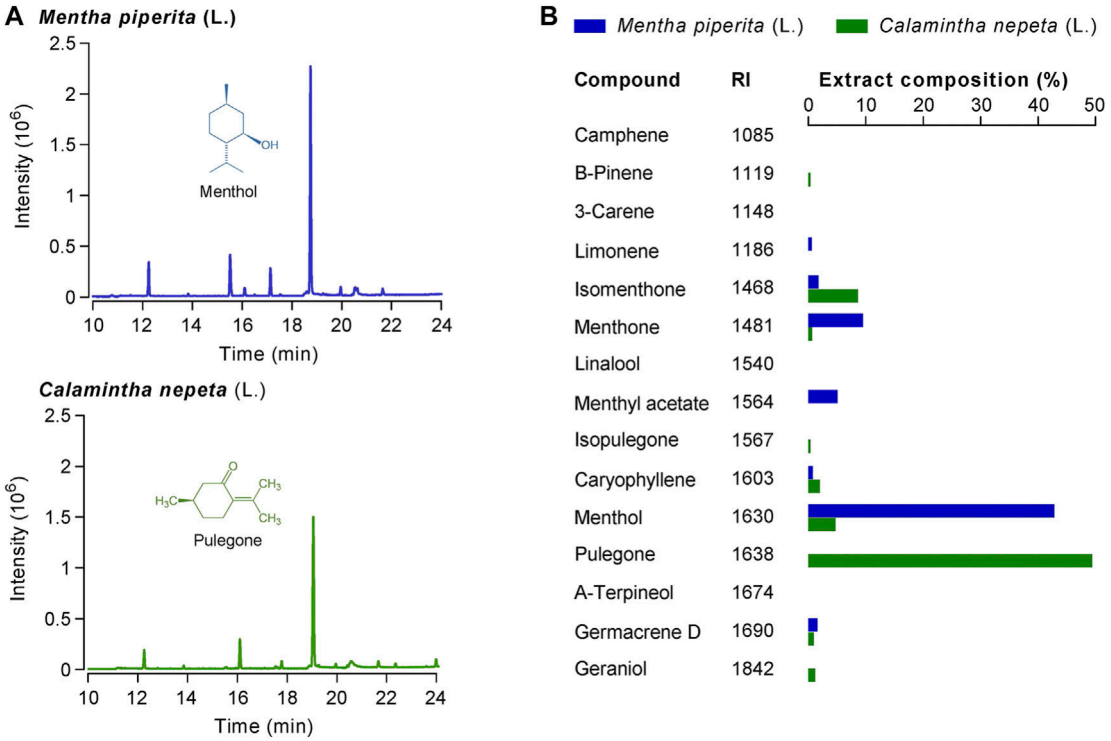

FIGURE 1 | (A) Chromatograms of *Calamintha nepeta* (L.) Savi and *Mentha piperita* L. PLE extracts 10-fold diluted were analyzed by GC-MS. On both chromatograms, the main components of each extract are identified: pulegone (T_R = 19.04 min) for *C. nepeta* and menthol (T_R = 18.75 min) for *M. piperita*. **(B)** Extract composition (in %) together with retention index (RI) of each found compound.

TNF-α, an effect that is blocked by celastrol (500 mM), a triterpene used as a positive control of the inhibition of the secretion of TNF-α (Allison et al., 2001); **Figure 2A**; ethanol 1%: 78.3 ± 0.7% vs. celastrol 500 mM: 1.1 ± 0.1%, n = 3, F(3;8)= 1,031.6, Dunnett Test $p < 0.001$). Interestingly, we observed a similar reduction of the secretion of TNF-α after incubation with menthol 3 mM (reduced to 1.2 ± 0.05% n = 3, $p < 0.001$) or pulegone 3 mM (reduced to 12.5 ± 2.2% n = 3, $p < 0.001$) (**Figure 2A**). We then evaluated the *in vitro* cytotoxicity of those different compounds. Interestingly, pulegone 3 mM presents a low cytotoxicity, comparable to the one of celastrol 500 mM, our positive control (5.6 ± 0.2% n = 3, and 1.4 ± 0.2% n = 3, respectively; **Figure 2D**). However, menthol 3 mM displayed a significant cytotoxicity (32.5 ± 11.1%, n = 3, F(3;8) = 6.22, Dunnett Test p = 0.017) compared to vehicle (1% ethanol; 8.4 ± 0.3%, n = 3, p = 0.038; **Figure 2D**). Therefore, pulegone showed a promising anti-inflammatory activity conjugated with low cytotoxicity.

To refine this gross characterization, we performed dose-response curves (0.03–13 mM) of the anti-inflammatory activity (**Figure 2B**) and the cytotoxicity (**Figure 2E**) of menthol and pulegone. The anti-inflammatory activity curve of each compound presents, notably, a similar distribution and an EC_{50} value in the same range (menthol: 1.5 ± 0.1 mM, n = 3; pulegone: 1.2 ± 0.2 mM, n= 3; **Figure 2C**; t-Test DF= 4, p = 0.09), suggesting equivalent anti-inflammatory activities of both, menthol and pulegone. However, the cytotoxicity curves were significantly different, showing a 100% cells death rate with a concentration of 12.8 mM of menthol (**Figure 2E**), while a similar pulegone concentration induced only 45.1% cells death rate. In accordance with this observation, the EC_{50} of the cytotoxicity was 3.5 ± 0.2 mM for menthol and 6.6 ± 0.3 mM for pulegone (t-Test DF= 4, p = 0.0001; **Figure 2F**). Taken together, those results indicate that THP-1 cells, which are among the first cells involved in the inflammation process, can withstand a higher concentration of pulegone than menthol.

To further characterize the effect on menthol and pulegone, we then investigated their potential pain-killer effects *in vivo* on nociceptive thresholds.

Menthol and Pulegone Induce *In Vivo* Anti-hyperalgesia

We first performed a dose-response curve of the putative analgesic effects of menthol and pulegone, measured on mechanical, thermal heat, and thermal cold sensitivities, 40 min after a single intraperitoneal (i.p.) injection itself performed 24 h after intra-plantar injection of complete Freund adjuvant (Hilfiger et al., 2020) (CFA; **Figure 3**;). CFA-model, similarly to other inflammatory-induced pain models, induces mechanical, thermal heat, and cold hyperalgesia, with a plateau in hyperalgesia observed between 24 and 48 h following CFA injection (Hilfiger et al., 2020). We selected several doses of monoterpene treatments within a range previously published in protocols (de Sousa et al., 2011; Pan et al., 2012).

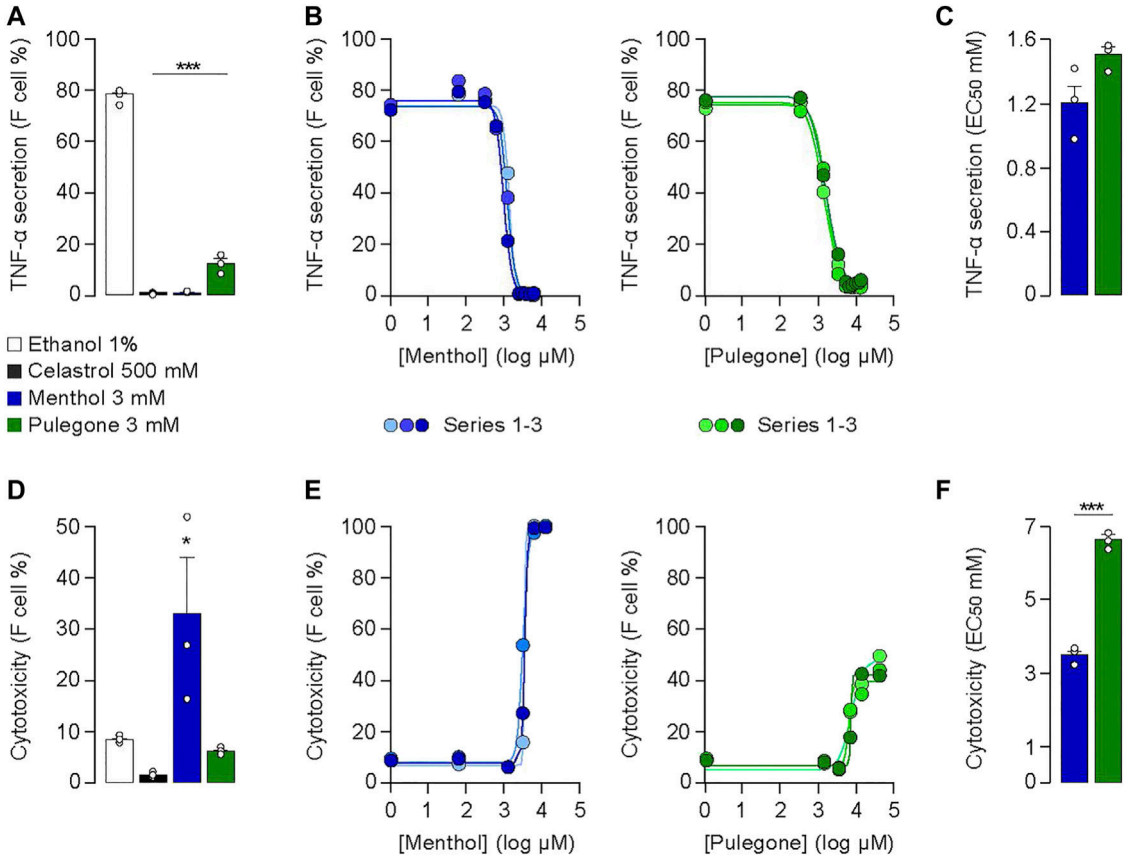

FIGURE 2 | (A) Anti-inflammatory activities and **(D)** cytotoxicities of pulegone and menthol at 3 mM in 1% ethanol after 4 h LPS-stimulation of THP-1 cells. Experiments (n = 3) were conducted on the same 96-well plate to compare to the same negative control (1% ethanol) (***p < 0.001; **p < 0.01; *p < 0.05). Celastrol at 500 mM was used as the positive control. **(B)** One-way ANOVA F(3;8) = 1,031.6, p < 0.001, **(E)** one-way ANOVA F(3;8) = 6.22 p = 0.05). Dose-response curves of **(B)** anti-inflammatory activity and **(E)** cytotoxicity of pulegone and menthol after 4 h LPS-stimulation of THP-1 cells. Concentration range: 0.03–13 mM. Each concentration was tested in triplicates on the same 96-well plate. **(C,F)** EC_{50} values calculated by the dose-response curves of **(C)** the anti-inflammatory activity and **(F)** cytotoxicity of menthol and pulegone. Ratios of the EC_{50} value of the anti-inflammatory activity over the EC_{50} value of the cytotoxicity for menthol (in blue) and pulegone (in green) compared with a t-test (***p < 0.001; **p < 0.01; *p < 0.05).

First, both menthol and pulegone induced dose-dependent increase of the mechanical threshold (Control vs. menthol: DF= 4, p = 0.0002; vs. pulegone: DF= 4, p < 0.001, Kruskal-Wallis and Dunn's comparisons **Figures 3A,B**), up to a plateau value obtained after 50 mg/kg for menthol (84.83 ± 17.87 Δg, n = 6; p = 0.0162 DF= 4, p < 0.001, Kruskal-Wallis and Dunn's comparisons) and 100 mg/kg for pulegone (150.2 ± 67.79 Δg, n = 8; p = 0.0007). Interestingly, while anti-hyperalgesic effects of menthol start at lower concentration than the one of pulegone (50 mg/kg vs. 100 mg/kg), the plateau effect induced by pulegone was slightly higher than the one induced by menthol. Secondly, both menthol and pulegone induced a dose-dependent increase of thermal heat withdrawal latency (Control vs. menthol: DF= 4, p < 0.0001; vs. pulegone: DF= 4, p =0.003, Kruskal-Wallis and Dunn's comparisons, **Figures 3C,D**), up to a plateau value obtained after 100 mg/kg (menthol: 1.713 ± 0.951 Δs, n = 8; p = 0.0016; pulegone 3.688 ± 0.852 Δs, n = 8; p = 0.0005). As previously, the anti-hyperalgesic effect of pulegone was significantly higher than the one induced by menthol (p = 0.0019). Thirdly, pulegone but not menthol induced a significant decrease in thermal cold acetone score (Control vs. menthol: DF= 4, p < 0.0001; vs. pulegone: DF= 4; p =0.1789, Kruskal-Wallis and Dunn's comparisons, **Figures 3E,F**) following 100 mg/kg injection (menthol: −1.25 ± 2.19 Δscore, n = 8; p = 0.0546; pulegone −1.63 ± 1.6 Δscore, n = 8; p = 0.0256). Finally, the anti-hyperalgesic effects of both terpenes were compared through their respective dose-response distribution, and showed that pulegone induced a significantly higher anti-hyperalgesic effect than menthol on all tested modalities (p < 0.001; **Figures 3B,D,F**). Interestingly, none of those observations were reproduced on contra-lateral paw (i.e., paw without inflammatory sensitization), suggesting an absence of potential deleterious anti-nociceptive effect (**Supplementary Figure S3**).

Along with this dose-response that allowed us to determine the optimal dose of i.p. terpene injection with regard to their anti-hyperalgesia effect (100 mg/kg), we next aimed to evaluate its duration. We thus monitored the mechanical, thermal heat, and thermal cold sensitivities every 20 min following i.p. injection of either menthol or pulegone at 100 mg/kg, carboxymethyl cellulose (CMC, 1%) in NaCl (0.9%) as a control vehicle

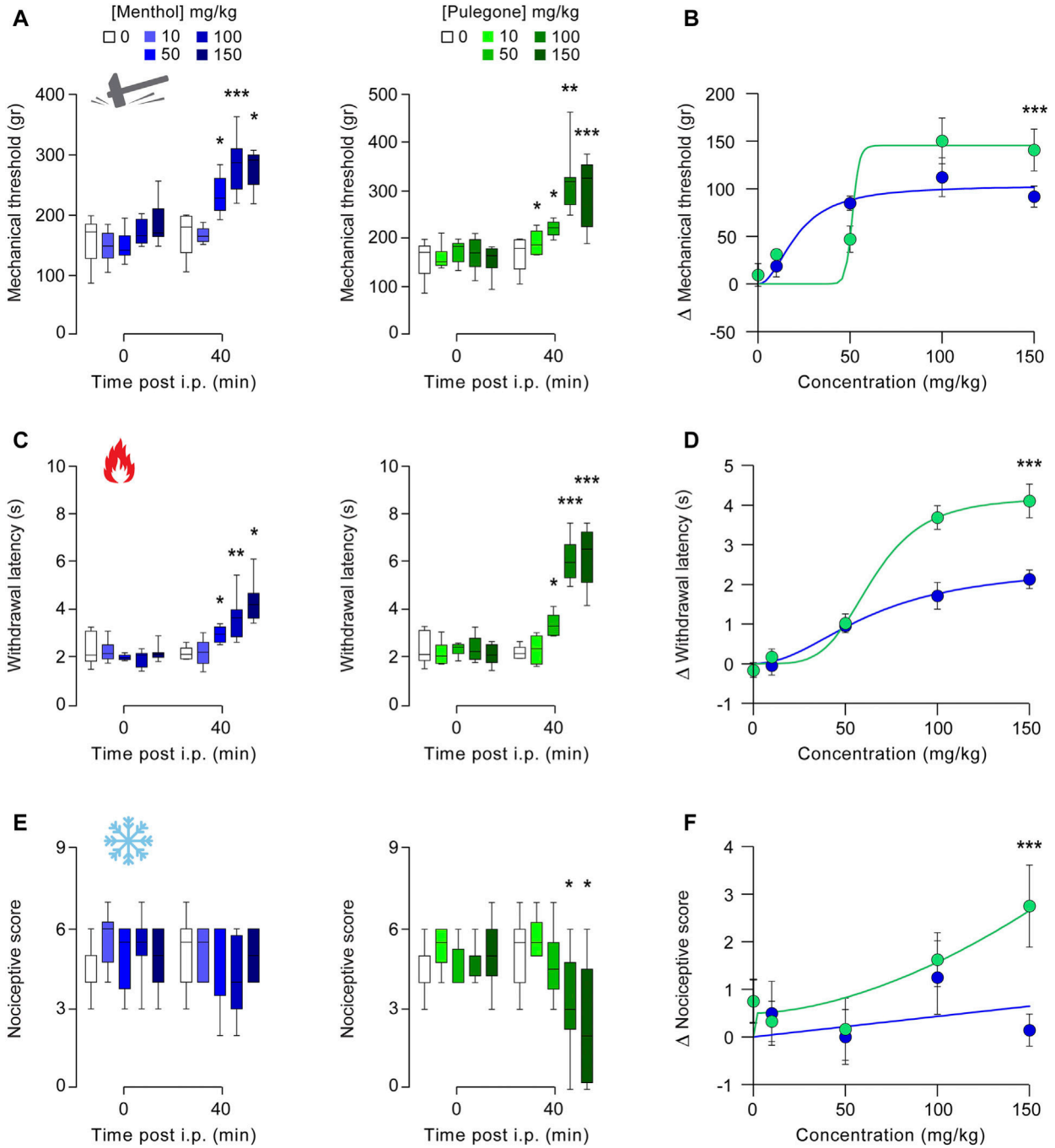

FIGURE 3 | Dose-response of the analgesic properties of menthol and pulegone on CFA-induced inflammatory pain model. Effect of menthol 10 ($n = 6$), 50 ($n = 6$), 100 ($n = 8$), and 150 mg/kg ($n = 7$) and pulegone 10 ($n = 6$), 50 ($n = 6$), 100 ($n = 8$), and 150 mg/kg ($n = 8$) or their vehicle ($n = 8$) measured 40 min after i.p. injection on mechanical **(A)**, thermal heat **(C)**, and thermal cold. **(E)** CFA-induced hyperalgesia. Dose-response distribution fits for menthol and pulegone on mechanical **(B)**, thermal heat **(D)**, and thermal cold **(F)**. Data are expressed as mean ± SD. Asterisks indicate statistical significance (***$p < 0.001$; **$p < 0.01$; *$p < 0.05$) using Kruskal-Wallis test followed by Dunn's multiple comparisons *post-hoc* test to compare each delta with the delta of the vehicle, to compare each treatment depending on the time post i.p. (0 vs. 40 min) it is a paired *t*-test or a Wilcoxon test, depending on the data's normal distribution.

(**Figure 4**; **Supplementary Figure S4**). The comparison of the AUC will be used to assess the global effect of each treatment.

Although, pulegone induced an anti-hyperalgesic effect on all measured modalities as soon as 20 min after i.p. injection on mechanical threshold (pulegone: 274.25 ± 68.89 g, $n = 8$; vehicle: 160.88 ± 35.17 g, $n = 8$, F (5, 110) = 45.47, $p < 0.0001$, two-way RM ANOVA and Dunnett's multiple comparisons, **Figures 4A,B**), as well on thermal heat

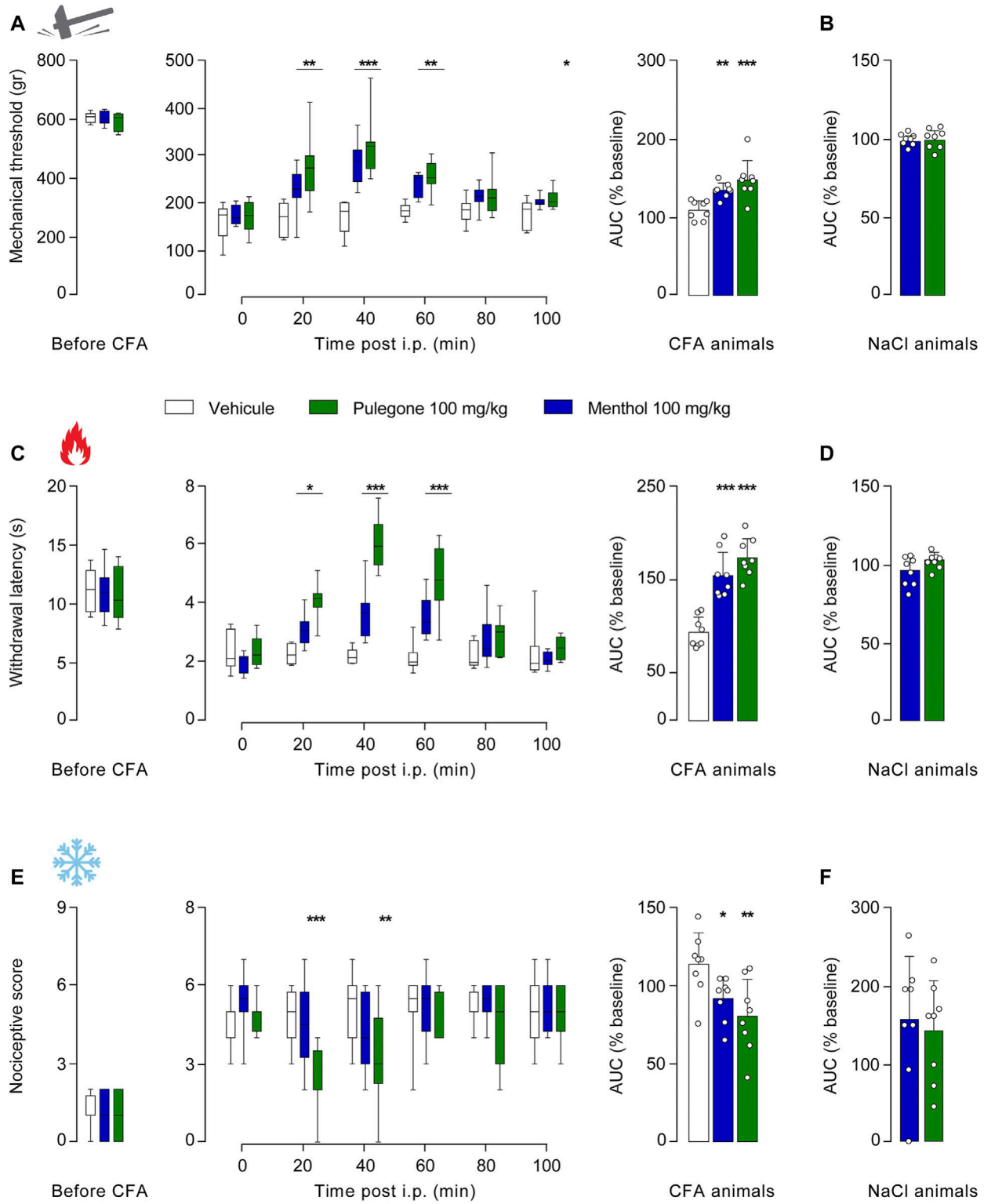

FIGURE 4 | Time-course of the analgesic properties of menthol and pulegone on CFA-induced inflammatory pain model. Baseline, time-course, and relative-to-baseline AUC (%) of the effects of i.p. menthol 100 mg/kg ($n = 8$), pulegone 100 mg/kg ($n = 8$), or the vehicle ($n = 8$) on CFA-induced mechanical **(A)**, thermal heat **(C),** and thermal cold **(E)** hyperalgesia. Relative-to-baseline AUC (%) of the effects of i.p. menthol 100 mg/kg ($n = 8$) and pulegone 100 mg/kg ($n = 8$) on mechanical **(B)**, thermal

(*Continued*)

FIGURE 4 | heat **(D),** and thermal cold **(F)** sensitivities of NaCl-injected hindpaw. Data are expressed as mean ± SD. Asterisks indicate statistical significance (***$p < 0.001$; **$p < 0.01$; *$p < 0.05$) using two-way ANOVA followed by Dunnett or Sidak multiple comparisons test for the time course, for the AUC is a one-way ANOVA followed by a Holm-Sidak multiple comparisons test or *t*-test, depending on the data's normal distribution giving the following statistic: mechanical: two-way ANOVA $F(5;110) = 45.47$, $p < 0.0001$ and one-way ANOVA $F(2;28) = 11.61$, $p < 0.0001$; thermal heat: two-way ANOVA $F(5;110) = 53.74$, $p < 0.0001$ and one-way ANOVA $F(2;28) = 24.47$, $p < 0.0001$ and thermal cold two-way ANOVA $F(5;110) = 11.75$, $p < 0.0001$ and one-way ANOVA $F(2;28) = 4.3$, $p = 0.0128$.

threshold (pulegone: 4.09 ± 0.62 s, $n = 8$; vehicle: 2.25 ± 0.34 s, $n = 8$, $F(5, 110) = 53.74$, $p < 0.0001$, two-way RM ANOVA with Dunnett's multiple comparisons test, **Figures 4C,D**), and also on thermal cold threshold (pulegone: 2.25 ± 1.28 score, $n = 8$; vehicle: 4.75 ± 1.04 score, $n = 8$, $F(5, 110) = 11.75$, $p < 0.0001$, RM ANOVA with Dunnett's multiple comparisons test, **Figures 4E,F**), significant effects of menthol were observable only after 40 min post i.p. injection (mechanical: menthol: 281.63 ± 45.52 g, $n = 8$; vehicle: 166.25 ± 35.4 g, $n = 8$, 8, $F(5, 110) = 45.47$, $p < 0.0001$ two-way RM ANOVA and Dunnett's multiple comparisons **Figure 4A**; thermal heat: menthol: 3.65 ± 0.88 s, $n = 8$; vehicle: 2.19 ± 0.26 s, $n = 8$, $F(5, 110) = 53.74$, $p < 0.000$, two-way RM ANOVA with Dunnett's multiple comparisons test **Figure 4C**).

Nevertheless, the effects of both terpenes fade 80 min after i.p. injection (mechanical: pulegone: 212 ± 42.46 g, $n = 8$; menthol: 209.38 ± 25.08 g, $n = 8$; versus vehicle: 179.92 ± 26.55 g, $n = 8$, $p = 0.1979$ and $p = 0.2579$, respectively, **Figure 4A**; thermal heat: pulegone: 2.84 ± 0.64 s, $n = 8$; menthol: 2.76 ± 0.89 s, $n = 8$; vehicle: 2.19 ± 0.44 s, $n = 8$, $p = 0.1155$ (pulegone), $p = 0.1951$ (menthol), **Figure 4C**; and thermal cold: pulegone: 4.5 ± 1.6 score, $n = 8$; vehicle: 5.13 ± 0.64 score, $n = 8$, $p = 0.6344$, **Figure 4E**).

Of note, menthol only slightly alleviated thermal cold hyperalgesia after i.p. injection (thermal cold: menthol: 91.39 ± 13.93%, $n = 8$, $p = 0.2696$, **Figure 4E**). Importantly, those effects were totally absent in non-hyperalgesic animals that received NaCl intraplantar injection (**Figures 4B,D,F**) as well as in the CFA contra-lateral hindpaw (**Supplementary Figure S4**), illustrating an anti-hyperalgesic action of those terpenes in absence of anti-nociceptive action. In addition, it is interesting to note that the anti-hyperalgesic effects of pulegone seem to be higher than those of menthol, especially for thermal heat modality (**Figure 4D**).

Altogether, these results indicate that a single i.p. injection of either menthol or pulegone exerts a significant and medium-lasting anti-hyperalgesic action on mechanical, thermal heat, and thermal cold sensitivities in an inflammatory-induced pain hypersensitivity rat model.

Menthol and Pulegone Are Devoid of *In Vivo* Locomotor Side Effects

Given that monoterpenes might have strong unwilling side-effects when injected at high doses (pulegone >200 mg/kg) (de Sousa et al., 2011; Silveira et al., 2014), we performed several controls to assess that the previous experiments are free of motor reflex bias. To do so, we quantified hindpaw diameter as well as the motor activity of the rats after the i.p. injection of either pulegone or menthol, at the highest dose of 150 mg/kg (**Figure 3**), using two different experimental paradigms.

In a few of monoterpenes known to have anti-inflammatory action (De Cássia Da Silveira E Sá et al., 2013; Souza et al., 2014), the hindpaw edema diameter due to CFA was not reduced by neither pulegone nor menthol i.p. injection (vehicle, 10.55 ± 0.86 mm, $n = 8$; menthol, 10.18 ± 0.66 mm, $n = 8$; pulegone, 10.29 ± 0.66 mm, $n = 8$; **Figure 5A**). This suggests that an acute terpene injection, at this stage of the CFA-induced inflammation, may have no or limited anti-inflammatory effect but rather acts directly on nociceptive thresholds through a mechanism that remains to be explained.

In order to verify that neither menthol nor pulegone i.p. injection affected the locomotor ability of the rats and consequently alters the assessment of the nociceptive thresholds during the experimentation, we monitored their locomotor functions after i.p. injection using the beam walk assay (**Figure 5B**) as well as the rotarod assay (**Figure 5C**). In those two tests, both menthol and pulegone failed to impair the locomotor abilities of the animals.

DISCUSSION

In the present study, we confirmed that the monoterpenes menthol and pulegone are the major monoterpenes present in *M. piperita* and *C. nepeta* extracts, respectively (**Figure 1**). We found that menthol and pulegone initiate very similar *in vitro* anti-inflammatory activities, while pulegone seems to display only limited *in vitro* cytotoxic effects on TPH-1 macrophages (**Figure 2**). Finally, we revealed anti-hyperalgesic properties of both menthol and pulegone, with a significant advantage for pulegone (**Figures 3**, **4**), without negative locomotor side effects (**Figure 5**).

Our results are in agreement with previous investigations, confirming that menthol and pulegone are the main monoterpenes present in *M. piperita* and *C. nepeta* extracts, respectively (Ristorcelli et al., 1996; Božović et al., 2017; Li et al., 2017). In addition, we confirmed the anti-inflammatory properties of pulegone and menthol, showing that both menthol and pulegone blocked the release of TNF-α from the LPS-stimulated THP-1 cell line (**Figure 2B**). Indeed, this result is in line with a previous report demonstrating on another macrophage cell line that menthol can suppress the LPS-induced TNF-a release (Shahid et al., 2018). A similar effect was observed with pulegone (Choi et al., 2018; Yang et al., 2019b, Yang et al., 2019a). Further experiments are required to take advantage of the significantly weaker cytotoxicity of pulegone observed in the THP-1 cell line (**Figure 2B**) especially to reduce pro-inflammatory cytokines release by these cells under chronic pain conditions.

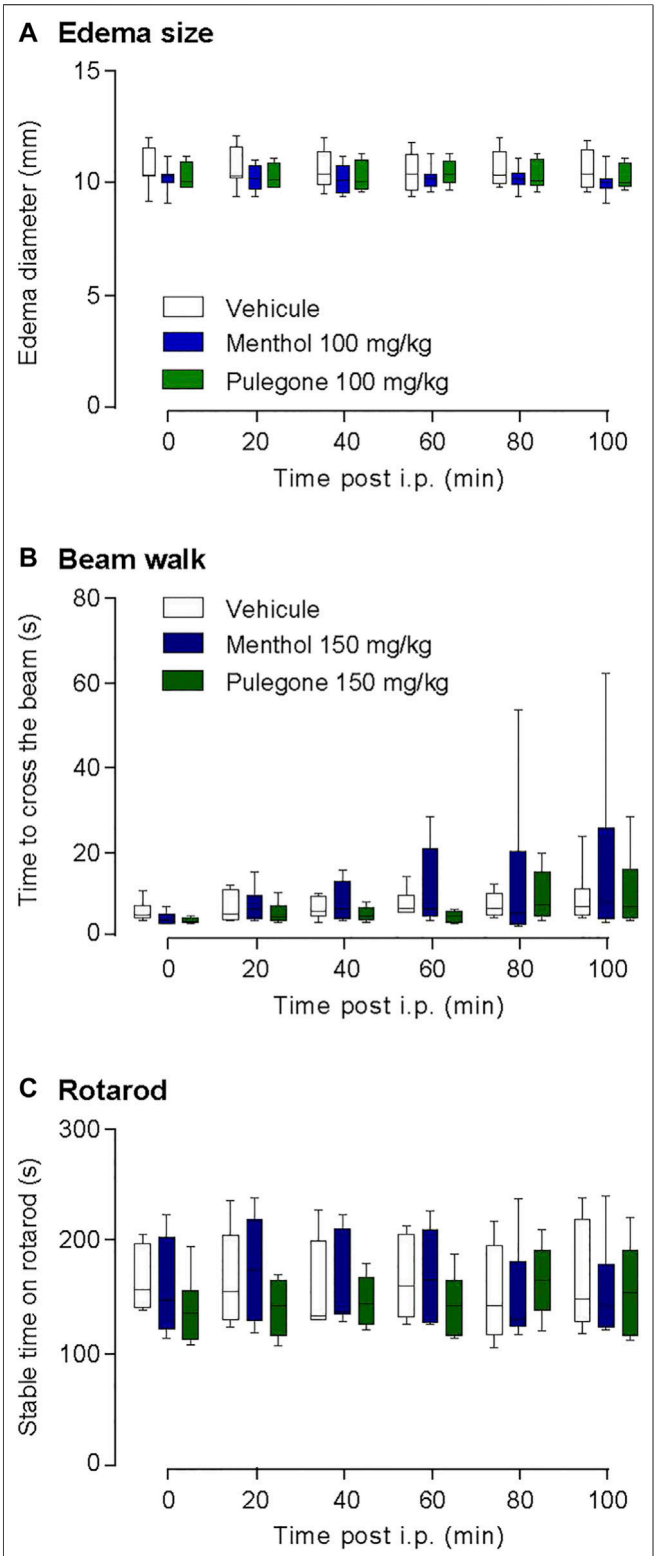

FIGURE 5 | Control of terpenes effect on edema and locomotor activity. **(A)** Time-course of the effects of i.p. menthol 100 mg/kg (n = 8), pulegone 100 mg/kg (n = 8), or the vehicle (n = 8) on CFA-induced edema size (two-way ANOVA F(5;75) = 1.643, p =0.1526). Time-course of the locomotor activity after an i.p. injection (Vehicle, n = 6; Menthol (150 mg/kg), n = 6; (*Continued*)

Investigating the analgesic properties of menthol and pulegone *in vitro* an *in vivo* on CFA-induced inflammatory hypersalgesia, we found, as expected, that both menthol (Pan et al., 2012; Liu et al., 2013) and pulegone were able to alleviate the mechanical and thermal heat hyperalgesia. However, only pulegone was able to alleviate thermal cold hyperalgesia. In addition, we showed that, at similar doses, pulegone has a higher anti-hyperalgesic potency than menthol, in both intensity and duration (**Figures 3**, **4**).

While the underlying mechanisms remain unknown, we propose a framework based on several hypotheses that remain to be explored. After peripheral inflammation, central sensitization leads to molecular and cellular changes in the central nervous systems where affinity and expression of channels and receptors like the gamma-aminobutyric acid receptor type A (GABA-A) increase and directly contribute to pain hypersensitivity (Latremoliere and Woolf, 2009). Thanks to their small molecular size and lipophilic properties, monoterpenes can cross the blood-brain-barrier (BBB) (Zhang et al., 2015; Weston-Green, 2019). Interestingly, other reports have shown that both menthol and pulegone can potentialize GABA-A receptors currents responsible for the inhibition of neuronal activity (Corvalán et al., 2009; Tong and Coats, 2012; Lau et al., 2014) and in this case, contribute to analgesia. Another possible pathway for menthol and pulegone to act as pain-killers might be to directly modulate the electrical activity of nociceptors, through the desensitization of their receptors targets involved in the sustenance of hypersensitivity states. Indeed, TRPM8 and TRPA1 are particularly involved in the detection and transduction of cold temperatures and noxious stimulations into neuronal activity (Basbaum et al., 2009; McKemy, 2013). TRPA1, a known target of menthol and pulegone (Majikina et al., 2018), is a cation channel contributing to transduce noxious temperatures above 42°C and involved in the propagation of nociceptive mechanical stimulation after inflammation (Brierley et al., 2011). In addition, it has been demonstrated that TRPA1 upregulation contributes to peripheral sensitization during inflammation and is responsible for both mechanical pain and thermal hypersensitivity (Petrus et al., 2007). Furthermore, high concentrations of agonists, such as monoterpenes, at the vicinity of sensory neurons can induce desensitization of both TRPM8 (Sarria et al., 2011; Liu and Rohacs, 2020) and TRPA1 (Akopian et al., 2007; Kühn et al., 2009). Therefore, one can hypothesize that monoterpenes could induce desensitization of TRPM8 and TRPA1, leading to a decrease of mechanical and cold thresholds, eventually leading to analgesia. Comparable mechanisms exists for the TRP vanilloid 1 (TRPV1), a channel involved in the detection of nociceptive hot temperatures and activated by the red chili pepper active compound, capsaicin

FIGURE 5 | Pulegone (150 mg/kg), n = 6) tested with the **(B)** rotarod two-way ANOVA F(5;75) = 0.2535, p =0.9367 and the **(C)** beam walk two-way ANOVA F(5;75) = 3.34, p =0.089. Data are expressed as mean ± SD. No statistical significance was observed, using two-way ANOVA followed by Dunnett multiple comparisons *post-hoc* test.

(Basbaum et al., 2009): Plantar capsaicin injection in naïve animals induces nocifensive reactions and pain hypersensitivities (Petitjean et al., 2014, 2020), while long exposure to capsaicin induces long-term desensitization of the TRPV1 contributing to capsaicin-induced analgesia.

If these concepts are valid and transposable to humans, monoterpenes might be key candidates for clinical use due to their capability to cross the BBB and interact with many different molecular targets during inflammation, with no or limited locomotor side effects, these compounds might be key candidates for clinical use. This work may lead to the development of easy to take drugs, to be administered every few hours in order to limit pain symptoms.

In conclusion, we showed that pulegone has a significantly higher effect than menthol on nociceptive sensory thresholds in an inflammatory-induced pain hypersensitivity rat model. We establish for the first time that pulegone acts as an anti-hyperalgesic compound in the setting of inflammatory pain conditions on mechanical and thermal pain hypersensitivities. Such properties of pulegone suggest that traditional treatments based on *C. nepeta* preparations have indeed the potential to reduce chronic inflammation and reduce pain conditions as it was described in ancient herbals (Fuchs, 1543; Mattioli, 1554). This work thus supports the interest and potential of ethnopharmacological research for the discovery of new innovative treatments to alleviate chronic pain conditions.

MATERIALS AND METHODS

All the protocols, tests, and use of living animals were performed in accordance with European committee council Direction, from the regional ethic committee (Comité Régional d'Ethique en Matière d'Expérimentation Animale de Strasbourg, CREMEAS) and with authorization from French Department of Agriculture (APAFIS# 19006-2019020714109922 v3).

Reagents and Chemicals

Ethanol was purchased from Sigma-Aldrich (Steinheim, Germany). Milli-Q water (18.2 MΩ) was generated by Millipore synergy system (Molsheim, France). Nitrogen was of 4.5 grade and helium of 6.0 grade (Sol France, Saint-Ouen l'Aumone, France). Pulegone (97%) and menthol (99%) were analytical standards obtained from Sigma-Aldrich (Steinheim, Germany). RPMI 1640 cell culture media was obtained from ATCC (LGC Standards, Molsheim, France). Penicilin and streptomycin were purchased from Cambrex Bio Science (St Beauzire, France). Fetal bovine serum (FBS) was obtained from Lonza BioWhittaker (Fisher Scientific, Illkirch, France). Lipopolysaccharide (LPS) from *Salmonella abortus equi* and celastrol were purchased from Sigma-Aldrich (Steinheim, Germany). Propidium iodide was obtained from Miltenyi Biotec Inc. (Auburn, AL, United States). For *in vivo* biological assays, terpenes were emulsified in warmed (37°C) carboxymethyl cellulose (CMC, 1%) - NaCl (0.9%) and administered at the temperature of 37°C. Pulegone, menthol, or vehicle was injected intraperitoneally (i.p.).

Plant Material

Plants. Calamintha nepeta (L.) Savi and *Mentha piperita* L. were obtained from the Ledermann-Mutschler nursery (Krautergersheim, France). Upon reception, leaves and stems of the plants were chopped and dried at room temperature and out of the light until constant weight was obtained, indicating that the drying process was done. Dry plants were then cryogenically grounded (6,870 Freeze/Mill, Spex CertiPrep, Stanmore, Royaume-Uni) into fine powders which were stored at 4°C and protected from the light before extraction.

Pressurized Liquid Extraction

Plant extracts were obtained by solid/liquid extraction under pressure using an ASE-350 system (Dionex, Sunnyvale, CA, United States). For the extraction, 3 g of finely grounded plant powder mixed with chemically inert Fontainebleau sand (previously heated at 600°C for 4 h and stored at room temperature) was placed into a 10 ml stainless steel extraction cell. Two 27 mm cellulose filters (Dionex, Sunnyvale, CA, United States) were placed one at the bottom and one at the top of the extraction cell. The extraction cell was then subjected to one cycle of extraction at 125°C under 100 bars for 7 min in the static extraction mode. The extraction solvent was a 50/50% (v/v) mixture of water and ethanol. The volume of the collected extract was about 15 ml. Between runs, the system was washed with 20 ml of the extraction solvent.

Gas Chromatography-Mass Spectrometer (GC-MS) Conditions

Plant extracts were analyzed on a 450-GC/240-MS system (Varian, Les Ulis, France) equipped with a DB-WAX capillary column (60 m × 0.25 mm × 0.15 µm) (Agilent Technologies, Les Ulis, France). Two microliters of the extract were injected in a split/splitless injector at 210°C and carried through the column by helium carrier gas (99.9999%) at 1 ml/min. The following temperature program was applied to the column oven to allow the separation of the different compounds: hold for 1 min at 40°C, increased to 100°C at 10°C/min, increased to 130°C at 5°C/min, increased to 150°C at 10°C/min, increased to 180°C at 5°C/min, heated to 230°C at 10°C/min, and finally held isothermal at 230°C for 5 min. For the MS parameters, the transfer line temperature was set to 200°C and the ion source at 150°C. The mass spectrometer was operated in electron impact (EI) mode, and the ionizing electron energy was set to 70 eV. The mass spectra were registered in a full scan acquisition mode in the range of 50–200 m/*z*. Peaks were identified by referring the mass spectra to the NIST (National Institute of Standards and Technology) mass spectral database and by comparing their retention time to the one of the analytical standard.

Drug Preparation

For *in vitro* assays, purified pulegone and menthol (Sigma-Aldrich (Steinheim, Germany) were prepared with a final 1% ethanol concentration for cell incubation.

For *in vivo* assays, purified pulegone and menthol (Sigma-Aldrich (Steinheim, Germany) were emulsified in warmed (37°C) carboxymethyl cellulose solution (CMC, 1%; in NaCl 0.9%) for subsequent intraperitoneal (i.p.) injections.

Cell Culture

THP-1 cell line, acute monocytic leukemia cells, was purchased from the American Type Culture Collection (ATCC TIB-202, LGC Standard, Molsheim, France). The cells were maintained in RPMI-1640 (ATCC) medium supplemented with 10% (v/v) fetal bovine serum and 1% (v/v) mixture of penicillin (1,000 UI/ml, Gibco^{TM}) and streptomycin (1,000 µg/ml, Gibco ^{TM}). Cells were grown in 75 cm^2 flasks in a humidified atmosphere with 5% CO_2 at 37°C and were replicated every 2–3 days before reaching a concentration of 1×10^6 cells/ml. Cells were sub-cultured at a concentration of approximately $2–3 \times 10^5$ cells/ml by adding fresh media to the flask.

TNF-α Secretion Assay

The TNF-α secreted by the THP-1 cells was measured in the culture medium using an assay kit (TNF-α secretion assay, Miltenyi Biotech, United States). TNF-α secretion was obtained by LPS activation of the THP-1 cells. THP-1 (180 µl) in suspension in the media at a concentration of 3×10^5 cells/ml was seeded in a 96-well plate. LPS (20 µl) was added in each well to reach a final concentration of 1 µg/ml. In appropriate wells, 20 µl of plant extract dissolved in 90/10 water/ethanol were added to the cell media. For the evaluation of the activities of the standards, 2 µl of a standard solution in ethanol were added to reach specified final concentrations (from 0.03 to 13 mM). Positive and negative controls were included in the TNF-α secretion assay. Celastrol, a triterpenoid known for its TNF-α inhibitor capacities in *in vitro* tests (Allison et al., 2001), was used as a positive control at a final concentration of 0.5 µM. LPS-stimulated cells with 1% of ethanol were used as a negative control. The 96-well plate was then incubated at 37°C in 5% CO_2 incubator for 2 h. After incubation, 2 µl of each antibody of the assay kit (catch reagent and detection reagent) were added in each well. The 96-well plate was once more incubated at 37°C in 5% CO_2 incubator for 2 h. Propidium iodide (2 µl) was then added to each well to reach a final concentration of 1 µg/ml. The 96-well plate was incubated one last time for 10 min at 37°C in 5% CO_2 incubator. Each terpene concentration was tested in triplicates on the same 96-well plate.

Flow Cytometry Parameters

Microcapillary flow cytometry system Guava® EasyCyte^{TM} 12HT (Merck Millipore, Darmstadt, Germany) with blue laser (488 nm) was used for the acquisition of the *in vitro* inflammation assay. The detection antibody of the assay contains *R*-phycoerythrin; thus, yellow fluorescence allows to tract the concentration of TNF-α secreted by the cells (F cell %, **Figure 2A**). Dead cells were detected by the red fluorescence of propidium iodide (F cell %, **Figure 2D**). The mean flow velocity used was 35 µl/min. Each well was agitated for 10 s before each analysis using a rotatory agitator. Between each sample, the microcapillary and the agitator were washed. Data were treated using GuavaSoft (InCyte 3.1.1.) software.

Animals

Male Wistar rats (300 g; Janvier Labs, Le Genest St. Isle, France) were used for this study. They were housed in groups of 3 or 4 under standard conditions (room temperature, 22°C; 12/12 h light/dark cycle) with *ad libitum* access to food and water and behavioral enrichment. All animals were manipulated and habituated to the tests and to the room for at least 2 weeks. All behavioral tests were done during the light period (i.e., between 7:00 and 19:00). A total number of 109 rats were used in this study (+1 who died during the procedure due to an abrupt overdose of isoflurane caused by a technical problem). They were divided into two main groups. The 91 rats that passed all three analgesic tests, calibrated forceps (mechanical sensitivity), plantar test (warm thermal sensitivity), and acetone test (cold thermal sensitivity) after one injection of monoterpene, composed a first group. The 18 rats that passed the two locomotor tests (rotarod assay and the beamwalk test) after one injection of monoterpenes composed a second group. The precise composition of the first group is as follows: CFA + Vehicle n = 8; CFA + Menthol (10 mg/kg) n = 6; CFA + Menthol (50 mg/kg) n = 6; CFA + Menthol (100 mg/kg) n = 8; CFA + Menthol (150 mg/kg) n = 7 (+1 how died); CFA + Pulegone (10 mg/kg) n = 6; CFA + Pulegone (50 mg/kg) n = 6; CFA + Pulegone (100 mg/kg) n = 8; CFA + Pulegone (150 mg/kg) n = 8; NaCl + Menthol (100 mg/kg) n = 8; NaCl + Menthol (150 mg/kg) n = 6; NaCl + Puleonge (100 mg/kg) n = 8; NaCl + Pulegone (150 mg/kg) n = 6. The precise composition of the second group is as follows: Vehicle n = 6; Menthol (150 mg/kg) n = 6; Pulegone (150 mg/kg) n = 6.

CFA Model of Inflammatory-Induced Hypersensitivities

To induce a peripheral inflammation, 100 µl of complete Freund adjuvant (CFA; Sigma, St. Louis, MO) was injected in the right hindpaw of the rat. All CFA injections were performed under light isoflurane anesthesia (3%). Edema was quantified by measuring the width of the dorsoplantar aspect of the hind paw before and after the injection of CFA with a caliper.

Behavioral Testing

Mechanical hyperalgesia. In all experimentation, to test the animal mechanical sensitivity, we used a calibrated forceps (Bioseb, Chaville, France). Briefly, the habituated rat is loosely restrained with a towel masking the eyes in order to limit stress by environmental stimulations. The tips of the forceps are placed at each side of the paw and a graduate force is applied. The pressure producing a withdrawal of the paw corresponded to the nociceptive threshold value. This manipulation was performed three times for each hindpaw, and the values were averaged.

Thermal hot hyperalgesia. To test the animal heat sensitivity, we used the Plantar test with Hargreaves method (Ugo Basile, Comerio, Italy) to compare the response of each hindpaw between healthy animals (unilateral intraplantar NaCl injection) and animals that received unilateral intraplantar CFA injection. The habituated rat was placed in a small box. We wait until the animal is calmed and then we exposed the hindpaw to a radiant heat. The latency time of paw withdrawal was measured. This manipulation was performed three times for each hindpaw, and the values were averaged.

Thermal cold hyperalgesia. To test the animal cold sensitivity, we used the acetone test to compare the response of each hindpaw between healthy animals (unilateral intraplantar NaCl injection) and animals that received unilateral intraplantar CFA injection. The habituated rat was placed in a small box, and once the animal is calm. Then, we put a drop of acetone (≥99%, Fisher Chemical) (between 50 and 100 µl) on the top of the hindpaw through a filed and curved needle without touching the hindpaw, and we scored the response of the animal during 20 s 0 no response, 1 a short response or fast movement of the hindpaw (<2 s), 2 a longer response (>2 s), and 3 licking of the hindpaw. This manipulation was performed three times for each hindpaw, and the values were summed.

Rotarod test. We used the Rotarod (IITC Life Science, Woodland Hills, CA). The speed of the roll increased progressively from 5 to 20 rpm in 4 min. The time spend by the animal on the rotarod before falling was measured. This test was repeated twice for each animal, and the values were averaged.

Beam walk test. The time needed by the rats to cross the beam (PVC bar of length: 130 cm; width: 4 cm, placed at 80 cm from the floor) was recorded. This test was repeated three times for each animal, and the values were averaged.

Statistical Analysis

Data are expressed as mean ± standard error of the mean (SEM). Statistical tests were performed with GraphPad Prism 7.05 (GraphPad Software, San Diego, California, United States). Sigmoid dose-response curves and EC_{50} values were calculated with the following equation:

$$Y = Bottom + (Top - Bottom)/ \\ (1 + 10\text{^}((LogEC_{50} - X)*HillSlope \quad (1)$$

with Y the response, X the concentration, Top (resp. Bottom) the plateaus at the top (resp. bottom) of the sigmoid in the units of the y axis, Hillslope the steepness of the curve, and EC_{50} the concentration that gives a concentration halfway between bottom and top.

Statistical analysis was performed using Student's t-test with a significance level of $\alpha = 0.05$, meaning that differences between the negative control and the sample were considered significant when $p < 0.05$. Results were considered to be statistically significant if p-values were below 0.05 (*), 0.01 (**), and 0.001 (***).

For behavioral tests, data were analyzed using repeated-measures two-way ANOVA for the time course experiments, with the following factors: treatment (between) and time (within); when four groups (treatment) were compared, the Dunnett's test was used for *post-hoc* multiple comparisons between individual groups, and when two groups (treatment) were compared, the Sidak's test was used for *post-hoc* multiple comparisons between individual groups. To compare dose-response results, a Shapiro-Wilk normality test was performed to evaluate the hypothesis of normality, and then we performed a nonparametric Kruskal-Wallis test supplemented with a *post-hoc* Dunn's test for multiple comparisons. For the comparison of each treatment depending on the time (0 vs. 40 min post i.p.), a Shapiro-Wilk normality test was performed. When the normality test was passed, we used the paired t-test, and when the normality test did not pass, we used the Wilcoxon matched-pairs signed-rank test. For the area under the curve (AUC), we tested the hypothesis of normality with a Shapiro-Wilk normality test. When it passed the normality test, we used an ordinary one-way ANOVA completed with a Holm-Sidak's test for *post-hoc* multiple comparisons. Otherwise, we performed a nonparametric Kruskal-Wallis test supplemented with a *post-hoc* Dunn's test for multiple comparisons. Results were considered to be statistically significant if p-values were below 0.05 (*), 0.01 (**), and 0.001 (***).

DATA AVAILABILITY STATEMENT

The original contributions presented in the study are included in the article/**Supplementary Material**, Further inquiries can be directed to the corresponding author.

ETHICS STATEMENT

The animal study was reviewed and approved by French Department of Agriculture (APAFIS# 19006-2019020714109922 v3).

AUTHOR CONTRIBUTIONS

Conceptualization: AC and HP. Methodology: AC, CM, EM, HP, LH, and ZT. Chemical analysis: CM, FE, and ZT. Behavior: LH. Writing: AC, HP, PD, and EH. Funding acquisition: AC and HP. Supervision: AC and HP. Project administration: AC and HP.

FUNDING

This work was supported by The Centre National de la Recherche Scientifique contract UPR3212, The Université de Strasbourg contract UPR3212, ANRT CIFRE grant no. 2018/1140 (to AC and HP) and no. 2016/047 (to CM, EM, and HP), and ANR JCJC 19-CE16-0011-0 (to AC).

ACKNOWLEDGMENTS

The authors thank the Chronobiotron (UMS 3512 for assistance in animal cares, experimentations, and surgeries).

SUPPLEMENTARY MATERIAL

The Supplementary Material for this article can be found online at: https://www.frontiersin.org/articles/10.3389/fphar.2021.753873/full#supplementary-material

REFERENCES

Adams, M., Berset, C., Kessler, M., and Hamburger, M. (2009). Medicinal Herbs for the Treatment of Rheumatic Disorders-Aa Survey of European Herbals from the 16th and 17th century. *J. Ethnopharmacol.* 121, 343–359. doi:10.1016/j.jep.2008.11.010

Akopian, A. N., Ruparel, N. B., Jeske, N. A., and Hargreaves, K. M. (2007). Transient Receptor Potential TRPA1 Channel Desensitization in Sensory Neurons Is Agonist Dependent and Regulated by TRPV1-Directed Internalization. *J. Physiol.* 583, 175–193. doi:10.1113/jphysiol.2007.133231

Allison, A. C., Cacabelos, R., Lombardi, V. R., Álvarez, X. A., and Vigo, C. (2001). Celastrol, a Potent Antioxidant and Anti-inflammatory Drug, as a Possible Treatment for Alzheimer's Disease. *Prog. Neuropsychopharmacol. Biol. Psychiatry* 25, 1341–1357. doi:10.1016/S0278-5846(01)00192-0

Bai, X., Liu, L., Zhang, J., Chen, L., Wu, T., Aisa, H. A., et al. (2021). Spectrum-effect Relationship between GC-QTOF-MS Fingerprint and Antioxidant, Anti-inflammatory Activities of Schizonepeta Tenuifolia Essential Oil. *Biomed. Chromatogr.* 35. doi:10.1002/bmc.5106

Basbaum, A. I., Bautista, D. M., Scherrer, G., and Julius, D. (2009). Cellular and Molecular Mechanisms of Pain. *Cell* 139, 267–284. doi:10.1016/j.cell.2009.09.028

Božović, M., Ragno, R., and Tzakou, O. (2017). *Calamintha Nepeta* (L.) Savi and its Main Essential Oil Constituent Pulegone: Biological Activities and Chemistry. *Molecules* 22, 290. doi:10.3390/molecules22020290

Brierley, S. M., Castro, J., Harrington, A. M., Hughes, P. A., Page, A. J., Rychkov, G. Y., et al. (2011). TRPA1 Contributes to Specific Mechanically Activated Currents and Sensory Neuron Mechanical Hypersensitivity. *J. Physiol.* 589, 3575–3593. doi:10.1113/jphysiol.2011.206789

Carović-Stanko, K., Petek, M., Grdiša, M., Pintar, J., Bedeković, D., Herak Ćustić, M., et al. (2016). Medicinal Plants of the Family Lamiaceae as Functional Foods - a Review. *Czech J. Food Sci.* 34, 377–390. doi:10.17221/504/2015-CJFS

Choi, Y. Y., Kim, M. H., Lee, H., Jo, S. Y., and Yang, W. M. (2018). (R)-(+)-pulegone Suppresses Allergic and Inflammation Responses on 2,4-Dinitrochlorobenzene-Induced Atopic Dermatitis in Mice Model. *J. Dermatol. Sci.* 91, 292–300. doi:10.1016/j.jdermsci.2018.06.002

Corvalán, N. A., Zygadlo, J. A., and García, D. A. (2009). Stereo-selective Activity of Menthol on GABA(A) Receptor. *Chirality* 21, 525–530. doi:10.1002/chir.20631

da Silveira, N. S., De Oliveira-Silva, G. L., Lamanes, Bde. F., Prado, L. C., and Bispo-da-Silva, L. B. (2014). The Aversive, Anxiolytic-like, and Verapamil-Sensitive Psychostimulant Effects of Pulegone. *Biol. Pharm. Bull.* 37, 771–778. doi:10.1248/bpb.b13-00832

de Cássia da Silveira e Sá, R., Andrade, L. N., and De Sousa, D. P. (2013). A Review on Anti-inflammatory Activity of Monoterpenes. *Molecules* 18, 1227–1254. doi:10.3390/molecules18011227

de Sousa, D. P., Júnior, E. V., Oliveira, F. S., De Almeida, R. N., Nunes, X. P., and Barbosa-Filho, J. M. (2007). Antinociceptive Activity of Structural Analogues of Rotundifolone: Structure-Activity Relationship. *Z. Naturforsch C J. Biosci.* 62, 39–42. doi:10.1515/znc-2007-1-207

de Sousa, D. P., Nóbrega, F. F., de Lima, M. R., and de Almeida, R. N. (2011). Pharmacological Activity of (R)-(+)-pulegone, a Chemical Constituent of Essential Oils. *Z. Naturforsch C J. Biosci.* 66, 353–359. doi:10.1515/znc-2011-7-806

Fuchs, L. (15432016). in *The New Herbal of 1543, Complete Coloured Edition*. Editors D. Dobat and W. Dressendorfer edition Taschen. Taschen, (ISBN: *9783836538022*)

Galeotti, N., Di Cesare Mannelli, L., Mazzanti, G., Bartolini, A., and Ghelardini, C. (2002). Menthol: A Natural Analgesic Compound. *Neurosci. Lett.* 322, 145–148. doi:10.1016/S0304-3940(01)02527-7

Govaerts, R. (2020). *World Checklist of Apocynaceae*. MIM, Deurne: R. Bot. Gard. Kew

Guimarães, A. G., Quintans, J. S., and Quintans, L. J. (2013). Monoterpenes with Analgesic Activity-Aa Systematic Review. *Phytother Res.* 27, 1–15. doi:10.1002/ptr.4686

Harborne, J. B. (1995). Dictionary of Natural Products. *Phytochemistry* 38. doi:10.1016/0031-9422(95)90037-3

Hilfiger, L., Zhao, Q., Kerspern, D., Inquimbert, P., Andry, V., Goumon, Y., et al. (2020). A Nonpeptide Oxytocin Receptor Agonist for a Durable Relief of Inflammatory Pain. *Sci. Rep.* 10, 3017. doi:10.1038/s41598-020-59929-w

Kühn, F. J., Kühn, C., and Lückhoff, A. (2009). Inhibition of TRPM8 by Icilin Distinct from Desensitization Induced by Menthol and Menthol Derivatives. *J. Biol. Chem.* 284, 4102–4111. doi:10.1074/jbc.M806651200

Latremoliere, A., and Woolf, C. J. (2009). Central Sensitization: a Generator of Pain Hypersensitivity by central Neural Plasticity. *J. Pain* 10, 895–926. doi:10.1016/j.jpain.2009.06.012

Lau, B. K., Karim, S., Goodchild, A. K., Vaughan, C. W., and Drew, G. M. (2014). Menthol Enhances Phasic and Tonic GABAA Receptor-Mediated Currents in Midbrain Periaqueductal Grey Neurons. *Br. J. Pharmacol.* 171, 2803–2813. doi:10.1111/bph.12602

Li, Y., Liu, Y., Ma, A., Bao, Y., Wang, M., and Sun, Z. (2017). *In Vitro* antiviral, Anti-inflammatory, and Antioxidant Activities of the Ethanol Extract of *Mentha Piperita* L. *Food Sci. Biotechnol.* 26, 1675–1683. doi:10.1007/s10068-017-0217-9

Liu, B., Fan, L., Balakrishna, S., Sui, A., Morris, J. B., and Jordt, S. E. (2013). TRPM8 Is the Principal Mediator of Menthol-Induced Analgesia of Acute and Inflammatory Pain. *Pain* 154, 2169–2177. doi:10.1016/j.pain.2013.06.043

Liu, L., and Rohacs, T. (2020). Regulation of the Cold-Sensing TRPM8 Channels by Phosphoinositides and Gq-Coupled Receptors. *Channels (Austin)* 14, 79–86. doi:10.1080/19336950.2020.1734266

Majikina, A., Takahashi, K., Saito, S., Tominaga, M., and Ohta, T. (2018). Involvement of Nociceptive Transient Receptor Potential Channels in Repellent Action of Pulegone. *Biochem. Pharmacol.* 151, 89–95. doi:10.1016/j.bcp.2018.02.032

Mattioli, P. A. (1554). Kreutterbuch Commentarii in Libros Sex Pedacii Dioscoridis, Tradional Herbal Also Known Commentari Published in *1554, French-latin Traduction* by Jean. Des Moulins, edition Cambridge Lvgdvni : Apud Gabrielem Coterium 1562, 1990.

McKemy, D. D. (2013). The Molecular and Cellular Basis of Cold Sensation. *ACS Chem. Neurosci.* 4, 238–247. doi:10.1021/cn300193h

Pan, R., Tian, Y., Gao, R., Li, H., Zhao, X., Barrett, J. E., et al. (2012). Central Mechanisms of Menthol-Induced Analgesia. *J. Pharmacol. Exp. Ther.* 343, 661–672. doi:10.1124/jpet.112.196717

Patel, R., Gonçalves, L., Leveridge, M., Mack, S. R., Hendrick, A., Brice, N. L., et al. (2014). Anti-hyperalgesic Effects of a Novel TRPM8 Agonist in Neuropathic Rats: A Comparison with Topical Menthol. *Pain* 155, 2097–2107. doi:10.1016/j.pain.2014.07.022

Perri, F., Coricello, A., and Adams, J. D. (2020). Monoterpenoids: the Next Frontier in the Treatment of Chronic Pain. *J* 3, 195–214. doi:10.3390/j3020016

Petitjean, H., Hugel, S., Barthas, F., Bohren, Y., Barrot, M., Yalcin, I., et al. (2014). Activation of Transient Receptor Potential Vanilloid 2-expressing Primary Afferents Stimulates Synaptic Transmission in the Deep Dorsal Horn of the Rat Spinal Cord and Elicits Mechanical Hyperalgesia. *Eur. J. Neurosci.* 40, 3189–3201. doi:10.1111/ejn.12688

Petitjean, H., Fatima, T., Mouchbahani-Constance, S., Davidova, A., Ferland, C. E., Orlowski, J., et al. (2020). Loss of SLC9A6/NHE6 Impairs Nociception in a Mouse Model of Christianson Syndrome. *Pain* 161, 2619–2628. doi:10.1097/j.pain.0000000000001961

Petrus, M., Peier, A. M., Bandell, M., Hwang, S. W., Huynh, T., Olney, N., et al. (2007). A Role of TRPA1 in Mechanical Hyperalgesia Is Revealed by Pharmacological Inhibition. *Mol. Pain* 3, 1744–8069. doi:10.1186/1744-8069-3-40

Quintans, J. S. S., Shanmugam, S., Heimfarth, L., Araújo, A. A. S., Almeida, J. R. G. D. S., Picot, L., et al. (2019). Monoterpenes Modulating Cytokines - A Review. *Food Chem. Toxicol.* 123, 233–257. doi:10.1016/j.fct.2018.10.058

Rehman, R., Hanif, M. A., Mushtaq, Z., and Al-Sadi, A. M. (2016). Biosynthesis of Essential Oils in Aromatic Plants: A Review. *Food Rev. Int.* 32, 117–160. doi:10.1080/87559129.2015.1057841

Ristorcelli, D., Tomi, F., and Casanova, J. (1996). Essential Oils ofCalamintha nepetasubsp.Nepetaand subsp.Glandulosafrom Corsica (France). *J. Essent. Oil Res.* 8, 363–366. doi:10.1080/10412905.1996.9700641

Salakhutdinov, N. F., Volcho, K. P., and Yarovaya, O. I. (2017). Monoterpenes as a Renewable Source of Biologically Active Compounds. *Pure Appl. Chem.* 89, 1105–1117. doi:10.1515/pac-2017-0109

Sarria, I., Ling, J., Zhu, M. X., and Gu, J. G. (2011). TRPM8 Acute Desensitization Is Mediated by Calmodulin and Requires PIP(2): Distinction from Tachyphylaxis. *J. Neurophysiol.* 106, 3056–3066. doi:10.1152/jn.00544.2011

Shahid, M., Lee, M. Y., Yeon, A., Cho, E., Sairam, V., Valdiviez, L., et al. (2018). Menthol, a Unique Urinary Volatile Compound, Is Associated with Chronic Inflammation in Interstitial Cystitis. *Sci. Rep.* 8, 10859. doi:10.1038/s41598-018-29085-3

Souza, M. T., Almeida, J. R., Araujo, A. A., Duarte, M. C., Gelain, D. P., Moreira, J. C., et al. (2014). Structure–activity Relationship of Terpenes with Anti-inflammatory Profile – a Systematic Review. *Basic Clin. Pharmacol. Toxicol.* 115, 244–256. doi:10.1111/bcpt.12221

Tissier, A., Ziegler, J., and Vogt, T. (2015). "Specialized Plant Metabolites: Diversity and Biosynthesis," in *Ecological Biochemistry: Environmental and Interspecies Interactions*, 14–37. doi:10.1002/9783527686063.ch2

Tong, F., and Coats, J. R. (2012). Quantitative Structure-Activity Relationships of Monoterpenoid Binding Activities to the Housefly GABA Receptor. *Pest Manag. Sci.* 68, 1122–1129. doi:10.1002/ps.3280

Turner, G. W., and Croteau, R. (2004). Organization of Monoterpene Biosynthesis in Mentha. Immunocytochemical Localizations of Geranyl Diphosphate Synthase, Limonene-6-Hydroxylase, Isopiperitenol Dehydrogenase, and Pulegone Reductase. *Plant Physiol.* 136, 4215–4227. doi:10.1104/pp.104.050229

Vavitsas, K., Fabris, M., and Vickers, C. E. (2018). Terpenoid Metabolic Engineering in Photosynthetic Microorganisms. *Genes (Basel)* 9. doi:10.3390/genes9110520

Weston-Green, K. (2019). "The United Chemicals of Cannabis: Beneficial Effects of Cannabis Phytochemicals on the Brain and Cognition," in *Recent Advances in Cannabinoid Research* (London, United Kingdom: IntechOpen). doi:10.5772/intechopen.79266

Wojtunik-Kulesza, K., Kasprzak-Drozd, K., Sajdlowski, D., Oniszczuk, A., Swiatkowski, W., and Waksmundzka-Hajnos, M. (2021). *Scutellaria Baicalensis* - A Small Plant with Large Pro-health Biological Activities. *Curr. Issues Pharm. Med. Sci.* 34, 55–59. doi:10.2478/cipms-2021-0010

Yang, Q., Luo, J., Lv, H., Wen, T., Shi, B., Liu, X., et al. (2019b). Pulegone Inhibits Inflammation via Suppression of NLRP3 Inflammasome and Reducing Cytokine Production in Mice. *Immunopharmacol. Immunotoxicol.* 41, 420–427. doi:10.1080/08923973.2019.1588292

Yang, Q., Liu, Q., Lv, H., Wang, F., Liu, R., and Zeng, N. (2019a). Effect of Pulegone on the NLPR3 Inflammasome during Inflammatory Activation of THP-1 C-ells. *Exp. Ther. Med.* 19. doi:10.3892/etm.2019.8327

Zhang, Q., Wu, D., Wu, J., Ou, Y., Mu, C., Han, B., et al. (2015). Improved Blood-Brain Barrier Distribution: Effect of Borneol on the Brain Pharmacokinetics of Kaempferol in Rats by *In Vivo* Microdialysis Sampling. *J. Ethnopharmacol.* 162, 270–277. doi:10.1016/j.jep.2015.01.003

Conflict of Interest: Authors HP, EH, LH, and ZT were employed by the company Benephyt.

The remaining authors declare that the research was conducted in the absence of any commercial or financial relationships that could be construed as a potential conflict of interest.

Publisher's Note: All claims expressed in this article are solely those of the authors and do not necessarily represent those of their affiliated organizations or those of the publisher, the editors, and the reviewers. Any product that may be evaluated in this article, or claim that may be made by its manufacturer, is not guaranteed or endorsed by the publisher.

SUPPLEMENTARY FIGURES

Figure S1: Composition of the *C. nepeta* and *M. piperita* extracts obtained by PLE and analyzed by GC-MS (RI: Retention Index).

Figure S2: Cytograms of THP-1 cells for the evaluation of the inhibition of TNF-α secretion and the cytotoxicities for the controls, the standards used to determine Figure 2. The cytograms are divided in 4: lower left corresponds to inactivated cells (low yellow fluorescence, control without LPS-stimulation), lower right corresponds to activated cells (higher yellow fluorescence with the maximum for the negative control) and upper right corresponds to dead cells (high red fluorescence).

Figure S3. Dose-response of the analgesic properties of menthol and pulegone on CFA-induced inflammatory pain model – contralateral hindpaw. Effect of menthol 10 (n = 6), 50 (n = 6), 100 (n = 8) and 150 mg/kg (n = 7) and pulegone 10 (n = 6), 50 (n = 6), 100 (n = 8) and 150 mg/kg (n = 8) or its vehicle (n = 8) or their vehicle (n = 8) measured 40 min after i.p. injection on mechanical (**a**), thermal heat (**c**) and thermal cold (**e**) sensitivities. Dose-response distribution fits for menthol and pulegone on mechanical (**b**), thermal heat (**d**) and thermal cold (**f**). Data are expressed as mean ± SD. Asterisks indicate statistical significance (** $p < 0.01$; * $p < 0.05$) using a paired t test or a Wilcoxon test, depending on the data's normal distribution.

Figure S4. Time-course of the analgesic properties of menthol and pulegone on CFA-induced inflammatory pain model – contralateral hindpaw. Baseline, time-course and relative-to-baseline AUC (%) of the effects of i.p. menthol 100 mg/kg (n = 8), pulegone 100 mg/kg (n = 8) or the vehicle (n = 8), on CFA-induced mechanical (**a**), thermal heat (**c**) and thermal cold (**e**) contralateral hindpaw sensitivities. Relative-to-baseline AUC (%) of the effects of i.p. menthol 100 mg/kg (n = 8), pulegone 100 mg/kg (n = 8) on mechanical (**b**), thermal heat (**d**) and thermal cold (**f**) sensitivities of NaCl-contralateral hindpaw. Data are expressed as mean ± SD.

A

Compound	RI	Extract composition (%)	
		Calamintha nepeta (L.) savi	*Mentha piperita* (L.)
Camphene	1085	-	<0.01
β-Pinene	1119	0.35	-
3-Carene	1148	-	<0.01
Limonene	1186	-	0.57
Isomenthone	1468	8.61	1.74
Menthone	1481	0.61	9.51
Linalool	1540	-	<0.01
Menthyl acetate	1564	-	5.07
Isopulegone	1567	0.37	-
Caryophyllene	1603	1.95	0.80
Menthol	1630	4.70	42.85
Pulegone	1638	49.41	-
α-Terpineol	1674	<0.01	<0.01
Germacrene D	1690	0.94	1.58
Geraniol	1842	1.17	-

Figure S1

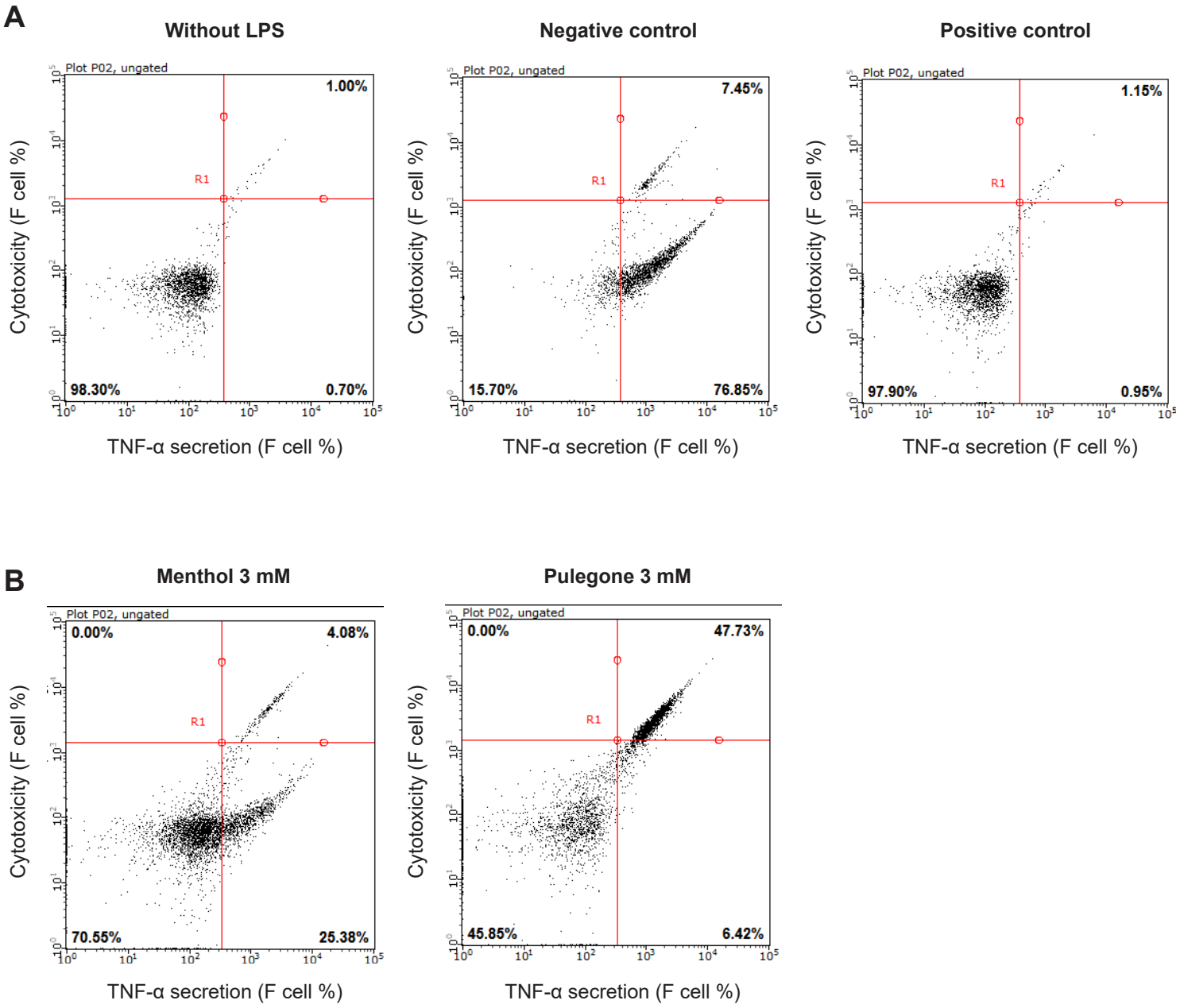
A
Without LPS
Negative control
Positive control
Plot P02, ungated
1.00%
R1
98.30%
0.70%
7.45%
15.70%
76.85%
1.15%
97.90%
0.95%
Cytotoxicity (F cell %)
TNF-α secretion (F cell %)
B
Menthol 3 mM
Pulegone 3 mM
0.00%
4.08%
70.55%
25.38%
47.73%
45.85%
6.42%

Figure S2

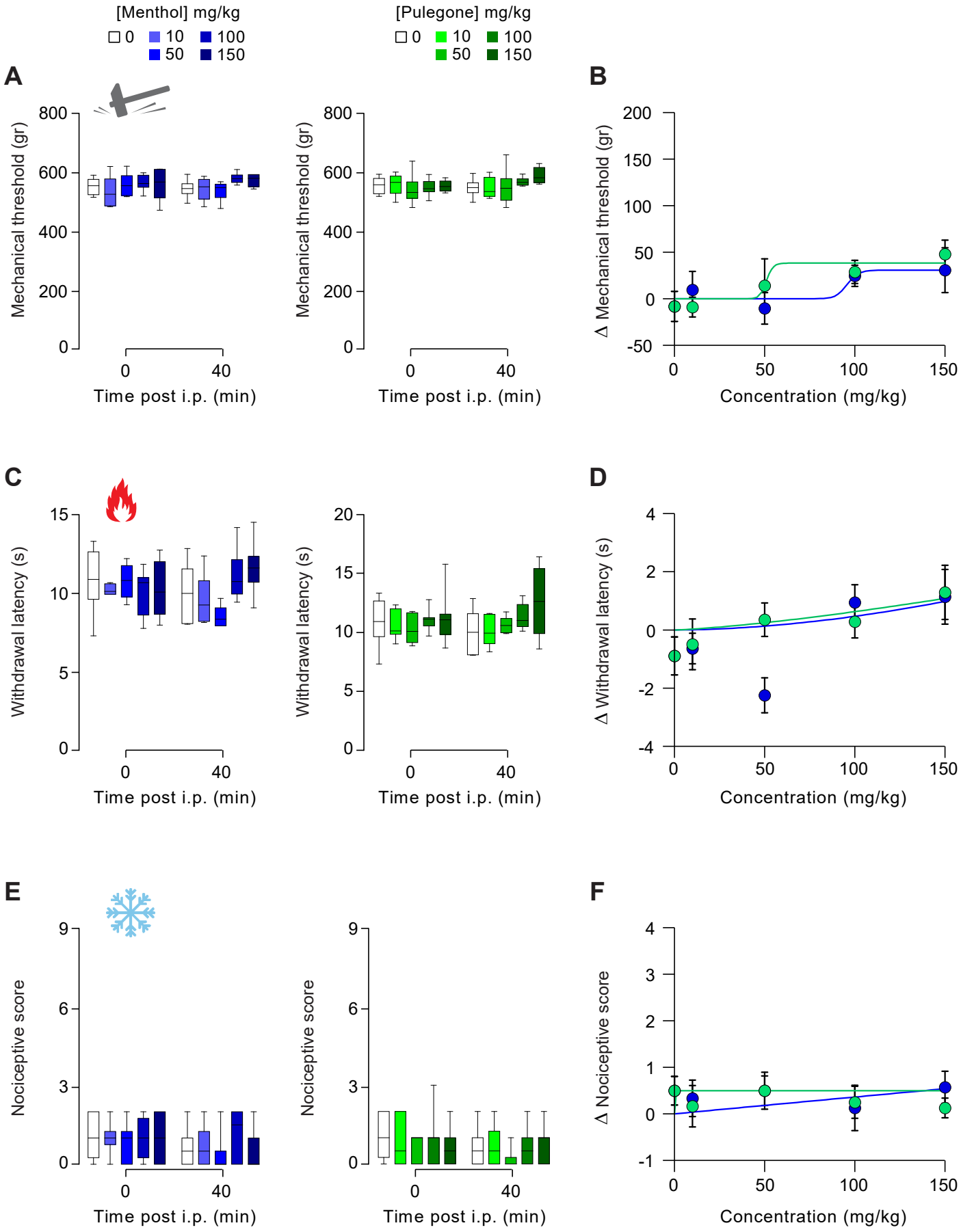
[Menthol] mg/kg
0
10
50
100
150
[Pulegone] mg/kg
0
10
50
100
150
A
B
C
D
E
F
Mechanical threshold (gr)
Δ Mechanical threshold (gr)
Withdrawal latency (s)
Δ Withdrawal latency (s)
Nociceptive score
Δ Nociceptive score
Time post i.p. (min)
Concentration (mg/kg)

Figure S3

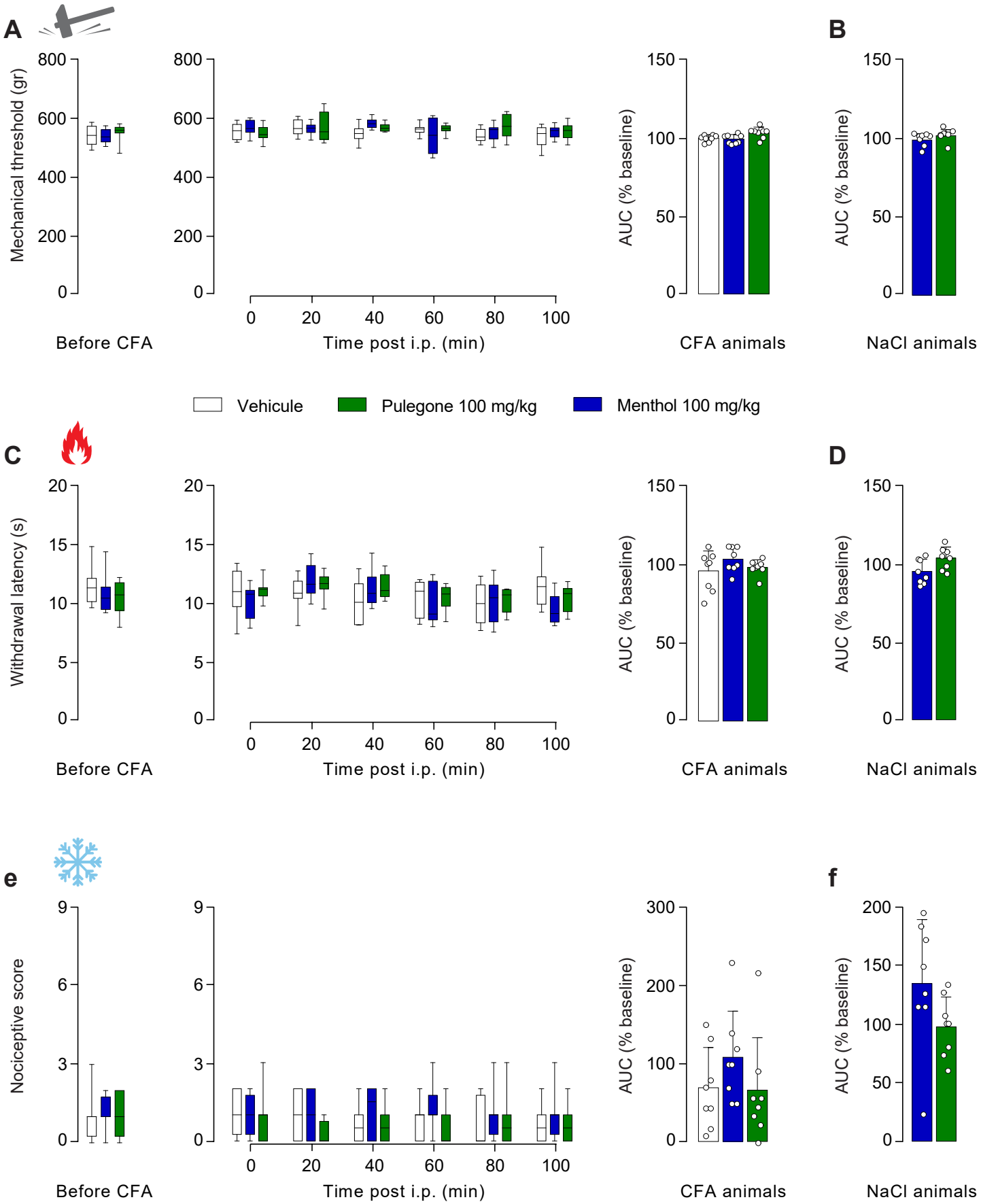
A
B
Mechanical threshold (gr)
800
600
400
200
0
Before CFA
0
20
40
60
80
100
Time post i.p. (min)
AUC (% baseline)
150
100
50
0
CFA animals
NaCl animals
Vehicule
Pulegone 100 mg/kg
Menthol 100 mg/kg
C
D
Withdrawal latency (s)
20
15
10
5
e
f
Nociceptive score
9
6
3
300
200

Figure S4

2. Article 2: A Nonpeptide Oxytocin Receptor Agonist for a Durable Relief of Inflammatory Pain

2.1. Overview

2.1.1. Introduction

It has been shown that OT induces antinociception and analgesia in different model (Grinevich and Charlet, 2017). Moreover, in nociception and pain, OT has both central and peripheral targets depending on the releasing pathway: plasmatic released OT mediates an antinociceptive action in vivo by reducing C fibre excitability, whereas OT released by PVN fibres directly inhibits sensory processing and produces analgesia (Juif and Poisbeau, 2013; Eliava et al., 2016). In inflammatory pain models, direct activation of parvOT neurons by optogenetics, resulting in central and peripheral release of endogenous OT, also produced a significant OTR dependent analgesia (Eliava et al., 2016). However, despite its interesting analgesic properties, OT is not used in the treatment of pain because of its inability to efficiently cross the BBB (Gimpl and Fahrenholz, 2001). In addition, OT is rapidly metabolized has as short half-life in the blood circulation and in the CSF (Mens et al., 1983; Morin et al., 2008). Finally, OT suffers from several additional drawbacks: a lack of specificity, notably an affinity for the V1aR (Chini et al., 1996), an extremely poor oral absorption and distribution and a lack of patentability.

Recently, a first non-peptide full agonist of OT (LIT-001) has been reported to improve social interactions in a mouse model of autism after peripheral administration (Frantz et al., 2018). Frantz et *al.* have shown that LIT-001 is a specific OTR agonist with high affinity and efficacy. Furthermore, the compound poorly antagonized AVP induced calcium release on V1aR and on V1bR.

Here we investigated the analgesic potential of the LIT-001 for thermal and mechanical sensitivity in a rat model of induced inflammatory pain (CFA).

2.1.2. Results

We first sharpened the pharmacological and functional profile of LIT-001. The selectivity of LIT-001 was assessed on classical off-targets: 24 GPCRs, 3 transporters,

10 enzymes and 6 ion channels. No significant agonist or antagonist activity was found on GPCRs and ion channels. Similarly, no significant uptake blockade is observed on NA, DA and 5-HT transporters. Furthermore, only an inhibitory activity for two enzymes (COX-2 and PDE4D2) was observed.

Before testing the properties of LIT-001, we started by characterizing the modifications induced by a single s.c. injection of CFA (100 µL) in the right hindpaw. Then we tested the putative anti-hyperalgesic properties of LIT-001 in the CFA-induced inflammatory pain model. Therefore, we performed a dose-response of the anti-hyperalgesic action of LIT-001 injected (i.p.) in order to get the optimal dose. We observed that the anti-hyperalgesic action of LIT-001 starts at 5 mg/kg which increases until reaching a plateau at 10 mg/kg, for both mechanical and thermal heat hypersensitivities. Next, we performed a time-course of the anti-hyperalgesic effect of i.p. LIT-001 at the optimal dose of 10 mg/kg. We revealed that LIT-001 exerts an anti-hyperalgesic action on mechanical and thermal threshold and this effect was significant from 1 to 5 hours after the injection, with a maximal effect at 3 h.

Considering that LIT-001 was engineered as an OTR specific agonist, we wanted to validate that these anti-hyperalgesic effects were indeed mediated by the OTR activation. Thus, we co-injected i.p. LIT-001 with a specific OTR antagonist, L-368,699. The anti-hyperalgesic action of LIT-001 was fully prevented by L-368,699. These results indicate that LIT-001 likely exerts its anti-hyperalgesic action through OTR binding.

A key point in the development of a clinically relevant anti-hyperalgesic compound is the absence of side effects such as anti-nociception. Noteworthy, we did not detect any alteration in the sensitivity of the contralateral hindpaw after LIT-001 administration. Similar observations were made in control animals (receiving 0.9 % NaCl instead of CFA). These results indicate that i.p. administration of LIT-001, as an analgesic, is only effective in cases of detectable hypersensitivity.

Finally, due to the long lasting anti-hyperalgesic effects of LIT-001 we analysed its distribution at key time points in plasma, CSF, brain and urine using Liquid Chromatography Mass Spectrometry. LIT-001 was found in plasma at its highest 30 min after i.p. injection then slowly decreased, but was still significantly present after 5 hours. Moreover, LIT-001 was found in significant amount in the brain and CSF 1 hour after injection (when its anti-hyperalgesic action is significant). After 5 hours, most of

LIT-001 was excreted in the urine and was barely detectable in the brain and CSF. These results indicate that the long-lasting anti-hyperalgesic effect of i.p. LIT-001 is likely due to its prolonged presence in plasma, with putative central effects.

In conclusion, we have shown that LIT-001 exerts a significant long-lasting anti-hyperalgesic effect on mechanical and thermal heat sensitivity. Furthermore, we highlighted that LIT-001 is a promising compound in the development of new therapies based on OTR targeting in the treatment of pain.

Author contribution:

This study was a collective work, I detail below my personal contribution to the following experiments (and consequent analysis):

- Behavioural experiments.
- Blood and tissue sampling.

SCIENTIFIC REPORTS
nature research

OPEN

A Nonpeptide Oxytocin Receptor Agonist for a Durable Relief of Inflammatory Pain

Louis Hilfiger[1], Qian Zhao[2], Damien Kerspern[1], Perrine Inquimbert[1], Virginie Andry[1], Yannick Goumon[1], Pascal Darbon[1], Marcel Hibert[2,3] & Alexandre Charlet[1,3*]

Oxytocin possesses several physiological and social functions, among which an important analgesic effect. For this purpose, oxytocin binds mainly to its unique receptor, both in the central nervous system and in the peripheral nociceptive terminal axon in the skin. However, despite its interesting analgesic properties and its current use in clinics to facilitate labor, oxytocin is not used in pain treatment. Indeed, it is rapidly metabolized, with a half-life in the blood circulation estimated at five minutes and in cerebrospinal fluid around twenty minutes in humans and rats. Moreover, oxytocin itself suffers from several additional drawbacks: a lack of specificity, an extremely poor oral absorption and distribution, and finally, a lack of patentability. Recently, a first non-peptide full agonist of oxytocin receptor (LIT-001) of low molecular weight has been synthesized with reported beneficial effect for social interactions after peripheral administration. In the present study, we report that a single intraperitoneal administration of LIT-001 in a rat model induces a long-lasting reduction in inflammatory pain-induced hyperalgesia symptoms, paving the way to an original drug development strategy for pain treatment.

Oxytocin (OT) is a 9–amino acid neuropeptide that plays an important role in several physiological and social functions. It was discovered by Sir Henry Dale for its role in lactation and parturition[1]. In the brain, OT is mainly synthesized in the paraventricular and supraoptic nuclei of the hypothalamus and released into the bloodstream by the neurons of the pituitary gland[2]. OT binds mainly to its unique receptor (OTR), a member of the G-protein coupled receptor (GPCRs) family. Its amino acid sequence was elucidated in 1953[3] and its receptor gene was isolated in 1992[4].

OT has been shown to induce antinociception as well as analgesia[5]. The antinociceptive and analgesic effects after intrathecal or systemic administration of OT are well-documented[6–8]. For instance, OT has a dose dependent analgesic effect in a rat model of inflammatory pain[8], and Petersson *et al*. have shown that OT was also able to reduce the size and volume of the inflammation[7]. In addition, one study proposed that OT can also bind OTR directly in the peripheral nociceptive terminal axon in the skin[9].

Interestingly, in nociception and pain, OT has central and peripheral targets depending on the releasing pathway: plasmatic released OT has *in vivo* antinociceptive action through reduction of C fiber excitability leading to a reduction of activity of wide dynamic range (WDR) spinal sensory neurons[10] whereas OT released by fibers originating from PVN directly on WDR neurons inhibits sensory processing and produces analgesia in inflammatory pain model[11,12]. In these models, direct activation of parvocellular OT neuron by optogenetics, resulting in central and peripheral release of endogenous OT, also produced a significant OTR-dependent analgesia[11].

In clinics, OT is used since many years in patients by the intravenous route for the initiation of labor and the final expulsion of the fetus[13]. It is also administered to women as a nasal spray to stimulate milk ejection. However, despite its interesting analgesic properties, OT is not used in pain treatment because it cannot efficiently penetrate the brain[14] and is rapidly metabolized. OT half-life in the blood circulation is estimated at 5 minutes in humans and rats[15] and around 20 minutes in rat cerebrospinal fluid (CSF)[16]. Moreover, OT suffers from several additional drawbacks: a lack of specificity, since this cyclic nonapeptide has very similar affinities for its receptor OTR, for the V1a vasopressin receptor (V1aR)[17,18] and for the Transient Receptor Potential Vanilloid type-1 (TRPV1) of the capsaicin ($EC_{50} = 0.316\,\mu M$)[19]; an extremely poor oral absorption and distribution since its high

[1]Centre National de la Recherche Scientifique and University of Strasbourg, UPR3212 Institute of Cellular and Integrative Neurosciences, Strasbourg, France. [2]Laboratoire d'Innovation Thérapeutique, Faculté de Pharmacie, UMR7200 CNRS/Université de Strasbourg, Illkirch, France. [3]These authors jointly supervised this work: Marcel Hibert and Alexandre Charlet. *email: acharlet@unistra.fr

molecular weight prevents or strongly limits its absorption from the gastro intestinal tract to the blood or from the blood to the brain; and finally, a lack of patentability.

Recently, a first non-peptide full agonist of oxytocin (LIT-001) has been reported to improve social interactions in a mouse model of autism after peripheral administration[20]. LIT-001 is a pyrazolobenzodiazepine derivative with a non-peptide chemical structure and a low molecular weight (MW) compared to oxytocin (MW = 531 vs. 1007, respectively, Fig. 1a). Frantz *et al*. have shown that LIT-001 is a specific oxytocin receptor agonist with high affinity (EC_{50} = 25 nM and EC_{50} = 18 nM) and efficacy (Emax = 96% and 95%) for human and mouse receptors, respectively. Furthermore, the compound poorly antagonized vasopressin induced calcium release on V1aR (IC_{50} = 5900 nM) and was devoid of agonist or antagonist effect on V1bR.

In the present study, we report that a single intraperitoneal administration of LIT-001 in a rat model induces a long-lasting reduction in inflammatory pain-induced hyperalgesia symptoms, paving the way to an original drug development strategy for pain treatment.

Results

LIT-001, a non-peptidergic oxytocin receptor agonist. The thermodynamic water solubility (S) of LIT-001 was measured in PBS buffer at pH 7.4: S = 0.53 ± 0.03 mM (0.34 mg/mL). Its lipophilicity in the same conditions was experimentally determined: $LogD_{7.4}$ = 2.0 ± 0.3 (Fig. 1a). The selectivity of LIT-001 (at 5 μM) has been tested on classical off-targets: 24 G-protein-coupled receptors (GPCRs), 3 transporters, 10 enzymes and 6 ion channels. No significant agonist or antagonist (Fig. 1b) activity was found at GPCRs levels or at the ionotropic TRPV1 receptor. Similarly, no significant uptake blockade is observed on noradrenaline, dopamine and serotonin transporters from rat brain synaptosomes (Fig. 1c). In addition, no enzyme inhibition activity was found on the human recombinant COX(1), PDE3A, Lck kinase, acetylcholinesterase and MAO-A from human placenta (6.4% to 9.5% inhibition, below significance) (Fig. 1c). Some inhibitory activity of COX(2) and PDE4D2 was however observed (24.6 and 23.1% at 5 μM, respectively) (Fig. 1c). On ion channels, no significant blockade activity was found on human hERG potassium, GABAA (alpha1/beta2/gamma2), Cav1.2 (L-type) calcium, Vav1.5 sodium, nAChR (alpha4/beta2) and KCNQ1/hminK potassium ion channels (Fig. S1). Finally, the lack of hERG inhibition was confirmed at two additional concentrations using patch clamp method (9.50% and 10.63% inhibition at 1 μM and 10 μM concentrations, respectively). *In vitro*, LIT-001 did not interact with CYP 2C9 and 2D6 cytochromes and weakly inhibited CYP 1A2, 2C19 and 3A4 (IC_{50} = 51, 21 and 11 μM, respectively). Interesting, tested at 1 μM, LIT-001 was very stable on human hepatocytes at 37 °C since no degradation was observed after 2 hours.

Altogether, these results indicates that LIT-001 is a very specific agonist for OTR, with limited off-targets and putative side-effects, and a long lasting (>2 h) half-life; all characteristics requested for a clinically-relevant compound.

Ten days' time course of long-term modifications induced by CFA subcutaneous injection. Before testing the putative analgesic action of LIT-001, we started by characterizing the long-term modifications induced by a single subcutaneous injection of complete Freund adjuvant (CFA, 100 μl) in the right hindpaw (Fig. 2a). We first measured the hindpaw diameter and observed that CFA, but not NaCl 0.9%, injection induced a major edema, whose size was maximum 24 h after the injection (CFA: 9.69 ± 0.22 mm, n = 14 vs NaCl: 5.73 ± 0.14 mm, n = 11; $p < 0.01$) and persistent for up to 10 days (Fig. 2b). On the other hand, the mechanical CFA-induced hyperalgesia was maximum 24 h after the injection (threshold pressure CFA: 122 ± 15 g, n = 14 vs NaCl: 520 ± 14 g, n = 18; $p < 0.01$) and, as the edema, was persistent up to 10 days (Fig. 2c1). Similarly, a thermal heat hyperalgesia was detected for up to 10 days and maximum 24 h after the CFA injection (withdrawal latency CFA: 2.5 ± 0.23 s, n = 14 vs NaCl: 10.31 ± 0.38 s, n = 18; $p < 0.01$; Fig. 2c2). Interestingly, the contralateral hindpaw to the CFA-injected one did not present any mechanical nor thermal heat hypersensitivity (Fig. S2). Based on these results, we decided to test the putative analgesic properties of LIT-001 at 24 h (D1) after the CFA injection.

Analgesic properties of LIT-001 on CFA-induced inflammatory pain model. We next aimed to test the putative analgesic properties of LIT-001 in the CFA-induced inflammatory pain model. For this purpose, we first performed a dose-response of the analgesic action of LIT-001 injected intraperitoneally (i.p.) at day 1 (D1) after the CFA injection, when the inflammatory pain symptoms were at their maximum (Fig. 3). We found a first analgesic action of i.p. LIT-001 at 5 mg/kg, an effect rising to reach a plateau at 10 mg/kg, that for both mechanical (Fig. 3a) and thermal heat (Fig. 3b) hypersensitivities. Importantly, none of the doses tested seem to exert an antinociceptive action, as measured on the contralateral hindpaw (Fig. S3).

Therefore, we performed a time-course of the analgesic effect of i.p. LIT-001 (10 mg/kg) injected at day 1 (D1) after the CFA injection (Fig. 4a). For that purpose, we analyzed the hindpaw size as well as the mechanical and thermal heat hypersensitivities for 24 h (Fig. 4b–d).

We first found that i.p. LIT-001, injected alone or with a specific oxytocin receptor antagonist, L-368,699 (L-368), had no effect on the CFA-induced edema size (CFA + Vehicle, 9.44 ± 0.18 mm, n = 7; CFA + LIT-001, 9.49 ± 0.23 mm, n = 8; CFA + LIT-001 + L-368, 10.32 ± 0.17 mm, n = 7; Fig. 4b). This suggests that acute LIT-001 injection, at this stage of the CFA-induced inflammation, may have no or limited anti-inflammatory effect *per se*.

However, we revealed that i.p. LIT-001 exerts an anti-hyperalgesic action on mechanical threshold (Fig. 4c1). This effect was significant from 1 to 5 h after i.p. injection, with a maximal effect at 3 h (CFA + Vehicle, 126 ± 29 g, n = 7 vs CFA + LIT-001, 246 ± 22 g, n = 8; $p < 0.001$), as reflected by an increase of the area under the curve (AUC) of 152 ± 11%. We observed a similar anti-hyperalgesic action on thermal heat latency (Fig. 4c2), significant from 1 to 5 h after i.p. injection, with a maximal effect at 3 h (CFA + Vehicle, 1.94 ± 0.18 s, n = 7 vs CFA + LIT-001, 5.83 ± 0.65 s, n = 8; $p < 0.001$), as reflected by an increase of the AUC of 135 ± 9%. These results indicate that i.p. LIT-001 exerts a strong significant and long-lasting anti-hyperalgesic action on both mechanical and thermal heat sensitivities.

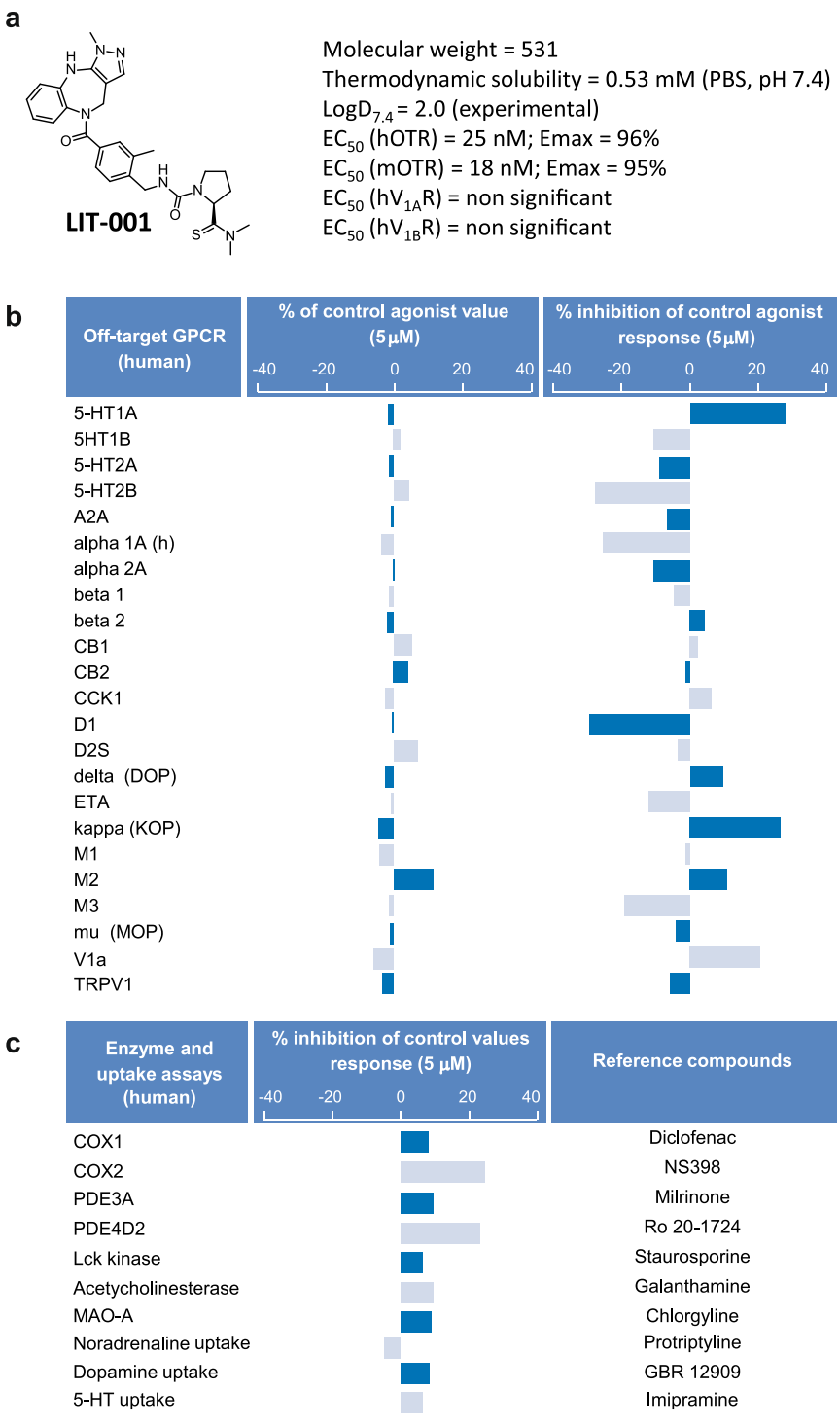

Figure 1. Pharmacological functional profile of LIT-001 on off-targets. (**a**) LIT-001 structure, physico-chemical properties and potency on target receptors. (**b**) *In vitro* agonist and antagonist profiles of LIT-001 on 24 off-target GPCRs. Cellular agonist and antagonist effects of LIT-001 were calculated as a % of control response to a known reference agonist for each target and cellular antagonist. Negative values are non significant in these assay setups. (**c**) Enzyme and transporter inhibition potency of LIT-001 on selected off-targets. Compound enzyme inhibition effect was calculated as a % inhibition of control enzyme activity. Compound uptake inhibition effect was calculated as a % inhibition of control uptake activity. Data are expressed as the mean value of 2 independent tests.

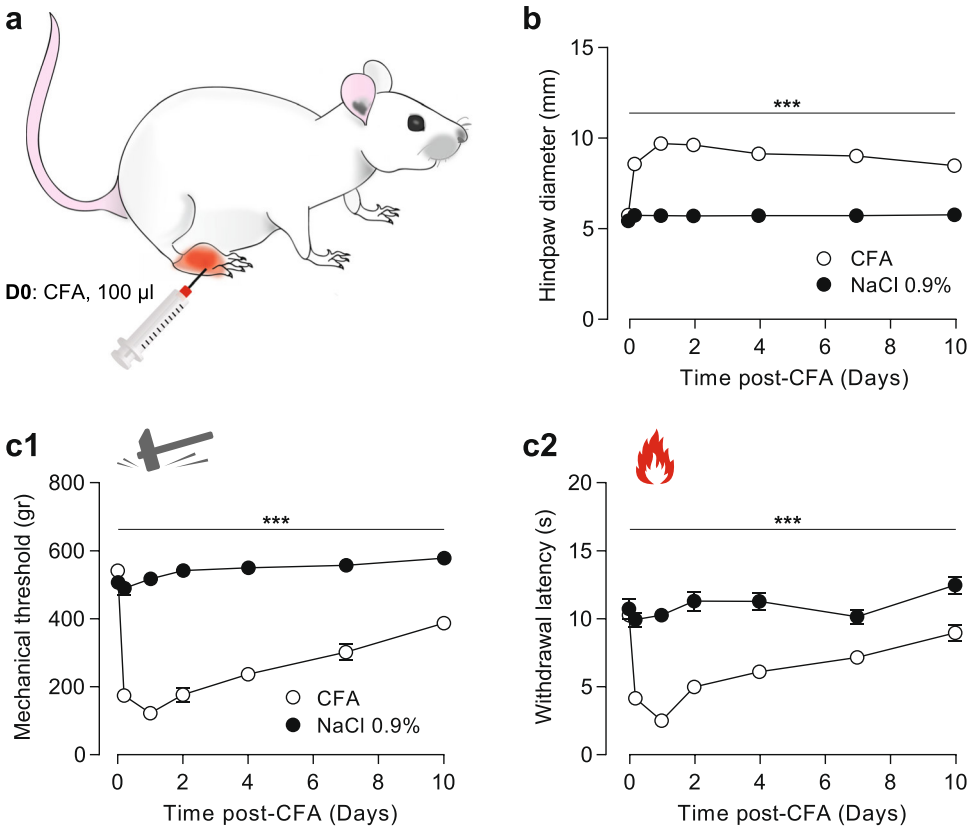

Figure 2. Ten days' time course of long-term modifications induced by CFA subcutaneous injection. (**a**) Scheme of the CFA-induced inflammatory pain model (100 µl). (**b**) Time-course of the CFA-induced edema size (CFA, n = 14; NaCl, n = 18). (**c**) Time-course of the CFA-induced mechanical (**c1**) and thermal heat (**c2**) hyperalgesia (CFA, n = 14; NaCl, n = 18). Data are expressed as mean ± SEM. Asterisks indicate statistical significance (***$p < 0.001$) using two-way ANOVA followed by Tukey multiple comparisons post-hoc test.

Given that LIT-001 was built as a specific agonist for OTR, we thought to validate that these anti-hyperalgesic effects were mediated by OTR activation. For this purpose, we co-injected LIT-001 with a specific OTR antagonist, L-368,699[11]. As expected, the anti-hyperalgesic action of i.p. LIT-001 was fully prevented by L-368,699, as displayed by the mechanical threshold (CFA + LIT-001 + L-368, 119 ± 12 g, n = 7) and thermal heat latency (CFA + LIT-001 + L-368, 3.08 ± 0.29 s, n = 7) and their relative AUC (90 ± 7% and 92 ± 8%, respectively) values 3 h post i.p. (Fig. 4c). These results indicate that i.p. LIT-001 likely exerts its anti-hyperalgesic action through OTR binding.

One important point in the development of a clinically-relevant anti-hyperalgesic compound is the limitation of its side effect, here the absence of anti-nociception. Noteworthy, we did not detect any alteration of contralateral hindpaw sensitivities after i.p. LIT-001, being on mechanical threshold (cCFA + LIT-001, 531 ± 25 g, n = 8; Fig. S4a1) or thermal heat latency (cCFA + LIT-001, 11 ± 0.53 s, n = 8; Fig. S4a2). Interestingly, we made similar observation on control animals, receiving NaCl 0.9% hindpaw injection and thus not presenting inflammatory pain symptoms (Figs. 4d, S4b). Here, i.p. LIT-001, injected alone or co-injected with the specific oxytocin receptor antagonist L-368,699, had no effect on mechanical (NaCl + LIT-001, 526 ± 20 g, n = 7; Figs. 4d1, S4b1) or thermal heat (NaCl + LIT-001, 8.14 ± 0.48 s, n = 7; Figs. 4d2, S4b2) hindpaw sensitivities, as reflected by the absence of increase of the AUC (Figs. 4d, S4b). These results indicate that i.p. LIT-001, as an analgesic, is only effective in case of detectable hypersensitivities.

LIT-001 distribution and clearance in the organism. Because the anti-hyperalgesic effects of i.p. LIT-001 10 mg/kg were long-lasting, up to 5 h, while oxytocin-induced analgesia usually only last for minutes, we analyzed its distribution at key time points in plasma, CSF, brain and urine (n = 5–6, Fig. 5) and performed a quantitative dosage by comparison to a dose-response curve, using Liquid Chromatography Mass Spectrometry (LC-MS/MS; Fig. S5). Interestingly, LIT-001 concentration was found in plasma at its highest 30 min after i.p. injection (650 ± 200 pmole/ml; Fig. 5b) then slowly decreased, but was still significantly present after 300 min (5 h; 95.2 ± 36.5 pmole/ml; Fig. 5b,c). In addition, LIT-001 was found in significant amount in both the brain and CSF 60 min after i.p. injection (1.6 ± 0.8 and 7.4 ± 4.4 pmole/ml, respectively; Fig. 5c) when its analgesic action is significantly observed. As expected according to its chemical structure and previous half-life evaluation, after 5 h most of LIT-001 was found in urine (188951 ± 8475 pmole/ml; Fig. 5c) and was hardly detectable in both CSF (1.5 ± 1.1 pmole/ml) and brain (0.6 ± 0.4 pmole/ml; Fig. 5c). These results indicate that the long-lasting

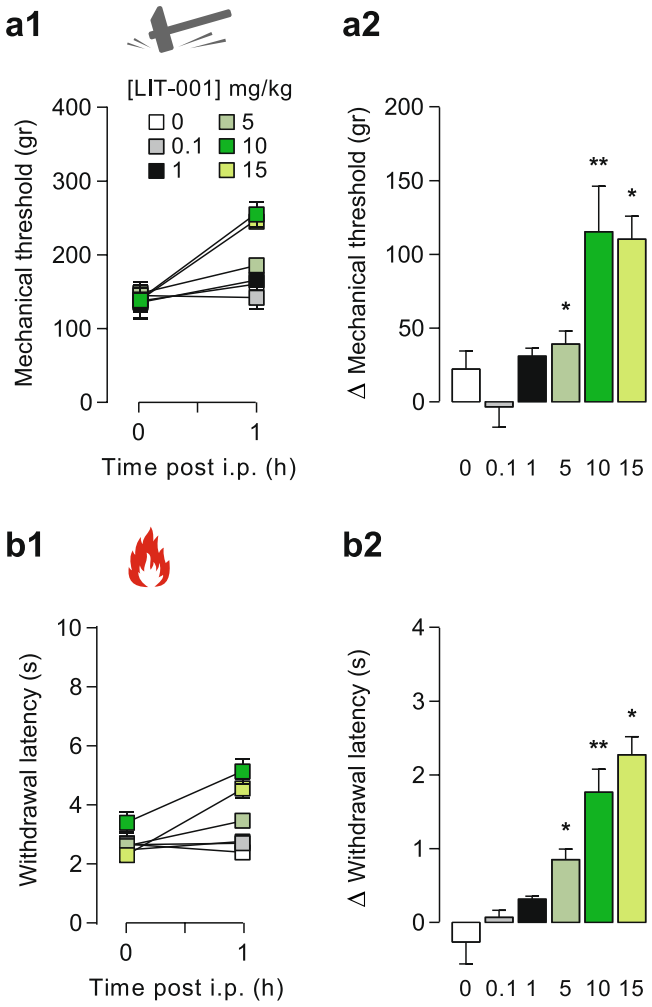

Figure 3. Dose-response of the analgesic properties of LIT-001 on CFA-induced inflammatory pain model. Effects of LIT-001 0.1 (n = 4), 1 (n = 6), 5 (n = 6), 10 (n = 8) and 15 mg/kg (n = 6) or its vehicule (n = 9) measured 1 hour after i.p. injection on mechanical (**a**) and thermal heat (**b**) CFA-induced hyperalgesia. Data are expressed as mean ± SEM. Asterisks indicate statistical significance (**p < 0.01; *p < 0.05) using paired Wilcoxon or T-test, depending on the data's normal distribution.

anti-hyperalgesic effect of i.p. LIT-001 is likely due to its prolonged presence in plasma, with putative central effects.

Discussion

In the present study, we show that LIT-001, a non-peptidergic specific agonist for OTR, exerts a significant long-lasting (>5 h) anti-hyperalgesic effect on both mechanical and thermal heat sensitivity.

Antinociceptive and analgesic action of OT is well documented[21–23]. It has been shown to act at both peripheric and central levels[10] mainly through final reduction of spinal wide dynamic range (WDR) neurons and C fiber excitability[11]. However, the main limitations of OT, or OTR peptidergic agonists, are (i) the short duration of the effect, (ii) the lack of permeability through the blood brain barrier (BBB), and (iii) the lack of specificity, which all are not compatible with clinical use.

Here, we show that a low molecular weight, non-peptidergic agonist, LIT-001, exerts a long lasting antihyperalgesic effect, up to 5 h. Two points may explain the prolonged effect of LIT-001. First, it has a long half-life (>2 h), by comparison to OT or OTR peptidergic agonists, which all have a very short half-life of less than 15 min. Second, it may reach its central and/or peripheral targets and trigger here long lasting mechanisms involving OTR. At this point, it is important to highlight that, for clinical purpose and mainly in case of chronic pain, a strong analgesic candidate should not only focus on nociception but also positively modulate all pain-induced disorders, such as anxiety, depression, loss of social interaction, impaired food intake or stress. Indeed, to attenuate this large variety of pain-relative symptoms may significantly improve the patient quality of life, one of the main goals of modern medicine. In this regard, to target the oxytocinergic system, in particular with specific OTR agonist such as LIT-001, may be particularly relevant. Indeed, activation of OTR is known to induce a variety of molecular cascades[24] resulting in an important modulation of nociception[25], social recognition and interactions[26,27], anxiety[28], feeding behavior[29], and stress[30], all important comorbidity factors in painful patients.

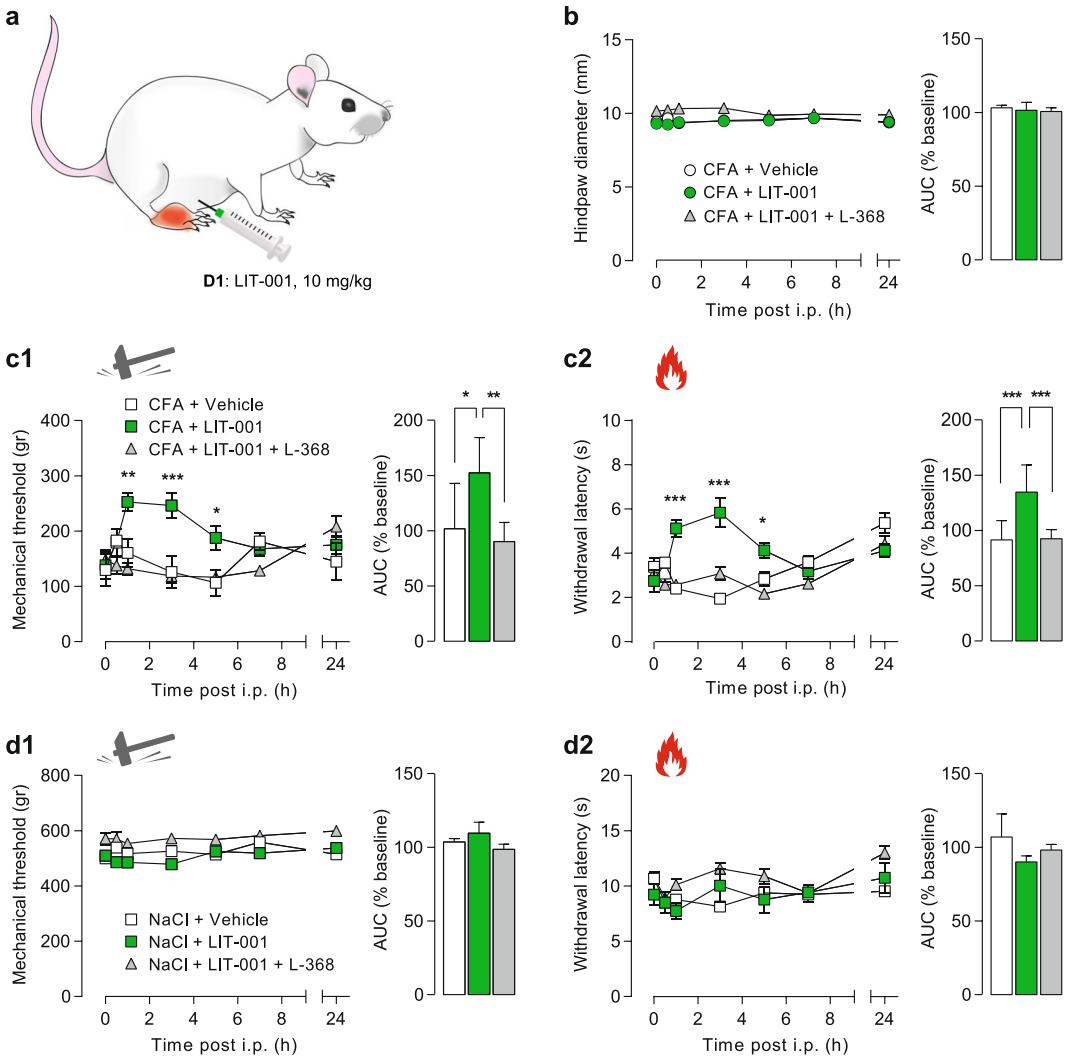

Figure 4. Time-course of the analgesic properties of LIT-001 on CFA-induced inflammatory pain model. (**a**) Scheme of the CFA-induced inflammatory pain model followed by i.p. LIT-001 injection. (**b**) Left, time-course of the effects of i.p. LIT-001 10 mg/kg (n = 8), its vehicule (n = 7) or co-injection with L-368,699 (n = 7), on CFA-induced edema size (CFA, n = 14; NaCl, n = 18). Right, relative-to-baseline AUC (%) of the effects. (**c**) Left, time-course of the effects of i.p. LIT-001 10 mg/kg (n = 7), its vehicule (n = 8) or co-injection with L-368,699 (n = 6) on CFA-induced mechanical (**c1**) and thermal heat (**c2**) hyperalgesia. Right, relative-to-baseline AUC (%) of the effects. (**d**) Left, time-course of the effects of i.p. LIT-001 10 mg/kg (n = 7), its vehicule (n = 8) or co-injection with L-368,699 (n = 6) on mechanical (**d1**) and thermal heat (**d2**) sensitivities of NaCl-injected hindpaw. Right, relative-to-baseline AUC (%) of the effects. Data are expressed as mean ± SEM. Asterisks indicate statistical significance (***$p < 0.001$; **$p < 0.01$; *$p < 0.05$) using two-way ANOVA followed by Tukey's multiple comparisons test.

Interestingly, a previous study has also shown that LIT-001 improved social interaction in a mouse model of autism[20], reinforcing its putative interest as an analgesic molecule.

Besides, we confirm the capability of LIT-001 to cross the blood brain barrier to exert its action in the central nervous system[20] (Fig. 5). In addition, we show that LIT-001 exerts long lasting anti-hyperalgesic effects. Importantly, LIT-001 does not accumulate in the body but is almost entirely excreted as such in the urine. While those data were obtained by intra-peritoneal injection, we hypothesize that similar results may be obtained using an oral administration of LIT-001. If true and transposable to human, it may lead to the development of a drug easy to take every few hours to limit pain symptoms. Those aspects point toward LIT-001, and future non-peptidergic agonists, as key candidates for clinical use. Although it displays a low micromolar affinity for this receptor, LIT-001 is a potent V2R agonist in functional assays[20]. The V2 receptor is peripheral and known to regulate water homeostasis. It is thus likely that LIT-001 will have some antidiuretic effect *in vivo* that will have to be studied and taken into account for a potential development toward clinical studies.

Because of its long half-life and its capability to cross the BBB, one may worried about the putative LIT-001 side effects: to design drugs with limited side-effects is a major challenge in chemical and pharmaceutical industries. Importantly, LIT-001 does not interact significantly with any classical off targets (G protein coupled

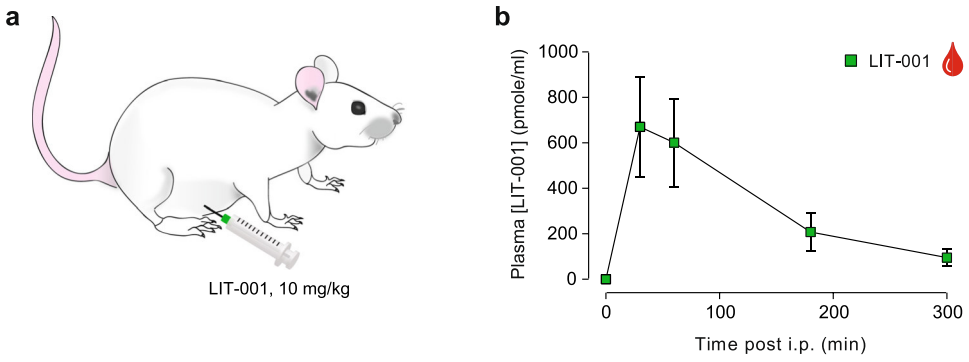

c

Time after i.p. injection (min)	[LIT-001] (pmole/ml +/- sem)			
	Brain	CSF	Plasma	Urine
60	1.6 ± 0.8	7.4 ± 4.4	626.1 ± 112.3	52498 ± 14244
300	0.6 ± 0.4	1.5 ± 1.1	95.2 ± 36.5	188951 ± 8475

Figure 5. LIT-001 distribution and clearance in the organism. (**a**) Scheme displaying the i.p. injection of LIT-001, 10 mg/kg in naïve animal. (**b**) Time course of the concentrations of LIT-001 present in the plasma of rats after an i.p. injection. (**c**) Concentrations of LIT-001 present at 60 and 300 min after i.p. injection, in the brain (60, n = 6; 300, n = 5), CSF (60, n = 4; 300, n = 4), plasma (60, n = 11; 300, n = 5) and urine (60, n = 6; 300, n = 5) 60 min and 300 min after i.p. injection. Data are expressed as mean ± SEM. Data are expressed as mean ± SEM of 5 animals.

receptors, transporters, enzymes, ion channels listed in Figs. 1, S1), neither as an agonist/activator nor an antagonist/inhibitor. Noteworthy, neither LIT-001 nor the OT antagonist L-368,699 displayed any significant agonist or antagonist activity at the TRPV1 receptor at 5 μM (Fig. 1b). Therefore, LIT-001 is a relatively specific OTR agonist likely exerting its analgesic effect via this receptor. This conclusion is strengthened by our results showing that the LIT-001 antihyperalgesic action is fully prevented in presence of L-368,699, a specific OTR antagonist that is also devoid of significant activity at TRPV1 receptor at 5 μM. In addition, an interesting aspect of LIT-001 seems to be its specific action on nociception and pain. Indeed, while LIT-001 shows limited inhibitory activity of COX2, which in a model of inflammatory pain could be relevant, we observed no modification of the size of the edema induced by CFA injection (Fig. 4), indicating that the LIT-001-induced reduction of pain symptoms is not based on a reduction of inflammation. However, we did not rule specific protocols to tests its anti-inflammatory action *per se*, and this should be done before any clinical trial. In addition, it is important to note that LIT-001 did not modify the mechanical/thermal heat sensitivities in control animals or contralateral paws, indicating that LIT-001 does not have antinociceptive effect, which, in a clinical perspective, is an important characteristic in order to limit undesired loss of sensitivities. At this stage, the only known drawback of LIT-001 is its action at the V2 vasopressin receptor (V2R).

In conclusion, we found that LIT-001 is a very useful probe to validate the oxytocin receptor as a target for the treatment of pain and represents a promising drug-like lead compound for the development of novel treatments.

Methods

All the protocols, tests and use and living animals were performed in accordance with European committee council Direction, authorization from French Department of Agriculture and from the regional ethic committee (Comité Régional d'Ethique en Matière d'Expérimentation Animale de Strasbourg, CREMEAS).

Drugs. LIT-001 was prepared as described in Frantz *et al.*[20]. For *in vivo* biological assays, it was dissolved in carboxymethyl cellulose (CMC, 1%) - NaCl (0.9%) and administered at the dose of 10 mg/kg. LIT-001 or vehicle were injected intraperitoneally (i.p.), in a volume of 10 ml/kg[20], 24 h after the induction of the CFA-induced painful inflammatory sensitization. To confirm the implication of the OTR we injected (i.p.) also L-368,899 (Sigma, St. Louis, MO) (1 mg/kg), an OTR antagonist, in combination with LIT-001 in another group of rats[11].

In vitro* physicochemical and pharmacological characterization.** ***Solubility of LIT-001 was determined from solution of about 1 mg of compound in 500 μl of PBS at pH 7.4. (Figs. 1, S1) The solution was stirred at room temperature for 24 h and centrifuged at 15.000 × *g* for 5 min. The supernatant was diluted with a mixture of acetonitrile and water and analyzed by HPLC with a diode detector (Gilson; Kinetex 2.6 μm C18 100 A 50 × 4.6 mm column). No degradation of LIT-001 was observed after 24 h. The lipophilicity ($LogD_{7.4}$) of LIT-001 was measured using 10 ml of a stock solution diluted with different concentrations of octanol and PBS to cover a LogP range from −2 to + 4.5 in a final volume of 1 ml. After stirring for 1 h at room temperature (≈ 20 °C), the

samples were centrifuged and the different phases were analyzed by HPLC (Gilson; diode detector, Kinetex 2.6 µ C18 100 A 50 × 4.6 mm column).

Stability of LIT-001 was determined in human hepatocytes. Cells were unfrozen and their viability measured (Tryptan blue). Cells are suspended (2 × 106 cells/ml) and dispensed in 96 well microtiterplates (50 µl/well). LIT-001 (50 µl of a 2 µM in the incubation media) was added. The final concentration of the compound was 1 µM in 1×10^6 cells/ml. The incubation volume was 100 µl/well. Incubations were stopped after 0, 4, 20, 40, 80 and 120 min in mixing the well content with 100 µl acetonitrile at 0 °C. A positive control (testosterone) was prepared in same conditions. All samples were analyzed by LC-MS/MS (UHPLC coupled to a triple quadripole Shimadzu LC-MS 8030). Each measurement was performed in triplicate.

In vitro profiling of LIT-001 was performed by Eurofins as described in the Eurofins SafetyScreen-Functional panel, 2018[31]. The hepatotoxicity of LIT-001 was studied with cryo-preserved mouse hepatocytes. After unfreezing (optiTHAW and optiINCUBATE media, Xenotech) and cell viability control, cells (2×10^6 cells/ml) were dispatched in 96 well microtiterplates. LIT-001 was added to reach a concentration 1 µM in the presence of 1 × 106 cells/mL in a volume of 100 µl/well. The incubation was stopped at 4, 20, 40, 80 and 120 min in adding 100 µl of acetonitrile at 0 °C. A positive control was treated in the same conditions. All samples were analyzed by UHPLC coupled to a mass spectrometer (Shimadzu LC-MS 8030).

Cytochrome inhibition by LIT-001 was studied as follows. A stock solution of LIT-001 at 10 mM in DMSO was prepared and stored at 4 °C. Solutions containing the cytochrome substrates and control inhibitors or LIT-001 were prepared. 2 µl of substrate-inhibitor solutions were mixed with 176 µl of phosphate buffer containing human liver microsomes (0.2 mg/ml), 1 mM of NADPH and 3 mM of $MgCl_2$. Height concentrations were tested: 0.03; 0.1; 0.3; 1; 3; 10; 30 and 100 µM. The reaction was initiated by addition of the co-factor after 5 min of incubation at 37 °C. After one hour of incubation, 200 µl of acetonitrile were added to stop enzymatic reactions and solubilize the products. Different control inhibitors were used and supernatants were analyzed by LC-MS/MS (UHPLC separation; Shimadzu LC-MS 8030).

- Furafylline (CYP 1A2 inhibitor): 0.03; 0.1; 0.3; 1; 3; 10; 30 and 100 µM
- Sulfaphenazole (CYP 2C9 inhibitor): 0.03; 0.1; 0.3; 1; 3; 10; 30 and 100 µM
- Tranylcypromine (CYP 2C19 inhibitor): 0.03; 0.1; 0.3; 1; 3; 10; 30 and 100 µM
- Quinidine (CYP 2C19 inhibitor): 0.003; 0.01; 0.1; 0.5; 1; 5; 10 and 50 µM
- Kétoconazole (CYP 3A4 inhibitor): 0.003; 0.01; 0.1; 0.5; 1; 5; 10 and 50 µM

Animals. Male Wistar rats (300 g; JANVIER LABS, Le Genest St. Isle, France) were used for this study. They were housed by groups of 3 or 4 under standard conditions (room temperature, 22 °C; 12/12 h light/dark cycle) with *ad libitum* access to food and water and behavioral enrichment. All animals were manipulated and habituated to the tests and to the room for at least 2 weeks. All behavioral tests were done during the light period (i.e., between 7:00 and 19:00). All the procedures were performed in accordance with European committee council Direction, authorization from French Department of Agriculture and from the regional ethic committee.

Behavioral testing. *Mechanical allodynia.* In all experimentations, to test the animal mechanical sensitivity, we used a calibrated forceps (Bioseb, Chaville, France) previously developed in our laboratory (Figs. 2, 3 and S2, S3)[32]. Briefly, the habituated rat is loosely restrained with a towel masking the eyes in order to limit stress by environmental stimulations. The tips of the forceps are placed at each side of the paw and a graduate force is applied. The pressure producing a withdrawal of the paw, or in some rare cases a vocalization of the animal, corresponded to the nociceptive threshold value. This manipulation was performed three times for each hindpaw and the values were averaged averaged.

Thermal allodynia/hyperalgesia. To test the animal heat sensitivity, we used the Plantar test with Hargreaves method (Ugo Basile, Comerio, Italy) to compare the response of each hindpaw[33] when we tested healthy animals (unilateral intraplantar NaCl injection) and animals having received unilateral intraplantar CFA (Freund's Complete Adjuvant) injection. The habituated rat is placed in a small box and we wait until the animal is calmed then we exposed the hindpaw to a radiant heat, the latency time of paw withdrawal was measured.

CFA model of inflammatory pain. In order to induce a peripheral inflammation, 100 µl of complete Freund adjuvant (CFA; Sigma, St. Louis, MO), was injected in the right hindpaw of the rat. All CFA injections were performed under light isoflurane anesthesia (3%). Animals were tested daily for 10 days after the paw injection, a period during which animals exhibited a clear mechanical allodynia and thermal heat hyperalgesia.

Pharmacokinetics of LIT-001. *Preparation of brain, cerebrospinal fluid, plasma and urine extracts.* Brains from rat injected with 10 mg/kg (18.8 µmol/kg) i.p. of LIT-001 were homogenized with an Ultra Turrax instrument (Ika, Staufen, Germany) in 2 ml of H_2O (Figs. 4, S4). The homogenates were then sonicated (3 times 10 s, 100 W) with a Vibra Cell apparatus (Sonics, Newtown, U.S.A.). Protein concentrations were determined using the Bradford method (Protein Assay, Bio-Rad, Marne-la-Coquette, France). 400 µl was mixed with 4 ml of ice cold acetonitrile (ACN) and let 30 min on ice. Samples were then centrifuged (20,000 × *g*, 30 min) at 4 °C. Supernatants were dried under vacuum and resuspended in 400 µl ACN 10%/H_2O 89.9%/formic acid 0.1% (v/v/v) and a volume of 5 µl was injected on the LC-MS/MS. For CSF, plasma and urine, 200 µl of fluids were mixed with 1 ml of ice cold acetonitrile (ACN) and let 30 min on ice. Samples were then centrifuged (20,000 × *g*, 30 min) at 4 °C.

Supernatants were dried under vacuum and suspended in 200 µl ACN 10%/H_2O 89.9%/formic acid 0.1% (v/v/v) and a volume of 5 µl was injected on the LC-MS/MS.

LC-MS/MS instrumentation and analytical conditions. Analyses were performed on a Dionex Ultimate 3000 HPLC system (Thermo Scientific, San Jose, USA) coupled with a triple quadrupole Endura mass spectrometer (Thermo Scientific). The system was controlled by Xcalibur v.2.0 software (Thermo Electron). Samples were loaded onto an Accucore C18 RP-MS column (ref 17126–151030; 150 × 1 mm 2.6 µm, Thermo Scientific) heated at 40 °C. The presence of LIT-001 was studied using the multiple reaction monitoring mode (MRM). Elution was performed at a flow rate of 150 µl/min by applying a linear gradient of mobile phases A/B. Mobile phase A corresponded to ACN 1%/H_2O 98.9%/formic acid 0.1% (v/v/v), whereas mobile phase B was ACN 99.9%/formic acid 0.1% (v/v). The gradient used is detailed in Fig. S4. Electrospray ionization was achieved in the positive mode with the spray voltage set at 3,500 V. Nitrogen was used as the nebulizer gas and the ionization source was heated to 210 °C. Desolvation (nitrogen) sheath gas was set to 27 Arb and Aux gas was set to 9 Arb. The ion transfer tube was heated at 312 °C. Q1 and Q2 resolutions were set at 0.7 FWHM, whereas collision gas (CID, argon) was set to 2 mTorr. Identification of the compounds was based on precursor ion, selective fragment ions and retention times obtained for LIT-001. Selection of the monitored transitions and optimization of collision energy and RF Lens parameters were manually determined (see Fig. S4 for details). Qualification and quantification were performed in MRM mode. Quantification was obtained using Quan Browser software (Thermo Scientific). For tissues and fluids, LIT-001 was quantified using calibration curves of external standards of LIT-001 (125 fmol to 100 pmol/injection; Fig. S4) added to urine, plasma or brain extracts of naive rat and submitted to the same procedure described for respective fluids and tissue recovery. The amounts of LIT-001 measured in samples fit within the standard curve limits, with typical analytical ranges (the range of amounts that can be accurately quantified) from 150 fmol to 120 pmol.

Statistical analysis. Data are expressed as mean ± standard error of the mean (SEM). Statistical tests were performed with GraphPad Prism 7.05 (GraphPas Software, San Diego, California, USA) using repeated-measures two-way ANOVA, with the following factors: treatment (between), and time (within); when the ANOVA test was significant, the Tukey test was used for *post-hoc* multiple comparisons between individual groups. Results were considered to be statistically significant if p values were below 0.05 (*), 0.01 (**), and 0.001 (***). For the area under the curve (AUC) comparisons, we used the one-way ANOVA (factors: treatment); when the ANOVA test was significant, the Tukey test was used for post hoc multiple comparisons.

Received: 7 October 2019; Accepted: 2 February 2020;
Published online: 20 February 2020

References

1. Dale, H. H. The action of extracts of pituitary body. *Biochem J.* **4**, 427–447 (1906).
2. Sawchenko, P. E., Swanson, L. W., Steinbusch, H. W. M. & Verhofstad, A. A. J. The distribution and cells of origin of serotonergic inputs to the paraventricular and supraoptic nuclei of the rat. *Brain Research* **277**, 355–360 (1983).
3. Du Vigneaud, V., Ressler, C. & Trippett, S. The sequence of aminoacids in oxytocin, with a proposal for the structure of oxytocin. *J. Biol. Chem.* **205**, 949–957 (1953).
4. Kimura, T., Tanizawa, O., Mori, K., Brownstein, M. J. & Okayama, H. Structure and expression of a human oxytocin receptor. *Nature* **356**, 526–529 (1992).
5. Grinevich, V. & Charlet, A. Oxytocin: pain relief in skin. *Pain* **158**, 2061–2063 (2017).
6. Lundeberg, T., Uvnäs-Moberg, K., Agren, G. & Bruzelius, G. Anti-nociceptive effects of oxytocin in rats and mice. *Neuroscience Letters* **170**, 153–157 (1994).
7. Petersson, M., Wiberg, U., Lundeberg, T. & Uvnäs-Moberg, K. Oxytocin decreases carrageenan induced inflammation in rats. *Peptides* **22**, 1479–1484 (2001).
8. Yu, S. Q., Lundeberg, T. & Yu, L. C. Involvement of oxytocin in spinal antinociception in rats with inflammation. *Brain Research* **983**, 13–22 (2003).
9. Gonzalez-Hernandez, A. *et al*. Peripheral oxytocin receptors inhibit the nociceptive input signal to spinal dorsal horn wide-dynamic-range neurons. *Pain* **158**, 2117–2128 (2017).
10. Juif, P. E. & Poisbeau, P. Neurohormonal effects of oxytocin and vasopressin receptor agonists on spinal pain processing in male rats. *Pain* **154**, 1449–1456 (2013).
11. Eliava, M. *et al*. A new population of parvocellular oxytocin neurons controlling magnocellular neuron activity and inflammatory pain processing. *Neuron* **89**, 1291–1304 (2016).
12. Jiang, C. Y., Fujita, T. & Kumamoto, E. Synaptic modulation and inward current produced by oxytocin in substantia gelatinosa neurons of adult rat spinal cord slices. *J. Neurophysiol.* **111**, 991–1007 (2013).
13. Heesen, M. *et al*. International consensus statement on the use of uterotonic agents during caesarean section. *Anaesthesia* **74**, 1219–1241 (2019).
14. Gimpl, G. & Fahrenholz, F. The oxytocin receptor system: structure, function, and regulation. *Physiological Reviews* **81**, 629–683 (2001).
15. Morin, V. *et al*. Evidence for non-linear pharmacokinetics of oxytocin in anesthetized rat. *J. Pharm. Pharm. Sci.* **11**, 12–24 (2008).
16. Mens, W., Witter, A. & Van Wimersma Greidanus, T. B. Penetration of neurohypophyseal hormones from plasma into cerebrospinalfluid (CSF): half-times of disappearance of these neuropeptidesfrom CSF. *Brain Res.* **262**, 143–152 (1983).
17. Chini, B. *et al*. Two aromatic residues regulate the response of the human oxytocin receptor to the partial agonist arginine vasopressin. *FEBS Letters* **397**, 201–206 (1996).
18. Kubo, A. *et al*. Oxytocin alleviates orofacial mechanical hypersensitivity associated with infraorbital nerve injury through vasopressin-1A receptors of the rat trigeminal ganglia. *Pain* **158**, 649–659 (2017).
19. Nersesyan, Y. *et al*. Oxytocin modulates nociception as an agonist of pain-sensing TRPV1. *Cell Rep.* **21**, 1681–1691 (2017).
20. Frantz, M. C. *et al*. LIT-001, the first nonpeptide oxytocin receptor agonist that improves social interaction in a mouse model of autism. *J. Med. Chem.* **61**, 8670–8692 (2018).
21. Boll, S., Almeida de Minas, A. C., Raftogianni, A., Herpertz, S. C. & Grinevich, V. Oxytocin and pain perception: from animal models to human research. *Neuroscience* **387**, 149–161 (2017).

22. Gonzalez-Hernandez, A. & Charlet, A. Oxytocin, GABA, and TRPV1, the analgesic triad? *Frontiers in Molecular Neuroscience*, https://doi.org/10.3389/fnmol.2018.00398 (2018).
23. Poisbeau, P., Grinevich, V. & Charlet, A. Oxytocin signaling in pain: cellular, circuit, system, and behavioral levels. *Current Topics in Behavioral Neurosciences* **35**, 193–221 *Behavioral Pharmacology of Neuropeptides: Oxytocin*, (2017).
24. Busnelli, M. & Chini, B. Molecular Basis of Oxytocin Receptor Signalling in the Brain: What we know and what we need to know. *Current Topics in Behavioral Neurosciences* **35**, 3–29 *Behavioral Pharmacology of Neuropeptides: Oxytocin*, (2017).
25. Juif, P. E. *et al*. Long-lasting spinal oxytocin analgesia is ensured by the stimulation of allopregnanolone synthesis which potentiates GABA(A) receptor-mediated synaptic inhibition. *J. Neurosci.* **33**, 16617–16626 (2013).
26. Andari, E. *et al*. Promoting social behavior with oxytocin in high-functioning autism spectrum disorders. *PNAS* **107**, 4389–4394 (2010).
27. Kosfeld, M., Heinrichs, M., Zak, P. J., Fischbacher, U. & Fehr, E. Oxytocin increases trust in humans. *Nature* **435**, 673–676 (2005).
28. Grund, T. *et al*. Neuropeptide S activates paraventricular oxytocin neurons to induce anxiolysis. *J. Neurosci.* **37**, 12214–12225 (2017).
29. Arletti, R., Benelli, A. & Bertolini, A. Influence of oxytocin on feeding behavior in the rat. *Peptides* **10**, 89–93 (1989).
30. Neumann, I. D. Involvement of the brain oxytocin system in stress coping: interactions with the hypothalamo-pituitary-adrenal axis. *Prog. Brain Res.* **139**, 147–162 (2002).
31. Eurofins SafetyScreen - Functional panel. https://www.eurofinsdiscoveryservices.com/ (2018)
32. Charlet, A., Lasbennes, F., Darbon, P. & Poisbeau, P. Fast non-genomic effects of progesterone-derived neurosteroids on nociceptive thresholds and pain symptoms. *Pain* **139**, 603–609 (2008).
33. Hargreaves, K., Dubner, R., Brown, F., Flores, C. & Joris, J. A new and sensitive method for measuring thermal nociception in cutaneous hyperalgesia. *Pain* **32**, 77–88 (1988).

Acknowledgements

This work was supported by the NARSAD Young Investigator Grant 24821 (to AC); the IDEX Interdisciplinary grant 2015 (to AC and MH); the French government under the specific ANR-14-CE-16-0005-01 project (OT-ism; to MH). The authors thank the Chronobiotron (UMS 3512 for assistance in animal cares, experimentations and surgeries), the PCBIS platform (UMS 3286 for physicochemical and pharmacokinetic studies) and the PACSI platform (GDS3670 for analytical chemistry).

Author contributions

Conceptualization, A.C., M.H.; Methodology, A.C., D.K., L.H., M.H., Q.Z., Y.G.; Chemical analysis, Q.Z.; Behavior, L.H.; Samples extracts, L.H., P.I.; H.P.L.C. dosages, V.A., Y.G.; Writing, A.C., L.H., M.H., P.D.; Funding acquisition, M.H., A.C.; Supervision, M.H., A.C.; Project administration, A.C.

Competing interests

The authors declare no competing interests.

Additional information

Supplementary information is available for this paper at https://doi.org/10.1038/s41598-020-59929-w.

Correspondence and requests for materials should be addressed to A.C.

Reprints and permissions information is available at www.nature.com/reprints.

Publisher's note Springer Nature remains neutral with regard to jurisdictional claims in published maps and institutional affiliations.

A Nonpeptide Oxytocin Receptor Agonist for a Durable Relief of Inflammatory Pain

Louis Hilfiger[1], Qian Zhao[2], Damien Kerspern[1], Perrine Inquimbert[1], Virginie Andry[1], Yannick Goumon[1], Pascal Darbon[1], Marcel Hibert[2#], Alexandre Charlet[1#*]

[1] Centre National de la Recherche Scientifique and University of Strasbourg, UPR3212 Institute of Cellular and Integrative Neurosciences, Strasbourg, France.
[2] Laboratoire d'Innovation Thérapeutique, Faculté de Pharmacie, UMR7200 CNRS/Université de Strasbourg, Illkirch, France.
[#] Equal senior author.
* Corresponding author.

Corresponding Author
Alexandre Charlet, PhD
CNRS UPR3112, INCI
8, Allée du Général Rouvillois
67000 Strasbourg, France
Phone: + 33 (0) 6070 825 06
E-mail: acharlet@unistra.fr

Supplementary table and figures

Channel	Compound	Concentration	Normalized percentage inhibition (mean, n=2)
Nav 1.5	LIT-001	5 mM	0.7
	Lidocaïne	100 mM	78.0
Cav 1.2	LIT-001	5 mM	-9.3
	Verapamil	50 mM	57.5
KCNQ1/minK	LIT-001	5 mM	7.1
	Chromanol 293B	10 mM	51.7
hERG	LIT-001	5 mM	2.1
	Cisapride	0.1 mM	35.9
			Normalized peak current (mean, n=2)
GABA A a1b2g2	LIT-001	5 mM	110.7
	Vehicle	0.33% DMSO	102.6
	Diazepam	0.1 mM	224.8
hnAChR a4b2	LIT-001	5 mM	2.7
	Vehicle	0.33% DMSO	4.5
	Acetylcholine	30 mM	66.1

Figure S1

Figure S1. Inhibition potency of LIT-001 on ion channel blockade. Normalized percentage inhibition values for each compound assayed on each channel specified below. The compound data was normalized to vehicle control (0% inhibition) and maximal inhibition control (100% inhibition).

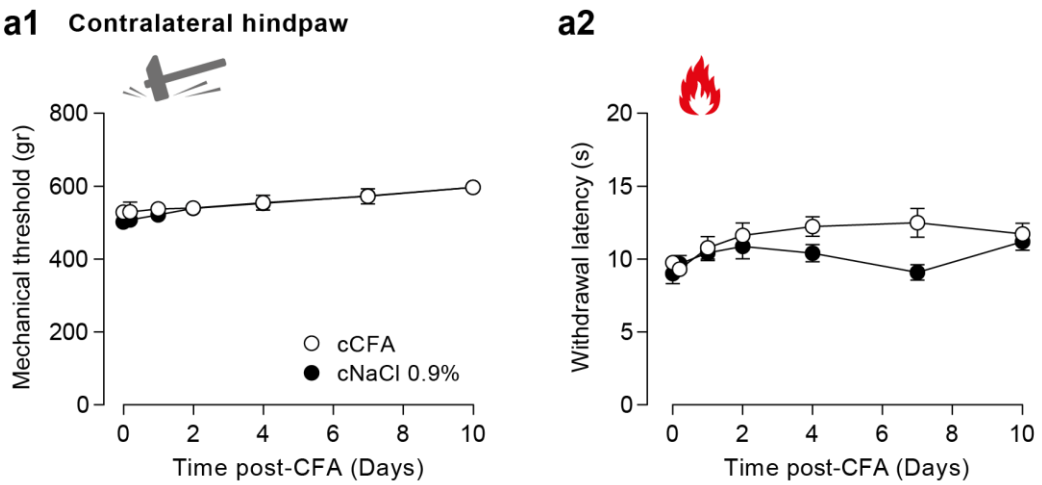

Figure S2

Figure S2. Ten days' time course of long-term modifications induced by CFA subcutaneous injection – contralateral hindpaw. (**a**) Time-course of the CFA-induced mechanical (**a1**) and thermal heat (**a2**) hyperalgesia (CFA, n = 14; NaCl, n = 18). Data are expressed as mean ± SEM. No statistical significance were detected using two-way ANOVA followed by Tukey multiple comparisons test.

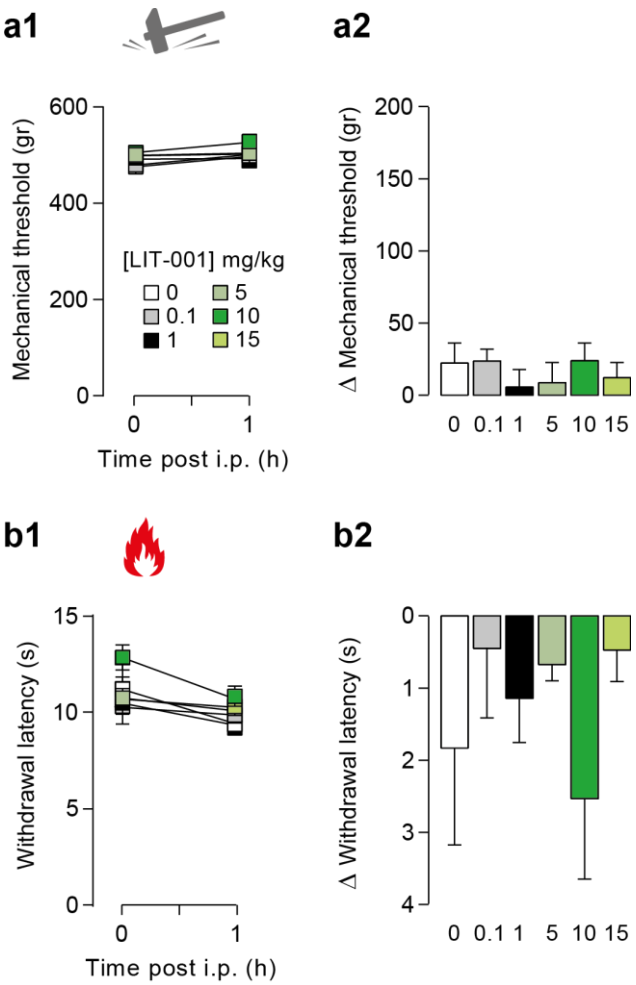

Figure S3

Figure S3. Dose-response of the analgesic properties of LIT-001 on CFA-induced inflammatory pain model – contralateral hindpaw. Effects of LIT-001 0.1 (n = 4), 1 (n = 6), 5 (n = 6), 10 (n = 8) and 15 mg/kg (n = 6) or its vehicule (n = 9) measured 1 hour after i.p. injection on CFA-contralateral hindpaw mechanical (**a**) and thermal heat (**b**) sensitivities. Data are expressed as mean ± SEM.

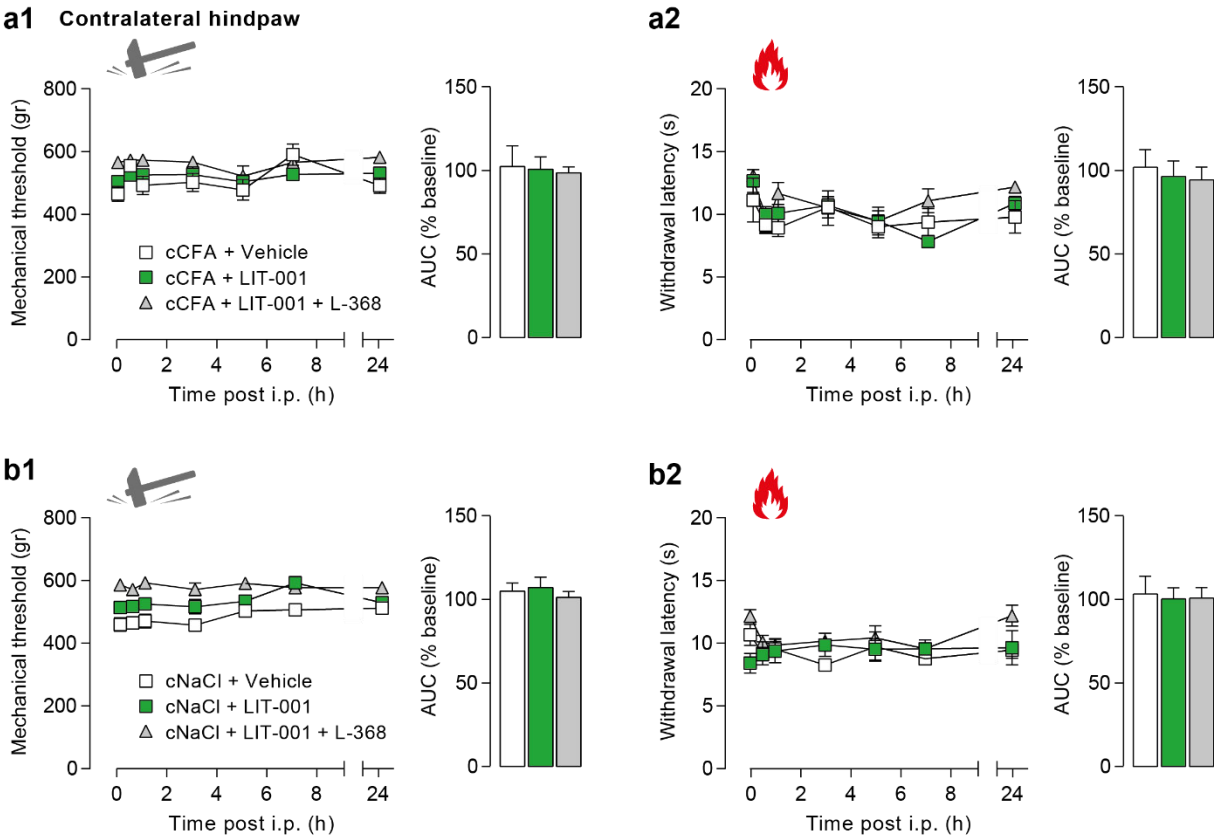

Figure S4

Figure S4. Time-course of the analgesic properties of LIT-001 on CFA-induced inflammatory pain model – contralateral hindpaw. (**a**) Left, time-course of the effects of i.p. LIT-001 10mg/kg (n = 7), its vehicule (n = 5) or co-injection with L-368,699 (n = 6) on CFA-contralateral hindpaw mechanical (**a1**) and thermal heat (**a2**) sensitivities. Right, relative-to-baseline AUC (%) of the effects. (**b**) Left, time-course of the effects of i.p. LIT-001 10mg/kg (n = 7), its vehicule (n = 5) or co-injection with L-368,699 (n = 6) on mechanical (**b1**) and thermal heat (**b2**) sensitivities of NaCl-contralateral hindpaw sensitivities. Right, relative-to-baseline AUC (%) of the effects. Data are expressed as mean ± SEM. No statistical significance were detected using two-way ANOVA followed by Tukey's multiple comparisons test.

a

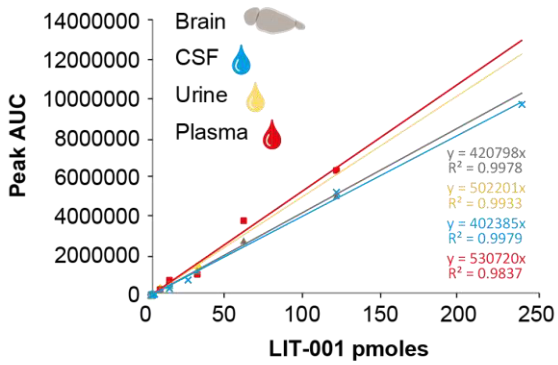

b HPLC gradient

Time (min)	0	3	8	11	14	15	19
B mobile phase	10	10	30	98	98	10	10

c MS ionization, selection, fragmentation and identification parameters

Compound	Polarity	Precursor (m/z)	Product (m/z)	Ion product type	Collision Energy (V)	RF Lens (V)
LIT-001	Positive	532.28	159.11	Quantification	19.05	242.05
LIT-001	Positive	532.28	185.07	Qualification	19.00	242.05
LIT-001	Positive	532.28	332.11	Qualification	22.49	242.05

Figure S5

Figure S5. LC-MS/MS dose response curves of increasing concentration of LIT-001 added to brain extracts, urine, plasma or water. (**a**) Samples were treated as described in the material and method section. (**b**-**c**) **LC and MS conditions for the purification and the detection of LIT-001.** Mobile phase A corresponded to ACN 1% / H_2O 98.9% / formic acid 0.1% (v/v/v), whereas mobile phase B was ACN 99.9 % / formic acid 0.1% (v/v).

3. Article 3: Projections from a novel population of parvocellular oxytocin neurons promote analgesia in the periaqueductal gray

3.1. Overview

3.1.1. Introduction

OT modulates several key neurophysiological functions, including pain modulation (Boll et al., 2018). It has been previously demonstrated that a small population of PVN parvOT neurons attenuates pain perception via two pathways (Eliava et al., 2016; González-Hernández et al., 2017). Through plasmatic release, OT mediates an antinociceptive action *in vivo* by reducing C fibre excitability. In the same time whereas OT released by PVN fibres directly inhibits sensory processing and produces analgesia. Moreover, the PAG plays a key role in descending analgesic pathways (Bell, 2018). It has been reported that both OT axons and OTR are found in the PAG (Campbell et al., 2009; Nasanbuyan et al., 2018) and the blocking of OTRs in the PAG decreased the pain threshold (Yang et al., 2011a).

Altogether, these studies suggest that OT may promote analgesia through the OT-mediated activation of PAG neurons. Thus, it is tempting to hypothesize that OT not only attenuates nociceptive signal at the level of peripheral nociceptors or spinal cord, but complementarily acts within the PAG to fine-tune additional descending pain-related pathways.

To address this question, we first generated a new knock-in rat line to label and manipulate OTR neurons in the PAG. Next, we employed cell-type-specific viral vectors and identified a new subpopulation of OT neurons, which projects to the PAG. Then we used *in vivo* electrophysiology combined with optogenetics to identify the role of OTR neurons of the PAG on the WDR neurons of the spinal cord. Finally, we assessed their analgesic function, by optogenetically-evoked OT release in the PAG and by chemogenetic activation of PAG OTR neurons, for thermal and mechanical sensitivity in a rat model of induced inflammatory pain.

3.1.2. Results

To study OTR-expressing neurons in the PAG, we generated a new transgenic line of rats expressing Cre in cells expressing OTR. In order to validate that these OTR-Cre rats correctly express functional OTRs and Cre within the same cells, we performed *ex vivo* electrophysiology recording. We showed that TGOT (OTR agonist) application induces a significant increase in firing of GFP+ OTR neurons, meaning that OTR and Cre are functional in PAG OTR neurons. We also found by performed staining (against GAD67) that the vast majority of GFP+/OTR+ neurons were GABAergic nature.

We determined by immunolabelling and histological analysis that OT projections activating PAG OTR neurons are coming exclusively from parvOT neurons of the PVN. Then, we characterized a function of PVN → PAG OT circuit *in vivo* by optogenetic stimulation of PVN OT neurons and recorded the effects in the PAG with a silicone tetrode. We thus observed that the stimulation of PVN OT neurons leads to an overall excitation of OTR+ PAG neurons. With complementary experiments, we also demonstrated that the stimulation of OTR+ PAG neuron leads to a decrease of the WDR neurons activity.

After the characterisation of the PVN → PAG OT circuit, we next assessed it role in the pain processing. For this purpose, we transfected OTR-Cre rats with a rAAV carrying a Cre-dependent sequence of hm3D(Gq) (chemogenetic activation). We then evaluated mechanical and thermal sensitivity in a CFA-induced inflammatory pain model during a chemogenetic stimulation of PAG OTR neurons. This stimulation induced an anti-hyperalgesia for mechanical or thermal sensitivities. No effects were observed in the contralateral paw nor in control animals.

A similar experiment gave us similar result with optogenetic stimulation of PAG OTR neurons in the same model. This experiment also confirmed the OTR implication *in vivo*, by injecting the OTR antagonist L-368,899, which completely blocked the anti-hyperalgesic effects of the optogenetic stimulation.

Finally, to understand whether the analgesia was caused by a modulation of the sensory and/or emotional component of pain, we performed a CPP test with the hm3D(Gq) OTR-Cre rats. We observed no modification in preference after the chemo stimulation of PAG OTR neurons.

In conclusion, we identified new population of parvOT neurons projecting to the PAG where they activate OTR neurons and a descending pain pathway, leading to a decrease in the response of spinal cord WDR neurons to nociceptive stimuli, thus reducing pain sensation. These findings have increased our knowledge of the key role of OT in the modulation of nociception and the potential of synthetic OT agonist that can cross the BBB, such as the LIT-001.

Author contribution:

This study was a collective work, I detail below my personal contribution to the following experiments (and consequent analysis):

- Stereotaxic surgery (viral transfection for *ex vivo* and behavioural experiments).
- Patch clamp *ex vivo.*
- Behavioural experiments (plantar, calibrated forceps and CPP).

Projections from a novel population of parvocellular oxytocin neurons promote analgesia in the periaqueductal gray

Mai Iwasaki[1*], Arthur Lefevre[1,2*], Ferdinand Althammer[3,@], Olga Lapies[1], Louis Hilfiger[1], Meggane Melchior[1], Damien Kerspern[1], Stéphanie Küppers[2], Quirin Krablicher[2], Ryan Patwell[2], Sabine Herpertz[2], Beate Ditzen[2], Kai Schoenig[2,@], Dusan Bartsch[2], Javier Stern[3], Pascal Darbon[1], Valery Grinevich[2,3,§,#], Alexandre Charlet[1,§,#]

[1] Centre National de la Recherche Scientifique and University of Strasbourg, Institute of Cellular and Integrative Neuroscience, 67000 Strasbourg, France
[2] Department of Neuropeptide Research in Psychiatry, Central Institute of Mental Health, University of Heidelberg, Mannheim 68159, Germany
[3] Center for Neuroinflammation and Cardiometabolic Diseases, Georgia State University, Atlanta, GA, USA
* Equal first authors
§ Senior authors
@ Present address: Institute of human genetics, University hospital Heidelberg, Germany

Correspondences:

Alexandre Charlet, PhD
Institute of Cellular and Integrative Neurosciences,
INCI CNRS UPR3212
8, Allée du Général Rouvillois
67000 Strasbourg
France
Phone: (33) 6070 825 06
E-mail: acharlet@unistra.fr

Valery Grinevich, MD, PhD
Department of Neuropeptide Research in Psychiatry
Central Institute of Mental Health
Medical Faculty Mannheim
University of Heidelberg
J5, Mannheim, 68159
Germany
Phone: (49) 621 1703 2995
E-mail: valery.grinevich@zi-mannheim.de

Highlights

- We generated a new line of transgenic knock-in rat (OTR-IRES-Cre)
- A distinct parvOT neuronal population projects to vlPAG but not the SON or spinal cord
- OT excites vlPAG OTR neurons which indirectly inhibits WDR neurons in the spinal cord
- This pathway alleviates nociception but not the affective component of pain

Abstract

The hypothalamic neuropeptide, oxytocin (OT), exerts prominent analgesic effects via central and peripheral action. Here we discovered a novel subset of OT neurons whose projections preferentially terminate on OT receptor (OTR)-expressing neurons in the ventrolateral periaqueductal gray (vlPAG). Using a newly generated line of transgenic rats (OTR-IRES-Cre), we determined that most of the vlPAG OTR expressing cells being targeted by OT projections are GABAergic in nature. Both optogenetically-evoked axonal OT release in the vlPAG as well as chemogenetic activation of OTR vlPAG neurons results in a long-lasting overall increase of vlPAG neuronal activity. This then leads to an indirect suppression of sensory neuron activity in the spinal cord and strong anti-hyperalgesia. Finally, we describe a novel OT→vlPAG→spinal cord circuit that is critical for analgesia in the context of both inflammatory and neuropathic pain.

Keywords: Oxytocin, oxytocin receptor, periaqueductal grey, spinal cord, inflammatory pain, neuropathic pain

Introduction

The hypothalamic neuropeptide oxytocin (OT) modulates several key neurophysiological functions, including pain modulation (Poisbeau et al., 2017). OT is produced in the hypothalamic supraoptic (SON) and paraventricular (PVN) nuclei by two major types of neurons: magnocellular (magnOT) and parvocellular (parvOT) neurons. MagnOT neurons of the SON and PVN are large cells that release OT into the bloodstream via axonal projections to the posterior pituitary. In contrast, parvOT neurons are smaller cells located exclusively in the PVN and project to the brainstem and spinal cord, but not the posterior pituitary (Althammer and Grinevich, 2017). It has been previously demonstrated that a small population of PVN parvOT neurons attenuates pain perception *via* two pathways: 1) through coordinated OT release into the bloodstream from magnOT neurons leading to the modulation of peripheral nociceptor activity in the dorsal root ganglion and skin and 2) by inhibiting sensory neurons in the spinal cord (Moreno-López et al., 2013; Eliava et al., 2016; González-Hernández et al., 2017).

The periaqueductal gray (PAG) plays a pivotal role in descending analgesic pathways (Melzack, 1975). Indeed, physiological suppression of pain seems to be primarily modulated by a top-down system comprised of the PAG, rostral ventromedial medulla (RVM), and dorsal horn of the spinal cord (SC) (Fields, 2000). For example, electrical stimulation of the PAG inhibits the firing rate of neurons in the dorsal horn of spinal cord (Basbaum et al., 1977; Liebeskind et al., 1973). In addition, both OT axons and OT receptors (OTR) have been reported in the PAG of mice (Campbell et al., 2009; Nasanbuyan et al., 2018; Saito et al 2021), where the administration of exogenous OT into the PAG enhances neuronal firing rates (Ogawa et al., 1992) and blocking OTRs in the PAG decreases pain threshold (Yang et al., 2011).

Altogether, these studies suggest that OT may promote analgesia through the OT-mediated activation of PAG neurons. It is therefore tempting to hypothesize two independent, yet complementary mechanisms of OT-mediated analgesia in which OT attenuates nociceptive signals at the level of peripheral nociceptors or the spinal cord (Eliava et al., 2016; Herpertz et al., 2019), and also acts within the PAG to fine-tune additional descending pain-related pathways.

However, neither the cellular circuitry nor the analgesic effects of endogenous OT signaling in the PAG have been studied. To address this gap, we first generated a new knock-in rat line to label and manipulate OT receptor (OTR) neurons in the PAG. Next, we employed cell-type-specific viral vectors to identify a new subpopulation of parvOT neurons projecting to the

ventrolateral subregion of the PAG (vlPAG). We then used *in vivo* electrophysiology combined with optogenetics in the vlPAG to reveal that activation of OTR neurons leads to inhibition of sensory wide dynamic range (WDR) neurons in the spinal cord (SC_{WDR}) of anesthetized rats. Finally, we found that optogenetically-evoked OT release in the vlPAG produces analgesia and this effect was recapitulated by chemogenetic activation of vlPAG OTR neurons. Altogether, we identified an independent parvOT→$vlPAG_{OTR}$→SC_{WDR} pathway that is distinct from the previously described direct parvOT→SC_{WDR} pathway (Eliava et al., 2016) and is capable of promoting analgesia in the context of both inflammatory and chronic neuropathic pain.

Results

vlPAG OTR-expressing neurons are GABAergic

To study OTR-expressing neurons in the vlPAG, we generated a new transgenic line of rats that express Cre recombinase exclusively in OTR expressing cells (OTR-IRES-Cre line, see Methods for details) (**Figure 1A1**, **S1A**). To label OTR neurons, we injected the PAG with a rAAV carrying a Cre-dependent sequence of GFP (rAAV1/2-pEF1a-DIO-GFP) in OTR-IRES-Cre female rats (n=4). We found a clustering of OTR neurons along the anteroposterior axis of the vlPAG (**Figure S1B-C**). To further assess the specificity of Cre expression in OTR-IRES-Cre line rats, we performed RNA scope using probes against both OTR and Cre mRNAs and found that 97.6% of Cre positive cells (n = 47) were also positive for OTR mRNAs and 90.4% of OTR positive cells (n = 42) also expressed Cre mRNAs (**Figure 1A2**).

Ex vivo electrophysiology in acute brain slices of PAG showed that application of the selective OTR agonist, [Thr^4Gly^7]-oxytocin (TGOT), induced a significant increase in firing of GFP+ OTR neurons which disappeared after wash out (Baseline 0.573 ±0.295 Hz vs TGOT 1.045 ±0.388 Hz vs Wash 0.514 ±0.298 Hz; n = 11; **Figure 1B1-B4**). There was no response to TGOT in recorded GFP- neurons (Baseline 0.119 ±0.046 Hz vs TGOT 0.108 ±0.049 Hz vs Wash 0.122 ±0.064 Hz, n = 9, **Figure 1B1-B4**). This result shows that OTR-iRES-Cre rats correctly express functional OTRs and Cre within the same cells.

We then quantified the number of vlPAG neurons expressing GFP and found that 396 out of 2135 (18.6%) cells were GFP-positive (**Figure 1C1-C2**), indicating that about a fifth of all vlPAG cells express OTR. Histochemical analysis of vlPAG slices further revealed that the vast majority of GFP+ cells stained positive for GAD-67, a marker of GABAergic neurons. This result indicates that virtually all of the vlPAG OTR+ neurons are GABA-ergic in nature

(94.7%, n = 174 cells, **Figure 1D1-D2**).

A discrete PVN parvOT neurons population projects to the vlPAG

To determine the origin of OT projections activating vlPAG OTR neurons, we injected a rAAV expressing mCherry under the control of the OT promotor (OTp-mCherry, Knobloch et al., 2012) into either the PVN or SON in addition to a Cre-dependent rAAV expressing GFP (Ef1A-DIO-GFP) into the vlPAG of OTR-iRES-Cre female rats (n=4; **Figure 2A1**). We found mCherry+ axons in close proximity to GFP+ OTR cells in the vlPAG after injection into the PVN (**Figure 2A2-A5**), but not the SON (not shown). This indicates that axons from OT neurons within the vlPAG originate exclusively from the PVN.

We confirmed these results with retrograde tracing by injecting wild type rats (n = 4) with CAV2-CMV-Cre into the vlPAG and rAAV-OTp-DIO-GFP into the PVN (**Figure 2B1**). We found that only a few, relatively small (n = 21 cells, 10 to 20 um diameter) OT neurons were labelled in the PVN (**Figure 2B2-B4**) whereas no labelling was detected in the SON (not shown). Furthermore, the retro-labeled cells were predominantly located at the latero-ventral edge of the PVN, although some GFP+ neurons were found in the caudal medio-dorsal region of the PVN.

Because this discrete population resembled the morphology of parvOT neurons (e.g. small size and spindle-like shape), we injected wild type rats (n=3) with a marker of magnOT cells, Fluorogold (FG, Santa Cruz Biotechnology, Dallas, 15 mg/kg, i.p.), to specifically label magnOT, but not parvOT neurons (Althammer and Grinevich, 2017). In parallel, the same rats received an injection of green latex Retrobeads (Lumafluor Inc., Durham, NC, USA) into the vlPAG (**Figure S2A1**) to retro-label only the OT neurons projecting to vlPAG. The histological analysis revealed that Fluorogold labelled PVN neurons did not contain the green puncta of Retrobeads in their cytoplasm (**Figure S2AB**), indicating that the OT cell projections to the vlPAG represent parvOT neurons, but not magnOT neurons.

Next, we asked whether these ParvOT $\rightarrow$ vlPAG$_{OTR}$ neurons belonged to the same population of parvOT we previously described (Eliava et al., 2016) as projecting to the SON and spinal cord (SC). We first injected wild type female rats (n = 3) with green Retrobeads into the vlPAG and red Retrobeads into the SC and found no OT-positive neurons in the PVN containing beads of both colors within the same cells (**Figure S2B1-B4**). We then analyzed whether ParvOT $\rightarrow$ vlPAG$_{OTR}$ neurons, identified in Figure 2B, are projecting axons to the SC or SON and found no detectable GFP+ axons in the cervical, thoracic or lumbar segments of the SC, nor in the SON (**Figure S2C1-C4**). Finally, we injected another cohort of wild type rats (n = 3

per group) with CAV2-CMV-Cre into the SON (**Figure S2D1**) or the SC (F**igure S2E2**) and rAAV-OTp-DIO-GFP into the PVN. Here, we found that PVN neurons projecting to the SON also send axons to the SC, but not to the vlPAG (**Figure S2D2**) and, similarly, PVN neurons projecting to the SC also send axons to the SON, but not to the vlPAG (**Figure S2E2**). Altogether, our results indicate the existence of two distinct populations of parvOT neurons, projecting either to the vlPAG (present study) or to the SC (Eliava et al., 2016).

PVN parvOT axons form direct contact with somatic and dendritic locations of vlPAG OTR neurons

Our next aim was to identify synaptic-like contacts between OT axons and OTR+ neurons in the vlPAG. First, we counted the number of OT fibers in close proximity to OTR+ neurons, relative to bregma (**Figure 3A**-**3C**), and found a positive correlation between the two parameters ($r = 0.575$, $p < 0.01$, **Figure 3D**), indicating that OT fibers specifically target OTR neurons in the vlPAG.

Next, we injected AAV-pEf1A-DIO-GFP into the vlPAG of OTR-IRES-Cre rats to label OTR neurons and then stained for OT, DAPI and synaptophysin (**Figure 3A**, **3E**). These sections were analyzed using Imaris software to quantify the OT innervation of GFP+ (37%) and GFP- (4%) cells (**Figure 3F**) as well as the percentage of synaptophysin-positive contacts between OT axons and GFP+ somas (7%) or dendrites (56%) (**Figure 3G**, **Figure S3A-D**). The latter indicated that the majority of OT axons predominantly form typical synaptic contacts on dendrites of PAG OTR+ neurons similar to the OT-containing synapses previously demonstrated in the brainstem and SC (Buijs, 1983).

Several reports have shown that OT is produced and released concomitantly with the conventional neurotransmitter, glutamate (Hasan et al., 2019; Knobloch et al., 2012). Therefore, we next tested whether OT-immunoreactive axons in the vlPAG also contained the glutamate transporter, vGluT2 (**Figure 3H-I**, **S3B**). This analysis revealed that only 5.3% of OT fibers were also positive for vGluT2 (**Figure 3H**). Importantly, we found synaptic-like contacts between GFP+ dendrites and both vGluT2+ (**Figure 3J1**) and vGluT2- OT fibers (**Figure 3J2**). These findings suggest that a small percentage of direct PVN OT $\rightarrow$ vlPAG contacts are glutamatergic, although the precise role of glutamate in these putative synapses remains unclear.

Evoked OT release in the vlPAG increases neuronal activity *in vivo*

We then wanted to characterize the function of the $PVN_{OT} \rightarrow$ vlPAG circuit *in vivo* by

expressing channelrhodopsin2 (ChR2) fused with mCherry ($rAAV_{1/2}$-pOT-ChR2-mCherry; **Figure 4A**) specifically in OT neurons of the PVN (Eliava et al., 2016; Knobloch et al., 2012). *In vivo* PAG neuronal firing was then recorded in anesthetized rats using silicone tetrodes coupled with a blue light (BL) that was used to stimulate PVN_{OT} axons in the vlPAG (20s at 30Hz, 10ms pulse width; **Figure 4A**, **S4A**). Out of 82 recorded neurons, 21 showed an increase in firing rate (mean ± SEM; from 1.05 ± 0.39 to 17.65 ± 6.45 Hz) (**Figure 4B-E**). In contrast, two neurons, whose spontaneous activity prior to BL onset was high, showed a decreased firing rate within 300 s after the onset of BL (one cell from 25.83 to 6.95 Hz, another from 40.20 to 0.19 Hz; **Figure 4B-C**). The remaining 59 neurons did not react to BL (**Figure 4C**). We found the normalized mean activity of the excited neuronal population remained elevated for at least 300 s following the onset of BL (**Figure 4D**). Notably, the time course of spike increase was diverse, as shown by the latency (1st quantile, median, 3rd quantile) for onset (1, 4, 40.25s), peak activity (116.25, 155, 280.25s) and offset (147.75, 296, 300) (**Figure S4B**). However, the total number of active neurons was maintained throughout the 300 s period following BL stimulation (**Figure S4C**). Therefore, we conclude that BL-evoked OT release in the vlPAG leads to an overall excitation of putative OTR+ vlPAG neurons.

Evoked OT release in vlPAG inhibits the activity of spinal cord WDR neurons *in vivo*

Next, we explored the downstream target of the $PVN_{OT} \rightarrow vlPAG_{OTR}$ circuit by performing *in vivo* BL stimulation of PVN_{OT} axons in vlPAG (vlPAG-BL) while simultaneously recording sensory wide dynamic range (WDR) neuronal responses to electrical stimulation of their hind paw receptive field (**Figure 5A**). We focused on WDR neurons in the spinal cord (SC_{WDR}) because they are modulated by vlPAG inputs and have also been identified as an important cell population for integrating pain related signals (Ritz and Greenspan, 1985). Indeed, peripheral sensory information converges from both fast (A-beta and delta type) and slow-conducting (C-type) primary afferent fibers, which are then integrated through WDR neurons in the deep laminae of the SC. Following repetitive electric stimulation to the hind paw WDR neuron receptive field, a short-term potentiation (wind-up; WU) occurs on the synapse made by C-type fibers onto WDR neurons that causes the spike rate of the cell to reach a plateau of maximal activity (**Figure 5B**, gray). This WU effect is typically enhanced during pain perception in animals with inflammation (Herrero et al., 2000), which suggests that WU can serve as an index of ongoing nociceptive processing (i.e. a measure of how sensitive the body is to nociceptive stimuli at a given moment). Therefore, we used WU (represented as the percentage of maximal spiking activity following electrical stimulation (1 Hz) to the hind paw receptive field) as our outcome measure for the effect of vlPAG-BL stimulation on WDR discharge, specifically from primary afferent C-fibers.

The results show that, prior to any vlPAG-BL stimulation, all cells exhibited the maximal WU effect 30 s after the onset of electrical stimulation (**Figure 5B**). In control animals (CTRL) that received vlPAG-BL in the absence of ChR2 expression, the WU remained stable up to 250 s after the plateau, despite a gradual reduction over time that was not statistically significant. In contrast, vlPAG-BL stimulation in animals expressing ChR2 in OT neurons showed a significant decrease in WU compared to control animals (**Figure 5B-C**; CTRL 30.12 ±8.60 vs ChR2 61.28 ±5.37 %, p = 0.0074, n = 8 and 14, respectively). This trend was maintained up to 600 s after the end of vlPAG-BL stimulation, as seen in a second series of recordings of the same neurons (**Figure 5B**, right panel, **Figure 5C**, bottom panel). While the magnitude of WU reduction was significantly larger in ChR2 animals than WT animals, there was no difference in the "inflection" timing of WU dynamics. Specifically, there was no significant difference between WT and ChR2 animals for latency (s) to reach the maximum WU [(1^{st} quartile, median, 3^{rd} quantile); WT:(26.00, 31.50, 46.00), ChR2: (26.25, 35.00, 55.75)]; latency to reach the half reduction of WU (s) [WT: (75.50, 96.50, 163.00), ChR2 (64.25, 83.00, 125.75)]; or latency to reach the maximum reduction of WU (s) [WT (183.00, 209.00, 263.00), ChR2 (198.50, 250, 269.75)] (**Figure S5**). Importantly, all recorded WDR neurons were impacted by vlPAG-BL (Figure to be included), highlighting the effectiveness of this circuit in gating the nociceptive signal at the spinal cord level.

In order to confirm that the recorded effect on WU was due to OT release in the vlPAG, we allowed the WU effect to dissipate over a 10 m interval following the initial stimulation protocols in the ChR2 group. We then infused the specific OTR antagonist, [d(CH2)5,Tyr(Me)2,Orn8]-vasotocin (dOVT), into the vlPAG prior to repeating the same protocol described above. We found that dOVT infusion caused a significant reduction of the vlPAG-BL stimulation effect such that WU was greater when dOVT was onboard than it was during the initial stimulation protocol (ChR2 + dOVT: 36.27 ± 4.80 %, p = 0.0313, n = 6) (**Figure 5B-5D**). Figure 5D summarizes the vlPAG-BL effect in the different groups during the period of maximum WU reduction (from 140 to 180 s), since dOVT lost its effectiveness after this period (**Figure 5B**, right panel), possibly due to diffusion out of the PAG region.

OT in the vlPAG induces analgesia during both inflammatory and neuropathic pain

Because the vlPAG is known to be a key component of an important descending pain modulatory system, and OT is known to exert an analgesic effect (Yang et al., 2011), we hypothesized that OTR+ neurons in the vlPAG are involved in pain processing. To test this hypothesis, we injected rAAV-pEF1A-DIO-GFP into the vlPAG of male OTR-iRES-Cre rats. The rats were subdivided into four groups (n = 7-8 per group) :1) no manipulation (Control), 2) inflammatory-induced pain sensitization after complete Freund adjuvant injection in the

posterior right paw (CFA), 3) acute mechanical nociception (Pain), 4) mechanical nociception 24h following hind paw CFA injection (CFA + Pain). Rats were euthanized 30min following each manipulation and brain sections containing vlPAG were collected. We next used c-Fos staining to compare the number of recently activated OTR (GFP+) expressing cells across the groups (**Figure 6A-B**). We found that rats exposed to either painful stimuli or painful stimuli following CFA injection had significantly more activated OTR neurons in vlPAG (38.1 ± 9.2% and 35.9 ± 3.4%, respectively) than rats not exposed to nociceptive stimulation (18.4 ± 9.6%). There was no statistically significant difference between the CFA group (26.0 ± 6.8%) and the control group (**Figure 6A**).

To verify the functional significance of vlPAG projecting OT neurons in the processing of inflammatory pain, a separate cohort of rats received vlPAG injections of rAAV$_{1/2}$-pOT-ChR2-mCherry. We then compared the within-subject effect of optogenetically-evoked OT release in the vlPAG (vlPAG-BL) on mechanical pain sensitivity both with and without the presence of CFA-induced inflammatory hyperalgesia (**Figure 6C-D**). We found that vlPAG-BL stimulation significantly, but not entirely, alleviated CFA-induced hyperalgesia as indicated by an increase in the mechanical pain threshold from 68.77 ± 9.39 g to 124.89 ±12.76 g (**Figure 6D1**; n = 10). Injection of the blood-brain barrier (BBB)-permeable OTR antagonist, L-368,899, completely blocked the effect of BL in the vlPAG (from 62.75 ± 5.31 g to 71.99 ± 5.14 g, **Figure 6D1**; n = 10). After complete wash out of L-368,899, the effect of vlPAG-BL returned to its baseline level (from 92.95 ± 8.89 g to 179.40 ± 19.13 g; **Figure 6D1**; n = 10). Finally, we found that vlPAG-BL had no effect on mechanical sensitivity in the absence of any peripheral sensitization when testing the contralateral paw (**Figure 6D2**).

To confirm that this effect was driven by vlPAG OTR neurons, we injected male and female OTR-Cre rats with viruses containing either an excitatory chemogenetic receptor, rAAV-Ef1a-DIO-hm3D(Gq)-mCherry, or a control virus rAAV-Ef1a-DIO-mCherry (n = 5-6 per group) (**Figure 6E**, **S6B**). We then repeated the CFA-induced inflammatory hyperalgesia experiments described above and found that chemogenetic excitation of vlPAG OTR neurons by i.p deschloroclozapine (DCZ) induced a significant increase mechanical pain threshold from 171.3 ± 12.5 g to 285.5 ± 14.2 g (**Figure 6F**). This effect was not observed in the contralateral paw of the same animals nor in the control virus group that received DCZ injection (**Figure 6F**). A similar effect was found in the hot plate test of thermal pain sensitivity, where DCZ increased the latency of response to thermal stimuli from 1.56 ± 0.13 s to 3.41 ± 0.73 s (**Figure 6G**), this was again not found in the contralateral paw of the same animals nor in the control group (**Figure 6G**). Finally, we repeated these experiments in male rats and found the same results (**Figure S6C**, **S6D**, n = 6 per group), ruling out a potential sexual dimorphism of this circuit.

We next sought to test if this novel $PVN_{OT} \rightarrow vlPAG_{OTR}$ circuit is involved in neuropathic pain, given that other pain-related OT pathways fail to affect such symptoms (Eliava et al., 2016; Wahis et al., 2021). To address this, we performed vlPAG-BL stimulation in the chronic constriction of the sciatic nerve (CCI) model of neuropathic pain (Austin et al., 2012). We found that BL-evoked OT release in the vlPAG increased the threshold of response to mechanical stimuli from 195.7 ± 72.3 g to 265.3 ± 58.9 g (**Figure S6A1-2**; n = 7). Similar to the previous experiment, injection of L-368,899 completely blocked the effect of BL in the vlPAG (from 174.6 ±56.4 g to 181.2 ± 29.7 g, **Figure S6A2**; n = 7) and the effect of vlPAG-BL was fully restored after wash out of L-368,899 (from 155.5 ± 43.1 g (baseline) to 218.3 ± 57.5 g (BL); **Figure S6A2**; n = 7). In addition, vlPAG-BL did not modulate the mechanical pain threshold of the contralateral paw (**Figures S6A3**).

Finally, to understand whether the analgesia was caused by a modulation of the sensory and/or emotional component of pain (King et al., 2009), we performed a conditioned place preference test using the same cohort from the chemogenetic experiments above (**Figure S6E**). The animals' baseline chamber preference was determined during habituation (see Methods for details) and used as the saline-paired control chamber. In contrast, the innately non-preferred chamber was paired with DCZ in order to stimulate vlPAG OTR cells expressing hm3D(Gq) (**Figure 6E**). Analysis of the rats´ behavior on test day revealed no significant change in preference for the DCZ-paired chamber (**Figure 6H-I**). Importantly, this was not due to an effect on locomotion as there were no differences between the test and the control group in the total distanced travel during the experiment (**Figure 6I**).

Discussion

Here we describe a new analgesic pathway recruited by newly discovered parvOT neurons projecting to the vlPAG (**Figure 1-2**), where they activate GABAergic OTR expressing neurons (**Figure 3-4**), which then leads to a decreased response to nociceptive stimuli in spinal cord WDR neurons (**Figure 5**). We further showed that activation of this novel circuit specifically reduces pain sensation (**Figure 6**), without alteration of the affective component of pain.

A vast amount of literature has shown that OT exerts analgesic effects by acting on various targets of pain-associated areas in the central and peripheral nervous systems (for review, see Boll et al., 2018). The contribution of OT to analgesia is generally attributed to two pathways. The first, is an ascending OT pathway that modulates the activity of brain regions

processing the emotional and cognitive components of pain, such as the amygdala, in which OT alleviates anxiety, especially in the context of chronic pain (Hasan et al., 2019; Knobloch et al., 2012; Wahis et al., 2021). The second is a descending OT pathway that indirectly promotes analgesia by reducing the activity of SC WDR neurons, which relay nociception in response to painful stimuli (DeLaTorre et al., 2009; Eliava et al., 2016). This specific OT descending pathway is powerful but restricted to inflammatory pain (Eliava et al 2016). Here we describe a particularly powerful OT descending pathway activating the diffuse PAG-RVM-SC descending control, efficient on both inflammatory and neuropathic pain, thermal and mechanical modalities, and male and female genders.

A novel and distinct parvOT neuronal population promotes analgesia *via* vlPAG

We identified a novel population of parvOT neurons that projects to the vlPAG, but not the SON nor the SC. Furthermore, we found that these neurons form synapses with little contribution of glutamate, thus supporting the idea of local axonal delivery of OT, as opposed to volume transmission (Chini et al., 2017; Landgraf and Neumann, 2004; van den Pol, 2012).

Consistent with previous reports showing that electric stimulation of PAG inhibits the firing of dorsal horn neurons in the SC (Liebeskind et al., 1973) and generates analgesia (Basbaum et al., 1977), we found that nociceptive transmission from C-type primary afferents to WDR neurons in the SC was effectively repressed by endogenous OT release in vlPAG. Notably, this effect peaked 250 s after OT release and was still observed 10 minutes after the cessation of blue light. This finding suggests that OT triggers a lasting activation of OTR expressing cells in the vlPAG, which then continually drives the regulation of SC WDR neurons for several minutes after initial OT release. Indeed, in a separate set of experiments, we showed that exogenously applied OTR agonist as well as endogenously evoked OT release excites neurons of the vlPAG and induces analgesia in the context of inflammatory pain. Notably, optogenetic release of OT in the vlPAG led to activation of individual neurons at various times, mostly within the first 40 seconds after the onset of blue light (BL) stimulation. The neurons' offset timings were also diverse and usually lasted for several minutes after the offset of BL stimulation. The reason for such variability in the offset times is still unclear. A first possibility may stem from the G-protein coupled metabotropic receptor nature of OTRs, which typically produce "slow" post synaptic currents lasting on the order of minutes (Knobloch et al., 2014). Furthermore, although OT axons in the midbrain make synapses (Buijs, 1978, 1983), direct release of OT into synaptic cleft has never been demonstrated. Thus, it is more likely that OT diffuses from axonal terminals or axonal varicosities *en passant* in the vicinity of OTR neurons (Chini et al., 2017). In which case, the action of OT could be synergized across multiple OTR expressing cells, resulting in long-lasting excitation driven by the sum

of different active timings. This leads to a complimentary possibility, which might be that the OT-induced modulation of this pathway relies on the influence of additional non neuronal cell types within the network, such as astrocytes, as it was shown in the amygdala (Wahis et al., 2021). While the specific mechanisms behind the lasting analgesic effect of OT release in the vlPAG are unclear, they would certainly play a critical role in its development as a potential therapeutic target and, therefore, warrant future research.

Importantly, we confirmed the uniqueness of this parvOT pathway by showing that the previously identified parvOT→SC_{WDR} and parvOT→SON pathways do not project to vlPAG. Interestingly, the level of reduction in nociception caused by optogenetic stimulation of parvOT neurons projecting to SON (Eliava et al., 2016) resembled the effect of stimulating vlPAG OT axons. Redundant, parallel circuits that play identical roles in the brain have been previously described (e.g. for feeding behavior (Betley et al., 2013)). Therefore, the direct projections from parvOT neurons to the SC and the indirect influence of parvOT neurons on sensory WDR neurons *via* the vlPAG can be interpreted as parallel circuits capable of independently promoting analgesia, particularly in the context of inflammatory pain. Although activation of both circuits results in similar electrophysiological inhibition of WDR neurons, they could be triggered by different situations, at different time points, or in different painful contexts. Indeed, we found that the PVN_{OT} → $vlPAG_{OTR}$ circuit promotes analgesia in the chronic neuropathic pain condition and in both male and female rats, whereas previous work found that the parvOT→SC_{WDR} circuit does not (Eliava et al., 2016). Moreover, considering that the vlPAG is an important area for the regulation of various defensive behaviors (Tovote et al., 2015), and that OT can mediate defensive behaviors, it will be important for future research to determine if vlPAG OTR neurons might be involved in other functions beyond nociception.

vlPAG OTR neurons reduce pain sensation, but not its affective component

We further found that painful stimulation increased c-fos levels in vlPAG OTR neurons, indicating that these neurons are endogenously recruited in the context of pain processing. Therefore, our finding confirms and clarifies the work of Saito et al (2021) showing that in mice PAG OTR neurons express c-fos after noxious stimulation.

By using our newly generated OTR-IRES-Cre transgenic rats, we were able to specifically activate OTR neurons in the vlPAG. We found that this activation led to a decrease in nociception in both inflammatory and neuropathic pain, but failed to alter place preference. This suggests the circuit we dissected here is not involved in the affective, memory component of pain (King et al., 2009). Interestingly, the opposite effect of OT on emotional

valence, but not on physical pain perception has been demonstrated in the central nucleus of amygdala (Wahis et al., 2021) and the anterior insular cortex (Küppers et al., unpublished). Taken together, these findings further emphasis the sheer variety of effects mediated by OT and highlight the need for continued efforts to dissect the precise anatomical and functional characteristics of the central OT system.

In conclusion, we identified a new subpopulation of parvocellular OT neurons that mediate analgesia by recruiting the PAG-controlled descending pain modulatory system (Figure 7). This study further describes and supports the role of OT as an analgesic molecule and points to the OTR as a potential therapeutic target. To this end, we generated the OTR-iRES-Cre line of rat, which will greatly enhance our ability to research this therapeutically relevant receptor. Finally, it should be noted that the inconsistent results found in human clinical studies of OTs effects on pain (Boll et al., 2018) may be due to the limitations of intranasal OT administration (Leng and Ludwig, 2015). Therefore, future research should be oriented towards developing synthetic OT agonists with the ability to cross the blood brain barrier more efficiently than OT itself (Busnelli and Chini, 2017; Busnelli et al., 2016; Hilfiger et al., 2020; Muttenthaler et al., 2017).

Acknowledgments

This work was supported by the University of Strasbourg Institute for Advanced Study (USIAS) fellowship 2014-15, Fyssen Foundation research grant 2015, NARSAD Young Investigator Grant 24821, ANR JCJC grant (to AC); ANR-DFG grant GR 3619/701, PHC PROCOPE and PICS07882 grants (to AC and VG); DFG grants GR 3619/15-1, GR 3619/16-1(to VG); SFB Consortium 1158-2 (to VG); French Japanese governments fellowship B-16012 JM/NH (to MI); Fyssen Foundation fellowship (to AL); Région Grand Est fellowship (to DK). The authors thank the Chronobiotron UMS 3415 for all animal care.

Authors contributions

Conceptualization, AC; Methodology, AC, AL, DK, FA, LH, MI, MM, OL, QK, VG; Analysis, AL, DK, FA, LH, MI; in situ hybridization, FA; Immunohistochemistry, AL, FA, SK; *Ex vivo* patch-clamp electrophysiology, DK, LH; *In vivo* electrophysiology, MI, MM, OL; Behavior LH, MI; transgenic rats line generation, KS, DB; Writing, AC, AL, BD, FA, JS, MI, OL, PD, SH, SK, VG; Funding acquisition AC, VG; Supervision AC, VG; Project administration, AC.

Materials and Methods

Animals

Adult female and male Wistar wild type and OTR-IRES-Cre rats (>8 weeks old; 250 - 350 g; Chronobiotron, Strasbourg, France) were used for this study. All animals were tattooed, sexed and genotyped (Kapa2G Robust HotStart PCR Kit, Kapa Biosystems; Hoffman La Roche) 1 week after birth. Animals were housed by sex, in groups of three under standard conditions (room temperature, 22 °C; 12 / 12 h light / dark cycle) with ad libitum access to food, water and behavioral enrichment. All animals that underwent behavioral testing were handled and habituated to the experimenter two weeks before stereotaxic surgery. After one week of post-surgical recovery, the rats were habituated to the applicable behavioral testing room and handling routines for an additional two weeks prior to the start of experiments. All behavioral tests were conducted during the light period (i.e., between 7:00 and 19:00). All experiments were conducted in accordance with European law, under French Ministery license 3668-2016011815445431 and 15541-2018061412017327, and German Animal Ethics Committee of the Baden Württemberg license G-102/17.

Viral cloning and packaging

Recombinant Adeno-associated virus (serotype 1/2) carrying either a conserved region of the OT promoter or Ef1A promoter and genes of interest in direct or “DIO” orientations were cloned and produced as reported previously (Knobloch et al., 2012). Briefly, HEK293T cells (#240073, Addgene, USA) were used for viral production. rAAVs produced included: rAAV-OTp-mCherry(or Venus), rAAV-OTp-ChR2-mCherry, rAAV-Ef1A-DIO-GFP (or mCherry), and rAAV-Ef1A-DIO-hM3Dq-mCherry. The canine adenovirus serotype 2 (CAV2-CMV-Cre) was purchased from the Institute of Molecular Genetics in Montpellier CNRS, France. rAAV genomic titers were determined with QuickTiter AAV Quantitation Kit (Cell Biolabs, Inc., San Diego, California, USA) and RT-PCR using the ABI 7700 cycler (Applied Biosystems, California, USA). rAAVs titers were between 10^9 - 10^{10} genomic copies/µl.

Stereotaxic injections

All surgeries were performed on rats anesthetized with 2.5% isoflurane and receiving Bupivacaine (s.c., 2mg/kg) or carprofen (i.p., 5mg/kg) and lidocaine applied locally (Tang et al., STAR protocols, in press). rAAVs were injected into the PVN, SON and vlPAG in different

combinations, as needed by each experiment, and allowed to express for four weeks. The coordinates were chosen using the Paxinos rat brain atlas [29](PVN: ML: +/-0.3 mm; AP: -1.4 mm; DV: -8.0 mm; SON: ML: +/-1.8 mm; AP: -1.2 mm; DV: -9.25 mm; PAG: ML: +/-0.5 mm; AP: -7.0 mm; DV: -5.9/-5.0 mm). Each site was injected with a total of 300nL of viral solution via a glass pipette at a rate of 150 nl/min using a syringe pump. Verification of injection and implantation sites, as well as expression of genes of interest were confirmed in all rats *post-hoc* (see "Histology" section). Rhodamine conjugated Retrobeads (Lumafluor Inc., Durham, NC, USA) were diluted 1:10 with 1x PBS and injected at a volume of 150 nl. Spinal cord Retrobeads injections was performed during the same surgery as virus injection (See "*In vivo* extracellular recording of WDR SC neurons" for details on the spinal cord surgery).

Generation of OTR-IRES-Cre rats

Cloning of the rat OXTR-Cre targeting vector

The OXTR-Cre targeting vector was cloned by modifying the plasmid Snap25-IRES2-Cre (Allen Institute for Brain Science (Harris et al., 2014)) The final vector contained the iRES2-Cre sequences, followed by a bovine growth hormone polyadenylation site, and homology arms for targeted integration of the oxytocin receptor locus, comprised of 1.3 kb and 1.4 kb genomic sequences. Homology arms were generated by PCR on genomic DNA from Sprague Dawley rats using the following primer pairs: OXTR_fwd_upper (5' GTCGACAGAAAACTGGTGGGTTTGCC 3') together with OXTR_rev_upper (5' GCTGCTAGCGAAGACTGGAGTCCACACCACC 3') and OXTR_fwd_lower (5' ACCCGGGAATTCTGTGCATGAAGCTGCATTAGG 3') together with OXTR_rev_lower (5' TAGTTTAAACGTGCATTCGTGTATGTTGTCTATCC 3'). The upper homology arm was inserted using the restriction enzymes SalI and NheI, while the lower arm was inserted using XmaI and PmeI. Vector sequences can be obtained upon request.

Design of gRNAs and functional testing

We used the online tool CRISPOR (http://crispor.org) for selection of the guide RNA (gRNA) target sites in the OXTR gene (Haeussler et al., 2016). Three gRNA target sites were chosen with high specificity scores (> 83, (Hsu et al., 2013)) for binding in the OXTR 3' UTR site where we aimed to introduce the IRES-Cre coding sequences.

For identification of the most effective gRNA, dual expression vectors based on px330 were cloned, harboring an expression cassette for the selected gRNAs and Cas9. In addition, the OXTR 3' UTR gRNA target regions were inserted into a nuclease reporter plasmid (pTAL-Rep, (Wefers et al., 2013)) in between a partly duplicated, nonfunctional β-galactosidase

gene. Hela cells were transfected with a combination of one of the px330 plasmids and the OXTR specific reporter vector. After transfection, the Cas9-nuclease-induced double-strand breaks stimulated the repair of the lacZ gene segments into a functional reporter gene, the activity of which was determined in cell lysates using an o-nitrophenyl-β-D-galactopyranosid (ONPG) assay. A luciferase expression vector was also added to the transfection mix and luciferase activity was measured for normalization. The most effective gRNA target site including PAM was determined as 5' ACTCCAGTCTTCCCCCGTGG**TGG** 3'

Specificity of the CRISPR/Cas induced genomic modification

The CRISPOR program was used to identify potential off-target sites for the selected OXTR gRNA (5'ACTCCAGTCTTCCCCCGTGGTGG 3'). No off-target sites were detected in an exonic sequence or on the same chromosome. In addition, only two potential target sites harboring at least four mismatches in the 12 bp adjacent to the PAM could be identified by the software.

Generation of transgenic rats

Sprague Dawley (SD) rats (Charles River) were bred in standard cages (Tecniplast) under a 12-h light/dark cycle in a temperature-controlled environment with free access to food and water at the Central Institute of Mental Health, Mannheim. All animal protocols were approved by the Regierungspräsidium Karlsruhe. SD single-cell embryos were injected using standard microinjection procedure. In brief, microinjections were performed in the cytoplasm and male pronuclei of zygotes with a mixture of Cas9 mRNA (10 ng·/µl), sgRNA expression vector (6 ng/µL) and the OXTR-Cre targeting vector (2 ng/µl) as the repair substrate. The injected embryos were cultured in M2 Medium at 37°C in 5% CO2 and 95% humidified air until the time of injection. Surviving oocytes were transferred to the oviducts of pseudo pregnant Sprague Dawley rats. Transgenic animals were identified by polymerase chain reaction of tail DNA (DNeasy kit, Qiagen, Hilden, Germany) using primers for Cre (Schönig et al., 2002).

DNA of Cre positive animals was further used for detection of homologous recombination at the OXTR locus. For this purpose, the targeted region was amplified by PCR using the Q5 polymerase (NEB) with 100 -200ng of genomic DNA as a template. Primers were selected which bind both up and downstream of the insertion site (outside of the homology arms), and were each combined with a primer located within the IRES2-Cre construct. For the 5' insertion site, the primers OXTR_check (5′ CAGCAAGAAGAGCAACTCATCC 3′) together with Cre_rev (5′ CATCACTCGTTGCATCGAC 3′) and, for the 3' site, CRISPR_bGH_fwd (5' GACAATAGCAGGCATGCTGG 3') together with OXTR_rev_check (5' AGCCAGGTGTCCAAGAGTCC 3') were used.

Histology

After transcardial perfusion with 4% paraformaldehyde (PFA) and post fixation overnight, brain sections (50 µm) were collected by vibratome slicing and immunohistochemistry was performed as previously described. The following primary antibodies were used: anti-OT (PS38, 1:2000; mouse; kindly provided by Harold Gainer), anti-Ds-Red (#632397, 1:1000; rabbit; Clontech), anti-GFP (ab13970, 1:1000, chicken, Abcam), anti *c-Fos* (#9F6, 1:500, rabbit, Cell Signaling), anti-Fluorogold (NM-101, 1:1000, guinea pig, Protos Biotech) anti-VGluT2 (1:2000; rabbit; SySy), or anti-NeuN (1:1000; rabbit; Abcam). For secondary antibodies, Venus/GFP signal was enhanced by Alexa488-conjugated IgGs. Other primary antibodies were visualized using CY3-conjugated or CY5-conjugated antibodies (1:500; Jackson Immuno-Research Laboratories). All images were acquired on a confocal Leica TCS microscope. Digitized images were processed with Fiji and analyzed using Adobe Photoshop. For the visualization of OT-ergic axonal projections within the PAG, we analyzed brain sections ranging from bregma -6.0mm to -8.4mm.

RNAScope in situ hybridization

RNAScope reagents (Advanced Cell Diagnostics, Inc., PN320881) and probes (OTR: 483671-C2 RNAscope Probe and Cre: 312281 RNAscope Probe) were used to detect the presence of specific mRNA expression using *in situ* hybridization. Brains were processed as described above using nuclease-free PBS, water, PBS and sucrose. We followed the manufacturer's protocol with a few modifications: 1) immediately after cryosectioning, slices were washed in nuclease-free PBS to remove residual sucrose and OCT compound. 2) Hydrogen peroxide treatment was performed with free-floating sections prior to slice mounting. 3) Sections were mounted in nuclease-free PBS at room temperature. 4) Pretreatment with Protease III was performed for 20 minutes at room temperature. 5) No target retrieval step was performed.

Three-dimensional reconstruction and analysis of OT-OTR contacts in the PAG

Confocal images were obtained using a Zeiss LSM 780 confocal microscope (1024x1024 pixel, 16-bit depth, pixel size 0.63-micron, zoom 0.7). For the three-dimensional reconstruction, 40µm-thick z-stacks were acquired using 1µm-steps. Imaris-assisted reconstruction was performed as previously described (Althammer et al., 2020; Tang et al., 2020; Wahis et al., 2021). In brief, surface reconstructions were created based on the four individual channels (DAPI, OT, OTR-GFP, SYN/vGlut2). Co-localization of OT signal with SYN or vGlut2 was confirmed both manually and through the association/overlap function of

IHC-labeled puncta in the Imaris software. IHC intensity of vGlut2 and SYN were assessed by creating spheres that precisely engulfed somata or dendrites as previously described (Tang et al., 2020).

Ex vivo patch-clamp recording of vlPAG-OTR neurons

Slice preparation

To validate the functionality of vlPAG OTR neurons in OTR-iRES-Cre rats using electrophysiology, 12-week old, female OTR-iRES-Cre rats (n = 4) received injections of the Cre dependent reporter virus, rAAV1/2-pEF1a-DIO-GFP, into the vlPAG. Following a 4-8 week recovery period, rats were anesthetized by administering i.p. ketamine (Imalgene 90 mg/kg) and xylazine (Rompun, 10 mg/kg). Transcardial perfusions were performed using an ice-cold, NMDG based aCSF was used containing (in mM): NMDG (93), KCl (2.5), NaH_2PO_4 (1.25), $NaHCO_3$ (30), $MgSO_4$ (10), $CaCl_2$ (0.5), HEPES (20), D-Glucose (25), L-ascorbic acid (5), Thiourea (2), Sodium pyruvate (3), N-acetyl-L-cysteine (10) and Kynurenic acid (2). The pH was adjusted to 7.4 using either NaOH or HCl, after bubbling in a gas comprised of 95 % O_2 and 5 % CO_2. Rats were then decapitated, brains were removed and 350 µm thick coronal slices containing the hypothalamus were obtained using a Leica VT1000s vibratome. Slices were warmed for 10 minutes in 35°C NMDG aCSF then placed in a room temperature holding chamber filled with normal aCSF for at least 1 hour. Normal aCSF was composed of (in mM): NaCl (124), KCl (2.5), NaH_2PO_4 (1.25), $NaHCO_3$ (26), $MgSO_4$ (2), $CaCl_2$ (2), D-Glucose (15), adjusted to pH 7.4 with HCL or NaOH and continuously bubbled in 95 % O_2-5 % CO_2 gas. Osmolarity of all aCSF solutions were maintained between 305-310 mOsm. Finally, slices were transferred from the holding chamber to an immersion-recording chamber and superfused at a rate of 2 ml/min.

Patch clamp recording

Next, we targeted GFP+ neurons in the vlPAG for whole-cell patch-clamp recording. The recording pipettes were visually guided by infrared oblique light video microscopy (DM-LFS; Leica). We used 4–9 MΩ borosilicate pipettes filled with a KMe based solution composed of (in mM): $KMeSO_4$ (135), NaCl (8), HEPES (10), $ATPNa_2$ (2), GTPNa (0.3). The pH was adjusted to 7.3 with KOH and osmolality was adjusted with sucrose to 300 mOsm/l, as needed. Data were acquired with an Axopatch 200B (Axon Instruments) amplifier and digitized with a Digidata 1440A (Molecular Devices, CA, USA). Series capacitances and resistances were compensated electronically. Data were sampled at 20 kHz and lowpass filtered at 5 kHz using the pClamp10 software (Axon Instruments). Further analysis was performed using Clampfit 10.7 (Molecular Devices; CA, USA) and Mini analysis 6 software (Synaptosoft, NJ, USA) in a semi-automated fashion (automatic detection of events with

chosen parameters followed by a visual validation).

TGOT stimulation

Finally, to validate the functionality of the putative OTR-Cre expressing cells in the vlPAG, we recorded GFP+ neurons in GAPfree (current clamp mode). Following a 5 min baseline recording period, a solution containing the OTR agonist, [Thr^4Gly^7]-oxytocin (TGOT, 0.4μM), was pumped into the bath for 20 s. The recording continued for a total of 20 min while the frequency of action potentials (APs) was quantified as the measure of neuronal activity. As a control, we repeated this procedure while patching GFP- neurons in the same vicinity. Neurons were held at ~50 mV by injecting between 0 and 10 pA of current throughout the recording and all *ex vivo* experiments were conducted at room temperature.

In vivo extracellular recording of vlPAG neurons

To test the effects of endogenous OT release on OTR cells of the vlPAG *in vivo*, female OTR-iRES-Cre rats were injected with $rAAV_{1/2}$-pOT-ChR2-mCherry into the PVN. After a 4-8 week recovery period, rats were anaesthetized with 4% isoflurane and placed in a stereotaxic frame before reducing the isoflurane level to 2%. A silicone tetrode coupled with an optical fiber (Neuronexus, USA) was inserted into the PAG to allow for stimulation of the ChR2 expressing axons of PVN-OT neurons projecting to vlPAG while recording the activity of putative OTR expressing neurons in the vicinity. Optical stimulation was delivered using a blue laser (λ 473 nm, output of 100 mW/mm², Dream Lasers, Shanghai, China) for 20 s at 1 Hz, with a pulse width of 5 ms. Extracellular neuronal activity was recorded using a silicone tetrode coupled with an optic fiber (Q1x1-tet-10mm-121-OAQ4LP; Neuronexus, USA). Data were acquired on an MC Rack recording unit (Multi Channel Systems), and spikes were sorted by Wave Clus (Chaure et al., 2018). Spike data was analyzed with custom MATLAB (MathWorks) scripts and the MLIB toolbox (Stüttgen Maik, Matlab Central File Exchange).

The firing rate of each recording unit was smoothed by convolution of Gaussian distribution, whose width was 10 s and standard deviation was 5. The mean firing rate of baseline period (BSmean) was defined as 0% activity and subtracted from the firing rates (FR) of the whole period (FR- BSmean). Maximum absolute activity (max(| FR- BSmean |)) was found using the highest absolute value among moving means of (FR- BSmean) with a time window of 21 s. When maximum absolute activity was found to exceed the BSmean, it was defined as 100% activity (cell#1~21), whereas when maximum absolute activity was found to be below BSmean, it was defined as -100% activity (cell#22~23).

In vivo extracellular recording of WDR SC neurons

Adult Wistar rats were anesthetized with 4% isoflurane and a then maintainted at 2% after being placed in a stereotaxic frame. A laminectomy was performed to expose the L4-L5 SC segments, which were then fixed in place by two clamps positioned on the apophysis of the rostral and caudal intact vertebras. The dura matter was then removed. To record wide-dynamic-range neurons (WDR), a silicone tetrode (Q1x1-tet-5mm-121-Q4; Neuronexus, USA) was lowered into the medial part of the dorsal horn of the SC, at a depth of around 500 -1100 µm from the dorsal surface (see Figure 5A2 for localization of recorded WDRs). We recorded WDR neurons of lamina V, receiving both noxious and non-noxious stimulus information from the ipsilateral hind paw.

We measured the action potentials of WDR neurons triggered by electrical stimulation of the hind paw. Such stimulation induced the activation of primary fibers, whose identities can be distinguished by their spike onset following each electrical stimuli (Aβ-fibers at 0-20 ms, Aδ-fibers at 20-90 ms, C-fibers at 90-300 ms and C-fiber post discharge at 300 to 800 ms). When the WDR peripheral tactile receptive fields are stimulated the intensity corresponding to 3 times the C-fiber threshold (1 ms pulse duration, frequency 1 Hz), a short-term potentiation effect, known as wind-up (WU), occurs that leads to an increased firing rate of WDR neurons (Mendell and Wall, 1965; Schouenborg, 1984). Because the value of WU intensity was highly variable among recorded neurons within and across animals, we averaged the raster plots two dimensionally across neurons within each group of rats. We further normalized these data so that the plateau phase of the maximal WU effect was represented as 100 percent activity. As WU is dependent on C-fiber activation, it can be used as a tool to assess nociceptive information in the SC and, in our case, the anti-nociceptive properties of OT acting in the vlPAG. We recorded WDR neuronal activity using the following protocol: 40 s of hind paw electric stimulation to induce maximal WU followed by continued electrical stimulation to maintain WU while simultaneously delivering 20 s of vlPAG blue light stimulation (30 Hz, 10ms pulse width, output ~100 mW/mm^2), followed by another 230 s of electrical stimulation alone to observe the indirect effects of OT on WU in WDR neurons. Electrical stimulation was ceased after the 290 s recording session to allow the WU effect to dissipate. Following a 300 s period of no stimulation, the ability of the WU effect to recover was assessed by resuming electrical stimulation of the hind paw for 60 s of WU. After another 10 min period without stimulation, we sought to confirm the effects of vlPAG OT activity on WU intensity by injecting 600 nl of the OTR antagonist, dOVT, (d(CH2)5-Tyr(Me)-[Orn8]-vasotocine; 1µM, Bachem, Germany) into the vlPAG of the rats expressing ChR2, and repeated the protocol described above.

The spikes of each recording unit were collected as raster plots with the vertical axis showing the time relative to electric shock, and the horizontal axis showing the number of electric shocks. Next, the raster plots were smoothed by convolution of the Gaussian distribution (horizontal width = 100 ms, vertical width = 20 ms, standard deviation = 20. The total number of C fiber derived spikes occurring between 90 and 800 ms after each electric shock was counted. The spike counts were smoothed with a moving average window of 21 s and the window containing the maximal activity was defined as '100% activity', which was then used to normalize the activity of each recording unit. Finally, the normalized percent activity from each recording unit was averaged for each experimental condition and plotted in figure 5.

Behavioral tests

Optogenetics

For *in vivo* optogenetic behavioral experiments, we used a blue laser (λ 473nm, 100 mW/mm², DreamLasers, Shanghai, China) coupled to optical fiber patch cables (BFL37-200-CUSTOM, EndA=FC/PC, EndB=Ceramic Ferrule; ThorLabs, USA). Optical fiber probes (CFMC12L10, Thorlabs, USA) were bilaterally implanted into the vlPAG (Coordinates relative to bregma: ML= ±2.0mm, AP= -6.7mm, DV=-7.0mm, medio-lateral angle=10°) under isoflurane anesthesia (4% induction, 2% maintenance), and then stabilized with dental cement. Following a two-week recovery period, all animals received special handling to habituate them to the fiber connection routine. Optical stimulation to the vlPAG was delivered using a series of pulse trains (intensity = ~10mW/mm², frequency = 30 Hz, pulse width = 10ms, duration = 20s) during all applicable behavioral experiments.

Chronic constriction of the sciatic nerve

To produce the model of chronic neuropathic pain, we surgically implanted a cuff around the sciatic nerve to induce a chronic constriction injury as previously described (Yalcin et al., 2014). Briefly, under isoflurane anesthesia (5%) via a facemask, an incision was made 3-4mm below the femur on the right hind limb, and 10mm of the sciatic nerve was exposed. A sterile cuff (2 mm section of split PE-20 polyethylene tubing; 0.38 mm ID / 1.09 mm OD) was positioned and then closed around the sciatic nerve. The skin was then sutured shut to enclose the cuff and allow chronic constriction to occur.

Mechanical hyperalgesia

Mechanical sensitivity was assessed using calibrated digital forceps (Bioseb®, France) as previously described (Wahis et al., 2021). Briefly, the habituated rat is loosely restrained with a towel masking the eyes in order to limit environmental stressors. The tips of the forceps are placed at each side of the paw and gradual force is applied. The pressure required to produce

a withdrawal of the paw was used as the nociceptive threshold value. This manipulation was performed three times for each hind paw and the values were averaged. After each trial, the device was cleaned with a disinfectant (Surfa'Safe, Anios laboratory®).

Inflammatory hyperalgesia

In order to induce peripheral inflammation, 100 µL of complete Freund adjuvant (CFA; Sigma, St. Louis, MO), was injected into the right hind paw of the rat. All CFA injections were performed under light isoflurane anesthesia (3 %). Edema was quantified by using a caliper to measure the width of the dorsoplantar aspect of the hind paw before and after the injection of CFA. In effort to reduce the number of animals used, we did not include an NaCl-injected group, as it has already been shown that the contralateral hind paw sensitivity is not altered by CFA injection (Hilfiger et al., 2020).

Thermal hyperalgesia

To test the animal thermal pain sensitivity threshold, we used the Plantar test with the Hargreaves method (Ugo Basile®, Comerio, Italy) to compare the response of each hind paw of animals having received unilateral intraplantar CFA injection. The habituated rat is placed in a small box and we wait until the animal is calmed then we exposed the hind paw to radiant heat, the latency time of paw withdrawal was measured. This manipulation was performed three times for each hind paw and the values were averaged. After each trial, the device was cleaned with a disinfectant (Surfa'Safe, Anios laboratory).

Conditioned Place Preference

The device is composed of two opaque conditioning boxes (rats: 30x32 cm; mice: 22x22 cm) and one clear neutral box (30x20 cm). Animals were tracked using a video-tracking system (Anymaze, Stoelting Europe, Ireland) and apparatus was cleaned with disinfectant (Surfa'Safe, Anios laboratory) after each trial. The animals underwent CPP as previously described (Wahis et al., 2021). Briefly, all rats underwent a three-day habituation period during which they were able to freely explore the entire apparatus for 30 min. On the 3rd habituation day, exploration behavior was recorded for 15 min to determine the animals' innate side preference. On the 4th day, animals were injected with saline (i.p, 1 mL/kg) and placed in their innately preferred chamber (unpaired box) for 15 min. Four hours later, animals were injected with DCZ (i.p, 100 µg/kg at 1 mL/kg) to stimulate vlPAG OTR neurons expressing hM3D(Gq), and then placed in the innately non-preferred chamber (paired box) for 15 min. On the 5th day, the animals were placed in the neutral chamber and allowed to explore the entire apparatus for 15 min. To control for potential locomotor effects, the total distance travelled during the test period was quantified and compared between all groups (Figure 6I).

Drugs

Deschloroclozapine (DCZ) (MedChemExpress®) is a potent, selective, metabolically stable agonist of muscarinic-based DREADDs and has already been administered i.p. in rodents (Nagai et al., 2020). In this study, we used it at concentration of 100 µg/kg, solubilized in (NaCl 0.9 % + DMSO 0.4 %) and injected at 1 mL/kg, i.p. The selective OTR agonist, [Thr^4Gly^7]-oxytocin (TGOT), was obtained from Bachem® (Fisher Scientific). Non-peptide oxytocin receptor (OTR) antagonist, L-368,899 (1-((7,7-Dimethyl-2(S)-(2(S)-amino-4-(methylsulfonyl)butyramido)bicyclo[2,2,1]heptan-1(S)-yl)methylsulfonyl)-4-(2-methylphenyl)piperazine hydrochloride), was obtained from (MERCK, Germany).

Statistical Analysis

For *ex vivo* electrophysiology data, one-way analysis of variance (ANOVA, Friedman test) followed by Dunn's post-hoc multiple comparisons test to compare averages across the three conditions (Baseline vs TGOT vs Wash). Differences were considered significant at $p<0.05$.
For *in vivo* electrophysiology data analysis, a paired-sample t-test was used to compare the average spike rates between the baseline and peak activity of PAG neurons in response to BL stimulation (**Figure 4**). A nonparametric, unpaired Wilcoxon rank sum test was used to compare the reduction in discharge of SC neurons between the wild type and the ChR2-expressing animals (**Figure 5**). A paired Wilcoxon signed rank test was used to compare the reduction discharge of SC neurons in the ChR2-expressing animals, between the "without dOVT" and "with dOVT" conditions (**Figure 5**). Wilcoxon rank sum tests were used to compare the latencies to reach the maximum, minimum, and the half value between the wild type and the ChR2-expressing rats (**Figure S5**).

Behavioral data are expressed as mean ± standard deviation (SD). Statistical tests were performed with GraphPad Prism 7.05 (GraphPad Software, San Diego, California, USA). All behavioral data failed the Shapiro-Wilk normality test. A Kruskall Wallis test with Dunn's post-hoc test was used to compare the percent co-localization of c-Fos+ and GFP+ cells across pain conditions (Figure 6A). A repeated-measures non parametric mixed model ANOVA was used to analyze the effect of DCZ on pain in PAG OTr/DREADDGq neurons with Dunnett's post-hoc multiple comparisons test to compare the effect of the (treatment) before (t = 0) and after the i.p. injection (20, 40, 60 and 180 min) (**Figure 6, S6**).
The ΔCPP score was calculated with the following formula in order to control for time spent in the neutral chamber: $\Delta CPP\ score = (paired_{postcond} - unpaired_{postcond}) - (paired_{hab} - unpaired_{hab})$. A Mann Whitney test was used to compare the effect of DCZ on CPP difference

score across the two groups as well as the distance travelled by the two groups (**Figure 6**). Differences were considered significant at $p<0.05$. Asterisks are used to indicate the significance level: * $0.01 \leq p < 0.05$, ** $0.001 \leq p < 0.01$, *** $p < 0.001$. All rats with off-target viral injection sites were removed from analysis.

Figure legends

Figure 1. Generation of KI OTR-Cre rats and identification of vlPAG OTR neurons

(A) Generation and confirmation of knock-in OTR-Cre rats. **A1** Schema of the OTR gene locus and the insertion site of the targeting vector containing the IRES-Cre sequence. **A2** Images of RNAscope in situ hybridization showing signal from Cre (n = 47 cells) and OTR (n = 42 cells) probes. Scale bar = 200 µm

(B) Electrophysical characterisation of OTR cells in the PAG. **B1** Schema of viral injection showing injection of rAAV-pEF1a-DIO-GFP in the PAG of OTR-Cre rats. **B2** Example image showing a GFP-positive cell during patch-clamp recordings. Scale bar = 20 µm. **B3** Example traces from a GFP-positive (left, Friedman's test = 14.97, $p < 0.0001$; Baseline vs TGOT ** $p = 0.0029$; TGOT vs Wash * $p = 0.0168$; Baseline vs Wash ns $p > 0.9999$, n = 11.) and a GFP negative (right, Friedman's test = 1.6, $p = 0.48$, n = 9) cell under baseline, TGOT application, and wash out conditions. **B4** Time course of GFP-positive cell activity (frequency distribution) under 3 conditions (baseline, TGOT application, wash). **B5** Plots showing individual and average nAP/t for GFP-positive (left) and negative (right) neurons under baseline, TGOT application, and wash out conditions.

(C) Quantitative analysis of OTR cells in the PAG. **C1** Images showing GFP (green) and DAPI (blue) staining of the vlPAG from OTR-Cre rats injected with Ef1a-DIO-GFP virus. Scale bar = 100 µm. Aq = Aqueduct. **C2** Bar plot showing the percentage of vlPAG cells expressing GFP.

(D) GAD67 staining of OTR cells in the vlPAG. **D1** Image of a vlPAG brain slice stained for GFP (green) and GAD67 (red). Scale bar = 100 µm, inset scale bar = 20 µm. **D2** Bar plot showing the percentage of GFP-positive neurons (n = 174 cells) in the vlPAG stained and not stained by GAD67 antibody.

Figure S1.

(A) Detailed schema of the generation of knock-in OTR-Cre rats, displaying the genomic structure of the OTR gene, the targeting vector, and the insertion site.

(B) Injection schema for the labelling of OTR neurons in the generated OTR-Cre rats. The rAAV-pEf1a-DIO-GFP is injected into the PAG, labelling exclusively OTR-neurons.

(C) Images showing GFP (green) and DAPI (blue) staining, at various distances from bregma, in the vlPAG of OTR-Cre rats injected with the Ef1a-DIO-GFP virus. Scale bar = 100µm. Aq = Aqueduct.

Figure 2. PVN ParvOT neurons send axonal projections to vlPAG.

(A) Anterograde tracing of projections from PVN OT-neurons to the vlPAG. **A1** Schema of viral injection showing injection of rAAV-pOT-mCherry in the PVN and rAAV-pEf1a-DIO-GFP in the PAG of OTR-Cre rats (n = 4 female rats). **A2** Image showing co-localization of rAAV-pOT-mCherry and OT in the PVN. Scale bar = 200 µm. 3v = third ventricle. **A3-5** Images of GFP (green, A3) and mCherry (red, A4) staining in the vlPAG showing PVN OT fibers surrounding vlPAG GFP neurons (A5). Scale bar = 300 µm, zoom scale bar = 40 µm. Aq = Aqueduct.

(B) Retrograde tracing of projections from PVN OT-neurons to the vlPAG. **B1** Schema of viral injection showing injection of rAAV-pOT-DIO-GFP in the PVN and rAAV-CAV2-Cre in the vlPAG of WT rats (n = 4 female rats). **B2** Image of the PVN from a rat injected with CAV2-Cre into the vlPAG and OTp-DIO-GFP into PVN, with OT stained in red. White arrows indicate co-localisation of GFP and OT. Scale bar = 200 µm. **B3-4** Magnified insets of the cells indicated by white arrows in the wide field image. Scale bar = 40 µM.

Figure S2.

(A) Distinction of parvocellular (parvOT) and magnocellular (magnOT) OT-neuron populations. **A1** Schema for the identification of magnOT and parvOT neurons: injection of green retrobeads into the PAG, staining for OT (red) and central application of fluorogold (FG, blue), which labels only magnOT neurons. **A2** Image of retrolabeled neurons containing fluorescent beads (green) as well as staining for Fluorogold (blue) and OT (red). White arrows indicate the co-localisation of OT and FG (magnOT neuron) and the white asterisk indicates the co-localisation of retrobeads and OT. Scale bars = 25 µm. n = 3 female rats.

(B) Retrograde labelling of projections from PVN OT-neurons to the vlPAG and SC. **B1** Schema of the experimental design with injection site of green retrobeads in the vlPAG (**B2**) and red retrobeads in the SC (L5, **B3**). Scale bars = 200 µm. **B4** Image of PVN OT-neurons (blue) projecting either to the vlPAG (green, white asterisk) or to the SC (red, white arrow). No OT neuron containing both red and green retrobeads was found. Aq = Aqueduct. 3v = third ventricle. Scale bar = 50µm. n = 4 female rats.

(C) PAG-projecting PVN OT-neurons from Figure 2B do not target the SC or SON. **C1** Schema of viral injection showing injection of rAAV-pOT-DIO-GFP in the PVN and rAAV-CAV2-Cre in the vlPAG of WT rats. **C2** Images of slices from the spinal cord at different levels (cervical, C3; thoracic, T7; lumbar, L4) and from the SON. No GFP fibers were found. Scale bars = 200 µm. n = 2 female rats.

(D) SON-projecting PVN OT-neurons do target the SC but not the vlPAG. **D1** Schema of viral injection showing injection of rAAV-pOT-DIO-GFP in the PVN and rAAV-CAV2-Cre in the SON of WT rats. **D2 Left** Images of PVN OT-neurons (red) expressing GFP (green) projecting fibers to the SC (L5, NeuN in red, scale bars = 100 µm). **Right** Image of the vlPAG showing no GFP positive fibers. Scale bar = 100 µm. n = 4 female rats.
(E) SC-projecting PVN OT-neurons do target the SON but not the vlPAG. E**1** Schema of viral injection showing injection of rAAV-pOT-DIO-GFP in the PVN and rAAV-CAV2-Cre in the SC of WT rats. **E2 Left** Images of PVN (scale bars = 40 µm) OT-neurons (red) expressing GFP (green) projecting fibers to the SON (scale bar = 100 µm). opt = optic tract. **Right** Image of the vlPAG showing no GFP positive fibers. Aq = aqueduct. Scale bar = 100 µm. n = 4 female rats.

Figure 3. OT fibers form synaptic and non-synaptic contacts with vlPAG OTR neurons.
(A) Schema of viral injection showing injection of rAAV-pEF1a-DIO-GFP in the PAG of OTR-Cre rats.
(B) Graph showing the relation between the number of OT fibers in the vlPAG and the bregma level. Blue area represents SEM.
(C) Graph showing the relation between the percentage of OTR neurons in the vlPAG and the bregma level. Blue area represents SEM.
(D) Correlation between the number of OTR neurons and the number of OT fibers within the same slice (n = 64 slices).
(E) Three-dimensional reconstruction of OT-ergic contacts with vlPAG OTR neurons via Imaris. **E1** Overview image showing OTR-neurons (green), OT-fibres (magenta) synaptophysin (SYN, red) and DAPI (blue). **E2** Magnified images from E1 showing contacts with or without SYN. White arrowheads indicate co-localization of OT (magenta) and SYN (red). while white arrowheads with an asterisk show a mismatch of OT and SYN. DAPI = blue, OTR = green.
(F) Bar graph showing the percentage of OTR positive (n = 496) and negative (n = 3840) cells receiving OT innervation (< 1 µm distance between fibers and cells). n = 4, 8 images per animal, p = 0.0055.
(G) Bar graph showings the percentage of contacts between OT and OTR-positive neurons at somatic and dendritic locations. n = 4, 8 images per animal, p < 0.0001.
(H) Imaris reconstruction of a vGluT2-positive (red) OT fiber (magenta) within the vlPAG.
(I) Bar graph showing that the vast majority of OT fibers within the vlPAG are vGluT2-negative (92.4%).
(J) 3D reconstruction of contacts between an OTR dendrite and OT fibers. **J1** Co-localisation

of OT (magenta) and vGluT2 (red) are indicated by white arrowheads. **J2** Mismatch of OT (magenta) and vGluT2 (red) are indicated by white arrowheads with an asterisk. DAPI = blue, OTR = green. n = 4 female rats.

Figure S3.

(A) Pipeline for Imaris-assisted 3D reconstruction based on raw IHC images.

(B) Confocal images showing OT fibers and OTR-positive neurons in the vlPAG. **B1** Images of OTR neurons (green), OT fibers (magenta), vGluT2 (red) and DAPI (blue). Scale bar = 100 µm. **B2** Overlay. Scale bar = 100 µm.

(C) Automated quantification of the number of SYN positive voxels in GFP-positive and negative neurons reveals no difference in overall synaptic input. n = 8 images per animal, p=0.6689.

(D) Analysis of somatic volume reveals no difference between OTR-positive (n = 496) and OTR-negative (n = 3840) soma sizes. n = 8 images per animal, p = 0.8104

Figure 4. Endogenous OT release in the vlPAG increases vlPAG neuron activity.

(A) Schema of the injection of rAAV-pOT-ChR2-mCherry in the PVN and setup for *in vivo* electrophysiological recordings (gray electrode), together with blue light (BL) stimulation (blue optic fiber) in the PAG. Recording site is shown on coronal drawings from anterior to posterior.

(B) Normalized firing rate of each vlPAG neuron (n = 23) that responded to BL in the vlPAG. 473 nm of BL was added as a 10 ms pulse at 30 Hz for 20 s, 100µW/mm². Dotted lines = BL stimulation.

(C) Recorded units' responsiveness. Out of 82 units, the spike rates of 21 units increased (red) and 2 units decreased (blue) as a result of BL stimulation.

(D) Mean percent activity (line) ± SEM (shaded) calculated from panel B.

(E) Difference in mean firing rate between the period before BL (-100 to 0 s) and the maximum activity period following BL stimulation (highest value among moving means with a time window of 21 s, between 0 to +300 s after the start of BL).

Figure S4.

(A) Image showing a representative recording site in the vlPAG. Dotted line indicated placement of the optic fibre. Aq = aqueduct.

(B) Onset, peak and offset of BL-induced excitation in the vlPAG. Onset is defined as the first time point when the spike rate exceeded the threshold (BS_{mean} + $4BS_{SD}$); BS_{mean} represents the mean firing rate of the baseline period, and BS_{SE} is the standard deviation of firing rate during the baseline period. Offset is defined as the last last time point when the spike rate fell

below the threshold for more than 20 s during the 300 s following BL.
(C) Number of active cells in each single second. “Active” defined by spike rate above the threshold (BS_{mean} + $4BS_{SD}$).

Figure 5. Endogenous OT release in vlPAG reduces WDR spinal cord neuronal activity.
(A) Schema of the injection of rAAV-pOT-ChR2-mCherry in the PVN and setup for *in vivo* electrophysiological recordings (gray electrode) of WDR neurons in the rat spinal cord (SC) at the lumbar 4 (L4) level during optogenetic BL stimulation (blue optic fiber) in the vlPAG to activate ChR2-expressing axons originating from PVN OT neurons. Recording sites in layer 5 are shown in the coronal drawing of L4 in the layer 5.
(B) Mean time course of the spike rate of WDR’s C-fiber discharge. CTRL rats (gray, n = 8), ChR2-expressing rats (blue, n = 14), or ChR2-expressing rats after dOVT injection in the vlPAG (red, n = 6). Left and right panels show two consecutive recordings separated by 300s. Line shadows represent SEM.
(C) Percentage of reduction expressed as the minimum level activity observed after a wind-up plateau phase. Minimum activity period: 140 - 180 s after the BL onset (shown in B). Top and bottom show two consecutive recordings separated by 300 s; * $p < 0.05$, ** $p < 0.01$.
(D) Mean smoothed raster plot of WDR discharge level along the relative timing to each single electric shock on the hind paw (vertical axis) and along the accumulating trials of electric shock (horizontal axis), in CTRL animals (top, n = 8), ChR2 animals (middle, n = 14), and ChR2 animals after dOVT injection in PAG (bottom, n = 6).

Figure S5.
Box plot showing maximum activity, minimum activity, and half activity latencies. Whiskers indicate the minimum and maximum latency. Coloured box shows the range between 1st and 3rd quantile, median is depicted as vertical line.

Figure 6. Evoked OT release in vlPAG reduces mechanical hyperalgesia.
(A) Percentage of c-Fos positive vlPAG OTR neurons under the control condition, painful stimulation, CFA inflammation, and painful stimulation combined with CFA. n = 7-8 per group, Kruskall Wallis test $H = 12.01$, $p < 0.01$, CTRL vs pain and CTRL vs pain + CFA $p < 0.05$, CTRL vs CFA $p > 0.05$. All results are expressed as average ± SEM.
(B) Examples of images showing c-Fos (red) and GFP (green) staining of vlPAG under the different experimental conditions (**B1-4**). Scale bar = 200 µm, inset scale bar = 75 µm. Aq = aqueduct.
(C) Schema of the injection of rAAV-pOT-ChR2-mCherry in the PVN and optic fiber

implantation in the PAG.
(D) Threshold of mechanical pain was raised by PAG-BL. The effect of vlPAG-BL was measured at 5 min, 1 h and 3 h after vlPAG-BL for the CFA-injected paw (**D1**) as well as contralateral paw (**D2**). Blue background represents BL stimulation. **** $p < 0.0001$, n = 10.
(E) Schema of the injection of rAAV-pEf1a-DIO-Gq-mCherry in the PAG.
(F) Mechanical pain threshold after DCZ administration in the CFA and contralateral paw of female rats expressing Gq-mCherry (blue) or mCherry only (gray) in vlPAG OTR neurons. All results are expressed as average ± SEM. * $p < 0.01$, *** $p < 0.0001$, n = 5-6 per group.
(G) Thermal pain threshold after DCZ administration under normal or inflammation (CFA) condition of female rats expressing Gq-mCherry (red) or mCherry only (gray) in vlPAG OTR neurons. All results are expressed as average ± SEM. * $p < 0.01$, *** $p < 0.0001$, n = 5-6 per group.
(H) Representative activity traces during the CPP test.
(I) Graphs showing the ΔCPP score (left) and total distance travelled (right) for the test and control groups. n = 6 per group

Figure S6.
(A) Optogenetic stimulation of the vlPAG in the chronic constriction of the sciatic nerve (CCI) model of neuropathic pain. **A1** Schema of the injection of rAAV-pOT-ChR2-mCherry in the PVN and optic fiber implantation in the PAG. **A2-3** Graphs showing the threshold response to mechanical stimuli in female rats optogenetically stimulated in vlPAG (as in Figure 6C and 6D). The effect of vlPAG-BL was measured at 5 min, 1 h and 3 h after vlPAG-BL on the CCI side (**A2**) as well as contralateral side (**A3**). All results are expressed as average ± SEM. * $p < 0.01$, ** $p < 0.01$, n = 7.
(B) Verification for the expression of Gq-mCherry in the vlPAG. **B1** Schema of the injection of rAAV-pEf1a-DIO-Gq-mCherry in the PAG. **B2** Image showing the expression of rAAV-Ef1A-DIO-Gq-mCherry (red) with staining for DAPI (blue). Scale bar = 100µm. Aq = aqueduct.
(C) Mechanical pain threshold after DCZ administration in the CFA (**C1**) and contralateral (**C2**) paw of male rats expressing Gq-mCherry (blue) or mCherry only (gray) in vlPAG OTR neurons. All results are expressed as average ± SEM. *** $p < 0.0001$, n = 6 per group.
(D) Thermal pain threshold after DCZ administration in the CFA (**D1**) and contralateral (**D2**) paw of male rats expressing Gq-mCherry (red) or mCherry only (gray) in vlPAG OTR neurons. All results are expressed as average ± SEM. *** $p < 0.0001$, n = 6 per group.
(E) Schema depicting the experimental timeline of the CPP protocol.

Figure 7. Two distinct ParvOT neuronal populations promote analgesia via release of OT in the vlPAG and in the blood and spinal cord.

We hypothesize that two parallel parvOT pathways are activated by pathological, painful stimuli. Both pathways release OT in various brain regions and the periphery, which then, leads to a reduction in nociception.

Figure 1

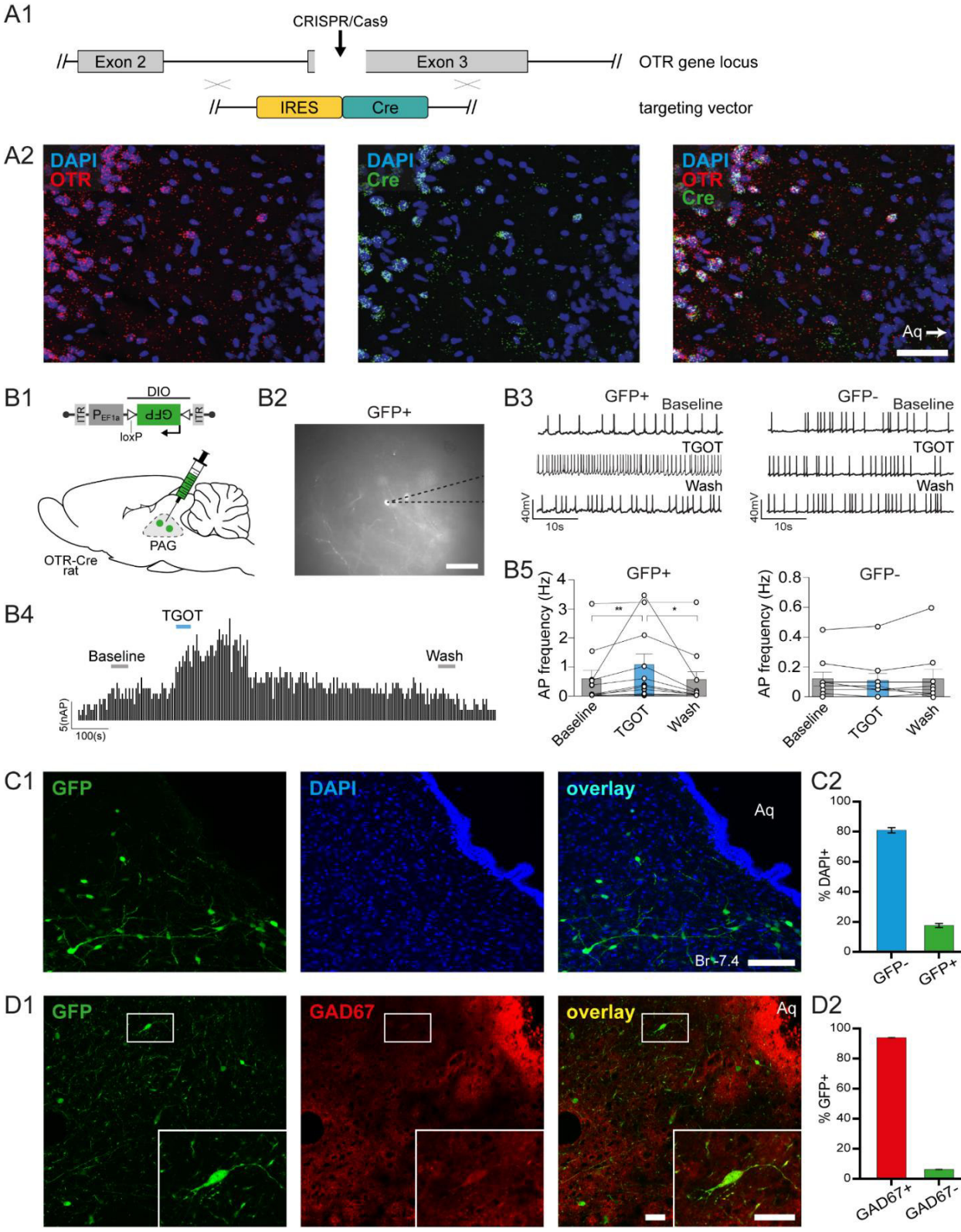
A1
CRISPR/Cas9
Exon 2
Exon 3
OTR gene locus
IRES
Cre
targeting vector
A2
DAPI
OTR
DAPI
Cre
DAPI
OTR
Cre
Aq
B1
DIO
ITR
PEF1a
GFP
ITR
loxP
PAG
OTR-Cre rat
B2
GFP+
B3
GFP+
Baseline
TGOT
Wash
GFP-
Baseline
TGOT
Wash
40mV
10s
B4
TGOT
Baseline
Wash
5(nAP)
100(s)
B5
GFP+
AP frequency (Hz)
Baseline
TGOT
Wash
GFP-
AP frequency (Hz)
Baseline
TGOT
Wash
C1
GFP
DAPI
overlay
Aq
Br -7.4
C2
% DAPI+
GFP-
GFP+
D1
GFP
GAD67
overlay
Aq
D2
% GFP+
GAD67+
GAD67-

Figure S1

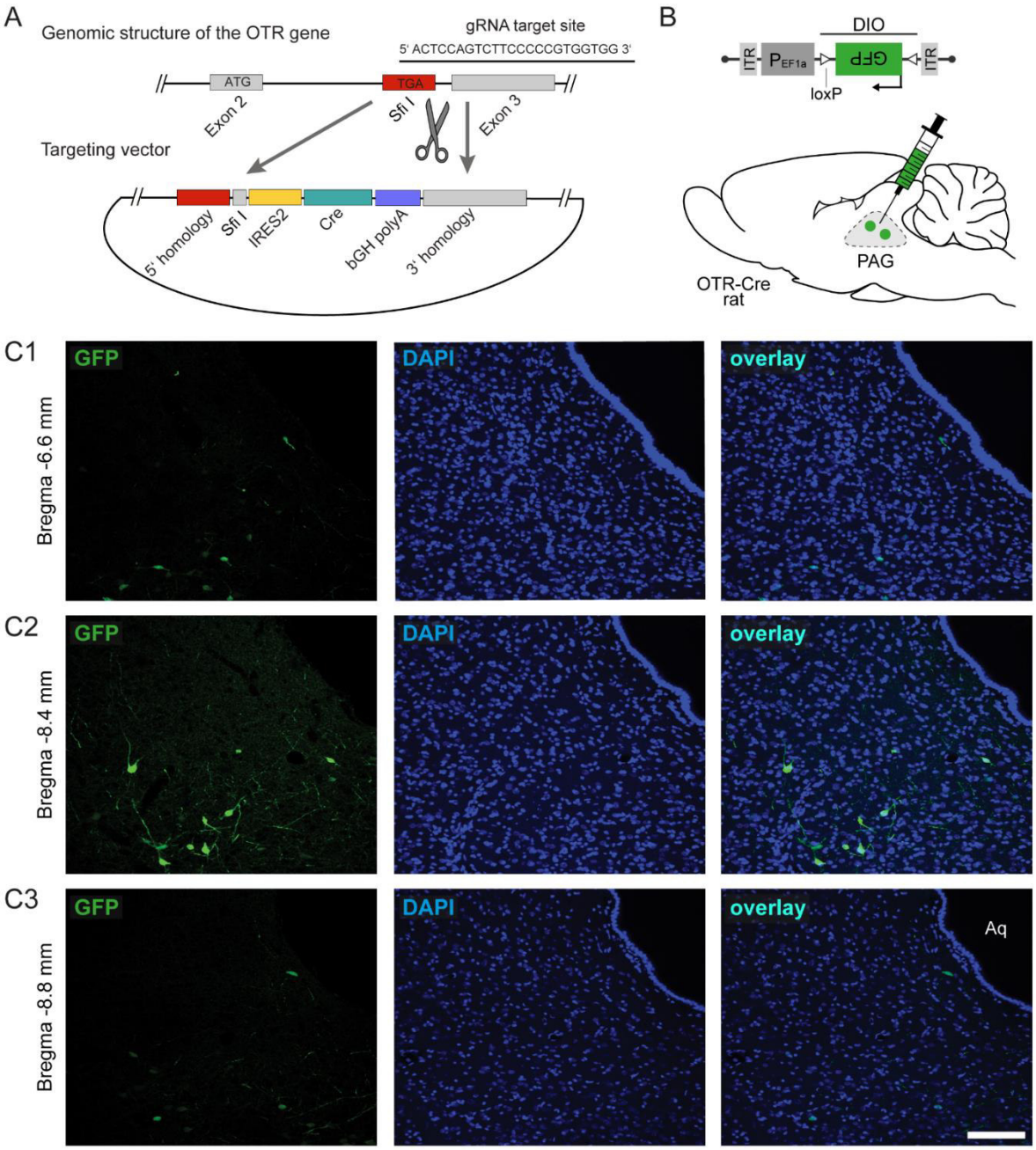
A
Genomic structure of the OTR gene
gRNA target site
5' ACTCCAGTCTTCCCCCGTGGTGG 3'
ATG
TGA
Exon 2
Sfi I
Exon 3
Targeting vector
5' homology
Sfi I
IRES2
Cre
bGH polyA
3' homology
B
DIO
ITR
PEF1a
GFP
ITR
loxP
PAG
OTR-Cre rat
C1
GFP
DAPI
overlay
Bregma -6.6 mm
C2
GFP
DAPI
overlay
Bregma -8.4 mm
C3
GFP
DAPI
overlay
Aq
Bregma -8.8 mm

Figure 2

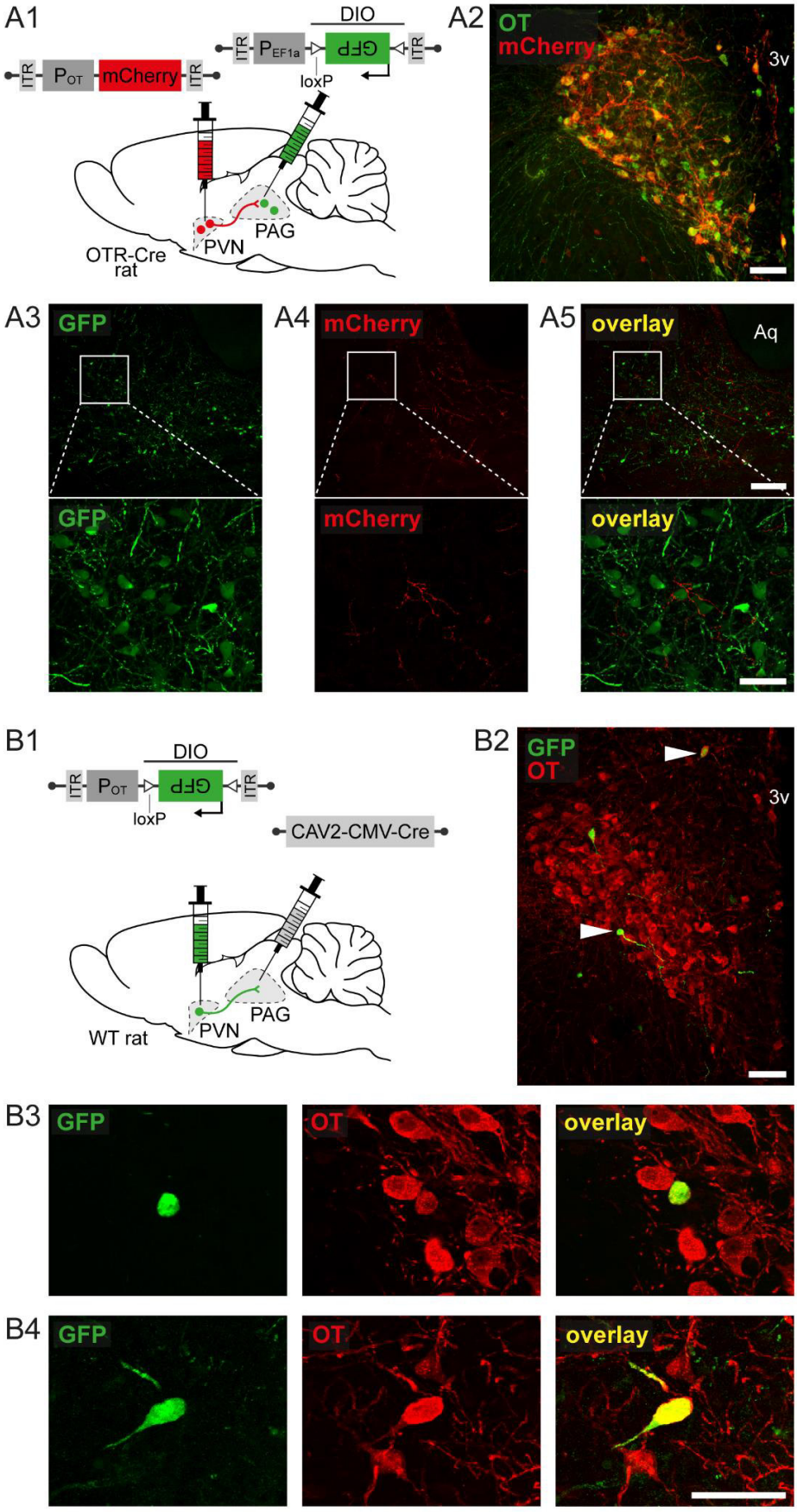
A1
DIO
ITR
P EF1a
GFP
ITR
ITR
P OT
mCherry
ITR
loxP
PAG
PVN
OTR-Cre
rat
A2
OT
mCherry
3v
A3
GFP
GFP
A4
mCherry
mCherry
A5
overlay
Aq
overlay
B1
DIO
ITR
P OT
GFP
ITR
loxP
CAV2-CMV-Cre
PAG
PVN
WT rat
B2
GFP
OT
3v
B3
GFP
OT
overlay
B4
GFP
OT
overlay

Figure S2

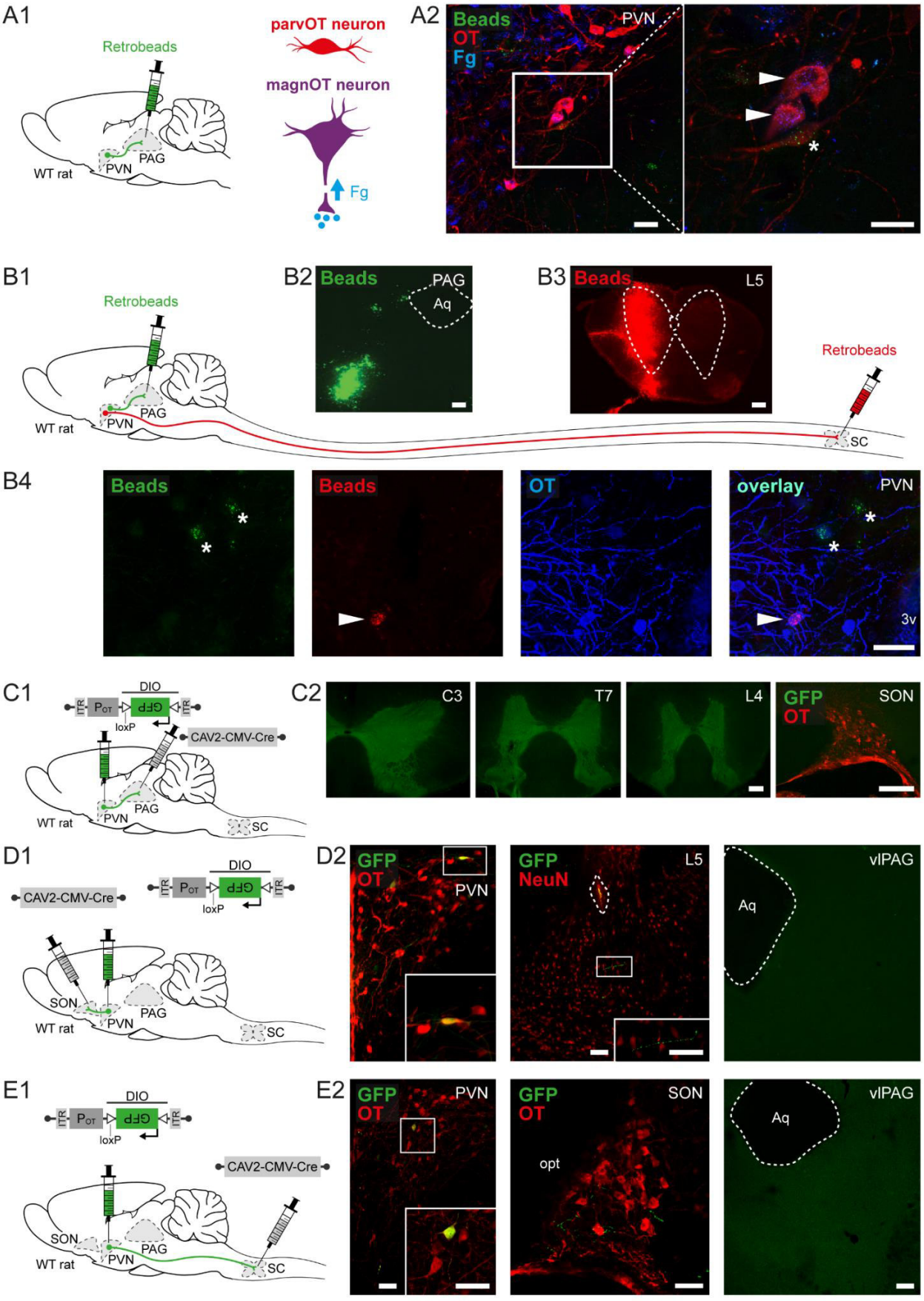
A1
Retrobeads
WT rat
PAG
PVN
parvOT neuron
magnOT neuron
Fg
A2
Beads
OT
Fg
PVN
B1
Retrobeads
WT rat
PAG
PVN
B2
Beads
PAG
Aq
B3
Beads
L5
Retrobeads
SC
B4
Beads
Beads
OT
overlay
PVN
3v
C1
DIO
POT
GFP
loxP
CAV2-CMV-Cre
WT rat
PAG
PVN
SC
C2
C3
T7
L4
GFP
OT
SON
D1
CAV2-CMV-Cre
DIO
POT
GFP
loxP
SON
PAG
WT rat
PVN
SC
D2
GFP
OT
PVN
GFP
NeuN
L5
vlPAG
Aq
E1
DIO
POT
GFP
loxP
CAV2-CMV-Cre
SON
PAG
WT rat
PVN
SC
E2
GFP
OT
PVN
GFP
OT
SON
opt
vlPAG
Aq

Figure 3

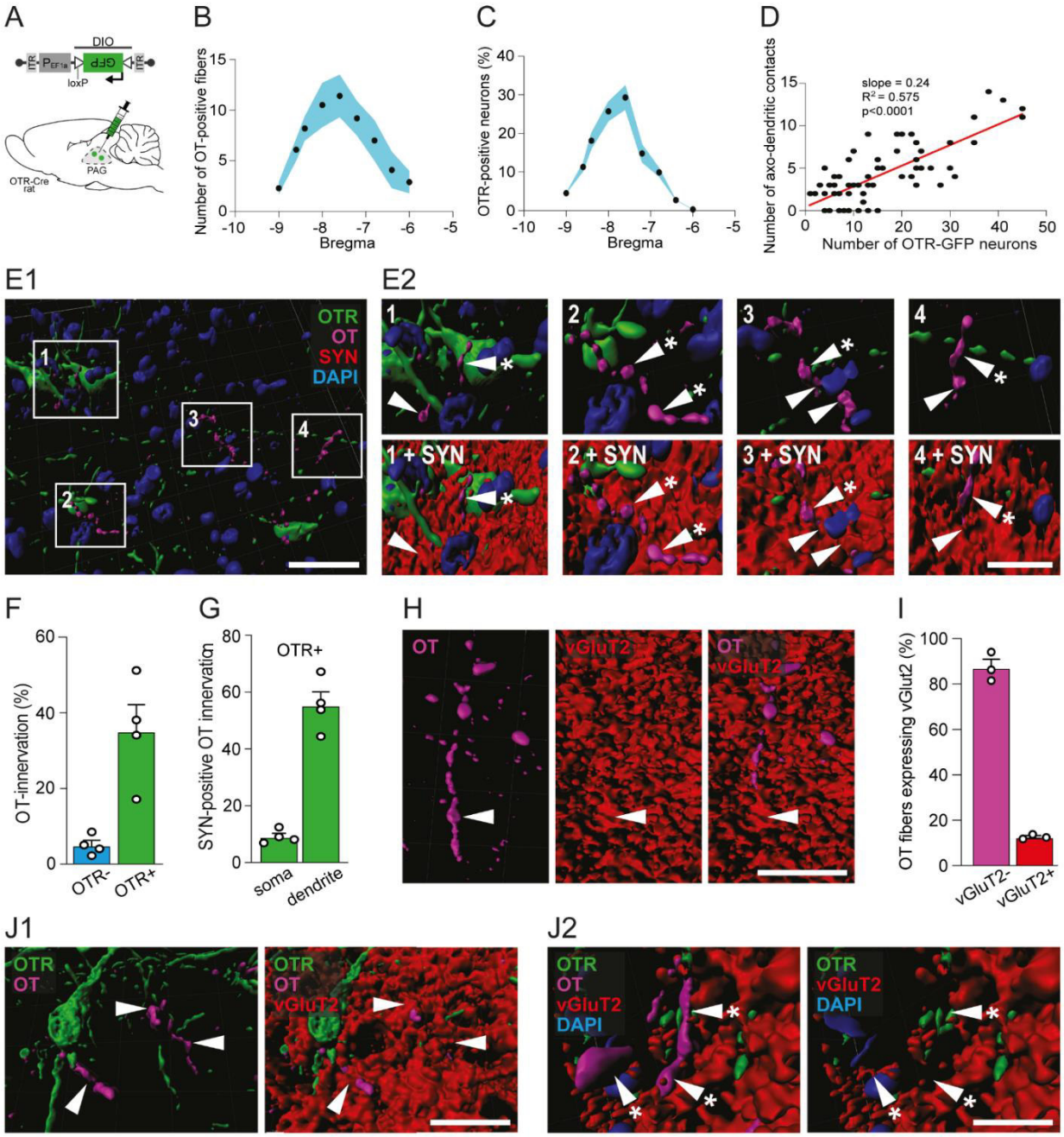
A
DIO
GFP
loxP
PAG
OTR-Cre rat
B
Number of OT-positive fibers
Bregma
C
OTR-positive neurons (%)
Bregma
D
slope = 0.24
R² = 0.575
p<0.0001
Number of axo-dendritic contacts
Number of OTR-GFP neurons
E1
OTR
OT
SYN
DAPI
E2
1 + SYN
2 + SYN
3 + SYN
4 + SYN
F
OT-innervation (%)
OTR-
OTR+
G
SYN-positive OT innervation
OTR+
soma
dendrite
H
OT
vGluT2
I
OT fibers expressing vGlut2 (%)
vGluT2-
vGluT2+
J1
J2

Figure S3

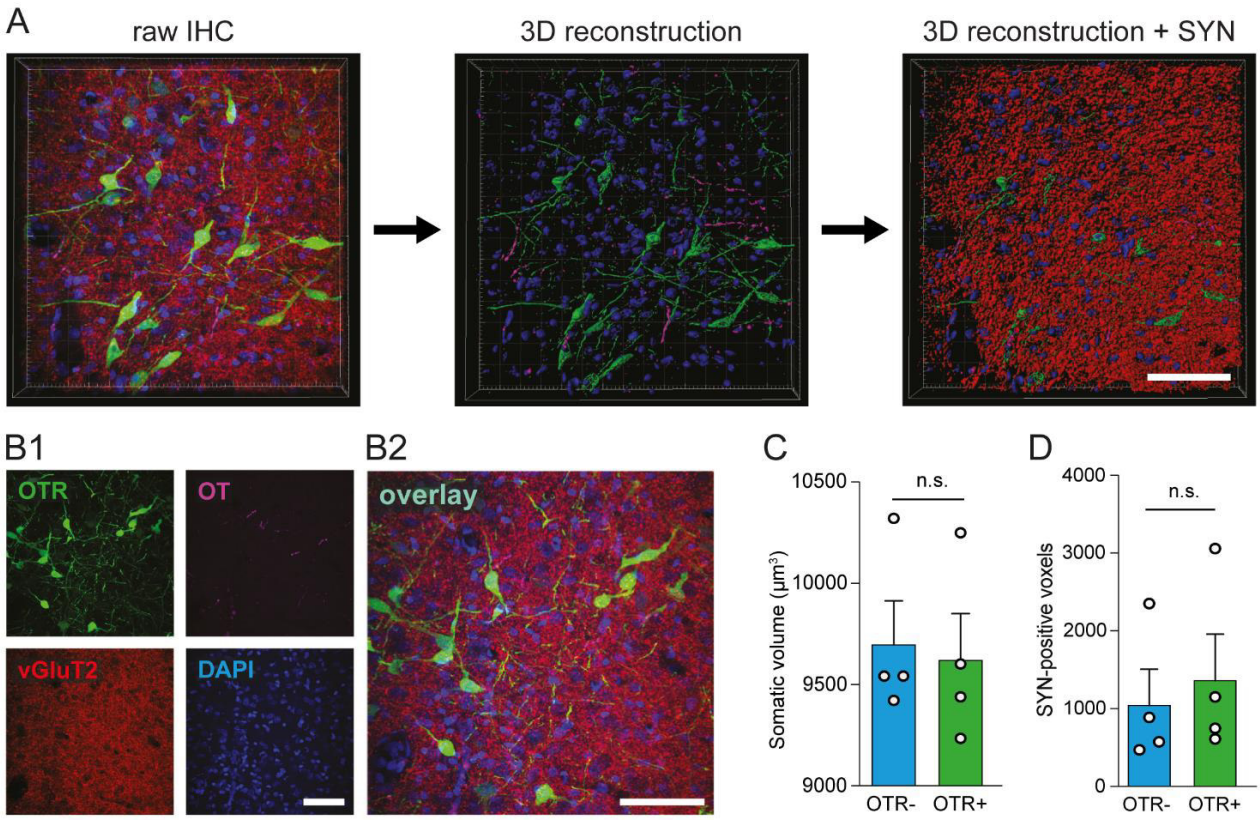
A
raw IHC
3D reconstruction
3D reconstruction + SYN
B1
OTR
OT
vGluT2
DAPI
B2
overlay
C
Somatic volume (µm³)
10500
10000
9500
9000
n.s.
OTR-
OTR+
D
SYN-positive voxels
4000
3000
2000
1000
0
n.s.
OTR-
OTR+

Figure 4

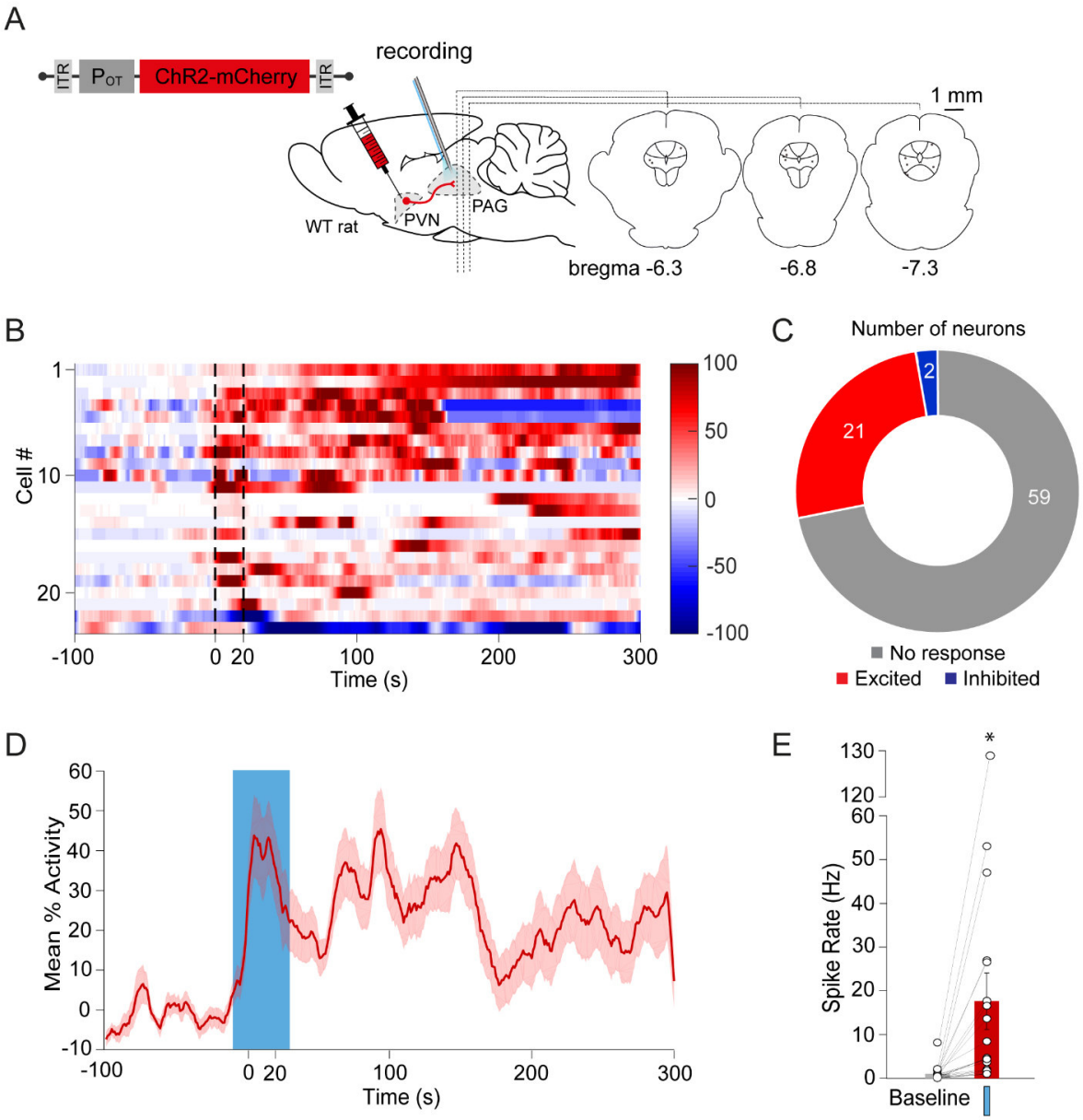
A
ITR
POT
ChR2-mCherry
ITR
recording
1 mm
WT rat
PVN
PAG
bregma -6.3
-6.8
-7.3
B
Cell #
Time (s)
C
Number of neurons
2
21
59
No response
Excited
Inhibited
D
Mean % Activity
Time (s)
E
Spike Rate (Hz)
Baseline
*

Figure S4

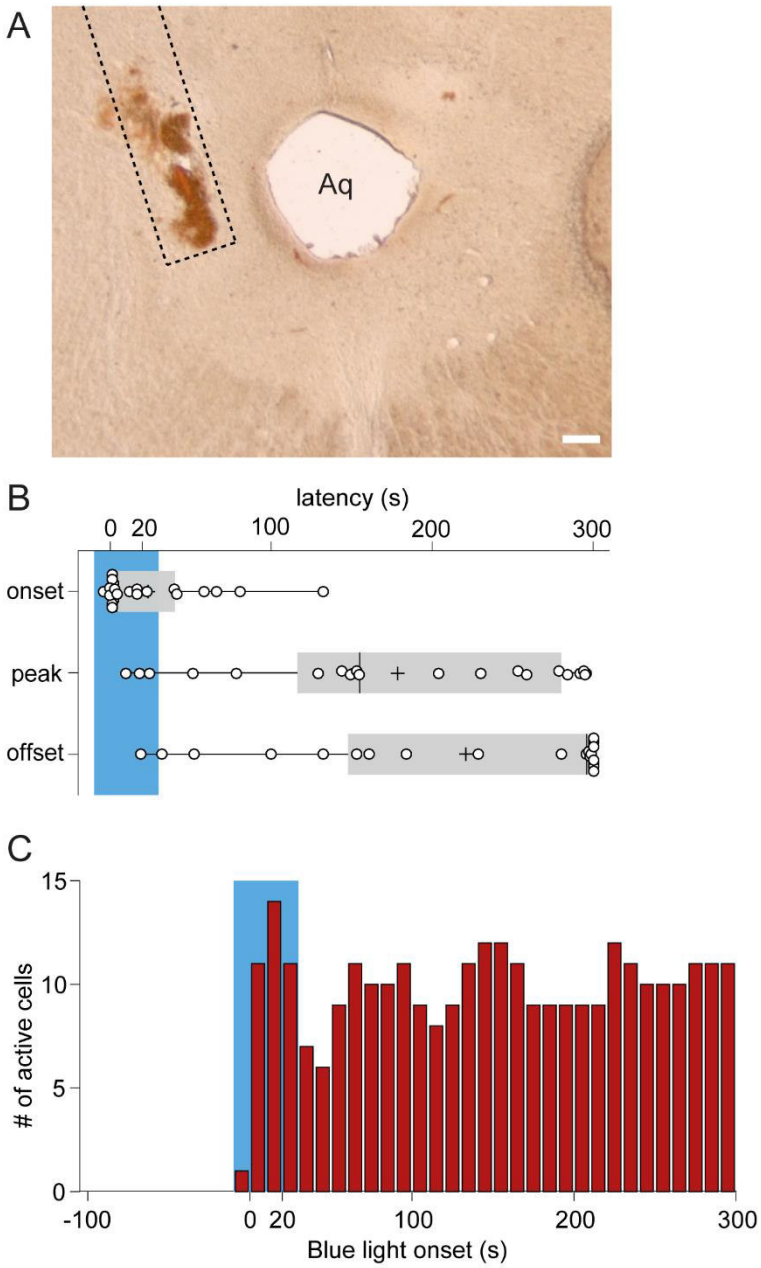
A
Aq
B
latency (s)
0 20
100
200
300
onset
peak
offset
C
15
10
5
0
# of active cells
-100
0 20
100
200
300
Blue light onset (s)

Figure 5

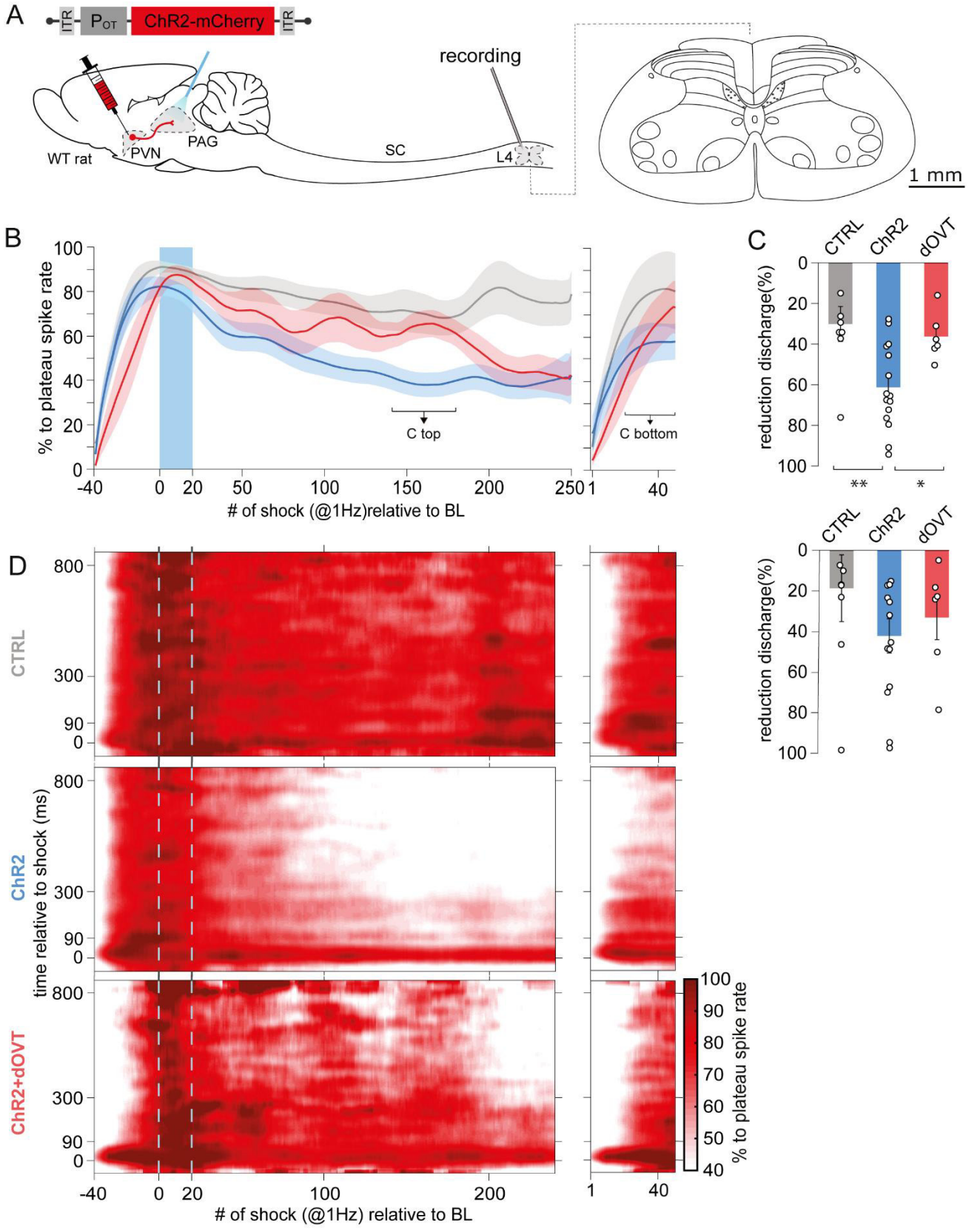
A
ITR
POT
ChR2-mCherry
ITR
recording
WT rat
PVN
PAG
SC
L4
1 mm
B
% to plateau spike rate
C top
C bottom
# of shock (@1Hz)relative to BL
C
CTRL
ChR2
dOVT
reduction discharge(%)
**
*
D
CTRL
ChR2
ChR2+dOVT
time relative to shock (ms)
# of shock (@1Hz) relative to BL
% to plateau spike rate

Figure S5

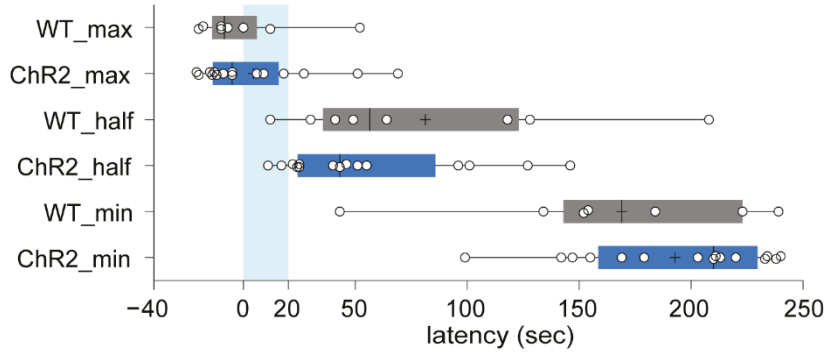
WT_max
ChR2_max
WT_half
ChR2_half
WT_min
ChR2_min
−40
0
20
50
100
150
200
250
latency (sec)

Figure 6

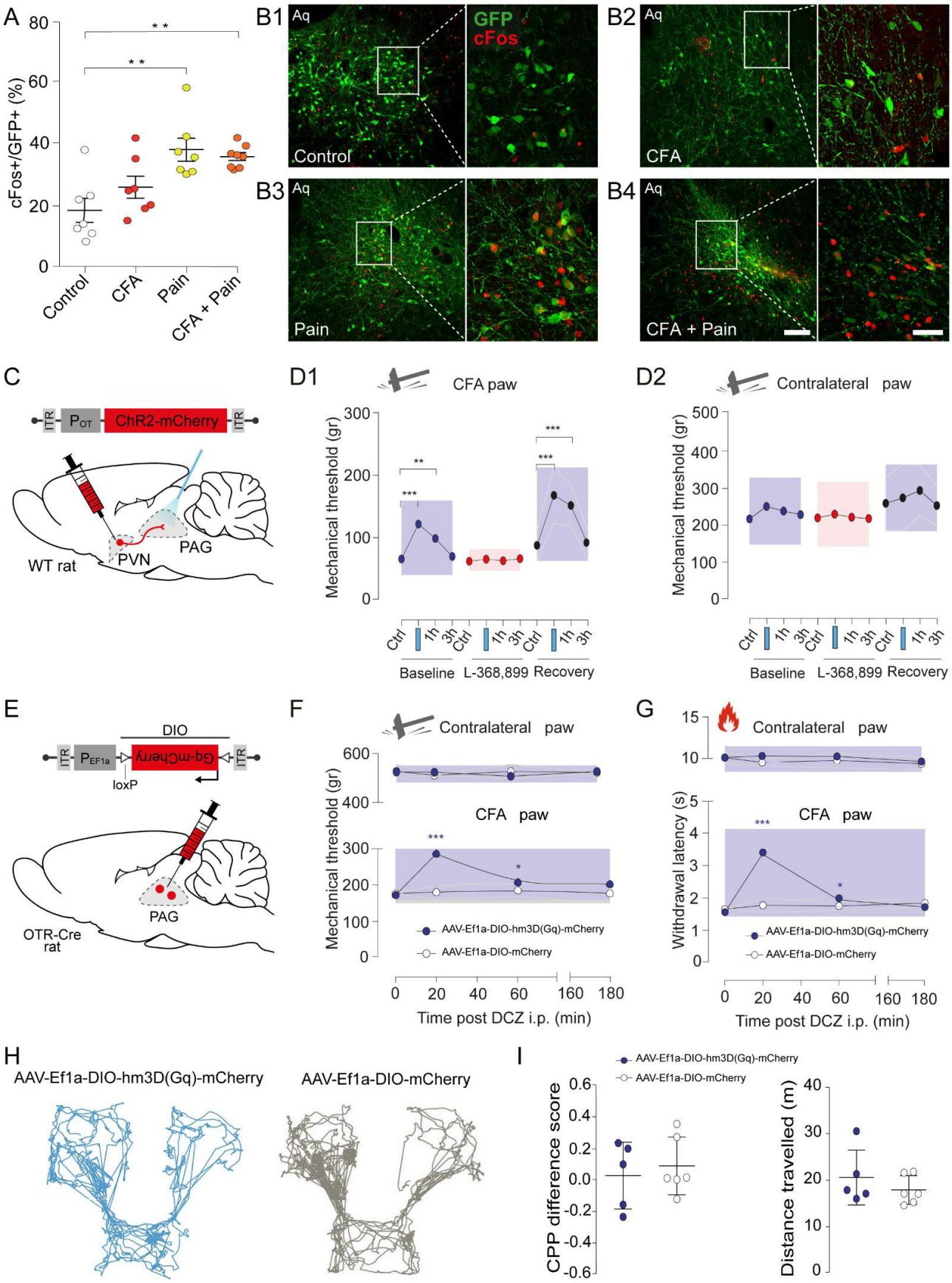
A
cFos+/GFP+ (%)
Control
CFA
Pain
CFA + Pain
B1
B2
B3
B4
Aq
GFP
cFos
Control
CFA
Pain
CFA + Pain
C
ITR
POT
ChR2-mCherry
PVN
PAG
WT rat
D1
CFA paw
Mechanical threshold (gr)
Ctrl
1h
3h
Baseline
L-368,899
Recovery
D2
Contralateral paw
E
DIO
PEF1a
Gq-mCherry
loxP
PAG
OTR-Cre rat
F
Contralateral paw
CFA paw
AAV-Ef1a-DIO-hm3D(Gq)-mCherry
AAV-Ef1a-DIO-mCherry
Time post DCZ i.p. (min)
G
Withdrawal latency (s)
H
AAV-Ef1a-DIO-hm3D(Gq)-mCherry
AAV-Ef1a-DIO-mCherry
I
CPP difference score
Distance travelled (m)

Figure S6

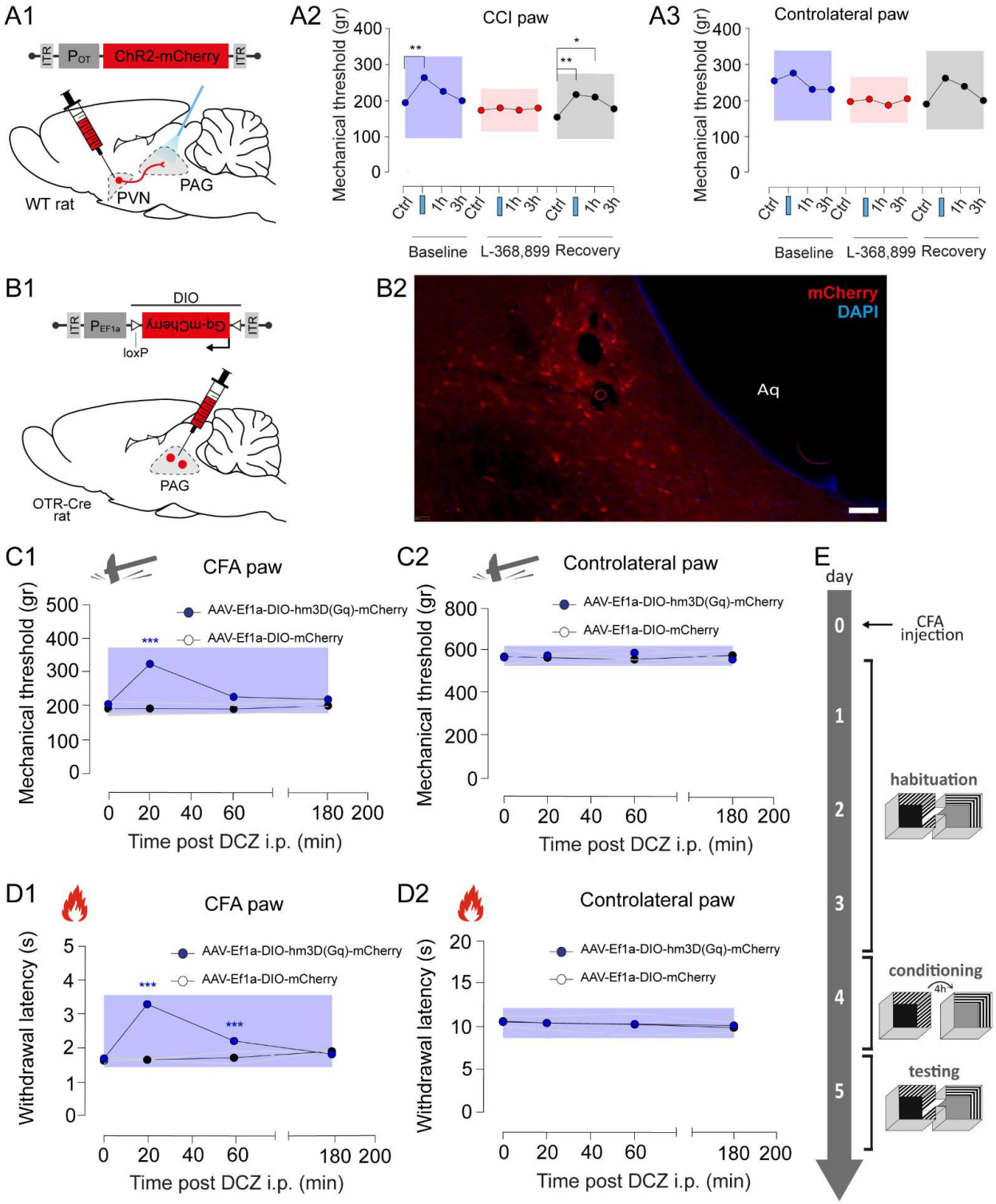
A1
ITR
POT
ChR2-mCherry
ITR
PAG
PVN
WT rat
A2
CCI paw
Mechanical threshold (gr)
400
300
200
100
0
**
*
**
Ctrl
1h
3h
Ctrl
1h
3h
Ctrl
1h
3h
Baseline
L-368,899
Recovery
A3
Controlateral paw
Mechanical threshold (gr)
400
300
200
100
0
Ctrl
1h
3h
Ctrl
1h
3h
Ctrl
1h
3h
Baseline
L-368,899
Recovery
B1
DIO
ITR
PEF1a
Gq-mCherry
ITR
loxP
PAG
OTR-Cre
rat
B2
mCherry
DAPI
Aq
C1
CFA paw
Mechanical threshold (gr)
500
400
300
200
100
0
AAV-Ef1a-DIO-hm3D(Gq)-mCherry
AAV-Ef1a-DIO-mCherry
***
0
20
40
60
180
200
Time post DCZ i.p. (min)
C2
Controlateral paw
Mechanical threshold (gr)
800
600
400
200
0
AAV-Ef1a-DIO-hm3D(Gq)-mCherry
AAV-Ef1a-DIO-mCherry
0
20
40
60
180
200
Time post DCZ i.p. (min)
E
day
0
CFA injection
1
habituation
2
3
conditioning
4h
4
testing
5
D1
CFA paw
Withdrawal latency (s)
5
4
3
2
1
0
AAV-Ef1a-DIO-hm3D(Gq)-mCherry
AAV-Ef1a-DIO-mCherry
***
***
0
20
40
60
180
200
Time post DCZ i.p. (min)
D2
Controlateral paw
Withdrawal latency (s)
20
15
10
5
0
AAV-Ef1a-DIO-hm3D(Gq)-mCherry
AAV-Ef1a-DIO-mCherry
0
20
40
60
180
200
Time post DCZ i.p. (min)

Figure 7

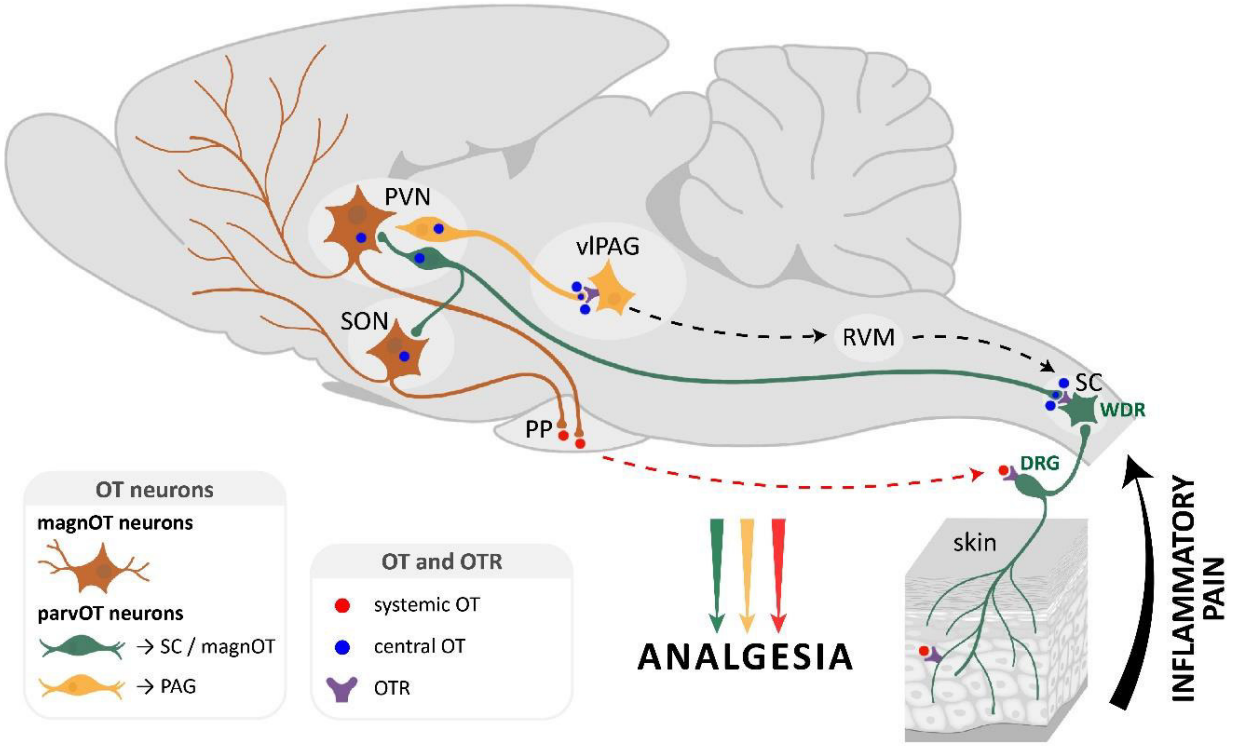
PVN
vlPAG
SON
RVM
SC
WDR
PP
DRG
skin
OT neurons
magnOT neurons
parvOT neurons
→ SC / magnOT
→ PAG
OT and OTR
systemic OT
central OT
OTR
ANALGESIA
INFLAMMATORY PAIN

Bibliography

Althammer, F., and Grinevich, V. (2017). Diversity of oxytocin neurons: beyond magno- and parvocellular cell types? J. Neuroendocrinol.

Althammer, F., Ferreira-Neto, H.C., Rubaharan, M., Roy, R.K., Patel, A.A., Murphy, A., Cox, D.N., and Stern, J.E. (2020). Three-dimensional morphometric analysis reveals time-dependent structural changes in microglia and astrocytes in the central amygdala and hypothalamic paraventricular nucleus of heart failure rats. J Neuroinflammation *17*, 221.

Austin, P.J., Wu, A., and Moalem-Taylor, G. (2012). Chronic Constriction of the Sciatic Nerve and Pain Hypersensitivity Testing in Rats. J Vis Exp 3393.

Basbaum, A.I., Marley, N.J.E., O'Keefe, J., and Clanton, C.H. (1977). Reversal of morphine and stimulus-produced analgesia by subtotal spinal cord lesions. Pain *3*, 43–56.

Betley, J.N., Cao, Z.F.H., Ritola, K.D., and Sternson, S.M. (2013). Parallel, redundant circuit organization for homeostatic control of feeding behavior. Cell *155*, 1337–1350.

Boll, S., Almeida de Minas, A.C., Raftogianni, A., Herpertz, S.C., and Grinevich, V. (2018). Oxytocin and Pain Perception: From Animal Models to Human Research. Neuroscience *387*, 149–161.

Buijs, R.M. (1978). Intra- and extrahypothalamic vasopressin and oxytocin pathways in the rat. Pathways to the limbic system, medulla oblongata and spinal cord. Cell Tissue Res. *192*, 423–435.

Buijs, R.M. (1983). Vasopressin and oxytocin—their role in neurotransmission. Pharmacology & Therapeutics *22*, 127–141.

Busnelli, M., and Chini, B. (2017). Molecular Basis of Oxytocin Receptor Signalling in the Brain: What We Know and What We Need to Know. Curr Top Behav Neurosci.

Busnelli, M., Kleinau, G., Muttenthaler, M., Stoev, S.B., Manning, M., Bibic, L., Howell, L.A., McCormick, P.J., Di Lascio, S., Braida, D., et al. (2016). Design and characterization of superpotent bivalent ligands targeting oxytocin receptor dimers via a channel-like structure. J. Med. Chem.

Campbell, P., Ophir, A.G., and Phelps, S.M. (2009). Central vasopressin and oxytocin receptor distributions in two species of singing mice. J Comp Neurol *516*, 321–333.

Chaure, F.J., Rey, H.G., and Quian Quiroga, R. (2018). A novel and fully automatic spike-sorting implementation with variable number of features. Journal of Neurophysiology *120*, 1859–1871.

Chini, B., Verhage, M., and Grinevich, V. (2017). The Action Radius of Oxytocin Release in the Mammalian CNS: From Single Vesicles to Behavior. Trends Pharmacol. Sci.

DeLaTorre, S., Rojas-Piloni, G., Martínez-Lorenzana, G., Rodríguez-Jiménez, J., Villanueva, L., and Condés-Lara, M. (2009). Paraventricular oxytocinergic hypothalamic prevention or interruption of long-term potentiation in dorsal horn nociceptive neurons: electrophysiological and behavioral evidence. Pain *144*, 320–328.

Eliava, M., Melchior, M., Knobloch-Bollmann, H.S., Wahis, J., da Silva Gouveia, M., Tang, Y., Ciobanu, A.C., Triana Del Rio, R., Roth, L.C., Althammer, F., et al. (2016). A New Population of Parvocellular Oxytocin Neurons Controlling Magnocellular Neuron Activity and Inflammatory Pain Processing. Neuron *89*, 1291–1304.

Fields, H.L. (2000). Pain modulation: expectation, opioid analgesia and virtual pain. Prog Brain Res *122*, 245–253.

González-Hernández, A., Manzano-García, A., Martínez-Lorenzana, G., Tello-García, I.A., Carranza, M., Arámburo, C., and Condés-Lara, M. (2017). Peripheral oxytocin receptors inhibit the nociceptive input signal to spinal dorsal horn wide dynamic range neurons. Pain.

Haeussler, M., Schönig, K., Eckert, H., Eschstruth, A., Mianné, J., Renaud, J.-B., Schneider-Maunoury, S., Shkumatava, A., Teboul, L., Kent, J., et al. (2016). Evaluation of off-target and on-target scoring algorithms and integration into the guide RNA selection tool CRISPOR. Genome Biol *17*, 148.

Harris, J.A., Hirokawa, K.E., Sorensen, S.A., Gu, H., Mills, M., Ng, L.L., Bohn, P., Mortrud, M., Ouellette, B., Kidney, J., et al. (2014). Anatomical characterization of Cre driver mice for neural circuit mapping and manipulation. Frontiers in Neural Circuits *8*, 76.

Hasan, M.T., Althammer, F., Silva da Gouveia, M., Goyon, S., Eliava, M., Lefevre, A., Kerspern, D., Schimmer, J., Raftogianni, A., Wahis, J., et al. (2019). A Fear Memory Engram and Its Plasticity in the Hypothalamic Oxytocin System. Neuron.

Herpertz, S.C., Schmitgen, M.M., Fuchs, C., Roth, C., Wolf, R.C., Bertsch, K., Flor, H., Grinevich, V., and Boll, S. (2019). Oxytocin Effects on Pain Perception and Pain Anticipation. J Pain.

Herrero, J.F., Laird, J.M., and López-García, J.A. (2000). Wind-up of spinal cord neurones and pain sensation: much ado about something? Prog Neurobiol *61*, 169–203.

Hilfiger, L., Zhao, Q., Kerspern, D., Inquimbert, P., Andry, V., Goumon, Y., Darbon, P., Hibert, M., and Charlet, A. (2020). A Nonpeptide Oxytocin Receptor Agonist for a Durable Relief of Inflammatory Pain. Sci Rep *10*, 3017.

Hsu, P.D., Scott, D.A., Weinstein, J.A., Ran, F.A., Konermann, S., Agarwala, V., Li, Y., Fine, E.J., Wu, X., Shalem, O., et al. (2013). DNA targeting specificity of RNA-guided Cas9 nucleases. Nat Biotechnol *31*, 827–832.

King, T., Vera-Portocarrero, L., Gutierrez, T., Vanderah, T.W., Dussor, G., Lai, J., Fields, H.L., and Porreca, F. (2009). Unmasking the tonic-aversive state in neuropathic pain. Nat Neurosci *12*, 1364–1366.

Knobloch, H.S., Charlet, A., Hoffmann, L.C., Eliava, M., Khrulev, S., Cetin, A.H., Osten, P., Schwarz, M.K., Seeburg, P.H., Stoop, R., et al. (2012). Evoked Axonal Oxytocin Release in the Central Amygdala Attenuates Fear Response. Neuron *73*, 553–566.

Knobloch, S., Charlet, A., Stoop, R., and Grinevich, V. (2014). Viral Vectors for Optogenetics of Hypothalamic Neuropeptides | Springer Nature Experiments.

Landgraf, R., and Neumann, I.D. (2004). Vasopressin and oxytocin release within the brain: a dynamic concept of multiple and variable modes of neuropeptide communication. Frontiers in Neuroendocrinology *25*, 150–176.

Leng, G., and Ludwig, M. (2015). Intranasal Oxytocin: Myths and Delusions. Biol. Psychiatry.

Liebeskind, J.C., Guilbaud, G., Besson, J.M., and Oliveras, J.L. (1973). Analgesia from electrical stimulation of the periaqueductal gray matter in the cat: behavioral observations and inhibitory effects on spinal cord interneurons. Brain Res *50*, 441–446.

Melzack, R. (1975). Prolonged relief of pain by brief, intense transcutaneous somatic stimulation. Pain *1*, 357–373.

Mendell, L.M., and Wall, P.D. (1965). RESPONSES OF SINGLE DORSAL CORD CELLS TO PERIPHERAL CUTANEOUS UNMYELINATED FIBRES. Nature *206*, 97–99.

Moreno-López, Y., Martínez-Lorenzana, G., Condés-Lara, M., and Rojas-Piloni, G. (2013). Identification of

oxytocin receptor in the dorsal horn and nociceptive dorsal root ganglion neurons. Neuropeptides *47*, 117–123.
Muttenthaler, M., Andersson, Å., Vetter, I., Menon, R., Busnelli, M., Ragnarsson, L., Bergmayr, C., Arrowsmith, S., Deuis, J.R., Chiu, H.S., et al. (2017). Subtle modifications to oxytocin produce ligands that retain potency and improved selectivity across species. Sci Signal *10*.
Nagai, Y., Miyakawa, N., Takuwa, H., Hori, Y., Oyama, K., Ji, B., Takahashi, M., Huang, X.-P., Slocum, S.T., DiBerto, J.F., et al. (2020). Deschloroclozapine, a potent and selective chemogenetic actuator enables rapid neuronal and behavioral modulations in mice and monkeys. Nat. Neurosci.
Nasanbuyan, N., Yoshida, M., Takayanagi, Y., Inutsuka, A., Nishimori, K., Yamanaka, A., and Onaka, T. (2018). Oxytocin-Oxytocin Receptor Systems Facilitate Social Defeat Posture in Male Mice. Endocrinology *159*, 763–775.
Ogawa, S., Kow, L.M., and Pfaff, D.W. (1992). Effects of lordosis-relevant neuropeptides on midbrain periaqueductal gray neuronal activity in vitro. Peptides *13*, 965–975.
Poisbeau, P., Grinevich, V., and Charlet, A. (2017). Oxytocin Signaling in Pain: Cellular, Circuit, System, and Behavioral Levels. Curr Top Behav Neurosci.
van den Pol, A.N. (2012). Neuropeptide transmission in brain circuits. Neuron *76*, 98–115.
Ritz, L.A., and Greenspan, J.D. (1985). Morphological features of lamina V neurons receiving nociceptive input in cat sacrocaudal spinal cord. J Comp Neurol *238*, 440–452.
Schönig, K., Schwenk, F., Rajewsky, K., and Bujard, H. (2002). Stringent doxycycline dependent control of CRE recombinase in vivo. Nucleic Acids Res *30*, e134.
Schouenborg, J. (1984). Functional and topographical properties of field potentials evoked in rat dorsal horn by cutaneous C-fibre stimulation. J Physiol *356*, 169–192.
Tang, Y., Benusiglio, D., Lefevre, A., Hilfiger, L., Althammer, F., Bludau, A., Hagiwara, D., Baudon, A., Darbon, P., Schimmer, J., et al. (2020). Social touch promotes interfemale communication via activation of parvocellular oxytocin neurons. Nat. Neurosci.
Tovote, P., Fadok, J.P., and Lüthi, A. (2015). Neuronal circuits for fear and anxiety. Nat. Rev. Neurosci. *16*, 317–331.
Wahis, J., Baudon, A., Althammer, F., Kerspern, D., Goyon, S., Hagiwara, D., Lefevre, A., Barteczko, L., Boury-Jamot, B., Bellanger, B., et al. (2021). Astrocytes mediate the effect of oxytocin in the central amygdala on neuronal activity and affective states in rodents. Nat Neurosci.
Wefers, B., Meyer, M., Ortiz, O., Angelis, M.H. de, Hansen, J., Wurst, W., and Kühn, R. (2013). Direct production of mouse disease models by embryo microinjection of TALENs and oligodeoxynucleotides. PNAS *110*, 3782–3787.
Yalcin, I., Megat, S., Barthas, F., Waltisperger, E., Kremer, M., Salvat, E., and Barrot, M. (2014). The Sciatic Nerve Cuffing Model of Neuropathic Pain in Mice. JoVE (Journal of Visualized Experiments) e51608.
Yang, J., Li, P., Liang, J.-Y., Pan, Y.-J., Yan, X.-Q., Yan, F.-L., Hao, F., Zhang, X.-Y., Zhang, J., Qiu, P.-Y., et al. (2011). Oxytocin in the periaqueductal grey regulates nociception in the rat. Regul Pept *169*, 39–42.

DISCUSSION

DISCUSSION

During my thesis, I participated in the study of the analgesic potential of new innovative molecules, which target endogenous analgesic systems. As these different points are already discussed independently in the previous articles, I will go here a step further and divide this discussion following the main studies exposed in this manuscript.

First, I will develop the potential of monoterpenes as analgesic compounds, their limitations, key points to be investigated and the synergy through a combination of different monoterpenes to produce new analgesic treatments. Secondly, I will discuss about the potential of LIT-001 as an analgesic compound as well as its drawbacks to improve it for therapeutic application. Furthermore, I will delve into the role of the OT system in the analgesia in order to propose hypothesis regarding the mechanisms of induction of the anti-hyperalgesic effects of LIT-001. Finally, I will propose in a global discussion to picture these compounds together in a multi pharmacological treatment, their potential effects, their cost and the transposition of all these observations from the animal model to humans.

1. Menthol and pulegone, two monoterpenes with anti-hyperalgesic properties, and their combination, an innovative analgesic treatment

In the study of the analgesic properties of menthol and pulegone, we confirm in our model of CFA induced hyperalgesia their anti-hyperalgesic potential. We also identified that pulegone was able to reduce mechanical, thermal, hot and cold hypersensitivity. In contrast, menthol was able to reduce mechanical and hot hypersensitivity, but was unable to reduce cold hypersensitivity. These finding are very interesting because menthol is a known agonist of TRPM8, the cold sensor. Furthermore, there are also studies that indicate the opposite, that menthol has effects on cold sensitivity (**Table 2**).

On the one hand, menthol could inhibit the nociceptive stimulus by activating $GABA_a$ R and inhibiting Na^+ / Ca^{2+} channels (**Figure 12**). This could explain the overall analgesic effects on mechanical and hot sensitivities. This, combined with the activation of TRPM8 and thus the non-nociceptive cold sensation induces phenomenon called cold analgesia (Dhaka et al., 2007). This would enhance these anti-hyperalgesic effects specially in an inflammatory pain model with TRPA1 / TRPV1 hyperexcitability (hypersensitivity for thermal hot modality). On the other hand, in the case of a thermal sensitivity test to cold, the activation of TRPM8 by menthol, would exacerbates this sensitivity and therefore does not allow us to observe a reduction in hypersensitivity to this modality. This could be a clue to the difference observed between the effects of menthol and pulegone. However, we did observe a slight non-significant tendency in the reduction of cold sensitivity for the optimal dose of 100 mg/kg, which may correspond, to the antinociceptive effects of the other menthol targets ($GABA_a$ R, Na^+, Ca^{2+} channels, etc.) (**Table 4**).

Another point to underline is that the acetone test we performed is based on four stages scoring (0, 1, 2 or 3). Maybe a more detailed scoring, for example in five stages, would have allowed us to observe more subtle significant differences. We also could have used another cold sensitivity test like the cold plate (Klein et al., 2010) (or the dynamic cold plate) with which we would have had a temporal value like for the plantar. However, studies showing effects on cold sensitivity have also used cold sensitivity tests (**Table 2**), but in other models with a topic application of menthol. The lack of effect observed in our study is perhaps due to these differences.

Although similar to menthol, pulegone has slightly more potent anti-hyperalgesic effects than menthol. Variations in target and affinity could explain these differences in potency. Regarding the effects of pulegone on ion channels, the lack of knowledge about the interactions really limits the possibilities of understanding. With only four articles and four known targets, it is complicated for the moment to go further in the comparison between menthol and pulegone (**Table 4**). However, it can be noted that both have an inhibitory effect on 5-HT_3 R and an activating effect on TRPV1 at similar concentrations. Menthol has inhibitory effects on TRPV1 at high concentrations (> 3 mM). Opposite effects have been identified for the K^+ channels, activator for menthol and inhibitor for pulegone. A biphasic effect on TRPM8 for pulegone has been identified (activator at low concentration and inhibitor at high concentration), which

could explain the difference in anti-hyperalgesic effects on cold sensitivity of pulegone compared to menthol observed in our study.

Based on the structural similarity with menthol and the shared targets of the majority of monoterpenes, it is possible to propose potential targets and mechanisms that could explain pulegone anti-hyperalgesic effects. It must be noted that these are hypotheses based on the data from **Table 4** and the synthesis made with the **Figure 12**.

Therefore, it can be envisaged that pulegone, at high concentration, blocks TRPA1 and TRPV1 like menthol does at high concentration (> 3 mM). Thus, by blocking the TRPs mostly involved in the perception of nociceptive signals (TRPV1 activated by noxious heat ≥ 43°C; TRPA1 activated by noxious cold ≤ 18°C) pulegone would then inhibit the generation of the nociceptive signal directly at the peripheral ending of nociceptors (for review; (Dai, 2016)). Moreover, by inhibiting TRPM8 (activated by non-noxious cold ≤ 25°C) at high dose, pulegone then blocks the detection of noxious cold stimuli. Indeed TRPM8, in basal condition is a non-nociceptive cold sensor, but its activation is essential for the detection of cold nociceptive signals by TRPA1 (Dhaka et al., 2007). This could explain the difference in anti-hyperalgesic effect for cold sensitivity between menthol and pulegone. TRPV3 (activated by non-nociceptive warm ≥ 34°C) is activated by menthol, could also be activated by pulegone. Thus, the opening of TRPV3 would activate the Aβ-fibres (non-nociceptive) leading to the activation of inhibitory interneurons, as proposed by GCT (**Figure 3**) and then promote an inhibition of the nociceptive signal at the level of the projection neurons (Melzack and Wall, 1965).

In addition to these effects on TRPs, it should also be taken into account that monoterpenes generally activate $GABA_a$ R and Gly R, which promote the inhibition of projection neurons in the spinal cord. This is completed by the inhibition of Ca^{2+} and Na^{+} channels by pulegone, which will therefore reduce depolarisation in neurons (nociceptors, projection neurons) and therefore the transmission of the nociceptive signal (Bell, 2018).

To summarise, the potential targets and mechanisms of pulegone and menthol, explaining their anti-hyperalgesic effects, are multiple and potentially involve all the targets listed in the previous section.

Taken as a pure analgesic compound, the interests of monoterpenes are limited due to their high cytotoxicity, and their lack of patentability. To address these drawbacks, we have developed a mix of menthol and pulegone with BENEPHYT. This is interesting because pulegone shows variations in targets and affinity (as seen previously) despite the close similarity with menthol. These variations may explain the differences in the anti-hyperalgesic effects of the two monoterpenes.

The results of the anti-hyperalgesic effects of the menthol and pulegone mix showed that they have synergic effects (**Annex 4 Terpene combination**). However, these effects differ depending on the modality studied (i.e. involving different TRP and nociceptors). For mechanical sensitivity at equivalent doses of terpenes (100 mg/kg pulegone or menthol and 50 mg/kg pulegone + 50 mg/kg menthol) there is no variation in effects. Therefore, it is very interesting because you decrease the concentration of each monoterpene needed and potentially reduce the side effects or increase the analgesic potential. However, it is possible that they act on the same sites of the channels/receptors to activate, potentiate, inhibit or block them, in which case it is not relevant in terms of synergistic effects to decrease the concentration. In addition, for thermal hot and cold sensitivities, in which anti-hyperalgesic effects of menthol are weaker than pulegone, we observe that the effect of the mix is in between the effects of menthol and pulegone seperatly. However, they are still far superior to pulegone and menthol alone at 50 mg/kg. It could be argued that what is observed is closer to a cumulative effect on the same or similar targets than a strong synergetic effect.

These results are interesting for their novelty but perhaps pulegone and menthol are structurally too close (pulegone is a precursor of menthone which is the precursor of menthol) (**Figure 10**) to have a potent synergetic effect. Presumably, combining monoterpenes with analgesic/anti-hyperalgesic properties from all three structural groups and having "compatible" effects on their targets would then induce stronger synergic effects.

For example, by mixing three analgesic terpenes (**Table 2**), borneol (bicyclic) with menthol or pulegone (cyclic) and geraniol (acyclic), we would have a diversity of chemical structures (**Figure 10**). This diversity would enable to target different binding sites on same channels/receptors (with more or less affinity depending on the monoterpene) and thus potentially have a synergic effect (**Figure 22**). With the data

from the **Table 4**, we may assume the overall effect of such mix (borneol x geraniol x menthol) on the ion channels involved in nociception (**Figure 22**).

Moreover, there is apparently no habituation effect, as a series of experiments has shown that the anti-hyperalgesic effects do not decrease during a repeated injection experiment (twice a day for 10 days) (Peana et al., 2002; Batista et al., 2010). This absence of habituation increases the potential interest of such anti-hyperalgesic mix of monoterpene especially when compared to morphine. The potential long-term hepatotoxicity of such a treatment (2 time a day for 2 weeks) should therefore be monitored, along with the anti-hyperalgesic effects, in order to control whether the mix is interesting for patenting and market launch.

Indeed, the hepatotoxicity (*in vivo*) of monoterpenes is established by the formation of metabolites and reactive oxygen species when high doses of monoterpenes (> 200 mg/kg i.p.) are administered (Zárybnický et al., 2018). In our study, we observed that the optimal dose of monoterpenes is 100 mg/kg, which is much lower than the hepatotoxic doses. On the other hand, given the rapid decrease in the anti-hyperalgesic effects of menthol and pulegone (approximately 1 hour), it is likely that they are rapidly metabolised (glucunorisation) and degraded to be excreted in the urine. It is therefore conceivable that taking the treatment several hours apart may induce little or no hepatotoxicity and therefore we are in a context similar to that of paracetamol, which must be taken at intervals to avoid hepatotoxicity (Mahadevan, 2005).

Additionally, in the development of a monoterpene mix, anti-inflammatory effects (**Figure 11**) must be taken into account in addition to the anti-nociceptive effects (**Figure 22**). Several studies have shown that pre-treatment (citral) (Quintans-Júnior et al., 2011) or chronic treatment with monoterpenes (linalool) (Peana et al., 2002) can inhibit the development of inflammation or reduce the volume of oedema in a CFA model (de Cássia da Silveira e Sá et al., 2013). Although not detected in our study, probably a single injection of monoterpene after the induction of oedema is not sufficient to significantly decrease its volume. The role of these anti-inflammatory effects has not to be neglected in the assessed anti-hyperalgesia.

Concerning the sedative effects of monoterpenes described in the literature at very high doses (≥ 150 mg/kg) (Sousa et al., 2007; Silveira et al., 2014) the most logical

hypothesis to explain these effects is that the very high concentration monoterpenes inhibit a consequent number of neurons. The inhibition of neurons could be due to the blocking of Ca^{2+}, Na^{+} channels and the activation of $GABA_a$ R and Gly R, which would then inhibit the nervous system of a given area, such as benzodiazepines, which are positive modulators of GABAa R and have sedative properties (classified as psychotropic) (Nielsen, 2015).

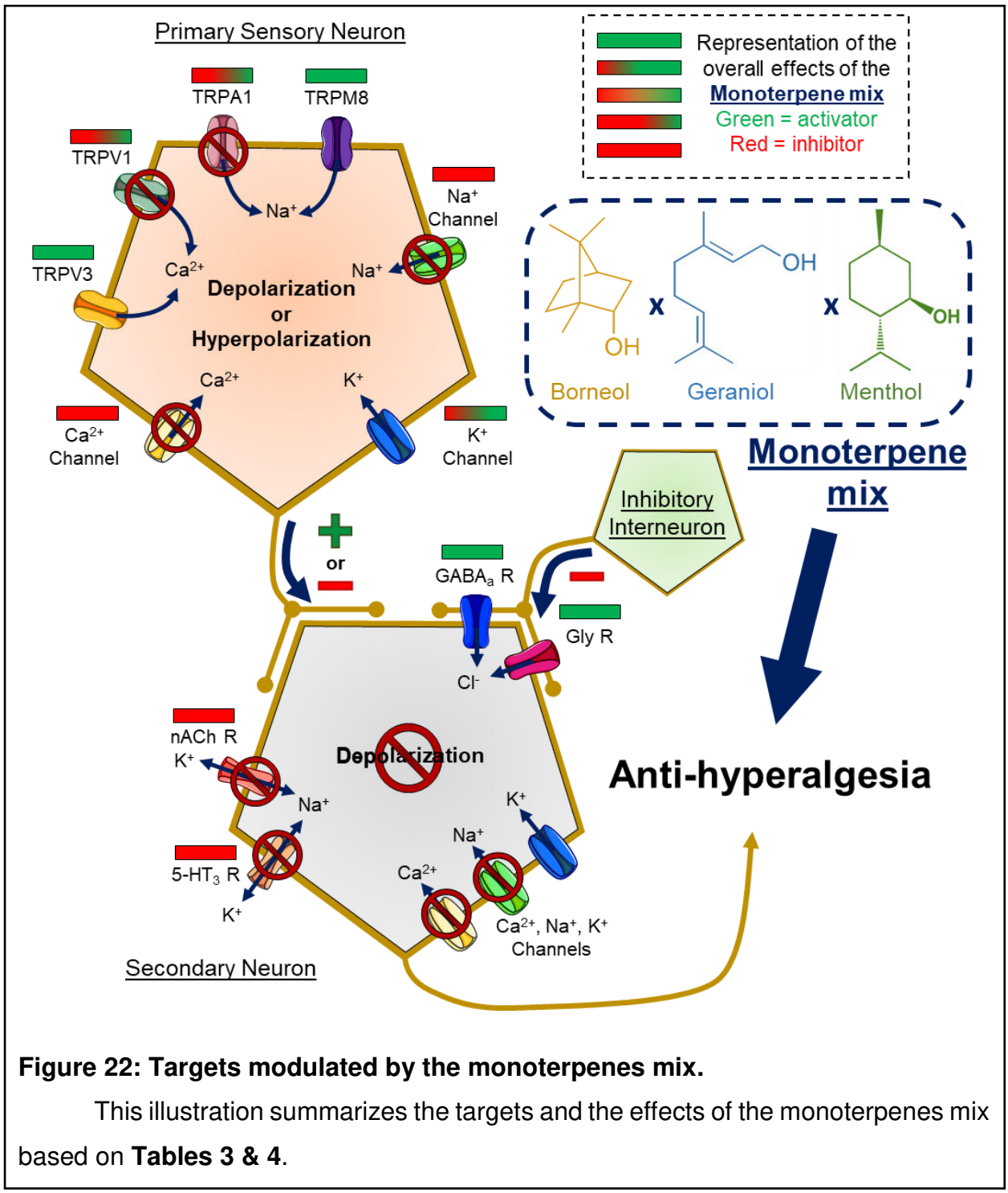

Figure 22: Targets modulated by the monoterpenes mix.

This illustration summarizes the targets and the effects of the monoterpenes mix based on **Tables 3 & 4**.

Monoterpenes as a whole are interesting but limited compounds due to their many drawbacks. However, the mixture of monoterpenes could address these drawbacks and even increase their potential with synergistic effects. Therefore, the use of monoterpene mixture is promising and innovative in the field of analgesic compounds.

2. LIT-001 the first non-peptidergic agonist of the oxytocin receptor that triggers the analgesic properties of the oxytocin system

In the study of the analgesic properties of LIT-001, we were able to identify its potential as an anti-hyperalgesic treatment. Taken as a pure analgesic molecule, its interest resides particularly on the duration of its effect (> 5 hours), which is similar if not slightly longer than the duration of the analgesic effects observed after an acute injection of morphine (in mice) (Bhalla et al., 2002). The long-lasting effects are probably due to its high stability and its distribution throughout the organism. However, it should be noted that the onset of analgesic effects starts between 30 minutes and 1 hour and is very much due to the activation of the OT system and OTR (highlighted by L-368,699), which by its GPCR nature has a synergy of activation, less instantaneous than an ion channels (Gimpl and Fahrenholz, 2001).

The analgesic or anti-hyperalgesic potency measured here in our CFA model indicates that LIT-001 leads to a decrease of around 50 % of the induced hypersensitivity (mechanical and thermal). LIT-001 therefore induces a very clear anti-hyperalgesic effect but not quite as powerful as an analgesia or even an anaesthesia induced by an opioid such as morphine (at equivalent relative dose) (Soignier et al., 2011). LIT-001 can therefore be considered as a first/second order analgesic therapeutic molecule (Hylands-White et al., 2017) that would offer an alternative to COX inhibitor and light opioids (VIDAL, 2021a).

A detailed understanding of the anti-hyperalgesic effects of LIT-001 also requires an understanding of the OT network and is necessary for clinical applications. The integration of the role of the PAG OTR neurons in Grinevich and Charlet figure

(2017) of OT-induced analgesia (**Figure 19**) is essential for the overall understanding of the OT system (**Figure 23**). Thus, based on the work of the role of the PVN → PAG → WDR circuit in analgesia, we were able to establish the role of a new population of PVN parvOT neurons that activates PAG OTR neurons, which activate inhibitory descending controls and consequently lead to inhibition of WDR neurons and analgesia (**Figure 23**). Additionally, a distinct population of PVN parvOT neurons, also plays a key role in the OT-induced analgesia system, by directly inhibiting WDR neurons through direct OT release at the spinal level and also leading to analgesia (**Figure 23**) (Eliava et al., 2016). These works allow us to realise that there are several central pathways that allow OT to regulate nociception. To these central pathways must be added the peripheral pathway that reaches the DRG OTR neurons and nociceptors endings through blood and dermal release of OT (**Figure 23**) (González-Hernández et al., 2017). This duplication of control pathways probably allows for a more precise regulation of analgesic effects and must play an essential role in mammalian life.

Thus with the help of these works we may assume sites of action of LIT-001 (**Figure 23**). Although, due to its ability to cross the BBB it can affect the OT system at all levels. We suppose that the majority of the analgesic effects are mediated by the nociceptors expressing OTR and the spinal WDR neurons especially after i.p. injection. However, the type of administration conditions those effects. For example, an intranasal administration of LIT-001 is expected to have more effect on CNS OTR neurons and supraspinal structures than an i.p. injection.

However, the potential interest of LIT-001 for clinical purposes is that beyond the anti-hyperalgesic effects, there is a modulation of pain-induced disorders, such as anxiety, depression, loss of social interaction, impaired food intake or stress (mainly in chronic pain) (Lumley et al., 2011). Indeed, alleviating this large variety of pain-related symptoms can significantly improve the patient's quality of life, one of the main goals of modern medicine. In this regard, targeting the OTR with LIT-001 is particularly relevant as OTR activation is known to induce a variety of molecular cascades resulting in significant positive modulation of nociception, social recognition and interactions, anxiety, eating behaviour and stress, all important comorbidity factors in painful patients (**Figure 17**) (Jurek and Neumann, 2018).

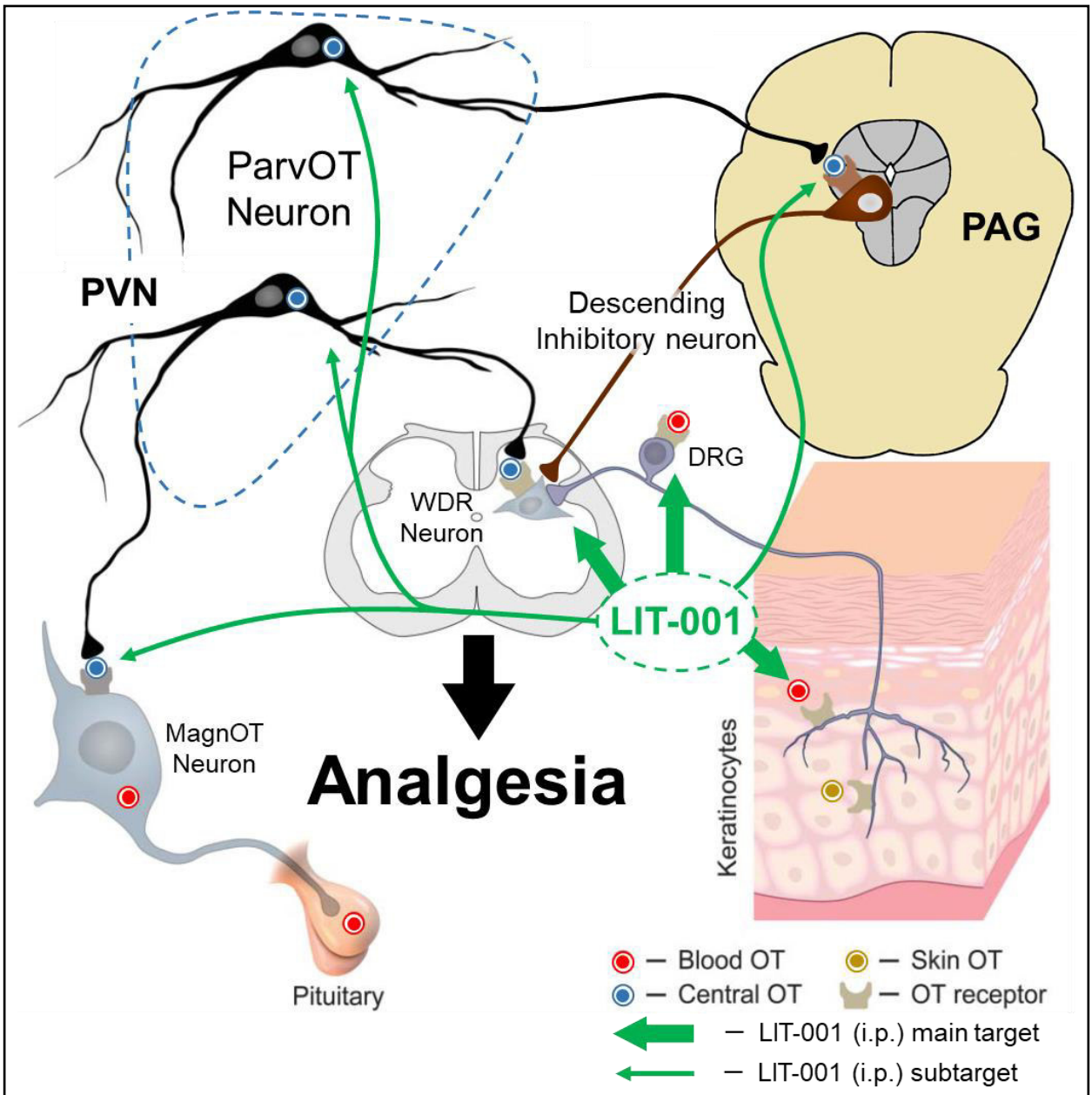

Figure 23: Updated oxytocin mediated peripheral and central analgesia.

LIT-001 (i.p.) acts on the OT system through major targets. On WDR neurons of the spinal cord, on the DRG cell body and peripheral ending of nociceptors. It also reaches subtargets, the descending inhibitory neurons of the PAG, the PVN parvOT and magnOT neurons. *Adapted from: Grinevich & Charlet (2017).*

Indeed, Frantz et *al.* study has already demonstrated that LIT-001 positively modulates behaviours by improving social interactions in a mouse model of autism (Frantz et al., 2018). Furthermore, we also point out in our study that LIT-001 crosses the BBB and is found in significant amounts in the brain and CSF (**Figure 23**). It is

therefore highly likely that LIT-001 has the potential to modulate such pain related disorders. We could have controlled the anxiety with an elevated plus maze test by injecting LIT-001 i.p. at anti-hyperalgesic doses (100 mg/kg). It is well known that an intracerebral injection of OT or TGOT (its agonist) decreases the time spent in the closed arms during the elevated plus maze test (Wahis et al., 2021). Potentially an i.p. injection of LIT-001 could induce a decrease in anxiety, although less marked than an intracerebral injection of OT or TGOT. Nevertheless, it is conceivable that these anxiolytic effects could be significant and potentially quite potent when administered intranasally.

As previously discussed, it is assumed that intranasal administration of LIT-001 would have a more pronounced effect on anxiety as it would reach supraspinal structures and OTR neurons more efficiently. However, it would also support a release of OT into the bloodstream from the pituitary magnOT neurons (**Figure 23**). Nevertheless, the intranasal administration of OT is currently very controversial.

Intranasal application of OT starts in 1958, to facilitate lactation in women (Newton and Egli, 1958). The postulate suggests that once administered intra-nasally, OT reaches the bloodstream through the mucosa, and then penetrates the brain via internalization into olfactory or trigeminal neurons, transported by axons and released centrally by exocytosis (Leng and Ludwig, 2016). However, Born et *al.* rejected this postulate because such a phenomenon would take hours, which is in contradiction with the raised concentration of peptides observed in the CSF of healthy subjects 30 minutes after intranasal administration. They also add that OT would be almost completely degraded during this interval (Born et al., 2002). Given the various critical points discussed in this section, the results and effects observed could be due to a direct modulation of brain circuits by exogenously administered OT (for review; (Leng and Ludwig, 2016)).

However, LIT-001 with its ability to cross the BBB and its half-life exceeding 2 hours makes possible to envisage that an intranasal administration of LIT-001 could reach OTR neurons in the CNS. LIT-001 found in the brain and CSF after an i.p. injection are evidence supporting this hypothesis. Indeed, it is likely that either LIT-001 goes into the brain directly with a "passive" crossing of the BBB at the olfactory nerve and olfactory bulb or with an internalisation by olfactory neurons, transported by axons and released centrally by exocytosis.

Furthermore, intranasal release of OT in humans and intracerebral injection of OT in rodents appears to be conducive to drug withdrawal in a context of addiction to a compound (methamphetamine, morphine, alcohol, etc.) (Russell et al., 1992; Carson et al., 2010; Pedersen et al., 2013; Cai et al., 2022). This potentially anti-addictive aspect is of particular interest in patients suffering from chronic pain who have been treated with opioids and suffer from an addiction disorder following this treatment. This would have a withdrawal effect in complement to the analgesic effects for example.

However, these effects are also potentially a disadvantage, as the risk of interacting with the OT system is to affect involuntarily other systems and induce side effects, such as reduced heart rate, blood pressure, modify renal activity, decreased food intake, and increased aggressivity (**Figure 17**) (Petersson et al., 1996; Morton et al., 2012). For example, concerning renal function, it has been shown that i.p. injection of OT in rats causes dose-dependent increases of the osmolality (Haanwinckel et al., 1995). This could be more problematic if LIT-001 (in long-term treatment) induces a dysregulation of the dopaminergic system, leading to behavioural modifications (Baracz and Cornish, 2013; László et al., 2020).

It is also very important to ensure that LIT-001 does not induce a habituation nor a modification of OT synthesis after repeated treatments. Indeed, OTR neurons over-stimulated during a long treatment could reduce OTR expression or OT synthesis by transcriptional modifications. Indeed, studies performing repeated intracerebral injections of OT (5 times per week) have shown a downregulation of OT and OTR in brain structures (Huang et al., 2014; Peters et al., 2014). Consequently, we would be in a similar situation as observed with opioids, where, as the treatment progresses, an increase in dose would be necessary (VIDAL, 2021c). Then when the treatment ended, the endogenous OT would potentially no longer be sufficient to have its analgesic effects and therefore there would be a risk of exacerbated hypersensitivity in the patient.

To assess all of these concerns, blood levels of OT should be monitored (each day) to ensure that OT synthesis does not change (in the same CFA model as used in our study). Then we should inject LIT-001 (i.p.) and measure the analgesic effects on thermal and mechanical sensitivity or measure anxiety via an elevated plus maze test, while monitoring food intake and repeating this operation for several days. If a

decrease in anti-hyperalgesic (or potential anxiolytic) effects is observed, this may be a habituation to the treatment. If behavioural changes in the animals or reductions in food intake would have been observed, this would indicate that LIT-001 is inducing behavioural changes as mentioned above.

Regarding potential OT/TRPV1 interactions, affinity tests performed by Dr. Marcel Hibert's team (unpublished data for the moment) showed that LIT-001 and OT have no affinity for TRPV1 either for agonist or antagonist effects. This supports the fact that LIT-001 is indeed specific for OTR and that OT does not affect TRPV1. Furthermore, it suggests that the conclusions of Nersesyan (2017) and Sun (2018) are probably erroneous (Gonzalez-Hernandez and Charlet, 2018).

The most likely hypothesis regarding these results are that TRPV1-expressing nociceptors also co-express OTR. Additionally, in the TRPV1 knockout mice model there would have been the establishment of compensatory mechanisms in the OTR neurons of the DRG. This might explain the reduced analgesic effects induced by OT. Indeed, TRP knockout models regularly show compensatory mechanisms and function modification of some sensitivity (for review; (Dai, 2016)). For example, the absence of TRPV1 in a TRPV1 knockout mice, greatly alters their thermal sensitivity to heat (Barton et al., 2006).

Finally, it has also been observed that LIT-001 has a slight affinity for V2R, which may induce side effects related to the activation of the AVP system, such as vasoconstriction, increased heart rate, antidiuretic (Pelletier et al., 2014). However, these effects on V2R remain to be determined *in vivo* and if these effects are observed *in vivo,* the only possibility is to upgrade LIT-001 in “LIT-002”, without affinity for V2R, by chemical engineering.

Overall, the LIT-001 is an innovative compound that is very interesting for its specific targeting of OTR and its non-peptidergic nature. As seen previously, the molecule itself has only one drawback, which is its affinity for V2R. The rest of the points discussed above concern the use of the OT system to induce analgesia.

3. Global discussion

3.1. Therapeutic and economic impact

In addition to studying the analgesic effects of two types of molecules, LIT- 001, and both menthol and pulegone, we considered the economic impact that these molecules could have. To do so first assessed the “production cost/effects” ratio of these molecules compared to current treatments such as opioids or monoclonal antibodies therapies for example (**Table 5**).

Table 5: Drug cost per gram.

Drug / Molecules	Cost/g	Supplier / Reference
Menthol	0.08 €	Sigma-Aldrich
Pulegone	0.85 €	Sigma-Aldrich
LIT-001	2 000 €	Marcel Hibert LIT platform
Paracetamol	0.15 €	Sanofi / Vidal
Tramadol	2.3 €	Mylan / Vidal
Codeine	62.5 €	UPSA / Vidal
Fentanyl	920 €	Sandoz / Vidal
Morphine	11.75 €	Aguettant / Vidal
Gabapentin	0.84 €	Pfizer / Vidal
Monoclonal antibodies	2 000 € /1 shot	Eli Lilly

Based on the **Table 5** it can be established that paracetamol is very inexpensive. However, it is a weak analgesic and ineffective for non-inflammatory related pain. Opioids have a variable cost but are relatively affordable, with the exception of fentanyl (**Table 5**). Although they are really efficient to reduce pain, they also have a tremendous amount of side effects. In addition, opioid misuse has created the Opioid crisis (**Figure 7**) that is severely affecting North America.

However, in addition to the "classical" analgesics such as morphine derivatives, or NSAIDs, there is a third category of analgesic treatments. These analgesic compounds are specific to a type of pain or disease, such as gabapentin, a GABA-related anti-epileptic drug that is also a specific analgesic for neuropathic pain. Gabapentin is not very expensive (**Table 5**) but is only used in neuropathic patients

and frequently (10 %) induces side effects ranging from somnolence to anxiety disorders and depression (VIDAL, 2021b). Another example is monoclonal antibodies therapies, which are particularly efficient in inflammatory diseases (e.g. rheumatoid arthritis, spondyloarthropathy, multiple sclerosis) (Basbaum et al., 2009). They act through the neutralization of TNF-α and NGF and have remarkable effect to suppress the associated hyperalgesia in these types of autoimmune diseases (Atzeni et al., 2005; Miller et al., 2017). However monoclonal antibodies are particularly expensive (**Table 5**) because patients need regular injections (2000 € / 1 shot) ranging from every 2 days to every month depending on the type of monoclonal antibody and the affliction (for review; (Bayer, 2019)).

Putting this into perspective, although monoterpenes require large doses to induce moderate analgesic effects, they remain particularly cheap to produce (**Table 5**). Moreover, due to the multitude of targets and mechanisms (anti-inflammatory and anti-nociceptive) monoterpenes may have positive effects in different types of pain, especially chronic and acute inflammatory pain. Additionally, interest in anti-inflammatory molecules against TNF-α or IL-6 has been on the rise over the last two decades, as promising treatments for numerous autoimmune diseases, including rheumatoid arthritis (Atzeni et al., 2005), and monoterpenes may be a major compound in these treatments. Regarding neuropathic pain, I suggest that monoterpenes are of limited interest because the anti-inflammatory effects and the TRPs modulations are not relevant in the treatment of neuropathic pain.

LIT-001 is a very expensive compound (**Table 5**), but it should also be taken into account that LIT-001 is produced on a small scale and that a larger scale production with an optimised synthesis process will likely make the cost lower. Nevertheless, it is a highly promising therapeutic molecule, not only to as a pain reliever, but for all diseases and conditions where the OT system is impaired. Moreover, by targeting an endogenous analgesic system (OT) with potentially positive effects on anxiety, LIT-001 has a potential therapeutic interest in all types of pain, inflammatory (chronic or acute) and neuropathic.

To summarise, monoterpenes and LIT-001 are molecules with a definite therapeutic and economic interest.

Indeed acute and chronic pain strongly affects our society, affecting the patient in his daily activities such as work, hobbies, social relationships and this constitutes a burden for the patients and society (Mick et al., 2013; Malfliet et al., 2017).

These afflictions are affecting the health care system in France in several ways, for example it has been shown that patients suffering from pain issues are going to medical consultations twice as often, are over-consuming analgesic drugs (misuses) and this induces an estimated over-cost to the French health care system of 1.163 billion € per years (Mick et al., 2013). Moreover, they also affect the socio-economic structure of our society; approximately 88 million working days are lost each year in France due to absenteeism, loss of productivity and work stoppages related to resistant chronic pain among workers. (for review; (Mick et al., 2013)).

The development of analgesic treatments such as the monoterpene mix or LIT-001 have economic and social implications that go beyond the “production cost/effects” ratio of treatments.

3.2. Multimodal pharmacological approach

Ultimately, we could imagine the pharmacotherapeutic combination of LIT-001 and the monoterpene mix in a multimodal therapeutic approach.

The first point of such a union is the diversity of molecular targets for which LIT-001 and the monoterpene mix should not interfere, knowing that LIT-001 is specific to OTR and monoterpenes affect almost exclusively ion channels. However, they can reach identical and/or similar nociceptive circuits, such as nociceptors that express TRP but also OTR in the DRG and in the peripheral endings (Moreno-López et al., 2013; Dai, 2016). In addition, both types of molecules pass the BBB, so they could act on WDR neurons at the spinal level for example and perhaps even at a supraspinal level (Wojtunik-Kulesza et al., 2017).

This difference in molecular targets within the same cells/neuronal networks enables us to envisage a synergy between the two components. For example, it can be hypothesized that the activation of GABAergic OTR+ (Gq) interneurons by LIT-001 would induce a release of GABA on $GABA_a$ R of (post-synaptic) projection neuron and the opening/activation of $GABA_a$ R would be potentiated by monoterpenes such as menthol. This would result in a synergy between the activation of the GABAergic OTR

interneuron by LIT-001 and the inhibition of the post-synaptic neuron by GABA coupled with the potentiation of $GABA_a$ R by the monoterpene mix. Additional synergies can be considered such as LIT-001 inhibition of nociceptor by OTR (Gi) combined with blocking of Ca^{2+}, Na^{+} ions channels by the monoterpene mix.

It should also be noted that both compounds have anti-inflammatory effects, OT decreases pro-inflammatory cytokine synthesis (Szeto et al., 2008) (**Figure 18**), as do monoterpenes (Quintans et al., 2019) (**Figure 11**). LIT-001 and the monoterpene mix could thus act synergistically against the inflammatory aspect of pain by lowering pro-inflammatory cytokine levels and thus reduce hyperalgesia.

In addition to these potential synergistic effects, another interesting point of such a combination is the temporal coverage. The effects of the monoterpenes start as early as 20 minutes, are maximal at 40 minutes, fade after 1 hour whereas the effects of the LIT start at around 30 minutes, last very effectively until 3 hours, and fade after 5 hours. We would therefore have a superposition of the rapid effects of the monoterpenes, which after 1 hour would pass to those of LIT-001 for a more prolonged effect.

The first question concerning such combination is whether the molecules will not interact chemically with each other. According to our collaborators in chemistry, there is no risk that these molecules will interact with each other due to their small size. Concerning the route of intake for preclinical tests in animals, the i.p. route will be preferred, as it has already been tested for LIT-001 and the monoterpenes. If the anti-hyperalgesic effects obtained with i.p. injections are successful, then it will be interesting to test these effects orally. Moreover, monoterpenes are already widely administered p.o. and with regard to LIT-001 due to its non-peptidergic nature, our chemist collaborators assumed that it should work orally.

Moreover, with these molecules, it is also possible to consider other, less conventional, intake routes than oral administration.

There is already the intranasal route, indeed as discussed in the previous chapter, it is likely that LIT-001 could be efficient in intranasal administration, due to its ability to cross the BBB. Monoterpenes can also reach supraspinal structures via orexin neurons. For example, monoterpene vapours induced analgesic effects in mice exposed to these vapours (Tashiro et al., 2016; Higa et al., 2021). Furthermore, the results of clinical trials conducted with inhalation of essential oils corroborate these

results (Sasannejad et al., 2012; Arslan et al., 2020). This suggests that the intranasal route for the administration of the combination of LIT-001 and the monoterpene mix is an avenue to explore for future therapeutical approaches. Indeed, the intranasal route could have advantages over the oral route, it may be easier to administer for some people (suffering from swallowing disorders, stomach sensitivity). However, it might also make it easier to reach the brain structures to induce (slightly) different effects compared to oral administration.

Regarding topical applications, for monoterpenes it is not problematic. They are frequently applied as balms to induce analgesic effects, either in animals (**Tables 2 & 3**) or in humans (Wang et al., 2017). Herman and Herman review the possible mechanisms of skin penetration by essential oils and monoterpenes. One of the mechanisms is an intercellular diffusion (i.e.: between the cells) (for review; (Herman and Herman, 2015)). However, for LIT-001 due to its chemical structure it is highly unlikely that such a possibility of skin penetration exists. Therefore, the combination cannot be carried out by topic application. Alternatively, LIT-001 can be taken orally or intranasally in combination with a topical application of the monoterpene mix directly on the painful area.

Diversifying the intake routes has a real therapeutic interest. Indeed, it has been shown that the intake route influences the effect of the coumpounds, which is mainly explained by a tissue-specific expression levels of the compounds targets. For example, there are more TRP channels involved in the effects of monoterpenes after a topical application or an oral intake than after an inhalation (for review; (Koyama and Heinbockel, 2020)).

This mixture is, of course, unconventional, but this does not make it any less interesting as a multimodal pharmacological treatment. Indeed, the targeting of different systems can increase the analgesic power and therefore reduce the doses of each compound, thus reducing their side effects. Moreover, the activation of endogenous systems is in some cases bounded by the “maximum activation” of this particular system. Therefore affecting different systems can help to break through this glass ceiling. With this kind of innovative approach, we may be able to make safer and/or more effective therapeutic treatments.

3.3. Animal models and transposition of preclinical to clinical research

I would like to address a last point on the use of animal models and the transposition of preclinical research to humans. Indeed, a large part of preclinical research is not conclusive when it is transferred to clinical studies. We know that the OT and OTR genes are not located on the same chromosomes in humans and rats, and there are some differences between rat and human OTR (number of, amino acids and site of N-glycolisation) (Gimpl and Fahrenholz, 2001). Concerning TRPs, we know that there are structural variations between species and variable expression (Ramsey et al., 2006). This raises the question of the relevance to use animal models if the targets are not identical to humans.

To address this question in the context of this thesis it must be taken into account that OT is identical between rat and human and OTR has only one amino acid difference. Furthermore, the affinity of OT for its receptor does not change (or hardly changes) between the two subtypes of OTR (human and rat) (Gimpl and Fahrenholz, 2001). Regarding TRPs, all the studies in **Table 4** using human and rodent TRPs show no difference between the two TRP strains.

Furthermore, although humans and rodents have diverged by 65 to 75 Myr, only 300 genes out of ~ 25 000 appear to be unique to either species (O'Leary et al., 2013). Moreover, numerous studies based on rodent models have provided a mechanistic understanding of the actual role of the target in the pathophysiology of pain (for review; (Mogil, 2019)).

Nevertheless, it is often argued that the notable differences in nociception (e.g. threshold, physiological response) and pain perception (e.g. context, pain expressions) between humans and rodents are a limitation to the translation of knowledge from pre-clinical to clinical research (Mogil, 2019). However, Mogil (2019) suggested that these differences in nociception and pain perception between rodents and humans are probably due to the approaches and ways used to assess nociception and pain.

Thus, structural differences exist between rats and humans, but they do not compromise our experimental findings. Moreover, in neuroscience, and particularly in behavioural studies, molecular targets are essential, but the integration of targets into a network that allows the observation of a behaviour is even more crucial. In addition, the nociceptive networks are well maintained between humans and rats.

Consequently, the animal model is relevant in the context of our studies and the transposition of the results to humans is credible in view of the clinical trials already conducted in humans with OT and monoterpenes (Alfvén, 2004; Wang et al., 2017).

The overall principle of behavioural experiments and their reliability can also be discussed.

Indeed, we may have made some interpretation shortcuts in our studies. For example, we refer to an analgesic/anti-hyperalgesic effect, but the tests and therefore the behavioural observations were based on a threshold of avoidance of an unpleasant and potentially nociceptive stimulus (or even painful). Therefore, during all the thermal or mechanical sensitivity tests, I measured the triggering of an avoidance response to a stimulus that we consider as nociceptive. I was never able to record nociception or even pain directly. Thus, potentially the animals were able to initiate avoidance behaviour without the inducement of a nociceptive stimulus and thus potentially the treatments had no anti-nociceptive effect.

However, this is highly unlikely, as in our studies I have observed modifications in these avoidance responses with the sensitisation induced by CFA resulting in an exacerbated sensitivity. Sensitisation was observed by comparing the thresholds before and after the injection of CFA. This explains the advantage of using an induced rather than a spontaneous pain model in our studies. The interest of measuring several modalities (thermal, mechanical) also allows us to report on a potential anti-nociceptive effect global or specific to a given modality.

Thus, in my opinion, the behavioural tests (measurement of thermal and mechanical sensitivities) and the induced pain model (CFA) that I used are relevant for the study of anti-nociceptive effects of potential therapeutic compounds.

Overall, the behavioural tests and animal models provide us a considerable amount of information and the "theoretical" transposability to humans appears to be favourable regarding the points discussed above. However, it is important to take into account the intrinsic limits of these models to temper the conclusions.

In order to go further in preclinical studies and then in clinical studies, it would be necessary to get rid of the pain avoidance measures and the problems mentioned previously. For this purpose, additional complementary measures such as operant

learning measures, spontaneous noxious behaviours and quality of life or physical activity measure can be performed (Abboud et al., 2021).

In addition, there is a risk of experimenter-designer bias. I think that in our studies, this is unlikely in view of the marked effects of our compounds, but it should be pointed out. The best way to avoid this is to carry out so-called double-blinded experiments, but this also requires much more organisation and human resources.

Finally, it is important to place the experiments in their context, as they are fundamental studies with the aim of observing effects that could pave the way for further studies.

3.4. Consideration of the ethical and professional context of the thesis

To take a step back I would like to address some personal considerations on the ethical and socio-professional context of the thesis.

3.4.1. Ethical issues in animal experimentation

Society today is generally turning away from animal experimentation. This refusal of experimentation began at the end of the 19th century and experienced a boom in the 1970-80s before regaining momentum in the years 2005-2010 until today.

From a personal point of view, I think that the overall movement that encompasses respect for animals, the integration of their legal status as sentient beings, is globally beneficial for society and research.

It is important to consider animals as sentient beings and therefore to limit their suffering whenever possible. We know that trauma (severe pain, stress) will induce behavioural modifications and physiological reactions, which can be a source of variability between animals within the same experiment (Rhudy and Meagher, 2000; Bailey, 2018). Thus, an animal that experiences intense suffering or distress in an experiment without the purpose of studying pain or stress will be a very poor experimental and scientific model. Therefore, it is essential to use analgesics in painful procedures in order to improve animal welfare and thus reduce biases related to pain, stress, etc.

The issue with these biases is that they can lead to particularly large variability in the results and therefore the experiment may require more animals to have a statistically viable result in addition to reducing the welfare of the animals. Indeed, as the 3Rs rule (Replace, Reduce, Refine) recommends, animal testing must be refined, thus limiting animal suffering and improving overall animal welfare. By doing so, we also reduce the variability and the number of animals needed to obtain a statistically exploitable result.

However, regarding replacement, it is currently impossible to do without the animal model in some fields of fundamental research. In 2019, 69% of the animals used for research purposes were used for basic research, particularly in neuroscience, oncology and immunology (Muraille, 2021). In neuroscience in particular, the use of animal models is essential for the understanding of cellular and neuronal mechanisms that allow a better understanding of diseases/illnesses and therefore the possibility to develop treatments.

Currently, *in vitro*, *in silico* and other so-called alternative models are not able to reflect the complexity of a neural network or a behaviour such as a nociceptive threshold to determine the analgesic potential of a compound. However, the use of so-called inferior animal models such as zebrafish and drosophila are particularly interesting as alternatives for studying specific phenomena, such as neurodevelopmental disorders (de Abreu et al., 2020) or drug discovery (Zanandrea et al., 2020). These are particularly interesting models for "paving the way" but the transition to the rodent and higher model remains essential before transposition to humans. Moreover, this does not reduce the number of animals used in research, it just transfers it to animals that are more distant from humans and therefore less “valuable” to a large part of the population.

The debate on the use of animals for medical purposes is particularly interesting in view of the recent news about xenotransplants with the first successful transplantation of a pig heart to a human (Reardon, 2022). This could be a solution to the organ shortage and a way out for all the people waiting for transplants (26,000 are waiting for transplants and 700 died for lack of an organ in France in 2019).

Based on the arguments developed above, I argue that animal experimentation is necessary to make progress in research and *in fine* in medicine. Moreover, the

majority of the public is in favour of animal experimentation as long it contributes to the improvement of human health and there is no other viable alternative (Muraille, 2021). However, this should not prevent us from questioning some practices and improving certain issues for the animal welfare.

Overall, the 3Rs rule is well applied (in the laboratories I have been able to visit) and pain management after procedures is generally well followed. However, one area for improvement is the consideration of the stress caused to the animal (Institute for Laboratory Animal Research (U.S.), 2008). Inappropriate handling, such as grabbing animals by the tail to hold them (especially for rats), can trigger this kind of stress (Institute for Laboratory Animal Research (U.S.), 2008). It is a stressful (and potentially painful) practice that should be avoided. Unfortunately, it is still used, although it can easily be replaced by the use of tunnels to move animals. Users can also be made aware to avoid "strong" scents (like tobacco smoke) and fragrances when they are in contact with animals with a particularly sensitive olfactory system such as rodents (Institute for Laboratory Animal Research (U.S.), 2008).

In conclusion, I think it is essential to apply the rules concerning replacement and reduction of animals as best as possible for animal welfare and sustainable science. It is also essential to communicate on the interest of our work, its issues and the importance of using the animal model to allow the society to form an opinion based on reliable infromations.

3.4.1. The importance of collaboration in research

To step back a little more I would like to address a point that was essential during my thesis, collaboration. Indeed, my thesis is a Cifre collaboration between company and academia. Moreover, all the projects in which I participated were the result of a collaboration.

The collaboration between BENEPHYT and the laboratory was more focused on a global vision of my thesis subject, i.e. analysing the potential of a molecule with the objective of valorisation and sharing technical and scientific knowledge between my two major projects (LIT-001 and monoterpenes). The collaboration between Dr. Alexandre Charlet and Dr. Hugues Petitjean was essential in my supervision. I personally learned a lot from this, because I was able to benefit from a double

supervision, and thus to have two distinct points of view. I was also able to study several different topics (OT, terpenes, nociception, pharmacology) thus allowing me to diversify my knowledge and skills (behavioural tests, patch-clamp).

Collaboration also has its constraints, such as the coexistence of different projects and schedules in parallel. Concerning the planning, I developed during my thesis a rigorous and efficient planning of my different projects, which often spread over several months. The problem that affected me the most was the regular change of subjects (every 5-6 months), which forced me to go back to my recaps of the bibliography to get back into the subject, although it was not a major concern.

Overall, the collaboration between BENEPHYT and the CNRS was very stimulating and allowed me to develop multiple professional and non-scientific skills (these points are developed in the **Annex 7**).

The pharmacological projects (LIT-001 and monoterpenes) were carried out in collaboration with chemists, in particular for the parts dealing with the chemical aspects of the compounds (pharmacological profile, chromatography, cytotoxicity) conducted *in vitro*. Indeed, our team is not equipped to conduct this type of *in vitro* experiment, and none of our team members has a recent experience in cell culture. Performing these experiments within our team would have been extremely time consuming. In addition, we would have missed the input of the expertise of the chemists for all the parts related to their speciality and their points of view on the entire projects.

These collaborations have been very valuable and allowed me to understand the issues and challenges that chemists can encounter during a project.

The studies related to the understanding of OT networks were carried out in collaboration with the team of Prof. Valery Grinevich from Mannheim. The situation is broadly the same, each team brings its own specificities, skills and point of view. The collaboration is particularly beneficial because it also allows for a variety of people and skills to be brought together to produce a more complete work/study/research. It should be noted that despite the geographical proximity and the facilities of Franco-German cooperation, visits, exchanges and transfer of scientific material between our laboratories could be difficult, especially during the COVID-19 crisis.

Finally, I consider collaborations in research essential, as they allow us to go further in our understanding by diversifying the approaches. However, this requires more organisation and communication and therefore takes more time.

CONCLUSION

During this thesis the data obtained allows us to highlight the analgesic potential of a non-peptidergic agonist of OTR, LIT-001. This opened the way for the preclinical and clinical development of this molecule, which relies on the endogenous OT system to induce anti-hyperalgesic effects. Additionally, we confirmed the anti-hyperalgesic effects of an understudied monoterpene, pulegone, extracted from a local pharmacopoeia plant, *Calamintha nepeta* (L.). Then we compared its effects with those of menthol, a reference monoterpene, and we made a mixture of both molecules in order to identify a synergistic effect between these two monoterpenes.

These studies enabled us to identify new and promising innovative molecules for the treatment of pain. In the future, these molecules could potentially be tangible alternatives to opiate-based analgesics. To reach this objective, we need to expand our knowledge about these molecules, their strengths and weaknesses, in order to undertake clinical studies. Furthermore, it also requires a strong knowledge of the nervous system networks and cellular actors involved in the analgesic effects.

REFERENCES

REFERENCES

Abboud, C., Duveau, A., Bouali-Benazzouz, R., Massé, K., Mattar, J., Brochoire, L., et al. (2021). Animal models of pain: Diversity and benefits. *Journal of Neuroscience Methods* 348, 108997. doi:10.1016/j.jneumeth.2020.108997.

Abe, J., Hosokawa, H., Okazawa, M., Kandachi, M., Sawada, Y., Yamanaka, K., et al. (2005). TRPM8 protein localization in trigeminal ganglion and taste papillae. *Molecular Brain Research* 136, 91–98. doi:10.1016/j.molbrainres.2005.01.013.

Abraira, V. E., and Ginty, D. D. (2013). The Sensory Neurons of Touch. *Neuron* 79, 618–639. doi:10.1016/j.neuron.2013.07.051.

Abraira, V. E., Kuehn, E. D., Chirila, A. M., Springel, M. W., Toliver, A. A., Zimmerman, A. L., et al. (2017). The Cellular and Synaptic Architecture of the Mechanosensory Dorsal Horn. *Cell* 168, 295-310.e19. doi:10.1016/j.cell.2016.12.010.

Adams, M., Berset, C., Kessler, M., and Hamburger, M. (2009). Medicinal herbs for the treatment of rheumatic disorders--a survey of European herbals from the 16th and 17th century. *J Ethnopharmacol* 121, 343–359. doi:10.1016/j.jep.2008.11.010.

Akerlund, M., Bossmar, T., Brouard, R., Kostrzewska, A., Laudanski, T., Lemancewicz, A., et al. (1999). Receptor binding of oxytocin and vasopressin antagonists and inhibitory effects on isolated myometrium from preterm and term pregnant women. *BJOG:An international journal of O&G* 106, 1047–1053. doi:10.1111/j.1471-0528.1999.tb08112.x.

Alfvén, G. (2004). Plasma Oxytocin in Children with Recurrent Abdominal Pain: *Journal of Pediatric Gastroenterology and Nutrition* 38, 513–517. doi:10.1097/00005176-200405000-00010.

Alfvén, G., Torre, B., and Uvnäs-Moberg, K. (1994). Depressed concentrations of oxytocin and cortisol in children with recurrent abdominal pain of non-organic origin. *Acta Paediatrica* 83, 1076–1080. doi:10.1111/j.1651-2227.1994.tb12989.x.

Allegri, M., Clark, M. R., De Andrés, J., and Jensen, T. S. (2012). Acute and chronic pain: where we are and where we have to go. *Minerva Anestesiol* 78, 222–235.

Almeida, J. R. G. da S., Souza, G. R., Silva, J. C., Saraiva, S. R. G. de L., Júnior, R. G. de O., Quintans, J. de S. S., et al. (2013). Borneol, a bicyclic monoterpene alcohol, reduces nociceptive behavior and inflammatory response in mice. *ScientificWorldJournal* 2013, 808460. doi:10.1155/2013/808460.

ANSM Nos missions - Médicaments à base de plantes et huiles essentielles - ANSM. Available at: https://ansm.sante.fr/qui-sommes-nous/notre-perimetre/les-medicaments/p/medicaments-a-base-de-plantes-et-huiles-essentielles [Accessed November 16, 2021].

Arazi, E., Blecher, G., and Zilberberg, N. (2020). Monoterpenes Differently Regulate Acid-Sensitive and Mechano-Gated K2P Channels. *Front Pharmacol* 11, 704. doi:10.3389/fphar.2020.00704.

Arslan, I., Aydinoglu, S., and Karan, N. B. (2020). Can lavender oil inhalation help to overcome dental anxiety and pain in children? A randomized clinical trial. *Eur J Pediatr* 179, 985–992. doi:10.1007/s00431-020-03595-7.

Ashoor, A., Nordman, J. C., Veltri, D., Yang, K.-H. S., Shuba, Y., Al Kury, L., et al. (2013). Menthol inhibits 5-HT3 receptor-mediated currents. *J Pharmacol Exp Ther* 347, 398–409. doi:10.1124/jpet.113.203976.

Atasoy, D., Betley, J. N., Su, H. H., and Sternson, S. M. (2012). Deconstruction of a neural circuit for hunger. *Nature* 488, 172–177. doi:10.1038/nature11270.

Atzeni, F., Turiel, M., Capsoni, F., Doria, A., Meroni, P., and Sarzi-Puttini, P. (2005). Autoimmunity and Anti-TNF-α Agents. *Annals of the New York Academy of Sciences* 1051, 559–569. doi:10.1196/annals.1361.100.

Aziz, Z. A. A., Ahmad, A., Setapar, S. H. M., Karakucuk, A., Azim, M. M., Lokhat, D., et al. (2018). Essential Oils: Extraction Techniques, Pharmaceutical And Therapeutic Potential - A Review. *CDM* 19, 1100–1110. doi:10.2174/1389200219666180723144850.

Bailey, J. (2018). Does the Stress of Laboratory Life and Experimentation on Animals Adversely Affect Research Data? A Critical Review. *Altern Lab Anim* 46, 291–305. doi:10.1177/026119291804600501.

Bakkali, F., Averbeck, S., Averbeck, D., and Idaomar, M. (2008). Biological effects of essential oils – A review. *Food and Chemical Toxicology* 46, 446–475. doi:10.1016/j.fct.2007.09.106.

Banerjee, P., Joy, K. P., and Chaube, R. (2017). Structural and functional diversity of nonapeptide hormones from an evolutionary perspective: A review. *General and Comparative Endocrinology* 241, 4–23. doi:10.1016/j.ygcen.2016.04.025.

Bannister, K., and Dickenson, A. H. (2017). The plasticity of descending controls in pain: translational probing: Top-down pain processing and monoaminergic imbalances. *J Physiol* 595, 4159–4166. doi:10.1113/JP274165.

Baracz, S. J., and Cornish, J. L. (2013). Oxytocin modulates dopamine-mediated reward in the rat subthalamic nucleus. *Hormones and Behavior* 63, 370–375. doi:10.1016/j.yhbeh.2012.12.003.

Barberis, C., Mouillac, B., and Durroux, T. (1998). Structural bases of vasopressin/oxytocin receptor function. *Journal of Endocrinology* 156, 223–229. doi:10.1677/joe.0.1560223.

Barton, N. J., McQueen, D. S., Thomson, D., Gauldie, S. D., Wilson, A. W., Salter, D. M., et al. (2006). Attenuation of experimental arthritis in TRPV1R knockout mice. *Experimental and Molecular Pathology* 81, 166–170. doi:10.1016/j.yexmp.2006.04.007.

Basbaum, A. I., Bautista, D. M., Scherrer, G., and Julius, D. (2009). Cellular and Molecular Mechanisms of Pain. *Cell* 139, 267–284. doi:10.1016/j.cell.2009.09.028.

Baskerville, T., and Douglas, A. (2008). "Interactions between dopamine and oxytocin in the control of sexual behaviour," in *Progress in Brain Research* (Elsevier), 277–290. doi:10.1016/S0079-6123(08)00423-8.

Batista, P. A., Werner, M. F. de P., Oliveira, E. C., Burgos, L., Pereira, P., Brum, L. F. da S., et al. (2010). The antinociceptive effect of (-)-linalool in models of chronic inflammatory and neuropathic hypersensitivity in mice. *J Pain* 11, 1222–1229. doi:10.1016/j.jpain.2010.02.022.

Bayer, V. (2019). An Overview of Monoclonal Antibodies. *Seminars in Oncology Nursing* 35, 150927. doi:10.1016/j.soncn.2019.08.006.

Behrendt, H.-J., Germann, T., Gillen, C., Hatt, H., and Jostock, R. (2004). Characterization of the mouse cold-menthol receptor TRPM8 and vanilloid receptor type-1 VR1 using a fluorometric imaging plate reader (FLIPR) assay. *Br J Pharmacol* 141, 737–745. doi:10.1038/sj.bjp.0705652.

Bell, A. (2018). The neurobiology of acute pain. *The Veterinary Journal* 237, 55–62. doi:10.1016/j.tvjl.2018.05.004.

Beltramini, A., Milojevic, K., and Pateron, D. (2017). Pain Assessment in Newborns, Infants, and Children. *Pediatr Ann* 46. doi:10.3928/19382359-20170921-03.

Benyamin, R., Trescot, A. M., Datta, S., Buenaventura, R., Adlaka, R., Sehgal, N., et al. (2008). Opioid complications and side effects. *Pain Physician* 11, S105-120.

Beran, F., Köllner, T. G., Gershenzon, J., and Tholl, D. (2019). Chemical convergence between plants and insects: biosynthetic origins and functions of common secondary metabolites. *New Phytol* 223, 52–67. doi:10.1111/nph.15718.

Bercy Infos (2020). Comment utiliser les huiles essentielles en toute sécurité ? Available at: https://www.economie.gouv.fr/particuliers/comment-utiliser-huiles-essentielles-en-toute-securite [Accessed November 16, 2021].

Bergman, M. E., Davis, B., and Phillips, M. A. (2019). Medically Useful Plant Terpenoids: Biosynthesis, Occurrence, and Mechanism of Action. *Molecules* 24, 3961. doi:10.3390/molecules24213961.

Berliocchi, L., Russo, R., Levato, A., Fratto, V., Bagetta, G., Sakurada, S., et al. (2009). (-)-Linalool attenuates allodynia in neuropathic pain induced by spinal nerve ligation in c57/bl6 mice. *Int Rev Neurobiol* 85, 221–235. doi:10.1016/S0074-7742(09)85017-4.

Bhalla, S., Matwyshyn, G., and Gulati, A. (2002). Potentiation of morphine analgesia by BQ123, an endothelin antagonist. *Peptides* 23, 1837–1845. doi:10.1016/S0196-9781(02)00141-9.

Blondell, R. D., Azadfard, M., and Wisniewski, A. M. (2013). Pharmacologic therapy for acute pain. *Am Fam Physician* 87, 766–772.

Blume, A., Bosch, O. J., Miklos, S., Torner, L., Wales, L., Waldherr, M., et al. (2008). Oxytocin reduces anxiety via ERK1/2 activation: local effect within the rat hypothalamic paraventricular nucleus. *Eur J Neurosci* 27, 1947–1956. doi:10.1111/j.1460-9568.2008.06184.x.

Blumenstein, M., Hruby, V. J., and Viswanatha, V. (1979). Investigation of the interactions of oxytocin with neurophysins at low pH using carbon-13 nuclear magnetic resonance and carbon-13-labeled hormones. *Biochemistry* 18, 3552–3557. doi:10.1021/bi00583a018.

Boll, S., Almeida de Minas, A. C., Raftogianni, A., Herpertz, S. C., and Grinevich, V. (2018). Oxytocin and Pain Perception: From Animal Models to Human Research. *Neuroscience* 387, 149–161. doi:10.1016/j.neuroscience.2017.09.041.

Booker, S. Q., and Herr, K. A. (2016). Assessment and Measurement of Pain in Adults in Later Life. *Clinics in Geriatric Medicine* 32, 677–692. doi:10.1016/j.cger.2016.06.012.

Born, J., Lange, T., Kern, W., McGregor, G. P., Bickel, U., and Fehm, H. L. (2002). Sniffing neuropeptides: a transnasal approach to the human brain. *Nat Neurosci* 5, 514–516. doi:10.1038/nn0602-849.

Breslow, E., and Burman, S. (1990). "Molecular, Thermodynamic, and Biological Aspects of Recognition and Function in Neurophysin-Hormone Systems: A Model System for the Analysis of Protein-Peptide Interactions," in *Advances in Enzymology - and Related Areas of Molecular Biology*, ed. A. Meister (Hoboken, NJ, USA: John Wiley & Sons, Inc.), 1–67. doi:10.1002/9780470123096.ch1.

Breton, J.-D., Veinante, P., Uhl-Bronner, S., Vergnano, A. M., Freund-Mercier, M. J., Schlichter, R., et al. (2008). Oxytocin-Induced Antinociception in the Spinal Cord is Mediated by a Subpopulation of Glutamatergic Neurons in Lamina I-II Which Amplify GABAergic Inhibition. *Mol Pain* 4, 1744-8069-4–19. doi:10.1186/1744-8069-4-19.

Burbach, J. P. H., Luckman, S. M., Murphy, D., and Gainer, H. (2001). Gene Regulation in the Magnocellular Hypothalamo-Neurohypophysial System. *Physiological Reviews* 81, 1197–1267. doi:10.1152/physrev.2001.81.3.1197.

Busnelli, M., Kleinau, G., Muttenthaler, M., Stoev, S., Manning, M., Bibic, L., et al. (2016). Design and Characterization of Superpotent Bivalent Ligands Targeting Oxytocin Receptor Dimers via a Channel-Like Structure. *J. Med. Chem.* 59, 7152–7166. doi:10.1021/acs.jmedchem.6b00564.

Cai, J., Che, X., Xu, T., Luo, Y., Yin, M., Lu, X., et al. (2022). Repeated oxytocin treatment during abstinence inhibited context- or restraint stress-induced reinstatement of methamphetamine-conditioned place preference and promoted adult hippocampal neurogenesis in mice. *Experimental Neurology* 347, 113907. doi:10.1016/j.expneurol.2021.113907.

Campbell, P., Ophir, A. G., and Phelps, S. M. (2009). Central vasopressin and oxytocin receptor distributions in two species of singing mice. *J. Comp. Neurol.* 516, 321–333. doi:10.1002/cne.22116.

Carović-Stanko, K., Petek, M., Grdiša, M., Pintar, J., Bedeković, D., Herak Ćustić, M., et al. (2016). Medicinal plants of the family Lamiaceae as functional foods – a review. *Czech J. Food Sci.* 34, 377–390. doi:10.17221/504/2015-CJFS.

Carson, D. S., Cornish, J. L., Guastella, A. J., Hunt, G. E., and McGregor, I. S. (2010). Oxytocin decreases methamphetamine self-administration, methamphetamine hyperactivity, and relapse to methamphetamine-seeking behaviour in rats. *Neuropharmacology* 58, 38–43. doi:10.1016/j.neuropharm.2009.06.018.

Caterina, M. J., Schumacher, M. A., Tominaga, M., Rosen, T. A., Levine, J. D., and Julius, D. (1997). The capsaicin receptor: a heat-activated ion channel in the pain pathway. *Nature* 389, 816–824. doi:10.1038/39807.

Chao, M. V. (2003). Neurotrophins and their receptors: A convergence point for many signalling pathways. *Nat Rev Neurosci* 4, 299–309. doi:10.1038/nrn1078.

Chini, B., Mouillac, B., Balestre, M.-N., Trumpp-Kallmeyer, S., Hoflack, J., Hibert, M., et al. (1996). Two aromatic residues regulate the response of the human oxytocin receptor to the partial agonist arginine vasopressin. *FEBS Letters* 397, 201–206. doi:10.1016/S0014-5793(96)01135-0.

Chiu, I. M., von Hehn, C. A., and Woolf, C. J. (2012). Neurogenic inflammation and the peripheral nervous system in host defense and immunopathology. *Nat Neurosci* 15, 1063–1067. doi:10.1038/nn.3144.

Choudhary, S., Marjianović, D. S., Wong, C. R., Zhang, X., Abongwa, M., Coats, J. R., et al. (2019). Menthol acts as a positive allosteric modulator on nematode levamisole sensitive nicotinic acetylcholine receptors. *International Journal for Parasitology: Drugs and Drug Resistance* 9, 44–53. doi:10.1016/j.ijpddr.2018.12.005.

Chuang, H., Prescott, E. D., Kong, H., Shields, S., Jordt, S.-E., Basbaum, A. I., et al. (2001). Bradykinin and nerve growth factor release the capsaicin receptor from PtdIns(4,5)P2-mediated inhibition. *Nature* 411, 957–962. doi:10.1038/35082088.

Claybaugh, J. R., and Uyehara, C. F. T. (1993). Metabolism of Neurohypophysial Hormones. *Ann NY Acad Sci* 689, 250–259. doi:10.1111/j.1749-6632.1993.tb55552.x.

Condés-Lara, M., Marina González, N., Martínez-Lorenzana, G., Luis Delgado, O., and José Freund-Mercier, M. (2003). Actions of oxytocin and interactions with glutamate on spontaneous and evoked dorsal spinal cord neuronal activities. *Brain Research* 976, 75–81. doi:10.1016/S0006-8993(03)02690-8.

Condés-Lara, M., Rojas-Piloni, G., Martínez-Lorenzana, G., and Rodríguez-Jiménez, J. (2009). Paraventricular hypothalamic oxytocinergic cells responding to noxious stimulation and projecting to the spinal dorsal horn represent a homeostatic analgesic mechanism. *European Journal of Neuroscience* 30, 1056–1063. doi:10.1111/j.1460-9568.2009.06899.x.

Condés-Lara, M., Rojas-Piloni, G., Martínez-Lorenzana, G., Rodríguez-Jiménez, J., López Hidalgo, M., and Freund-Mercier, M. J. (2006). Paraventricular hypothalamic influences on spinal nociceptive processing. *Brain Research* 1081, 126–137. doi:10.1016/j.brainres.2006.01.050.

Coste, B., Mathur, J., Schmidt, M., Earley, T. J., Ranade, S., Petrus, M. J., et al. (2010). Piezo1 and Piezo2 Are Essential Components of Distinct Mechanically Activated Cation Channels. *Science* 330, 55–60. doi:10.1126/science.1193270.

Cox, J. J., Reimann, F., Nicholas, A. K., Thornton, G., Roberts, E., Springell, K., et al. (2006). An SCN9A channelopathy causes congenital inability to experience pain. *Nature* 444, 894–898. doi:10.1038/nature05413.

Cox-Georgian, D., Ramadoss, N., Dona, C., and Basu, C. (2019). "Therapeutic and Medicinal Uses of Terpenes," in *Medicinal Plants*, eds. N. Joshee, S. A. Dhekney, and P. Parajuli (Cham: Springer International Publishing), 333–359. doi:10.1007/978-3-030-31269-5_15.

d'Alessio, P., Mirshahi, M., Bisson, J.-F., and Bene, M. (2014). Skin Repair Properties of d-Limonene and Perillyl Alcohol in Murine Models. *AIAAMC* 13, 29–35. doi:10.2174/18715230113126660021.

Dafni, A., and Böck, B. (2019). Medicinal plants of the Bible—revisited. *J Ethnobiology Ethnomedicine* 15, 57. doi:10.1186/s13002-019-0338-8.

Dai, Y. (2016). TRPs and pain. *Semin Immunopathol* 38, 277–291. doi:10.1007/s00281-015-0526-0.

Dale, H. H. (1906). On some physiological actions of ergot. *The Journal of Physiology* 34, 163–206. doi:10.1113/jphysiol.1906.sp001148.

Dale, R., and Stacey, B. (2016). Multimodal Treatment of Chronic Pain. *Medical Clinics of North America* 100, 55–64. doi:10.1016/j.mcna.2015.08.012.

Daumas, F. (1961). Review of Wörterbuch der Aegyptischen Drogennamen (Grundriss der Medizin der Alten Ägypter, VI). *Revue de l'histoire des religions* 160, 87–89.

Dawes, J. M., Anderson, D. A., Bennett, D., Bevan, S., and McMahon, S. B. (2013). "Inflammatory mediators and modulators of pain.," in *Wall and Melzack's Textbook of Pain*, 48–67.

de Abreu, M. S., Genario, R., Giacomini, A. C. V. V., Demin, K. A., Lakstygal, A. M., Amstislavskaya, T. G., et al. (2020). Zebrafish as a Model of Neurodevelopmental Disorders. *Neuroscience* 445, 3–11. doi:10.1016/j.neuroscience.2019.08.034.

de Araujo, A. D., Mobli, M., Castro, J., Harrington, A. M., Vetter, I., Dekan, Z., et al. (2014). Selenoether oxytocin analogues have analgesic properties in a mouse model of chronic abdominal pain. *Nat Commun* 5, 3165. doi:10.1038/ncomms4165.

de Cássia da Silveira e Sá, R., Andrade, L., and de Sousa, D. (2013). A Review on Anti-Inflammatory Activity of Monoterpenes. *Molecules* 18, 1227–1254. doi:10.3390/molecules18011227.

de Cássia da Silveira e Sá, R., Lima, T., da Nóbrega, F., de Brito, A., and de Sousa, D. (2017). Analgesic-Like Activity of Essential Oil Constituents: An Update. *IJMS* 18, 2392. doi:10.3390/ijms18122392.

de Santana, M. F., Guimarães, A. G., Chaves, D. O., Silva, J. C., Bonjardim, L. R., de Lucca Júnior, W., et al. (2015). The anti-hyperalgesic and anti-inflammatory profiles of p-cymene: Evidence for the involvement of opioid system and cytokines. *Pharm Biol* 53, 1583–1590. doi:10.3109/13880209.2014.993040.

De Sousa, D. P. (2011). Analgesic-like Activity of Essential Oils Constituents. *Molecules* 16, 2233–2252. doi:10.3390/molecules16032233.

de Sousa, D. P., Nóbrega, F. F. F., de Lima, M. R. V., and de Almeida, R. N. (2011). Pharmacological activity of (R)-(+)-pulegone, a chemical constituent of essential oils. *Z Naturforsch C J Biosci* 66, 353–359. doi:10.1515/znc-2011-7-806.

Deepa, B., and Venkatraman Anuradha, C. (2013). Effects of linalool on inflammation, matrix accumulation and podocyte loss in kidney of streptozotocin-induced diabetic rats. *Toxicology Mechanisms and Methods* 23, 223–234. doi:10.3109/15376516.2012.743638.

DeLaTorre, S., Rojas-Piloni, G., Martínez-Lorenzana, G., Rodríguez-Jiménez, J., Villanueva, L., and Condés-Lara, M. (2009). Paraventricular oxytocinergic hypothalamic prevention or interruption of long-term potentiation in dorsal horn nociceptive neurons: Electrophysiological and behavioral evidence. *Pain* 144, 320–328. doi:10.1016/j.pain.2009.05.002.

Denda, S., Takei, K., Kumamoto, J., Goto, M., Tsutsumi, M., and Denda, M. (2012). Oxytocin is expressed in epidermal keratinocytes and released upon stimulation with adenosine 5′-[γ-thio]triphosphate in vitro. *Exp Dermatol* 21, 535–537. doi:10.1111/j.1600-0625.2012.01507.x.

Deuis, J. R., Dvorakova, L. S., and Vetter, I. (2017). Methods Used to Evaluate Pain Behaviors in Rodents. *Front. Mol. Neurosci.* 10, 284. doi:10.3389/fnmol.2017.00284.

Dhaka, A., Murray, A. N., Mathur, J., Earley, T. J., Petrus, M. J., and Patapoutian, A. (2007). TRPM8 Is Required for Cold Sensation in Mice. *Neuron* 54, 371–378. doi:10.1016/j.neuron.2007.02.024.

Dineley, K. T., Pandya, A. A., and Yakel, J. L. (2015). Nicotinic ACh receptors as therapeutic targets in CNS disorders. *Trends in Pharmacological Sciences* 36, 96–108. doi:10.1016/j.tips.2014.12.002.

Djenane, D. (2015). Chemical Profile, Antibacterial and Antioxidant Activity of Algerian Citrus Essential Oils and Their Application in Sardina pilchardus. *Foods* 4, 208–228. doi:10.3390/foods4020208.

Dogrul, A., Ossipov, M. H., and Porreca, F. (2009). Differential mediation of descending pain facilitation and inhibition by spinal 5HT-3 and 5HT-7 receptors. *Brain Research* 1280, 52–59. doi:10.1016/j.brainres.2009.05.001.

Donaldson, Z. R., and Young, L. J. (2008). Oxytocin, Vasopressin, and the Neurogenetics of Sociality. *Science* 322, 900–904. doi:10.1126/science.1158668.

Donatello, N. N., Emer, A. A., Salm, D. C., Ludtke, D. D., Bordignon, S. A. S. R., Ferreira, J. K., et al. (2020). Lavandula angustifolia essential oil inhalation reduces mechanical hyperalgesia in a model of inflammatory and neuropathic pain: The involvement of opioid and cannabinoid receptors. *Journal of Neuroimmunology* 340, 577145. doi:10.1016/j.jneuroim.2020.577145.

Dragunow, M., and Faull, R. (1989). The use of c-fos as a metabolic marker in neuronal pathway tracing. *Journal of Neuroscience Methods* 29, 261–265. doi:10.1016/0165-0270(89)90150-7.

Duan, B., Cheng, L., Bourane, S., Britz, O., Padilla, C., Garcia-Campmany, L., et al. (2014). Identification of Spinal Circuits Transmitting and Gating Mechanical Pain. *Cell* 159, 1417–1432. doi:10.1016/j.cell.2014.11.003.

Dubin, A. E., and Patapoutian, A. (2010). Nociceptors: the sensors of the pain pathway. *J. Clin. Invest.* 120, 3760–3772. doi:10.1172/JCI42843.

Duque-Wilckens, N., Steinman, M., Grinevich, V., and Trainor, B. (2017). The Role of Oxytocin Neurons in the Bed Nucleus of the Stria Terminalis in Mediating Social Withdrawal. *Biological Psychiatry* 81, S44–S45. doi:10.1016/j.biopsych.2017.02.118.

Eccles, R. (1994). Menthol and Related Cooling Compounds. *Journal of Pharmacy and Pharmacology* 46, 618–630. doi:10.1111/j.2042-7158.1994.tb03871.x.

Eliava, M., Melchior, M., Knobloch-Bollmann, H. S., Wahis, J., da Silva Gouveia, M., Tang, Y., et al. (2016). A New Population of Parvocellular Oxytocin Neurons Controlling Magnocellular Neuron Activity and Inflammatory Pain Processing. *Neuron* 89, 1291–1304. doi:10.1016/j.neuron.2016.01.041.

Engle, M. P., Ness, T. J., and Robbins, M. T. (2012). Intrathecal Oxytocin Inhibits Visceromotor Reflex and Spinal Neuronal Responses to Noxious Distention of the Rat Urinary Bladder: *Regional Anesthesia and Pain Medicine* 37, 515–520. doi:10.1097/AAP.0b013e318266352d.

Ermisch, A., Rühle, H.-J., Landgraf, R., and Hess, J. (1985). Blood—Brain Barrier and Peptides. *J Cereb Blood Flow Metab* 5, 350–357. doi:10.1038/jcbfm.1985.49.

Estacion, M., Dib-Hajj, S. D., Benke, P. J., Te Morsche, R. H. M., Eastman, E. M., Macala, L. J., et al. (2008). NaV1.7 gain-of-function mutations as a continuum: A1632E displays physiological changes associated with erythromelalgia and paroxysmal extreme pain disorder mutations and produces symptoms of both disorders. *J Neurosci* 28, 11079–11088. doi:10.1523/JNEUROSCI.3443-08.2008.

Fanelli, F., Barbier, P., Zanchetta, D., de Benedetti, P. G., and Chini, B. (1999). Activation Mechanism of Human Oxytocin Receptor: A Combined Study of Experimental and Computer-Simulated Mutagenesis. *Mol Pharmacol* 56, 214–225. doi:10.1124/mol.56.1.214.

Fatt, P., and Katz, B. (1953). The electrical properties of crustacean muscle fibres. *The Journal of Physiology* 120, 171–204. doi:10.1113/jphysiol.1953.sp004884.

Favaretto, A. L. V., Ballejo, G. O., Albuquerque-Araújo, W. I. C., Gutkowska, J., Antunes-Rodrigues, J., and McCann, S. M. (1997). Oxytocin Releases Atrial Natriuretic Peptide from Rat Atria In Vitro that Exerts Negative Inotropic and Chronotropic Action. *Peptides* 18, 1377–1381. doi:10.1016/S0196-9781(97)00209-X.

Feng, J., and Hu, H. (2019). A novel player in the field: Merkel disc in touch, itch and pain. *Exp Dermatol* 28, 1412–1415. doi:10.1111/exd.13945.

Figueira, R. J., Peabody, M. F., and Lonstein, J. S. (2008). Oxytocin receptor activity in the ventrocaudal periaqueductal gray modulates anxiety-related behavior in postpartum rats. *Behavioral Neuroscience* 122, 618–628. doi:10.1037/0735-7044.122.3.618.

Foster, E., Wildner, H., Tudeau, L., Haueter, S., Ralvenius, W. T., Jegen, M., et al. (2015). Targeted Ablation, Silencing, and Activation Establish Glycinergic Dorsal Horn Neurons as Key Components of a Spinal Gate for Pain and Itch. *Neuron* 85, 1289–1304. doi:10.1016/j.neuron.2015.02.028.

Franklin, K. B. J. (1998). Analgesia and Abuse Potential: An Accidental Association or a Common Substrate? *Pharmacology Biochemistry and Behavior* 59, 993–1002. doi:10.1016/S0091-3057(97)00535-2.

Frantz, M.-C., Pellissier, L. P., Pflimlin, E., Loison, S., Gandía, J., Marsol, C., et al. (2018). LIT-001, the First Nonpeptide Oxytocin Receptor Agonist that Improves Social Interaction in a Mouse Model of Autism. *J. Med. Chem.* 61, 8670–8692. doi:10.1021/acs.jmedchem.8b00697.

Freyd, M. (1923). The Graphic Rating Scale. *Journal of Educational Psychology* 14, 83–102. doi:10.1037/h0074329.

Galeotti, N., Di Cesare Mannelli, L., Mazzanti, G., Bartolini, A., and Ghelardini, C. (2002). Menthol: a natural analgesic compound. *Neurosci Lett* 322, 145–148. doi:10.1016/s0304-3940(01)02527-7.

García-Añoveros, J., and Nagata, K. (2007). "TRPA1," in *Transient Receptor Potential (TRP) Channels* Handbook of Experimental Pharmacology., eds. V. Flockerzi and B. Nilius (Berlin, Heidelberg: Springer Berlin Heidelberg), 347–362. doi:10.1007/978-3-540-34891-7_21.

Geenen, V., Legros, J.-J., Franchimont, P., Baudrihaye, M., Defresne, M.-P., and Boniver, J. (1986). The Neuroendocrine Thymus: Coexistence of Oxytocin and Neurophysin in the Human Thymus. *Science* 232, 508–511. doi:10.1126/science.3961493.

Geenen, V., Martens, H., Brilot, F., Renard, C., Franchimont, D., and Kecha, O. (2000). Thymic Neuroendocrine Self-Antigens: Role in T-Cell Development and Central T-Cell Self-Tolerance. *Annals of the New York Academy of Sciences* 917, 710–723. doi:10.1111/j.1749-6632.2000.tb05435.x.

Gimpl, G., and Fahrenholz, F. (2001). The Oxytocin Receptor System: Structure, Function, and Regulation. *Physiological Reviews* 81, 629–683. doi:10.1152/physrev.2001.81.2.629.

Godoi, M. M., Junior, H. Z., da Cunha, J. M., and Zanoveli, J. M. (2020). Mu-opioid and CB1 cannabinoid receptors of the dorsal periaqueductal gray interplay in the regulation of fear response, but not antinociception. *Pharmacology Biochemistry and Behavior* 194, 172938. doi:10.1016/j.pbb.2020.172938.

Gonçalves, E. C. D., Assis, P. M., Junqueira, L. A., Cola, M., Santos, A. R. S., Raposo, N. R. B., et al. (2020). Citral Inhibits the Inflammatory Response and Hyperalgesia in Mice: The Role of TLR4, TLR2/Dectin-1, and CB2 Cannabinoid Receptor/ATP-Sensitive K+ Channel Pathways. *J Nat Prod* 83, 1190–1200. doi:10.1021/acs.jnatprod.9b01134.

Gong, L., Gao, F., Li, J., Li, J., Yu, X., Ma, X., et al. (2015). Oxytocin-induced membrane hyperpolarization in pain-sensitive dorsal root ganglia neurons mediated by Ca2+/nNOS/NO/KATP pathway. *Neuroscience* 289, 417–428. doi:10.1016/j.neuroscience.2014.12.058.

Gonzalez-Hernandez, A., and Charlet, A. (2018). Oxytocin, GABA, and TRPV1, the Analgesic Triad? *Front. Mol. Neurosci.* 11, 398. doi:10.3389/fnmol.2018.00398.

González-Hernández, A., Manzano-García, A., Martínez-Lorenzana, G., Tello-García, I. A., Carranza, M., Arámburo, C., et al. (2017). Peripheral oxytocin receptors inhibit the nociceptive input signal to spinal dorsal horn wide-dynamic-range neurons. *Pain* 158, 2117–2128. doi:10.1097/j.pain.0000000000001024.

Gravati, M., Busnelli, M., Bulgheroni, E., Reversi, A., Spaiardi, P., Parenti, M., et al. (2010). Dual modulation of inward rectifier potassium currents in olfactory neuronal cells by promiscuous G protein coupling of the oxytocin receptor: Dual regulation of potassium currents by oxytocin. *Journal of Neurochemistry*, no-no. doi:10.1111/j.1471-4159.2010.06861.x.

Greiner, J. F.-W., Müller, J., Zeuner, M.-T., Hauser, S., Seidel, T., Klenke, C., et al. (2013). 1,8-Cineol inhibits nuclear translocation of NF-κB p65 and NF-κB-dependent transcriptional activity. *Biochimica et Biophysica Acta (BBA) - Molecular Cell Research* 1833, 2866–2878. doi:10.1016/j.bbamcr.2013.07.001.

Grinevich, V., and Charlet, A. (2017). Oxytocin: pain relief in skin. *Pain* 158, 2061–2063. doi:10.1097/j.pain.0000000000001006.

Grinevich, V. V., and Polenov, A. L. (1998). Morphofunctional specialization of the main and accessory magnocellular neuroendocrine nuclei of the hypothalamus. *Neurosci Behav Physiol* 28, 710–714. doi:10.1007/BF02462994.

Guan, X., Li, X., Yang, X., Yan, J., Shi, P., Ba, L., et al. (2019). The neuroprotective effects of carvacrol on ischemia/reperfusion-induced hippocampal neuronal impairment by ferroptosis mitigation. *Life Sciences* 235, 116795. doi:10.1016/j.lfs.2019.116795.

Guimarães, A. G., Quintans, J. S. S., and Quintans-Júnior, L. J. (2013). Monoterpenes with Analgesic Activity-A Systematic Review. *Phytother. Res.* 27, 1–15. doi:10.1002/ptr.4686.

Guimarães, A. G., Xavier, M. A., de Santana, M. T., Camargo, E. A., Santos, C. A., Brito, F. A., et al. (2012). Carvacrol attenuates mechanical hypernociception and inflammatory response. *Naunyn-Schmiedeberg's Arch Pharmacol* 385, 253–263. doi:10.1007/s00210-011-0715-x.

Güler, A. D., Lee, H., Iida, T., Shimizu, I., Tominaga, M., and Caterina, M. (2002). Heat-Evoked Activation of the Ion Channel, TRPV4. *J. Neurosci.* 22, 6408–6414. doi:10.1523/JNEUROSCI.22-15-06408.2002.

Haanwinckel, M. A., Elias, L. K., Favaretto, A. L., Gutkowska, J., McCann, S. M., and Antunes-Rodrigues, J. (1995). Oxytocin mediates atrial natriuretic peptide release and natriuresis after volume expansion in the rat. *Proceedings of the National Academy of Sciences* 92, 7902–7906. doi:10.1073/pnas.92.17.7902.

Haefeli, M., and Elfering, A. (2006). Pain assessment. *Eur Spine J* 15, S17–S24. doi:10.1007/s00586-005-1044-x.

Hall, A. C., Turcotte, C. M., Betts, B. A., Yeung, W.-Y., Agyeman, A. S., and Burk, L. A. (2004). Modulation of human GABAA and glycine receptor currents by menthol and related monoterpenoids. *Eur J Pharmacol* 506, 9–16. doi:10.1016/j.ejphar.2004.10.026.

Han, Y., and Yu, L.-C. (2009). Involvement of oxytocin and its receptor in nociceptive modulation in the central nucleus of amygdala of rats. *Neuroscience Letters* 454, 101–104. doi:10.1016/j.neulet.2009.02.062.

Hasan, M. T., Althammer, F., Silva da Gouveia, M., Goyon, S., Eliava, M., Lefevre, A., et al. (2019). A Fear Memory Engram and Its Plasticity in the Hypothalamic Oxytocin System. *Neuron* 103, 133-146.e8. doi:10.1016/j.neuron.2019.04.029.

Heesen, M., Carvalho, B., Carvalho, J. C. A., Duvekot, J. J., Dyer, R. A., Lucas, D. N., et al. (2019). International consensus statement on the use of uterotonic agents during caesarean section. *Anaesthesia* 74, 1305–1319. doi:10.1111/anae.14757.

Herman, A., and Herman, A. P. (2015). Essential oils and their constituents as skin penetration enhancer for transdermal drug delivery: a review. *Journal of Pharmacy and Pharmacology* 67, 473–485. doi:10.1111/jphp.12334.

Higa, Y., Kashiwadani, H., Sugimura, M., and Kuwaki, T. (2021). Orexinergic descending inhibitory pathway mediates linalool odor-induced analgesia in mice. *Sci Rep* 11, 9224. doi:10.1038/s41598-021-88359-5.

Hilfiger, L., Triaux, Z., Marcic, C., Héberlé, E., Emhemmed, F., Darbon, P., et al. (2021). Anti-Hyperalgesic Properties of Menthol and Pulegone. *Front. Pharmacol.* 12, 753873. doi:10.3389/fphar.2021.753873.

Hilfiger, L., Zhao, Q., Kerspern, D., Inquimbert, P., Andry, V., Goumon, Y., et al. (2020). A Nonpeptide Oxytocin Receptor Agonist for a Durable Relief of Inflammatory Pain. *Sci Rep* 10, 3017. doi:10.1038/s41598-020-59929-w.

Hotta, M., Nakata, R., Katsukawa, M., Hori, K., Takahashi, S., and Inoue, H. (2010). Carvacrol, a component of thyme oil, activates PPARα and γ and suppresses COX-2 expression. *Journal of Lipid Research* 51, 132–139. doi:10.1194/jlr.M900255-JLR200.

Hua, R., Pease, J. E., Cheng, W., Sooranna, S. R., Viney, J. M., Nelson, S. M., et al. (2013). Human Labour is Associated with a Decline in Myometrial Chemokine Receptor Expression: The Role of Prostaglandins, Oxytocin and Cytokines. *Am J Reprod Immunol* 69, 21–32. doi:10.1111/aji.12025.

Huang, H., Michetti, C., Busnelli, M., Managò, F., Sannino, S., Scheggia, D., et al. (2014). Chronic and Acute Intranasal Oxytocin Produce Divergent Social Effects in Mice. *Neuropsychopharmacol* 39, 1102–1114. doi:10.1038/npp.2013.310.

Hylands-White, N., Duarte, R. V., and Raphael, J. H. (2017). An overview of treatment approaches for chronic pain management. *Rheumatol Int* 37, 29–42. doi:10.1007/s00296-016-3481-8.

IASP Terminology. *International Association for the Study of Pain (IASP)*. Available at: https://www.iasp-pain.org/resources/terminology/ [Accessed November 28, 2021].

Institut Pasteur de Lille Douleurs chroniques : la recherche d'un traitement efficace. Available at: https://pasteur-lille.fr/actualites/dossiers/douleurs-chroniques/ [Accessed December 3, 2021].

Institute for Laboratory Animal Research (U.S.) ed. (2008). *Recognition and alleviation of distress in laboratory animals*. Washington, D.C: National Academies Press Available at: https://www.ncbi.nlm.nih.gov/books/NBK4039/.

Iwaszkiewicz, K. S., Schneider, J. J., and Hua, S. (2013). Targeting peripheral opioid receptors to promote analgesic and anti-inflammatory actions. *Front. Pharmacol.* 4. doi:10.3389/fphar.2013.00132.

Ji, R.-R., Samad, T. A., Jin, S.-X., Schmoll, R., and Woolf, C. J. (2002). p38 MAPK activation by NGF in primary sensory neurons after inflammation increases TRPV1 levels and maintains heat hyperalgesia. *Neuron* 36, 57–68. doi:10.1016/s0896-6273(02)00908-x.

Jo, Y.-H., Stoeckel, M.-E., Freund-Mercier, M.-J., and Schlichter, R. (1998). Oxytocin Modulates Glutamatergic Synaptic Transmission between Cultured Neonatal Spinal Cord Dorsal Horn Neurons. *J. Neurosci.* 18, 2377–2386. doi:10.1523/JNEUROSCI.18-07-02377.1998.

Jójárt, J., Jójárt, I., Boda, K., Gálfi, M., Mihály, A., B.-Baldauf, Zs., et al. (2009). Distribution of oxytocin-immunoreactive neuronal elements in the rat spinal cord. *Acta Biologica Hungarica* 60, 333–346. doi:10.1556/ABiol.60.2009.4.1.

Juhás, S., Cikos, S., Czikková, S., Veselá, J., Il'ková, G., Hájek, T., et al. (2008). Effects of borneol and thymoquinone on TNBS-induced colitis in mice. *Folia Biol (Praha)* 54, 1–7.

Juif, P.-E., Breton, J.-D., Rajalu, M., Charlet, A., Goumon, Y., and Poisbeau, P. (2013). Long-Lasting Spinal Oxytocin Analgesia Is Ensured by the Stimulation of Allopregnanolone Synthesis Which Potentiates GABAA Receptor-Mediated Synaptic Inhibition. *Journal of Neuroscience* 33, 16617–16626. doi:10.1523/JNEUROSCI.3084-12.2013.

Juif, P.-E., and Poisbeau, P. (2013). Neurohormonal effects of oxytocin and vasopressin receptor agonists on spinal pain processing in male rats. *Pain* 154, 1449–1456. doi:10.1016/j.pain.2013.05.003.

Julius, D. (2013). TRP channels and pain. *Annu Rev Cell Dev Biol* 29, 355–384. doi:10.1146/annurev-cellbio-101011-155833.

Jurek, B., and Neumann, I. D. (2018). The Oxytocin Receptor: From Intracellular Signaling to Behavior. *Physiological Reviews* 98, 1805–1908. doi:10.1152/physrev.00031.2017.

Kamm, O. (1928). The Dialysis of Pituitary Extracts. *Science* 67, 199–200. doi:10.1126/science.67.1729.199.

Kang, Y.-S., and Park, J.-H. (2000). Brain uptake and the analgesic effect of oxytocin— Its usefulness as an analgesic agent. *Arch Pharm Res* 23, 391–395. doi:10.1007/BF02975453.

Kato, F., Sugimura, Y. K., and Takahashi, Y. (2018). "Pain-Associated Neural Plasticity in the Parabrachial to Central Amygdala Circuit: Pain Changes the Brain, and the Brain Changes the Pain," in *Advances in Pain Research: Mechanisms and Modulation of Chronic Pain* Advances in Experimental Medicine and Biology., eds. B.-C. Shyu and M. Tominaga (Singapore: Springer Singapore), 157–166. doi:10.1007/978-981-13-1756-9_14.

Katsukawa, M., Nakata, R., Takizawa, Y., Hori, K., Takahashi, S., and Inoue, H. (2010). Citral, a component of lemongrass oil, activates PPARα and γ and suppresses COX-2 expression. *Biochimica et Biophysica Acta (BBA) - Molecular and Cell Biology of Lipids* 1801, 1214–1220. doi:10.1016/j.bbalip.2010.07.004.

Katsuyama, S., Otowa, A., Kamio, S., Sato, K., Yagi, T., Kishikawa, Y., et al. (2015). Effect of plantar subcutaneous administration of bergamot essential oil and linalool on formalin-induced nociceptive behavior in mice. *Biomed Res* 36, 47–54. doi:10.2220/biomedres.36.47.

Kender, R. G., Harte, S. E., Munn, E. M., and Borszcz, G. S. (2008). Affective analgesia following muscarinic activation of the ventral tegmental area in rats. *J Pain* 9, 597–605. doi:10.1016/j.jpain.2008.01.334.

Kimura, T., Makino, Y., Saji, F., Takemura, M., Inoue, T., Kikuchi, T., et al. (1994). Molecular characterization of a cloned human oxytocin receptor. *European Journal of Endocrinology* 131, 385–390. doi:10.1530/eje.0.1310385.

Kita, I., Yoshida, Y., and Nishino, S. (2006). An activation of parvocellular oxytocinergic neurons in the paraventricular nucleus in oxytocin-induced yawning and penile erection. *Neuroscience Research* 54, 269–275. doi:10.1016/j.neures.2005.12.005.

Klein, A. H., Sawyer, C. M., Carstens, M. I., Tsagareli, M. G., Tsiklauri, N., and Carstens, E. (2010). Topical application of L-menthol induces heat analgesia, mechanical allodynia, and a biphasic effect on cold sensitivity in rats. *Behav Brain Res* 212, 179–186. doi:10.1016/j.bbr.2010.04.015.

Knobloch, H. S., Charlet, A., Hoffmann, L. C., Eliava, M., Khrulev, S., Cetin, A. H., et al. (2012). Evoked Axonal Oxytocin Release in the Central Amygdala Attenuates Fear Response. *Neuron* 73, 553–566. doi:10.1016/j.neuron.2011.11.030.

Knobloch, H. S., and Grinevich, V. (2014). Evolution of oxytocin pathways in the brain of vertebrates. *Front. Behav. Neurosci.* 8. doi:10.3389/fnbeh.2014.00031.

Kobayashi, K., Fukuoka, T., Obata, K., Yamanaka, H., Dai, Y., Tokunaga, A., et al. (2005). Distinct expression of TRPM8, TRPA1, and TRPV1 mRNAs in rat primary afferent neurons with aδ/c-fibers and colocalization with trk receptors. *J. Comp. Neurol.* 493, 596–606. doi:10.1002/cne.20794.

Kolodny, A., Courtwright, D. T., Hwang, C. S., Kreiner, P., Eadie, J. L., Clark, T. W., et al. (2015). The prescription opioid and heroin crisis: a public health approach to an epidemic of addiction. *Annu Rev Public Health* 36, 559–574. doi:10.1146/annurev-publhealth-031914-122957.

Koohsari, S., Sheikholeslami, M. A., Parvardeh, S., Ghafghazi, S., Samadi, S., Poul, Y. K., et al. (2020). Antinociceptive and antineuropathic effects of cuminaldehyde, the major constituent of Cuminum cyminum seeds: Possible mechanisms of action. *Journal of Ethnopharmacology* 255, 112786. doi:10.1016/j.jep.2020.112786.

Kowalczyk, A., Przychodna, M., Sopata, S., Bodalska, A., and Fecka, I. (2020). Thymol and Thyme Essential Oil—New Insights into Selected Therapeutic Applications. *Molecules* 25, 4125. doi:10.3390/molecules25184125.

Koyama, S., and Heinbockel, T. (2020). The Effects of Essential Oils and Terpenes in Relation to Their Routes of Intake and Application. *IJMS* 21, 1558. doi:10.3390/ijms21051558.

Kubo, A., Shinoda, M., Katagiri, A., Takeda, M., Suzuki, T., Asaka, J., et al. (2017). Oxytocin alleviates orofacial mechanical hypersensitivity associated with infraorbital nerve injury through vasopressin-1A receptors of the rat trigeminal ganglia. *Pain* 158, 649–659. doi:10.1097/j.pain.0000000000000808.

La Rocca, V., da Fonsêca, D. V., Silva-Alves, K. S., Ferreira-da-Silva, F. W., de Sousa, D. P., Santos, P. L., et al. (2017). Geraniol Induces Antinociceptive Effect in Mice Evaluated in Behavioural and Electrophysiological Models. *Basic Clin Pharmacol Toxicol* 120, 22–29. doi:10.1111/bcpt.12630.

László, K., Péczely, L., Géczi, F., Kovács, A., Zagoracz, O., Ollmann, T., et al. (2020). The role of D2 dopamine receptors in oxytocin induced place preference and anxiolytic effect. *Hormones and Behavior* 124, 104777. doi:10.1016/j.yhbeh.2020.104777.

Lee, H. J., Jeong, H. S., Kim, D. J., Noh, Y. H., Yuk, D. Y., and Hong, J. T. (2008). Inhibitory effect of citral on NO production by suppression of iNOS expression and NF-κB activation in RAW264.7 cells. *Arch. Pharm. Res.* 31, 342–349. doi:10.1007/s12272-001-1162-0.

Lee, H.-J., Macbeth, A. H., Pagani, J., and Young, W. S. (2009). Oxytocin: The Great Facilitator of Life. *Progress in Neurobiology*, S030100820900046X. doi:10.1016/j.pneurobio.2009.04.001.

Lee, M. S., Choi, J., Posadzki, P., and Ernst, E. (2012). Aromatherapy for health care: An overview of systematic reviews. *Maturitas* 71, 257–260. doi:10.1016/j.maturitas.2011.12.018.

Lee, S. K., Ryu, P. D., and Lee, S. Y. (2013). Differential distributions of neuropeptides in hypothalamic paraventricular nucleus neurons projecting to the rostral ventrolateral medulla in the rat. *Neuroscience Letters* 556, 160–165. doi:10.1016/j.neulet.2013.09.070.

Leng, G., and Ludwig, M. (2016). Intranasal Oxytocin: Myths and Delusions. *Biological Psychiatry* 79, 243–250. doi:10.1016/j.biopsych.2015.05.003.

Li, J., Zhang, X., and Huang, H. (2014). Protective effect of linalool against lipopolysaccharide/d-galactosamine-induced liver injury in mice. *International Immunopharmacology* 23, 523–529. doi:10.1016/j.intimp.2014.10.001.

Li, T., Wang, P., Wang, S. C., and Wang, Y.-F. (2017a). Approaches Mediating Oxytocin Regulation of the Immune System. *Front. Immunol.* 7. doi:10.3389/fimmu.2016.00693.

Li, Y., Liu, Y., Ma, A., Bao, Y., Wang, M., and Sun, Z. (2017b). In vitro antiviral, anti-inflammatory, and antioxidant activities of the ethanol extract of Mentha piperita L. *Food Sci Biotechnol* 26, 1675–1683. doi:10.1007/s10068-017-0217-9.

Lidierth, M. (2006). Local and diffuse mechanisms of primary afferent depolarization and presynaptic inhibition in the rat spinal cord: Local and diffuse PAD. *The Journal of Physiology* 576, 309–327. doi:10.1113/jphysiol.2006.110577.

Liktor-Busa, E., Keresztes, A., LaVigne, J., Streicher, J. M., and Largent-Milnes, T. M. (2021). Analgesic Potential of Terpenes Derived from *Cannabis sativa*. *Pharmacol Rev* 73, 98–126. doi:10.1124/pharmrev.120.000046.

Lima, M. da S., Quintans-Júnior, L. J., de Santana, W. A., Martins Kaneto, C., Pereira Soares, M. B., and Villarreal, C. F. (2013a). Anti-inflammatory effects of carvacrol: Evidence for a key role of interleukin-10. *European Journal of Pharmacology* 699, 112–117. doi:10.1016/j.ejphar.2012.11.040.

Lima, P. R., de Melo, T. S., Carvalho, K. M. M. B., de Oliveira, Í. B., Arruda, B. R., de Castro Brito, G. A., et al. (2013b). 1,8-cineole (eucalyptol) ameliorates cerulein-induced acute pancreatitis via modulation of cytokines, oxidative stress and NF-κB activity in mice. *Life Sciences* 92, 1195–1201. doi:10.1016/j.lfs.2013.05.009.

Liu, B., Fan, L., Balakrishna, S., Sui, A., Morris, J. B., and Jordt, S.-E. (2013). TRPM8 is the principal mediator of menthol-induced analgesia of acute and inflammatory pain. *Pain* 154, 2169–2177. doi:10.1016/j.pain.2013.06.043.

Lumley, M. A., Cohen, J. L., Borszcz, G. S., Cano, A., Radcliffe, A. M., Porter, L. S., et al. (2011). Pain and emotion: a biopsychosocial review of recent research. *J. Clin. Psychol.* 67, 942–968. doi:10.1002/jclp.20816.

Lummis, S. C. R. (2012). 5-HT3 Receptors. *Journal of Biological Chemistry* 287, 40239–40245. doi:10.1074/jbc.R112.406496.

Lumpkin, E. A., and Caterina, M. J. (2007). Mechanisms of sensory transduction in the skin. *Nature* 445, 858–865. doi:10.1038/nature05662.

Lundeberg, T., Uvnäs-Moberg, K., Ågren, G., and Bruzelius, G. (1994). Anti-nociceptive effects of oxytocin in rats and mice. *Neuroscience Letters* 170, 153–157. doi:10.1016/0304-3940(94)90262-3.

Luo, Y., Sun, W., Feng, X., Ba, X., Liu, T., Guo, J., et al. (2019). (−)-menthol increases excitatory transmission by activating both TRPM8 and TRPA1 channels in mouse spinal lamina II layer. *Biochemical and Biophysical Research Communications* 516, 825–830. doi:10.1016/j.bbrc.2019.06.135.

Luttrell, L. M., Maudsley, S., and Bohn, L. M. (2015). Fulfilling the Promise of "Biased" G Protein–Coupled Receptor Agonism. *Mol Pharmacol* 88, 579–588. doi:10.1124/mol.115.099630.

Lv, Y., Zhang, L., Li, N., Mai, N., Zhang, Y., and Pan, S. (2017). Geraniol promotes functional recovery and attenuates neuropathic pain in rats with spinal cord injury. *Can. J. Physiol. Pharmacol.* 95, 1389–1395. doi:10.1139/cjpp-2016-0528.

Mack, S. O., Kc, P., Wu, M., Coleman, B. R., Tolentino-Silva, F. P., and Haxhiu, M. A. (2002). Paraventricular oxytocin neurons are involved in neural modulation of breathing. *Journal of Applied Physiology* 92, 826–834. doi:10.1152/japplphysiol.00839.2001.

Macpherson, L. J., Geierstanger, B. H., Viswanath, V., Bandell, M., Eid, S. R., Hwang, S., et al. (2005). The Pungency of Garlic: Activation of TRPA1 and TRPV1 in Response to Allicin. *Current Biology* 15, 929–934. doi:10.1016/j.cub.2005.04.018.

Macpherson, L. J., Hwang, S. W., Miyamoto, T., Dubin, A. E., Patapoutian, A., and Story, G. M. (2006). More than cool: promiscuous relationships of menthol and other sensory compounds. *Mol Cell Neurosci* 32, 335–343. doi:10.1016/j.mcn.2006.05.005.

Madrid, R., de la Peña, E., Donovan-Rodriguez, T., Belmonte, C., and Viana, F. (2009). Variable threshold of trigeminal cold-thermosensitive neurons is determined by a balance between TRPM8 and Kv1 potassium channels. *J Neurosci* 29, 3120–3131. doi:10.1523/JNEUROSCI.4778-08.2009.

Mahadevan, S. B. K. (2005). Paracetamol induced hepatotoxicity. *Archives of Disease in Childhood* 91, 598–603. doi:10.1136/adc.2005.076836.

Majikina, A., Takahashi, K., Saito, S., Tominaga, M., and Ohta, T. (2018). Involvement of nociceptive transient receptor potential channels in repellent action of pulegone. *Biochem Pharmacol* 151, 89–95. doi:10.1016/j.bcp.2018.02.032.

Malfliet, A., Coppieters, I., Van Wilgen, P., Kregel, J., De Pauw, R., Dolphens, M., et al. (2017). Brain changes associated with cognitive and emotional factors in chronic pain: A systematic review. *Eur J Pain* 21, 769–786. doi:10.1002/ejp.1003.

Marchese, E., D'onofrio, N., Balestrieri, M. L., Castaldo, D., Ferrari, G., and Donsì, F. (2020). Bergamot essential oil nanoemulsions: antimicrobial and cytotoxic activity. *Zeitschrift für Naturforschung C* 75, 279–290. doi:10.1515/znc-2019-0229.

Martínez-Lorenzana, G., Espinosa-López, L., Carranza, M., Aramburo, C., Paz-Tres, C., Rojas-Piloni, G., et al. (2008). PVN electrical stimulation prolongs withdrawal latencies and releases oxytocin in cerebrospinal fluid, plasma, and spinal cord tissue in intact and neuropathic rats. *Pain* 140, 265–273. doi:10.1016/j.pain.2008.08.015.

McKemy, D. D., Neuhausser, W. M., and Julius, D. (2002). Identification of a cold receptor reveals a general role for TRP channels in thermosensation. *Nature* 416, 52–58. doi:10.1038/nature719.

Medicherla, K., Sahu, B. D., Kuncha, M., Kumar, J. M., Sudhakar, G., and Sistla, R. (2015). Oral administration of geraniol ameliorates acute experimental murine colitis by inhibiting pro-inflammatory cytokines and NF-κB signaling. *Food Funct.* 6, 2984–2995. doi:10.1039/C5FO00405E.

Melzack, R., and Casey, K. (1968). "Sensory, motivational and central control determinants of pain.," in *The Skin Senses.* (Charles C Thomas), 423–443.

Melzack, R., and Wall, P. D. (1965). Pain Mechanisms: A New Theory: A gate control system modulates sensory input from the skin before it evokes pain perception and response. *Science* 150, 971–979. doi:10.1126/science.150.3699.971.

Mens, W. B. J., Witter, A., and Van Wimersma Greidanus, T. B. (1983). Penetration of neurohypophyseal hormones from plasma into cerebrospinal fluid (CSF): Half-times of disappearance of these neuropeptides from CSF. *Brain Research* 262, 143–149. doi:10.1016/0006-8993(83)90478-X.

Mick, G., Perrot, S., Poulain, P., Serrie, A., Eschalier, A., Langley, P., et al. (2013). Impact sociétal de la douleur en France : résultats de l'enquête épidémiologique National Health and Wellness Survey auprès de plus de 15 000 personnes adultes. *Douleurs : Evaluation - Diagnostic - Traitement* 14, 57–66. doi:10.1016/j.douler.2012.12.014.

Miller, R. E., Malfait, A.-M., and Block, J. A. (2017). Current status of nerve growth factor antibodies for the treatment of osteoarthritis pain. *Clin Exp Rheumatol* 35 Suppl 107, 85–87.

Miranda-Cardenas, Y., Rojas-Piloni, G., Martínez-Lorenzana, G., Rodríguez-Jiménez, J., López-Hidalgo, M., Freund-Mercier, M. J., et al. (2006). Oxytocin and electrical stimulation of the paraventricular hypothalamic nucleus produce antinociceptive effects that are reversed by an oxytocin antagonist. *Pain* 122, 182–189. doi:10.1016/j.pain.2006.01.029.

Mogil, J. S. (2019). The translatability of pain across species. *Phil. Trans. R. Soc. B* 374, 20190286. doi:10.1098/rstb.2019.0286.

Morán, A., Montero, M. J., Martín, M. L., and San Román, L. (1989). Pharmacological screening and antimicrobial activity of the essential oil of Artemisia caerulescens subsp. Gallica. *Journal of Ethnopharmacology* 26, 197–203. doi:10.1016/0378-8741(89)90067-6.

Moreno-López, Y., Martínez-Lorenzana, G., Condés-Lara, M., and Rojas-Piloni, G. (2013). Identification of oxytocin receptor in the dorsal horn and nociceptive dorsal root ganglion neurons. *Neuropeptides* 47, 117–123. doi:10.1016/j.npep.2012.09.008.

Morin, V., Del Castillo, J. R. E., Authier, S., Ybarra, N., Otis, C., Gauvin, D., et al. (2008). Evidence for Non-Linear Pharmacokinetics of Oxytocin in Anesthetizetized Rat. *J Pharm Pharm Sci* 11, 12. doi:10.18433/J3PK5X.

Morton, G. J., Thatcher, B. S., Reidelberger, R. D., Ogimoto, K., Wolden-Hanson, T., Baskin, D. G., et al. (2012). Peripheral oxytocin suppresses food intake and causes weight loss in diet-induced obese rats. *American Journal of Physiology-Endocrinology and Metabolism* 302, E134–E144. doi:10.1152/ajpendo.00296.2011.

Muraille, E. (2021). Débat : Pourquoi l'Europe veut interdire l'expérimentation animale et avec quelles conséquences ? *The Conversation*. Available at: http://theconversation.com/debat-pourquoi-leurope-veut-interdire-lexperimentation-animale-et-avec-quelles-consequences-167139 [Accessed January 25, 2022].

Murthy, S. E., Dubin, A. E., and Patapoutian, A. (2017). Piezos thrive under pressure: mechanically activated ion channels in health and disease. *Nat Rev Mol Cell Biol* 18, 771–783. doi:10.1038/nrm.2017.92.

Nagai, Y., Miyakawa, N., Takuwa, H., Hori, Y., Oyama, K., Ji, B., et al. (2020). Deschloroclozapine, a potent and selective chemogenetic actuator enables rapid neuronal and behavioral modulations in mice and monkeys. *Nat Neurosci* 23, 1157–1167. doi:10.1038/s41593-020-0661-3.

Nagoor Meeran, M. F., Seenipandi, A., Javed, H., Sharma, C., Hashiesh, H. M., Goyal, S. N., et al. (2021). Can limonene be a possible candidate for evaluation as an agent or adjuvant against infection, immunity, and inflammation in COVID-19? *Heliyon* 7, e05703. doi:10.1016/j.heliyon.2020.e05703.

Nail-Billaud, S. (2020). Régime : les huiles essentielles qui vous font maigrir ! Available at: https://www.docmorris.fr/conseils-de-pharmacien/article/regime-les-huiles-essentielles-pour-maigrir [Accessed November 16, 2021].

Nasanbuyan, N., Yoshida, M., Takayanagi, Y., Inutsuka, A., Nishimori, K., Yamanaka, A., et al. (2018). Oxytocin–Oxytocin Receptor Systems Facilitate Social Defeat Posture in Male Mice. *Endocrinology* 159, 763–775. doi:10.1210/en.2017-00606.

National Institute on Drug Abuse (2021a). Opioid Overdose Crisis. *National Institute on Drug Abuse*. Available at: https://www.drugabuse.gov/drug-topics/opioids/opioid-overdose-crisis [Accessed November 1, 2021].

National Institute on Drug Abuse (2021b). Overdose Death Rates. *National Institute on Drug Abuse*. Available at: https://www.drugabuse.gov/drug-topics/trends-statistics/overdose-death-rates [Accessed October 28, 2021].

Nersesyan, Y., Demirkhanyan, L., Cabezas-Bratesco, D., Oakes, V., Kusuda, R., Dawson, T., et al. (2017). Oxytocin Modulates Nociception as an Agonist of Pain-Sensing TRPV1. *Cell Reports* 21, 1681–1691. doi:10.1016/j.celrep.2017.10.063.

Neugebauer, V., Galhardo, V., Maione, S., and Mackey, S. C. (2009). Forebrain pain mechanisms. *Brain Research Reviews* 60, 226–242. doi:10.1016/j.brainresrev.2008.12.014.

Newton, M., and Egli, G. E. (1958). The Effect of Intranasal Administration of Oxytocin on the Let-Down of Milk in Lactating Women. *American Journal of Obstetrics and Gynecology* 76, 103–107. doi:10.1016/S0002-9378(16)36872-7.

Nguyen, T. H. D., Itoh, S. G., Okumura, H., and Tominaga, M. (2021). Structural basis for promiscuous action of monoterpenes on TRP channels. *Commun Biol* 4, 293. doi:10.1038/s42003-021-01776-0.

Nielsen, S. (2015). "Benzodiazepines," in *Non-medical and illicit use of psychoactive drugs* Current Topics in Behavioral Neurosciences., eds. S. Nielsen, R. Bruno, and S. Schenk (Cham: Springer International Publishing), 141–159. doi:10.1007/7854_2015_425.

Nishijima, C. M., Ganev, E. G., Mazzardo-Martins, L., Martins, D. F., Rocha, L. R. M., Santos, A. R. S., et al. (2014). Citral: a monoterpene with prophylactic and therapeutic anti-nociceptive effects in experimental models of acute and chronic pain. *Eur J Pharmacol* 736, 16–25. doi:10.1016/j.ejphar.2014.04.029.

Nobel Prize (2021). The Nobel Prize in Physiology or Medicine 2021. *NobelPrize.org*. Available at: https://www.nobelprize.org/prizes/medicine/2021/summary/ [Accessed November 30, 2021].

Noël, J., Zimmermann, K., Busserolles, J., Deval, E., Alloui, A., Diochot, S., et al. (2009). The mechano-activated K+ channels TRAAK and TREK-1 control both warm and cold perception. *EMBO J* 28, 1308–1318. doi:10.1038/emboj.2009.57.

OECD (2019). *Addressing Problematic Opioid Use in OECD Countries*. OECD doi:10.1787/a18286f0-en.

O'Leary, M. A., Bloch, J. I., Flynn, J. J., Gaudin, T. J., Giallombardo, A., Giannini, N. P., et al. (2013). The Placental Mammal Ancestor and the Post–K-Pg Radiation of Placentals. *Science* 339, 662–667. doi:10.1126/science.1229237.

Oz, M., El Nebrisi, E. G., Yang, K.-H. S., Howarth, F. C., and Al Kury, L. T. (2017). Cellular and Molecular Targets of Menthol Actions. *Front. Pharmacol.* 8, 472. doi:10.3389/fphar.2017.00472.

Oz, M., Lozon, Y., Sultan, A., Yang, K.-H. S., and Galadari, S. (2015). Effects of monoterpenes on ion channels of excitable cells. *Pharmacology & Therapeutics* 152, 83–97. doi:10.1016/j.pharmthera.2015.05.006.

Pan, R., Tian, Y., Gao, R., Li, H., Zhao, X., Barrett, J. E., et al. (2012). Central mechanisms of menthol-induced analgesia. *J Pharmacol Exp Ther* 343, 661–672. doi:10.1124/jpet.112.196717.

Patel, R., Gonçalves, L., Leveridge, M., Mack, S. R., Hendrick, A., Brice, N. L., et al. (2014). Anti-hyperalgesic effects of a novel TRPM8 agonist in neuropathic rats: a comparison with topical menthol. *Pain* 155, 2097–2107. doi:10.1016/j.pain.2014.07.022.

Peana, A. T., D'Aquila, P. S., Panin, F., Serra, G., Pippia, P., and Moretti, M. D. L. (2002). Anti-inflammatory activity of linalool and linalyl acetate constituents of essential oils. *Phytomedicine* 9, 721–726. doi:10.1078/094471102321621322.

Pedersen, C. A., Smedley, K. L., Leserman, J., Jarskog, L. F., Rau, S. W., Kampov-Polevoi, A., et al. (2013). Intranasal Oxytocin Blocks Alcohol Withdrawal in Human Subjects. *Alcohol Clin Exp Res* 37, 484–489. doi:10.1111/j.1530-0277.2012.01958.x.

Peier, A. M., Moqrich, A., Hergarden, A. C., Reeve, A. J., Andersson, D. A., Story, G. M., et al. (2002a). A TRP channel that senses cold stimuli and menthol. *Cell* 108, 705–715. doi:10.1016/s0092-8674(02)00652-9.

Peier, A. M., Reeve, A. J., Andersson, D. A., Moqrich, A., Earley, T. J., Hergarden, A. C., et al. (2002b). A Heat-Sensitive TRP Channel Expressed in Keratinocytes. *Science* 296, 2046–2049. doi:10.1126/science.1073140.

Pelletier, J.-S., Dicken, B., Bigam, D., and Cheung, P.-Y. (2014). Cardiac Effects of Vasopressin: *Journal of Cardiovascular Pharmacology* 64, 100–107. doi:10.1097/FJC.0000000000000092.

Pergolizzi, J. V., Taylor, R., LeQuang, J.-A., Raffa, R. B., and the NEMA Research Group (2018). The role and mechanism of action of menthol in topical analgesic products. *J Clin Pharm Ther* 43, 313–319. doi:10.1111/jcpt.12679.

Perri, F., Coricello, A., and Adams, J. D. (2020). Monoterpenoids: The Next Frontier in the Treatment of Chronic Pain? *J* 3, 195–214. doi:10.3390/j3020016.

Peters, S., Slattery, D. A., Uschold-Schmidt, N., Reber, S. O., and Neumann, I. D. (2014). Dose-dependent effects of chronic central infusion of oxytocin on anxiety, oxytocin receptor binding and stress-related parameters in mice. *Psychoneuroendocrinology* 42, 225–236. doi:10.1016/j.psyneuen.2014.01.021.

Petersson, M., Alster, P., Lundeberg, T., and Uvnäs-Moberg, K. (1996). Oxytocin Causes a Long-Term Decrease of Blood Pressure in Female and Male Rats. *Physiology & Behavior* 60, 1311–1315. doi:10.1016/S0031-9384(96)00261-2.

Pethő, G., and Reeh, P. W. (2012). Sensory and Signaling Mechanisms of Bradykinin, Eicosanoids, Platelet-Activating Factor, and Nitric Oxide in Peripheral Nociceptors. *Physiological Reviews* 92, 1699–1775. doi:10.1152/physrev.00048.2010.

Petrovska, B. (2012). Historical review of medicinal plants' usage. *Phcog Rev* 6, 1. doi:10.4103/0973-7847.95849.

Pogorzala, L. A., Mishra, S. K., and Hoon, M. A. (2013). The Cellular Code for Mammalian Thermosensation. *Journal of Neuroscience* 33, 5533–5541. doi:10.1523/JNEUROSCI.5788-12.2013.

Proudfoot, C. J., Garry, E. M., Cottrell, D. F., Rosie, R., Anderson, H., Robertson, D. C., et al. (2006). Analgesia Mediated by the TRPM8 Cold Receptor in Chronic Neuropathic Pain. *Current Biology* 16, 1591–1605. doi:10.1016/j.cub.2006.07.061.

Pugh, G., Smith, P. B., Dombrowski, D. S., and Welch, S. P. (1996). The role of endogenous opioids in enhancing the antinociception produced by the combination of delta 9-tetrahydrocannabinol and morphine in the spinal cord. *J Pharmacol Exp Ther* 279, 608–616.

Pulido, P., Perello, C., and Rodriguez-Concepcion, M. (2012). New Insights into Plant Isoprenoid Metabolism. *Molecular Plant* 5, 964–967. doi:10.1093/mp/sss088.

Quintans, J. S. S., Shanmugam, S., Heimfarth, L., Araújo, A. A. S., Almeida, J. R. G. da S., Picot, L., et al. (2019). Monoterpenes modulating cytokines - A review. *Food and Chemical Toxicology* 123, 233–257. doi:10.1016/j.fct.2018.10.058.

Quintans-Júnior, L. J., Guimarães, A. G., Santana, M. T. de, Araújo, B. E. S., Moreira, F. V., Bonjardim, L. R., et al. (2011). Citral reduces nociceptive and inflammatory response in rodents. *Rev. bras. farmacogn.* 21, 497–502. doi:10.1590/S0102-695X2011005000065.

Quintans-Júnior, L., Moreira, J. C. F., Pasquali, M. A. B., Rabie, S. M. S., Pires, A. S., Schröder, R., et al. (2013). Antinociceptive Activity and Redox Profile of the Monoterpenes (+)-Camphene, p-Cymene, and Geranyl Acetate in Experimental Models. *ISRN Toxicol* 2013, 459530. doi:10.1155/2013/459530.

R. Campbell Thompson (1949). *A Dictionary of Assyrian Botany*. Available at: http://archive.org/details/CampbellThompson1949 [Accessed November 22, 2021].

Rajan, J., and Behrends, M. (2019). Acute Pain in Older Adults: Recommendations for Assessment and Treatment. *Anesthesiol Clin* 37, 507–520. doi:10.1016/j.anclin.2019.04.009.

Ramsey, I. S., Delling, M., and Clapham, D. E. (2006). An Introduction to TRP Channels. *Annu. Rev. Physiol.* 68, 619–647. doi:10.1146/annurev.physiol.68.040204.100431.

Rash, J. A., Aguirre-Camacho, A., and Campbell, T. S. (2014). Oxytocin and Pain: A Systematic Review and Synthesis of Findings. *The Clinical Journal of Pain* 30, 453–462. doi:10.1097/AJP.0b013e31829f57df.

Reardon, S. (2022). First pig-to-human heart transplant: what can scientists learn? *Nature*, d41586-022-00111–9. doi:10.1038/d41586-022-00111-9.

Rehman, M. U., Tahir, M., Khan, A. Q., Khan, R., Oday-O-Hamiza, Lateef, A., et al. (2014). D-limonene suppresses doxorubicin-induced oxidative stress and inflammation via repression of COX-2, iNOS, and NFκB in kidneys of Wistar rats. *Exp Biol Med (Maywood)* 239, 465–476. doi:10.1177/1535370213520112.

Reiter, M. K., Kremarik, P., Freund-Mercier, M. J., Stoeckel, M. E., Desaulles, E., and Feltz, P. (1994). Localization of Oxytocin Binding Sites in the Thoracic and Upper Lumbar Spinal Cord of the Adult and Postnatal Rat: A Histoautoradiographic Study. *European Journal of Neuroscience* 6, 98–104. doi:10.1111/j.1460-9568.1994.tb00251.x.

Reversi, A., Rimoldi, V., Marrocco, T., Cassoni, P., Bussolati, G., Parenti, M., et al. (2005). The Oxytocin Receptor Antagonist Atosiban Inhibits Cell Growth via a “Biased Agonist” Mechanism. *Journal of Biological Chemistry* 280, 16311–16318. doi:10.1074/jbc.M409945200.

Rexed, B. (1952). The cytoarchitectonic organization of the spinal cord in the cat. *J. Comp. Neurol.* 96, 415–495. doi:10.1002/cne.900960303.

Rhodes, C. H., Morriell, J. I., and Pfaff, D. W. (1981). Immunohistochemical analysis of magnocellular elements in rat hypothalamus: Distribution and numbers of cells containing neurophysin, oxytocin, and vasopressin. *J. Comp. Neurol.* 198, 45–64. doi:10.1002/cne.901980106.

Rhudy, J. L., and Meagher, M. W. (2000). Fear and anxiety: divergent effects on human pain thresholds. *Pain* 84, 65–75. doi:10.1016/S0304-3959(99)00183-9.

Ribeiro-Da-Silva, A., and Coimbra, A. (1982). Two types of synaptic glomeruli and their distribution in laminae I-III of the rat spinal cord. *J. Comp. Neurol.* 209, 176–186. doi:10.1002/cne.902090205.

Robinson, D. R., and Gebhart, G. F. (2008). Inside Information: The Unique Features of Visceral Sensation. *Molecular Interventions* 8, 242–253. doi:10.1124/mi.8.5.9.

Rojas-Piloni, G., Gerardo, R.-P., Mejía-Rodríguez, R., Rosalinda, M.-R., Martínez-Lorenzana, G., Guadalupe, M.-L., et al. (2010). Oxytocin, but not vassopressin, modulates nociceptive responses in dorsal horn neurons. *Neurosci Lett* 476, 32–35. doi:10.1016/j.neulet.2010.03.076.

Rousselot, P., Papadopoulos, G., Merighi, A., Poulain, D. A., and Theodosis, D. T. (1990). Oxytocinergic innervation of the rat spinal cord. An electron microscopic study. *Brain Research* 529, 178–184. doi:10.1016/0006-8993(90)90825-V.

Rozen, F., Russo, C., Banville, D., and Zingg, H. H. (1995). Structure, characterization, and expression of the rat oxytocin receptor gene. *Proceedings of the National Academy of Sciences* 92, 200–204. doi:10.1073/pnas.92.1.200.

Rozza, A. L., Meira de Faria, F., Souza Brito, A. R., and Pellizzon, C. H. (2014). The Gastroprotective Effect of Menthol: Involvement of Anti-Apoptotic, Antioxidant and Anti-Inflammatory Activities. *PLoS ONE* 9, e86686. doi:10.1371/journal.pone.0086686.

Rudomin, P., and Schmidt, R. F. (1999). Presynaptic inhibition in the vertebrate spinal cord revisited. *Experimental Brain Research* 129, 1–37. doi:10.1007/s002210050933.

Russell, J., Neumann, I., and Landgraf, R. (1992). Oxytocin and vasopressin release in discrete brain areas after naloxone in morphine-tolerant and -dependent anesthetized rats: push-pull perfusion study. *J. Neurosci.* 12, 1024–1032. doi:10.1523/JNEUROSCI.12-03-01024.1992.

Russo, E. B. (2019). The Case for the Entourage Effect and Conventional Breeding of Clinical Cannabis: No “Strain,” No Gain. *Front. Plant Sci.* 9, 1969. doi:10.3389/fpls.2018.01969.

Sabogal-Guáqueta, A. M., Osorio, E., and Cardona-Gómez, G. P. (2016). Linalool reverses neuropathological and behavioral impairments in old triple transgenic Alzheimer’s mice. *Neuropharmacology* 102, 111–120. doi:10.1016/j.neuropharm.2015.11.002.

Sah, P., Faber, E. S. L., Lopez De Armentia, M., and Power, J. (2003). The Amygdaloid Complex: Anatomy and Physiology. *Physiological Reviews* 83, 803–834. doi:10.1152/physrev.00002.2003.

Salehi, B., Mishra, A. P., Shukla, I., Sharifi-Rad, M., Contreras, M. del M., Segura-Carretero, A., et al. (2018). Thymol, thyme, and other plant sources: Health and potential uses: Thymol, health and potential uses. *Phytotherapy Research* 32, 1688–1706. doi:10.1002/ptr.6109.

Sandkühler, J. (2009). Models and Mechanisms of Hyperalgesia and Allodynia. *Physiological Reviews* 89, 707–758. doi:10.1152/physrev.00025.2008.

Santiago, M., Sachdev, S., Arnold, J. C., McGregor, I. S., and Connor, M. (2019). Absence of Entourage: Terpenoids Commonly Found in *Cannabis sativa* Do Not Modulate the Functional Activity of Δ^{9}-THC at Human CB_{1} and CB_{2} Receptors. *Cannabis and Cannabinoid Research* 4, 165–176. doi:10.1089/can.2019.0016.

Sasannejad, P., Saeedi, M., Shoeibi, A., Gorji, A., Abbasi, M., and Foroughipour, M. (2012). Lavender Essential Oil in the Treatment of Migraine Headache: A Placebo-Controlled Clinical Trial. *Eur Neurol* 67, 288–291. doi:10.1159/000335249.

Savino, W., Arzt, E., and Dardenne, M. (1999). Immunoneuroendocrine Connectivity: The Paradigm of the Thymus-Hypothalamus/Pituitary Axis. *Neuroimmunomodulation* 6, 126–136. doi:10.1159/000026372.

Schoenen, J., Van Hees, J., Gybels, J., de Castro Costa, M., and Vanderhaeghen, J. J. (1985). Histochemical changes of substance P, FRAP, serotonin and succinic dehydrogenase in the spinal cord of rats with adjuvant arthritis. *Life Sciences* 36, 1247–1254. doi:10.1016/0024-3205(85)90269-3.

Scott, J., and Huskisson, E. C. (1976). Graphic representation of pain. *Pain* 2, 175–184.

Sendemir, E., Kafa, I. M., Schäfer, H. H., and Jirikowski, G. F. (2013). Altered oxytocinergic hypothalamus systems in sepsis. *Journal of Chemical Neuroanatomy* 52, 44–48. doi:10.1016/j.jchemneu.2013.05.001.

Shamay-Tsoory, S. G., Fischer, M., Dvash, J., Harari, H., Perach-Bloom, N., and Levkovitz, Y. (2009). Intranasal Administration of Oxytocin Increases Envy and Schadenfreude (Gloating). *Biological Psychiatry* 66, 864–870. doi:10.1016/j.biopsych.2009.06.009.

Shen, Y., Sun, Z., and Guo, X. (2015). Citral inhibits lipopolysaccharide-induced acute lung injury by activating PPAR-γ. *European Journal of Pharmacology* 747, 45–51. doi:10.1016/j.ejphar.2014.09.040.

Sherkheli, M. A., Benecke, H., Doerner, J. F., Kletke, O., Vogt-Eisele, A. K., Gisselmann, G., et al. (2009). Monoterpenoids induce agonist-specific desensitization of transient receptor potential vanilloid-3 (TRPV3) ion channels. *J Pharm Pharm Sci* 12, 116–128. doi:10.18433/j37c7k.

Sikandar, S., Ronga, I., Iannetti, G. D., and Dickenson, A. H. (2013). Neural coding of nociceptive stimuli—from rat spinal neurones to human perception. *Pain* 154, 1263–1273. doi:10.1016/j.pain.2013.03.041.

Silveira, N. S. da, Oliveira-Silva, G. L. de, Lamanes, B. de F., Prado, L. C. da S., and Bispo-da-Silva, L. B. (2014). The Aversive, Anxiolytic-Like, and Verapamil-Sensitive Psychostimulant Effects of Pulegone. *Biological & Pharmaceutical Bulletin* 37, 771–778. doi:10.1248/bpb.b13-00832.

Sofroniew, M. V. (1983). “Morphology of Vasopressin and Oxytocin Neurones and Their Central and Vascular Projections,” in *Progress in Brain Research* (Elsevier), 101–114. doi:10.1016/S0079-6123(08)64378-2.

Soignier, R. D., Taylor, B. K., Baiamonte, B. A., Lee, F. A., Paul, D., and Gould, H. J. (2011). Measurement of CFA-Induced Hyperalgesia and Morphine-Induced Analgesia in Rats: Dorsal vs Plantar Mechanical Stimulation of the Hindpaw. *Pain Med* 12, 451–458. doi:10.1111/j.1526-4637.2011.01066.x.

Soleimani, M., Sheikholeslami, M. A., Ghafghazi, S., Pouriran, R., and Parvardeh, S. (2019). Analgesic effect of α-terpineol on neuropathic pain induced by chronic constriction injury in rat sciatic nerve: Involvement of spinal microglial cells and inflammatory cytokines. *Iranian Journal of Basic Medical Sciences* 22. doi:10.22038/ijbms.2019.14028.

Sousa, D. P. de, Raphael, E., Brocksom, U., and Brocksom, T. J. (2007). Sedative Effect of Monoterpene Alcohols in Mice: A Preliminary Screening. *Zeitschrift für Naturforschung C* 62, 563–566. doi:10.1515/znc-2007-7-816.

Souto-Maior, F. N., Fonsêca, D. V. da, Salgado, P. R. R., Monte, L. de O., de Sousa, D. P., and de Almeida, R. N. (2017). Antinociceptive and anticonvulsant effects of the monoterpene linalool oxide. *Pharm Biol* 55, 63–67. doi:10.1080/13880209.2016.1228682.

Souza, M. C., Siani, A. C., Ramos, M. F. S., Menezes-de-Lima, O. J., and Henriques, M. G. M. O. (2003). Evaluation of anti-inflammatory activity of essential oils from two Asteraceae species. *Pharmazie* 58, 582–586.

Stedronsky, K., Telgmann, R., Tillmann, G., Walther, N., and Ivell, R. (2002). The affinity and activity of the multiple hormone response element in the proximal promoter of the human oxytocin gene. *J Neuroendocrinol* 14, 472–485. doi:10.1046/j.1365-2826.2002.00799.x.

Stojanović, N. M., Randjelović, P. J., Mladenović, M. Z., Ilić, I. R., Petrović, V., Stojiljković, N., et al. (2019). Toxic essential oils, part VI: Acute oral toxicity of lemon balm (Melissa officinalis L.) essential oil in BALB/c mice. *Food and Chemical Toxicology* 133, 110794. doi:10.1016/j.fct.2019.110794.

Story, G. M., Peier, A. M., Reeve, A. J., Eid, S. R., Mosbacher, J., Hricik, T. R., et al. (2003). ANKTM1, a TRP-like Channel Expressed in Nociceptive Neurons, Is Activated by Cold Temperatures. *Cell* 112, 819–829. doi:10.1016/S0092-8674(03)00158-2.

Sun, W., Zhou, Q., Ba, X., Feng, X., Hu, X., Cheng, X., et al. (2018). Oxytocin Relieves Neuropathic Pain Through GABA Release and Presynaptic TRPV1 Inhibition in Spinal Cord. *Front. Mol. Neurosci.* 11, 248. doi:10.3389/fnmol.2018.00248.

Swanson, L. W., and McKellar, S. (1979). The distribution of oxytocin- and neurophysin-stained fibers in the spinal cord of the rat and monkey. *J. Comp. Neurol.* 188, 87–106. doi:10.1002/cne.901880108.

Swanson, L. W., and Sawchenko, P. E. (1983). Hypothalamic Integration: Organization of the Paraventricular and Supraoptic Nuclei. *Annu. Rev. Neurosci.* 6, 269–324. doi:10.1146/annurev.ne.06.030183.001413.

Szeto, A., Nation, D. A., Mendez, A. J., Dominguez-Bendala, J., Brooks, L. G., Schneiderman, N., et al. (2008). Oxytocin attenuates NADPH-dependent superoxide activity and IL-6 secretion in macrophages and vascular cells. *American Journal of Physiology-Endocrinology and Metabolism* 295, E1495–E1501. doi:10.1152/ajpendo.90718.2008.

Takaishi, M., Uchida, K., Suzuki, Y., Matsui, H., Shimada, T., Fujita, F., et al. (2016). Reciprocal effects of capsaicin and menthol on thermosensation through regulated activities of TRPV1 and TRPM8. *J Physiol Sci* 66, 143–155. doi:10.1007/s12576-015-0427-y.

Tan, R., Zheng, W., and Tang, H. (1998). Biologically Active Substances from the Genus *Artemisia*. *Planta Med* 64, 295–302. doi:10.1055/s-2006-957438.

Tan, Z. J., Wei, J. B., Li, Z. W., Shao, M., Hu, Q. S., and Peng, B. W. (2000). [Modulation of GABA-activated currents by oxytocin in rat dorsal root ganglion neurons]. *Sheng Li Xue Bao* 52, 381–384.

Tang, Y., Benusiglio, D., Lefevre, A., Hilfiger, L., Althammer, F., Bludau, A., et al. (2020). Social touch promotes interfemale communication via activation of parvocellular oxytocin neurons. *Nat Neurosci* 23, 1125–1137. doi:10.1038/s41593-020-0674-y.

Tashiro, S., Yamaguchi, R., Ishikawa, S., Sakurai, T., Kajiya, K., Kanmura, Y., et al. (2016). Odour-induced analgesia mediated by hypothalamic orexin neurons in mice. *Sci Rep* 6, 37129. doi:10.1038/srep37129.

Tetali, S. D. (2018). Terpenes and isoprenoids: a wealth of compounds for global use. *Planta* 249, 1–8. doi:10.1007/s00425-018-3056-x.

Tholl, D. (2015). "Biosynthesis and Biological Functions of Terpenoids in Plants," in *Biotechnology of Isoprenoids* Advances in Biochemical Engineering/Biotechnology., eds. J. Schrader and J. Bohlmann (Cham: Springer International Publishing), 63–106. doi:10.1007/10_2014_295.

Todd, A. J. (2010). Neuronal circuitry for pain processing in the dorsal horn. *Nat Rev Neurosci* 11, 823–836. doi:10.1038/nrn2947.

Todd, A. J. (2017). Identifying functional populations among the interneurons in laminae I-III of the spinal dorsal horn. *Mol Pain* 13, 174480691769300. doi:10.1177/1744806917693003.

Ton, H. T., Smart, A. E., Aguilar, B. L., Olson, T. T., Kellar, K. J., and Ahern, G. P. (2015). Menthol Enhances the Desensitization of Human α3β4 Nicotinic Acetylcholine Receptors. *Mol Pharmacol* 88, 256–264. doi:10.1124/mol.115.098285.

Tracy, L. M., Georgiou-Karistianis, N., Gibson, S. J., and Giummarra, M. J. (2015). Oxytocin and the modulation of pain experience: Implications for chronic pain management. *Neuroscience & Biobehavioral Reviews* 55, 53–67. doi:10.1016/j.neubiorev.2015.04.013.

Treede, R.-D., Rief, W., Barke, A., Aziz, Q., Bennett, M., Benoliel, R., et al. (2019). Chronic pain as a symptom or a disease: the IASP Classification of Chronic Pain for the International Classification of Diseases (ICD-11). *Pain* 160, 19–27. doi:10.1097/j.pain.0000000000001384.

Triaux, Z., Petitjean, H., Marchioni, E., Boltoeva, M., and Marcic, C. (2020). Deep eutectic solvent–based headspace single-drop microextraction for the quantification of terpenes in spices. *Anal Bioanal Chem* 412, 933–948. doi:10.1007/s00216-019-02317-9.

Triaux, Z., Petitjean, H., Marchioni, E., Steyer, D., and Marcic, C. (2021). Comparison of Headspace, Hydrodistillation and Pressurized Liquid Extraction of Terpenes and Terpenoids from Food Matrices—Qualitative and Quantitative Analysis. *J Anal Chem* 76, 284–295. doi:10.1134/S1061934821030151.

Tsuchiya, H. (2017). Anesthetic Agents of Plant Origin: A Review of Phytochemicals with Anesthetic Activity. *Molecules* 22, 1369. doi:10.3390/molecules22081369.

Turner, P. V., Pang, D. S., and Lofgren, J. L. (2019). A Review of Pain Assessment Methods in Laboratory Rodents. *comp med* 69, 451–467. doi:10.30802/AALAS-CM-19-000042.

Tzabazis, A., Mechanic, J., Miller, J., Klukinov, M., Pascual, C., Manering, N., et al. (2016). Oxytocin receptor: Expression in the trigeminal nociceptive system and potential role in the treatment of headache disorders. *Cephalalgia* 36, 943–950. doi:10.1177/0333102415618615.

van Loon, J. P. A. M., de Grauw, J. C., van Dierendonck, M., L'Ami, J. J., Back, W., and van Weeren, P. R. (2010). Intra-articular opioid analgesia is effective in reducing pain and inflammation in an equine LPS induced synovitis model: Analgesic and anti-inflammatory effects of intra-articular opioids in equine synovitis. *Equine Veterinary Journal* 42, 412–419. doi:10.1111/j.2042-3306.2010.00077.x.

Vavitsas, K., Fabris, M., and Vickers, C. (2018). Terpenoid Metabolic Engineering in Photosynthetic Microorganisms. *Genes* 9, 520. doi:10.3390/genes9110520.

VIDAL (2021a). Les médicaments des douleurs modérées à sévères. *VIDAL*. Available at: https://www.vidal.fr/maladies/douleurs-fievres/prise-charge-douleur/douleur-moderee-severe.html [Accessed December 8, 2021].

VIDAL (2021b). NEURONTIN. Available at: https://www.vidal.fr/medicaments/gammes/neurontin-6598.html [Accessed January 22, 2022].

VIDAL (2021c). Quels médicaments contre la douleur ? *VIDAL*. Available at: https://www.vidal.fr/maladies/douleurs-fievres/prise-charge-douleur/medicaments.html [Accessed December 7, 2021].

Vierck, C. J., Whitsel, B. L., Favorov, O. V., Brown, A. W., and Tommerdahl, M. (2013). Role of primary somatosensory cortex in the coding of pain. *Pain* 154, 334–344. doi:10.1016/j.pain.2012.10.021.

Viero, C., Shibuya, I., Kitamura, N., Verkhratsky, A., Fujihara, H., Katoh, A., et al. (2010). REVIEW: Oxytocin: Crossing the Bridge between Basic Science and Pharmacotherapy: From Neuropeptide to Happiness Chemical. *CNS Neuroscience & Therapeutics* 16, e138–e156. doi:10.1111/j.1755-5949.2010.00185.x.

Vigan, M. (2010). Essential oils: renewal of interest and toxicity. *Eur J Dermatol* 20, 685–692. doi:10.1684/ejd.2010.1066.

Vogt-Eisele, A. K., Weber, K., Sherkheli, M. A., Vielhaber, G., Panten, J., Gisselmann, G., et al. (2007). Monoterpenoid agonists of TRPV3. *Br J Pharmacol* 151, 530–540. doi:10.1038/sj.bjp.0707245.

Von Deines, H., and Grapow, H. (1959). *Wörterbuch der ägyptischen Drogennamen*. Berlin: Akademie-Verlag.

Wahis, J., Baudon, A., Althammer, F., Kerspern, D., Goyon, S., Hagiwara, D., et al. (2021). Astrocytes mediate the effect of oxytocin in the central amygdala on neuronal activity and affective states in rodents. *Nat Neurosci* 24, 529–541. doi:10.1038/s41593-021-00800-0.

Waldherr, M., and Neumann, I. D. (2007). Centrally released oxytocin mediates mating-induced anxiolysis in male rats. *Proceedings of the National Academy of Sciences* 104, 16681–16684. doi:10.1073/pnas.0705860104.

Walstab, J., Wohlfarth, C., Hovius, R., Schmitteckert, S., Röth, R., Lasitschka, F., et al. (2014). Natural compounds boldine and menthol are antagonists of human 5-HT3 receptors: implications for treating gastrointestinal disorders. *Neurogastroenterol Motil* 26, 810–820. doi:10.1111/nmo.12334.

Wang, G., Tang, W., and Bidigare, R. R. (2005a). "Terpenoids As Therapeutic Drugs and Pharmaceutical Agents," in *Natural Products*, eds. L. Zhang and A. L. Demain (Totowa, NJ: Humana Press), 197–227. doi:10.1007/978-1-59259-976-9_9.

Wang, G., Tang, W., and Bidigare, R. R. (2005b). "Terpenoids As Therapeutic Drugs and Pharmaceutical Agents," in *Natural Products*, eds. L. Zhang and A. L. Demain (Totowa, NJ: Humana Press), 197–227. doi:10.1007/978-1-59259-976-9_9.

Wang, P., Yang, H.-P., Tian, S., Wang, L., Wang, S. C., Zhang, F., et al. (2015). Oxytocin-secreting system: A major part of the neuroendocrine center regulating immunologic activity. *Journal of Neuroimmunology* 289, 152–161. doi:10.1016/j.jneuroim.2015.11.001.

Wang, S., Zhang, D., Hu, J., Jia, Q., Xu, W., Su, D., et al. (2017). A clinical and mechanistic study of topical borneol-induced analgesia. *EMBO Mol Med* 9, 802–815. doi:10.15252/emmm.201607300.

Wang, V. C., and Mullally, W. J. (2020). Pain Neurology. *The American Journal of Medicine* 133, 273–280. doi:10.1016/j.amjmed.2019.07.029.

Wasner, G. (2004). Topical menthol--a human model for cold pain by activation and sensitization of C nociceptors. *Brain* 127, 1159–1171. doi:10.1093/brain/awh134.

West, S. J., Bannister, K., Dickenson, A. H., and Bennett, D. L. (2015). Circuitry and plasticity of the dorsal horn – Toward a better understanding of neuropathic pain. *Neuroscience* 300, 254–275. doi:10.1016/j.neuroscience.2015.05.020.

Wilke, B. U., Kummer, K. K., Leitner, M. G., and Kress, M. (2020). Chloride – The Underrated Ion in Nociceptors. *Front. Neurosci.* 14, 287. doi:10.3389/fnins.2020.00287.

Witschi, R., Punnakkal, P., Paul, J., Walczak, J.-S., Cervero, F., Fritschy, J.-M., et al. (2011). Presynaptic 2-GABAA Receptors in Primary Afferent Depolarization and Spinal Pain Control. *Journal of Neuroscience* 31, 8134–8142. doi:10.1523/JNEUROSCI.6328-10.2011.

Wojtunik-Kulesza, K. A., Targowska-Duda, K., Klimek, K., Ginalska, G., Jóźwiak, K., Waksmundzka-Hajnos, M., et al. (2017). Volatile terpenoids as potential drug leads in Alzheimer's disease. *Open Chemistry* 15, 332–343. doi:10.1515/chem-2017-0040.

Woo, S.-H., Lukacs, V., de Nooij, J. C., Zaytseva, D., Criddle, C. R., Francisco, A., et al. (2015). Piezo2 is the principal mechanotransduction channel for proprioception. *Nat Neurosci* 18, 1756–1762. doi:10.1038/nn.4162.

Xu, L., Han, Y., Chen, X., Aierken, A., Wen, H., Zheng, W., et al. (2020). Molecular mechanisms underlying menthol binding and activation of TRPM8 ion channel. *Nat Commun* 11, 3790. doi:10.1038/s41467-020-17582-x.

Yaksh, T. L., Woller, S. A., Ramachandran, R., and Sorkin, L. S. (2015). The search for novel analgesics: targets and mechanisms. *F1000Prime Rep* 7. doi:10.12703/P7-56.

Yang, H., Tenorio Lopes, L., Barioni, N. O., Roeske, J., Incognito, A. V., Baker, J., et al. (2021). The molecular makeup of peripheral and central baroreceptors: stretching a role for Transient Receptor Potential (TRP), Epithelial Sodium Channel (ENaC), Acid Sensing Ion Channel (ASIC), and Piezo channels. *Cardiovascular Research*, cvab334. doi:10.1093/cvr/cvab334.

Yang, H.-P., Wang, L., Han, L., and Wang, S. C. (2013). Nonsocial Functions of Hypothalamic Oxytocin. *ISRN Neuroscience* 2013, 1–13. doi:10.1155/2013/179272.

Yang, J. (1994). Intrathecal Administration of Oxytocin Induces Analgesia in Low Back Pain Involving the Endogenous Opiate Peptide System: *Spine* 19, 867–871. doi:10.1097/00007632-199404150-00001.

Yang, J., Li, P., Liang, J.-Y., Pan, Y.-J., Yan, X.-Q., Yan, F.-L., et al. (2011a). Oxytocin in the periaqueductal grey regulates nociception in the rat. *Regulatory Peptides* 169, 39–42. doi:10.1016/j.regpep.2011.04.007.

Yang, J., Liang, J.-Y., Zhang, X.-Y., Qiu, P.-Y., Pan, Y.-J., Li, P., et al. (2011b). Oxytocin, but not arginine vasopressin is involving in the antinociceptive role of hypothalamic supraoptic nucleus. *Peptides* 32, 1042–1046. doi:10.1016/j.peptides.2011.02.001.

Yang, J., Yang, Y., Chen, J.-M., Liu, W.-Y., Wang, C.-H., and Lin, B.-C. (2007). Central oxytocin enhances antinociception in the rat. *Peptides* 28, 1113–1119. doi:10.1016/j.peptides.2007.03.003.

Yang, P., and Zhu, M. X. (2014). "TRPV3," in *Mammalian Transient Receptor Potential (TRP) Cation Channels* Handbook of Experimental Pharmacology., eds. B. Nilius and V. Flockerzi (Berlin, Heidelberg: Springer Berlin Heidelberg), 273–291. doi:10.1007/978-3-642-54215-2_11.

Zanandrea, R., Bonan, C. D., and Campos, M. M. (2020). Zebrafish as a model for inflammation and drug discovery. *Drug Discovery Today* 25, 2201–2211. doi:10.1016/j.drudis.2020.09.036.

Zárybnický, T., Boušová, I., Ambrož, M., and Skálová, L. (2018). Hepatotoxicity of monoterpenes and sesquiterpenes. *Arch Toxicol* 92, 1–13. doi:10.1007/s00204-017-2062-2.

Zgheib, R., Chaillou, S., Ouaini, N., Kassouf, A., Rutledge, D., El Azzi, D., et al. (2016). Chemometric Tools to Highlight the Variability of the Chemical Composition and Yield of Lebanese *Origanum syriacum* L. Essential Oil. *Chem. Biodiversity* 13, 1326–1347. doi:10.1002/cbdv.201600061.

Zhang, X.-F., Chen, J., Faltynek, C. R., Moreland, R. B., and Neelands, T. R. (2008). Transient receptor potential A1 mediates an osmotically activated ion channel. *Eur J Neurosci* 27, 605–611. doi:10.1111/j.1460-9568.2008.06030.x.

ANNEXES

ANNEXES

1. References: Table 2 Monoterpenes and analgesia

Adriana Estrella, G.-R., María Eva, G.-T., Alberto, H.-L., María Guadalupe, V.-D., Azucena, C.-V., Sandra, O.-S., et al. (2021). Limonene from Agastache mexicana essential oil produces antinociceptive effects, gastrointestinal protection and improves experimental ulcerative colitis. *Journal of Ethnopharmacology* 280, 114462. doi:10.1016/j.jep.2021.114462.

Almeida, J. R. G. da S., Souza, G. R., Silva, J. C., Saraiva, S. R. G. de L., Júnior, R. G. de O., Quintans, J. de S. S., et al. (2013). Borneol, a bicyclic monoterpene alcohol, reduces nociceptive behavior and inflammatory response in mice. *ScientificWorldJournal* 2013, 808460. doi:10.1155/2013/808460.

Angeles-López, G., Pérez-Vásquez, A., Hernández-Luis, F., Déciga-Campos, M., Bye, R., Linares, E., et al. (2010). Antinociceptive effect of extracts and compounds from Hofmeisteria schaffneri. *Journal of Ethnopharmacology* 131, 425–432. doi:10.1016/j.jep.2010.07.009.

Batista, P. A., Werner, M. F. de P., Oliveira, E. C., Burgos, L., Pereira, P., Brum, L. F. da S., et al. (2010). The antinociceptive effect of (-)-linalool in models of chronic inflammatory and neuropathic hypersensitivity in mice. *J Pain* 11, 1222–1229. doi:10.1016/j.jpain.2010.02.022.

Berliocchi, L., Russo, R., Levato, A., Fratto, V., Bagetta, G., Sakurada, S., et al. (2009). (-)-Linalool attenuates allodynia in neuropathic pain induced by spinal nerve ligation in c57/bl6 mice. *Int Rev Neurobiol* 85, 221–235. doi:10.1016/S0074-7742(09)85017-4.

Brito, R. G., Dos Santos, P. L., Quintans, J. S. S., de Lucca Júnior, W., Araújo, A. A. S., Saravanan, S., et al. (2015). Citronellol, a natural acyclic monoterpene, attenuates mechanical hyperalgesia response in mice: Evidence of the spinal cord lamina I inhibition. *Chem Biol Interact* 239, 111–117. doi:10.1016/j.cbi.2015.06.039.

Brito, R. G., Santos, P. L., Prado, D. S., Santana, M. T., Araújo, A. A. S., Bonjardim, L. R., et al. (2013). Citronellol reduces orofacial nociceptive behaviour in mice - evidence of involvement of retrosplenial cortex and periaqueductal grey areas. *Basic Clin Pharmacol Toxicol* 112, 215–221. doi:10.1111/bcpt.12018.

Cavalcante Melo, F. H., Rios, E. R. V., Rocha, N. F. M., Citó, M. do C. de O., Fernandes, M. L., de Sousa, D. P., et al. (2012). Antinociceptive activity of carvacrol (5-isopropyl-2-methylphenol) in mice. *J Pharm Pharmacol* 64, 1722–1729. doi:10.1111/j.2042-7158.2012.01552.x.

de Almeida, A. A. C., Silva, R. O., Nicolau, L. A. D., de Brito, T. V., de Sousa, D. P., Barbosa, A. L. dos R., et al. (2017). Physio-pharmacological Investigations About the Anti-inflammatory and Antinociceptive Efficacy of (+)-Limonene Epoxide. *Inflammation* 40, 511–522. doi:10.1007/s10753-016-0496-y.

de Santana, M. F., Guimarães, A. G., Chaves, D. O., Silva, J. C., Bonjardim, L. R., de Lucca Júnior, W., et al. (2015). The anti-hyperalgesic and anti-inflammatory profiles of p-cymene: Evidence for the involvement of opioid system and cytokines. *Pharm Biol* 53, 1583–1590. doi:10.3109/13880209.2014.993040.

de Santana, M. T., de Oliveira, M. G. B., Santana, M. F., De Sousa, D. P., Santana, D. G., Camargo, E. A., et al. (2013). Citronellal, a monoterpene present in Java citronella oil, attenuates mechanical nociception response in mice. *Pharm Biol* 51, 1144–1149. doi:10.3109/13880209.2013.781656.

de Sousa, D. P., Júnior, E. V. M., Oliveira, F. S., de Almeida, R. N., Nunes, X. P., and Barbosa-Filho, J. M. (2007). Antinociceptive activity of structural analogues of rotundifolone: structure-activity relationship. *Z Naturforsch C J Biosci* 62, 39–42. doi:10.1515/znc-2007-1-207.

de Sousa, D. P., Nóbrega, F. F. F., de Lima, M. R. V., and de Almeida, R. N. (2011). Pharmacological activity of (R)-(+)-pulegone, a chemical constituent of essential oils. *Z Naturforsch C J Biosci* 66, 353–359. doi:10.1515/znc-2011-7-806.

Galeotti, N., Di Cesare Mannelli, L., Mazzanti, G., Bartolini, A., and Ghelardini, C. (2002). Menthol: a natural analgesic compound. *Neurosci Lett* 322, 145–148. doi:10.1016/s0304-3940(01)02527-7.

Gonçalves, E. C. D., Assis, P. M., Junqueira, L. A., Cola, M., Santos, A. R. S., Raposo, N. R. B., et al. (2020). Citral Inhibits the Inflammatory Response and Hyperalgesia in Mice: The Role of TLR4, TLR2/Dectin-1, and CB2 Cannabinoid Receptor/ATP-Sensitive K+ Channel Pathways. *J Nat Prod* 83, 1190–1200. doi:10.1021/acs.jnatprod.9b01134.

González-Ramírez, A. E., González-Trujano, M. E., Orozco-Suárez, S. A., Alvarado-Vásquez, N., and López-Muñoz, F. J. (2016). Nerol alleviates pathologic markers in the oxazolone-induced colitis model. *European Journal of Pharmacology* 776, 81–89. doi:10.1016/j.ejphar.2016.02.036.

Guimarães, A. G., Oliveira, G. F., Melo, M. S., Cavalcanti, S. C. H., Antoniolli, A. R., Bonjardim, L. R., et al. (2010). Bioassay-guided evaluation of antioxidant and antinociceptive activities of carvacrol. *Basic Clin Pharmacol Toxicol* 107, 949–957. doi:10.1111/j.1742-7843.2010.00609.x.

Hilfiger, L., Triaux, Z., Marcic, C., Héberlé, E., Emhemmed, F., Darbon, P., et al. (2021). Anti-Hyperalgesic Properties of Menthol and Pulegone. *Frontiers in Pharmacology* 12, 3248. doi:10.3389/fphar.2021.753873.

Jiang, J., Shen, Y. Y., Li, J., Lin, Y. H., Luo, C. X., and Zhu, D. Y. (2015). (+)-Borneol alleviates mechanical hyperalgesia in models of chronic inflammatory and neuropathic pain in mice. *Eur J Pharmacol* 757, 53–58. doi:10.1016/j.ejphar.2015.03.056.

Kaimoto, T., Hatakeyama, Y., Takahashi, K., Imagawa, T., Tominaga, M., and Ohta, T. (2016). Involvement of transient receptor potential A1 channel in algesic and analgesic actions of the organic compound limonene. *Eur J Pain* 20, 1155–1165. doi:10.1002/ejp.840.

Katsuyama, S., Otowa, A., Kamio, S., Sato, K., Yagi, T., Kishikawa, Y., et al. (2015). Effect of plantar subcutaneous administration of bergamot essential oil and linalool on formalin-induced nociceptive behavior in mice. *Biomed Res* 36, 47–54. doi:10.2220/biomedres.36.47.

Klein, A. H., Sawyer, C. M., Carstens, M. I., Tsagareli, M. G., Tsiklauri, N., and Carstens, E. (2010). Topical application of L-menthol induces heat analgesia, mechanical allodynia, and a biphasic effect on cold sensitivity in rats. *Behav Brain Res* 212, 179–186. doi:10.1016/j.bbr.2010.04.015.

Koohsari, S., Sheikholeslami, M. A., Parvardeh, S., Ghafghazi, S., Samadi, S., Poul, Y. K., et al. (2020). Antinociceptive and antineuropathic effects of cuminaldehyde, the major constituent of Cuminum cyminum seeds: Possible mechanisms of action. *Journal of Ethnopharmacology* 255, 112786. doi:10.1016/j.jep.2020.112786.

La Rocca, V., da Fonsêca, D. V., Silva-Alves, K. S., Ferreira-da-Silva, F. W., de Sousa, D. P., Santos, P. L., et al. (2017). Geraniol Induces Antinociceptive Effect in Mice Evaluated in Behavioural and Electrophysiological Models. *Basic Clin Pharmacol Toxicol* 120, 22–29. doi:10.1111/bcpt.12630.

Liapi, C., Anifantis, G., Chinou, I., Kourounakis, A., Theodosopoulos, S., and Galanopoulou, P. (2007). Antinociceptive Properties of 1,8-Cineole and β-Pinene, from the Essential Oil of *Eucalyptus camaldulensis* Leaves, in Rodents. *Planta Med* 73, 1247–1254. doi:10.1055/s-2007-990224.

Lima, D. F., Brandão, M. S., Moura, J. B., Leitão, J. M. R. S., Carvalho, F. A. A., Miúra, L. M. C. V., et al. (2011). Antinociceptive activity of the monoterpene α-phellandrene in rodents: possible mechanisms of action. *J Pharm Pharmacol* 64, 283–292. doi:10.1111/j.2042-7158.2011.01401.x.

Liu, B., Fan, L., Balakrishna, S., Sui, A., Morris, J. B., and Jordt, S.-E. (2013). TRPM8 is the principal mediator of menthol-induced analgesia of acute and inflammatory pain. *Pain* 154, 2169–2177. doi:10.1016/j.pain.2013.06.043.

Lorenzetti, B. B., Souza, G. E., Sarti, S. J., Santos Filho, D., and Ferreira, S. H. (1991). Myrcene mimics the peripheral analgesic activity of lemongrass tea. *J Ethnopharmacol* 34, 43–48. doi:10.1016/0378-8741(91)90187-i.

Nishijima, C. M., Ganev, E. G., Mazzardo-Martins, L., Martins, D. F., Rocha, L. R. M., Santos, A. R. S., et al. (2014). Citral: a monoterpene with prophylactic and therapeutic anti-nociceptive effects in experimental models of acute and chronic pain. *Eur J Pharmacol* 736, 16–25. doi:10.1016/j.ejphar.2014.04.029.

Pan, R., Tian, Y., Gao, R., Li, H., Zhao, X., Barrett, J. E., et al. (2012). Central mechanisms of menthol-induced analgesia. *J Pharmacol Exp Ther* 343, 661–672. doi:10.1124/jpet.112.196717.

Passos, F. F. de B., Lopes, E. M., de Araújo, J. M., de Sousa, D. P., Veras, L. M. C., Leite, J. R. S. A., et al. (2015). Involvement of Cholinergic and Opioid System in γ-Terpinene-Mediated Antinociception. *Evid Based Complement Alternat Med* 2015, 829414. doi:10.1155/2015/829414.

Patel, R., Gonçalves, L., Leveridge, M., Mack, S. R., Hendrick, A., Brice, N. L., et al. (2014). Anti-hyperalgesic effects of a novel TRPM8 agonist in neuropathic rats: a comparison with topical menthol. *Pain* 155, 2097–2107. doi:10.1016/j.pain.2014.07.022.

Peana, A. T., De Montis, M. G., Nieddu, E., Spano, M. T., D'Aquila, P. S., and Pippia, P. (2003). Profile of spinal and supra-spinal antinociception of (−)-linalool. *European Journal of Pharmacology* 485, 165–174. doi:10.1016/j.ejphar.2003.11.066.

Quintans-Júnior, L., Moreira, J. C. F., Pasquali, M. A. B., Rabie, S. M. S., Pires, A. S., Schröder, R., et al. (2013). Antinociceptive Activity and Redox Profile of the Monoterpenes (+)-Camphene, p-Cymene, and Geranyl Acetate in Experimental Models. *ISRN Toxicol* 2013, 459530. doi:10.1155/2013/459530.

Quintans-Júnior, L., Rocha, R. F. da, Caregnato, F. F., Moreira, J. C. F., Silva, F. A. da, Araújo, A. A. de S., et al. (2011). Antinociceptive Action and Redox Properties of Citronellal, an Essential Oil Present in Lemongrass. *Journal of Medicinal Food* 14, 630–639. doi:10.1089/jmf.2010.0125.

Rahbar, I., Abbasnejad, M., Haghani, J., Raoof, M., Kooshki, R., and Esmaeili-Mahani, S. (2018). The effect of central administration of alpha-pinene on capsaicin-induced dental pulp nociception. *Int Endod J* 52, 307–317. doi:10.1111/iej.13006.

Rao, V. S. N., Menezes, A. M. S., and Viana, G. S. B. (1990). Effect of myrcene on nociception in mice. *Journal of Pharmacy and Pharmacology* 42, 877–878. doi:10.1111/j.2042-7158.1990.tb07046.x.

Silva, R. O., Salvadori, M. S., Sousa, F. B. M., Santos, M. S., Carvalho, N. S., Sousa, D. P., et al. (2014). Evaluation of the anti-inflammatory and antinociceptive effects of myrtenol, a plant-derived monoterpene alcohol, in mice. *Flavour and Fragrance Journal* 29, 184–192. doi:10.1002/ffj.3195.

Soleimani, M., Sheikholeslami, M. A., Ghafghazi, S., Pouriran, R., and Parvardeh, S. (2019). Analgesic effect of α-terpineol on neuropathic pain induced by chronic constriction injury in rat sciatic nerve: Involvement of spinal microglial cells and inflammatory cytokines. *Iranian Journal of Basic Medical Sciences* 22. doi:10.22038/ijbms.2019.14028.

Souto-Maior, F. N., Fonsêca, D. V. da, Salgado, P. R. R., Monte, L. de O., de Sousa, D. P., and de Almeida, R. N. (2017). Antinociceptive and anticonvulsant effects of the monoterpene linalool oxide. *Pharm Biol* 55, 63–67. doi:10.1080/13880209.2016.1228682.

Wang, S., Zhang, D., Hu, J., Jia, Q., Xu, W., Su, D., et al. (2017). A clinical and mechanistic study of topical borneol-induced analgesia. *EMBO Mol Med* 9, 802–815. doi:10.15252/emmm.201607300.

2. References: Table 3 Monoterpenes *in vivo* targets

Andrade, J. C., Monteiro, Á. B., Andrade, H. H. N., Gonzaga, T. K. S. N., Silva, P. R., Alves, D. N., et al. (2021). Involvement of GABAA Receptors in the Anxiolytic-Like Effect of Hydroxycitronellal. *BioMed Research International* 2021, 1–17. doi:10.1155/2021/9929805.

Bianchini, A. E., Garlet, Q. I., da Cunha, J. A., Bandeira, G., Brusque, I. C. M., Salbego, J., et al. (2017). Monoterpenoids (thymol, carvacrol and S-(+)-linalool) with anesthetic activity in silver catfish (Rhamdia quelen): evaluation of acetylcholinesterase and GABAergic activity. *Braz J Med Biol Res* 50, e6346. doi:10.1590/1414-431X20176346.

da Silveira, N. S., de Oliveira-Silva, G. L., Lamanes, B. de F., Prado, L. C. da S., and Bispo-da-Silva, L. B. (2014). The aversive, anxiolytic-like, and verapamil-sensitive psychostimulant effects of pulegone. *Biol Pharm Bull* 37, 771–778. doi:10.1248/bpb.b13-00832.

de Almeida, A. A. C., Silva, R. O., Nicolau, L. A. D., de Brito, T. V., de Sousa, D. P., Barbosa, A. L. dos R., et al. (2017). Physio-pharmacological Investigations About the Anti-inflammatory and Antinociceptive Efficacy of (+)-Limonene Epoxide. *Inflammation* 40, 511–522. doi:10.1007/s10753-016-0496-y.

de Santana, M. F., Guimarães, A. G., Chaves, D. O., Silva, J. C., Bonjardim, L. R., de Lucca Júnior, W., et al. (2015). The anti-hyperalgesic and anti-inflammatory profiles of p-cymene: Evidence for the involvement of opioid system and cytokines. *Pharm Biol* 53, 1583–1590. doi:10.3109/13880209.2014.993040.

de Santana, M. T., de Oliveira, M. G. B., Santana, M. F., De Sousa, D. P., Santana, D. G., Camargo, E. A., et al. (2013). Citronellal, a monoterpene present in Java citronella oil, attenuates mechanical nociception response in mice. *Pharm Biol* 51, 1144–1149. doi:10.3109/13880209.2013.781656.

Galeotti, N., Di Cesare Mannelli, L., Mazzanti, G., Bartolini, A., and Ghelardini, C. (2002). Menthol: a natural analgesic compound. *Neurosci Lett* 322, 145–148. doi:10.1016/s0304-3940(01)02527-7.

Gonçalves, E. C. D., Assis, P. M., Junqueira, L. A., Cola, M., Santos, A. R. S., Raposo, N. R. B., et al. (2020). Citral Inhibits the Inflammatory Response and Hyperalgesia in Mice: The Role of TLR4, TLR2/Dectin-1, and CB2 Cannabinoid Receptor/ATP-Sensitive K+ Channel Pathways. *J Nat Prod* 83, 1190–1200. doi:10.1021/acs.jnatprod.9b01134.

Jiang, J., Shen, Y. Y., Li, J., Lin, Y. H., Luo, C. X., and Zhu, D. Y. (2015). (+)-Borneol alleviates mechanical hyperalgesia in models of chronic inflammatory and neuropathic pain in mice. *Eur J Pharmacol* 757, 53–58. doi:10.1016/j.ejphar.2015.03.056.

Kaimoto, T., Hatakeyama, Y., Takahashi, K., Imagawa, T., Tominaga, M., and Ohta, T. (2016). Involvement of transient receptor potential A1 channel in algesic and analgesic actions of the organic compound limonene. *Eur J Pain* 20, 1155–1165. doi:10.1002/ejp.840.

Katsuyama, S., Otowa, A., Kamio, S., Sato, K., Yagi, T., Kishikawa, Y., et al. (2015). Effect of plantar subcutaneous administration of bergamot essential oil and linalool on formalin-induced nociceptive behavior in mice. *Biomed Res* 36, 47–54. doi:10.2220/biomedres.36.47.

Koohsari, S., Sheikholeslami, M. A., Parvardeh, S., Ghafghazi, S., Samadi, S., Poul, Y. K., et al. (2020). Antinociceptive and antineuropathic effects of cuminaldehyde, the major constituent of Cuminum cyminum seeds: Possible mechanisms of action. *Journal of Ethnopharmacology* 255, 112786. doi:10.1016/j.jep.2020.112786.

Liapi, C., Anifantis, G., Chinou, I., Kourounakis, A., Theodosopoulos, S., and Galanopoulou, P. (2007). Antinociceptive Properties of 1,8-Cineole and β-Pinene, from the Essential Oil of *Eucalyptus camaldulensis* Leaves, in Rodents. *Planta Med* 73, 1247–1254. doi:10.1055/s-2007-990224.

Lima, D. F., Brandão, M. S., Moura, J. B., Leitão, J. M. R. S., Carvalho, F. A. A., Miúra, L. M. C. V., et al. (2012). Antinociceptive activity of the monoterpene α-phellandrene in rodents: possible mechanisms of action. *J Pharm Pharmacol* 64, 283–292. doi:10.1111/j.2042-7158.2011.01401.x.

Liu, B., Fan, L., Balakrishna, S., Sui, A., Morris, J. B., and Jordt, S.-E. (2013). TRPM8 is the principal mediator of menthol-induced analgesia of acute and inflammatory pain. *Pain* 154, 2169–2177. doi:10.1016/j.pain.2013.06.043.

Nishijima, C. M., Ganev, E. G., Mazzardo-Martins, L., Martins, D. F., Rocha, L. R. M., Santos, A. R. S., et al. (2014). Citral: a monoterpene with prophylactic and therapeutic anti-nociceptive effects in experimental models of acute and chronic pain. *Eur J Pharmacol* 736, 16–25. doi:10.1016/j.ejphar.2014.04.029.

Passos, F. F. de B., Lopes, E. M., de Araújo, J. M., de Sousa, D. P., Veras, L. M. C., Leite, J. R. S. A., et al. (2015). Involvement of Cholinergic and Opioid System in γ-Terpinene-Mediated Antinociception. *Evid Based Complement Alternat Med* 2015, 829414. doi:10.1155/2015/829414.

Patel, R., Gonçalves, L., Leveridge, M., Mack, S. R., Hendrick, A., Brice, N. L., et al. (2014). Anti-hyperalgesic effects of a novel TRPM8 agonist in neuropathic rats: a comparison with topical menthol. *Pain* 155, 2097–2107. doi:10.1016/j.pain.2014.07.022.

Peana, A. T., De Montis, M. G., Nieddu, E., Spano, M. T., D'Aquila, P. S., and Pippia, P. (2004). Profile of spinal and supra-spinal antinociception of (−)-linalool. *European Journal of Pharmacology* 485, 165–174. doi:10.1016/j.ejphar.2003.11.066.

Rahbar, I., Abbasnejad, M., Haghani, J., Raoof, M., Kooshki, R., and Esmaeili-Mahani, S. (2019). The effect of central administration of alpha-pinene on capsaicin-induced dental pulp nociception. *Int Endod J* 52, 307–317. doi:10.1111/iej.13006.

Rao, V. S. N., Menezes, A. M. S., and Viana, G. S. B. (1990). Effect of myrcene on nociception in mice. *Journal of Pharmacy and Pharmacology* 42, 877–878. doi:10.1111/j.2042-7158.1990.tb07046.x.

Santos-Miranda, A., Gondim, A. N., Menezes-Filho, J. E. R., Vasconcelos, C. M. L., Cruz, J. S., and Roman-Campos, D. (2014). Pharmacological evaluation of R(+)-pulegone on cardiac excitability: role of potassium current blockage and control of action potential waveform. *Phytomedicine* 21, 1146–1153. doi:10.1016/j.phymed.2014.05.007.

Vieira, G., Cavalli, J., Gonçalves, E. C. D., Braga, S. F. P., Ferreira, R. S., Santos, A. R. S., et al. (2020). Antidepressant-Like Effect of Terpineol in an Inflammatory Model of Depression: Involvement of the Cannabinoid System and D2 Dopamine Receptor. *Biomolecules* 10, E792. doi:10.3390/biom10050792.

Wang, S., Zhang, D., Hu, J., Jia, Q., Xu, W., Su, D., et al. (2017). A clinical and mechanistic study of topical borneol-induced analgesia. *EMBO Mol Med* 9, 802–815. doi:10.15252/emmm.201607300.

Yang, H., Woo, J., Pae, A. N., Um, M. Y., Cho, N.-C., Park, K. D., et al. (2016). α-Pinene, a Major Constituent of Pine Tree Oils, Enhances Non-Rapid Eye Movement Sleep in Mice through GABAA-benzodiazepine Receptors. *Mol Pharmacol* 90, 530–539. doi:10.1124/mol.116.105080.

3. References: Table 4 Monoterpenes *ex vivo* and *in vitro* targets

Almanaitytė, M., Jurevičius, J., and Mačianskienė, R. (2020). Effect of Carvacrol, TRP Channels Modulator, on Cardiac Electrical Activity. *Biomed Res Int* 2020, 6456805. doi:10.1155/2020/6456805.

Arazi, E., Blecher, G., and Zilberberg, N. (2020). Monoterpenes Differently Regulate Acid-Sensitive and Mechano-Gated K2P Channels. *Front Pharmacol* 11, 704. doi:10.3389/fphar.2020.00704.

Ashoor, A., Nordman, J. C., Veltri, D., Yang, K.-H. S., Shuba, Y., Al Kury, L., et al. (2013). Menthol inhibits 5-HT3 receptor-mediated currents. *J Pharmacol Exp Ther* 347, 398–409. doi:10.1124/jpet.113.203976.

Behrendt, H.-J., Germann, T., Gillen, C., Hatt, H., and Jostock, R. (2004). Characterization of the mouse cold-menthol receptor TRPM8 and vanilloid receptor type-1 VR1 using a fluorometric imaging plate reader (FLIPR) assay. *Br J Pharmacol* 141, 737–745. doi:10.1038/sj.bjp.0705652.

Cheang, W. S., Lam, M. Y., Wong, W. T., Tian, X. Y., Lau, C. W., Zhu, Z., et al. (2013). Menthol relaxes rat aortae, mesenteric and coronary arteries by inhibiting calcium influx. *Eur J Pharmacol* 702, 79–84. doi:10.1016/j.ejphar.2013.01.028.

Choudhary, S., Marjianović, D. S., Wong, C. R., Zhang, X., Abongwa, M., Coats, J. R., et al. (2019). Menthol acts as a positive allosteric modulator on nematode levamisole sensitive nicotinic acetylcholine receptors. *International Journal for Parasitology: Drugs and Drug Resistance* 9, 44–53. doi:10.1016/j.ijpddr.2018.12.005.

Czyzewska, M. M., and Mozrzymas, J. W. (2013). Monoterpene α-thujone exerts a differential inhibitory action on GABA(A) receptors implicated in phasic and tonic GABAergic inhibition. *Eur J Pharmacol* 702, 38–43. doi:10.1016/j.ejphar.2013.01.032.

de Menezes-Filho, J. E. R., Gondim, A. N. S., Cruz, J. S., de Souza, A. A., Santos, J. N. A. dos, Conde-Garcia, E. A., et al. (2014). Geraniol Blocks Calcium and Potassium Channels in the Mammalian Myocardium: Useful Effects to Treat Arrhythmias. *Basic Clin Pharmacol Toxicol* 115, 534–544. doi:10.1111/bcpt.12274.

Deiml, T., Haseneder, R., Zieglgänsberger, W., Rammes, G., Eisensamer, B., Rupprecht, R., et al. (2004). Alpha-thujone reduces 5-HT3 receptor activity by an effect on the agonist-reduced desensitization. *Neuropharmacology* 46, 192–201. doi:10.1016/j.neuropharm.2003.09.022.

García, D. A., Bujons, J., Vale, C., and Suñol, C. (2006). Allosteric positive interaction of thymol with the GABAA receptor in primary cultures of mouse cortical neurons. *Neuropharmacology* 50, 25–35. doi:10.1016/j.neuropharm.2005.07.009.

Gaudioso, C., Hao, J., Martin-Eauclaire, M.-F., Gabriac, M., and Delmas, P. (2012). Menthol pain relief through cumulative inactivation of voltage-gated sodium channels. *Pain* 153, 473–484. doi:10.1016/j.pain.2011.11.014.

Ghosh, M., Schepetkin, I. A., Özek, G., Özek, T., Khlebnikov, A. I., Damron, D. S., et al. (2020). Essential Oils from Monarda fistulosa: Chemical Composition and Activation of Transient Receptor Potential A1 (TRPA1) Channels. *Molecules* 25, 4873. doi:10.3390/molecules25214873.

Gonçalves, J. C. R., Alves, A. de M. H., de Araújo, A. E. V., Cruz, J. S., and Araújo, D. A. M. (2010). Distinct effects of carvone analogues on the isolated nerve of rats. *Eur J Pharmacol* 645, 108–112. doi:10.1016/j.ejphar.2010.07.027.

Gonçalves, J. C. R., Silveira, A. L., de Souza, H. D. N., Nery, A. A., Prado, V. F., Prado, M. A. M., et al. (2013). The monoterpene (-)-carvone: A novel agonist of TRPV1 channels. *Cytometry* 83A, 212–219. doi:10.1002/cyto.a.22236.

Granger, R. E., Campbell, E. L., and Johnston, G. A. R. (2005). (+)- And (-)-borneol: efficacious positive modulators of GABA action at human recombinant alpha1beta2gamma2L GABA(A) receptors. *Biochem Pharmacol* 69, 1101–1111. doi:10.1016/j.bcp.2005.01.002.

Haeseler, G., Maue, D., Grosskreutz, J., Bufler, J., Nentwig, B., Piepenbrock, S., et al. (2002). Voltage-dependent block of neuronal and skeletal muscle sodium channels by thymol and menthol. *Eur J Anaesthesiol* 19, 571–579. doi:10.1017/s0265021502000923.

Hall, A. C., Turcotte, C. M., Betts, B. A., Yeung, W.-Y., Agyeman, A. S., and Burk, L. A. (2004). Modulation of human GABAA and glycine receptor currents by menthol and related monoterpenoids. *Eur J Pharmacol* 506, 9–16. doi:10.1016/j.ejphar.2004.10.026.

Hans, M., Wilhelm, M., and Swandulla, D. (2012). Menthol suppresses nicotinic acetylcholine receptor functioning in sensory neurons via allosteric modulation. *Chem Senses* 37, 463–469. doi:10.1093/chemse/bjr128.

Henderson, B. J., Grant, S., Chu, B. W., Shahoei, R., Huard, S. M., Saladi, S. S. M., et al. (2018). Menthol Stereoisomers Exhibit Different Effects on α4β2 nAChR Upregulation and Dopamine Neuron Spontaneous Firing. *eNeuro* 5, ENEURO.0465-18.2018. doi:10.1523/ENEURO.0465-18.2018.

Jansen, C., Shimoda, L. M. N., Kawakami, J. K., Ang, L., Bacani, A. J., Baker, J. D., et al. (2019). Myrcene and terpene regulation of TRPV1. *Channels (Austin)* 13, 344–366. doi:10.1080/19336950.2019.1654347.

Jarvis, G. E., Barbosa, R., and Thompson, A. J. (2016). Noncompetitive Inhibition of 5-HT3 Receptors by Citral, Linalool, and Eucalyptol Revealed by Nonlinear Mixed-Effects Modeling. *J Pharmacol Exp Ther* 356, 549–562. doi:10.1124/jpet.115.230011.

Joca, H. C., Cruz-Mendes, Y., Oliveira-Abreu, K., Maia-Joca, R. P. M., Barbosa, R., Lemos, T. L., et al. (2012). Carvacrol decreases neuronal excitability by inhibition of voltage-gated sodium channels. *J Nat Prod* 75, 1511–1517. doi:10.1021/np300050g.

Kaimoto, T., Hatakeyama, Y., Takahashi, K., Imagawa, T., Tominaga, M., and Ohta, T. (2016). Involvement of transient receptor potential A1 channel in algesic and analgesic actions of the organic compound limonene. *Eur J Pain* 20, 1155–1165. doi:10.1002/ejp.840.

Lansdell, S. J., Sathyaprakash, C., Doward, A., and Millar, N. S. (2015). Activation of human 5-hydroxytryptamine type 3 receptors via an allosteric transmembrane site. *Mol Pharmacol* 87, 87–95. doi:10.1124/mol.114.094540.

Lau, B. K., Karim, S., Goodchild, A. K., Vaughan, C. W., and Drew, G. M. (2014). Menthol enhances phasic and tonic GABAA receptor-mediated currents in midbrain periaqueductal grey neurons. *Br J Pharmacol* 171, 2803–2813. doi:10.1111/bph.12602.

Leal-Cardoso, J. H., da Silva-Alves, K. S., Ferreira-da-Silva, F. W., dos Santos-Nascimento, T., Joca, H. C., de Macedo, F. H. P., et al. (2010). Linalool blocks excitability in peripheral nerves and voltage-dependent Na+ current in dissociated dorsal root ganglia neurons. *European Journal of Pharmacology* 645, 86–93. doi:10.1016/j.ejphar.2010.07.014.

Lee, S. P., Buber, M. T., Yang, Q., Cerne, R., Cortés, R. Y., Sprous, D. G., et al. (2008). Thymol and related alkyl phenols activate the hTRPA1 channel. *Br J Pharmacol* 153, 1739–1749. doi:10.1038/bjp.2008.85.

Legrand, C., Merlini, J. M., de Senarclens-Bezençon, C., and Michlig, S. (2020). New natural agonists of the transient receptor potential Ankyrin 1 (TRPA1) channel. *Sci Rep* 10, 11238. doi:10.1038/s41598-020-68013-2.

Li, A. S., Iijima, A., Huang, J., Li, Q. X., and Chen, Y. (2020). Putative Mode of Action of the Monoterpenoids Linalool, Methyl Eugenol, Estragole, and Citronellal on Ligand-Gated Ion Channels. *Engineering* 6, 541–545. doi:10.1016/j.eng.2019.07.027.

Liu, B., Fan, L., Balakrishna, S., Sui, A., Morris, J. B., and Jordt, S.-E. (2013). TRPM8 is the principal mediator of menthol-induced analgesia of acute and inflammatory pain. *Pain* 154, 2169–2177. doi:10.1016/j.pain.2013.06.043.

Luo, Q.-T., Fujita, T., Jiang, C.-Y., and Kumamoto, E. (2014). Carvacrol presynaptically enhances spontaneous excitatory transmission and produces outward current in adult rat spinal substantia gelatinosa neurons. *Brain Res* 1592, 44–54. doi:10.1016/j.brainres.2014.10.021.

Luo, Y., Sun, W., Feng, X., Ba, X., Liu, T., Guo, J., et al. (2019). (−)-menthol increases excitatory transmission by activating both TRPM8 and TRPA1 channels in mouse spinal lamina II layer. *Biochemical and Biophysical Research Communications* 516, 825–830. doi:10.1016/j.bbrc.2019.06.135.

Macpherson, L. J., Hwang, S. W., Miyamoto, T., Dubin, A. E., Patapoutian, A., and Story, G. M. (2006). More than cool: promiscuous relationships of menthol and other sensory compounds. *Mol Cell Neurosci* 32, 335–343. doi:10.1016/j.mcn.2006.05.005.

Magyar, J., Szentandrássy, N., Bányász, T., Fülöp, L., Varró, A., and Nánási, P. P. (2002). Effects of thymol on calcium and potassium currents in canine and human ventricular cardiomyocytes. *Br J Pharmacol* 136, 330–338. doi:10.1038/sj.bjp.0704718.

Magyar, J., Szentandrássy, N., Bányász, T., Fülöp, L., Varró, A., and Nánási, P. P. (2004). Effects of terpenoid phenol derivatives on calcium current in canine and human ventricular cardiomyocytes. *Eur J Pharmacol* 487, 29–36. doi:10.1016/j.ejphar.2004.01.011.

Majikina, A., Takahashi, K., Saito, S., Tominaga, M., and Ohta, T. (2018). Involvement of nociceptive transient receptor potential channels in repellent action of pulegone. *Biochem Pharmacol* 151, 89–95. doi:10.1016/j.bcp.2018.02.032.

Mohammadi, B., Haeseler, G., Leuwer, M., Dengler, R., Krampfl, K., and Bufler, J. (2001). Structural requirements of phenol derivatives for direct activation of chloride currents via GABA(A) receptors. *Eur J Pharmacol* 421, 85–91. doi:10.1016/s0014-2999(01)01033-0.

Moqrich, A., Hwang, S. W., Earley, T. J., Petrus, M. J., Murray, A. N., Spencer, K. S. R., et al. (2005). Impaired thermosensation in mice lacking TRPV3, a heat and camphor sensor in the skin. *Science* 307, 1468–1472. doi:10.1126/science.1108609.

Nguyen, P. T. T., Jang, S. H., Rijal, S., Park, S. J., and Han, S. K. (2020). Inhibitory actions of borneol on the substantia gelatinosa neurons of the trigeminal subnucleus caudalis in mice. *Korean J Physiol Pharmacol* 24, 433–440. doi:10.4196/kjpp.2020.24.5.433.

Nguyen, T. H. D., Itoh, S. G., Okumura, H., and Tominaga, M. (2021). Structural basis for promiscuous action of monoterpenes on TRP channels. *Commun Biol* 4, 293. doi:10.1038/s42003-021-01776-0.

Ortar, G., Schiano Moriello, A., Morera, E., Nalli, M., Di Marzo, V., and De Petrocellis, L. (2014). Effect of acyclic monoterpene alcohols and their derivatives on TRP channels. *Bioorg Med Chem Lett* 24, 5507–5511. doi:10.1016/j.bmcl.2014.10.012.

Pan, R., Tian, Y., Gao, R., Li, H., Zhao, X., Barrett, J. E., et al. (2012). Central mechanisms of menthol-induced analgesia. *J Pharmacol Exp Ther* 343, 661–672. doi:10.1124/jpet.112.196717.

Park, T.-J., Park, Y.-S., Lee, T.-G., Ha, H., and Kim, K.-T. (2003). Inhibition of acetylcholine-mediated effects by borneol. *Biochem Pharmacol* 65, 83–90. doi:10.1016/s0006-2952(02)01444-2.

Park, T.-J., Seo, H.-K., Kang, B.-J., and Kim, K.-T. (2001). Noncompetitive inhibition by camphor of nicotinic acetylcholine receptors. *Biochemical Pharmacology* 61, 787–793. doi:10.1016/S0006-2952(01)00547-0.

Parnas, M., Peters, M., Dadon, D., Lev, S., Vertkin, I., Slutsky, I., et al. (2009). Carvacrol is a novel inhibitor of Drosophila TRPL and mammalian TRPM7 channels. *Cell Calcium* 45, 300–309. doi:10.1016/j.ceca.2008.11.009.

Peier, A. M., Moqrich, A., Hergarden, A. C., Reeve, A. J., Andersson, D. A., Story, G. M., et al. (2002). A TRP channel that senses cold stimuli and menthol. *Cell* 108, 705–715. doi:10.1016/s0092-8674(02)00652-9.

Priestley, C. M., Williamson, E. M., Wafford, K. A., and Sattelle, D. B. (2003). Thymol, a constituent of thyme essential oil, is a positive allosteric modulator of human GABA(A) receptors and a homo-oligomeric GABA receptor from Drosophila melanogaster. *Br J Pharmacol* 140, 1363–1372. doi:10.1038/sj.bjp.0705542.

Re, L., Barocci, S., Sonnino, S., Mencarelli, A., Vivani, C., Paolucci, G., et al. (2000). Linalool modifies the nicotinic receptor–ion channel kinetics at the mouse neuromuscular junction. *Pharmacological Research* 42, 177–181. doi:10.1006/phrs.2000.0671.

Reiner, G. N., Delgado-Marín, L., Olguín, N., Sánchez-Redondo, S., Sánchez-Borzone, M., Rodríguez-Farré, E., et al. (2013). GABAergic pharmacological activity of propofol related compounds as possible enhancers of general anesthetics and interaction with membranes. *Cell Biochem Biophys* 67, 515–525. doi:10.1007/s12013-013-9537-4.

Santos-Miranda, A., Gondim, A. N., Menezes-Filho, J. E. R., Vasconcelos, C. M. L., Cruz, J. S., and Roman-Campos, D. (2014). Pharmacological evaluation of R(+)-pulegone on cardiac excitability: role of potassium current blockage and control of action potential waveform. *Phytomedicine* 21, 1146–1153. doi:10.1016/j.phymed.2014.05.007.

Selescu, T., Ciobanu, A. C., Dobre, C., Reid, G., and Babes, A. (2013). Camphor activates and sensitizes transient receptor potential melastatin 8 (TRPM8) to cooling and icilin. *Chem Senses* 38, 563–575. doi:10.1093/chemse/bjt027.

Shen, A.-Y., Huang, M.-H., Wang, T.-S., Wu, H.-M., Kang, Y.-F., and Chen, C.-L. (2009). Thymol-evoked Ca+ mobilization and ion currents in pituitary GH3 cells. *Nat Prod Commun* 4, 749–752.

Sherkheli, M. A., Benecke, H., Doerner, J. F., Kletke, O., Vogt-Eisele, A. K., Gisselmann, G., et al. (2009). Monoterpenoids induce agonist-specific desensitization of transient receptor potential vanilloid-3 (TRPV3) ion channels. *J Pharm Pharm Sci* 12, 116–128. doi:10.18433/j37c7k.

Sidell, N., Verity, M. A., and Nord, E. P. (1990). Menthol blocks dihydropyridine-insensitive Ca2+ channels and induces neurite outgrowth in human neuroblastoma cells. *J Cell Physiol* 142, 410–419. doi:10.1002/jcp.1041420226.

Stotz, S. C., Vriens, J., Martyn, D., Clardy, J., and Clapham, D. E. (2008). Citral sensing by Transient [corrected] receptor potential channels in dorsal root ganglion neurons. *PLoS One* 3, e2082. doi:10.1371/journal.pone.0002082.

Takaishi, M., Fujita, F., Uchida, K., Yamamoto, S., Sawada (Shimizu), M., Hatai (Uotsu), C., et al. (2012). 1,8-Cineole, a TRPM8 Agonist, is a Novel Natural Antagonist of Human TRPA1. *Mol Pain* 8, 1744-8069-8–86. doi:10.1186/1744-8069-8-86.

Takaishi, M., Uchida, K., Fujita, F., and Tominaga, M. (2014). Inhibitory effects of monoterpenes on human TRPA1 and the structural basis of their activity. *J Physiol Sci* 64, 47–57. doi:10.1007/s12576-013-0289-0.

Takaishi, M., Uchida, K., Suzuki, Y., Matsui, H., Shimada, T., Fujita, F., et al. (2016). Reciprocal effects of capsaicin and menthol on thermosensation through regulated activities of TRPV1 and TRPM8. *J Physiol Sci* 66, 143–155. doi:10.1007/s12576-015-0427-y.

Ton, H. T., Smart, A. E., Aguilar, B. L., Olson, T. T., Kellar, K. J., and Ahern, G. P. (2015). Menthol Enhances the Desensitization of Human α3β4 Nicotinic Acetylcholine Receptors. *Mol Pharmacol* 88, 256–264. doi:10.1124/mol.115.098285.

Vatanparast, J., Bazleh, S., and Janahmadi, M. (2017). The effects of linalool on the excitability of central neurons of snail Caucasotachea atrolabiata. *Comp Biochem Physiol C Toxicol Pharmacol* 192, 33–39. doi:10.1016/j.cbpc.2016.12.004.

Vogt-Eisele, A. K., Weber, K., Sherkheli, M. A., Vielhaber, G., Panten, J., Gisselmann, G., et al. (2007). Monoterpenoid agonists of TRPV3. *Br J Pharmacol* 151, 530–540. doi:10.1038/sj.bjp.0707245.

Walstab, J., Wohlfarth, C., Hovius, R., Schmitteckert, S., Röth, R., Lasitschka, F., et al. (2014). Natural compounds boldine and menthol are antagonists of human 5-HT3 receptors: implications for treating gastrointestinal disorders. *Neurogastroenterol Motil* 26, 810–820. doi:10.1111/nmo.12334.

Wang, S., Zhang, D., Hu, J., Jia, Q., Xu, W., Su, D., et al. (2017). A clinical and mechanistic study of topical borneol-induced analgesia. *EMBO Mol Med* 9, 802–815. doi:10.15252/emmm.201607300.

Wang, W., Wang, H., Zhao, Z., Huang, X., Xiong, H., and Mei, Z. (2020). Thymol activates TRPM8-mediated Ca2+ influx for its antipruritic effects and alleviates inflammatory response in Imiquimod-induced mice. *Toxicology and Applied Pharmacology* 407, 115247. doi:10.1016/j.taap.2020.115247.

Xu, H., Blair, N. T., and Clapham, D. E. (2005). Camphor activates and strongly desensitizes the transient receptor potential vanilloid subtype 1 channel in a vanilloid-independent mechanism. *J Neurosci* 25, 8924–8937. doi:10.1523/JNEUROSCI.2574-05.2005.

Xu, H., Delling, M., Jun, J. C., and Clapham, D. E. (2006). Oregano, thyme and clove-derived flavors and skin sensitizers activate specific TRP channels. *Nat Neurosci* 9, 628–635. doi:10.1038/nn1692.

Xu, Z.-H., Wang, C., Fujita, T., Jiang, C.-Y., and Kumamoto, E. (2015). Action of thymol on spontaneous excitatory transmission in adult rat spinal substantia gelatinosa neurons. *Neurosci Lett* 606, 94–99. doi:10.1016/j.neulet.2015.08.042.

Yang, H., Woo, J., Pae, A. N., Um, M. Y., Cho, N.-C., Park, K. D., et al. (2016). α-Pinene, a Major Constituent of Pine Tree Oils, Enhances Non-Rapid Eye Movement Sleep in Mice through GABAA-benzodiazepine Receptors. *Mol Pharmacol* 90, 530–539. doi:10.1124/mol.116.105080.

Ye, C.-J., Li, S.-A., Zhang, Y., and Lee, W.-H. (2019). Geraniol targets KV1.3 ion channel and exhibits anti-inflammatory activity in vitro and in vivo. *Fitoterapia* 139, 104394. doi:10.1016/j.fitote.2019.104394.

Zhang, X.-B., Jiang, P., Gong, N., Hu, X.-L., Fei, D., Xiong, Z.-Q., et al. (2008). A-type GABA receptor as a central target of TRPM8 agonist menthol. *PLoS One* 3, e3386. doi:10.1371/journal.pone.0003386.

Zolfaghari, Z., and Vatanparast, J. (2020). Thymol provokes burst of action potentials in neurons of snail Caucasotachea atrolabiata. *Comp Biochem Physiol C Toxicol Pharmacol* 228, 108654. doi:10.1016/j.cbpc.2019.108654.

4. Results: Terpene combination - Confidential data

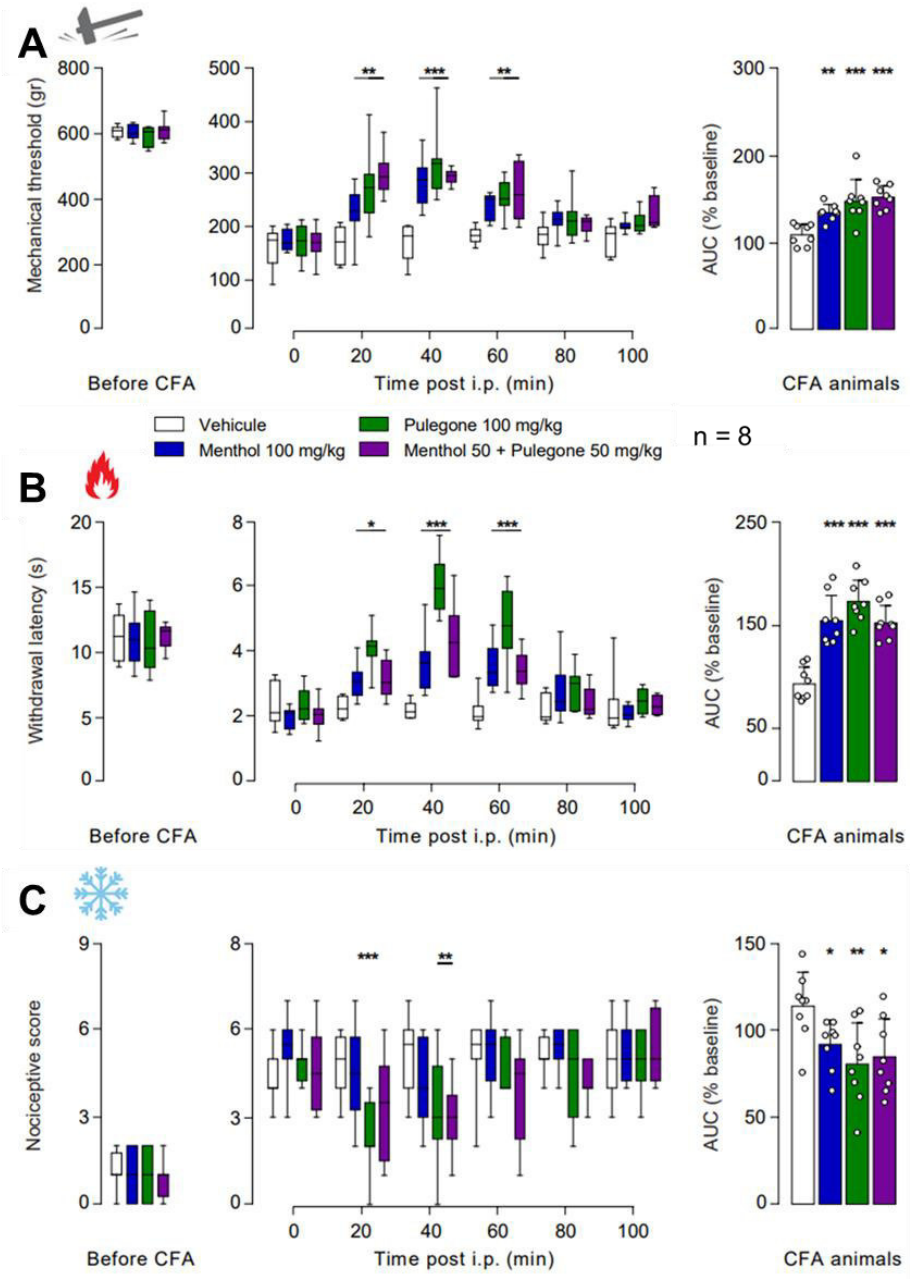

Time-course of the analgesic properties of menthol, pulegone and monterpene mix (menthol + pulegone) on CFA-induced inflammatory pain model. Baseline, time-course, and relative-to-baseline AUC (%) of the effects of i.p. menthol 100 mg/kg (n = 8), pulegone 100 mg/kg (n = 8), menthol 50 mg/kg + pulegone 50 mg/kg (n = 8) or the vehicle (n = 8) on CFA-induced mechanical (**A**), thermal heat (**B**), and thermal cold (**C**) hyperalgesia (for the methods, see Hilfiger et al., 2021). Data are expressed as mean ± SD. Asterisks indicate statistical significance (***p < 0.001; **p < 0.01; *p < 0.05).

5. Article S1: Social touch promotes interfemale communication via activation of parvocellular oxytocin neurons

Publication not directly related to the thesis

nature neuroscience

ARTICLES

https://doi.org/10.1038/s41593-020-0674-y

Check for updates

Social touch promotes interfemale communication via activation of parvocellular oxytocin neurons

Yan Tang[1,9,10], Diego Benusiglio[1,10], Arthur Lefevre[1,2,10], Louis Hilfiger[2,10], Ferdinand Althammer[1,3], Anna Bludau[4], Daisuke Hagiwara[1], Angel Baudon[2], Pascal Darbon[2], Jonas Schimmer[1], Matthew K. Kirchner[3], Ranjan K. Roy[3], Shiyi Wang[1], Marina Eliava[1], Shlomo Wagner[5], Martina Oberhuber[6], Karl K. Conzelmann[6], Martin Schwarz[7], Javier E. Stern[3], Gareth Leng[8], Inga D. Neumann[4,11], Alexandre Charlet[2,11] ✉ and Valery Grinevich[1,3,11] ✉

Oxytocin (OT) is a great facilitator of social life but, although its effects on socially relevant brain regions have been extensively studied, OT neuron activity during actual social interactions remains unexplored. Most OT neurons are magnocellular neurons, which simultaneously project to the pituitary and forebrain regions involved in social behaviors. In the present study, we show that a much smaller population of OT neurons, parvocellular neurons that do not project to the pituitary but synapse onto magnocellular neurons, is preferentially activated by somatosensory stimuli. This activation is transmitted to the larger population of magnocellular neurons, which consequently show coordinated increases in their activity during social interactions between virgin female rats. Selectively activating these parvocellular neurons promotes social motivation, whereas inhibiting them reduces social interactions. Thus, parvocellular OT neurons receive particular inputs to control social behavior by coordinating the responses of the much larger population of magnocellular OT neurons.

The hypothalamic neuropeptide OT promotes various types of social behavior[1–3]. OT is mainly synthesized in neurons of the paraventricular nuclei (PVN) and supraoptic nuclei (SON) of the hypothalamus. The vast majority of these neurons project to the posterior pituitary, where OT is secreted into the blood for essential physiological effects, such as suckling-induced milk letdown and regulation of uterine contractions during birth[4]. In parallel, these neurons project axonal collaterals to forebrain regions[5] that express OT receptors (OTRs), including the central nucleus of the amygdala, nucleus accumbens, lateral septum, hippocampus and medial prefrontal cortex[6,7]. Studies employing microdialysis to measure OT concentrations within socially relevant brain regions revealed that OT is released in the bed nucleus of the stria terminalis, lateral septum and central nucleus of the amygdala during social investigation of a conspecific[2,8,9]. However, to date, no direct measurement of OT neuron activity during actual social interaction of freely moving conspecifics has been performed, although it was recently reported that social approach triggers calcium release in PVN OT neurons in immobilized, head-fixed male mice[10].

Several studies suggest that female–female interactions are predominantly mediated via somatosensory inputs[11,12], whereas other interactions such as male–male, male–female or parental contact may rely on other sensory modalities. However, whether these sensory stimulations can activate OT neurons is unknown because, to date, there has been no direct recording of activity from identified OT neurons during actual social behavior. In an attempt to address these points, in the present study, we performed ex vivo and in vivo manipulation of OT neuron activity primarily in the PVN—the main source of OT in the brain[5]—to decipher their involvement in the modulation of social interaction in freely moving female rats.

Results

PVN OT neurons are activated on social interaction. To identify OT neurons electrophysiologically, we injected a recombinant adeno-associated virus (rAAV-OTp-ChR2-mCherry) bilaterally into the PVN to induce expression of the light-sensitive ion channel Channelrhodopsin-2 (ChR2) under the control of the OT promoter[5,13]. This resulted in 90.4% of ChR2-expressing neurons being OT positive, showing the high specificity of the infection in the PVN (Extended Data Fig. 1a). We then recorded individual neurons in the PVN using implanted tetrodes combined with an optic fiber to identify the OT neurons by their electrophysiological response to blue-laser pulses, similar to methods described previously[14].

In total, we recorded 90 neurons in 10 adult female rats at the diestrus phase of the ovarian cycle, while monitoring the behavior of the rats and their ultrasonic vocalizations during both open field (OF) exploration and free social interactions (FSIs) (Fig. 1a,b). Of these neurons, 15 (in 5 animals) were stringently identified as single OT neurons (Extended Data Fig. 1e). In the OF arena, the patterns of spiking activity of these neurons (Fig. 1d and Extended

[1]Department of Neuropeptide Research in Psychiatry, Central Institute of Mental Health, Medical Faculty Mannheim, University of Heidelberg, Mannheim, Germany. [2]Centre National de la Recherche Scientifique, Institute of Cellular and Integrative Neurosciences, University of Strasbourg, Strasbourg, France. [3]Center for Neuroinflammation and Cardiometabolic Diseases, Georgia State University, Atlanta, GA, USA. [4]Department of Neurobiology and Animal Physiology, University of Regensburg, Regensburg, Germany. [5]Sagol Department of Neurobiology, University of Haifa, Mount Carmel, Haifa, Israel. [6]Max von Pettenkofer-Institute Virology, Faculty of Medicine and Gene Center, Ludwig Maximilian University, Munich, Germany. [7]Institute for Experimental Epileptology and Cognition Research, University of Bonn Medical Center, Bonn, Germany. [8]Centre for Discovery Brain Sciences, University of Edinburgh, Edinburgh, UK. [9]Present address: Centre de Neurosciences Psychiatriques, Centre Hospitalier Universitaire Vaudois (CHUV) , Prilly (Lausanne), Switzerland. [10]These authors contributed equally: Yan Tang, Diego Benusiglio, Arthur Lefevre, Louis Hilfiger. [11]These authors jointly supervised this work: Inga D. Neumann, Alexandre Charlet, Valery Grinevich. ✉e-mail: acharlet@unistra.fr; valery.grinevich@zi-mannheim.de

Data Fig. 2d) were indistinguishable from those of OT neurons observed under basal conditions in anesthetized rats, because these neurons displayed typical OT neuron characteristics[15]. Specifically, they all display a low rate of tonic firing (~1 Hz) with a low index of dispersion of spikes (<1), and a distribution of interspike intervals consistent with random spike generation subject to a prolonged relative refractory period. In contrast, during episodes of FSI with an unfamiliar conspecific, the same neurons fired at a higher rate (mean increase 1.5 ± 0.4 spikes s^{-1}, $P = 0.001$, $n = 15$; Fig. 1c,d) and more irregularly; the second-by-second firing rates showed a high index of dispersion, reflecting the prominent occurrence of clusters of spikes (Fig. 1d and Extended Data Fig. 1n).

As revealed by cross-correlation analysis, OT neurons also displayed increased synchronicity during FSI (mean pairwise correlation: OF, 0.10 ± 0.04; FSI, 0.40 ± 0.08, $P = 0.001$; Extended Data Fig. 1k–l). In anesthetized rats, adjacent OT neurons showed no such cross-correlated activity. We also recorded local field potentials in the PVN and found a substantial increase of oscillatory power in the theta (5–10 Hz) frequency band during FSI (Extended Data Fig. 1f–h). The spike activity of OT neurons tended to be phase-locked with theta oscillations during FSI, but not in the OF arena (Extended Data Fig. 1i,j). In contrast to OT neurons, non-OT PVN neurons did not show an increase in spiking activity when comparing exploratory behavior and social interaction (Extended Data Fig. 2e–g).

Thus, during FSI with actual physical contact, OT neurons in the PVN were more active and exhibited frequent clusters of spikes, and this activity was correlated among the OT neurons.

Social physical contact increases PVN OT neuron activity. To examine which component of social interaction activates these neurons, we first recorded their neuronal activity during a chambered social interaction (CSI)[16]. In this setup, experimental and stimulus rats were separated by a transparent wall with small holes (7.5 mm), allowing rats to see, sniff and hear, but not touch, each other (Fig. 1e).

OT neurons showed little change in spiking activity between CSI and baseline recordings in an OF (CSI: 1.4 ± 0.4 spikes s^{-1}; OF: 1.0 ± 0.2 spikes s^{-1}, $P = 0.14$; Fig. 1f). When the wall was removed to allow FSI, the same OT neurons displayed a significant increase in activity (FSI: 3.0 ± 0.4 spikes s^{-1}, $P < 0.001$; Fig. 1f), accompanied by an increase in index of dispersion (FSI 3.2 ± 0.4, CSI 1.3 ± 0.3, $P = 0.006$ versus FSI; OF 0.9 ± 0.2, $P = 0.004$ versus FSI). To estimate the amount of OT axonal release due to the increase in firing rate, together with the altered firing pattern, we employed an activity (spike)-dependent model of OT secretion[17] (Extended Data Fig. 2h–j) that quantitatively captures the features of stimulus secretion coupling at the nerve terminals.

To dissect which sensory modalities activate OT neurons during FSI, we categorized rat social behaviors into 'sniffing', 'head-to-head' and 'crawled on top' or 'being crawled' events and constructed peristimulus time histograms (PSTHs) of spiking activity before, during and after the onset of each sequence (Fig. 1g,h). 'Crawled on top' and 'being crawled' induced the greatest increases in firing rates ($P = 0.036$ and 0.024, respectively; Supplementary Video 1), whereas 'sniffing', 'chasing' and 'head-to-head' events induced lesser, non-significant changes (Fig. 1h and Extended Data Fig. 2a–c). In addition, ultrasonic vocalizations during FSI revealed the appearance of bands between 40 and 90 kHz known to be related to social communication in rats[18] (Extended Data Fig. 3a,b), but we found no time-locked (in ranges up to ±5 s) correlation between OT neuron activity and ultrasonic vocalizations (Extended Data Fig. 3c–e). Although we could not discriminate individual ultrasonic vocalizations between the two conspecifics, we hypothesized that OT neurons were activated mainly by physical contacts and investigated this further by modeling gentle, non-nociceptive mechanical stimuli.

Gentle non-nociceptive mechanical stimuli trigger OT neuron activation. To test whether somatosensory stimulation itself is sufficient to increase OT cell activity, we performed controlled tactile stimulations using compressed air delivery (airpuffs) in isoflurane-anesthetized rats as described previously[19] (Fig. 2a). Stimulation of the skin on the dorsal body region by airpuffs (at three sites) reproducibly activated 19 of 23 (83%) recorded PVN OT neurons (mean increase 1.3 ± 0.5 spikes s^{-1}, mean $P = 0.021$; Fig. 2a,b and Extended Data Fig. 4a,b).

Airpuffs applied to the abdominal skin produced few or no changes in their activity (mean change 0.5 ± 0.3 spikes s^{-1}, $P = 0.33$), and there were no detected effects after stimulation of the anogenital area or the whiskers pad (Extended Data Fig. 4c). For potential involvement of the olfactory system in PVN OT neuron activation during social interaction, we exposed female rats to either a neutral odor (clean bedding) or a socially relevant odor (urinated-on female bedding). We found that the exposure to odorants did not elicit significant changes in either firing rate or spike distribution ($P = 0.34$ or 0.48, respectively; Extended Data Fig. 4d–f) in any of the recorded OT neurons. There was also no difference on presentation of neutral odor. Hence, we concluded that somatosensory inputs are the dominant signals that activate PVN OT neurons during social interactions.

ParvOT neurons respond to gentle non-nociceptive mechanical stimuli. Although the overwhelming majority of OT neurons in the PVN (97%) are magnocellular OT (magnOT) neurons, there is also a population of parvocellular OT (parvOT) neurons (~3%) that do not project to the pituitary[20], but that are crucial for the transmission of nociceptive signals to the magnOT cells[13].

Fig. 1 | In vivo recording of individual OT neurons in the PVN. a, Setup for recordings of behavior, ultrasonic vocalizations and neural activity. **b**, Video-tracking and electrophysiological recording from a rat alone in the OF arena (top) and during FSI (bottom): animal movement path (blue line), location of prominent OT cell activity (colored dots), heatmap of time spent by the rat in different locations. **c**, Example firing rate of four identified OT neurons recorded simultaneously during FSI. Red bars indicate periods of social interaction. **d**, Average firing rate of 15 OT neurons from 5 rats: OF baseline 1.1 ± 0.4 Hz, not socially interacting (not-SI) 1.6 ± 0.3 Hz and SI 2.6 ± 0.2 Hz (OF not-SI, $P = 0.07$; OF SI, $P = 0.001$; not-SI SI, $P = 0.03$; one-way ANOVA). Average index of dispersion on 1-s time bins of 15 OT neurons: OF 0.9 ± 0.2, not-SI 1.4 ± 0.3, SI 3.4 ± 0.4 (OF not-SI, $P = 0.16$; OF SI, $P = 0.0004$; not-SI SI, $P = 0.001$; one-way ANOVA). Average pairwise Pearson's correlation of spiking activity (1-s time bins) of 17 OT neuron pairs recorded in OF and SI ($P = 0.005$, unpaired, two-sided Student's *t*-test). **e**, Frames of recorded videos (top) of experimental rats that were placed either alone (OF), or with a mesh between rats (CSI) or for FSI with a stimulus rat; representative spike raster plots of an OT cell in each condition (bottom). **f**, Average firing rate of 15 OT neurons while rats underwent OF, CSI and FSI tests (OF CSI $P = 0.14$; OF FSI, $P = 0.004$; CSI FSI, $P = 0.006$; $n = 15$ cells; one-way ANOVA). Average index of dispersion on 1-s time bins (OF CSI, $P = 0.21$; OF FSI, $P = 0.001$; CSI FSI, $P = 0.003$; $n = 15$ cells; one-way ANOVA). Average pairwise Pearson's correlation of spiking activity (1-s time bins) of 17 OT neuron pairs (OF CSI, $P = 0.39$; OF FSI, $P = 0.002$; CSI FSI, $P = 0.003$; one-way ANOVA). **g**, Normalized firing rates of OT neurons during each behavior; 'crawling on top' and 'being crawled' elicited the strongest responses (*$P = 0.036$, **$P = 0.024$; $n = 8$ cells, one-way ANOVA, followed by Tukey's post hoc test). **h**, Representative spike raster plots, averaged response and PSTHs of OT cell activity during 'crawling on top' (increased response, $P = 0.036$, $n = 6$ cells, Wilcoxon's test) and 'being crawled' (increased response, $P = 0.024$, $n = 6$ cells; Wilcoxon's test) behaviors. Data represented as mean ± s.e.m.

To study whether parvOT neurons are also activated by non-nociceptive stimuli, we applied airpuffs to conscious rats trained and adapted for short-term immobilization. For this purpose, we first used rats that had been injected systemically with the retrograde tracer Fluorogold to label all neurons in the brain that project outside the blood–brain barrier, including in particular magnOT,

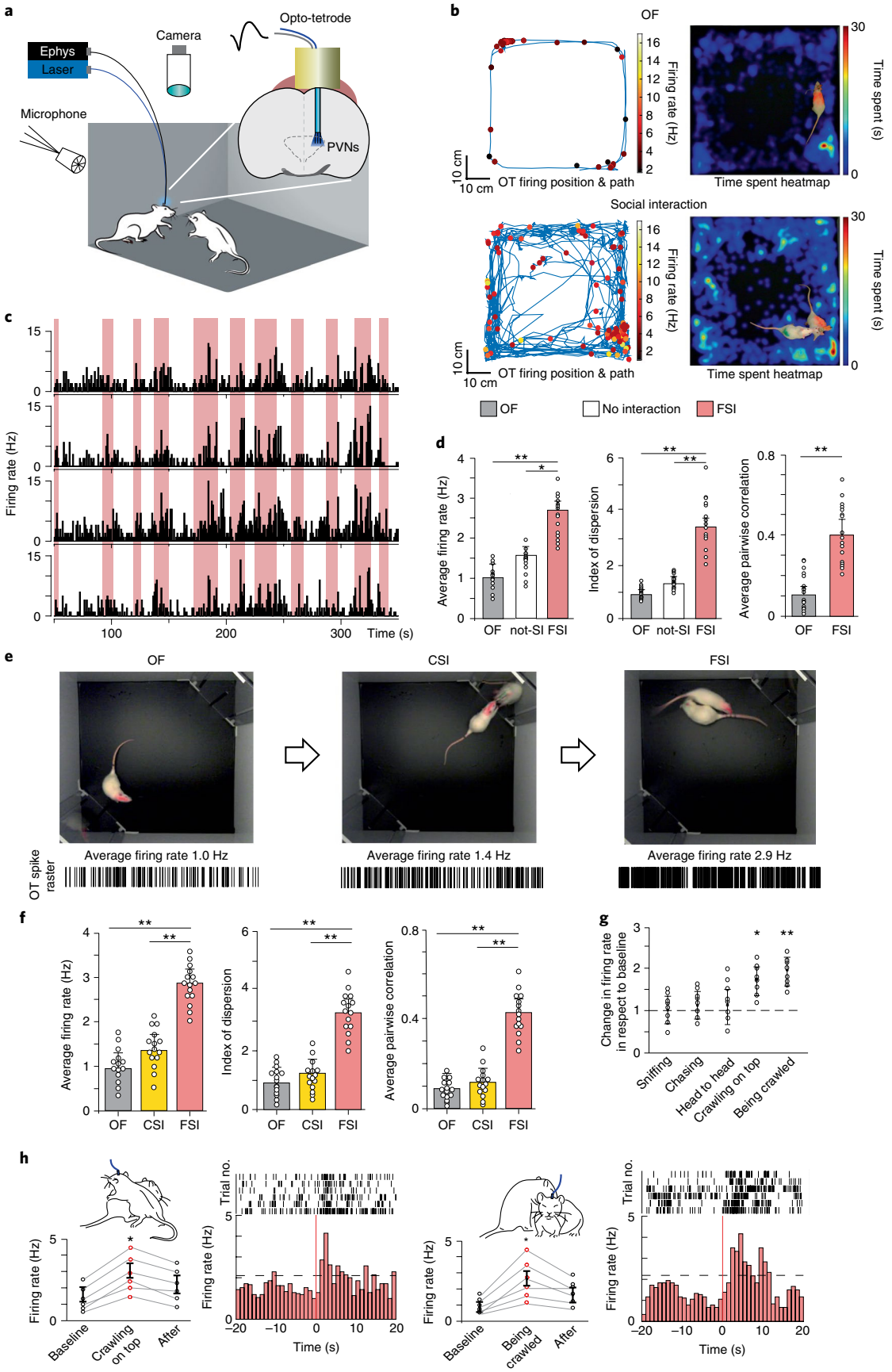

but not parvOT, neurons. To identify neurons strongly activated by airpuffs, we used the expression of *c-fos* as an indicator of activated OT neurons. Previous studies have found that *c-fos* expression is activated in a non-identified OT neuron cell type after social interaction in voles[21], mice[22] and rats[23]. Immunocytochemistry revealed the presence of *c-fos* in 30% of parvOT neurons in the PVN of stimulated rats (average 12.4 ± 3 neurons per PVN per hemisphere, $n = 4$; Fig. 2c and Supplementary Table 1a), but not in magnOT neurons or in any OT neurons in nonstimulated control rats, indicating that airpuffs specifically applied to the dorsal body region seem to predominantly activate parvOT neurons. In a second step, we labeled parvOT neurons retrogradely by injecting the canine adenovirus serotype 2 (CAV2-Cre)[24] into the SON, and concomitantly injected the Cre-responder rAAV-expressing mCherry under the control of the OT promoter into the PVNs. In line with our previous results, airpuffs induced *c-fos* expression exclusively in retrogradely labeled mCherry-positive OT neurons (average 47.6%, 7.5 ± 3 neurons per PVN per hemisphere, $n = 4$; Fig. 2d and Supplementary Table 1b).

To explore the role of parvOT neurons in social interaction and their response to gentle non-nociceptive mechanical stimuli (airpuffs), we chose to manipulate their activity via virally expressed, designer receptors exclusively activated by designer drugs (DREADDs). To this end, we used a similar Cre-dependent viral-based strategy employing OTp-DIO-hM4D(Gi)-mCherry and OTp-DIO-hM3D(Gq)-mCherry rAAVs (Fig. 2e,f). As a first step, we verified the efficiency of DREADDs in modulating of parvOT neuron activity ex vivo, showing that hM3D(Gq)-CNO-induced parvOT activation significantly increased the spontaneous action potential (AP) frequency (baseline 0.85 ± 0.39 Hz versus clozapine *N*-oxide (CNO) 1.31 ± 0.51 Hz, $n = 9$; $P = 0.0039$; Extended Data Fig. 5a–c) and the number of evoked APs (16.18 ± 3.89 APs versus CNO 22.55 ± 5.66 APs, $n = 11$; $P = 0.0314$; Extended Data Fig. 5d–f). Consistent with this, hM4D(Gi)-CNO-induced inhibition (10 µM, 6 min) significantly decreased both the spontaneous AP frequency (baseline 1.38 ± 0.38 Hz versus CNO 0.36 ± 0.18 Hz, $n = 7$; $P = 0.0469$; Extended Data Fig. 5g–i) and the number of evoked APs (baseline 13 ± 2.02 APs versus CNO 7.75 ± 2.03 APs, $n = 11$; $P = 0.0007$; Extended Data Fig. 5j–l).

After the ex vivo results, we next performed in vivo recording in anesthetized animals to better understand the airpuff-induced activation of parvOT. For this purpose, PVN parvOT activity was imaged using the GCaMP6s reporter and fiber photometry[25] (Fig. 2e–h). Then, rats were injected with the DREADD ligand CNO (3 mg kg^{-1} intraperitoneally) and OT neuron Ca^{2+} transients were analyzed. Chemogenetic activation of the parvOT neurons enhanced the Ca^{2+} response to airpuffs (45 ± 9% increase of area under the curve (AUC; $P = 0.03$; Fig. 2i). Conversely, chemogenetic inhibition of the parvOT neurons reduced the response to airpuffs (65 ± 5% decrease of AUC; $P = 0.009$ compared with control; Fig. 2j).

Thus, we concluded that gentle non-nociceptive mechanical stimulation of the dorsal region activates parvOT neurons, which we hypothesized may drive the activity of the larger population of magnOT neurons.

Intra-PVN connectivity of parvOT and magnOT neurons. To validate this hypothesis, we first looked for direct synaptic contact of parvOT neurons on to magnOT somata and/or dendrites via injection of OTp-DIO-GFP rAAV into the PVN and Cav2-Cre into the SON to specifically label parvOT neurons (Extended Data Fig. 6a,b) in analogy to a previous study[13]. For three-dimensional (3D) reconstruction of interposition between axons of parvOT neurons and somatodendritic domains of magnOT neurons, we employed the IMARIS technique[26,27]. This approach allows precise identification of the location of synaptic contact by quantifying overlap with SYN-immunoreactive puncta. By performing IMARIS-assisted Sholl analysis, we found synaptic-like contacts of parvOT neurons with magnOT somata and dendrites (Fig. 3a and Extended Data Fig. 6; 6 dendritic contacts, 124 somatic contacts, $n = 354$) as well as an average chance of innervation of 34.9% (Fig. 3b), indicating that approximately a third of PVN magnOT neurons receive parvOT input. Based on these anatomical observations, we performed patch-clamp recording for functional validation of parvOT–magnOT neuron connection via rAAV-OTp-DIO-ChR2-mCherry (to label specifically parvOT) and rAAV-OTp-Venus (to label all OT neurons) injected into the PVN and Cav2-Cre injected into the SON (Fig. 3g). First, we confirmed the magnOT nature of recorded neurons through the presence of a hyperpolarizing transient outward rectification, as well as a weak low-threshold depolarization (Fig. 3h), by comparison to the electrophysiological properties of identified parvOT neurons (Fig. 3c–f). We observed that stimulation of parvOT neurons evoked responses in 45% of recorded magnOT neurons (9 of 20; Fig. 3i) with a significant increase in postsynaptic current (PSC) frequencies (baseline 0.158 ± 0.055 Hz versus ChR2 0.346 ± 0.15 Hz, $n = 9$; $P < 0.01$; Fig. 3i). Next, we aimed to visualize Ca^{2+} variations in magnOT neurons on DREADD-mediated activation of parvOT neurons via rAAV-OTp-DIO-hM3D(Gq)-mCherry and rAAV-OTp-GCaMP6s injected into the PVN and Cav2-Cre into the SON (Fig. 4a–d). After application of CNO (10 µM, 1 min), we observed that 40 ± 8% of recorded magnOT neurons responded to parvOT hM3D(Gq) stimulation, again confirming described

Fig. 2 | Gentle non-nociceptive mechanical stimuli trigger OT neuron activation. a, Head-fixed rats injected with rAAV-pOT-ChR2-mCherry were stimulated with airpuffs at anterior, central and posterior portions of the dorsal body region, whereas OT neurons were recorded with an opto-electrode. Top: PSTH example of OT neuron responses to airpuffs. Bottom: normalized PSTHs of 10 (of 23) recorded OT neuron responses to airpuffs in three dorsal body regions ((i) anterior; (ii) central; (iii) posterior); red indicates high spiking activity. ITR, inverted terminal repeat; NS, not significant. **b**, Top: statistics of average firing rate of OT neuron responses to airpuff stimulations (peak versus baseline, $^*P = 0.017$, $^{**}P = 0.025$, $^{***}P = 0.021$; $n = 23$ cells from 8 rats; one-way ANOVA followed by Bonferroni's post hoc comparison) indicates a significant increase above basal rate (dashed line). Bottom: latency of OT neuron responses to airpuffs. All data shown as average ± s.e.m. **c**, Fluorogold-injected rats received continuous airpuffs for 10 min and were killed and perfusion-fixed 90 min later. PVN slices were triple stained with antibodies against OT (blue), Fluorogold (red) and *c-fos* (green). The confocal image shows a Fluorogold-negative parvocellular OT neuron expressing *c-fos* (1 of 99 such double-labeled neurons observed in 4 rats). Scale bars, 100 and 10 µm (inset). **d**, Rats injected bilaterally with CAV2-Cre into the SON and rAAV-OTp-DIO-mCherry into the PVN were exposed to airpuffs for 10 min and killed 90 min later. The confocal image shows *c-fos* expression in a parvOT neuron (mCherry-positive, labeled via the retrograde CAV2-Cre, and is 1 of 60 such triple-labeled neurons observed in 4 rats). Scale bars, 100 and 10 µm (inset). **e**,**f**, Viral vectors for recording Ca^{2+} signals in GCaMP6s-expressing OT neurons during chemogenetic activation (**e**) or silencing (**f**) of parvocellular OT neurons. **g**,**h**, Examples of fiber photometry-based Ca^{2+} signals of PVN OT neuron population during airpuff stimulation (orange bars). Top: response to airpuffs 30–60 min after saline injection (control); bottom: response to airpuffs 30–60 min after CNO-induced activation (**g**) or silencing (**h**) of parvOT neurons. **i**, Average traces of Ca^{2+} responses to airpuffs 30–60 min after injection of either CNO to activate (Gq) parvOT neurons or saline (control). Each graphic is the average of 33 airpuff responses (11 airpuffs per animal, $n = 3$; AUC 0–30 s after airpuffs, relative to control; $^*P = 0.03$, paired, two-sided Student's *t*-test). **j**, Average traces of Ca^{2+} responses to airpuffs 30–60 min after injection of either CNO to silence (Gi) parvOT neurons or saline (control). Each graphic is the average of 33 airpuff responses (11 airpuffs per animal, $n = 3$; AUC 0–30 s after airpuffs, relative to control; $^{**}P = 0.007$, paired, two-sided Student's *t*-test). All data show average ± s.e.m.

anatomical connectivity (Figs. 3b,i and 4d). In responsive neurons, the number of Ca^{2+} transients was significantly increased, a result mirrored by the increase of AUCs (Fig. 4d). However, the width of these Ca^{2+} transients did not show any significant change, indicating that parvOT-induced magnOT activity does not trigger long-lasting Ca^{2+} transients, but several bursts of sharp Ca^{2+} peaks, as observed

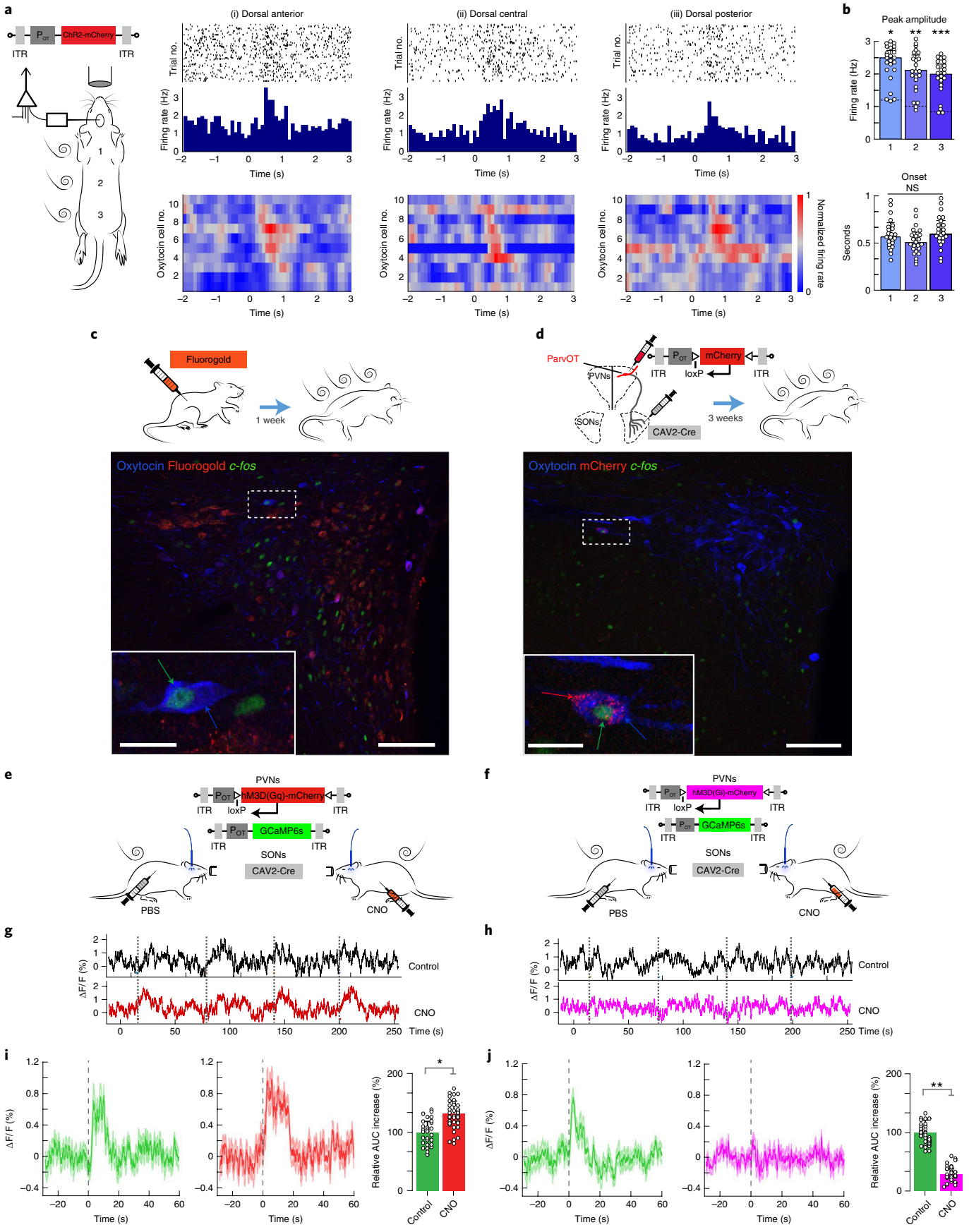

in the example traces (Fig. 4b). This feature was further confirmed by plotting the time course of Ca^{2+} event probability, showing that the probability of observing magnOT Ca^{2+} transients is increased over the 4 min after the ex vivo CNO treatment (Fig. 4c). These data indicate that parvOT neurons synapse on magnOT neurons within the PVN to drive their activity, as similarly reported for SON magnOT neurons in vivo[13].

Magnocellular neurons and their release of OT into blood, controlled by parvOT neurons. Using similar viral strategies, we expressed DREADDs—hM3D(Gq) or hM4D(Gi)—specifically in parvOT neurons and injected rAAV-OTp-GCaMP6s into the PVNs to express the Ca^{2+} indicator GCaMP6s in all PVN OT neurons (1,193 of 1,371 OT neurons expressed GCaMP6s, 87 ± 4%, $n = 4$; Fig. 4p). This allowed us to monitor the global activity of PVN OT neurons via fiber photometry in isoflurane-anesthetized rats on activation/inhibition of parvOT neurons. Activation of parvOT cells induced an increase in Ca^{2+} fluorescent signal of the PVN OT neuron population approximately 30 min after CNO injection (intraperitoneal 3 mg kg^{-1}) and lasting for >2 h (Fig. 4e–h). Conversely, inhibition of parvOT neurons decreased Ca^{2+} fluorescent signals of the general population 30 min after CNO injection and the effect lasted for more than 2 h (Fig. 4i–l). Administration of CNO did not have any effect on the Ca^{2+} signal in control animals lacking the DREADD receptors (Fig. 4m–o). Considering that the contribution of parvOT neurons to the OT population Ca^{2+} signal is negligible (Extended Data Fig. 7a–e), those results suggest that changes in parvOT neuron activity directly influence the firing pattern of large populations of PVN magnOT neurons. The similar kinetics of Ca^{2+} signal fluctuations after CNO activation of parvOT PVN neurons, together with airpuff application, were detected during recording of magnOT neurons in the SON, which do not contain parvOT neurons (Extended Data Fig. 7f–o).

To investigate whether parvOT-induced magnOT activity is followed by actual OT release, we analyzed neurohypophyseal OT release after chemogenetic activation of parvOT neurons. We performed blood sampling from the jugular vein before and after CNO injection (3 mg kg^{-1}; Fig. 4q) and found a significant increase in plasma OT 45 min ($P = 0.00093$ versus basal; $P = 0.0036$ versus OTp-mCherry control) and 90 min ($P = 0.002$ versus basal; $P = 0.0017$ versus OTp-mCherry control; Fig. 4r) after intraperitoneal CNO injections.

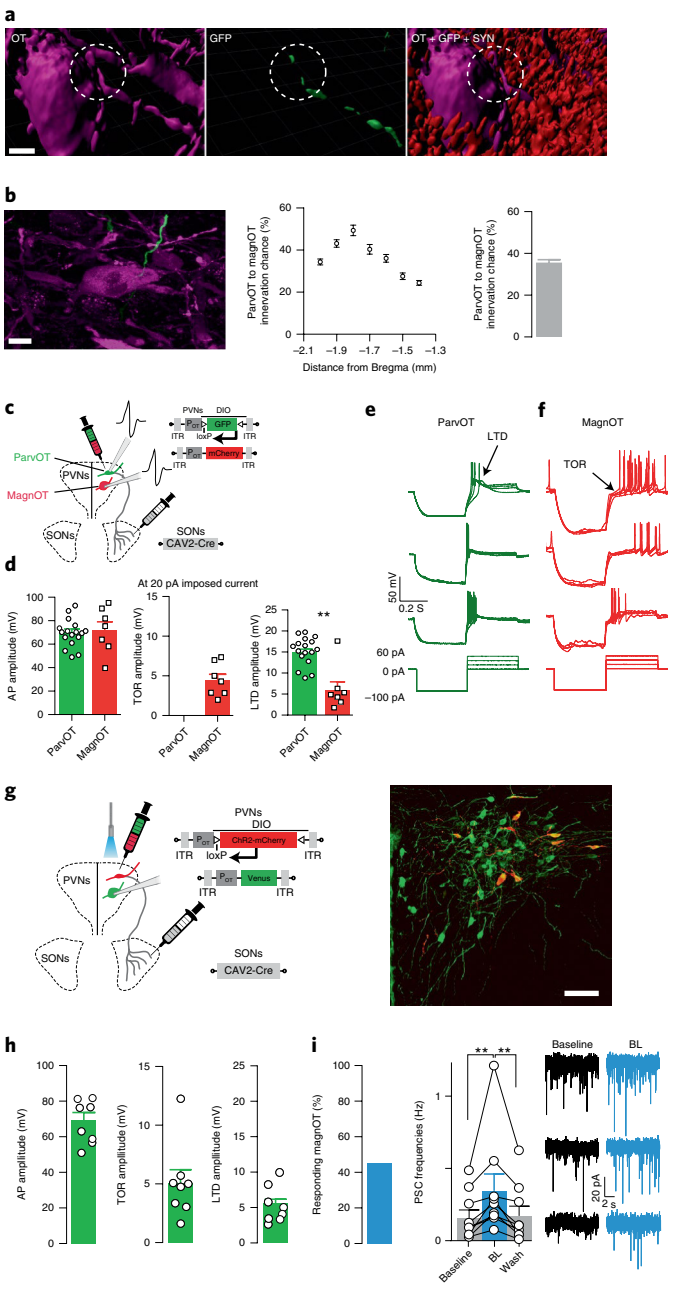

Fig. 3 | Intra-PVN connectivity of parvOT and magnOT neurons. a, Images show the 3D surface reconstruction of OT, GFP and SYN. Circles with dashed lines indicate the overlap of OT, GFP and SYN. Scale bar, 10 µm. **b**, Confocal image shows a single magnOT neuron (purple) innervated by a parvOT fiber (green). Scale bar, 10 µm. Dot-plot graph shows that the chance of innervation by parvOT neurons depends on the anatomical location of magnOT neurons within the PVN. Bar graph shows the average chance for magnOT PVN neurons to be innervated by parvOT axons ($n = 214$ cells from 3 rats). **c**, Schema of the viral injection into the SON and PVN plus the electrophysiological recording in the PVN (with pipette) for the recording of parvOT neurons (expressing mCherry + GFP) and magnOT neurons (expressing mCherry). **d**, Comparison of average and individual points of voltage amplitude between parvOT neurons ($n = 17$ cells from 4 rats) and magnOT neurons ($n = 7$ cells from 4 rats) for different electrophysiological parameters (AP; parvOT 70.12 ± 2.87 mV versus magnOT 71.65 ± 7.414 mV; $P = 0.82$, unpaired, two-sided Student's t-test; transient outward rectification (TOR): magnOT = 4.39 ± 0.79 mV; low threshold depolarization (LTD): parvOT 14.88 ± 0.81 mV versus magnOT 5.93 ± 1.98 mV; $^{**}P = 0.0019$, two-sided Mann–Whitney U-test). **e**, Example responses of three parvOT neurons to a hyperpolarizing current at −100 pA followed by four current injections starting from 0 to 60 pA. **f**, Example responses of three magnOT neurons to a hyperpolarizing current at −100 pA followed by four current injections starting from 0 pA to 60 pA. **g**, Left: schematic representation of viral vectors injected in the PVN (OTp-DIO-ChR2-mCherry and OTp-Venus) and the SON (CAV2-Cre) to transduce the expression of ChR2-mCherry in parvOT neurons and of Venus in PVN OT neurons. Right: image showing viral expression in the PVN in one of four rats. Scale bar, 100 µm. **h**, Average and individual points of voltage amplitude of magnOT neurons ($n = 8$ cells from 4 rats) for different electrophysiological parameters: AP, TOR and LTD. **i**, Average percentage (45%) of responding magnOT neurons ($n = 9$ cells) in all the magnOT neurons that have been recorded ($n = 20$ cells from 4 rats). MagnOT PSC frequency reversibly increases after parvOT ChR2 photostimulation ($n = 9$ cells). Example responses of three magnOT neurons in voltage clamp configuration at −70 mV before and after the ChR2 optogenetic stimulation of parvOT neurons. Baseline versus BL: $^{**}P < 0.001$; baseline versus wash: $^{**}P < 0.001$, Friedman's test followed by Dunn's post hoc test. BL, blue light. All data are represented as mean + s.e.m.

Taken collectively, these results indicate that parvOT neurons tightly control magnOT neuron activity in vivo to regulate peripheral OT release.

Differential neural inputs to parvOT and PVN magnOT neurons. These findings suggest that parvOT neurons act as 'first responders to somatosensory input', conveying information to the rest of the PVN OT neuronal population (that is, magnOT neurons). Hence, we asked whether parvOT neurons receive more synaptic inputs than magnOT ones in the PVN. In an attempt to assess potential differences of synaptic inputs to parvOT and magnOT neurons, we used IMARIS to quantify the total amount of SYN fluorescence at somata and dendrites. To perform an unbiased analysis, we created spheres that precisely engulfed magnOT and parvOT somata and accounted for individual variances in cell roundness and surface area (Methods). We found statistically significant differences at both the soma (Fig. 5a) and dendritic locations (Fig. 5b, at two different locations, 5 and 20 µm from the soma) and analyzed a total of 104 neurons (parvOT = 56, magnOT = 48), suggesting that parvOT neurons might receive more overall synaptic input.

Next, to uncover the origin of synaptic inputs to parvOT and magnOT neurons, we employed the retrograde trans-synaptic, EnvA-pseudotyped, G-deletion-mutant rabies virus (Rb-GFP[28]). To specifically distinguish inputs to parvOT and magnOT neurons, we used a double-conditional approach, which allows retrotracing of inputs to OT neurons that project to an area of choice (SON for parvOT and posterior pituitary for magnOT) (Methods; Fig. 5c,e).

In both groups of rats, we found green fluorescent protein (GFP)-expressing neurons in numerous brain regions, including the septum, medial preoptic area and amygdala (Fig. 5d,f and Extended Data Fig. 8h), demonstrating that parvOT and magnOT neurons receive a large number of common inputs (Supplementary Table 2). However, we detected the presence of GFP neurons in the paraventricular nucleus of thalamus, insula and habenula only after infection of parvOT neurons (Extended Data Fig. 8i), whereas GFP neurons in the substantia nigra were found only after primary infection of magnOT neurons (Extended Data Fig. 8j). In line with the IMARIS analysis, the total number of neurons projecting to parvOT and magnOT neurons was 1,963.6 ± 710 and 694.8 ± 121 neurons, respectively ($P = 0.02$; Fig. 5g). Although we did not find between-group differences in the proportion of inputs coming from hypothalamic and extrahypothalamic areas (Fig. 5h), the periqueductal gray and subfornical organ showed preferential innervation of parvOT and magnOT neurons, respectively (Fig. 5i). This indicates that parvOT neurons receive at least partially distinct, and more pronounced neuronal inputs than magnOT neurons.

ParvOT neurons modulate social behavior. To test whether this small population of parvOT neurons can modulate social behavior by their effects on the activity of the much more abundant magnOT neurons, we used the previously described chemogenetic approach to silence or activate them during behavioral tests (Fig. 6a). Then 3 weeks after viral injection, rats were injected intraperitoneally with either CNO (3 mg kg^{-1}) or saline 60 min before social interaction tests (Fig. 6b). Selective inhibition of the parvOT neurons resulted in less social interaction: in the FSI test, the time spent with a conspecific was reduced by 37 ± 6 s (over 5-min sessions, $P < 0.001$; Supplementary Video 2). By contrast, in the CSI test, where no physical contact is allowed, the time spent by the experimental rat approaching the stimulus rat was unchanged (Fig. 6c–e; $n = 15$ rats). Conversely, CNO-induced activation of parvOT neurons led to more social interaction: in the FSI test, the time spent with a conspecific increased

Fig. 4 | Magnocellular neurons and their release of OT into blood are controlled by parvOT neurons. a, To allow the expression of hM3D(Gq) on parvOT PVN to SON projecting neurons, rats' SON are infected with a CAV2-Cre rAAV and the PVN are infected with an AAV, allowing the Cre-dependent expression of hM3D(Gq) under the control of the OT promoter. We also make PVN OT neurons express the calcium indicator GCaMP6s to monitor calcium transients in parvOT neurons. **b**, Example traces of the effect of CNO (10 µM, 6 min) on PVN oxytocinergic neuron calcium activity. **c**, CNO application increases the number of calcium transients by 5-fold ± 1-fold (solid line: average, shaded area: s.e.m., $P = 0.0019$, Wilcoxon's test) and the AUC by 15- ± 9-fold ($P = 0.0043$, Wilcoxon's test) in 40 ± 8% of recorded magnOT neurons ($n = 20$ slices from 7 rats, 70 cells). **d**, Calcium event probability, fraction of responses, number of peaks, AUC and peak duration of calcium events in PVN OT neurons. After CNO application, the probability of observing a calcium peak is increased over ~4 min, but the duration of those peaks remains unchanged (ratio = 2 ± 0.7, $P = 0.46$, paired, two-sided Student's t-test). Bar plots show mean ± s.e.m. **e**–**h**, Schema of viral vectors injected and implanted optic fiber-for-fiber photometry recording (**e**) of PVN OT neurons with concomitant DREADD-Gq activation of parvOT neurons. Example traces (**f**) of recorded GCaMP6s signal from PVN OT neurons before and after CNO-induced activation of parvOT neurons. Normalized AUC of GCaMP6s signal (**g**, solid line: average, shaded area: s.e.m., 1-min bin size) of PVN OT neurons showing increase of cellular activity after parvOT activation mediated by CNO intraperitoneal injection (indicated by arrow). The 30-min averaged AUC (**h**) showing a gradual increase of cellular activity (baseline AUC versus 0–30 min, $P = 0.0606$, versus 30–60 min, $^{*}P = 0.0403$) that lasts at least 120 min (baseline AUC versus 60–90 min, $^{*}P = 0.028$; versus 90–120 min, $^{*}P = 0.0325$, $n = 6$ rats, two-way ANOVA and Tukey's corrected post hoc comparison). **i**–**l**, Schema of viral vectors injected and implanted optic fiber for fiber photometry recording (**i**) of PVN OT neurons with concomitant DREADD-Gi inhibition of parvOT neurons. Example traces (**j**) of recorded GCaMP6s signal from PVN OT neurons before and after CNO-induced inhibition of parvOT neurons. Normalized AUC of GCaMP6s signal (**k**, solid line: average, shaded area: s.e.m., 1-min bin size) of PVN OT neurons showing decrease of cellular activity after parvOT inhibition mediated by intraperitoneal CNO injection (indicated by arrow). The 30-min averaged AUC (**l**) showing a gradual decrease of cellular activity (baseline AUC versus 0–30 min, $P = 0.058$, versus 30–60 min, $^{***}P = 0.00013$) that lasts at least 120 min (baseline AUC versus 60–90 min, 90–120 min, $^{***}P = 0.00019$, $n = 3$ rats, two-way ANOVA and Tukey's corrected post hoc comparison). **m**–**o**, Schema of viral vectors injected and implanted optic fiber-for-fiber photometry recording (**m**) of PVN OT neurons in control animals (DREADD free) expressing GFP in parvOT neurons. Normalized AUC of GCaMP6s signal (**n**, solid line: average, shaded area: s.e.m., 1-min bin size) of PVN OT neurons showing no significant changes in Ca^{2+} signal on CNO injection. No significant changes are detected in 30-min averaged AUC (**o**) up to 120 min ($P = 0.109$, $n = 2$ rats, two-way ANOVA and Tukey's corrected post hoc comparison). **p**, Panels of immunostained section of the PVN showing post hoc verification of implanted optic fiber above the PVN and co-localization of immunoreactive GCaMP6s (green, top left), DIO-hM3D(Gq)-mCherry (red, bottom left) and OT (blue, right) in one of six rats. Arrows indicate mCherry-positive parvOT neurons. Scale bars, 100 µm and 10 µm (inset). **q**, Schema of viral vectors injected for DREADD-Gq activation of parvOT neurons and blood sampling from the jugular vein. **r**, Chemogenetic activation of parvOT neurons evokes peripheral OT release. Plasma OT (pg ml^{-1}) taken under basal conditions and 45 and 90 min after intraperitoneal CNO (3 mg kg^{-1}; depicted by arrow; $n = 8$ rats parvOT Gq group, $n = 6$ rats control group). At 45 min, $^{++}P = 0.00093$ versus basal (−45 min), $^{**}P = 0.0036$ versus control (OTp-mCherry) and, at 90 min, $^{++}P = 0.002$ versus basal, $^{**}P = 0.0017$ versus control. Two-way repeated-measures ANOVA with Bonferroni post hoc correction. Data are presented as mean ± s.e.m.

by 10±6 s (P=0.04). In the CSI test, no significant difference in approaching time was measured between saline- and CNO-injected rats (Fig. 6f–h; n=9 rats).

Inhibition and activation of parvOT neurons also had opposite effects on crawling behavior (Fig. 6e,h). Moreover, after inhibiting parvocellular OT neurons, rats often actively avoided

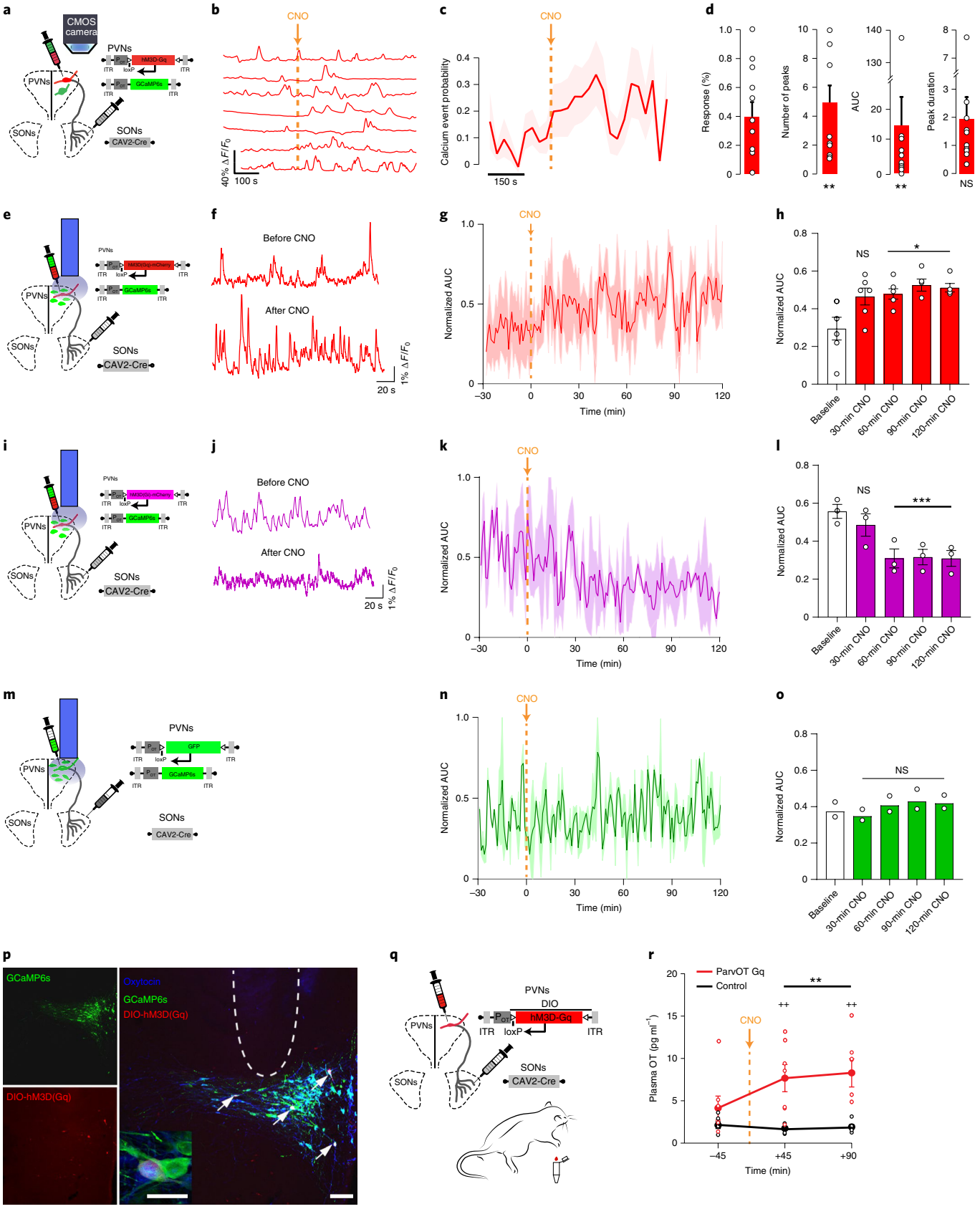

the stimulus rat, a behavior never observed in the control group (Extended Data Fig. 9c). Control rats injected with control virus rAAV-OTp-DIO-GFP receiving saline or CNO showed no behavioral differences (Extended Data Fig. 9a).

To show that alterations of social behaviors induced by DREADD-based manipulation of parvOT neuron activity were indeed an effect mediated by central OT release, the parvOT activation (Gq) experiment was repeated while applying an OTR antagonist[29] by intracerebroventricular infusion (0.75 µg per 5 µl)[30]. Compared with saline-infused control animals, OTR antagonist-infused animals showed a strong reduction in social interactions (37 ± 18% reduction, $P = 0.007$, $n = 12$ rats), regardless of CNO administration, whereas, without OTR antagonist, CNO application caused increased social interactions (16 ± 3% increase, $P = 0.04$, $n = 12$; Fig. 6i and Extended Data Fig. 9h). We did not observe a CNO- or OTR antagonist-induced effect on locomotor activity (Extended Data Fig. 9b,d–e). This result confirms that the downstream effect on CNO-induced activation of parvOT neurons of social behavior is indeed mediated by OT and its receptors. In a second group of rats ($n = 10$) expressing GFP in parvOT neurons, administration of an OTR antagonist also had a comparable effect in reducing social behavior; as expected, CNO itself did not have any effect on social interaction of animals (Fig. 6j and Extended Data Fig. 9i).

Discussion

In the present study, we provide evidence that somatosensory stimulation in female rats activates parvOT neurons, which subsequently drive the activation of the much larger population of magnOT neurons. Using ex vivo and in vivo approaches, we demonstrated that parvOT neurons synapse on magnOT neurons to elicit a central effect of OT to promote interfemale communication.

Social touch evokes OT neuronal activity. The use of single-unit in vivo recording precludes discrimination between parvOT and magnOT neurons. However, considering the limited number of parvOT neurons (~30 parvOT cells[13] versus ~1,200 magnOT cells[31] in the PVN of each hemisphere), it is highly likely that we exclusively recorded from magnOT cells. In support, we found that nonaggressive social interactions of female rats and, in particular, physical contacts elicited a coordinated, clustered spiking activity of PVN OT neurons—a pattern that strongly facilitates activity-dependent secretion of OT from nerve terminals of magnOT cells in the pituitary[17] (Extended Data Fig. 2h–j). This activity is almost synchronous across recorded OT neurons, and is highly correlated with theta rhythmicity of PVN local field potentials. These coordinated changes in OT neuronal electrical activity occurred only during FSI, allowing physical contacts between conspecifics, but not during CSI, where physical touch between animals was prevented by a barrier. Moreover, detailed analysis of PVN OT neuron activity during social behaviors revealed that the highest increase in neuronal firing occurred immediately after (0–10 s) crawling on top or being crawled behaviors (Fig. 1), that is, social contacts involving activation of cutaneous sensory nerves.

To test whether non-noxious repetitive somatosensory stimulations directly influence PVN OT neuron activity, even in the absence of other stimuli, we applied airpuff stimulations to the skin of the dorsal area of the rat, in lightly anesthetized conditions, while measuring action potentials of PVN neurons. Notably, airpuffs induced a significant increase in spiking activity of most (83%) recorded putative magnOT neurons, but had little or no effect on the activity of non-OT PVN neurons, reinforcing the idea that somatosensory inputs selectively activate magnOT neurons. This finding is in line with previous studies[32] that reported increased OT plasma levels in rats after 10 min of massage-like stroking. Furthermore, the stimulation of low-threshold mechanoreceptors, particularly the touch-sensitive nerve fiber C-tactile afferents is known to trigger OT release, and has been associated with increased social motivation in rodents and humans[33].

ParvOT neurons control PVN magnOT neuron activity. To shed light on the causal link between somatosensory stimulation and social behavior, we focused our research on a specific subtype of 'parvocellular' OT neurons. These neurons communicate with various autonomic centers in the brain stem and spinal cord[20], and are involved in analgesia during acute pain[13].

When we applied low-intensity, non-noxious cutaneous stimulation (airpuff) in awake rats, we observed a sustained increase of *c-fos* expression in parvOT neurons in the PVN (Fig. 2). Of note, we found that airpuffs induced *c-fos* expression in parvOT, but not in magnOT, neurons. However, the absence of *c-fos* expression in magnOT cells does not necessarily indicate the absence of their increasing activity[34–36]. Indeed, only dramatic physiological challenges such as hemorrhage, salt loading or fear evoke *c-fos* expression in magnOT neurons[34,37]. Importantly, during lactation magnOT neurons release a large amount of OT into the peripheral circulation although an increase in *c-fos* expression was never found. In analogy, our findings demonstrate increased OT plasma concentrations after chemogenetic activation of parvOT neurons (Fig. 4) via a demonstrated parvOT → magnOT connectivity, although without detectable *c-fos* immunosignal in magnOT neurons releasing the neuropeptide into the blood.

Furthermore, chemogenetic activation or inhibition of parvOT neurons via DREADDs resulted, respectively, in an increase or decrease in OT neuron activity in response to the airpuff stimulation (Fig. 2). This suggests that parvOT neurons can be activated by both nociceptive[13] and non-nociceptive stimuli (in the present study) and subsequently promote analgesia as well as social behavior. Such pleotropic effects of OT originating from the same parvOT neurons require further investigation.

To provide additional evidence that parvOT neurons modulate magnOT neuron activity within the PVN, we employed a

Fig. 5 | ParvOT neurons receive more inputs than magnOT neurons. a, Three-dimensional reconstruction of parvOT and magnOT neurons and the quantification of SYN fluorescence. Asterisks (white) indicate the placement of the spheres (yellow) used to quantify the total amount of SYN fluorescence (red). Top: the placement of a sphere around a magnOT neuron soma; bottom: the placement of a sphere on to a parvOT neuron dendrite. Scale bars, 5 µm. **b**, Quantification of SYN fluorescence in close proximity to parvOT ($n = 56$ cells from 3 rats) and magnOT ($n = 48$ cells from 3 rats) neurons at somatic (top) and dendritic locations (bottom) considering differences in cellular roundness and surface area (adjusted) (unpaired, two-sided Student's *t*-test, $^{***}P < 0.0001$). **c**,**e**, Virus injection strategy to retrotrace inputs from parvOT (**c**) and magnOT (**e**) neurons, respectively. **d**,**f**, Schema representing the proportion of inputs (number of inputs from one brain area/total number of inputs) from each brain area to parvOT (**d**) and magnOT (**f**) neurons, respectively. Brain areas projecting only to parvOT or magnOT neurons are circled in green or purple, respectively. See Supplementary Table 2 for a full list of abbreviations for structures in **d** and **f**. **g**, Quantification of the total number of inputs to parvOT and magnOT neurons (two-sided Student's *t*-test, $^{*}P = 0.0223$, $n = 5$ rats per group). **h**, Proportion of inputs to parvOT and magnOT neurons located in or outside the hypothalamus. Numbers indicate average number of neurons. **i**, Bar graphs showing the proportion of inputs coming from brain areas that show preferential innervation of parvOT or magnOT neurons. Two-sided Student's *t*-test; asterisks indicate significant difference: $^{*}P = 0.0315$, $^{**}P = 0.0153$, $^{***}P = 0.0264$, $^{****}P = 0.0299$, $^{*****}P = 0.0453$ and $^{******}P = 0.0011$; $n = 5$ rats per group. Data represented as mean ± s.e.m.

combination of immunohistochemistry and 3D anatomical reconstruction. We found 1.5- to 4-fold more synaptic-like contacts on parvOT somata and dendrites compared with the respective compartments of magnOT neurons (Fig. 5). This finding is supported by retrograde tracing data, which demonstrate substantially more inputs to parvOT neurons than to magnOT neurons (Fig. 5).

Do parvOT neurons control social behavior?. To investigate how parvOT neurons modulate social behavior, we performed chemogenetic manipulation of parvOT neurons by viral means. We found that targeted activation or inhibition of parvOT neurons increased or decreased the total time of social interaction with a conspecific, respectively. Furthermore, the intracerebroventricular

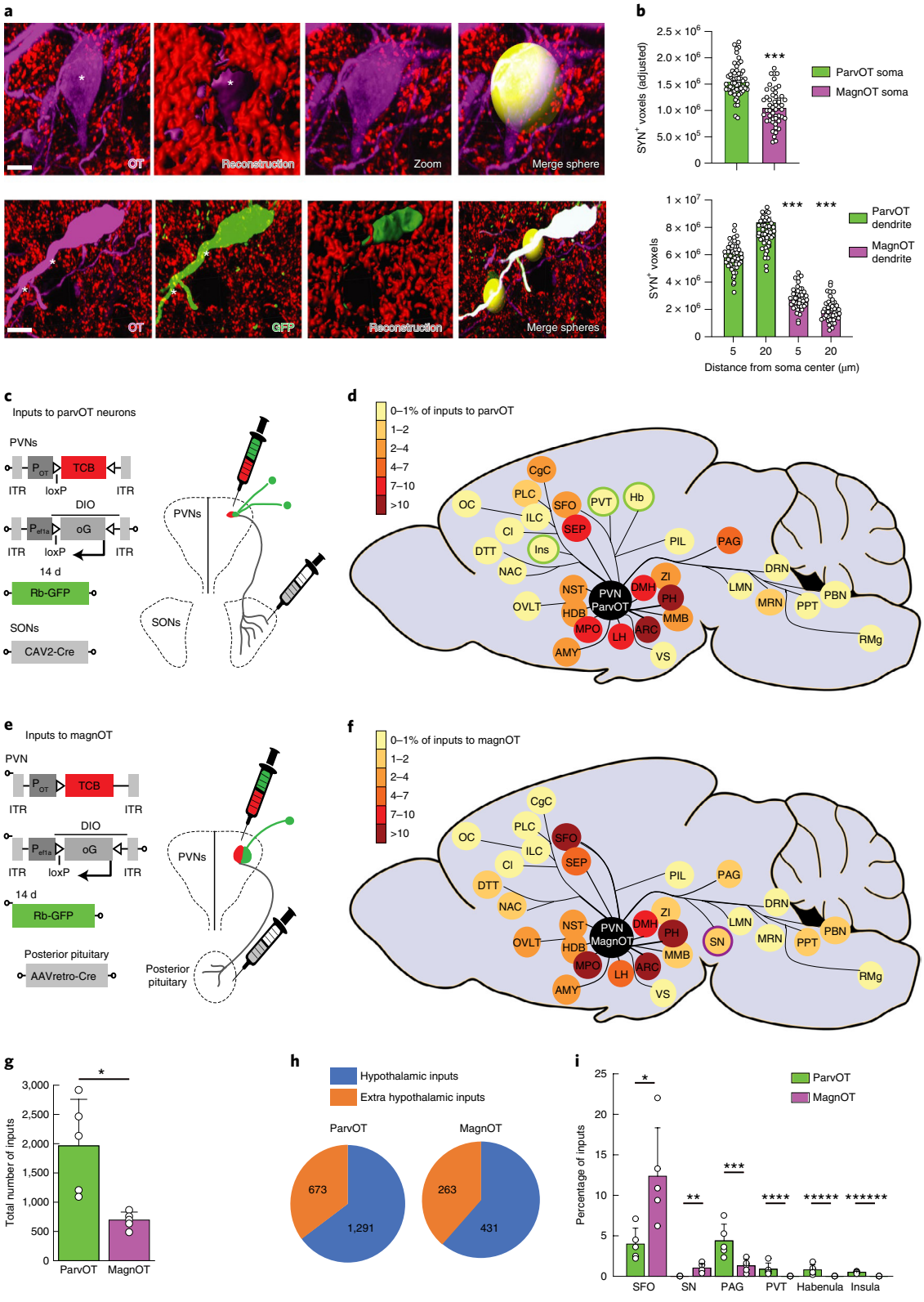

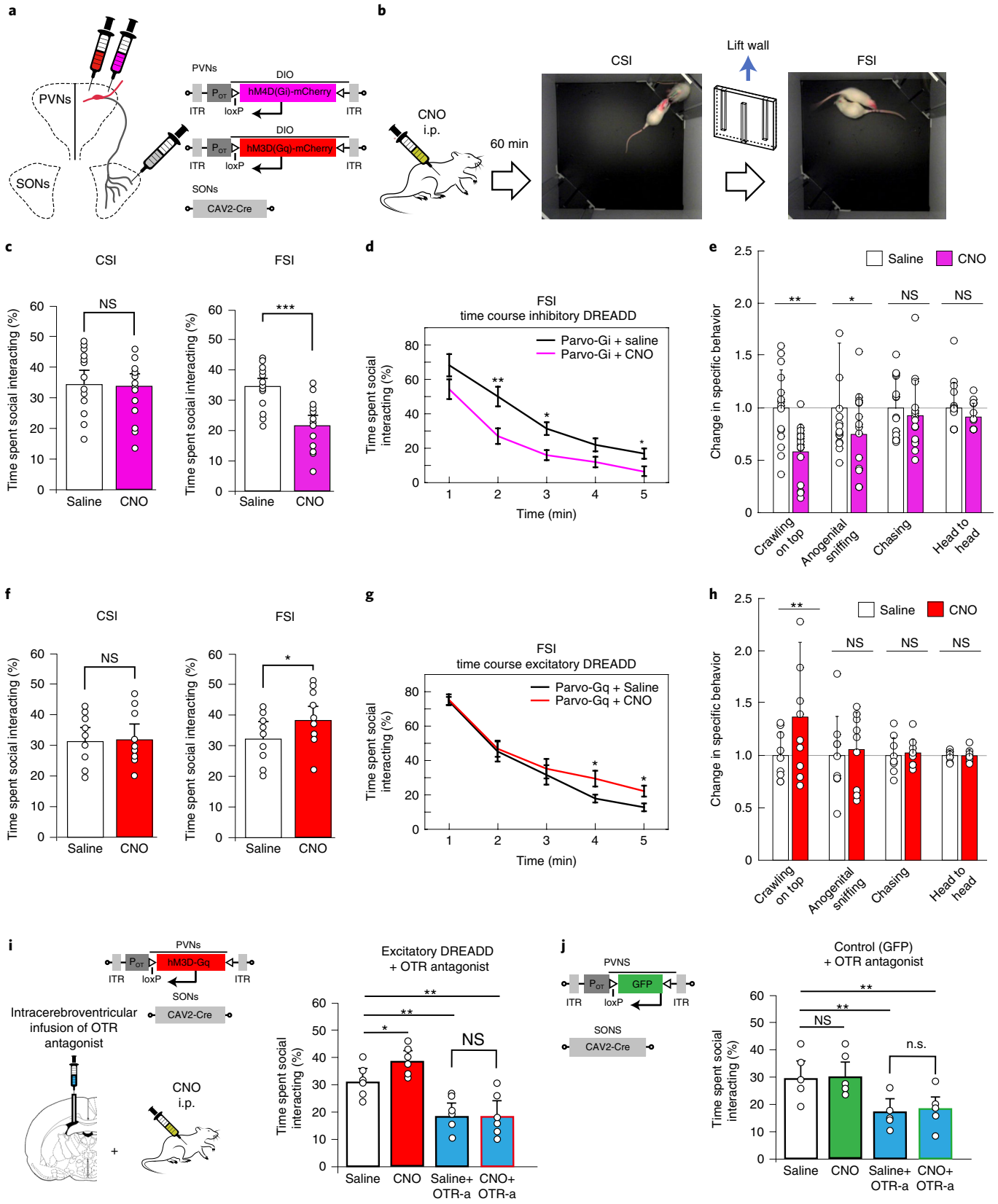

application of an OTR antagonist prevented CNO-induced social interaction after chemogenetic activation of parvOT neurons (Fig. 6). This suggests that the excitation of parvOT neurons is transmitted to magnOT cells, which, in turn, project axonal collaterals to numerous forebrain regions[5,7]. Given that parvOT neurons exclusively project to the brain stem and spinal cord[38], our results allow the hypothesis that the OTR antagonist blocks the action of OT released from magnOT axons in socially relevant brain regions, resulting in the attenuation of social communication between female conspecifics.

Fig. 6 | Modulation of parvocellular OT neurons alters social behavior. a, Viral vectors used to express genes of interest (hM4D(Gi)-mCherry or hM3D(Gq)-mCherry) in parvOT neurons. **b**, CNO or saline was injected intraperitoneally (i.p.) 60 min before the behavioral tests. **c**, Silencing parvOT neurons (Parvo-Gi group): percentage of time spent by an experimental rat injected with saline or CNO socially interacting with a conspecific in CSI ($P=0.41$) and FSI ($n=15$ rats, $^{***}P=0.0001$, paired, two-sided Student's t-test), calculated over the 5-min session. **d**, Temporal dynamics of time spent in social interaction in 1-min bins (second minute, $^{**}P=0.01$; third minute $^{*}P=0.03$; fifth minute $^{*}P=0.04$; $n=15$ rats, two-way ANOVA time × treatment). **e**, Parvo-Gi group: time spent in different social behaviors in rats injected with saline or CNO: crawling on top ($^{**}P=0.008$), sniffing ($^{*}P=0.012$), chasing ($P=0.13$), head to head ($P=0.31$) ($n=15$ rats, one-way ANOVA, Tukey's corrected post hoc comparison). **f**, Activation of parvOT neurons (Parvo-Gq group): average time spent in social interaction with conspecific stimulus in CSI ($P=0.32$) and FSI ($n=9$ rats, $^{*}P=0.04$, paired, two-sided Student's t-test) after CNO or saline injection. **g**, Temporal dynamics of time spent in social interaction in 1-min bins for rats injected with CNO or saline (fourth minute, $P=0.03$; fifth minute, $n=9$ rats, $P=0.05$, two-way ANOVA time × treatment). **h**, Parvo-Gq group: time spent in different social behaviors in rats injected with saline or CNO: mounting ($^{**}P=0.006$), sniffing ($P=0.44$), chasing ($P=0.27$), head to head ($P=0.11$) ($n=9$ rats, one-way ANOVA, Tukey's corrected post hoc comparison). **i**, OTR antagonist intracerebroventricular infusion decreases social interaction even in the presence of pharmacological activation (hM3D-Gq) of parvOT neurons. Percentage of social interaction time is shown in different conditions: saline (control), CNO, OTR antagonist (OTR-a) or CNO + OTR antagonist administration. Time spent social interacting over 5-min sessions. Saline intraperitoneally and intracerebroventricularly: 90 ± 19 s; CNO intraperitoneally and saline intracerebroventricularly: 105 ± 15 s, $^{*}P=0.04$, $n=6$ rats; saline intraperitoneally and OTR antagonist intracerebroventricularly: 54 ± 17 s, $^{**}P=0.007$; CNO intraperitoneally and OTR antagonist intracerebroventricularly: 56 ± 16 s, $^{**}P=0.009$, $n=6$ rats (one-way ANOVA and Tukey's corrected post hoc comparison). **j**, Control group in which parvOT neurons express GFP. Saline intraperitoneally and intracerebroventricularly: 88 ± 18 s; CNO intraperitoneally and saline intracerebroventricularly: 89 ± 14 s, $n=5$ rats; saline intraperitoneally and OTR antagonist intracerebroventricularly: 53 ± 14 s, $^{**}P=0.008$; CNO intraperitoneally and OTR antagonist intracerebroventricularly: 57 ± 15 s, $^{**}P=0.001$, $n=5$ rats (one-way ANOVA and Tukey's corrected post hoc comparison). All data are represented as mean ± s.e.m.

A stable OT-mediated social interaction throughout female life?. Although we exclusively used virgin females in our present study, it will be important to investigate how pregnancy and lactation change the OT-dependent response to somatosensory stimulation. Given the drastic activation of the OT system and close physical contact with the offspring peripartum[39–41], it is plausible that the reward of tactile stimulation changes as well. Moreover, due to the interaction of OT and prolactin during the milk letdown reflex[42,43], the nipples might become more sensitive to the suckling of pups, which could translate into a more rewarding experience for mothers. Further studies are needed to assess the intricate interrelationship of social touch, social behavior and social motivation, which requires concomitant actions of OT, serotonin and dopamine within the nucleus accumbens and ventral tegmental area[22,44], in females as well as males. Accordingly, we found that parvOT, but not magnOT, neurons are innervated by neurons of the insular cortex, which is a critical region processing social touch[45], and could thus be potentially involved in the recruitment of the oxytocinergic system during social tactile stimulation.

Taken together, our data extend the current knowledge of the interrelationship of intracerebral OT release, social touch and its behavioral correlates. Our results suggest that parvOT neurons translate mechanosensory information from the periphery into social behavior (Extended Data Fig. 10), but the precise ascending pathways from cutaneous nerves—via the parvOT → magnOT circuit—to forebrain regions controlling social behaviors await further investigation.

Although intranasal OT application has improved clinical outcomes of schizophrenia, post-traumatic stress disorders and autism spectrum disorders, there is still an ongoing debate about the validity of these findings[46], suggesting that evoking endogenous OT release might be a more reliable way to exploit the benefits of this neuropeptide. Thus, a combination of gentle touch, social interaction and/or intranasal OT application might be a powerful tool to treat human mental diseases, in which the OT system is compromised[47,48].

Online content

Any methods, additional references, Nature Research reporting summaries, extended data, supplementary information, acknowledgements, peer review information; details of author contributions and competing interests; and statements of data and code availability are available at https://doi.org/10.1038/s41593-020-0674-y.

Received: 10 January 2019; Accepted: 18 June 2020;
Published online: 27 July 2020

References

1. Lee, H.-J., Macbeth, A. H., Pagani, J. & Scott Young, W. 3rd. Oxytocin: the great facilitator of life. *Prog. Neurobiol.* **88**, 127–151 (2010).
2. Jurek, B. & Neumann, I. D. The oxytocin receptor: from intracellular signaling to behavior. *Physiol. Rev.* **98**, 1805–1908 (2018).
3. Walum, H. & Young, L. J. The neural mechanisms and circuitry of the pair bond. *Nat. Rev. Neurosci.* **19**, 643–654 (2018).
4. Russell, J. A., Leng, G. & Douglas, A. J. The magnocellular oxytocin system, the fount of maternity: adaptations in pregnancy. *Front. Neuroendocrinol.* **24**, 27–61 (2003).
5. Knobloch, H. S. et al. Evoked axonal oxytocin release in the central amygdala attenuates fear response. *Neuron* **73**, 553–566 (2012).
6. Marlin, B. J. & Froemke, R. C. Oxytocin modulation of neural circuits for social behavior. *Dev. Neurobiol.* **77**, 169–189 (2017).
7. Grinevich, V. & Stoop, R. Interplay between oxytocin and sensory systems in the orchestration of socio-emotional behaviors. *Neuron* **99**, 887–904 (2018).
8. Dumais, K. M., Alonso, A. G., Immormino, M. A., Bredewold, R. & Veenema, A. H. Involvement of the oxytocin system in the bed nucleus of the stria terminalis in the sex-specific regulation of social recognition. *Psychoneuroendocrinology* **64**, 79–88 (2016).
9. Dumais, K. M., Alonso, A. G., Bredewold, R. & Veenema, A. H. Role of the oxytocin system in amygdala subregions in the regulation of social interest in male and female rats. *Neuroscience* **330**, 138–149 (2016).
10. Resendez, S. L. et al. Social stimuli induce activation of oxytocin neurons within the paraventricular nucleus of the hypothalamus to promote social behavior in male mice. *J. Neurosci.* **40**, 2282–2295 (2020).
11. Bobrov, E., Wolfe, J., Rao, R. P. & Brecht, M. The representation of social facial touch in rat barrel cortex. *Curr. Biol.* **24**, 109–115 (2014).
12. Chen, P. & Hong, W. Neural circuit mechanisms of social behavior. *Neuron* **98**, 16–30 (2018).
13. Eliava, M. et al. A new population of parvocellular oxytocin neurons controlling magnocellular neuron activity and inflammatory pain processing. *Neuron* **89**, 1291–1304 (2016).
14. Lima, S. Q., Hromádka, T., Znamenskiy, P. & Zador, A. M. PINP: a new method of tagging neuronal populations for identification during in vivo electrophysiological recording. *PLoS ONE* **4**, e6099 (2009).
15. Leng, T., Leng, G. & MacGregor, D. J. Spike patterning in oxytocin neurons: capturing physiological behaviour with Hodgkin–Huxley and integrate-and-fire models. *PLoS ONE* **12**, e0180368 (2017).
16. Netser, S., Haskal, S., Magalnik, H. & Wagner, S. A novel system for tracking social preference dynamics in mice reveals sex- and strain-specific characteristics. *Mol. Autism* **8**, 53 (2017).
17. Maícas-Royo, J., Leng, G. & MacGregor, D. J. A predictive, quantitative model of spiking activity and stimulus-secretion coupling in oxytocin neurons. *Endocrinology* **159**, 1433–1452 (2018).
18. Portfors, C. V. Types and functions of ultrasonic vocalizations in laboratory rats and mice. *J. Am. Assoc. Lab. Anim. Sci.* **46**, 28–34 (2007).

19. Lenschow, C. et al. Sexually monomorphic maps and dimorphic responses in rat genital cortex. *Curr. Biol.* **26**, 106–113 (2016).
20. Althammer, F. & Grinevich, V. Diversity of oxytocin neurones: beyond magno- and parvocellular cell types? *J. Neuroendocrinol.* **30**, e12549 (2018).
21. Johnson, Z. V. et al. Central oxytocin receptors mediate mating-induced partner preferences and enhance correlated activation across forebrain nuclei in male prairie voles. *Horm. Behav.* **79**, 8–17 (2016).
22. Hung, L. W. et al. Gating of social reward by oxytocin in the ventral tegmental area. *Science* **357**, 1406–1411 (2017).
23. Okabe, S., Yoshida, M., Takayanagi, Y. & Onaka, T. Activation of hypothalamic oxytocin neurons following tactile stimuli in rats. *Neurosci. Lett.* **600**, 22–27 (2015).
24. Bru, T., Salinas, S. & Kremer, E. J. An update on canine adenovirus type 2 and its vectors. *Viruses* **2**, 2134–2153 (2010).
25. Gunaydin, L. A. et al. Natural neural projection dynamics underlying social behavior. *Cell* **157**, 1535–1551 (2014).
26. VanRyzin, J. W. et al. Microglial phagocytosis of newborn cells is induced by endocannabinoids and sculpts sex differences in juvenile rat social play. *Neuron* **102**, 435–449.e6 (2019).
27. Erny, D. et al. Host microbiota constantly control maturation and function of microglia in the CNS. *Nat. Neurosci.* **18**, 965–977 (2015).
28. Wickersham, I. R. et al. Monosynaptic restriction of transsynaptic tracing from single, genetically targeted neurons. *Neuron* **53**, 639–647 (2007).
29. Manning, M., Stoev, S., Cheng, L. L., Ching Wo, N. & Chan, W. Y. Design of oxytocin antagonists, which are more selective than atosiban. *J. Pept. Sci.* **7**, 449–465 (2001).
30. Grund, T. et al. Neuropeptide S activates paraventricular oxytocin neurons to induce anxiolysis. *J. Neurosci.* **37**, 12214–12225 (2017).
31. Rhodes, C. H., Morriell, J. I. & Pfaff, D. W. Immunohistochemical analysis of magnocellular elements in rat hypothalamus: Distribution and numbers of cells containing neurophysin, oxytocin, and vasopressin. *J. Comp. Neurol.* **198**, 45–64 (1981).
32. Uvnäs-Moberg, K., Handlin, L. & Petersson, M. Self-soothing behaviors with particular reference to oxytocin release induced by non-noxious sensory stimulation. *Front. Psychol.* **5**, 1529 (2015).
33. Walker, S. C., Trotter, P. D., Swaney, W. T., Marshall, A. & Mcglone, F. P. C-tactile afferents: Cutaneous mediators of oxytocin release during affiliative tactile interactions? *Neuropeptides* **64**, 27–38 (2017).
34. Brown, C. H., Bains, J. S., Ludwig, M. & Stern, J. E. Physiological regulation of magnocellular neurosecretory cell activity: integration of intrinsic, local and afferent mechanisms. *J. Neuroendocrinol.* **25**, 678–710 (2013).
35. Hoffman, G. E. & Lyo, D. Anatomical markers of activity in neuroendocrine systems: are we all 'Fos-ed out'? *J. Neuroendocrinol.* **14**, 259–268 (2002).
36. Hoffman, G. E., Smith, M. S. & Verbalis, J. G. c-Fos and related immediate early gene products as markers of activity in neuroendocrine systems. *Front. Neuroendocrinol.* **14**, 173–213 (1993).
37. Hasan, M. T. et al. A fear memory engram and its plasticity in the hypothalamic oxytocin system. *Neuron* **103**, 133–146.e8 (2019).
38. Stern, J. E. Electrophysiological and morphological properties of pre-autonomic neurones in the rat hypothalamic paraventricular nucleus. *J. Physiol.* **537**, 161–177 (2001).
39. Bosch, O. J. Brain oxytocin correlates with maternal aggression: link to anxiety. *J. Neurosci.* **25**, 6807–6815 (2005).
40. Fenelon, V. S., Poulain, D. A. & Theodosis, D. T. Fos synthesis and neuronal activation: analysis of Fos immunoreactivity in identified magnocellular neurons during lactation. *Ann. N.Y. Acad. Sci.* **689**, 508–511 (1993).
41. Neumann, I., Douglas, A. J., Pittman, Q. J., Russell, J. A. & Landgraf, R. Oxytocin released within the supraoptic nucleus of the rat brain by positive feedback action is involved in parturition-related events. *J. Neuroendocrinol.* **8**, 227–233 (1996).
42. Augustine, R. A. et al. Prolactin regulation of oxytocin neurone activity in pregnancy and lactation. *J. Physiol.* **595**, 3591–3605 (2017).
43. Kennett, J. E. & McKee, D. T. Oxytocin: an emerging regulator of prolactin secretion in the female rat. *J. Neuroendocrinol.* **24**, 403–412 (2012).
44. Dölen, G., Darvishzadeh, A., Huang, K. W. & Malenka, R. C. Social reward requires coordinated activity of nucleus accumbens oxytocin and serotonin. *Nature* **501**, 179–184 (2013).
45. McGlone, F., Wessberg, J. & Olausson, H. Discriminative and affective touch: sensing and feeling. *Neuron* **82**, 737–755 (2014).
46. Leng, G. & Ludwig, M. Reply to: Improving research standards to restore trust in intranasal oxytocin. *Biol. Psychiatry* **79**, e55–e56 (2016).
47. Meyer-Lindenberg, A., Domes, G., Kirsch, P. & Heinrichs, M. Oxytocin and vasopressin in the human brain: social neuropeptides for translational medicine. *Nat. Rev. Neurosci.* **12**, 524–538 (2011).
48. Grinevich, V. & Neumann, I. D. How puzzle stones from animal studies translate into psychiatry. *Mol. Psychiatry* https://doi.org/10.1038/s41380-020-0802-9 (2020).

Methods

Animals. Female Wistar rats aged 4–8 weeks were purchased from Janvier and housed under standard laboratory conditions (12-h light:dark cycle, lights on at 07:00, 22–24 °C, 50 ± 5% humidity, free access to food and water). All experiments were conducted under license G-102/17 (authorized by the German Animal Ethics Committee of the Baden Württemberg, Regierungspräsidium Karlsruhe) and in accordance with German law, under license 3668-2016011815445431 from the French Ministry and EU regulations. In total, 194 rats were used, of which 15 were excluded due to mistargeting or insufficient expression of viral vectors (Supplementary Table 3).

Viruses. The rAAVs (serotype 1/2) used in the present study (carrying the conserved region of the OT promoter and genes of interest in direct or 'floxed' orientations) were cloned and produced as reported previously[5,13,30,49]. HEK293T cells (Addgene, catalog no. 240073) were used for the virus production. The rAAVs produced included: rAAV-OTp-mCherry/Venus, rAAV-OTp-ChR2-mCherry, rAAV-OTp-DIO-ChR2-mCherry, rAAV-OTp-DIO-hM3D(Gq)-mCherry, rAAV-OTp-DIO-hM4D(Gi)-mCherry, rAAV-OTp-DIO-GFP, rAAV-OTp-DIO-ChR2-EYFP, rAAV-OTp-GCaMP6s, rAAV-OTp-TCB (TVA fused mCherry) and rAAV-Ef1A-DIO-oG. The CAV2-CMV-Cre was purchased from the Institute of Molecular Genetics[24]. The rAAVretro-Ef1A-Cre was purchased from the Salk Institute Viral Vector Core. Modified rabies virus was produced at the Gene Center Rabies laboratory, Ludwig Maximilian University.

Stereotactic injections of viral vectors. For stereotactic injections of viruses, rats were anesthetized with a mixture of ketamine (65 mg per kg birth weight) and xylazine (14 mg per kg birth weight). The rAAV genomic titers were determined using QuickTiter AAV Quantitation Kit (Cell Biolabs, Inc.) and reverse transcription PCR using the ABI 7700 cycler (Applied Biosystems). The rAAV titers were between 10^9 and 10^{10} genomic copies µl^{-1}. We injected 300 nl per PVN. CAV2-Cre was purchased from the Institute of Molecular Genetics (diluted to 10^9 genomic copies µl^{-1}, 300 nl per SON). Viruses were injected via a glass pipette into the target regions at 150 nl min^{-1} using a syringe pump as previously described[50]. Coordinates were chosen in accordance with a rat brain atlas[51] for PVN (anteroposterior (A/P): −1.8 mm; mediolateral (M/L): ±0.3 mm; dorsoventral (D/V): −8 mm), SON (A/P: −1.8 mm, M/L: ±1.2 mm, D/V: −9.25 mm) and posterior pituitary (A/P: −5.6 mm, M/L: ±0.1 mm, D/V: −10.5 mm). Verification of injection and implantation sites and expression of genes of interest was confirmed in all rats post hoc in 50-µm sections containing the PVN and SON (Histology).

Ex vivo experiments. *Slice preparation.* Some 4–8 weeks after injection of the viruses into the PVN and SON of 5-week-old virgin female rats, animals were anesthetized using ketamine (Imalgene 90 mg kg^{-1}) and xylazine (Rompun, 10 mg kg^{-1}) administered intraperitoneally. Then, intracardiac perfusion was performed with an ice-cold, *N*-methyl-D-glucamine (NMDG)-based artificial cerebrospinal fluid (aCSF), which contained (in mM): NMDG (93), KCl (2.5), NaH_2PO_4 (1.25), $NaHCO_3$ (30), $MgSO_4$ (10), $CaCl_2$ (0.5), 4-(2-hydroxyethyl)-1-piperazine-ethanesulfonic acid (Hepes) (20), D-glucose (25), L-ascorbic acid (5), thiourea (2), sodium pyruvate (3), *N*-acetyl-L-cysteine (10) and kynurenic acid (2). The pH was adjusted to 7.4 using either NaOH or HCl, after bubbling in 95% O_2/5% CO_2 gas. Rats were then decapitated, the brains removed and 350-µm-thick coronal slices containing the hypothalamus were obtained using a Leica VT1000s vibratome. Slices were warmed for 10 min in 35 °C NMDG aCSF and placed for a minimum of 1 h in a holding chamber at room temperature, containing normal aCSF. Normal aCSF, also used during all ex vivo experiments, is composed of (in mM): NaCl (124), KCl (2.5), NaH_2PO_4 (1.25), $NaHCO_3$ (26), $MgSO_4$ (2), $CaCl_2$ (2) and D-glucose (15), adjusted to a pH value of 7.4 with HCl or NaOH, and continuously bubbled with 95% O_2/5% CO_2 gas. All aCSF was checked for osmolality and kept to a value of between 305 and 310 mosmol. In electrophysiology or calcium-imaging experiments, slices were transferred from the holding chamber to an immersion recording chamber and superfused at a rate of 2 ml min^{-1}. CNO-containing solution (10 µM) was applied in a bath through a 6-min-long pumping episode, corresponding to several times the volume of the recording chamber (two applications per slice maximum). All ex vivo experiments were conducted at room temperature.

Patch-clamp recording. Whole-cell patch-clamp recordings were visually guided by infrared oblique light videomicroscopy (DM-LFS; Leica), using 4- to 9-MΩ borosilicate pipettes filled with a $KMeSO_4$-based intrapipette solution composed of (in mM): $KMeSO_4$ (135), NaCl (8), Hepes (10), $ATPNa_2$ (2) and GTPNa (0.3). The pH was adjusted to 7.3 with KOH and osmolality checked to be 300 mosmol l^{-1}, and adjusted with sucrose if needed. Data were acquired with an Axopatch 200B (Axon Instruments) amplifier and digitized with a Digidata 1440A (Molecular Devices). Series capacitances and resistances were compensated electronically. Data were sampled at 20 kHz and low-pass filtered at 5 kHz using the pClamp10 software (Axon Instruments). Further analysis was performed using Clampfit 10.7 (Molecular Devices) and Mini analysis v.6 software (Synaptosoft) in a semi-automated fashion (automatic detection of events with chosen parameters followed by a visual validation).

Evoked activity. To test the effects of CNO on neuronal excitability ex vivo, we used a current step method. For this purpose, we make PVN → SON projecting neurons express the DREADD receptors by injecting rats' SON with a CAV2-Cre virus (rAAV-CAV-Cre) and PVN with an OT-specific Cre-inducible DREADD construct (rAAV-OTp-DIO-hM4D(Gi)-mCherry or OTp-DIO-hM3D(Gq)-mCherry). Then, 6–8 weeks after infection, coronal slices were prepared and fluorescent neurons (indicative of the viral expression) were selected for whole-cell patch-clamp recordings. After establishing the clamp, neurons were recorded in current clamp mode with 0 pA injected. To test the effects of DREADD activation—hM4D(Gi) or hM3D(Gq)—neurons were subjected to the following current steps: for hM4D(Gi), neurons received an injection of an −100 pA negative current to hyperpolarize the neuron membrane (reaching −100 mV) before each step. These steps start at −80 pA and increase by 20 pA, reaching +120 pA. For hM3D(Gq), steps start at −20 pA and increase by 10 pA, reaching 80 pA. To quantify the effects of DREADD activation, the number of APs triggered by these steps was evaluated.

Spontaneous activity. To evaluate the effect of DREADD activation on neuronal activity, neurons were also recorded 2 min before and after CNO exposure in voltage or current clamp mode. In these cases, the frequency of the PSCs or APs was quantified.

Identification of parvOT and magnOT. The identity of PVN OT neurons was verified through a current step protocol[52]; this method has been used in several other studies to allow discrimination between parvocellular and magnocellular neurons[13,53–56]. Neurons received an injection of an −100 pA current to hyperpolarize the neuron membrane (reaching −100 mV) before each step. These steps start at 0 pA and increase by 20 A, reaching +60 pA. To discriminate between parvOT and magnOT, we have measured the hyperpolarizing notch and the T-outward rectification.

ChR2 stimulation of SON's parvOT neurons. To decipher the connection between SON parvOT neurons and PVN magnOT neurons, we used an optogenetic strategy. First, we identified PVN OT neurons by injecting rats' PVN with an rAAV containing the coding sequence of the fluorescent marker Venus, under the control of the OT promoter (OTp-Venus). Then, we aimed to specifically activate SON → PVN projection by using a combination of two rAAVs: the first was injected in the SON and induces the expression of the Cre recombinase in SON-targeting neurons, and the second was injected into the PVN to allow the expression of the ChR2 in OT neurons after a Cre-dependent recombination (OTp-DIO-ChR2-mCherry). Then, 6–8 weeks after infection, coronal slices containing the PVN were prepared and the Venus$^+$/mCherry$^-$ neurons were selected for whole-cell patch-clamp recordings. This combination of fluorescent markers allows us to select PVN OT neurons that are not directly targeting the SON.

Neurons were recorded for 2 min in the voltage clamp to establish the baseline frequency of PSCs and, then, we performed an optogenetic stimulation of ChR2-expressing oxytocinergic neurons by applying light pulses (10 ms at 30 Hz for 20 s) using light source X-Cite 110LED from Excelitas Technologies, through a GFP filter, controlled with a Clampex-driven TTL. Neurons were also recorded during the ChR2 stimulation to observe that the neurons were not expressing ChR2 itself. Finally, we continued to recorded 10 min after the stimulation to observe the effect of the SON parvOT neuron stimulation on the PSC frequency of the recorded neurons. PSCs were detected using Mini analysis v.6 software (Synaptosoft).

Calcium imaging. To test whether the chemogenetic activation of PVN → SON projecting oxytocinergic neurons can modify the intra-PVN microcircuit activity, we used an ex vivo calcium-imaging approach. To this end, rats' SON were infected with CAV2-Cre and the PVN with a virus allowing the expression of hM3D(Gq) under the control of OT promoter after a Cre-dependent recombination (OTp-DIO-hM3D(Gq)-mCherry). We also made PVN OT neurons express the calcium indicator GCaMP6s using a third viral vector (rAAV-OTp-GCaMP6s). Then, 6–8 weeks after infection, coronal slices containing the PVN were prepared and neurons that were positive for GCaMP, but negative for mCherry, were recorded. To perform this fluorescence microscopy, we used a Zeiss Axio examiner microscope with a ×40 water immersion objective (numerical aperture of 1.0), mounted with an X-Light Confocal unit—CRESTOPT spinning disk. Images were acquired at 5 Hz with an optiMOS sCMOS camera (Qimaging). Neurons within a confocal plane were illuminated for 100 ms at wavelength λ = 475 nm using a Spectra 7 LUMENCOR. The different hardware elements were synchronized through the MetaFluor software (Molecular Devices, LLC). Neuron calcium levels were measured in a hand-drawn region of interest (ROI). In all recordings, the Fiji rolling ball algorithm was used to increase the signal:noise ratio. Recordings in which movements/drifts were visible were discarded.

Offline data analysis was performed using a customized python-based script.

First, a linear regression and a median filter were applied to each trace. Peaks were then detected using the 'find_peaks' function of the SciPy library.

More precisely, fluorescence variation was identified as a calcium peak if its prominence exceeded twice the s.d. and if the maximum peak value surpasses three fluorescence units. The ROIs with zero calcium variations were excluded from the analysis. The remaining ROIs were considered as living neurons and the number of peaks quantified before and after the drug application. The AUC was estimated as the sum of the local area of each peak to avoid a biased AUC estimation due to baseline drift. All these data were normalized according to the duration of the recording and neurons were labeled as 'responsive' when their AUC or number of peaks was increased by at least 20% after drug application. As the time post-stimulation is longer than the baseline, the probability of observing a spontaneous calcium peak is stronger post-stimulation. To avoid this bias, neurons with only one calcium peak during the whole recording were removed from responsive neurons. The response probability was calculated as the number of responsive neurons with a least 1 calcium event per time bin (30 s) divided by the number of responsive neurons in each recording. Finally, all data were normalized per slice and this result was used as the statistical unit. All data were compared using paired statistical analysis (before versus after drug application) and the results are expressed as a ratio (baseline:drug effect), with a ratio of 1 meaning neither an increase nor a decrease in the measured parameter.

In vivo opto-electrode recordings. *Implantation of opto-electrodes.* Silicon probes (A1x32-Poly3-10mm, NeuroNexus) containing a 32-channel single shank combined with an optic fiber (diameter: 100 µm, Thorlabs) (opto-electrodes) were used in acute (anesthetized and head-fixed) recordings. For freely moving recordings, 32-channel chronic opto-electrodes were hand made, consisting of 8 tetrodes and 1 specially designed microdrive. The microdrives and tetrodes were manually assembled as described previously[57]. The tetrodes were made with 0.0005-inch tungsten wires (Stablohm 675, California Fine Wire Company). Eight tetrodes and an optic fiber (200 µm, Thorlabs) were loaded into the microdrive via a guiding tube and were arranged in parallel order. Assembled opto-electrodes were gold plated and the impedance of each channel was measured between 250 and 350 kΩ. For implantation, rats were anesthetized with 2% isoflurane and placed in a stereotaxic frame. Bregma position and horizontal level were aligned during the implantation. Opto-electrode tips were implanted into the target location and the microdrive was fixed on the skull by six microscrews (Knupfer) and dental cement (Paladur, Heraeus Kulzer).

Optogenetic identification of OT neurons. Electrophysiological signals were acquired by an Open-Ephys acquisition board and sampled at 30 kHz. To identify ChR2$^+$ OT neurons in the PVN, pulses of blue light (λ = 473 nm, DreamLasers) were delivered by the optic fiber while recording extracellular electrical activity of the neurons. The pulse train was controlled by a pulse generator (Master9, A.M.P.I.), and pulses had a duration of 10 ms and were applied at stimulation frequencies of 1, 5 and 10 Hz. In each session, the laser output at the optic fiber terminal was measured as 20 mW mm^{-2}. Neurons with a clear time-locked response to light pulses (spikes within 2–8 ms from onset of pulses) were classified as OT neurons (Extended Data Fig. 1e).

Analysis of spike waveforms. Spike sorting was done manually in Plexon Offline Sorter v.4.0 (Plexon, Inc.), with tetrode mode. The raw data were filtered at 250 Hz with a Butterworth high-pass filter, and waveform detection thresholds were placed at −0.5 to +0.8% of the analog-to-digital converter range (or −0.32 or ~−0.51 mV), depending on the signal:noise ratio. Magnocellular neurons have spikes with a width at half-amplitude of about 0.5 ms, an absolute refractory period of about 2.5 ms and a long relative refractory period, reflecting a prominent hyperpolarizing afterpotential[17]. Therefore, the sample length in waveform detection was set to 1.4 ms (400 µs pre-threshold period; at the 30-kHz sampling rate, a single waveform consists of 42 data points and, in the tetrode waveform, each unit detected 168 data points), and dead time was set to 1.2 ms. Next, the detected waveforms were aligned at the valley point, when the neurons were depolarized at their maximum, and principal component analysis and slice features of waveform were plotted and projected into 3D space for visual separation of clusters into presumptive single units. The timestamp feature was used to exclude mechanical noise recorded at the same time across four channels among the tetrodes. In different recording sessions (for example, OF and social interaction), we analyzed whether the features of spike waveforms remain consistent with the 3D plot results. After clustering, units with a minimum interevent interval exceeding 2,500 µs were accepted as single hypothalamic neurons. Units displaying minimum interevent intervals between 1,200 and 2,500 µs were recognized as arising from multiple neurons and excluded from the statistics of the study.

Statistical analyses of spike patterning. From segments of stationary activity recorded in OF conditions, interspike interval distributions were constructed to verify that these were consistent with distributions characteristic of OT neurons under basal conditions recorded in anesthetized rats[58]. To quantify the regularity of spike firing, we calculated the index of dispersion (IoD) of firing rate in 1-s bins as the ratio of the variance to the mean. For events that arise as a result of a random process that is invariant in time, the IoD will be equal to 1, independent of the mean rate and the binwidth. If events arise more regularly than chance, the IoD will be <1, and if they are more variable than expected by chance—as when spikes occur in clusters or bursts—the IoD will be >1.

In OT neurons, spikes cannot arise purely randomly because of the refractory period, and the IoD reduces slightly with increasing firing rate because, at higher rates, the relative refractory period is larger as a proportion of the mean interspike interval. The IoD also reduces with increasing binwidth because OT neurons also display a prolonged activity-dependent afterhyperpolarization that acts to stabilize mean firing rates over a timescale of seconds. Collectively the known intrinsic membrane properties of rat OT neurons, as tested through computational models, imply that, if spikes arise as a result of a purely random and time-invariant process, then the IoD of the firing rate in 1-s bins will be in the range 0.3–1.0 for neurons firing at up to 6 spikes s^{-1}, depending on firing rate and individual variability in membrane properties[17,58].

LFPs in the PVN. Local field potentials (LFPs) were sampled at 1 kHz with a low-pass filter. Subsequent analysis was done using customized MATLAB (MathWorks) scripts. We estimated the power spectrum density of the LFP signal using a multi-tapper approach, based on Thomson's method ('pmtm' function). Spectrograms were computed for each recording using a standard 'spectrogram' function. The power of theta oscillations was calculated as an average of power spectrum densities in the range 5–10 Hz. Phase-lock analysis was performed to investigate the relationship between theta oscillations in the PVN and the timing of spikes in OT neurons. The phase of the oscillatory activity was extracted with Hilbert's transformation ('Hilbert's' function) and converted into angle degrees. Then, we used Rayleigh's tests for circular uniformity, which indicate whether there is a significant correlation between the timing of spikes and a specific phase of the theta cycle (Extended Data Fig. 1h–j).

In vivo fiber photometry. *Optic-guided implantation of optic fibers.* We injected a modified adenovirus (AAV-OTp-GCaMP6s) bilaterally into the PVN or SON to transduce expression of the Ca^{2+} indicator GCaMP6s in OT neurons, and verified that this was expressed cell specifically (87 ± 4% of OT neurons, $n = 1{,}371$ neurons, $n = 4$ rats, Fig. 4p). Optic fibers (M127L01 diameter 400 µm, numerical aperture 0.50, length 10 mm, Thorlabs) were implanted ~100 µm above the dorsal border of the PVN (A/P: −1.8 mm; M/L: 0.35 mm; D/V: −7.85 mm) or SON (A/P: −1.25 mm; M/L: 1.90 mm; D/V: −9.0 mm) under 1.5% isoflurane anesthesia. Four 1-mm screws (Knupfer) and a metal implant guide (OGL, Thorlabs) were attached to the skull with OptiBond FL (Kerr) and fixed using dental cement (Paladur, Heraeus Kulzer).

During implantation, the implantable cannula was fixed in an adaptor (ADAL3, Thorlabs) attached to a stereotactic holder, whereas the other end of the cannula was connected through a pre-bleached Patch cord (Thorlabs, FP400URT) to the photodetector and light-emitting diode (LED) of the fiber photometry system (FOM, NPI Electronic). The digitized photometry signal was monitored and recorded via a digital input/output board (Open-Ephys) to the DAQ system (Open Ephys) with 0.1- to 20-Hz bandpass filter and 20-s timescale set in to visualize the Ca^{2+} signal online, while the cannula tip was gradually lowered into the PVN at 1 mm min^{-1}. When the optic fiber tip was close to the PVN where GCaMP6s was expressed, a slight increase in the signal baseline and a minor spontaneous fluctuation could be visually detected. During implantation, rats were under 1.5% isoflurane anesthesia and the body temperature was kept stable at 37 °C by a heating plate (Temperature controller 69001, RWD Life Science). The LED power in the fiber photometry system was set at a constant value between 5 and 10 mW mm^{-2}. The fiber photometry recordings were conducted after 1 week of recovery from the implantation. Fiber photometry raw data were sampled at 30 kHz in Open-Ephys GUI and analyzed with customized MATLAB scripts.

Fiber photometry data analysis. Digitized optical signal acquired from the fiber photometry system was first downsampled at 3,000 Hz and then low-pass filtered (MATLAB 'butterworth' function) at 10 Hz to exclude noise at higher frequency. Second, to correct the baseline drifting due to photo-bleaching of fluorophores, we fitted the signal with a polynomial curve (MATLAB 'polyfit' function) and subtracted it from the signal. Next, we smoothed the signal with a Savitzky–Golay filter (MATLAB 'smooth' function, option 'sgolay'). For each experiment, the signal F was converted to $\Delta F/F_0$ by:

$$\Delta F/F(t) = \frac{F(t) - F_0}{F_0}$$

where t is time and F_0 was calculated as the average value of F of a 600-s recording at the start of the experiment. The data were subdivided into 1-min bins and the mean $\Delta F/F_0$ was calculated for each bin. We detected calcium transients similar to those reported in our previous study[59]. Finally, we calculated the AUC of the Ca^{2+} signal (MATLAB 'trapz' function) to estimate the cumulative fluorescence for each bin and normalized the AUC to values from 0 to 1. Values of normalized AUC were displayed in a 1-min bin and averaged in 30-min bins. The ratios of AUCs between experimental and control conditions were used for quantitative analysis and called 'relative AUC increase'.

Application of airpuffs and OT neuron response. Airpuffs from a pressurized air can (Toolcraft, 20793T, 400 ml) were applied through a stiff micropipette tip with a 2-mm opening positioned 10–15 mm above the skin in an area of ~2 cm^2. A plastic cover with 2-cm holes was placed above the rat's body to restrict the area of stimulation. The controlled air pressure was 1.139 g cm^{-3}. During in vivo electrophysiology recordings, in each stimulation point, five airpuffs (duration 0.2 s, interval between puffs 1 s) were delivered in sequence with intervals of 1 min between sequences (Fig. 2a and Extended Data Fig. 4). During fiber photometry recordings, one airpuff (duration 1 s) was applied every 1 min (Fig. 2e–j).

OT neuron response to airpuff stimulations. We applied airpuffs to the skin of three regions of the rat's dorsal body area (anterior, central and posterior parts), two regions of the rat's ventral area (abdomen and anogenital area) and the whiskers on both sides. We considered a recorded neuron as responsive to airpuff stimulations if the average firing rate after (from 0 s to 2 s) stimulus onset increased by at least twice the s.d. of the baseline activity (2 s before stimulus onset). Onset of the response was calculated as the time at which the firing rate of a responsive neuron increased by 1× the s.d. of the baseline activity. We recorded the activity of $n = 23$ OT neurons in response to airpuffs applied to the rat's dorsal body area, which showed variable response latencies of up to 30 s (Extended Data Fig. 4a,b); 10 of those neurons exhibited a response within 1 s after stimulus onset and are shown in Fig. 2a,b.

Blood sampling and plasma OT measurements. To monitor neurohypophyseal OT release after chemogenetic activation of hypothalamic parvOT neurons, we performed blood sampling from the jugular vein in urethane-anesthetized rats. After surgery, rats were placed on a heating pad for the rest of the experiment to maintain constant body temperature. The jugular vein catheter was connected to a 1-ml syringe containing sterile heparinized saline (30 U ml^{-1}); 45 min before, and 45 min as well as 90 min after, intraperitoneal CNO, 500 µl blood was drawn (Fig. 4q,r), which was replaced by 500 µl sterile saline. After each sample, the catheter was filled with heparinized saline to avoid blood clotting. Blood samples were collected in ethylenediaminetetraacetic acid (EDTA) tubes (Bayer) on ice, centrifuged (5,000*g*, for 10 min at 4 °C), and 200-µl plasma samples were stored at −80 °C before extraction and OT quantification by radioimmunoassay. The OT content in extracted plasma was analyzed by a highly sensitive radioimmunoassay with a detection limit of 0.1 pg and cross-reactivity <0.7% (RIAgnosis)[60,61].

Behavior. Starting from 14 d before behavioral tests, vaginal smears were collected to monitor ovarian cycle. Rats in the metestrus, proestrus and estrus phases were excluded from the experiments and reintroduced once they reached diestrus.

Behavioral tests were conducted in an arena (material nonabsorbent to odors) with dimensions 60 × 60 × 60 cm^3 under dim light conditions (<20 lux; lux-meter SO 200K, Sauter). On the day before the test, the experimental rat was exposed to the arena for 15 min for habituation. The arena was cleaned with 70% ethanol after each session to eliminate residual odors. Experimental and stimulus rats were housed in separate cages and had not previous encountered each other before the social interaction tests. The same rat was exposed to social interaction tests twice on separate days, each time with a different social stimulus rat so that the experimental paradigm always represented interaction with a novel, unfamiliar conspecific.

OF test. The experimental rat was placed in a corner of the arena and was allowed to freely explore the environment. These tests served as a 'baseline' for social interaction tests.

FSI test. The experimental and the stimulus rats were placed in opposite corners of the arena at the same time and were allowed to freely interact with each other and/or explore the environment.

CSI test. For this test, two Plexiglas transparent meshes (dimensions 20 × 30 × 1 cm^3) provided with three openings/holes (dimensions 15 × 0.75 cm^2) were placed in two opposite corners of the arena. The mesh separated a little triangular area (14 × 14 × 20 cm^3, corresponding to ~3% of the total area of the arena) from the rest of the arena (central compartment). The experimental rat was placed in the central compartment whereas the stimulus rat was placed in one of the two little compartments. The two rats were able to see, hear and smell each other through the openings, but they were not able to touch each other.

Chemogenetic inhibition or activation of parvocellular OT neurons by DREADD. To selectively activate or inhibit parvocellular OT neurons, rats were injected with rAAV-OTp-DIO-hM3D(Gq)-mCherry (Parvo-Gq group), rAAV-OTp-DIO-hM4D(Gi)-mCherry (Parvo-Gi group) or rAAV-OTp-DIO-GFP (Parvo-GFP control group) into the PVN and CAV2-Cre into the SON, as previously described[13].

All groups (Parvo-Gq, Parvo-Gi and Parvo-GFP) were subjected to the same protocol. On day 1 experimental rats were exposed to the OF arena for 15 min for habituation. On day 2, the experimental rat was injected intraperitoneally with either CNO or saline solution 60 min before starting the tests, and was then subjected to one CSI and one FSI session for 5 min each.

Intracerebroventricular administration of OTR antagonist. Guide cannulas were implanted above the lateral ventricle for intracerebroventricular infusion of the OTR antagonist *des*-Gly-NH_2,*d*$(CH_2)_5$(Tyr(Me)^2,Thr^4)OVT[29]. OTR antagonist 0.75 µg per 5 µl (ref. [30,62]) was infused 15 min before the behavioral tests. Four groups of rats were studied, which received intraperitoneal injection and intracerebroventricular infusion of saline/saline, CNO/saline, saline/OTR antagonist or CNO/OTR antagonist, respectively.

Video and audio analyses of behavior. The videos were recorded using a GigE color HD camera (Basler AG). The tracks of the experimental and stimulus rats were extracted from videos using two software packages: Ethovision XT v.11.5 (Noldus) and MATLAB Toolbox idTracker (MathWorks). The results of the two software packages were compared and crossvalidated. The distance moved by each rat, the velocity, time spent in different areas of the arena, and distance between rats and time spent in close proximity were calculated automatically. Social interactions were also analyzed manually to classify social behaviors into different categories: 'sniffing', 'chasing', 'crawling on top', 'being crawled' and 'head-to-head' approaching; the time spent by the experimental rat for each behavioral category was used for all analyses. Manual scoring of social behavior scoring was done by a researcher (different from the person who performed the experiment) who was blind to treatment conditions.

Ultrasonic vocalizations were recorded with an ultrasound microphone (Avisoft-Bioacustic) and analyzed using Avisoft-SASlab Pro v.5.2 software. After calculation of a sound spectrogram, the vocalization time, duration and frequency were extracted. Each 'call' was classified into a non-social (peak frequency ~22 kHz) or an appetitive/social (peak frequency ~50 kHz) call. Social vocalizations were further classified into trills (<10 ms), single component calls (>10 ms, not modulated) and complex vocalizations (>10 ms, frequency modulated or combined)[63].

Freely moving single unit recordings: experimental groups. Open field and FSI groups: experimental rats implanted with opto-electrodes for single-unit recordings in the PVN were subjected to one OF session and one FSI session for 10 min each. Between the two sessions the rat was placed in the home cage (single housed) for 15 min.

Open field, CSI and FSI groups: experimental rats implanted with opto-electrodes for single-unit recordings in the PVN were subjected to one OF, one CSI and one FSI session for 10 min each, without pauses in between. Stimulus rats were placed in one of the little chambers separated by a Plexiglas mesh at the start of the CSI session; the wall was then lifted up (Fig. 6b) at the start of the FSI session, allowing the stimulus rat to join the experimental rat in the central compartment.

Histology. Anesthetized rats were transcardially perfused with phosphate-buffered saline (PBS) followed by 4% paraformaldehyde (PFA). Brains were dissected out and post-fixed overnight in 4% PFA at 4 °C with gentle agitation. Then, 50-µm vibratome coronal sections containing the PVN and the SON were cut and collected. Immunohistochemistry was performed on free-floating sections using the following antibodies: anti-OT (PS38, 1:2,000; mouse; kindly provided by H. Gainer), anti-OT (T-5021, 1:50,000, Peninsula, guinea-pig), anti-SYN (Abcam, anti-rabbit, ab32127, 1:1,000), anti-Ds-Red (Clontech, catalog no. 632397, 1:1,000; rabbit), anti-GFP (Abcam, ab13970, 1:1,000, chicken), anti-*c-fos* (Cell Signaling, catalog no. 9F6, 1:500, rabbit), anti-Fluorogold (Protos Biotech. catalog no. NM-101, 1:1,000, guinea-pig) and anti-Cre (Novagen, catalog no. 69050, 1:2,000, mouse). Further information on validation of primary antibodies can be found in the Nature Research Reporting Summary. The signals were visualized with the following secondary antibodies: CysTyr3 conjugate (711-165-152) or CysTyr5 conjugate (Jackson Immuno-Research Laboratories, 115-175-146) or Alexa 488 (Invitrogen, A11039) and Alexa 594 (Invitrogen, A11012) and Alexa-594 (Jackson Immuno-Research Laboratories, 715-585-151) and Alexa-647 (Jackson Immuno-Research Laboratories, 713-645-147). All secondary antibodies were diluted 1:500.

Fluorogold treatment and visualization. To discriminate between magnOT and parvOT neurons, rats received a single injection of Fluorogold (Santa Cruz Biotechnology, 15 mg per kg birth weight intraperitoneally) 7 d before the perfusion. Brain sections were stained with a primary antibody for Fluorogold (guinea-pig anti-FG, dilution 1:1,000, Protos Biotech Corp) and Fluorogold immunosignal was visualized by secondary antibodies conjugated with CysTyr3 (Jackson Immuno-Research Laboratories, goat anti-rabbit, dilution 1:500). The co-localization of Fluorogold, OT and *c-fos* signals was manually quantified in the PVN ($n = 4$ rats, 6 sections per brain).

Images of immunostained tissue sections. All images were acquired on a Leica TCS SP5 (DKFZ Light Microscopy Facility), confocal laser-scanning microscope. Digitized images were analyzed using Fiji (National Institute of Mental Health) and Adobe Photoshop CS5 (Adobe).

Confocal microscopy and 3D IMARIS analysis. For the 3D reconstruction of OT neurons, we took *z*-stack images (50 µm depth, 1-µm steps, ×40 magnification) of PVN and SON using a Zeiss LSM 780 confocal microscope (1,024 × 1,024 pixels, 16-bit depth, pixel size 0.63 µm, zoom 0.7). Raw czi files were used for further analysis with IMARIS[26,27,64] software (v.9.31, Oxford Instruments: https://imaris.oxinst.com). First, IMARIS was used to reconstruct the cellular surface using the following customized settings: surface detail 0.700 µm (smooth); thresholding background subtraction (local contrast), diameter of largest sphere, which fits into the object: 2.00; color: base; diffusion transparency: 65%. After surface reconstruction, we used the filter function to remove unspecific background signals: filter: volume maximum 400 µm^3. After deletion of all background signals the 'mask all' function was used to create the final surface reconstruction. Next, the surface reconstruction was used as the template for the filament reconstruction using the following customized settings: detect new starting points: largest diameter 7.00 µm, seed points 0.300 µm; remove seed points around starting points: diameter of sphere regions: 15 µm. Seed points were corrected for (either placed in or removed from the center of the somata) manually if the IMARIS algorithm placed them incorrectly. All surface and filament parameters were exported into separate Excel files and used for data analysis. For all quantifications, we used 6–8 ×40 *z*-stacks per animal (2 *z*-stacks per brain hemisphere). We used a computer suited for IMARIS analysis (Intel Core i7 8700 @ 3.2 GHz, 64 GB RAM, x-64-bit, Windows 10 Enterprise). All images used for analysis were taken with the same confocal settings (pinhole, laser intensity, digital gain and digital offset). Sholl analysis was performed using IMARIS in the filament reconstruction mode and individual datasets were exported into separate Excel files for further analysis. To assess the number of SYN$^+$/GFP$^+$ axons, we used a simplified version of the Sholl analysis, where we included only the first two to eight spheres (starting in the soma center) until either we could detect SYN$^+$/GFP intersections or they were >2 µm apart from the border of the respective soma. The total amount of immunofluorescence (SYN) was calculated using the extract intensity/number of spots function. First, we created spheres that precisely engulfed the respective somata (parvOT and magnOT neurons) so that both ends of the cell soma (maximum diameter) touched the border of the respective sphere. To account for individual variability in roundness and surface area, we calculated the surface area for each individual OT cell using the surface reconstruction mode. Given that cells with a larger surface area occupy more 3D space within the artificially constructed sphere, which could confound precise quantification of SYN fluorescence, we adjusted each calculated value (SYN$^+$ voxels per sphere) based on the surface area. Assuming an inverse almost-linear relationship between cell volume and the total amount of SYN fluorescence within a sphere, we calculated the degree of occupancy (that is, percentage) for each soma within the respective sphere. Finally, we calculated the final SYN$^+$ voxels using the following equation: (Number of SYN$^+$ voxels) × (Degree of occupancy). For the quantification along the dendrites we used spheres with a 10-µm radius along the dendrite for both parvOT and magnOT neurons.

Projection-specific, trans-synaptic retrograde tracing. Input tracing experiments were performed in female Wistar rats (aged 10–12 weeks). We used Rb-GFP[28] to monosynaptically retrogradely trace neurons projecting to parvOT and magnOT neurons. Rb-GFP selectively enters neurons expressing the avian sarcoma and leukosis virus receptor (TVA), and can spread presynaptically only from neurons expressing the rabies virus glycoprotein (we used the optimized glycoprotein, oG, used previously[65]). We injected a 300 nl mixture of 1:1 rAAV-OTp-TCB:rAAV-Ef1A-DIO-oG into the right PVN of female rats. Then, to specifically trace inputs to parvOT neurons, we injected rats ($n = 5$) with CAV2-CMV-Cre into the right SON (Extended Data Fig. 8a). In another group of rats ($n = 5$), we employed a similar strategy to express oG only in magnOT neurons: we injected an AAV retrograde-expressing Cre (rAAVretro-Ef1A-Cre) into the posterior pituitary (Extended Data Fig. 8c, based on previous work[66]). This strategy makes Rb-GFP selectively enter all OT neurons, but specifically spread retrogradely from neurons expressing oG (that is, parvOT or magnOT neurons). After 2 weeks, we injected 300 nl EnvA ΔG-EGFP into the right PVN, and, 7 d later, animals were perfused with 4% PFA. The number of projecting neurons was quantified from brain sections as follows: every third 50-µm section was imaged and neurons were counted, and then multiplied by three, to estimate the real number of inputs. GFP$^+$ neurons on the injected hemisphere were counted and assigned to brain areas based on classifications of the Paxinos Mouse Brain Atlas[37], using anatomical landmarks in the sections visualized by tissue autofluorescence. Very few contralateral inputs were noticed and we therefore decided to neglect them. Although we had good infection at injection sites for both parvOT and magnOT groups (Extended Data Fig. 8g), starter neurons could not be reliably counted, because rabies virus toxicity prevented us correctly visualizing mCherry in the PVN. Thus, the analysis presented here does not take into account inputs to OT neurons from within the PVN. The percentage of inputs from each region was obtained by dividing the number of inputs from one region by the total number of inputs. Input regions that were detected in a subset of animals only were discarded from the analysis. We used unpaired, two-sided Student's *t*-tests to compare the total number of inputs with parvOT and magnOT neurons and χ^2 tests to compare proportions of inputs between regions.

We controlled TVA being selectively expressed in OT neurons by injecting control rats ($n = 2$) with rAAV-OTp-TCB in the PVN, and staining for OT. This revealed that most OT neurons expressed mCherry and no non-OT neurons expressed mCherry (Extended Data Fig. 8e). Furthermore, we verified that Rb-GFP was selectively entering OT neurons by injecting control rats ($n = 2$) with rAAV-OTp-TCB, and Rb-GFP 2 weeks later. This resulted in specific expression of GFP in PVN OT neurons (Extended Data Fig. 8f).

In each rat, we confirmed the SON injection site by staining for Cre for the parvOT neurons tracing (Extended Data Fig. 8a,b) and injecting a virus Cre-dependently expressing mCherry in the SON of magnOT neuron tracing, which led to expression of mCherry in SON magnocellular neurons (Extended Data Fig. 8c,d).

OT secretion model. The OT secretion model[17] simulates stimulus-secretion coupling in OT neurons. The model is a continuous approximation of the stochastic release process from all neuronal compartments. It is based on extensive studies on activity-dependent hormone secretion from magnocellular neurosecretory neurons[58] and it matches experimental data closely. In the model, when spikes invade the secretory terminals, exocytosis occurs in response to fast rising Ca^{2+} concentrations (e). At higher frequencies, the spikes broaden, producing a larger increase in e. The rate of secretion is modeled as the product of: e raised to the power of φ (which accounts for the cooperativeness of the Ca^{2+} activation), of the pool of releasable OT p, and a secretion-scaling factor α, and is calculated as:

$$s = e^{\varphi} \times \alpha \times p$$

where $\varphi = 2$ and $\alpha = 0.003\ \mathrm{pg\,s^{-1}}$.

The nonlinear dependence of the secretion rate gives high secretion probability on short spike intervals. To infer OT secretion arising from the spike trains observed in the present study, the recorded event timings were used to drive the secretion model described fully elsewhere[17]. The published model is scaled to quantitatively match secretion from the pituitary nerve terminals of a single OT neuron. The scaling factor α cannot be used for absolute quantitative estimates of release within the brain, but the relative efficacy of two firing patterns can be compared using the model, because α is eliminated in the ratio.

Statistics. Statistical analyses were performed using SigmaPlot v.11 (Systat) and GraphPad Prism v.7.05 (GraphPad Software). The two-sided, Wilcoxon's signed-rank *W*-test was used to compare the variation of spike frequencies measured for the same neuron in different conditions. The two-sided Mann–Whitney *U*-test was used to compare low threshold depolarization in different cells. Two-sided Student's *t*-tests were used to compare average values in two conditions when the data satisfied assumptions of normality. Pearson's correlation coefficient was used to measure the linear correlation between firing rate and animals' distance. One-way analysis of variance (ANOVA), followed by a multiple comparison post hoc test, was used to compare averages in three or more conditions. Two-way ANOVA, followed by a multiple comparison post hoc test, was used to analyze electrophysiological or behavioral data with repeated measures and CNO/saline/OTR antagonist treatment (time × treatment). No statistical methods were used to predetermine sample size, but our sample sizes are similar to those reported in previous publications[5,13,30].

Differences were considered significant for $P < 0.05$. Asterisks were used to indicate the significance level: $^*0.01 \le P < 0.05$, $^{**}0.001 \le P < 0.01$, $^{***}P < 0.001$. Statistical analyses of neuronal spike trains and local field potentials, such as PSTHs, auto- and cross-correlation, spike burst analysis, power spectrum density and phase locking were performed using NeuroExplorer 3 (Nex Technologies) and customized MATLAB scripts.

Randomization and blinding. Randomization was used to assign brain samples and animals to experimental groups whenever possible, with the constraint that, in social behavior experiments, interacting rats had to be unfamiliar conspecifics, as described under Methods.

Most of the measurements were made using a machine, and are not subject to operator bias, with the exception of manual scoring of social behaviors from videos; in this case, all scorings were done by a researcher (different from the one who performed the experiment) who was blind to treatment conditions.

Reporting Summary. Further information on research design is available in the Nature Research Reporting Summary linked to this article.

Data and code availability

Python code (used for ex vivo calcium-imaging data analysis in Fig. 4a–d) and MATLAB code (used for in vivo fiber photometry data analysis in Fig. 4e–o and Extended Data Fig. 7a–n) can be found in Supplementary Software. All data that support the findings of the present study, as well as MATLAB codes for the analysis of extracellular recording data, are available from the corresponding author upon reasonable request.

References

49. Menon, R. et al. Oxytocin signaling in the lateral septum prevents social fear during lactation. *Curr. Biol.* **28**, 1066–1078.e6 (2018).
50. Grinevich, V. et al. Somatic transgenesis. *Viral Vectors* **3**, 243–274 (2016).
51. Paxinos, G. & Watson, C. *The Rat Brain in Stereotaxic Coordinates*, 7th edn (Elsevier Acad. Press, 2014).
52. Tasker, J. G. & Dudek, F. E. Electrophysiological properties of neurones in the region of the paraventricular nucleus in slices of rat hypothalamus. *J. Physiol.* **434**, 271–293 (1991).
53. Chu, C.-P. et al. Effects of stresscopin on rat hypothalamic paraventricular nucleus neurons in vitro. *PLoS ONE* **8**, e53863 (2013).
54. Luther, J. A. & Tasker, J. G. Voltage-gated currents distinguish parvocellular from magnocellular neurones in the rat hypothalamic paraventricular nucleus. *J. Physiol.* **523**, 193–209 (2000).
55. Luther, J. A. et al. Neurosecretory and non-neurosecretory parvocellular neurones of the hypothalamic paraventricular nucleus express distinct electrophysiological properties. *J. Neuroendocrinol.* **14**, 929–932 (2002).
56. Yuill, E. A., Hoyda, T. D., Ferri, C. C., Zhou, Q.-Y. & Ferguson, A. V. Prokineticin 2 depolarizes paraventricular nucleus magnocellular and parvocellular neurons. *Eur. J. Neurosci.* **25**, 425–434 (2007).
57. Tang, Y., Benusiglio, D., Grinevich, V. & Lin, L. Distinct types of feeding related neurons in mouse hypothalamus. *Front. Behav. Neurosci.* **10**, 91 (2016).
58. Maícas Royo, J., Brown, C. H., Leng, G. & MacGregor, D. J. Oxytocin neurones: intrinsic mechanisms governing the regularity of spiking activity. *J. Neuroendocrinol.* **28**, 28 (2016).
59. Grund, T. et al. Chemogenetic activation of oxytocin neurons: temporal dynamics, hormonal release, and behavioral consequences. *Psychoneuroendocrinology* **106**, 77–84 (2019).
60. de Jong, T. R. et al. Salivary oxytocin concentrations in response to running, sexual self-stimulation, breastfeeding and the TSST: the Regensburg Oxytocin Challenge (ROC) study. *Psychoneuroendocrinology* **62**, 381–388 (2015).
61. Landgraf, R., Neumann, I., Holsboer, F. & Pittman, Q. J. Interleukin-1β stimulates both central and peripheral release of vasopressin and oxytocin in the rat. *Eur. J. Neurosci.* **7**, 592–598 (1995).
62. Neumann, I. D., Maloumby, R., Beiderbeck, D. I., Lukas, M. & Landgraf, R. Increased brain and plasma oxytocin after nasal and peripheral administration in rats and mice. *Psychoneuroendocrinology* **38**, 1985–1993 (2013).
63. Ishiyama, S. & Brecht, M. Neural correlates of ticklishness in the rat somatosensory cortex. *Science* **354**, 757–760 (2016).
64. Althammer, F., Ferreira-Neto, H. C., Rubaharan, M., Roy, K. R. & Stern, J. E. Three-dimensional morphometric analysis reveals time-dependent structural changes in microglia and astrocytes in the central amygdala and hypothalamic paraventricular nucleus of heart failure rats. *Res. Sq.* https://doi.org/10.21203/rs.3.rs-22630/v1 (2020).
65. Kim, E. J., Jacobs, M. W., Ito-Cole, T. & Callaway, E. M. Improved monosynaptic neural circuit tracing using engineered rabies virus glycoproteins. *Cell Rep.* **15**, 692–699 (2016).
66. Zhang, B. et al. Reconstruction of the hypothalamo-neurohypophysial system and functional dissection of magnocellular oxytocin neurons in the brain. Preprint at *bioRxiv* https://doi.org/10.1101/2020.03.26.007070 (2020).

Acknowledgements

We thank T. Grund and X. Liu for initial contribution to this study, R. Stoop for valuable comments on the manuscript, J. Müller for packaging viral vectors, E. Kremer for the canine virus, J. Maicos-Roya for contributing to the modeling of OT release, S. Netser for his comments on the manuscript, C. Pitzer and the Interdisciplinary Neurobehavioral Core Facility of Heidelberg University for some of the behavioral experiments performed there, and T. Splettstoesser (www.scistyle.com) for composing Extended Data Fig. 10. The work was supported by Chinese Scholarship Council No. 201406140043 (to Y.T.), the German Research Foundation (DFG) within the Collaborative Research Center (SFB) 1158 seed grant for young researchers and Fyssen Foundation (to A.L.), DFG postdoctoral fellowship AL 2466/1-1 (to F.A.), Alexander von Humboldt research fellowship (to D.H.), Human Frontier Science Program RGP0019/2015 (to V.G. and S.W.), Israel Science Foundation (grant nos. 1350/12 and 1361/17), Milgrom Foundation and the Ministry of Science, Technology and Space of Israel (grant no. 3-12068, to S.W.), NIH grant (no. R01NS094640, to J.E.S.), BBSRC grant (no. BB/S000224/1, to G.L.), DFG grant (nos. NE 465/27, NE 465/31 and NE 465/34, to I.D.N.), ANR-DFG grant and PICS grant (no. GR 3619/701 and no. GR 07882, to A.C. and V.G.), NARSAD Young Investigator grant (no. 24821) and ANR JCJC grant (no. GR 19-CE16-0011-01, to A.C.), DFG grant (no. GR 3619/4-1), SFB 1158, SNSF-DFG grant (no. GR 3619/8-1) and Fritz Thyssen Foundation grant (no. 10.16.2.018 MN) (all to V.G.).

Author contributions

Y.T., D.B., A.L., A.C. and V.G. designed and conceived the project. L.H. and P.D. performed the ex vivo electrophysiology. L.H. and A. Baudon did the ex vivo calcium imaging. Y.T., D.B. and S.W. performed the in vivo electrophysiology. Y.T. and A.L. did the fiber photometry. Y.T., D.B. and S.W. performed the behavioral experiments and analyses. D.B., M.E., D.H. and F.A. did the immunohistochemistry and confocal microscopy. A.L. and J.S. performed the trans-synaptic labeling of OT neuron inputs. M.S., M.O. and K.K.C. assisted with virus design for trans-synaptic labeling. F.A., M.K.K., R.K.R. and J.E.S. did the 3D reconstruction and analysis. A. Bludau and I.D.N. calculated the plasma OT dosages. G.L. did the modeling. Y.T., D.B., A.L., L.H., F.A., I.D.N., A.C. and V.G. prepared the manuscript. I.D.N., A.C. and V.G. supervised and administered the project, and acquired the funding.

Competing interests

The authors declare no competing interests.

Additional information

Extended data is available for this paper at https://doi.org/10.1038/s41593-020-0674-y.

Supplementary information is available for this paper at https://doi.org/10.1038/s41593-020-0674-y.

Correspondence and requests for materials should be addressed to A.C. or V.G.

Peer review information *Nature Neuroscience* thanks Dayu Lin, Jeffrey Tasker and the other, anonymous, reviewer(s) for their contribution to the peer review of this work.

Reprints and permissions information is available at www.nature.com/reprints.

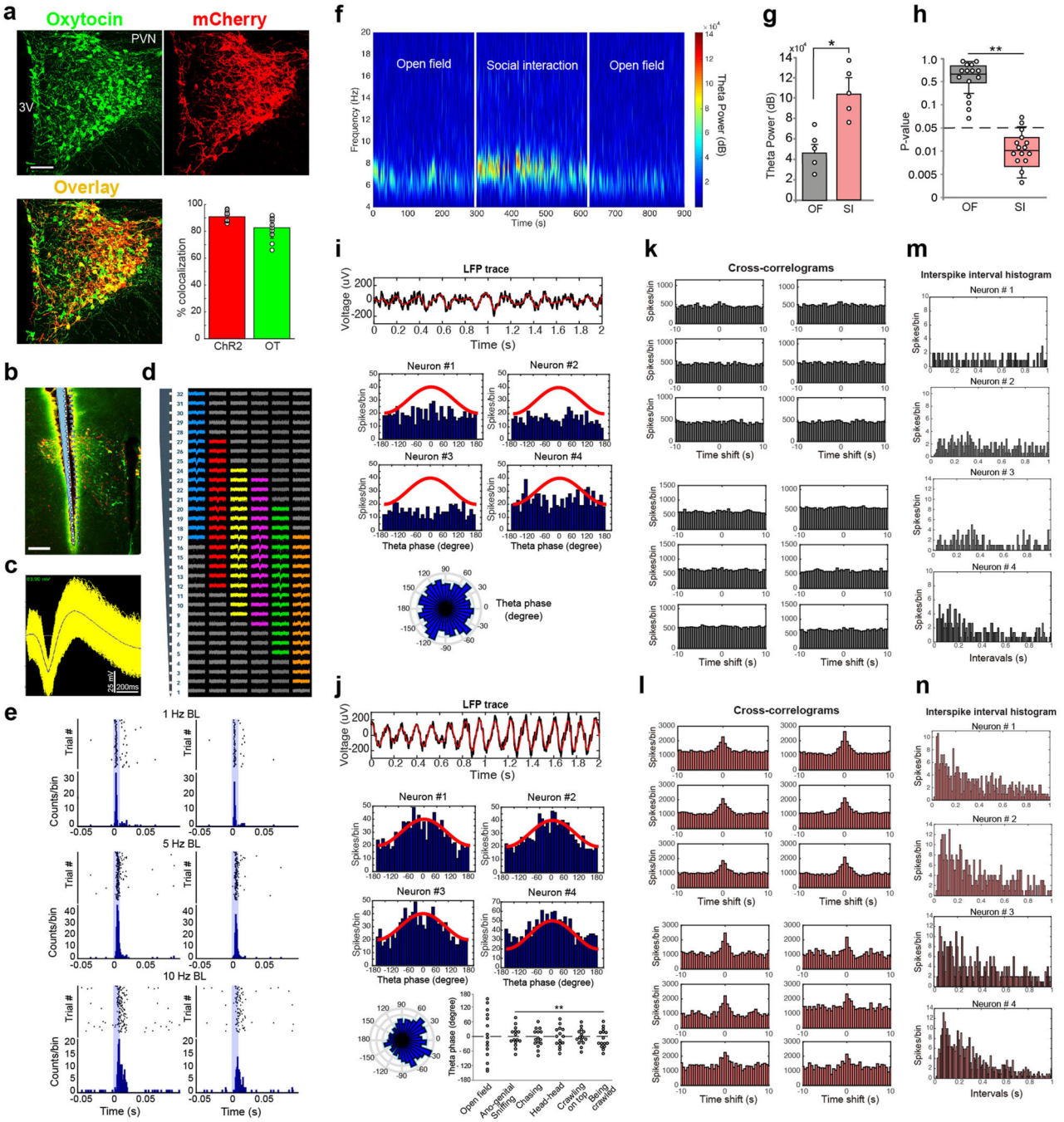

Extended Data Fig. 1 | See next page for caption.

Extended Data Fig. 1 | Recording of optogenetically identified oxytocin neurons, local field potential, phase locking, synchronization and spike distribution. a, The cell type specificity of rAAV-OTp-ChR2-mCherry expression in OT cells. OT-immunosignal (green) colocalizes with ChR2-mCherry (red) signal; the overlay appears in yellow. Scale bar = 100 μm. Bottom, right: quantification of the colocalization mCherry/ChR2 (red bar, 90.8 ± 3.9 %) and mCherry/OT immnoreactive cells (green bar, 82.6 ± 7.7 %). Bar plots show mean ± SEM. **b**, Post-hoc verification of implanted optoprobe location in the PVN in a representative animal (one of five rats). Scale bar = 100 μm. **c**, Sorted extracellular spike waveforms (n = 175 action potentials) of a representative single unit optically-identified as OT neurons. **d**, Silicon probe (NeuroNexus) with 32-channel single shank were used in acute (anesthetized) single units recording. Sorted units and their location in the channels map were visualized with Phy-GUI (klusta, Python). Spike sorting was manually done in Plexon Offline Sorter 4.0 (Plexon, Inc.). **e**, PSTHs illustrating two optogenetically-identified oxytocin neurons by their response to blue light pulses (1 Hz, 5 Hz and 10 Hz laser stimulation, 10 ms, λ=473 nm, 10 mW/mm^2). In both neurons, low frequency stimulation evoked spikes with a relatively constant short latency of 2-10 ms. **f**, Power spectrogram of the local field potential (LFP) in the PVN recorded before (open field, OF), during and after (OF) a free social interaction (FSI) session. **g**, Average theta (5-10 Hz) power recorded during and FSI session is significantly higher than before FSI session ($p = 0.03$, n = 5 rats, paired two-sided t test). All data represented as mean + SEM. **h**, P value distribution of phase-locking between theta (5-10 Hz) oscillations and OT cells spikes during exploratory (OF) or social (FSI) behavior (** $p = 0.0089$, n = 15 cells from 5 rats, paired two-sided t test; box plot shows median 10th, 25th, 75th, and 90th percentiles; min/max: OF, 0.07/0.99; SI, 0.002/0.08). **i, j**, Example traces (black) of LFP in the PVN and band-pass (5-10 Hz) filtered theta oscillations (red) during exploratory (OF) or social (FSI) behavior. Examples of distribution of four OT neurons firing in relation to LFP theta oscillations; OT neurons spikes are phase-locked with theta oscillations (** $P = 0.0014$, n = 15 cells) during social interaction (FSI, **j**), but not during exploratory behavior (**i**). Circular representation of OT neurons firing in relation to theta oscillation phase shows phase locking during social behavior (**l**) exclusively. No significant difference of spike-phase coupling between social behavior subtypes ($P = 0.28$). Significance of phase locking are determined by Rayleigh test for circular uniformity. **k, l**, Cross-correlation of pairs of oxytocin neurons recorded simultaneously. During open field (**k**) test there is no detectable correlation between oxytocin neurons spiking activity, but during social interaction (**l**) there is a significant increase ($P = 0.0038$, n = 12 cell pairs) of temporally correlated spikes within a time window of $\tau = 1.2 \pm 0.5$ s (mean correlation half-time). **m, n**, Examples of interspike interval (ISI, time bins = 10 ms) histograms of four OT neurons recorded during exploratory behavior (OF, **m**) and during social interaction (FSI, **n**). During FSI there is a prominent increase of spikes with short intervals due to increased spike clustering.

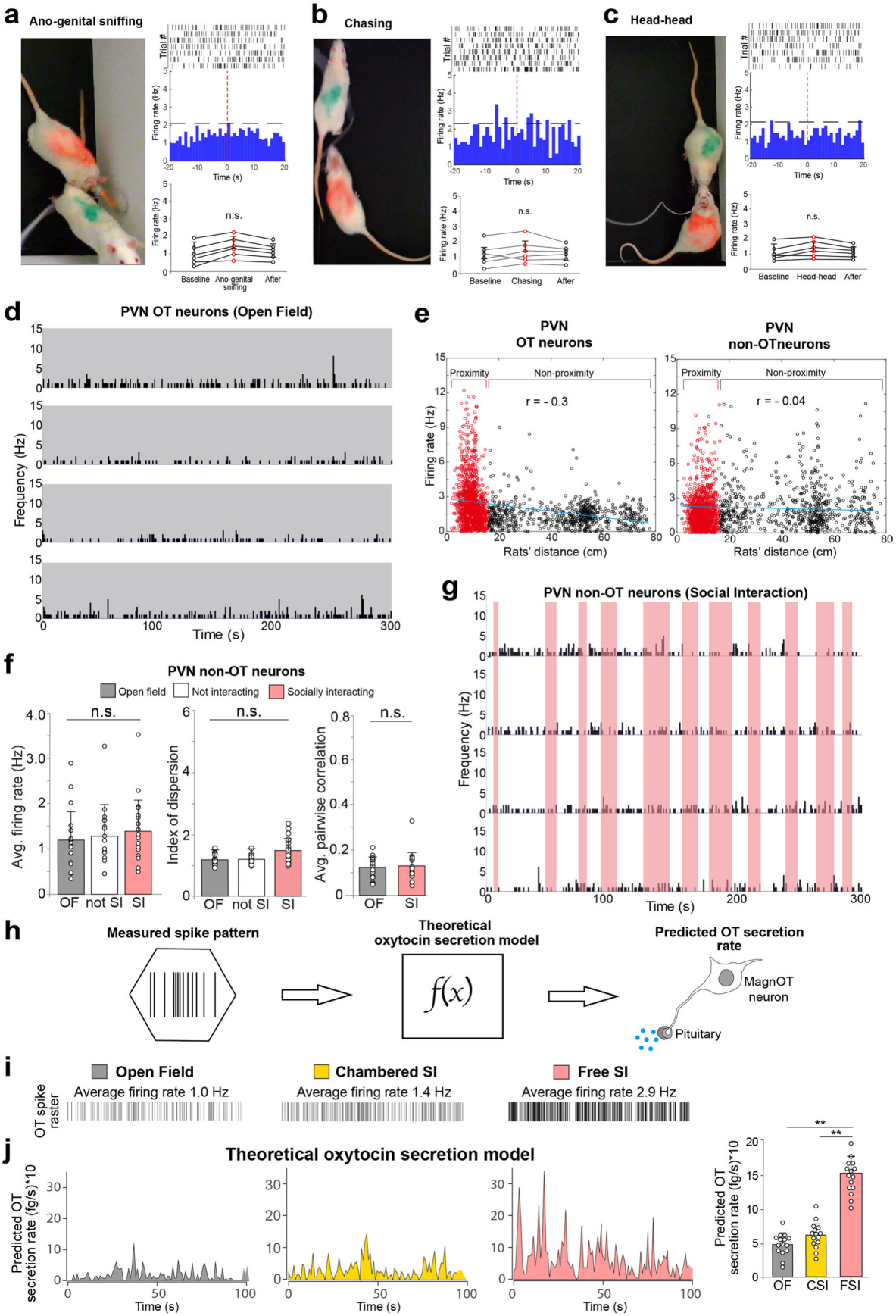

Extended Data Fig. 2 | See next page for caption.

Extended Data Fig. 2 | Analysis of social interactions, the firing rate of oxytocin and non-oxytocin PVN neurons, and activity-dependent model of oxytocin secretion. a-c, Examples of manually classified social interaction behaviors: *ano-genital sniffing*, *chasing*, *head-to-head* events. PSTHs of a single unit identified as oxytocin neurons aligned to the onset of the specific behavior. Averaged (10 s time bin) PSTHs responses before, during, and after each behavior (0 to +10 s vs. basal $P = 0.12$, $P = 0.45$, $P = 0.88$, respectively, n = 6 cells per behavior, two-sided Wilcoxon test). **d**, Example firing rate of four PVN OT neurons recorded during exploratory (OF) behavior. **e**, Linear regression of PVN OT and non-OT neuronal firing rate in relation to rat's distance in the area during FSI. OT neuronal activity shows a moderate negative correlation with distance (r = -0.3, p = 0.0092), while non-OT neurons do not show any significant correlation (r = −0.04, $P = 0.11$). **f**, Example firing rate of four PVN non-OT neurons recorded during social interaction. **g**, Average firing rate of 21 non-OT neurons from five rats (OF baseline 1.2 ± 0.2 Hz, not socially interacting (not SI) firing rate 1.2 ± 0.2 Hz, and social interacting (SI) firing rate 1.4 ± 0.2 Hz; $P = 0.83$, $P = 0.23$, $P = 0.34$, one-way ANOVA). Average index of dispersion on 1-s time bins of 21 non-OT cells (OF 1.1 ± 0.2, not SI 1.1 ± 0.2, SI 1.4 ± 0.3, $P = 0.78$, $P = 0.07$, $P = 0.11$, one-way ANOVA). Average pairwise Pearson correlation of spiking activity (1-s time bins) of 21 non-OT neurons' pairs recorded in OF and FSI ($P = 0.98$, paired two-sided t test). All data show average + SEM. **h**, Schematic illustration of the theoretical model used to estimate the amount of secreted oxytocin from axonal terminals given the measured neuronal spike pattern. **i**, Average firing rate of OT cells from rats that underwent open field (OF), CSI, and FSI tests. **j**, Predicted OT secretion rate for a representative OT cell in each condition (left). Average OT predicted secretion rate (right) in each condition (OF-CSI, $P = 0.11$, OF-FSI, ** $P = 0.005$, OF-CSI, ** $P = 0.007$, spike pattern data used for prediction are from n = 15 cells from 5 rats, one-way ANOVA followed by Tukey's post hoc test). Data represented as mean + SEM.

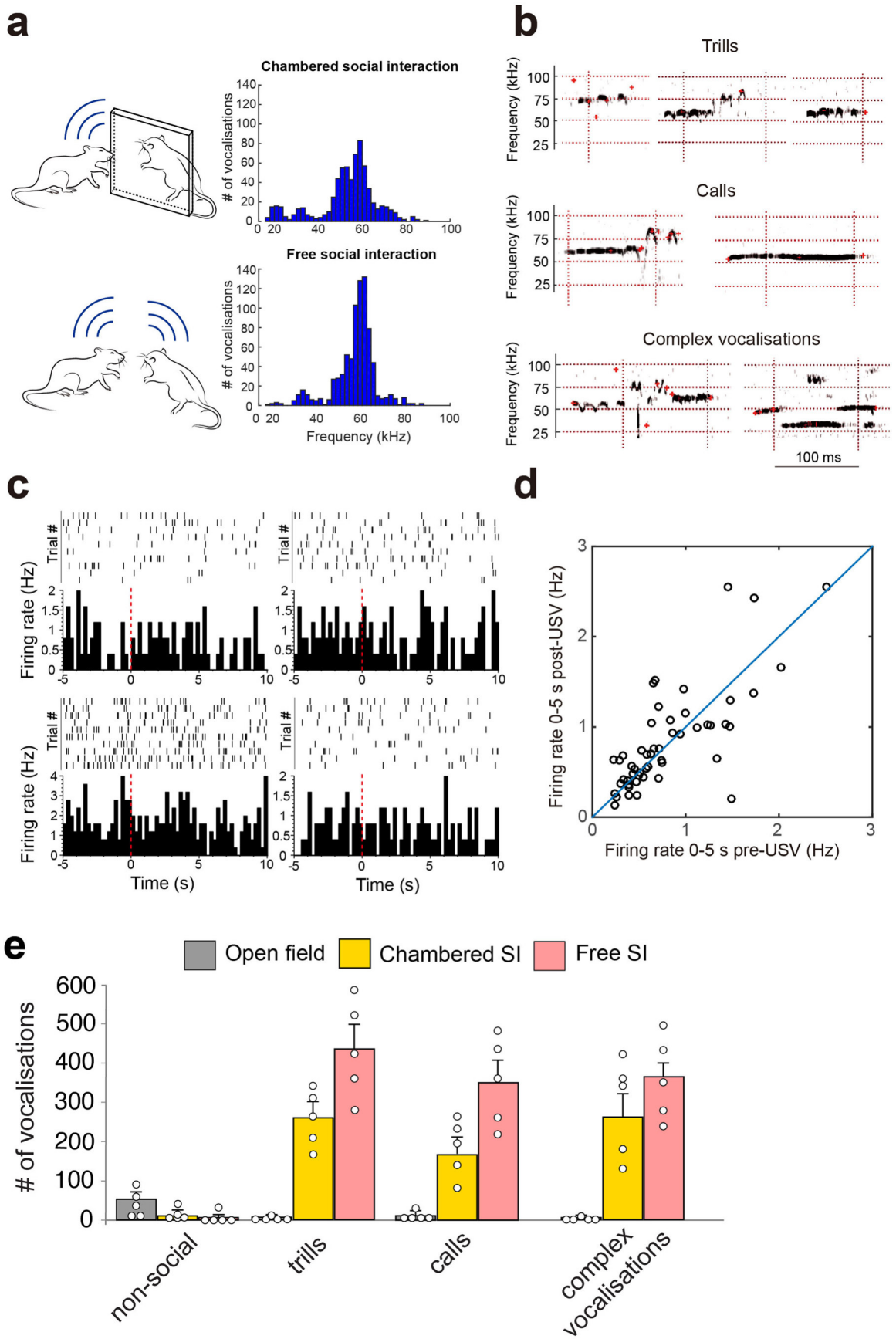

Extended Data Fig. 3 | See next page for caption.

Extended Data Fig. 3 | Ultra Sound Vocalizations (USVs) and OT neuronal activity. a, Histograms of USVs peak frequency distribution during CSI (top) and FSI (bottom). **b**, Examples of sound spectrograms showing USVs events classified as whistles, calls, or complex vocalizations. **c**, PSTHs of oxytocin neurons spiking activity aligned to USVs onset (red dashed line) show no significant time-locked correlation between them. **d**, Firing rate of oxytocin neurons 0-5 s before USV events versus 0-5 s after USV events showing no significant correlation ($P = 0.24$, n = 53 vocalisations, two-sided Wilcoxon test). **e**, Total number of USVs registered in 5 pairs (experimental and stimulus animal) of rats during OF, CSI, and FSI tests divided - according to their frequency and duration – in non-social (< 25 kHz), trills (< 10 ms), calls (> 10 ms, not modulated), and complex vocalizations (> 10 ms, frequency modulated or mixed). All data represented as mean + SEM.

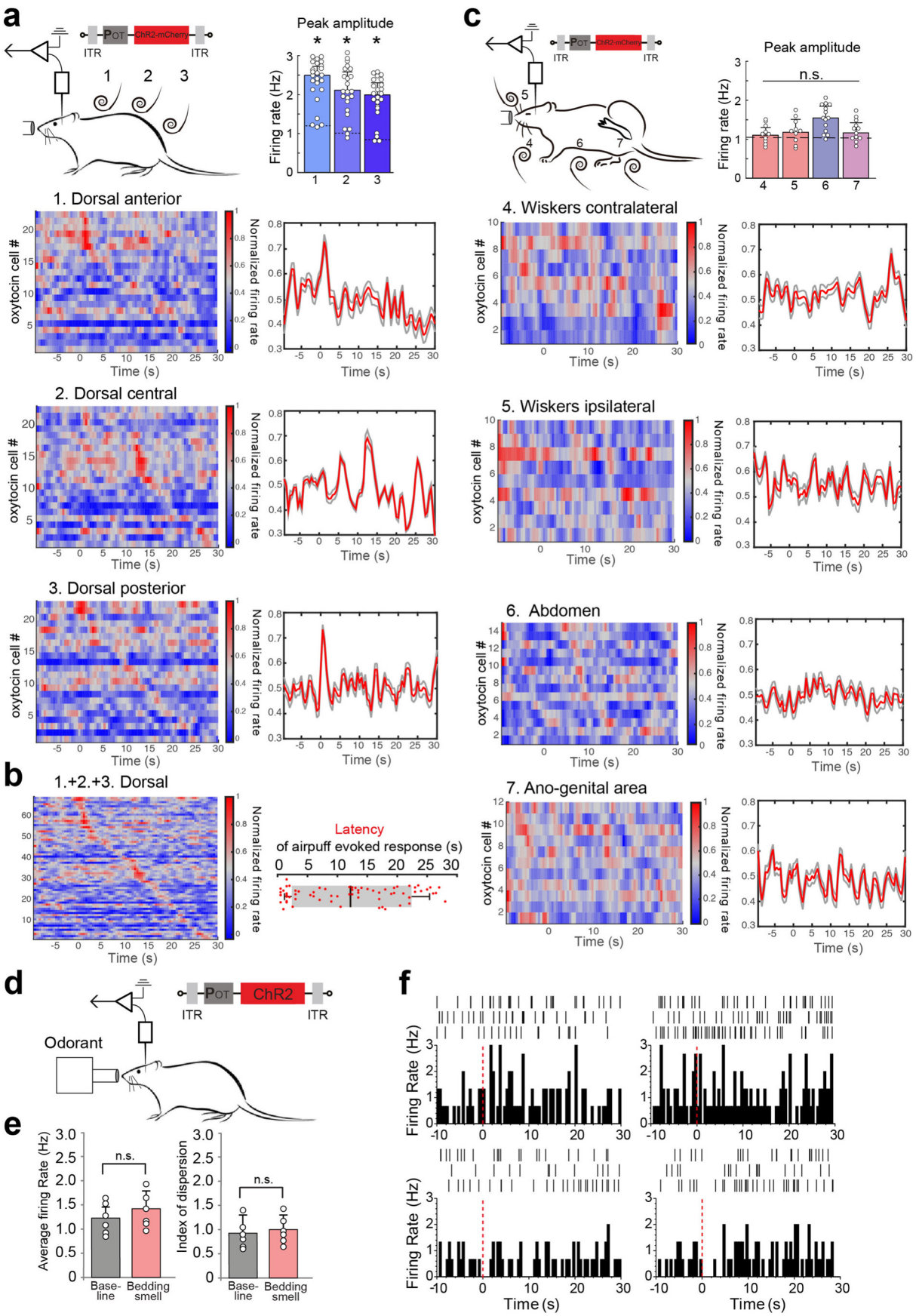

Extended Data Fig. 4 | See next page for caption.

Extended Data Fig. 4 | Oxytocin neurons response to airpuffs and to socially-related olfactory stimuli. a, Illustration of single-unit recordings of oxytocin neurons during airpuffs applied to 1. anterior, 2. central, 3. posterior (n = 23 cells from 8 rats) part of the dorsal body region. Average increase response of oxytocin neurons compared to baseline for different stimulations regions (*P = 0.017, *P = 0.025, *P = 0.021 respectively, n = 23 cells from 8 rats, one-way ANOVA followed by Bonferroni post hoc comparison). PSTHs showing single oxytocin neurons (left) and averaged (right) and response to repeated airpuffs in all stimulation sites. **b**, Combined PSTHs of 1., 2., 3., showing different response latency of oxytocin neuron to airpuff stimulations on the dorsal body area. **c**, Single-unit recordings of oxytocin neurons during airpuff stimulations on: whiskers (n = 10 cells), abdomen (n = 14 cells), and anogenital area (n = 12 cells). Average increase response of oxytocin neurons compared to baseline for different stimulation regions. PSTHs showing single oxytocin neurons (left) and averaged (right) and response to repetitive airpuff stimulations in all stimulation sites. All data represented as mean + SEM. **d**, Illustration of the experimental setup for recording oxytocin neurons activity (opto-electrodes) during presentation of olfactory stimuli. **e**, Average firing rate and index of dispersion of six oxytocin neurons 10 s before presentation of the olfactory stimuli vs 10 s after; no significant changes are detected (P = 0.34, P = 0.48, n = 6 cells from 3 rats, paired two-sided t test). Data represented as average + SEM. **f**, PSTHs of 4 (out of 6 recorded) oxytocin neurons spiking activity aligned to onset of olfactory cues (red dashed line) - urinated bedding smell; no significant changes in firing rate are detected.

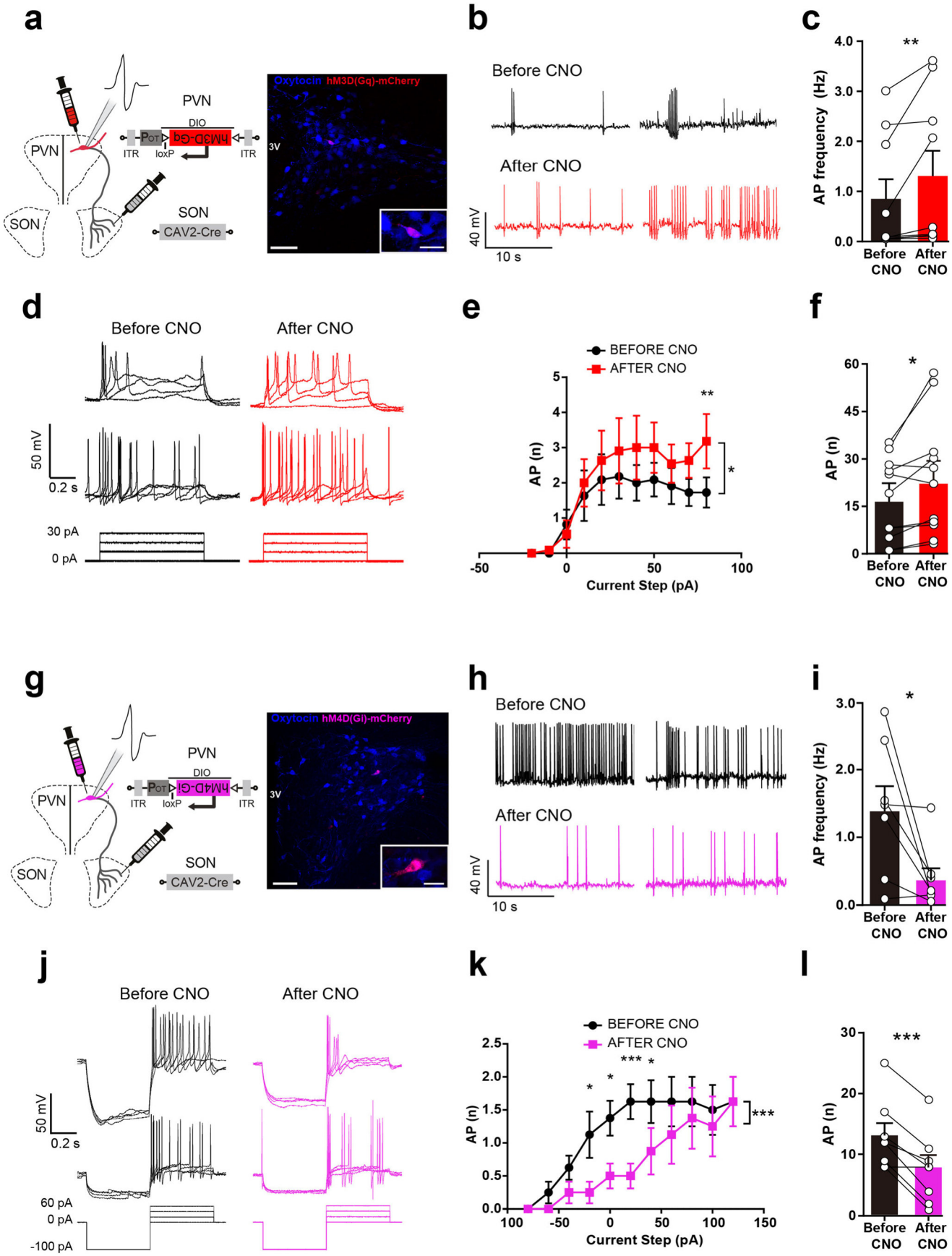

Extended Data Fig. 5 | See next page for caption.

Extended Data Fig. 5 | *Ex vivo* effects of excitatory hM3D(Gq) and inhibitory hM4D(Gi) DREADD in parvOT neurons. a, Schema of viral vectors injected for *ex vivo* recording of parvOT neurons with concomitant DREADD-Gq activation. The picture shows hM3D(Gq) (purple) and OT (blue) immunoreactivities in the PVN of one out five rats. Scale bar = 100 µm and (inset) 10 µm. **b-c**, Spontaneous response from parvOT neurons expressing hM3D(Gq) in before and after the CNO bath application; b example traces, c quantification (baseline 0.85 ± 0.39 Hz vs CNO 1.31 ± 0.51 Hz, n = 9 cells from 5 rats; $P = 0.0039$). **d-f**, Evoked responses from parvOT neurons expressing hM3D(Gq) to current injections before and after the CNO bath application; (**d**) example traces, (**e**) quantification per step (before CNO current step 80 pA 1.727 ± 0.428 nAP vs after CNO current step 80 pA 3.182 ± 0.772 nAP, n = 11; $^{**}P < 0.01$); (**f**) quantification of the average response (16.18 ± 3.89 AP vs CNO 22.55 ± 5.66 AP, n = 11 cells from 5 rats; $P = 0.0314$). **g**, Schema of viral vectors injected for *ex-vivo* recording of parvOT neurons with concomitant DREADD-Gi excitation. The picture shows hM4D(Gi) (purple) and OT (blue) immunoreactivities in the PVN of one out seven rats. Scale bar = 100 µm and (inset) 10 µm. **h-i**, Spontaneous response from parvOT neurons expressing hM4D(Gi) in before and after the CNO bath application; b example traces, c quantification (baseline 1.38 ± 0.38 Hz vs CNO 0.36 ± 0.18 Hz, n = 7 cells from 7 rats; $P = 0.0469$). **j-l**, Evoked responses from parvOT neurons expressing hM4D(Gi) to current injections before and after the CNO bath application; (**j**) example traces, (**k**) quantification per step (before CNO current step 20 pA 1.625 ± 0.263 nAP vs after CNO current step 20 pA 0.5 ± 0.189 nAP, n = 8; $^{***}P < 0.001$); **l**, quantification of the average response (baseline 13 ± 2.02 AP vs CNO 7.75 ± 2.03 AP, n = 8 cells from 7 rats; p = 0.0007). All results are expressed as average ± SEM. The statistical significances: * $P < 0.05$; ** $P < 0.01$; *** $P < 0.001$ (two-sided Wilcoxon test: c and i; Two-way ANOVA followed by a Holm-Sidak post hoc test: e and k; Paired two-sided t test: f and l). Open circles indicate individual cells.

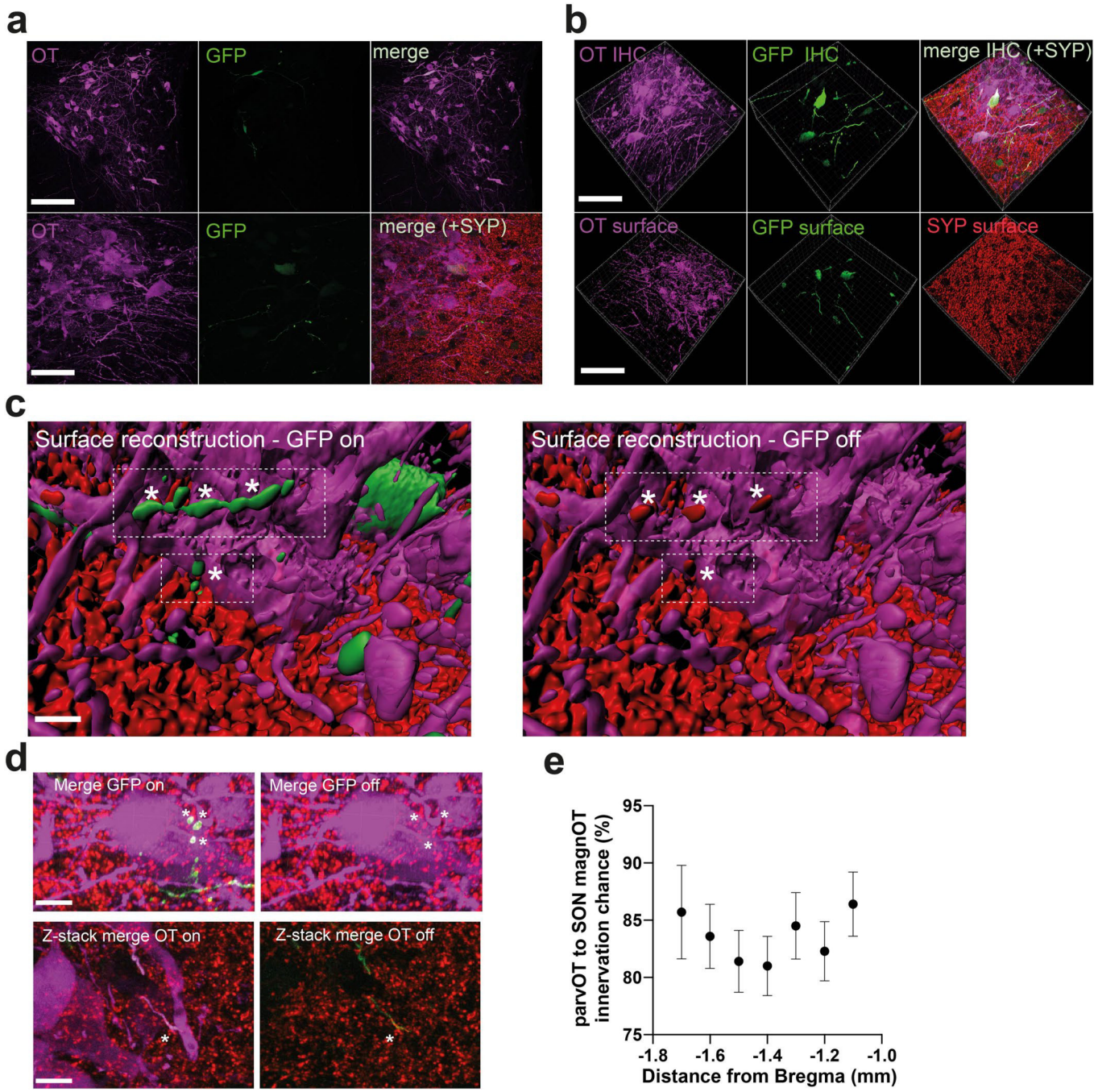

Extended Data Fig. 6 | Three-dimensional reconstruction and assessment of parvOT-magnOT connectivity. a, Confocal images show specific labeling of parvOT neurons using CAV2-Cre in combination with OTp-DIO-GFP. Top panel shows a representative PVN (one out of three independent experiments, n = 3 rats) image with 2 labeled parvOT neurons. Bottom panel shows an image with higher magnification and overlay with synaptophysin (SYN). OT = purple, GFP = green, SYN = red. Scale bars = 200 µm (top panel) and 50 µm (bottom panel). **b**, Images show raw fluorescent confocal z-stacks and surface reconstruction of individual fluorescent channels (one out of three independent experiments, n = 3 rats). The top panel shows fluorescent signals of OT, GFP and merge (+SYN). The bottom panel shows the same channels with applied surface reconstruction. Bottom images have been vertically flipped to enhance visualization of the reconstructed channels. Scale bars = 75 µm. **c**, Images show the IMARIS three-dimensional surface reconstruction of OT, GFP and SYN. Boxes with dashed lines and asterisks indicate the overlap of GFP and SYN. In the right panel the overlap between OT (purple) and GFP (green) has been manually removed to visualize the GFP/SYN (green/red) overlap (n = 169 cells from 3 rats). Scale bar = 10 µm. **d**, Confocal images show synaptic contact of parvOT neurons with magnOT somata and dendrites. Top panel shows axo-somatic contact. Bottom panel shows axo-dendritic contact using a high magnification confocal z-stack. Asterisks indicate synaptic contact. Scale bars = 10 µm. **e**, Quantification of SON OT neuron chance to receive innervation by parvOT neurons in respect to their rostro-caudal location (n = 169 cells from 3 rats). All data are presented as mean ± SEM.

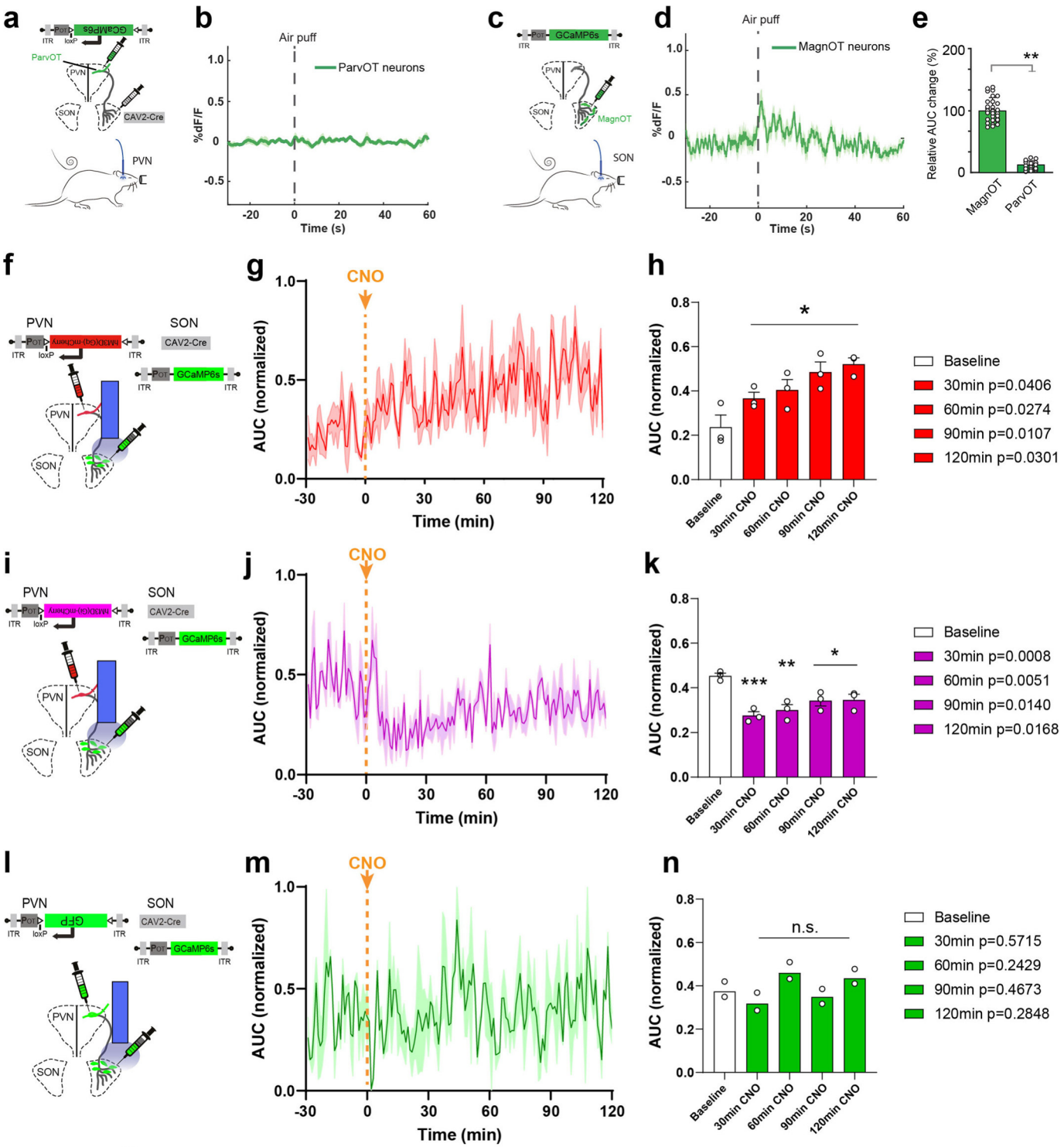

Extended Data Fig. 7 | See next page for caption.

Extended Data Fig. 7 | Fiber photometry recording of PVN parvOT neurons and SON magnOT neurons with chemogenetic manipulation of parvOT neurons. a-b, Schema of viral vectors injected (CAV2-Cre in the SON and OTp-DIO-GCaMP6s in the PVN) and implanted optic fiber for fiber photometry recording of PVN parvOT neurons (a). No Ca^{2+} transient nor changes in Ca^{2+} signal upon 'airpuff' stimulation were detected when recording parvOT neurons exclusively (b, solid line: average, shaded area: SEM, n = 3 rats). **c-d**, Schema of viral vectors injected and implanted optic fiber for fiber photometry recording of SON magnOT neurons (c). Examples of fiber photometry-based Ca^{2+} signals of SON magnOT population during airpuff stimulation (d); the graphic is an average of 33 airpuff responses (11 airpuffs per animal, n = 3 rats). **e**, Relative change in the area under the curve (AUC) 0-30 s after airpuffs with respect to 30 s before the stimuli, of SON magnOT vs. parvOT neurons (solid line: average, shaded area: SEM, n = 33 airpuffs from 3 rats, ** $P = 0.008$, unpaired two-sided t test). Data show mean + SEM. **f-g-h**, Schema of viral vectors injected and implanted optic fiber for fiber photometry recording (f) of SON OT neurons with concomitant DREADD-Gq activation of parvOT neurons. Normalized area under the curve (AUC) of GCaMP6s signal (g, solid line: average, shaded area: SEM, 1 min bin size) of SON OT neurons showing increase of cells activities after parvOT activation mediated by CNO i.p. injection (indicated by arrow). 30-min averaged AUC (h) showing a gradual increase in cellular activity and lasting at least 120 min (* $P = 0.0406$, * $P = 0.0274$, * $P = 0.0107$, * $P = 0.0301$, n = 3 rats, two-way ANOVA Tukey's corrected post-hoc comparison). Data show mean + SEM. **i-j-k**, Schema of viral vectors injected and implanted optic fiber for fiber photometry recording (i) of SON OT neurons with concomitant DREADD-Gi inhibition of parvOT neurons. Normalized area under the curve (AUC) of GCaMP6s signal (j, solid line: average, shaded area: SEM, 1 min bin size) of PVN OT neurons showing a decrease of cellular activity after parvOT inhibition mediated by i.p. CNO injection (indicated by arrow). 30-min averaged AUC (k) shows a sharp decrease in cellular activity that lasts at least 60 min and then gradually recovers (*** $P = 0.0008$, ** $P = 0.0051$, * $P = 0.0140$, * $P = 0.0168$, n = 3 rats, two-way ANOVA Tukey's corrected post-hoc comparison). Data show mean + SEM. **l-m-n**, Schema of viral vectors injected and implanted optic fiber for fiber photometry recording (l) of SON OT neurons in control animals (DREADD-free) expressing GFP in parvOT neurons. Normalized area under the curve (AUC) of GCaMP6s signal (m, solid line: average, shaded area: SEM, 1 min bin size) of PVN OT neurons showing no significant changes in Ca^{2+} signal upon CNO injection. No significant changes are detected in 30-min averaged AUC (n) up to 120 min ($P = 0.5715$, $P = 0.2429$, $P = 0.4673$, $P = 0.2848$, n = 2 rats, two-way ANOVA Tukey's corrected post-hoc comparison). Data show mean values. **o**, Panels of an immunostained section of the SON (one of out of eight independent experiments) showing post-hoc verification of implanted optic fiber above the SON and co-localization of immunoreactive, GCaMP6s (green), oxytocin (blue), and merged channels. Scale bar 100 μm and 10 μm (inset).

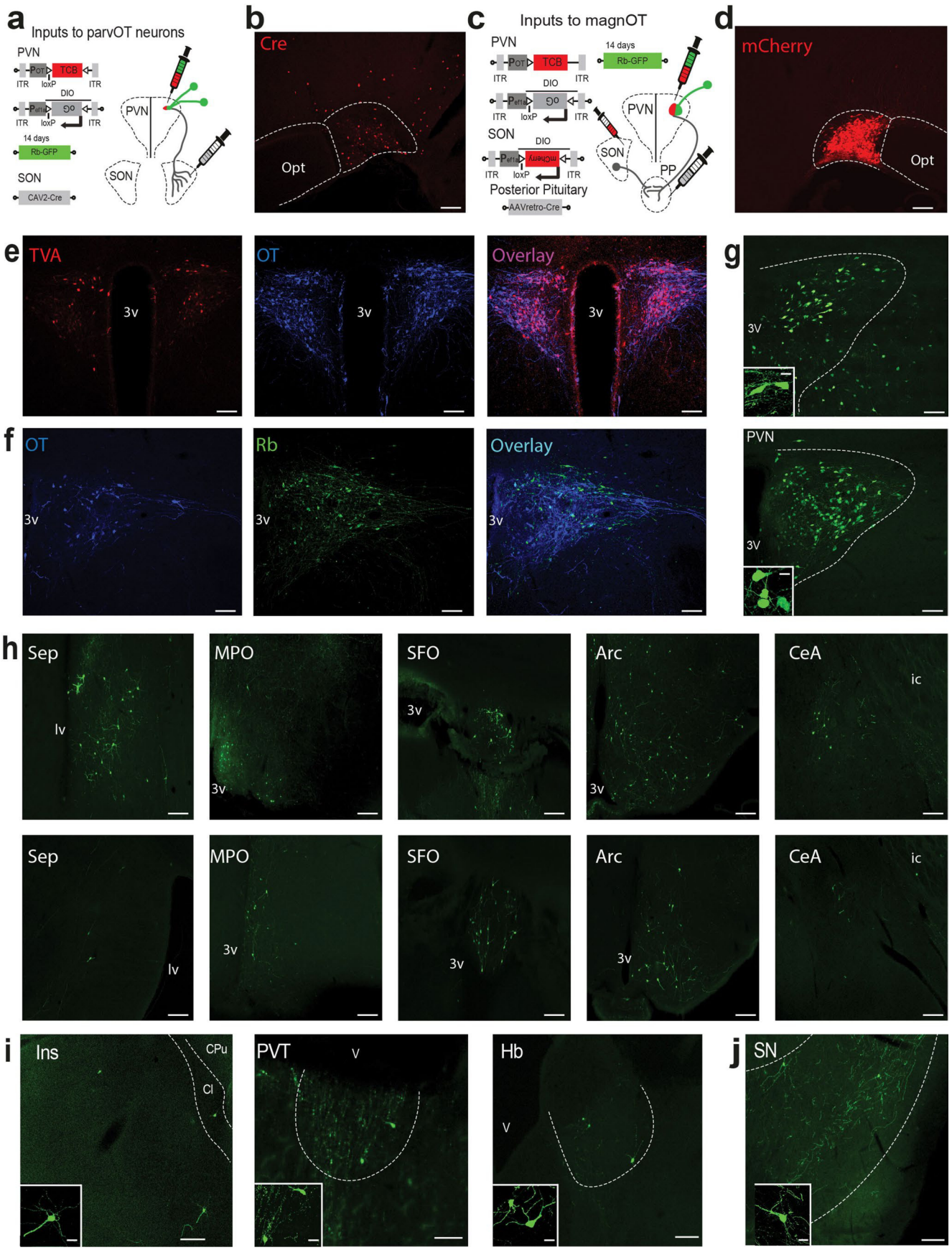

Extended Data Fig. 8 | See next page for caption.

Extended Data Fig. 8 | Inputs to parvOT and magnOT neurons. a, c, Virus injection strategy to retrotrace inputs from parvOT and magnOT neurons, respectively and to control injection sites of Cre (n = 5 rats). **b, d**, Injection site of CAV2-Cre in SON and of AAVretro-Cre in PP were confirmed by staining for Cre or mCherry in SON (n = 5 rats). **e**, Immunofluorescence for mCherry (red, fused to TVA), OT (blue) and overlay of the PVN from a rat injected with rAAV-OTp-TCB (n = 2 rats). **f**, Immunofluorescence for OT (blue), GFP (Green) and overlay of the PVN from a rat injected with rAAV-OTp-TCB, and Rb-GFP two weeks later (n = 2 rats). **g**, Injection site of rabies in parvOT (Top) and magnOT (bottom) groups (n = 5 rats). **h**, Epifluorescence microscope images showing neurons monosynaptically retrolabelled by Rabies-GFP in various brain areas projecting to both parvOT and magnOT neurons. Top line: neurons projecting to parvOT neurons; Bottom line: neurons projecting to magnOT neurons (n = 5 rats). **i, j**, Epifluorescence microscope images showing neurons monosynaptically retrolabelled by Rabies-GFP in brain areas projecting specifically to parvOT (i) or magnOT neurons (j) (n = 5 rats). All scale bars = 100 μm. All scale bars in insert = 10 μm. Brain areas legend: Amygdala: AMY, Arcuate hypothalamic nucleus: Arc, Bed nucleus of stria terminalis: NST, Cingulate cortex: CgC, Claustrum: Cl, Dorsal raphe nucleus: DRN, Dorsal tenia tecta: DTT, Dorsomedial hypothalamic area: DMH, Habenular nucleus: Hb, Horizontal limb of diagonal band nucleus: HDB, Infralimbic cortex: ILC, Insular cortex: Ins, Lateral hypothalamic area: LH, Lateral lemniscus nucleus: LMN, Lateral septal nucleus: SEP, Mammillary body: MMB, Medial preoptic area: MPO, Median raphe nucleus: MRN, Nucleus accumbens: NAC, Orbital cortex: OC, Parabrachial nucleus: PBN, Paraventricular thalamus: PVT, Pedunculopontine tegmental nucleus: PPT, Periaqueductal gray area: PAG, Posterior hypothalamic nucleus: PH, Posterior intralaminar thalamus: PIL, Prelimbic cortex: PLC, Raphe magnus nucleus: RMg, Subfornical organ:SFO, Substancia nigra: SN, Vascular organ of lamina terminalis: OVLT, Ventral Subiculum: VS, Zona incerta: ZI.

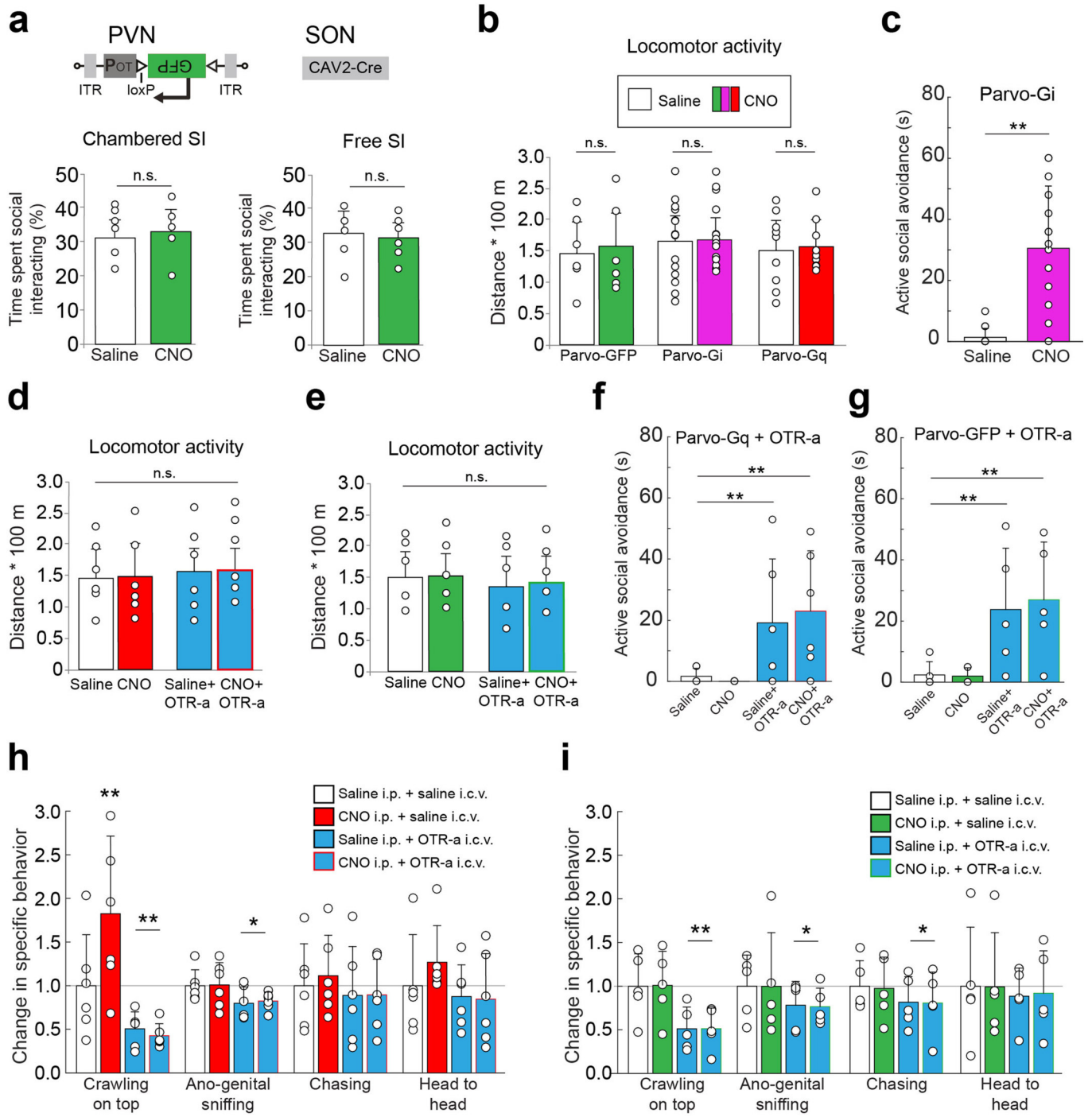

Extended Data Fig. 9 | Effects of DREADD activation of parvocellular oxytocin neurons on social behaviors. a, Parvocellular oxytocin-GFP control group: time spent by rats injected with saline or CNO socially interacting with conspecific stimulus in CSI ($P=0.34$) and FSI session ($P=0.29$, n=6 rats, paired two-sided t test). **b**, CNO does not affect locomotor activity: average distance run by experimental rats (n=6 rats GFP group, n=15 rats Parvo-Gi group, n=9 rats Parvo-Gq group) injected with saline or CNO during an open field (OF) test. No significant changes were detected, one-way ANOVA Tukey's corrected post-hoc comparison. **c**, Quantification of 'active social avoidance' behavior of experimental rat (actively escaping from stimulus rat, which is trying to interact) expressing inhibitory DREADD hM4D(Gi) in parvOT neurons and injected either with saline (control) or CNO. The total time of free social interaction session is 5 minutes. ** $P=0.0096$, n=15 rats, paired two-sided t test). **d-e**, OT receptor antagonist (OTR-a), CNO, or both do not affect locomotor activity: average distance run by experimental rats (d: $P=0.79$, n=6 rats saline/CNO/saline, P=0.92 n=6 rats saline/CNO/OTR-a; e: $P=0.73$, n=5 rats saline/CNO/saline, p=0.64, n=5 rats saline/CNO/OTR-a) injected with saline/CNO/OTR-a during an open field (OF) test. One-way ANOVA Tukey's corrected post-hoc comparison. **f-g**, Quantification of 'active social avoidance' behavior of experimental rat after administration of saline/CNO/OTR-a. Infusion of OTR-a induced an increase of avoidance behavior (Parvo-Gq: **$P=0.0027$, **$P=0.0018$, n=6 rats per group, Parvo-GFP: **$P=0.0042$, **$P=0.0013$, n=5 rats per group, one-way ANOVA Tukey's corrected post-hoc comparison). **h-i**, Time spent in different subtype of social behavior of experimental rat expressing excitatory DREADD hM3D(Gq) (h) or GFP (i) in parvOT neurons after administration of saline/CNO/OTR-a. Crawling on top behavior was the subtype most affected by parvOT neurons chemogenetic activation and by infusion of OTR-a (Parvo-Gq: ** $P=0.01$, **$P=0.004$, *$P=0.023$, n=6 rats per group, Parvo-GFP: **$P=0.006$, *$P=0.035$, *$P=0.047$, one-way ANOVA Tukey's corrected post-hoc comparison). All data represented as mean + SEM.

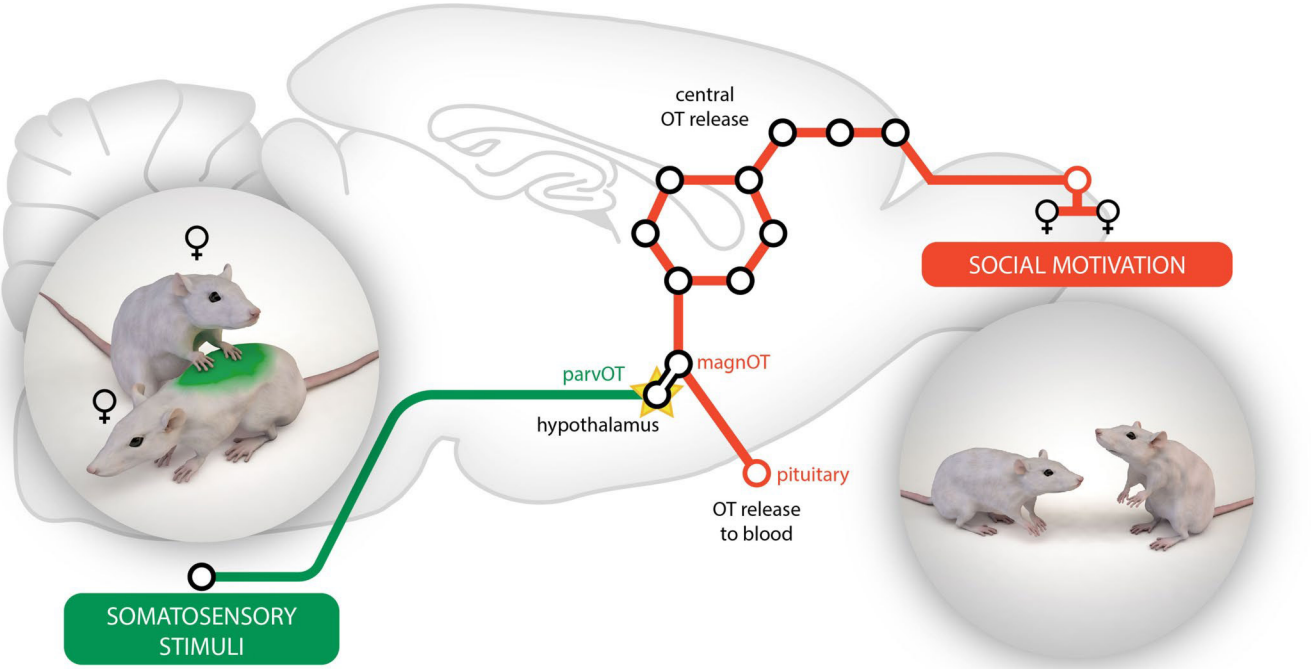

Extended Data Fig. 10 | Working hypothesis. Non-nociceptive signals ('social touch') arising from stimulation of dorsal body parts of interacting virgin female rats converge onto hypothalamic parvocellular oxytocin neurons via ascending pathways. As a consequence, the somatosensory-driven activation of parvocellular oxytocin neurons is transmitted to magnocellular oxytocin neurons inducing central oxytocin release in the social-relevant forebrain areas (as schematically depicted by circles representing nine amino acids in the oxytocin molecule), to support motivated social communication between female conspecifics.

6. Article S2: Le toucher favorise les interactions sociales *via* l'ocytocine

Publication not directly related to the thesis

mis à la souris d'apprendre à retourner dans le compartiment où ses neurones dopaminergiques ont été stimulés (un apprentissage par renforcement).

Le G5-MNI-glutamate possède donc toutes les qualités photochimiques et pharmacologiques requises pour la manipulation des circuits neuronaux chez la souris dans des tâches comportementales. Contrairement aux techniques optogénétiques de stimulation neuronale, fondées sur l'expression d'opsines microbiennes, le décageage ne nécessite pas de manipulation génétique, et permet donc le photocontrôle de tissus natifs [1]. Un autre atout de la cape de dendrimère est qu'elle augmente considérablement la solubilité des composés auxquels elle est attachée [9], un avantage considérable pour les cages, qui sont des composés chimiques généralement hydrophobes. Nous prévoyons la possibilité que la cape de dendrimère soit facilement greffée sur n'importe quel neurotransmetteur cagé, ouvrant la voie à la manipulation optique de l'activité synaptique *in vivo*. ◊

A cloaked caged glutamate for in vivo optical activation of synapses

LIENS D'INTÉRÊT

Les auteurs déclarent n'avoir aucun lien d'intérêt concernant les données publiées dans cet article.

RÉFÉRENCES

1. Paoletti P, Ellis-Davies GCR, Mourot A. Optical control of neuronal ion channels and receptors. *Nat Rev Neurosci* 2019 ; 20 : 514-32.
2. Ellis-Davies GCR. Caged compounds: photorelease technology for control of cellular chemistry and physiology. *Nat Methods* 2007 ; 4 : 619-28.
3. Ellis-Davies GCR. Two-photon uncaging of glutamate. *Front Synaptic Neurosci* 2019 ; 10 : 48.
4. Canepari MM, Nelson LL, Papageorgiou G, *et al.* Photochemical and pharmacological evaluation of 7-nitroindolinyl-and 4-methoxy-7-nitroindolinyl-amino acids as novel, fast caged neurotransmitters. *J Neurosci Methods* 2001 ; 112 : 29-42.
5. Matsuzaki M, Ellis-Davies GCR, Nemoto T, *et al.* Dendritic spine geometry is critical for AMPA receptor expression in hippocampal CA1 pyramidal neurons. *Nat Neurosci* 2001 ; 4 : 1086-92.
6. Warther D, Gug S, Specht A, *et al.* Two-photon uncaging: new prospects in neuroscience and cellular biology. *Bioorg Med Chem Lett* 2010 ; 18 : 7753-8.
7. Durand-de Cuttoli R, Chauhan PS, Pétriz Reyes A, *et al.* Optofluidic control of rodent learning using cloaked caged glutamate. *Proc Natl Acad Sci USA* 2020 ; 117 : 6831-5.
8. Feliu N, Walter MV, Montañez MI, *et al.* Stability and biocompatibility of a library of polyester dendrimers in comparison to polyamidoamine dendrimers. *Biomaterials* 2012 ; 33 : 1970-81.
9. Richers MT, Amatrudo JM, Olson JP, Ellis-Davies GCR. Cloaked caged compounds: chemical probes for two-photon optoneurobiology. *Angew Chem Int Ed Engl* 2017 ; 56 : 193-7.
10. Durand-de Cuttoli R, Mondoloni S, Marti F, *et al.* Manipulating midbrain dopamine neurons and reward-related behaviors with light-controllable nicotinic acetylcholine receptors. *eLife* 2018 ; 7 : 15991.

NOUVELLE

Le toucher favorise les interactions sociales *via* l'ocytocine

Arthur Lefevre[1,2], Louis Hilfiger[1], Alexandre Charlet[1]

[1]CNRS et Université de Strasbourg, Institut des neurosciences cellulaires et intégratives, 8 allée du Général Rouvillois, 67000 Strasbourg, France.
[2]Department of neuropeptide research for psychiatry, Central institute of mental health, Université de Heidelberg, Mannheim, Allemagne.
acharlet@unistra.fr

› Il est désormais largement admis que la qualité et la quantité des contacts sociaux influent sur la santé physique de l'individu et son espérance de vie, et peuvent jouer un rôle dans l'apparition ou l'évolution de maladies graves comme les dépressions et les maladies cardio-vasculaires [1]. Cependant, les mécanismes physiologiques sous-jacents restent obscurs. Aussi est-il important de tenter de comprendre comment les stimulus sensoriels qui accompagnent une interaction sociale agissent sur le corps humain. La résultante est probablement multifactorielle, et il est possible que chaque modalité sensorielle (visuelle, auditive, tactile, olfactive ou gustative) ait des effets différents. Si de nombreuses études se sont intéressées aux rôles de la vision et de l'audition dans le comportement social [2], le rôle du toucher, en revanche, a été peu exploré. Une équipe internationale coordonnée par Alexandre Charlet (France) et Valery Grinevich (Allemagne) a récemment montré l'importance du toucher et sa capacité à provoquer la libération d'une neurohormone, l'ocytocine, qui agit sur le « cerveau social » [3].

Ocytocine et comportement social

Connue depuis plus d'un siècle pour son rôle dans l'accouchement et la lactation, l'ocytocine, isolée en 1927, est une neurohormone nonapeptidique synthétisée principalement dans l'hypothalamus, et agissant à la fois dans le système nerveux central et dans d'autres organes [4]. Ses effets sont très divers, puisqu'elle agit aussi sur la mobilité gastrique, l'appétit, le rythme cardiaque, ou encore la douleur. Cependant, depuis la découverte de son importance dans l'attachement affectif, le contrôle des émotions, ou les comportement sexuels et parentaux, l'attention des chercheurs et des cliniciens s'est portée principalement sur son rôle dans les interactions sociales [2].

https://doi.org/10.1051/medsci/2021073

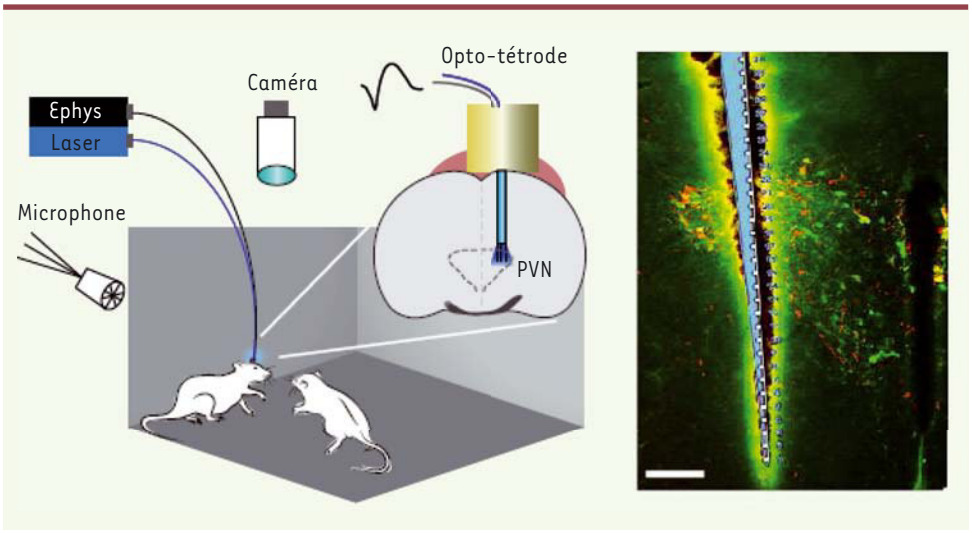

Figure 1. ***À gauche : représentation schématique de l'expérience, montrant l'activation des neurones produisant l'ocytocine lors d'interactions sociales.*** Deux rats femelles interagissent pendant que l'activité de neurones à ocytocine est enregistrée grâce à une opto-tétrode. PVN : noyau paraventriculaire. ***À droite : image par microscopie à épifluorescence montrant le site d'implantation de l'opto-tétrode dans l'hypothalamus et les neurones à ocytocine*** (en vert). Barre d'échelle : 100 µm

De nombreuses études ont permis de caractériser l'action de l'ocytocine dans le comportement social, et, depuis une quinzaine d'année, ce peptide est administré par voie nasale chez des individus sains ou atteints de diverses maladies mentales perturbant la sociabilité, telles que les troubles du spectre de l'autisme et la schizophrénie [5]. Cependant, on ne comprend toujours pas comment cette neurohormone est libérée lors d'une interaction sociale.

Le contact physique libère de l'ocytocine

Pour tenter de répondre à cette question, une étude a été menée chez l'animal. Pour identifier, chez des rats se déplaçant librement, les neurones produisant l'ocytocine et enregistrer leur activité électrophysiologique, nous avons utilisé une technique d'optogénétique qui permet également, en activant des canaux ioniques artificiels par la lumière, de stimuler ces neurones *(Figure 1)* [3]. Cette approche a d'abord permis de montrer que les neurones ocytocinergiques ne sont pas activés par une exploration libre d'un environnement inerte, mais uniquement lors d'une interaction entre individus. En analysant plus finement le comportement des rats, nous avons découvert que c'était lors des contacts tactiles que ces neurones étaient le plus activés. Nous avons montré que les stimulus olfactifs, auditifs ou visuels n'avaient pas autant d'effet sur l'activité de ces neurones qu'une stimulation tactile, alors que l'olfaction joue pourtant un rôle majeur dans la communication chez les rongeurs [3].

Des neurones ocytocinergiques aux rôles différents

Il existe au moins deux sous-populations de neurones produisant l'ocytocine : les neurones magnocellulaires, majoritaires, qui sont de grandes cellules projetant leurs axones dans de nombreuses régions du cerveau, ainsi que vers la glande pituitaire (hypophyse) postérieure afin d'y sécréter l'hormone ocytocine dans le sang, et les neurones parvocellulaires, plus petits et très peu nombreux (environ 5 % des neurones ocytocinergiques), qui ne libèrent pas l'ocytocine dans le sang mais dans le tronc cérébral et la moelle épinière [6]. En nous fondant sur les résultats de précédents travaux [7, 8] (➜), nous avons émis l'hypothèse que les neurones parvocellulaires exerçaient un contrôle sur l'activité des neurones magnocellulaires. Par différentes techniques (imagerie calcique, *patch-clamp*, chimiogénétique, traçage anatomique rétroviral), nous avons montré que les neurones parvocellulaires 1) reçoivent, depuis de nombreuses régions cérébrales, bien plus d'entrées synaptiques que les neurones magnocellulaires, et 2) établissent des connexions fonctionnelles avec les neurones magnocellulaires afin de controler leur activité [3]. Cela indique que les neurones parvocellulaires exercent vraisemblablement une fonction d'intégration de signaux, en recevant les informations sensorielles pour les relayer aux neurones magnocellulaires.

(➜) Voir la Nouvelle de A. Baudon et A. Charlet, *m/s* n° 1, janvier 2020, page 9

Par ailleurs, nous avons montré que l'inhibition sélective des neurones ocytocinergiques parvocellulaires bloque l'activité des neurones magnocellulaires en réponse à un stimulus tactile : ces derniers ne sécrètent alors plus d'ocytocine, ce qui a pour conséquence de diminuer l'interaction sociale. Inversement, l'activation des neurones parvocellulaires augmente l'activité des neurones magnocellulaires, la libération d'ocytocine dans le sang, et la durée des interactions sociales [3].

L'ensemble de ces résultats montre qu'une petite population de neurones ocytocinergiques, les neurones parvocellulaires, est activée lors d'une interaction sociale comportant des contacts tactiles, et transmet cette information au reste des neurones ocytocinergiques, les neurones magnocellulaires. Ces derniers libèrent alors de l'ocytocine dans le cerveau et dans le sang, ce qui promeut les interactions sociales *(Figure 2)*.

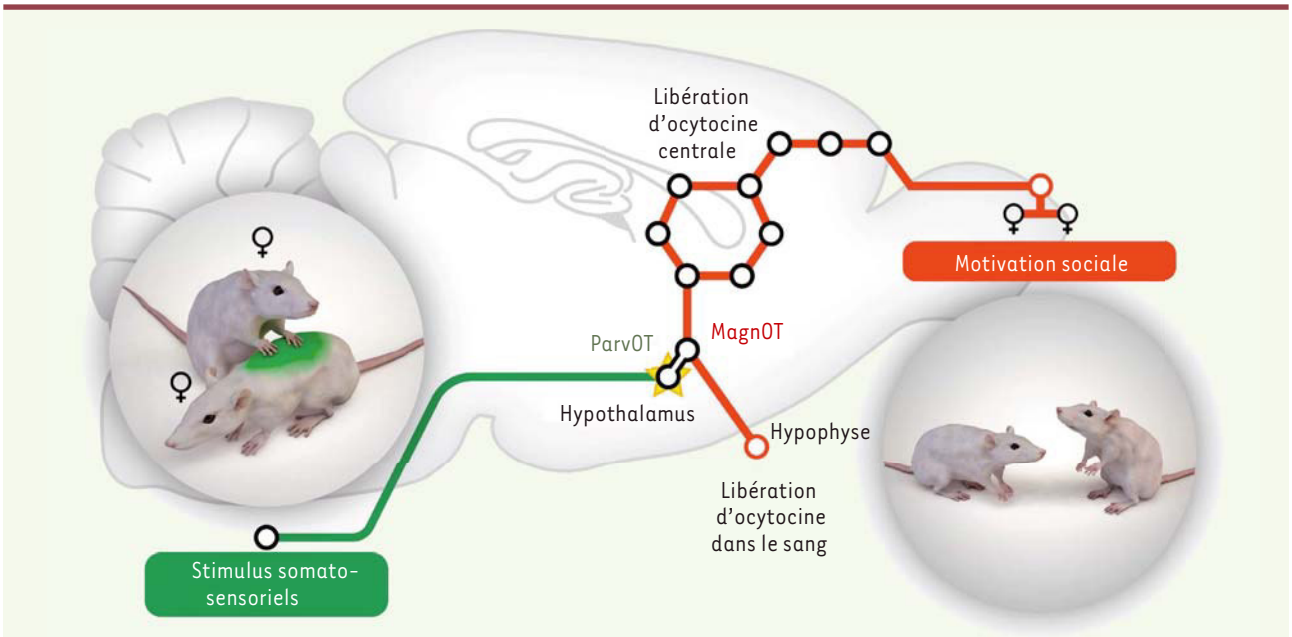

Figure 2. ***L'ocytocine induit un comportement social à partir d'une stimulation tactile.*** Un réseau de neurones capte les informations sensorielles tactiles et provoque la libération d'ocytocine dans le sang, en tant que neurohormone, et dans les régions cérébrales contrôlant le comportement social, en tant que neuromodulateur.

Vers des thérapies tactiles ?

Sous réserve que les résultats de cette étude effectuée chez un rongeur soient transposables à l'espèce humaine (le système ocytocinergique est très conservé chez les mammifères), savoir que le contact tactile provoque la libération d'ocytocine pourrait faire évoluer la prise en charge thérapeutique de certaines maladies psychiatriques. L'administration d'ocytocine est en effet utilisée comme traitement expérimental depuis plusieurs années, mais le manque de résultats probants [9] a incité les chercheurs à développer de nouvelles approches pour activer le système ocytocinergique. Il est probable que la faible capacité de l'ocytocine à pénétrer dans le cerveau en quantité suffisante constitue le principal frein à son utilisation thérapeutique [5]. Aussi, l'administration de nouveaux agonistes du récepteur de l'ocytocine dénués de ces limitations [10], combinée à des stimulations tactiles ou des massages doux, pourrait constituer un outil thérapeutique puissant pour les troubles psychiques dans lesquels le système ocytocinergique est dysfonctionnel.

Enfin, concernant les mesures de distanciation physique entre personnes qui sont en vigueur dans de nombreux pays pour lutter contre l'actuelle pandémie de COVID-19, il n'est sans doute pas inutile de rappeler l'importance du maintien de relations sociales directes pour la santé mentale et physique des individus, mais aussi d'alerter sur le risque que la présente situation détériore durablement le comportement social chez une partie de la population. Ce phénomène requiert une attention particulière, et plusieurs études sont en cours pour évaluer les taux d'ocytocine dans la population. ◊

Tactile contacts increase social interactions by releasing oxytocin

LIENS D'INTÉRÊT

Les auteurs déclarent n'avoir aucun lien d'intérêt concernant les données publiées dans cet article.

RÉFÉRENCES

1. Holt-Lunstad J, Smith TB, Layton JB. Social relationships and mortality risk: a meta-analytic review. *PLoS Med* 2010 ; 7 : e1000316.
2. Lee HJ, Macbeth AH, Pagani JH, Young WS. Oxytocin: the great facilitator of life. *Prog Neurobiol* 2009 ; 88 : 127-51.
3. Tang Y, Benusiglio D, Lefevre A, *et al.* Social touch promotes interfemale communication via activation of parvocellular oxytocin neurons. *Nat Neurosci* 2020 ; 23 : 1125-37.
4. Gimpl G, Fahrenholz F. The oxytocin receptor system: structure, function, and regulation. *Physiol Rev* 2001 ; 81 : 629-83.
5. Lefevre A, Sirigu A. The two fold role of oxytocin in social developmental disorders: a cause and a remedy? *Neurosci Biobehav Rev* 2016 ; 63 : 168-76.
6. Eliava M, Melchior M, Knobloch-Bollmann HS, *et al.* A new population of parvocellular oxytocin neurons controlling magnocellular neuron activity and inflammatory pain processing. *Neuron* 2016 ; 89 : 1291-304.
7. Hasan MT, Althammer F, Silva da Gouveia M, *et al.* A fear memory engram and its plasticity in the hypothalamic oxytocin system. *Neuron* 2019 ; 103 : 133-46.
8. Baudon A, Charlet A. Un engramme ocytocinergique pour apprendre et contrôler sa peur. *Med Sci (Paris)*. 2020 ; 36 : 9-11.
9. Keech B, Crowe S, Hocking DR. Intranasal oxytocin, social cognition and neurodevelopmental disorders: a meta-analysis. *Psychoneuroendocrinology*. 2017 ; 87 : 9-19.
10. Hilfiger L, Zhao Q, Kerspern D, *et al.* A nonpeptide oxytocin receptor agonist for a durable relief of inflammatory pain. *Sci Rep* 2020 ; 10 : 3017.

7. Synthèse NCT : Etudier les molécules actives des plantes médicinales pour créer de nouveaux antidouleurs

Synthesis realized during the doctoral training “New Chapter of the Thesis”

Université de Strasbourg

Ecole doctorale des sciences de la vie et de la santé

ED 414

Louis HILFIGER

Mentor : Anna DYNGOSZ

Synthèse NCT :

Etudier les molécules actives des plantes médicinales pour créer de nouveaux antidouleurs

Sujet de thèse :

« Caractérisation de nouveaux composés analgésiques : analogue de l'ocytocine et terpènes »

Directeur de thèse : Dr. Alexandre CHARLET, INCI (Institut des Neurosciences Cellulaires et Intégratives) – UPR3212 – CNRS

Encadrant professionnel de thèse : Dr. Hugues PETITJEAN, BENEPHYT

BenePhyt

cnrs

INCI

Partie 1 : Cadre général et enjeux de la thèse

1.1 Contexte de la thèse et de sa thématique

Ma thèse est une thèse CIFRE, c'est-à-dire en partenariat entre mon laboratoire au CNRS dirigé par le Dr. Alexandre CHARLET et une start-up Strasbourgeoise BENEPHYT dirigée par le Dr. Hugues PETITJEAN. Compte tenu de ce contexte atypique j'ai deux sujets principaux répartis à 50/50 entre le CNRS et BENEPHYT, regroupés dans une grande thématique ; les nouvelles molécules analgésiques.

Aujourd'hui, en médecine, l'essentiel des molécules analgésiques sont des dérivées des opiacés et au cours de la dernière décennie, l'utilisation abusive d'analgésiques à base d'opioïdes a initié l'une des plus grandes crises sanitaires en Amérique du Nord. En 2017, près de 50 000 Américains sont morts d'une overdose d'opioïdes et environ 1,7 million de personnes aux États-Unis ont souffert de troubles liés à l'utilisation d'opioïdes prescrits sur ordonnance. Au vu des puissants effets secondaires et du risque de mortalité par overdose, il est urgent d'identifier et de développer de nouvelles molécules analgésiques impliquant d'autres voies que celles utilisées par les opiacés.

1.2 BENEPHYT et nos objectifs

Mon projet avec BENEPHYT prend la suite d'une précédente thèse CIFRE en Chimie soutenue en 2019 par Dr. Zélie TRIAUX qui a eu pour objectif d'identifier, de caractériser et d'extraire des petites molécules issues de plantes poussant dans la région rhénane, les monoterpènes. Ces molécules sont très utilisées en agroalimentaire mais très peu caractérisées pour leurs effets anti-inflammatoires et analgésiques.

L'objectif principal de mon projet est de caractériser les effets analgésiques de différents monoterpènes identifiés lors de cette précédente thèse et de repérer quelles combinaisons pourront avoir les meilleurs effets. Dans mon projet je dispose d'une autonomie très importante quant au choix des expériences, de l'organisation, de la planification et dans une moindre mesure de la gestion des budgets. Les rapports réguliers sur les expériences, résultats et objectifs sont effectués avec les Dr. Alexandre CHARLET et Dr. Hugues PETITJEAN, afin de maintenir un cadre et d'assurer un suivit autour du projet et de ses évolutions.

L'objectif pour BENEPHYT est d'acquérir des informations sur les effets des monoterpènes en vue d'une éventuelle future commercialisation pour des traitements analgésiques, notamment des douleurs inflammatoires.

1.3 La thématique ocytocine

Au sein de l'équipe du Dr. Alexandre CHARLET mes travaux ont porté sur la compréhension des mécanismes du système ocytocinergique. L'ocytocine est une neuro-hormone très impliquée dans les relations sociales mais également dans les réponses à la douleur. Cette implication dans les réponses à la douleur a poussé des chercheurs à synthétiser des agonistes au récepteur à l'ocytocine. Dans ce projet j'ai pu, d'une part, étudier l'activité électriques des réseaux de neurones ocytocinergique et, d'autre part, évaluer les propriétés analgésiques des agonistes au récepteurs à l'ocytocine. Ces travaux ont été réalisés en collaboration avec le chimiste Dr. Marcel HIBERT et notamment l'anatomiste Pr. Valery GRINEVICH de l'université de Mannheim.

1.4 La thèse un objectif personnel et professionnel

La thèse, depuis mon entrée à la faculté, a toujours été mon objectif, peu importe le travail et le temps que cela prendrait. J'avais confiance en mes capacités de travail, que j'ai réussi à développer au long d'un parcours scolaire moyen et pas toujours évident au début.

La thèse est pour moi un mélange entre la volonté de prouver aux autres et à moi-même que la dyslexie n'empêche pas d'atteindre le plus haut niveau scolaire, d'un goût prononcé pour les sciences, d'une curiosité insatiable depuis toujours et enfin de beaucoup d'abnégation et de travail. Pour moi la thèse est similaire à la fable du lièvre et de la tortue, cependant l'essentiel n'est pas de partir à point mais de garder le cap. D'un point de vue plus pragmatique la thèse est une opportunité d'acquérir de l'expérience, d'être une transition entre la vie étudiante et la vie professionnelle et accéder à un panel vaste de postes et de métiers notamment à l'international.

Partie 2 : Projet, encadrement et conduite de la thèse

2.1 Le projet LIT, une expérience formatrice

Au début de ma thèse, je n'ai pas pu travailler de suite sur mon sujet de thèse parce que j'ai dû faire face à des délais administratifs entre le CNRS et BENEPHYT. Ce temps a été mis à contribution pour la réalisation d'autres projets, notamment un projet de valorisation d'une molécule agoniste (le LIT-001) du récepteur à l'ocytocine. Un agoniste est une molécule activant le récepteur de manière similaire à la molécule endogène ici l'ocytocine.

L'objectif de ce projet est d'étudier les effets analgésiques sur les sensibilités mécanique et thermique de cette molécule dans un modèle de douleur inflammatoire. Le modèle de douleur est modélisé par un rat dans lequel nous avons induit une réaction inflammatoire via l'injection de fragment de bactérie inactivée dans la patte arrière. L'organisme réagit localement par une importante inflammation locale de la patte, sans toutefois avoir de réelle infection. Le second objectif de ce projet est d'acquérir de l'expérience dans la gestion et la conduite de projet de recherche. Etant donné qu'il s'agissait de mon premier projet les grandes lignes ont été décidé par le Dr. Alexandre CHARLET, j'ai eu toutefois les pleines responsabilités pour la gestion de la partie expérimentale et organisationnelle de ce projet. Ces résultats ont fait l'objet d'une publication dans un article de recherche.

2.2 Le projet TerPain, projet de recherche et de valorisation

2.2.1 L'initiation et l'organisation du projet

L'initiation du projet TerPain est issu de la précédente thèse CIFRE de BENEPHYT, dont les résultats ont permis d'obtenir une liste de terpènes pouvant être facilement extraits de plantes de la région. Les terpènes sont une famille de molécules issues de plantes étant principalement exploitées dans l'industrie agro-alimentaire et dans les médecines non-conventionnelles notamment dans les huiles essentielles. Le terpène le plus connu est le menthol, il est responsable du goût de la menthe et aussi de son effet rafraichissant via une activation chimique des récepteurs au froid.

Au début de ma thèse, nous avons eu un premier échange avec le Dr. Hugues PETITJEAN pour définir la stratégie de BENEPHYT vis-à-vis des objectifs et attentes de ma thèse. L'objectif est de caractériser les effets analgésiques de terpènes issus de cette liste précédemment établie. Les

attentes sont portées sur le développement et le brevetage de mélanges de terpènes dans un but thérapeutique.

Suite à cet échange où la direction du projet a été fixée par BENEPHYT, j'ai pu réaliser une première recherche bibliographique me permettant d'avoir une idée assez précise de l'état de l'art dans ce domaine. Cela m'a permis de pouvoir cibler les terpènes les plus intéressant de la liste (menthol et pulégone) pour approfondir leurs effets analgésiques et d'évaluer qu'il serait plus intéressant pour BENEPHYT, d'orienter les études uniquement sur la sensibilité mécanique et thermique.

2.2.2 Planification et réalisation des expériences

Dès lors que les terpènes cibles ont été sélectionnés, j'ai pu commencer à établir un plan expérimental permettant de répondre aux questions que nous nous posions. A partir de mon expérience et de la bibliographie j'ai proposé différentes options de plans expérimentaux aux Dr. Alexandre CHARLET et Dr. Hugues PETITJEAN qui seront réalisés au seins des locaux du Chronobiotronc (plate-forme CNRS/Inserm d'hébergement d'animaux).

Nous avons décidé de tester 2 modalités (sensibilité mécanique et thermique) sur un modèle de douleur inflammatoire, ce qui nous permet d'étudier les effets analgésiques dans un contexte de douleur. En effet au vu des objectifs thérapeutiques il est important que les molécules soient efficaces dans le contexte dans lequel elles seront potentiellement appliquées. De plus j'ai déjà pu maitriser le modèle lors du précédent projet. Pour ce faire nous avons utilisé 3 tests de sensibilité à la douleur (mécanique, thermique chaud et froid) et mesuré les réponses des animaux à différents moments suivant l'injection de terpènes (dit : time-course). Nous avons également testé différentes concentrations de terpènes pour observer des effets doses réponses afin d'avoir une idée de la dose optimale. Ces expériences ont également été complétées avec des contrôles, notamment des rats sans douleurs inflammatoire et des rats avec douleurs inflammatoire mais sans traitement.

Il a donc été convenu de premièrement tester une cohorte peu nombreuses d'animaux afin d'évaluer le potentiel des expériences, afin de ne pas utiliser tout le budget et de pouvoir se retourner financièrement si les expériences n'étaient pas concluantes. Fort heureusement les premiers résultats se sont montrés très prometteurs. Nous avons analysé les résultats rapidement afin d'observer les tendances pour avoir le moins de délais entre chaque série d'expérimentation. En effet nous sommes tributaires des disponibilités de notre fournisseur d'animaux (Janvier-Labs), et de la période d'habituation à la manipulation. La fréquence des tests impose une anticipation du calendrier, élément très important dans la gestion de ces expériences.

2.2.3 Suivit des résultats et ajustement des expériences

J'ai échangé tout au long de ces expériences avec le Dr. Alexandre CHARLET et le Dr. Hugues PETITJEAN pour qu'ils valident financièrement mes propositions d'ajustement de cohorte expérimentale, nécessaire pour avoir un nombre suffisant d'animaux pour chaque dose afin d'avoir des résultats statistiquement exploitables. Un résultat statistiquement exploitable est dit d'un résultat dont la reproductibilité étant suffisamment importante et que la variabilité suffisamment faible pour pouvoir affirmer que la probabilité que ce résultat est dû au hasard est inférieur à 5%, 1% où 0,1% (selon les types d'expériences et les tests statistiques utilisés). Dans notre cas il s'agit toujours de comparer les groupes tests avec les groupes contrôles pour pouvoir affirmer que les réductions de sensibilité dans les différentes modalités sont bien dues aux injections de terpènes.

Lors de ces réunions, suite à des observations des premières cohortes et d'une étude bibliographique, nous avons établi qu'il serait nécessaire d'étudier les effets des terpènes sur la locomotion et l'activité musculaire. En effet certaines études ont mis en évidence que les terpènes ont des effets sédatifs à haute dose, il est donc nécessaire de contrôler que les doses utilisées n'altèrent pas les capacités musculaires et motrices de nos animaux. Cela pourrait non seulement influer sur les effets analgésiques mais aussi induire des effets indésirables compromettant pour la poursuite de recherche. Nous avons utilisé des animaux sans inflammation et testé via deux expériences, l'activité motrice, sans effets significatif pour les deux terpènes.

2.2.4 Résultats, publication scientifique et valorisation

De manière générale, l'ensemble de ces données sont en cours de publication dans un article de recherche qui permet de caractériser finement les effets analgésiques du menthol et de la pulegone dans un modèle de douleur inflammatoire.

Cette publication nous sert également de support pour atteindre la dernière étape du projet, qui est l'élaboration d'un mélange de différents terpènes. Cela nous permettra d'évaluer des potentiels effets synergiques entre les différentes molécules. Le but étant l'éventuelle mise sur le marché de ce cocktail thérapeutique.

Pour identifier les mélanges de terpènes les plus intéressant, j'ai effectué un important travail bibliographique, qui fera par ailleurs à la fin de ma thèse l'objet d'une publication d'un article de synthèse bibliographique. Les effets analgésiques de ce mélange, toujours dans le modèle de douleur inflammatoire, sont comparés aux effets analgésiques des terpènes individuels. Les résultats sont très prometteurs pour BENEPHYT qui a décidé de valoriser les données expérimentales et de breveter le mélange en partenariat avec la SATT Conectus et le CNRS. Il est envisagé de tester encore de nouvelles combinaison de terpènes d'ici la fin de ma thèse, toujours dans la même optique de valorisation de mélange à vocation thérapeutique.

Partie 3 : Compétences et expertises développées

3.1 L'expertise scientifique

3.1.1 Neuroscience, pharmacologie et biologie

Lors de la thèse l'expertise que l'on développe le plus est l'expertise de son sujet de thèse/domaine. Dans mon cas grâce à mes différents projets sur des sujets différents, j'ai pu développer une expertise scientifique variée. Elle est particulièrement pointue dans la connaissance des terpènes, qui va de leur synthèse à leurs effets pharmacologiques notamment sur la douleur. Cette connaissance est appuyée par la publication d'un article de recherche en premier auteur, d'une présentation à un congrès international des résultats de ces expériences et d'une review de la littérature sur le sujet. Ces publications me permettent de me positionner parmi mes pairs comme expert de ce sujet.

Les projets ocytocines m'ont quant à eux permis d'accroitre ma connaissance de ce domaine spécifique des neurosciences, très important dans la recherche sur les troubles du spectre autistique et d'actualité dans le contexte de restriction de contact sociaux. Grâce à deux/trois publications

d'articles de recherche en co-premier auteur et de deux présentations à des congrès internationaux, j'ai pu échanger avec des chercheurs reconnus dans ce domaine.

Au-delà de la connaissance bibliographique et académique de mes deux sujets principaux j'ai aussi lors de ma thèse pu développer mon expertise de manière plus générale dans les domaines des neurosciences, de la pharmacologie et plus globalement dans la biologie. Cela s'est fait par la lecture d'article, de participation à des présentations, des congrès etc…. Mais cette expertise se reflète aussi par la maitrise de techniques d'expériences, dans ces domaines. Par exemple la maitrise du modèle de douleur et des tests de douleurs, de l'électrophysiologie, du génotypage. Tout cela représente donc l'ensemble de l'expertise que j'ai pu développer dans le contexte de ma thèse.

3.1.2 Chimie, électronique, informatique

Lors de ma thèse en complément des connaissances acquises dans mes domaines d'expertises, j'ai aussi pu développer des connaissances annexes à mon sujet par exemple des connaissances en électronique, en chimie, en informatique mais aussi en physique. Cela est dû à nos expériences qui nécessitent une connaissance générale des phénomènes physico-chimique et électrique pour maitriser les outils et les techniques. Par exemple les techniques en électrophysiologie nécessitent des connaissances en électronique pour enregistrer le signal électrique des neurones mais aussi en informatique pour le traitement des données etc…

3.2 Méthodologie de travail

3.2.1 La démarche scientifique, une méthodologie transposable

La recherche se développe par l'acquisition de compétences scientifiques qui sont pour la plupart des connaissances soit théorique, soit technique. Cependant la compétence à la base de toute la recherche depuis plus d'un siècle, n'est ni théorique ni technique, c'est celle qui rend la science crédible, reproductible et échangeable avec ses pairs, c'est la démarche scientifique (Annexe n°2). La démarche scientifique régule l'ensemble de mon travail de recherche pendant ma thèse et toute ma vie future, c'est une démarche qui peut être considéré comme une méthodologie de travail transposable à de nombreux métiers.

Par exemple lors de ma thèse j'ai soulevé une question initiale « *Est-ce que les terpènes extrait des plantes ont des effets analgésiques lorsqu'ils sont utilisés purs et peuvent-ils avoir des effets synergiques lorsque combinés entre eux ?* ». J'ai donc émis des hypothèses sur le sujet pour répondre à cette question. Dès lors à partir de ces hypothèses alimentées par une recherche bibliographique, (fonder une hypothèse nécessite une observation, connaissance ou recherche initiale) j'ai réalisé des expériences qui permettaient de confirmer ou d'infirmer tels ou tels éléments de mes hypothèses comme « *Tester la sensibilité mécanique et thermique de manière distinct pour mieux discerner les effets analgésiques des terpènes* ». Puis l'observation et l'analyse statistique des résultats me permettent d'interpréter ces derniers et de conclure « *Il n'y a pas de différence entre la sensibilité thermique et mécanique dans les effets analgésiques de terpènes* ». Cette conclusion intermédiaire me permet de me poser une nouvelle question de laquelle découlera une nouvelle hypothèse et ainsi de nouvelles expériences et études seront nécessaires. Ce processus sera répété jusqu'à ce que je puisse conclure quant à la validité ou non de mon hypothèse qui permet de répondre à ma question initiale. Et cela quel que soit les résultats obtenus, c'est la déontologie de la recherche.

Cette démarche d'observation, de réflexion, de recherche, d'hypothèse et d'analyse, je l'applique également dans mon travail hors recherche afin de me renouveler dans ma manière de m'organiser, de planifier, de gérer le flux de travail et d'anticiper les imprévus.

3.2.2 La planification et gestion de deux projets parallèles

Du fait de la coexistence simultanée de mes deux principaux projets de recherche, j'ai pendant ma thèse appris à planifier mon emploi du temps en fonction des besoins et des contraintes intrinsèques à mes expériences. Par exemple, pour le lancement des expériences sur l'analgésie des terpènes, j'ai réalisé des plannings de 3-4 mois qui doivent prendre en compte tous les paramètres de mes expériences, la croissance des animaux pour avoir une homogénéité des gabarits, le temps de récupération des chirurgies et le nombre d'animaux qu'il est possible de tester dans une journée. Dans le même temps j'ai aussi dû prendre en compte le temps d'analyse des résultats des expériences pour observer s'il fallait lancer une nouvelle série d'expériences, sans se trouver dans 1 mois sans activité car les animaux ne sont pas encore adultes. Il a aussi fallu composer avec les deadlines de soumission des articles des projets Ocytocines. L'année 2020 a aussi rajouté à tout cela la problématique des pénuries et problèmes d'acheminement du matériel expérimental suite à la crise sanitaire et aux répercutions du premier confinement.

Au-delà de mes projets, je suis en charge dans mon équipe du génotypage (c-a-d ; faire le suivit des animaux génétiquement modifiés pour s'assurer que les nouvelles générations portent toujours les modifications génétiques), des commandes du matériel, des consommables et des demandes de devis, qui sont toujours envoyé au Dr. Alexandre Charlet pour une validation finale. De plus pour le projet terpènes je suis aussi responsable du budget pour la réalisation des expériences. Dans l'ensemble au vu de la problématique du financement de la recherche publique en France, nous avons toujours comme objectif d'éviter au maximum les coûts inutiles en optimisant les dépenses et les achats.

Cette gestion des achats, devis et budget à nécessité que je développe des compétences administratives dans le contexte particulier de la recherche. Pour la gestion des demandes de stages, d'ordre de mission et de suivit de thèse notamment.

3.3 La communication

3.3.1 La communication scientifique

La communication en science est tout autant important que la méthodologie, c'est elle qui permet de transmettre les connaissances acquises et de pouvoir avancer dans le domaine. Une bonne communication scientifique est une communication qui s'adapte à son auditoire et non l'inverse. La communication scientifique pour les spécialistes est toujours faite en anglais.

Les principales communications scientifiques sont les articles de recherche, les reviews et dans une moindre mesure les thèses (le document), il s'agit donc d'une communication écrite. Ce sont des documents techniques ou bibliographiques destinés à des spécialistes du domaine et des chercheurs d'autres domaines dont le socle de connaissance permet la compréhension du document. Dans ce contexte, j'aurai pour la fin de ma thèse co-écrit trois/quatres articles de recherche et une review. Ces documents me servent à communiquer à mes paires la recherche et les expériences que je produis. J'ai aussi eu l'occasion de participer à l'écriture de quelques articles de vulgarisation scientifique en français pour des revues de vulgarisation scientifique (Médecine

science, Journal du CNRS). J'ai donc dû adapter le discours pour que celui-ci soit compréhensible pour le public cible.

La deuxième manière de communiquer est donc la communication orale, qu'elle soit supportée par une présentation de type PowerPoint ou d'un poster. C'est une communication qui généralement découle des articles et review et qui est synthétisée à l'aide de schémas et de points clés pour que l'auditoire bénéficie d'un message clair. Personnellement dans l'équipe nous avons toujours régulièrement réalisé des présentations au sein de l'équipe et de l'institut pour échanger sur nos avancées récentes et les problèmes rencontrés.

Et enfin la participation aux congrès et symposiums nationaux et internationaux sont des évènements importants dans la vie de la recherche et auquels j'ai eu l'occasion de participer à trois reprise pour donner un speech et présenter deux poster. Ces expériences m'ont permis d'être à l'aise dans la création du support mais aussi dans le discours et dans l'échange avec les participants au congrès notamment avec des questions qui peuvent êtres déstabilisantes.

3.3.2 La hiérarchie et la gestion de confit

Bien qu'en recherche académique et dans les strat-up la hiérarchie est généralement assez horizontale, j'ai eu l'opportunité d'expérimenter cette hiérarchie sous deux aspects via les rapports et suivis réguliers avec mes différents chefs. J'ai pu apprendre à savoir quoi et comment communiquer avec différents chefs puis m'adapter en fonction de leurs sensibilités propres.

J'ai aussi vécu une période de tension et de conflits avec une thésarde en fin de thèse quand j'étais encore en stage de master deux (dans la même équipe qu'actuellement). Pour résoudre ce problème d'encadrement j'ai demandé au Dr. Alexandre Charlet d'être éloigné de cette personne en terme d'encadrement, il a accepté à condition que d'autres doctorants valident mes compétences techniques, ce qui été fait, prouvant ainsi à mon chef par le biais d'autres acteurs de confiance que j'étais apte à être en autonomie quasi intégrale pour la réalisation des expériences. Les tensions et conflits ont fortement diminuer pour le reste du stage. Cette expérience m'a montré qu'il est important d'anticiper les problèmes relationnels et qu'il est presque toujours possible de trouver une solution qui apaise les tensions.

Partie 4 : Pistes professionnelles

4.1 Discovery Scientist in Protein Degradation at Roche (Offre n°1, Annexe n°4)

4.1.1 Le poste

L'offre est un poste de recherche en neuroscience au sein de l'entreprise Roche à Bâle. Il porte sur l'identification et la caractérisation de composés permettant de moduler la dégradation des protéines dans les neurones et les cellules gliales. Il est attendu du candidat/e qu'il/elle participe activement à la recherche et la découverte de nouvelles molécules et de leurs fonctionnements. Notamment en s'impliquant par du travail de paillasse (50% du temps), de l'écriture d'article de recherche, de présentation des résultats a des congrès. Il est également attendu une implication intellectuelle dans les autres projets de « drug discovery » en participant aux réunions de recherche, en proposant des nouvelles approches (techniques, modèles) ou des hypothèses quant au mécanismes d'action de ces molécules. L'objectif en complément de l'activité de recherche est, en

étant aidé et formé par d'autres membres de la division préclinique, d'apprendre à gérer des projets, encadrer des stagiaires, doctorants, post-doctorant. Le but à terme est de manager une équipe pour devenir un chef d'équipe dans la division Neuroscience et Rare Diseases.

4.1.2 Les prérogatives

La première prérogative concerne le parcours, un PhD (doctorant) en Biochimie, Neuroscience, ou en Science de la Vie puis d'avoir travaillé durant la thèse ou un post-doctorat dans le domaine des protéinopathies (maladies associé à la dégradation des protéines) idéalement sur des maladies neurodégénératives. Il est nécessaire d'avoir une bonne connaissance/expérience dans les domaines de la biochimie, de la pharmacologie et des modèles cellulaires et animaux. Il est important d'avoir une bonne rigueur scientifique et d'avoir écrit des articles scientifiques de recherche dans les domaines cités précédemment. En plus de ces compétences de recherche il est essentiel d'avoir un très bon niveau d'anglais, d'être bon communicant, organisé et apte à gérer plusieurs projets. En plus de tout cela il est également préférable d'avoir eu une expérience dans un projet de « drug discovery » dans une start-up ou dans l'industrie pharmaceutique. Certaines techniques spécifiques au projet sont également considérées comme un plus mais non essentiels.

4.1.3 Le poste dans mon projet professionnel et personnel

Le poste correspond parfaitement à mes envies en terme de projet professionnel. Il répond parfaitement à mon envie personnelle de travailler et d'habiter dans la région environnante de Bâle, d'où moi et ma conjointe sommes originaire. C'est un poste de chercheur dans le domaine des neurosciences ce qui correspond parfaitement à mon parcours et mon souhait de continuer à travailler dans la recherche mais du côté de l'industrie. De plus c'est un poste où l'on me permettrait de continuer à progresser dans la gestion de projet et d'équipe, tout en me laissant encore un peu d'activité de paillasse. De plus l'employeur Roche est un employeur très apprécié de ses employés car malgré son statut de grande multinationale pharmaceutique elle fonctionne et a toujours des valeurs d'une entreprise familiale. Enfin dans ce genre d'entreprise avec un PhD et quelques années d'expériences, il est toujours possible d'évoluer et de changer de poste si par exemple dans une dizaine d'année je souhaite m'éloigner de la recherche dite de « paillasse » et m'orienter vers le project management scientifique, la gestion de laboratoire, la communication scientifique, etc.…

Les contraintes de ce poste sont pour moi les horaires de travail qui peuvent ne plus avoir de limite durant les phases de rush mais également la compétition en interne pour atteindre tel ou tel poste. Malgré ces contraintes (que je pense plus associer à la fonction et au niveau de compétence bien plus que ce poste en particulier) les avantages selon moi sont bien plus important que les contraintes dans mon projet professionnel et personnel.

Cependant malgré que mon profil valide de nombreuses prérogatives, il me manque l'expérience d'un post-doctorat dans le domaine des protéinopathies. Je pourrais si cela est un problème pour l'employeur proposer de réaliser un contrat de post-doctorat de 2 ou 3 ans chez eux afin d'acquérir l'expérience nécessaire en termes de connaissance dans le domaine des protéinopathies et maladie neurodégénératives tout en perfectionnant les autres points, la gestion de projet, la maitrise de la langue etc.…

4.2 Associate Project Manager at ThermoFischer (Offre n°2, Annexe n°4)

4.2.1 Le poste

L'offre concerne un poste d'associate project manager chez ThermoFisher à Bâle. Le poste consiste à manager et fournir un support pour les clients qui achètent du matériel, des appareils, du consommable etc… pour leurs études/projets dans la recherche médicale et l'industrie pharmaceutique. L'objectif est d'être proactif auprès du client, assister aux réunions avec le client pour comprendre ses besoins, impératifs, mais aussi proposer des alternatives pertinentes lorsque celles-ci existent et donc avoir une culture scientifique importante pour comprendre les tenants et les aboutissant des projets. Il faudra aussi assurer le suivi des commandes des produits compétant pour assurer le respect des délais et des deadlines des projets tout en communicant de manière efficace afin de respecter le planning du client. Au-delà du service client il faudra aussi communiquer entre les différents services internes de l'entreprise pour assurer l'expédition des produits et suivre ces expéditions.

4.2.2 Les prérogatives

En termes de parcours le post est ouvert à différents profils, un diplôme dans les services aux clients ou bien dans les sciences de la vie sont acceptés pour postuler, il est demandé d'avoir 2 à 3 ans d'expérience dans la gestion de projet plus particulièrement dans la coordination de projet. Les autres compétences portent sur les compétences plus générales, tels que les compétences informatiques avec les gestions des outils de bases, mais aussi sur la capacité a communiquer et à échanger (en anglais) et sur la gestion de planning. Un plus non négligeable est une expérience dans un service de vente.

4.2.3 Le poste dans mon projet professionnel et personnel

Ce poste comme le précédent répond à mon envie personnelle de travailler et d'habiter dans la région environnante de Bâle. Il me permettrait également de rester au contact de la recherche avec ces contacts avec l'industrie pharmaceutique et de participer à la gestion de projet varié. Je pense également qu'il y a des possibilités de progression surtout avec un profil PhD qui me permettra d'avoir du crédit auprès des clients.

Les contraintes selon moi pour ce poste sont multiples, je n'ai jamais eu d'expérience en vente ce qui peut être un problème si jamais cette partie du travail ne me correspond pas. L'autre contrainte majeure pour moi est la communication écrite sans faute, étant dyslexique il est compliqué pour moi d'écrire surtout en anglais sans faire de faute, ce qui risque de me faire perdre beaucoup de temps en terme de relecture.

Il est également demandé une expérience de 3 ans en gestion de projet mais pour répondre à ce point je mettrai en avant ma thèse pendant laquelle j'ai effectué de la gestion de plus de 3 projets différents.

Annexe n°1 : Budget de thèse

Ressources Humaines / Salaires	
Doctorant	72000
Charges patronal	25265
Prime	7200
Frais de scolarité	1888
Encadrant 1	23040
Encadrant 2	5760
Consommables/matériel informatique	
Fourniture de bureau	140
Matériel informatique	830
Logiciels	640
Infrastructure	
Charges du bâtiment	57600
Déplacement/formation	
Congrès	645
Mission étranger	740
Formations	1000
Communication	
Adhésion société de recherche	90
Frais de publication	5480
Support poster	70
Edition de la thèse	200
Consommables expérimentales	
Produits chimiques	2555,18
Consommable patch	481,01
Consommable de laboratoire	850,12
Matériel expérimentales	
Tondeuse	25,4
Trousse de dissection	251,49
Pompe péristaltique	295,25
Bain Marie	92,86
Set up patch	15000
Set up Ca2+	12000
Poste de chirurgie	4000
Poste d'isoflurane	2000
Vibratome	2800
Pince calibré	800
Plantar	2400
Rotarod	50
Beam walk	50
Animaux et animalerie	
Animaux janvier	4138,83
Animaux + frais chronobiotronc	3355,14

Total : 253733,3 €

Annexe n° 2 : Schéma de la méthodologie/démarche scientifique

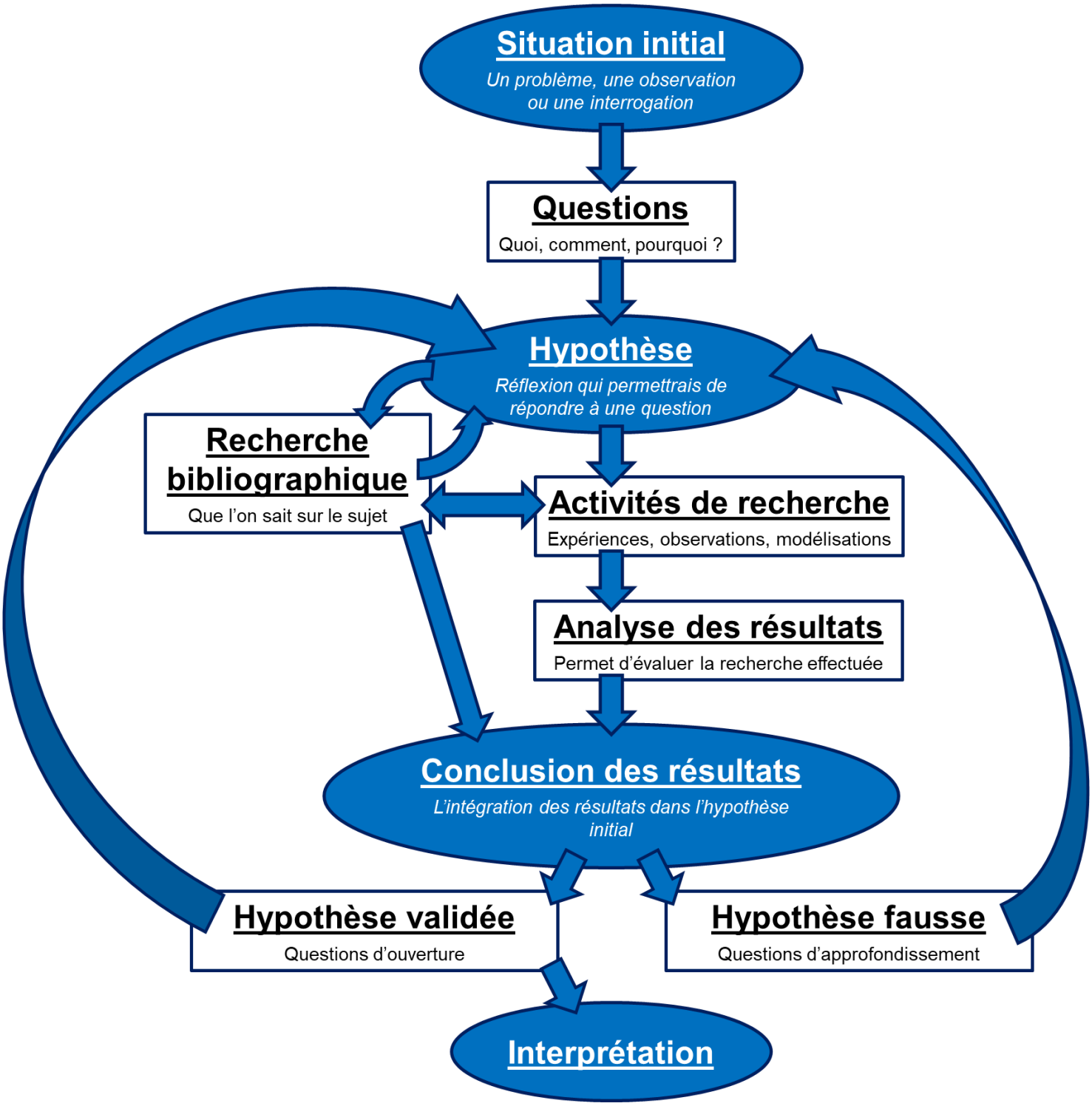

Annexe n° 3 : Synthèse des entretiens réseaux

Entretiens n°1 : Dr.Méggane Melchior (20/04/2021)

Entreprise/structure : CNRS – INCI Poste/fonction : Manager de projet

Contexte : Méggane a soutenu sa thèse dans la même équipe que moi en Mars 2018, elle est partie directement chez Idorsia à Bâle à la fin de sa thèse. Puis après 2 ans, pour des raisons personnelles elle est revenue au laboratoire en qualité de manager de projet. C'est donc une personne facilement contactable avec laquelle je m'entends bien qui est passée par l'industrie pharmaceutique en Suisse directement après sa thèse. Son parcours était donc très intéressant pour moi c'est dans ce contexte que je l'ai contactée.

Résumé : Méggane après sa thèse a donc été recrutée par Idorsia via un ancien membre du labo (Pierre-Eric Juif) en tant que « *clinical pharmacologist junior* ». Elle s'est donc occupé de la gestion de projet de recherche clinique de phase 1 et 2 (phase précoce de la recherche clinique), ses missions étaient d'écrire des protocoles, d'analyser les documents, les datas, de suivre les réunions avec les médecins et la pré-clinique, en somme de gérer toute la partie scientifique. Son background de connaissances en neurosciences n'a pas été primordiale, le plus important sont les connaissances globales en biologie et la méthode de travail scientifique. Malgré une proposition de CDI elle a choisi de ne pas prolonger et de revenir sur Strasbourg. Elle a donc contacté son ancien directeur de thèse pour avoir des contacts et il lui a proposé un poste de Manager de projet. Elle coordonne les projets, les budgets, les commandes, gère les stagiaires et occasionnellement réalise des expériences. Elle aimerait maintenant développer la partie enseignement et devenir maitre de conférence.

Suite : Méggane m'a donné le contact de Pierre-Eric Juif (Responsable de recherche clinique chez Idorsia) et de Safia Ayachi (Domain therapeutics).

Entretiens n°2 : Dr.Pascal Darbon (04/05/2021)

Entreprise/structure : CNRS – INCI Poste/fonction : Enseignant chercheur et Directeur adjoint d'unité

Contexte : Pascal est un enseignant chercheur très impliqué dans l'école doctorale et a vu passer beaucoup d'étudiants, il a donc beaucoup de contact. Je sais aussi qu'il a été en post-doctorat (CDD jeune chercheur) à Bern en Suisse.

Résumé : Pascal a soutenu sa thèse en 1998 à Besançon puis a été en post-doctorat pendant 7 ans dont 5 ans à Bern. En 2006 il obtient un poste de maitre de conférence à Strasbourg. Il a encadré 4 doctorant depuis et il enseigne beaucoup à différents niveaux, Licence, Master. Il a été pendant longtemps responsable au sein de l'école doctorale des sciences de la vie et de la santé et est maintenant directeur adjoint de notre institut.

Suite : Pascal m'a informé des démarches et des bonnes pratiques pour réaliser un post doctorat en Suisse. Il m'a aussi donné des contacts dans la recherche et des anciens doctorants qui sont maintenant dans l'industrie à l'international.

Entretiens n°3 : Dr.Pierre-Eric Juif (25/05/2021)

Entreprise/structure : Idorsia Poste/fonction : Associate Director, Project Clinical Pharmacologist

Contexte : Méggane nous a mis en contact car elle sait que Pierre-Eric apprécie rencontrer et échanger avec les jeunes doctorants en particulier ceux de sa précédente équipe. Nous avons donc convenu d'un entretien par visio pour échanger dans le cadre de ces entretiens réseaux.

Résumé : Pierre-Eric a soutenu sa thèse au Luxembourg en 2009 puis a réalisé 4 ans de post-doctorat, 1 ans dans son équipe du Luxembourg et 3 ans dans mon équipe a l'INCI à Strasbourg. Son objectif était de postuler dans la recherche académique, mais il s'est rendu compte de la difficulté d'obtenir un poste dans la recherche académique ou même privé avec uniquement une thèse et un post-doctorat. En dernière année de post-doctorat il a donc réalisé un DU (diplôme universitaire) pour se former et approfondir la recherche clinique, avec 6 mois de cours et un stage pratique pour valider la formation. Il a ensuite postulé à de nombreuses offres de post-doctorats. Il entre en post-doctorant en études cliniques pharmacologique chez Actelion en 2014 (dont la branche R&D deviendra Idorsia en 2017) et progresse depuis lors jusqu'à devenir directeur associé depuis 2019. Ses projets portent notamment sur les projets Neuro-inflammation. Une journée type consiste à faire un peu de littérature, beaucoup d'écriture de protocole, un peu d'analyse et de relecture d'articles et surtout beaucoup de réunions avec les médecins cliniciens.

Suite : Pierre-Eric a accepté de m'ajouter sur son réseaux Linkedin mais aussi de partager mes potentiels publications de recherche d'emplois. Il m'a suggéré de réaliser des formations ou du moins de mettre en valeur mes compétences transversales et hors de mon domaine d'expertise des neurosciences. Il m'a aussi beaucoup conseillé sur les manières d'aborder les post-doctorats pour rentrer dans le domaine de l'industrie et m'a convié à le recontacter quand je commencerai la recherche d'emploi pour m'aider.

Annexe n° 4 : Offres d'emplois/pistes professionelles

Offre n°1 : Discovery Scientist in Protein Degradation at Roche

1

Discovery Scientist in Protein Degradation in Neuroscience & Rare Diseases Research

de fr es ru tr it pt zh ja

At Roche, we believe it is urgent to deliver medical solutions now – even as we develop innovations for the future. We are passionate about improving the lives of patients with brain diseases, and strive for ambitious ideas, innovative approaches and urgent action. Our belief is that our success as a company will come from developing therapies for patients in need, which is why we come to work every single day. We commit ourselves to scientific rigor, unassailable ethics, and access to medical innovations for all. We do this today to build a better tomorrow.

Within Roche's Pharma Research and Early Development (pRED), Neuroscience & Rare Diseases represents a major focus area where we are committed to realizing our long-term vision of changing lives of patients with severe brain disorders. Our preclinical research and early clinical development activities center around large and rare indications within the four major pillars of neurodevelopmental disorders, movement disorders, dementias, and multiple sclerosis. With unparalleled strengths across diverse disciplines, Roche is uniquely positioned to lead in transforming science to medicines for patients with disorders of the nervous system.

To achieve our goals, Roche pRED Neuroscience & Rare Diseases is currently undergoing a major and exciting recruitment effort for a large number of new positions to further build our discovery engine for the next generation of transformative therapies. Among these we are seeking a Discovery Scientist in Protein Degradation in the Section of Neural Signalling within the Department of Neuroscience & Rare Diseases Research. All positions are based in the Roche Innovation Center Basel in Switzerland.

The position

As Discovery Scientist you will be an integral part of the Protein Degradation Lab within the Neural Signalling Section in the Neuroscience & Rare Diseases Research department. In this 100% permanent position you will perform la research roughly 50% of your time while leading research and early portfolio

2

projects for drug discovery efforts towards the goal of targeting pathways related to protein degradation in neurons and glia. In our highly collaborative and multidisciplinary pharma research matrix environment you will perform exploratory activities focusing on various intracellular protein degradation mechanisms and pathways with respect to Neuroscience & Rare Diseases indications. In addition you are expected to provide support for assay development, establish screens for early drug discovery projects, provide intellectual input towards understanding of disease mechanisms, and propose new drug targets and approaches to target proteins in the brain in specific cell types. In this single contributor role with initially no direct reports you will be mentored and trained to lead an early drug discovery project and project team of 8-10 people with the goal to develop you towards an independent preclinical pharma research scientist, lab head and Roche Research Project Leader. This position is ideal for individuals with relevant technical expertise who are motivated to switch from an early academic position (postdoc level) to a pharma industry research career and to get introduced to the new way of working in such an environment.

Your main responsibilities

- While performing substantial hands-on lab work (~50% of the time), you also will be the subject matter expert on proteasomal and related protein degradation pathways and lead, perform and build up efforts in Neuroscience and Rare Diseases Research towards state-of-the-art methodology and approaches in this field with a focus on applications to drug discovery.
- Under mentorship of an experienced Roche Research Project Leader you will lead an early drug discovery research project team of roughly 8-10 people (no direct reports)
- You will propose new drug targets and therapeutic approaches and lead research aimed at advancing drug discovery projects through the pipeline starting from identification of protein degradation targets, target validation, design of in vitro assays for screening, design and execution of proof of mechanism studies.
- You will support development and characterization of relevant biochemical, cellular and rodent models to explore and test protein degradation.

3

- You will effectively, design, plan, execute, document and communicate scientific research and results both within the departments as well as to supporting functions.
- You will summarize scientific novelty from your research, submit patent applications and present your results at conferences and publish in peer-reviewed journals
- You will also join a vibrant multicultural team of scientists, associates, postdocs and students working towards innovative approaches to drug discovery in CNS disorders. In that environment you will be asked to train or supervise as non-line manager research associates, postdocs, students and trainees.

Who you are

Must haves

- You have a PhD in Biochemistry, Life Sciences, Molecular and Cellular Biology, Medical Biotechnologies/Biology, Neuroscience, or a related field
- You are working or have been working as a postdoc related to protein degradation (UPS related pathways preferred) or proteinopathies, ideally on a CNS or neurodegeneration related topic or have proficient hands-on technical experience in proteasomal protein degradation in non-CNS cell types (e.g. in cancer biology) that can be applied to the brain too
- You have strong hands-on protein biochemistry expertise and apply this in cells and tissue
- You are proficient in animal and cellular modeling of proteinopathies or protein degradation and ideally have experience with viral vectors in this context; hands-on experience with mammalian or primary cell culture techniques is expected
- You have a deep understanding of cutting-edge methodologies for studying/assessing subcellular compartments/mechanisms including fluorescent or other reporter-based live-cell imaging (i.e. Incucyte, Operetta, or similar), confocal microscopy or other high resolution imaging of cell culture experiments or immunostaining of brain tissue and you are proficient in related image analysis and quantification

4

- You are passionate about Neuroscience & Rare Disease drug discovery, scientific rigor is a genuine part of your working style, and you bring a flexible mindset to an agile department with fast-paced project work
- You have a proven scientific publication track record in the field of proteinopathy or protein degradation, ideally with links to Alzheimer's disease or other neurodegenerative disorders
- Experience with working in drug discovery projects in biotech / pharmaceutical industry is a plus but not a prerequisite
- You are well self-organized and -driven and have excellent communication skills in English (speaking and writing) and are proficient at planning, recording, and executing experiments and data analysis.
- You have strong interpersonal skills to lead collaborative research work in a multi-disciplinary matrix structure and the motivation to grow eventually into an independent lab head and people leader

Desirable

- You are familiar with disease mechanisms related to proteinopathies of the CNS including tauopathies, synucleinopathies or related disorders and have experience with in vivo models for Alzheimer's and Parkinson's disease; having a Swiss LTK1/2 or respective European Felasa or similar certificate is a plus
- basic understanding of principles of pharmacology (e.g. potency / efficacy, measures of receptor occupancy / target engagement, strategies to define a pharmacologically active dose etc.) is a plus;
- Knowledge of iPSC or co-culture systems and methods is a plus;
- You are tech savvy and keen to learn or develop novel methods (including single cell multi-omics) and implement them in your work process. Associated with this, you are also used to interact with bioinformaticians or data scientists or are trained in handling large data-sets yourself; experience in structural biology and EM is a plus

Are you ready to apply? Roche embraces diversity and equal opportunity in a serious way. We are committed to building teams that represent a range of backgrounds, perspectives, and skills.

If you still have questions then please check our FAQs and videos on careers.roche.ch/faq.

5 *For non-EU / EFTA citizens: Please state your eligibility status to work in Switzerland (e.g. B-Permit, C-Permit) and note that if you do not own a valid Swiss work permit, Roche cannot guarantee your final employment due to authority regulations.*

Who we are

At Roche, 100,000 people across 100 countries are pushing back the frontiers of healthcare. Working together, we've become one of the world's leading research-focused healthcare groups. Our success is built on innovation, curiosity and diversity.

Roche is an equal opportunity employer.

Job facts

Location **Switzerland, Basel-City, Basel** | Function **Research & Development** | Subfunction **Research** | Schedule **Full time** | Job level **Individual contributor** | Job type **Regular** | Division **Roche Pharmaceuticals** | Posted since **2021/03/05** | Job-ID **202102-104144**

Get in touch

Mrs. Mélodie Lee Mairon

Offre n°2 : Associate Project Manager at ThermoFischer

1

Associate Project Manager, Labeling

Thermo Fisher Scientific ★★★½☆ 3,411 avis
Bâle, BS

When you're part of the team at Thermo Fisher Scientific, you'll do important work, like helping customers in finding cures for cancer, protecting the environment or making sure our food is safe. Your work will have real-world impact, and you'll be supported in achieving your career goals.

Fisher Clinical Services GmbH is part of Thermo Fisher Scientific Corporation, a world-class company serving the scientific community and healthcare industry. We are leaders in providing clinical supply chain management services and clinical supplies distributed to patients worldwide. For more information about our site in Allschwil please visit: www.fisherclinicalservices.com

Associate Project Manager (Labeling)

The Associate Project Manager manages projects and studies for customers. You will work with various departments, proactively working with all the parties involved in the study and in timeline management, milestone tracking and weekly updates to the customer. Taking on full study management of a project coordinating across all technical and service aspects of a project. The Associate Project Manager is mainly working on accounts which are already established Customers.

Responsibilities:

- Works with the Client to finalize Specifications. This may include meetings at the client's premises.
- Setting up and maintaining study filing systems and maintains accurate records for all work undertaken.
- Coordination and communication of all relevant activities, both internal and external to ensure that all services and products are ready for the start of the study or as required by the customer.

2

- Use of appropriate project planning tools to communicate milestones and critical path activities and responsibilities.
- Timely provision of reports and other information to customers if applicable.
- Creates and supports creation of Label Specifications, Label proofs and print documentation using internal systems.
- Provides back-up support to other Associate and Project managers.
- Responsible for quote correctness and financial forecasting.
- Monitors project activities and day to day business as well as establishment of a customer approved Job Specification.
- Collects all the information on a study design including correct label texts and all other relevant information.
- Coordinates shipments through the logistics department.
- Responsible to log issues into Trackwise and work on the investigation.
- Applies Good Manufacturing Principles in all areas.

Your Profile:

- Professional degree, preferably in a health related field or in customer service.
- 2-3 years of successful experience in project management as a Project Coordinator or equivalent.
- Proficiency in personal computer applications (e.g. Microsoft Word, Excel, PowerPoint, Access, Outlook).
- Proven experience with customers in a dynamic environment.
- Excellent communication, organizational skills, relationship building and project co-ordination skills.
- Understanding and competent use of SOPs required by company Quality standards.
- Excellent organizational, planning, verbal, written and numerical skills with the ability to analyze and define solutions and manage multiple tasks to meet strict deadlines.
- Requires ability to develop strong customer management skills; proactively anticipates, understands, and responds to the needs of clients to meet or exceed their expectations.

At Thermo Fisher Scientific, each one of our 75,000 extraordinary minds has a unique story to tell. Join us and contribute to our singular mission—enabling our customers to make the world healthier, cleaner and safer.

Thermo Fisher Scientific

Université de Strasbourg

Louis HILFIGER

École Doctorale des Sciences de la Vie et de la Santé STRASBOURG

Analyse *in vivo* de l'activité anti-hyperalgésique de molécules innovantes.

Résumé :

Le traitement des douleurs est l'un des enjeux important du 21ème siècle, en effet le nombre de personne souffrant de douleurs chroniques dans le monde dépasse les 100 millions. Cependant le traitement de ces douleurs est complexe et la médecine est aujourd'hui extrêmement dépendante des analgésiques dérivés des opiaces, qui ont pourtant des effets secondaires particulièrement délétères. Ainsi, pour continuer à traiter les douleurs il est essentiel de développer des traitements alternatifs.

Dans ce contexte, mon travail de thèse a consisté à explorer le potentiel analgésique de nouvelles molécules innovantes ciblant les systèmes analgésiques endogènes. J'ai ainsi pendant ma thèse pu caractériser le potentiel anti-hyperalgésique de deux molécules innovantes, le LIT-001 une issue de l'ingénierie du récepteur de l'ocytocine et la pulégone, un monoterpène analogue du menthol et pourtant largement sous étudié. Cette recherche s'est principalement basé sur une approche comportementale *in vivo* basé sur un modèle de douleur induite.

Mots-clefs : Douleur, analgésie, anti-hyperalgésie, pharmacologie, ocytocine, terpène, menthol, pulégone, évaluation comportementale.

Summary:

The treatment of pain is one of the major challenges of the 21st century, as the number of people suffering from chronic pain in the world exceeds 100 million. However, pain treatment is complex and medicine is currently extremely dependent on opiate-based analgesics, which have particularly severe side effects. Thus, in order to be able to continue managing pain, it is essential to develop alternatives treatments.

In this context, the aim of my thesis work was to explore the analgesic potential of new innovative molecules targeting endogenous analgesic systems. During my thesis, I was able to characterise the anti-hyperalgesic potential of two innovative molecules, LIT-001, a molecule derived from the engineering of the oxytocin receptor, and pulegone, a monoterpene analogue of menthol, although it remains considerably understudied. The research was mainly based on an *in vivo* behavioural approach using an induced pain model.

Key words: Pain, analgesia, anti-hyperalgesia, pharmacology, oxytocin, terpene, menthol, pulegone, behavioural assessment.